VOLUME 75 AUGUST 19, 1971 NUMBER 17

JPCHAx

THE JOURNAL OF PHYSICAL CHEMISTRY

PUBLISHED BIWEEKLY BY THE AMERICAN CHEMICAL SOCIETY

Molecular Sieve Zeolites

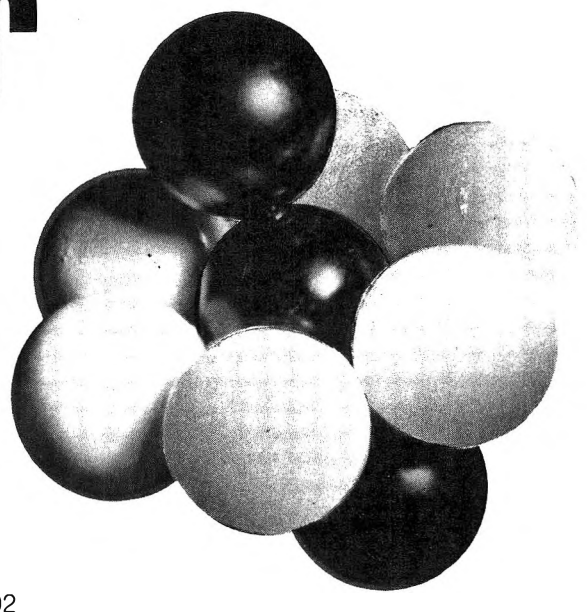

ADVANCES IN CHEMISTRY SERIES No. 101 and 102

Seventy-seven papers from a symposium co-sponsored by the Divisions of Colloid and Surface Chemistry, Petroleum Chemistry, and Physical Chemistry of the American Chemical Society and Worcester Polytechnic Institute, Edith M. Flanigen and Leonard B. Sand, co-chairmen.

Do you need a group of substances that can remove radioactive isotopes from nuclear wastes, remove ammonia from secondary sewage effluents, remove sulfur dioxide from waste gases, foster formation of actinides, or disrupt bacterial cells? These and many other possibilities are available through research on molecular sieve zeolites. For example, they are used for

- separating hydrogen isotopes
- solubilizing enzymes
- carrying active catalysts in curing of plastics
- transporting soil nutrients in fertilizers
- filtering tars from cigarette smoke

"Molecular Sieve Zeolites" reports recent advances in this rapidly developing field. Volume I offers 41 papers devoted to the synthesis, structure, mineralogy, and modification of sieve zeolites. These are followed in Volume II by 36 papers discussing sorption and catalysts.

Volume I: 526 pages with index. Cloth bound (1971) $16.00
Volume II: 459 pages with index. Cloth bound (1971) $16.00
No. 101 and 102 ordered together $30.00
Postpaid in U.S. and Canada; plus 35 cents elsewhere.
Set of L.C. cards with library orders upon request.

Other books in the ADVANCES IN CHEMISTRY SERIES of interest to colloid and surface, petroleum, and physical chemists include:

No. 97 Refining Petroleum for Chemicals
293 pages Cloth bound (1970) $11.50

No. 89 Isotope Effects in Chemical Processes
278 pages Cloth bound (1969) $13.00

No. 87 Interaction of Liquids at Solid Substrates
212 pages Cloth bound (1968) $9.50

No. 86 Pesticidal Formulations Research. Physical and Colloidal Chemical Aspects
212 pages Cloth bound (1969) $9.50

No. 79 Adsorption from Aqueous Solution
212 pages Cloth bound (1968) $10.00

No. 43 Contact Angle, Wettability, and Adhesion
389 pages Cloth bound (1964) $10.50

No. 31 Critical Solution Temperatures
246 pages Cloth bound (1961) $8.00

No. 29 Physical Properties of Chemical Compounds—III
489 pages Cloth bound (1961) $10.00

No. 22 Physical Properties of Chemical Compounds—II
491 pages Cloth bound (1959) $10.00

No. 20 Literature of the Combustion of Petroleum
295 pages Paper bound (1958) $8.00

No. 15 Physical Properties of Chemical Compounds
536 pages Cloth bound (1955) $10.00

Order from:

Special Issues Sales
American Chemical Society
1155 16th St., N.W.
Washington, D.C. 20036

THE JOURNAL OF

PHYSICAL CHEMISTRY

AMERICAN CHEMICAL SOCIETY, *1155 Sixteenth St., N.W., Washington, D. C. 20036*
FREDERICK T. WALL, *Executive Director*

Books and Journals Division
JOHN K CRUM, *Director (Acting)*
JOSEPH H. KUNEY, *Head, Business Operations Department*
RUTH REYNARD, *Assistant to the Director*

 Published biweekly by the American Chemical Society at 20th and Northampton Sts., Easton, Pa. 18042. Second-class postage paid at Washington, D. C., and at additional mailing offices.

All manuscripts should be sent to *The Journal of Physical Chemistry*, Department of Chemistry, University of Minnesota, Minneapolis, Minn. 55455.

Additions and Corrections are published once yearly in the final issue. See Volume 74, Number 26 for the proper form.

Extensive or unusual alterations in an article after it has been set in type are made at the author's expense, and it is understood that by requesting such alterations the author agrees to defray the cost thereof.

The American Chemical Society and the Editor of *The Journal of Physical Chemistry* assume no responsibility for the statements and opinions advanced by contributors.

Correspondence regarding accepted copy, proofs, and reprints should be directed to Editorial Production Office, American Chemical Society, 20th and Northampton Sts., Easton, Pa. 18042. Manager: CHARLES R. BERTSCH. Assistant Editor: EDWARD A. BORGER. Editorial Assistant: EVELYN J. UHLER.

Advertising Office: Century Communications Corporation, 142 East Avenue, Norwalk, Conn. 06851.

Business and Subscription Information

Remittances and orders for subscriptions and for single copies, notices of changes of address and new professional connections, and claims for missing numbers should be sent to the Subscription Service Department, American Chemical Society, 1155 Sixteenth St., N.W., Washington, D. C. 20036. Allow 4 weeks for changes of address. Please include an old address label with the notification.

Claims for missing numbers will not be allowed (1) if received more than sixty days from date of issue, (2) if loss was due to failure of notice of change of address to be received before the date specified in the preceding paragraph, or (3) if the reason for the claim is "missing from files."

Subscription rates (1971): members of the American Chemical Society, $20.00 for 1 year; to nonmembers, $40.00 for 1 year. Those interested in becoming members should write to the Admissions Department, American Chemical Society, 1155 Sixteenth St., N.W., Washington, D. C. 20036. Postage to Canada and countries in the Pan-American Union, $4.00; all other countries, $5.00. Single copies for current year: $2.00. Rates for back issues from Volume 56 to date are available from the Special Issues Sales Department, 1155 Sixteenth St., N.W., Washington, D. C. 20036.

This publication and the other ACS periodical publications are now available on microfilm. For information write to: MICROFILM, Special Issues Sales Department, 1155 Sixteenth St., N.W., Washington, D. C. 20036.

Notice to Authors last printed in the issue of June 10, 1971

TRACE INORGANICS IN WATER ADVANCES IN CHEMISTRY SERIES NO. 73

Twenty-one papers from a symposium by the Division of Water, Air, and Waste Chemistry of the American Chemical Society, chaired by Robert A. Baker. Includes:

Five surveys on broad topics—

- Transport properties of electrolytes
- Anions in aqueous solution
- Effects of trace inorganics on the ice/water system
- Aluminum species in water
- The role of hydrous Mn and Fe oxides in fixation of metals in soils and sediments

Eleven papers on analytical developments, such as:

- Atomic absorption (3 papers)
- Atomic fluorescence
- Flame emission
- Neutron activation

And five research reports.

396 pages with index Cloth (1968) **$12.50**

Set of L.C. Cards free with library orders.

Other books in the **ADVANCES IN CHEMISTRY SERIES** on inorganic chemistry include:

No. 72 Mass Spectrometry in Inorganic Chemistry. A basic tool for chemical manipulations, the mass spectrometer is a conventional monitor for any stage in a research problem to help establish what is going on. 21 Research reports. 329 pages with index
Cloth (1968) $12.00

No. 71 Lanthanide/Actinide Chemistry. The two series share similarities in chemical properties, magnetism, and radiant energy absorption and emission characteristic of *f*-electron species. But important differences exist—oxidation states, bonding, and complex ion formation. Lanthanides—13 papers; actinides—12 papers. 359 pages with index
Cloth (1968) $11.00

No. 62 Werner Centennial. Four biographical papers on Alfred Werner, systematizer of coordination chemistry, and 38 papers that report current research and survey progress in his field since he died 50 years ago. 661 pages with index
Cloth (1967) $17.50

No. 54 Advanced Propellant Chemistry. Primarily directed toward the search for new oxidizers. Twenty-six papers survey theory of advanced oxidizers, oxygen oxidizers, fuels and binders, fluorine systems, and liquid systems. 290 pages with index
Cloth (1966) $10.50

No. 49 Mechanisms of Inorganic Reactions. Ten lectures by top authorities with extensive discussion prepared and presented by 20 more authorities. Topics include ion association in octahedral complexes, bridging groups in electron transfer reactions, kinetic patterns of ligand reactivity, acid-base reactions in fused salts. 266 pages with index
Cloth (1965) $10.00

No. 42 Boron-Nitrogen Chemistry. Thirty-two papers on theoretical and preparative aspects of molecules containing B-N bonds, including many heterocyclic ring compounds. 330 pages with index
Cloth (1964) $10.00

No. 39 Nonstoichiometric Compounds. Twenty-three papers survey the field and give new work on structural aspects of nonstoichiometric oxides, hydrides, chalcogenides, and miscellaneous compounds. 253 pages
Paper (1963) $9.00

No. 37 Reactions of Coordinated Ligands and Homogeneous Catalysis. Directs attention to changes in ligand groups when they attach to metal ions and to the role of coordination compounds in organic syntheses. 255 pages
Paper (1963) $9.50

No. 36 Free Radicals in Inorganic Chemistry. Surveys methods for investigating inorganic free radicals and details studies on several species, including the new difluoramine radical. 175 pages with index
Paper (1962) $7.50

No. 32 Borax to Boranes. Twenty-eight papers from symposia sponsored by the Boron Committee of the ACS Division of Inorganic Chemistry during the peak years of interest in boron chemistry. Covers history and personalities in the field, chemistry of boron and its compounds, including the superfuels. 244 pages
Paper (1961) $8.00

No. 21 Ozone Chemistry and Technology. Sixty papers from the International Ozone Conference cover: ozone chemistry, high concentration ozone, organic chemistry of ozone, ozone analysis and technology, atmospheric ozone, formation in electrical discharge, toxicity, sterilization and water purification, reaction kinetics. 465 pages
Cloth (1959) $10.00

No. 19 Handling and Uses of Alkali Metals. Nineteen articles on the chemistry, manufacture, and use of the alkali metals; five are devoted solely or partly to lithium, two to potassium, the remainder to sodium. 177 pages
Paper (1957) $7.00

All books postpaid in U.S. and Canada, plus 30 cents foreign and PUAS

Order from **SPECIAL ISSUES SALES**

AMERICAN CHEMICAL SOCIETY
1155 SIXTEENTH ST., N.W.
WASHINGTON, D.C. 20036

THE JOURNAL OF
PHYSICAL CHEMISTRY

Volume 75, Number 17 August 19, 1971

Platinum Group Metals and Compounds

ADVANCES IN CHEMISTRY SERIES
NO. 98

Eleven papers from a symposium by the Division of Inorganic Chemistry of the American Chemical Society chaired by U. V. Rao.

What new complexes of the platinum group metals have been synthesized? Here is a collection of papers presenting data on chalcogenides, oxides, nitrido and hydrido complexes, as well as the catalytic properties of these metals and their alloys. Information is included on

- synthesis
- structure
- magnetic susceptibility
- double bond migration

The platinum group metals are considered from the viewpoints of both industry and research. Their magnetic and thermodynamic properties are explored, as well as recent chemistry of σ- and π-bonded complexes. Crystal structure is discussed by several authors, with data presented in the form of

- x-ray scattering data
- absorption spectra
- crystal spectra
- infrared spectra
- Mossbauer spectra
- vibrational spectra

165 pages with index. Cloth bound (1971) $9.00
Postpaid in U.S. and Canada; plus 35 cents elsewhere.
Set of L. C. cards with library orders upon request.

Other books in the ADVANCES IN CHEMISTRY SERIES of interest to inorganic chemists include:

No. 89 Isotope Effects in Chemical Processes
278 pages Cloth bound (1969) $13.00

No. 82 Radiation Chemistry — II
558 pages Cloth bound (1968) $16.00

No. 81 Radiation Chemistry — I
616 pages Cloth bound (1968) $16.00

No. 81 and No. 82 ordered together $30.00

No. 78 Literature of Chemical Technology
732 pages Cloth bound (1968) $17.50

No. 73 Trace Inorganics in Water
396 pages Cloth bound (1968) $12.50

No. 72 Mass Spectrometry in Inorganic Chemistry
329 pages Cloth bound (1968) $12.00

Order from:
Special Issues Sales
American Chemical Society
1155 16th St., N. W.
Washington, D. C. 20036

NOTES

COMMUNICATIONS TO THE EDITOR

AUTHOR INDEX

In papers with more than one author the name of the author to whom inquiries about the paper should be addressed is marked with an asterisk in the by-line.

THE JOURNAL OF
PHYSICAL CHEMISTRY

VOLUME 75, NUMBER 17 AUGUST 19, 1971

Dynamic Sampling of the Deuterium Hydride Self-Exchange behind Reflected Shock Waves[1]

by R. D. Kern* and G. G. Nika[2]

Department of Chemistry, Louisiana State University in New Orleans, New Orleans, Louisiana 70122
(Received March 5, 1971)

Publication costs assisted by the National Science Foundation

The self-exchange reaction of deuterium hydride diluted in neon has been studied over the temperature range 1800–2800°K. Dynamic sampling of the reflected shock zone at 20-μsec intervals was performed with a time-of-flight mass spectrometer. Sixty-one experiments covering a total density range 1.7–3 $\times$ 10^{-6} mol cm^{-3} were analyzed during typical reaction times of 500 μsec. During the observation period of runs exceeding 2600°K, an equilibrium condition was observed. The time dependence of product formation was found to be nonlinear. An average mole fraction basis was used for product formation. The reaction profiles were fit to the equation $[1 - 4f_{av}] = \exp(-k'[M]t^2)$; $k' = 10^{16.67\pm0.21}\exp(-40{,}980 \pm 2250/RT)$ cm^3 mol^{-1} sec^{-2}. The equilibrium constant for the $H_2 + D_2 \rightleftarrows 2HD$ system was obtained using the previously reported rate constant for the forward reaction along with the self-exchange rate constant reported here. Agreement with the calculated equilibrium constant was obtained within the experimental errors associated with the kinetic results.

Introduction

The homogeneous isotopic exchange reactions of HCl + D_2[3] and H_2 + D_2[4] in the shock tube have recently been studied in this laboratory by a variety of dynamic sampling techniques. The Arrhenius parameters for these reactions are E^* = 34.3 and 44.4 kcal mol^{-1} and log A = 16.1 and 16.9 cm^3 mol^{-1} sec^{-2}, respectively. Both systems exhibited similar order exponents. Reaction profiles of product formation were found to be a nonlinear function of time and both systems were fitted to quadratic time-dependent rate expressions.

The H_2–D_2 reaction has also been studied by Bauer and Ossa[5] and by Burcat and Lifshitz.[6] Using the single-pulse shock tube technique, these workers reported activation energies of 42.3 and 40.0 kcal mol^{-1}, respectively. The reaction orders determined from ref 5 were H_2(0.38), D_2(0.66), Ar(0.98) and from ref 6 H_2 + D_2(1.3), Ar(0.65). The self-exchange reaction has been studied by Lewis and Bauer,[7] who reported E^* = 35.9 kcal mol^{-1}, 1.43-order dependence for HD and 0.57 order for argon. The measurement of the time dependence of product formation was not attempted in the single-pulse shock tube experiments.[5-7]

The investigation of the HD self-exchange provides two opportunities to check the consistency of the experimental results reported for the forward reaction.[4] First, the magnitude of the activation energy should be the same since the overall reaction is thermoneutral.

(1) Support of this work by the National Science Foundation under Grant GP-23137 and also funds for equipment from NSF Departmental Science Development Program GU-2632 are gratefully acknowledged.

(2) NDEA Fellow.

(3) R. D. Kern and G. G. Nika, *J. Phys. Chem.*, **75**, 171 (1971).

(4) R. D. Kern and G. G. Nika, *ibid.*, **75**, 1615 (1971).

(5) S. H. Bauer and E. Ossa, *J. Chem. Phys.*, **45**, 434 (1966).

(6) A. Burcat and A. Lifshitz, *ibid.*, **47**, 3079 (1967).

(7) D. Lewis and S. H. Bauer, *J. Amer. Chem. Soc.*, **90**, 5390 (1968).

Second, a nonlinear time dependence for the growth of products H_2 and D_2 should be observed.

Experimental Section

The shock tube used in this study has been described previously.[3] All test gas mixtures had a maximum residence time of 30 sec in the shock tube prior to shock initiation. During this period an analog signal for O_2 was compared to background. Improvements in the vacuum system produced a background O_2 level of 15 ppm. This lower limit was established by using neon gas mixtures in which known ppm O_2 levels were added. On this basis no experiment was performed at oxygen levels greater than 20 ppm. Outgassing rates in the shock tube–TOF system were less than 0.01 μ/min. Typical ultimate vacuums were 7×10^{-7} Torr in the shock tube, 5×10^{-7} Torr in the ion source ballast volume, and 2×10^{-7} Torr in the TOF main chamber.

Deuterium hydride was purchased from Merck Sharp and Dohme and further purified as follows. A liquid nitrogen trap was added to the gas handling system, filled with Matheson Coleman and Bell activated "Linde" Type 4A (4–8 mesh) molecular sieve. The trap was baked until outgassing could no longer be detected by a thermocouple gauge during a 12-hr room temperature period. The entire trap was cooled by liquid nitrogen; HD was introduced and collected upon the lower region of the trap. Successive fractions of the condensed gas were analyzed with the mass spectrometer. Those fractions which exhibited O_2 levels less than 20 ppm were diluted with Matheson research grade neon (99.995%) and allowed to stand in 5-l. storage bulbs prior to use. A Toepler pump was used to compress the remaining HD into a 1-l. storage bulb.

Focusing of the TOF for static equalization of analog outputs from m/e 2 and 4 signals was maintained by use of an equimolar $H_2 + D_2$ gas mixture diluted in neon. The low mass signal heights relative to one another were kept within 2% for all runs. The ionizing voltage was 35 eV.

Reflected shock zone temperatures were calculated from measurements of the incident shock velocity at four equally spaced stations. Extrapolations of the slightly decelerating incident wave velocities to the end wall were performed as reported in ref 3.

Results

For the self-exchange, $2HD \underset{k_1}{\overset{k_{-1}}{\rightleftarrows}} H_2 + D_2$, the reaction profile for HD reacting at temperatures where $k_{-1}/k_1 = {}^1/_4$ is represented by the equation

$$[1 - 4f_{H_2}] = \exp(-4k_{-1}[HD]_0 t) \qquad (1)$$

where

$$f_{H_2} = \frac{[H_2]}{[HD]_0}$$

The initial concentration is given by $[HD]_0$, and the rate constant for the self-exchange is k_{-1}. The rate of product formation is defined by

$$\text{rate} = \frac{d[H_2]}{dt}$$

Equation 1 was modified to test experimentally by setting $4k_{-1} = k'[M]^y$ to allow for any inert gas dependence of order y and setting $[HD]_0 = [HD]_0^x$ and $t = (t - t_{ind})^z$ to evaluate values for x and z other than unity. Since an induction time, t_{ind}, was not detected, t was equated to t^z. The working expression for the mole fraction of products, f_{av}, for a given mass spectrum recorded during the observation period was taken to be the arithmetical average of the peak heights of m/e 2 and 4 divided by the sum of the peak heights of m/e 2, 3, and 4. The experimental form of eq 1 is

$$[1 - 4f_{av}] = \exp(-k'[HD]_0^x[M]^y t^z) \qquad (2)$$

At early times, eq 2 reduces to a form which neglects the back reaction

$$f_{av} = \frac{k'}{4}[HD]_0^x[M]^y t^z = k_{obsd} t^z \qquad (3)$$

A preliminary value of z was determined by plotting $\log f_{av}$ *vs.* $\log t$. The average of the preliminary values was greater than three-halves and, as explained below, is about 1.7. However, since a nonintegral time dependence does not have any simple mechanistic interpretation, z was taken to be 2. An initial estimate for k_{obsd} ($= k'[HD]_0^x[M]^y/4$) was obtained by plotting f_{av} *vs.* t^2.

The initial estimate for k_{obsd} was used as input for the computer. The computer searched for the value of k_{obsd} which reproduced the entire experimental profile with the lowest standard deviation. The equation for the entire profile was

$$[1 - 4f_{av}] = \exp(-k_{obsd} t^2) \qquad (4)$$

Average mole fraction profiles calculated on a DEC PDP-10 were plotted on a Houston Instruments Corp. DP-3 Digital Plotter through an XY-10 controller.

The experimental value for z was derived from plots of $\log(-\ln[1 - 4f_{av}])$ *vs.* $\log t$. The graphical values were about 1.7 although the individual reaction profiles were fit satisfactorily by z equal to 2. Linear extrapolation of these plots to early reaction times ($\lesssim 10$ μsec) clearly indicates the absence of an induction period. Figure 1 depicts a best-fit reaction profile generated by eq 4 along with the experimental points.

The $\log(-\ln[1 - 4f_{av}])$ *vs.* $\log t$ plot corresponding to the first figure is shown in Figure 2. The rejection of the data point at early reaction time is a general result of errors in measuring small signal peak heights on the Polaroid film records. Measurements of the peak heights have been described elsewhere.[3] The rejected point corresponds to $f_{av} \simeq 0.025$. Typical initial peak

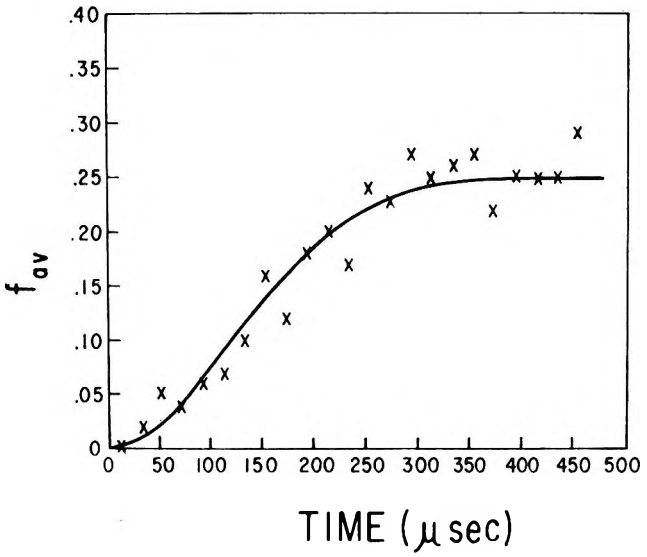

Figure 1. Fit of quadratic time dependence profile to TOF data for a run at 2695°K: ×, experimental points; ——, calculated profile.

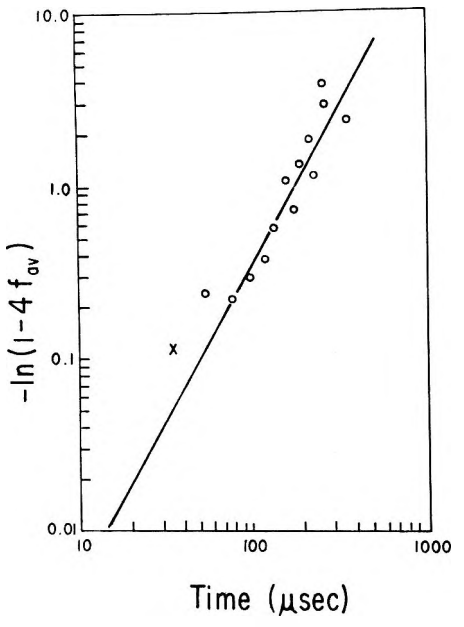

Figure 2. Plot of log ($-\ln [1 - 4f_{av}]$) *vs.* log t from TOF data for a run at 2695°K: O, experimental points; ×, rejected point; z (slope) = 1.8.

heights for m/e 3 were 8 mm; thus signal heights for m/e 2 and 4 were about 0.2 mm for $f_{av} \simeq 0.025$. Statistical fluctuations and the microscope graticule divisions combine to establish a lower limit of 0.1 mm for peak height measurements. Thus, the rejection of a point involving a possible error of 100% is justified. Those values of $f_{av} = 0$ and $\geq 1/4$ were not used since the log function is discontinuous at those values.

The reaction was studied at different initial concentrations to determine the value of x and at a different initial pressure to determine y. A twofold variation in HD concentration, 6 to 3%, yielded a value of $x = 0$ on

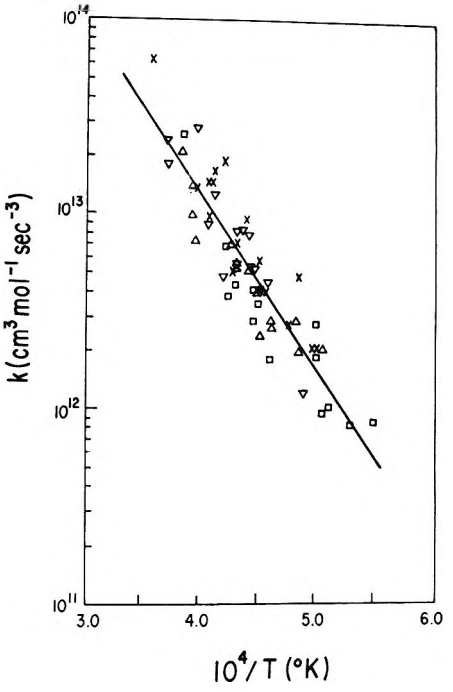

Figure 3. Arrhenius plot of data in Table I: ×, mixture A; △, B; □, C; ▽, D.

a mole fraction basis. On a concentration basis, the order with respect to HD is 1. This value is consistent with the results from the forward reaction.[4] The inert gas dependence was studied by varying the initial pressure from 4.8 to 7.5 Torr on a mixture in which the HD concentration was held constant at 4%. The variation of [M] was limited to 64% due to operational difficulties precipitated by excessive pressures in the ion source. The value of y was found to be 0.57 although the error associated with the measurement will allow a value of 1.

The determination of y has been a problem in previous work[3,4] and is the least accurately determined quantity in the rate equation. To compare the forward reaction rate constants with single-pulse data, y was taken to be 1 even though the experimental value was ≤ 0.5. The uncertainty in the determination permitted a value of 1 to be used. In the same spirit of comparison, the data for the self-exchange is treated with $y = 1$ using the equation

$$[1 - 4f_{av}] = \exp(-k'[M]t^2] \quad (5)$$

The results are listed in Table I for the four mixtures. An Arrhenius plot of the data is shown in Figure 3. Least-squares treatment of the rate constants yielded values of $E^* = 40.98 \pm 2.25$ kcal mol^{-1} and log $A = 16.67 \pm 0.21$ cm^3 mol^{-1} sec^{-2}.

The rate constant expression from the single-pulse experiments[7] was recalculated for a quadratic time dependence by dividing the expression by the residence time, 1 msec. The Arrhenius parameters for this recalculated rate constant are $E^* = 35.94 \pm 2$ kcal mol^{-1} and log $A = 15.39$ cm^3 mol^{-1} sec^{-2}. To collate

Table I: Rate Constants for Self-Exchange of Deuterium Hydride

Mixture (neon diluent)	T_5, °K	$\rho_5 \times 10^6$, mol cm^{-3}	$k \times 10^{-11}$, cc mol^{-1} sec^{-2}
A. 6% HD	2007	1.77	20.6
P_1 = 4.8 Torr	2018	1.78	20.1
	2069	1.80	46.9
	2096	1.80	27.2
	2191	1.87	40
	2220	1.92	57.8
	2226	1.88	40.8
	2274	1.95	93.4
	2324	1.91	70.7
	2337	1.93	51
	2423	1.95	165
	2450	1.99	154
	2450	1.93	143
	2457	1.93	96.9
	2464	1.92	144
	2528	1.98	136
	2813	2.04	611
B. 4% HD	1890	1.73	20.2
P_1 = 4.8 Torr	2077	1.73	28.4
	2087	1.77	19.6
	2164	1.79	26.1
	2175	1.83	28.2
	2215	1.82	23.9
	2233	1.79	39.7
	2275	1.89	50.6
	2318	1.86	54.2
	2318	1.87	63.9
	2344	1.81	69.3
	2541	1.94	73.5
	2548	1.90	139
	2548	1.96	97.6
	2608	1.92	204
C. 4% HD	1820	2.65	8.63
P_1 = 7.5 Torr	1891	2.70	8.25
	1956	2.72	10.2
	1975	2.74	9.69
	2005	2.76	27.1
	2010	2.77	18.7
	2181	2.85	18.1
	2227	2.89	34.9
	2245	2.91	41.1
	2245	2.90	28.5
	2337	2.94	43.8
	2363	2.98	38.3
	2369	2.95	69.8
	2608	3.05	256
D. 3% HD	2049	1.72	12
P_1 = 4.8 Torr	2190	1.82	44.4
	2225	1.78	40
	2242	1.80	53.3
	2260	1.80	53.3
	2260	1.80	77.2
	2290	1.81	80.7
	2309	1.81	80.4
	2315	1.83	55.1
	2385	1.86	47.7
	2425	1.85	123
	2459	1.85	87.1
	2522	1.87	274
	2695	1.92	180
	2703	1.92	237

with the results reported here, E^* was fixed at 37.94 kcal mol^{-1}, and the mean temperature of the single pulse work was used to adjust the rate constant expression. Several Arrhenius plots of the forward and reverse reactions are displayed in Figure 4. Points on the extremities of the solid lines mark the temperature range of the experiments. Extrapolated portions are indicated by dashed lines.

The values of log A for k' (this work) and k[4,5] were modified for use in Figure 4 and to calculate the equilibrium constant for the $H_2 + D_2 = 2HD$ reaction. In the integrations to arrive at the equations

$$[1 - 2f_{HD}] = \exp(-k[M]t^2) \quad (6)$$

and

$$[1 - 4f_{av}] = \exp(-k'[M]t^2) \quad (5)$$

a factor of 2 is incorporated in k and a factor of 4 in k'. Correcting for these factors the equilibrium constant is expressed as

$$K = k_1/k_{-1} = 10^{(16.63-16.07)\pm0.43} \times \exp(-[44.37 - 40.98] \pm 4.76)$$

Taking the preexponential and 10% of the standard deviation, $K = 10^{0.6} = 4$, in agreement with the calculated equilibrium constant.

Discussion

The conclusions reached in the consideration of three mechanisms to explain the forward reaction[4] apply also to the self-exchange. A summary of these conclusions follows. A four-center molecular mechanism predicts an activation energy $\geq$ 148 kcal/mol,[8] zero-order dependence for the inert gas concentration, and a linear time dependence for product formation. An atomic mechanism requires a combined order dependence of one for reactants expressed on a mole fraction basis, first order for [M], quadratic time dependence for product formation, and an activation energy of about 110 kcal mol^{-1}. A vibrational energy chain mechanism is consistent with the same order dependence as the atomic mechanism but requires a linear time dependence for product formation.

(8) C. W. Wilson, Jr., and W. A. Goddard, III, *J. Chem. Phys.*, 51, 716 (1969).

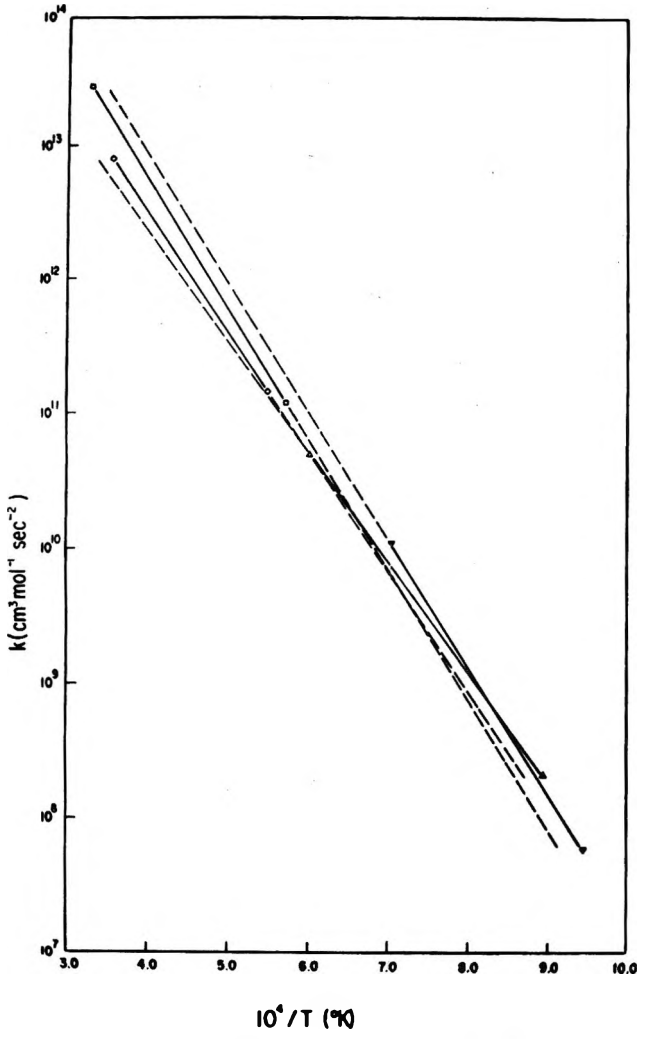

Figure 4. Arrhenius plots for 2HD = H_2 + D_2: ◇—◇, this work; △—△, ref 7; for H_2 + D_2 = 2HD: □—□, ref 4; ▽—▽, ref 5.

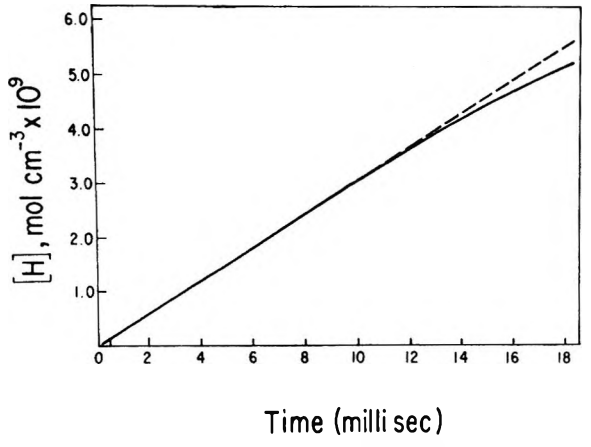

Figure 5. Atomic profile for the H_2 dissociation at 2500°K: - - - - -, neglect of back reaction; ——, back reaction included.

Support of the two critical assumptions involved in the atomic and vibrational chain mechanisms is presented here in graphical form.

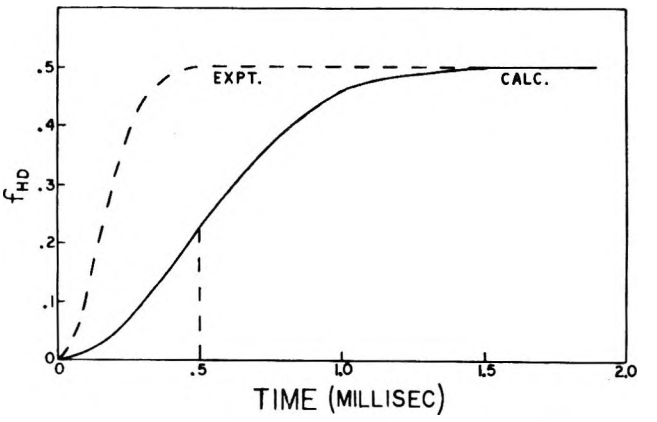

Figure 6. Comparison of f_{HD} reaction profiles at 2500°K: - - - -, ref 4; ——, atomic mechanism.

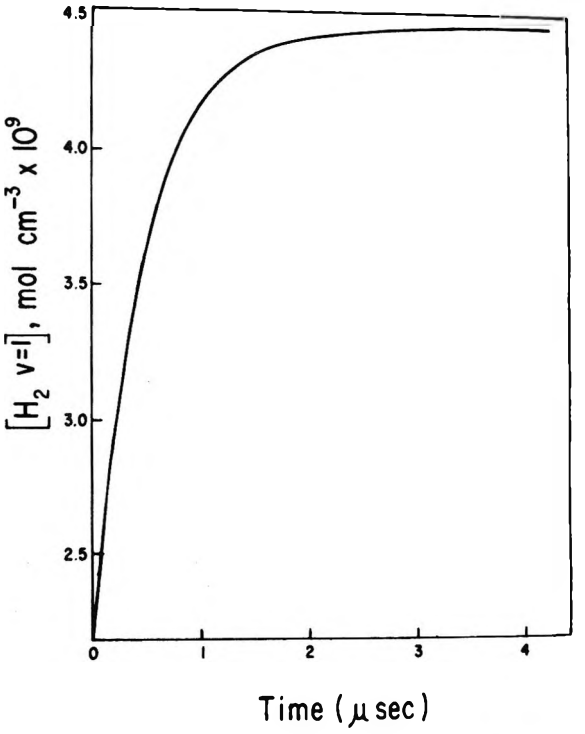

Figure 7. Vibrational energy profile for $H_2(v = 0) \rightleftarrows H_2(v = 1)$ at 2500°K.

In developing the atomic mechanism, the back reaction for H_2 decomposition was neglected. Justification of this is demonstrated in Figure 5. The conditions were 2500°K, k_{diss},[9] $[H_2]_0 = 6 \times 10^{-8}$, $[M] = 2 \times 10^{-6}$, and $[H]_{equil} = 1.3 \times 10^{-8}$ mol cm^{-3} (calculated from the "JANAF Thermochemical Tables"[10]). At 500 μsec, $[H] = 1.6 \times 10^{-10}$ mol cm^{-3}. Equilibrium occurs at about 150 msec, much longer than the observation period of 0.5 msec for the runs reported here. Figure 6 compares the reaction profile derived from the atomic mechanism with the experimental results of

(9) R. L. Belford and R. A. Strehlow, *Annu. Rev. Phys. Chem.*, **20**, 260 (1967).

(10) "JANAF Thermochemical Tables," The Dow Chemical Co., Midland, Mich., 1965.

ref 4. The dotted line was derived from eq 6 while the solid line was based on

$$1 - 2f_{HD} = \exp(-2k_{diss}k_{ex}[H_2]_0[M]t^2)$$

where k_{diss}[9] and k_{ex}[11] were calculated at 2500°K.

A similar assumption was made in the vibrational energy chain mechanism in which the back reaction for vibrational excitation was neglected. Figure 7 displays the reaction profile for $H_2(v = 0 \rightarrow 1)$ at 2500°K. The value for $k_{vib}(v = 0 \rightarrow 1)$[12] was used and the back reaction included. Equilibrium occurs at about 4 μsec which necessitates consideration of the back reaction. When included, the time dependence of product formation becomes linear. This is not supported by the experimental results.[4]

This investigation of the self-exchange supports the nonlinear time dependence of product formation reported previously for isotopic exchange reactions.[3,4] It further permits an appraisal of the equilibrium constant in good agreement with the calculated value.

Acknowledgments. The assistance of Mr. Darryl Olivier in the operation and maintenance of the equipment is greatly appreciated. The authors wish to thank Mr. Joe N. Brown for his help in computer programming and the LSUNO Computer Research Center (NSF Grant No. GP-2964 and GJ-131) for financial assistance. Miss Mary Ellen May and Mr. Richmond Tankersley contributed notably to the data reduction and handling process.

(11) A. A. Westenberg and N. deHaas, *J. Chem. Phys.*, **47**, 1393 (1967).

(12) J. H. Kiefer and R. W. Lutz, *ibid.*, **44**, 668 (1966).

Chemical HF Lasers from Flash Photolysis of Various N_2F_4 + RH Systems

by L. E. Brus* and M. C. Lin

U. S. Naval Research Laboratory, Washington, D. C. 20390 *(Received March 5, 1971)*

Publication costs assisted by the U. S. Naval Research Laboratory

HF stimulated emission has been observed from flash-photolyzed mixtures of N_2F_4 with a number of hydrogen sources: HCl, CH_4, CH_3F, CH_2F_2, CH_3Br, C_2H_6, C_2H_5F, and C_2H_5I. The vibrational–rotational transitions $P_{21}(4)$–$P_{21}(8)$ and $P_{10}(6)$–$P_{10}(9)$ were found in all cases examined with one exception. Under present conditions the emission is believed to result predominantly from the abstraction reaction

$$F + RH \longrightarrow HF^{\dagger} + R\cdot$$

Detailed analysis of the photoproducts indicates two other reactions yielding HF are occurring. The first has been recently studied by Padrick and Pimentel[1]

$$R\cdot + N_2F_4 \longrightarrow RNF_2^{\dagger} + NF_2$$

$$RNF_2^{\dagger} \longrightarrow R'CN + 2HF^{\dagger}$$

The second is a proposed new NF radical insertion–elimination reaction

$$NF + RH \longrightarrow RNHF^{\dagger} \longrightarrow HF^{\dagger} + R'—CH{=}NH$$

It is noted that uv photodissociation of NF_2 could yield metastable $NF(^1\Delta)$ radical.

Introduction

HF vibrational–rotational stimulated emission from flashlamp-initiated $N_2F_4 + H_2$ mixtures was first reported by Pearson, *et al.*[2] Padrick and Pimentel[1] have recently reported HF lasing in flashlamp-initiated $N_2F_2 + CH_4$ and $N_2F_4 + CH_3I$ mixtures over the temperature range 205–298°K; the emission was attributable to both abstraction and elimination reactions. These workers were able to show *via* the equal gain technique[3] that HF produced by elimination from chem-

(1) T. D. Padrick and G. C. Pimentel, *J. Chem. Phys.*, **54**, 720 (1971).

(2) R. K. Pearson, D. W. Gregg, E. B. Huss, S. J. Thomas, R. E. Niver, and J. R. Creighton, Lawrence Radiation Laboratory Report UCRL-72433, April 1970; *Chem. Phys. Lett.*, **8**, 609 (1971).

(3) J. H. Parker and G. C. Pimentel, *J. Chem. Phys.*, **51**, 91 (1969).

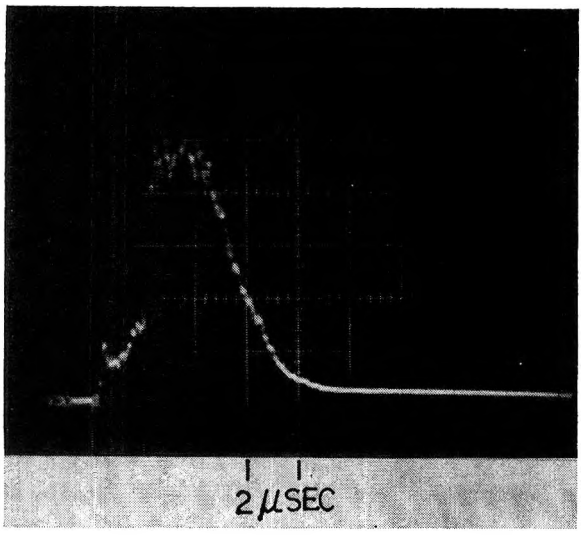

Figure 1. Total emission from N_2F_4 laser at 298°K. Pressure: 3 Torr of N_2F_4 and 3 Torr of CH_4. Sweep rate, 2 μsec/div.

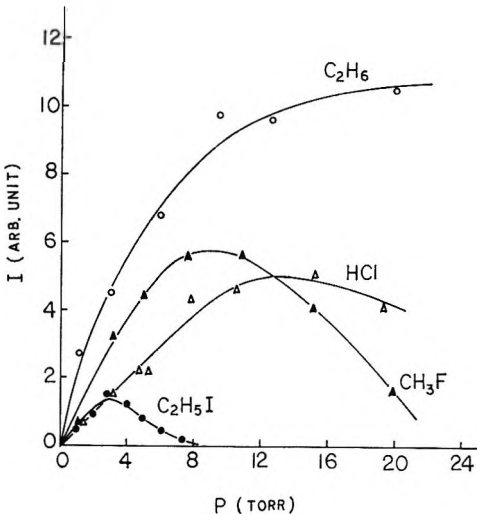

Figure 2. Relative total emission intensity as a function of pressure for various N_2F_4 + RH (3:2) mixtures.

ically activated $CH_3NF_2^{\dagger}$ has an initial population ratio of $N_1/N_0 = 0.35 \pm 0.02$, where N_v is the HF population in the vth vibrational level. In this work we report lasing action from mixtures of N_2F_4 with CH_4, C_2H_6, HCl, and a number of partially halogenated hydrocarbons. The dependence of lasing intensity upon various experimental parameters is given, and the chemistry of the various reactive species involved is discussed in detail.

Experimental Apparatus and Observations

The laser tube was a 1.0-m long, 2.5-cm i.d. quartz pipe; both ends were sealed with NaCl flats at Brewster's angle. The optical cavity was formed by two 1.0-in. diameter, 3-m radius gold-coated mirrors at a separation of 1.3 m; one of the mirrors had a 1-mm coupling hole at its center. Six 50 cm long Xe quartz flashlamps were placed coaxially around the laser tube in an alumina housing.[4] Unless otherwise noted, a 1200-J flash (~6 μsec half-width) was used. The laser beam passed through a 0.5-m Minuteman Model 305-SMP grating monochromator and was observed by an Au:Ge detector at 77°K in conjunction with a Tektronix Model 556 oscilloscope. Gas samples were of commercial grade; all impurities not condensable at 77°K were pumped off. Experiments were conducted at room temperature.

HF-stimulated emission was observed from the flash photolysis of N_2F_4 with CH_4, CH_3F, CH_2F_2, CH_3Br, C_2H_6, C_2H_5F, C_2H_5I, and HCl; as a general rule the lasing characteristics of these different systems were similar. Figure 1 shows the total laser pulse observed for a mixture of 3 Torr of N_2F_4 and 3 Torr of CH_4; pulses from other mixtures had much the same shape.

Figure 2 shows the pulse intensity as a function of total pressure for several different N_2F_4 + RH mixtures (3:2 relative proportions). The signal for C_2H_6 was the strongest and increased out to 20 Torr; the signal from C_2H_5I was considerably weaker and reached a maximum at only 3 Torr. CH_3F and HCl represent intermediate cases. Data were also obtained for CH_4 and CH_2F_2; CH_4 is much the same as C_2H_6 while CH_2F_2 has the same shape as C_2H_6 but only about $^1/_2$ the intensity. The addition of He or Ar to N_2F_4 + RH mixtures (3:2 relative proportions) at 6 Torr pressure, where RH = C_2H_6, CH_3F, and CH_2F_2, produced no change in the intensity to within ±20% for added inert gas pressures up to 13 Torr.

Figure 3 compares the emission intensities observed at 6 Torr total pressure for the different N_2F_4 + RH mixtures at various relative proportions. C_2H_6 and CH_4 generally give the strongest signals; with the exception of C_2H_5I and C_2H_5F the observed intensities for a given relative proportion are all within a factor of 2 or 3 of each other. C_2H_5F is, furthermore, atypical in that it will lase only if the partial pressure of N_2F_4 is higher than that of C_2H_5F.

The individual vibrational-rotational transition emitting were identified[5] in the cases of C_2H_5I, C_2H_5F, CH_4, and C_2H_6 under varying conditions of pressure and relative proportion. Under all circumstances $P_{21}(4)$–$P_{21}(8)$ and $P_{10}(6)$–$P_{10}(9)$ were observed except as noted below. Occasionally, $P_{32}(5)$ as well as additional P_{21} and P_{10} lines were found in mixtures either flashed at a higher energy (2000 J) or with a high relative proportion of N_2F_4. The P_{21} transitions were stronger and appeared first. C_2H_5F was again atypical in that for a 3:2 N_2F_4 + C_2H_5F mixture, when lasing is close to threshold, only P_{21} transitions were observed.

(4) We thank Drs. W. H. Lupton and J. Emmett for design of the flashlamp and electrical system.

(5) $P_{21}(4)$ stands for the rotational line P(4) of the (2 → 1) HF vibrational band; identification was made by comparison with the HF spectral data of D. E. Mann, B. A. Thrush, D. R. Lide, Jr., J. J. Ball, and N. Acquista, *J. Chem. Phys.*, 34, 420 (1961).

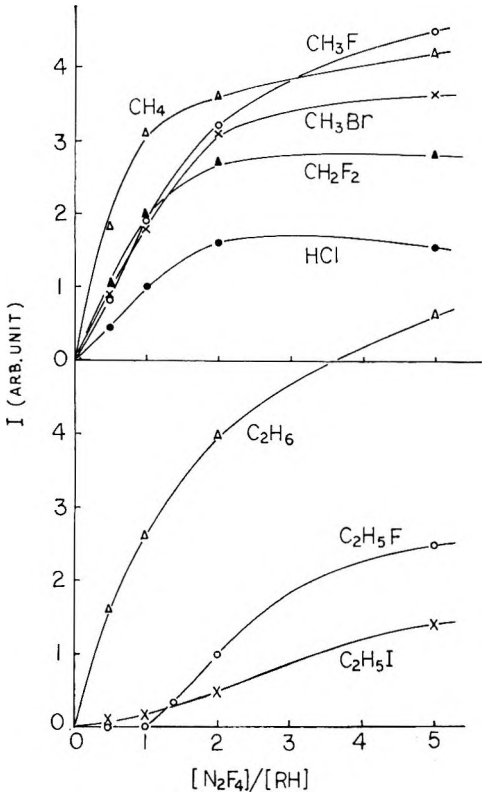

Figure 3. Relative total emission intensity as a function of $[N_2F_4]/[RH]$ at a total pressure of 6 Torr.

Discussion

A. Flash Initiation and Reaction Mechanism. An equilibrium[6] exists between NF_2 and N_2F_4 such that at room temperature and at a few Torr of pressure, ~2% of the N_2F_4 is in the form of the free radical NF_2. NF_2 has a relatively strong ($\epsilon_{max} \simeq 550$ l./mol cm), diffuse absorption[7] in the region 2500–2700 Å (108–114 kcal/mol), which results in photodissociation into $F(^2P)$ + NF. The bond dissociation energy $D_0°(FN-F)$ is known to be 70.6 ± 4 kcal/mol.[8] The NF radical thus produced is isoelectronic with O_2 and has a similar electronic term manifold with a $^3\Sigma$ ground state and low lying metastable $^1\Delta$ and $^1\Sigma$ excited states. Douglas and Jones[9] have observed these two metastable states in emission and determined that they lie 32.7 kcal/mol ($^1\Delta$) and 54.1 kcal/mol ($^1\Sigma$) above the ground $^3\Sigma$ state. The NF_2 absorption lies then just above the threshold (103 ± 4 kcal/mol) of photodissociation producing NF ($^1\Delta$); two processes are energetically possible under electric dipole selection rules

$$NF_2(^2B_1) \begin{cases} \nearrow F(^2P) + NF(^1\Delta) \\ \searrow F(^2P) + NF(^3\Sigma) \end{cases}$$

In addition, Padrick and Pimentel[1] report that F atoms can be produced by a weak absorption of N_2F_4, itself, below 2100 Å.

The general kinetic scheme for photodecomposition of N_2F_4 vapor has not been previously studied. We find that mass spectroscopic analysis of the products formed from flash photolysis of pure N_2F_4 at 6 Torr of pressure indicates the presence of N_2, F_2, N_2F_2, and NF_3. The following reaction scheme is proposed to account for their production

$$N_2F_4 \rightleftarrows 2NF_2 \qquad K_{eq}$$

$$N_2F_4 + h\nu \longrightarrow N_2F_3 + F \qquad I_1$$

$$NF_2 + h\nu \longrightarrow NF(^3\Sigma \text{ or } ^1\Delta) + F \qquad I_2$$

$$2NF \longrightarrow N_2 + 2F \qquad (1)$$

$$F + N_2F_4 \longrightarrow NF_3 + NF_2 \qquad (2)$$

$$NF + N_2F_4 \longrightarrow NF_2 + N_2F_2 + F \qquad (3)$$

$$2F + M \longrightarrow F_2 + M \qquad (4)$$

It is to be noted that reaction 3 is not an F-atom abstraction reaction; rather, it is a bimolecular displacement reaction, such as

$$NF + N_2F_4 \longrightarrow FN\cdots\underset{\displaystyle F\ \ F}{\overset{\displaystyle F\ \ F}{N{-}N}} \longrightarrow N_2F_3 + NF_2$$

$$(\Delta H° \simeq -5 \text{ kcal/mol})$$

which is followed by a very fast unimolecular decomposition of N_2F_3

$$N_2F_3 \longrightarrow N_2F_2 + F \qquad (\Delta H° \simeq -14 \text{ kcal/mol})$$

Reaction 1 has been studied by Diesen[10] and is known to be very fast ($k_1 = 2.5 \times 10^{13}$ cc/mol sec).

In our N_2F_4 + RH lasing mixtures, however, reactions 1–4 will be minimized by reactions with RH. Mass spectrometric analysis of the reaction products in different N_2F_4 + RH flash-photolyzed mixtures (5 Torr of N_2F_4 and 1 Torr of RH) is shown in Table I. On the basis of the present study and earlier works,[1,11–13] we propose the following general mechanism for the photolysis of N_2F_4 in the presence of hydrocarbons

$$F + RH \longrightarrow HF^\dagger + R \qquad (5)$$

$$R + N_2F_4 \longrightarrow RNF_2^\dagger + NF_2 \qquad (6)$$

$$RNF_2^\dagger \longrightarrow 2HF^\dagger + R'CN \qquad (6a)$$

$$RNF_2^\dagger + M \longrightarrow RNF_2 + M \qquad (6b)$$

(6) F. A. Johnson and C. B. Colburn, *J. Amer. Chem. Soc.*, **83**, 3043 (1961).

(7) P. L. Goodfriend and H. P. Woods, *J. Mol. Spec.*, **13**, 63 (1964).

(8) A. N. Zercheninov, V. I. Chesnokov, and A. V. Pankratov, *Zh. Fiz. Khim.*, **43**, 390 (1969).

(9) A. E. Douglas and W. E. Jones, *Can. J. Phys.*, **44**, 2251 (1966); W. E. Jones, *ibid.*, **45**, 21 (1967).

(10) D. W. Diesen, *J. Chem. Phys.*, **41**, 3256 (1964).

(11) C. L. Bumgardner, *Tetrahedron Lett.*, 3683 (1964).

(12) C. L. Bumgardner, E. L. Lawton, and H. Carmichael, *Chem. Commun.*, 1079 (1968).

(13) J. W. Frazer, *J. Inorg. Nucl. Chem.*, **16**, 63 (1960).

Table I: Mass Spectrometric (CEC Model 21-620) Analysis of Products Formed during a Single Flash of Various N_2F_4 + RH (5 Torr:1 Torr) Lasing Mixtures. (Spectra were taken before and after the flash: we list the principal new peaks observed after the flash.)

RH	*m/e*	Tentative ion assignment	Possible molecular sources
C_2H_6	41–38	CH_3CN^+, CH_2CN^+, $CHCN^+$	CH_3CN
	43–42	$CH_2CH{=}NH^+$, $C_2H_3N^+$	$CH_2CH{=}NH$, $C_2H_5NF_2$, C_2H_5NFH
C_2H_5F	41–38	CH_3CN^+, CH_2CN^+, $CHCN^+$	CH_3CN, C_2H_4FNFH
	57	CH_2FCN^+	CH_2FCN, $CH_2FCH_2NF_2$
	66	$C_2H_4F_2^+$	$C_2H_4F_2$
CH_4	27–26	HCN^+, CN^+	HCN
	29	$CH_2{=}NH^+$	$CH_2{=}NH$, CH_3NHF
CH_3F	47–46	$CHF{=}NH^+$, CH_2FN^+	$CHFNH$, CH_2FNF_2
	45	FCN^+	FCN, CH_2FNF_2
	27–26	HCN^+, CN^+	HCN
	85	$CH_2FNF_2^+$	CH_2FNF_2
	65–64	$CHFNF^+$, $CFNF^+$	CH_2FNF_2
	51–50	CHF_2^+, CF_2^+	CH_2F_2
CH_2F_2	47–46	$CHF{=}NH^+$, $CHFN^+$	CHF_2NFH
	45	FCN^+	FCN, CHF_2NFH
	85	CHF_2NFH^+	CHF_2NFH
	65–64	CF_2NH^+ or CHF_2N^+	CHF_2NFH, CHF_2NF_2
	69	CF_3^+	CHF_3

$$R + N_2F_4 \longrightarrow RF + N_2F_2 + F \quad (7)$$

$$NF + RH \longrightarrow RNFH^\dagger \quad (8)$$

$$RNFH^\dagger \longrightarrow HF^\dagger + R''{-}CH{=}NH \quad (8a)$$

$$RNFH^\dagger + M \longrightarrow RNFH + M \quad (8b)$$

The reaction of the alkyl radical, R, with NF_2 is neglected because of the low concentration of NF_2.

Reaction 5 is quite fast and has been employed as an HF laser chemical pumping mechanism in numerous studies. Reaction 6 in the case of $RH{=}CH_4$ has been studied by Frazer[13] and by Bumgardner, *et al.*[12] The results of Bumgardner, *et al.*,[12] indicate that at a total pressure of 6 Torr, over 90% of the chemically activated $CH_3NF_2^*$ in reaction 6 should eliminate 2HF *via* reaction 6a. The mass spectrometric data substantiate the occurrence of this reaction. The dissociation energy of the C–N bond in RNF_2 is about 60 kcal/mol if R is a small alkyl group.[14] Accordingly, ΔH_r° for reaction 6 is about 40 kcal/mol; this would imply that the critical activation energy for HF elimination in reaction 6a is less than or equal to 40 kcal/mol. The activation energy cannot be considerably less than 40 kcal/mol because of the known thermal stability[13] of CH_3NF_2.

The occurrence of reaction 7 is supported by the data of Table I. Reaction 7 is exothermic by about 35 kcal/mol; it can serve as a chain propagation step to replenish F atoms.

The occurrence of reaction 8 has not been previously reported but is supported by the data of Table I. In the cases of CH_3F and C_2H_5F, NF insertion into these compounds with subsequent elimination of 2HF seems to be the only reasonable source of the products HCN (mass 27) and CH_3CN (mass 41). The reaction in the C_2H_5F case is

$$NF + C_2H_5F \longrightarrow CH_3{-}CHF{-}N(F^\dagger, H) \longrightarrow CH_3CN + 2HF \quad (\Delta H_r^\circ \simeq -106 \text{ kcal/mol}^{15})$$

In the case of CH_4, the cracking pattern of CH_3NF_2 is known[13] and, judging from the absence of the principal fragment peak mass 67, almost no stabilized CH_3NF_2 was formed. Thus, the product peak at mass 29 in this system is not a fragment of CH_3NF_2 but more likely the imine formed *via* reaction 8

$$NF + CH_4 \longrightarrow CH_3{-}N(H^\dagger, F) \longrightarrow HF + CH_2{=}N{-}H$$

Reaction 8 is spin-allowed and exothermic by an additional 33 kcal/mol if the NF radical is actually in the metastable $^1\Delta$ state. Conversely, the fact that reaction 8 does occur supports the initial creation of NF in the $^1\Delta$ state. The chemically activated $CH_3NHF^\dagger$ formed above will then have over 100 kcal/mol internal excitation energy and should lie far above the critical energy necessary for the elimination of HF.

B. HF Laser Chemical Pumping and Pressure Effect. Although HF can be produced by the three reactions

(14) This estimate is based on the alkyl–NF_2 bond dissociation energy reported by (a) A. J. Dijkstra, J. A. Kerr, and A. F. Trotman-Dickenson, *J. Chem. Soc. A*, 105 (1967), and (b) M. C. Lin, unpublished data.

(15) Calculated from thermodynamic tables in S. W. Benson, "Thermochemical Kinetics," Wiley, New York, N. Y., 1968.

5, 6, and 8, reaction 5 is believed to be the principal pumping reaction under the present conditions. It is known that HF* produced by reaction 5 in the case of RH=H_2 has population ratios $N_2/N_1 = 3.2$[16] and $N_1/N_0 > 1$.[17] The F-atom abstraction reaction yields complete $2 \rightarrow 1$ and $1 \rightarrow 0$ population inversions with resulting high gain. On the other hand, Padrick and Pimentel[1] have shown that $N_1/N_0 = 0.35$ for $HF^\dagger$ eliminated *via* reaction 6 from $CH_3NF_2^\dagger$; elimination reactions typically produce only a weak partial inversion with resulting low gain. As a numerical example, we have calculated[18] that the transition with maximum gain, $P_{10}(6)$, in the case of $N_1/N_0 = 0.35$ has only 5% of the gain shown by the maximum gain transition in the case of $N_1/N_0 = 1$, $P_{10}(3)$.

In our N_2F_4 + RH lasing mixtures, strong $2 \rightarrow 1$ and $1 \rightarrow 0$ population inversions will be established by reaction 5. However, if either of the two elimination reactions 6 and 8 is fast enough to occur simultaneously with reaction 5, there will be increased population of HF ($v = 0$ and 1) and reduction of stimulated emission. In our kinetic scheme, reaction 6 is a secondary reaction and probably has a rate constant 1 or 2 orders of magnitude slower than (5); therefore, there should not be much production of HF *via* reaction 6 during the first few microseconds of the flash when stimulated emission is observed to occur. However, reaction 8 is a primary reaction and, if sufficiently fast, could alter the observed stimulated emission.

As previously indicated, NF_2 is in very low concentration (~2%); we find the conversion of RH per flash from mass spectrometric analysis is much less than 1%. In Figure 2 the increase of laser intensity with increasing N_2F_4 (and NF_2) partial pressure simply reflects the increasing density of F-atom sources and also indicates that reaction 2 is slow compared with reaction 5. One might propose that the different intensities in Figure 2 for different RH principally result from varying vibrational relaxation of HF by RH. However, if this were the case, these differences would tend to decrease as the partial pressure of N_2F_4 increased at constant total pressure. This behavior is not observed; in fact, the variation of intensity we observe for 5:1 N_2F_4 + RH mixtures must be principally due to differing degrees of $HF^\dagger$ inversion produced by the sum of reactions 5, 8, and, less likely, 6.

In the absence of detailed data on the rates of reaction 6 and 8 and on the rates of vibrational relaxation of $HF^\dagger$, any explanation for the anomalous behavior of C_2H_5F would be rather speculative.

The case of HCl is interesting; here the abstraction reaction is the only one occurring. A preliminary study[19] of abstraction of H from HCl by F-atom shows the HF N_3/N_2 and N_2/N_1 population ratios to be lower than in the case of abstraction from H_2 or CH_4, and we do, in fact, observe weaker emission with HCl than with CH_4.

In Figure 1, as the total pressure is increased at fixed relative proportions of N_2F_4 to RH, both the density of F and NF sources, as well as the vibrational relaxation rate of $HF^\dagger$, will increase. Stimulated emission from CH_4 and C_2H_6 mixtures increases at least up to 20 Torr—clearly, relaxation by these hydrocarbons or N_2F_4 itself is not significant. Emission maxima as a function of pressure are observed for HCl and CH_3F mixtures, however. In the case of HCl, it appears that fast vibrational relaxation of $HF^\dagger$ by HCl is lowering the gain. Relaxation could also be occurring in the CH_3F case, but here another process is also possible: the rates of the elimination reactions 6 and 8, if relatively low at low pressure, could be increased sufficiently at high pressure to produce appreciable HF during the period of observed stimulated emission and hence lower the gain.

C_2H_5I + N_2F_4 mixtures are a special case: the flash will strongly dissociate the C_2H_5I yielding C_2H_5 + I*. There will be a high rotational temperature as well as strong relaxation of HF by C_2H_5 and I atoms. In addition, elimination from $C_2H_5NF_2^\dagger$ is now a primary reaction in the kinetic scheme and should strongly perturb the HF inversion from reaction 5. All of these effects will decrease HF lasing intensity in N_2F_4 + C_2H_5I mixtures. A 1.3-μm emission was not observed under our present conditions; this fact indicates that either the electronic quenching of $I^*(^2P_{1/2})$ or a chemical reaction with N_2F_4, such as

$$I^* + N_2F_4 \longrightarrow NF_2I + NF_2,$$

is comparably faster than the laser buildup time.[20]

Acknowledgments. We wish to express our appreciation to W. R. Sooy and J. Emmett for the use of their facilities under ARPA Order 660. We also thank J. McCaffery for the loan of an infrared detector.

(16) K. G. Anlauf, P. E. Charters, D. S. Horne, R. G. Macdonald, D. H. Maylotte, J. C. Polanyi, W. J. Skrlac, D. C. Tardy, and K. B. Woodall, *J. Chem. Phys.*, **53**, 4091 (1970).

(17) W. H. Green and M. C. Lin, *ibid.*, **54**, 3222 (1971).

(18) This calculation uses eq 4 of ref 1 and assumes equal densities of HF ($v = 0$) molecules at 298°K.

(19) N. Jonathan, C. M. Melliar-Smith, and D. H. Slater, *Chem. Phys. Lett.*, **7**, 257 (1970).

(20) Note Added in Proof. Recently, Ross and Shaw (D. S. Ross and R. Shaw, *J. Phys. Chem.*, **75**, 1170 (1971)) have studied the reaction

$$CH_3 + NF_2 \rightarrow CH_3NF_2^{\dagger\dagger}$$

with subsequent elimination of 2HF yielding HCN. A standard RRKM calculation by one of us (M. C. L.) using data of ref 12 and 20 indicates that $k_6/k_9 \simeq 10^{-2}$ at 300°K. Additionally, the activation energy for elimination of HF is found to be $E_0 = 38$ kcal/mol (Ross and Shaw obtain 42 kcal/mol). As the exothermicity of reaction 6 when R is CH_3 is only 40 kcal/mol, elimination from $CH_3NF_2^\dagger$ will be slow, if it occurs at all, as compared with elimination from $CH_3NF_2^{\dagger\dagger}$ in reaction 9 where $\Delta H_r = -60$ kcal/mol. These considerations suggest that in this work and ref 1, CH_3 radicals lead to HCN + 2HF *via* reaction 9 instead of reaction 6, despite the low concentration of NF_2 relative to N_2F_4. In these systems, reaction 6 can serve as a source of NF_2 for reaction 9, even if reaction 6 rarely leads to HF elimination *via* reaction 6a.

Chemical Effects of the Nuclear Reaction $N^{14}(n,p)C^{14}$ in Potassium Azide[1]

by John D. Vaughan,* Richard L. Springborn, and Virginia L. Vaughan

Department of Chemistry, Colorado State University, Fort Collins, Colorado 80521 *(Received February 1, 1971)*

Publication costs borne completely by The Journal of Physical Chemistry

The distribution of labeled products resulting from $N^{14}(n,p)C^{14}$ in potassium azide was investigated. The chief products found with water dissolution of the target were $C^{14}N^-$, $C^{14}N_2^{2-}$, and $C^{14}H_3NH_2$. Thermal anneal at 300° for periods of 1 to 8 hr resulted in a large increase in $C^{14}N_2^{2-}$ and in decreases in other products. Thermal decomposition of target at 400° gave principally $C^{14}N_2^{2-}$.

Introduction

The chemical effects of (n,p) nuclear reactions are of particular interest because the recoil atom is different from the target atom. Thus, a highly energetic recoil atom is produced within a chosen atomic environ at thermal energies. In the case of the $N^{14}(n,p)C^{14}$ reaction, long periods of thermal neutron irradiation of the nitrogeneous target are required in order that sufficient radioactivity in long-lived C^{14} be produced. Such long periods of irradiation enhance the probability that concomitant radiation may alter[2] the chemical fate of the recoil atom. Because of reduced diffusion, the effect of radiation is less for solid than for liquid or gaseous targets;[2a,3] accordingly, studies of C^{14} recoil chemistry are usually restricted to solids. In general, the labeled species within target crystals are released by dissolving the target in a solvent. This dissolution then introduces the possibility of secondary reactions between crystal-entrapped recoil products and the solvent. The identities of labeled products in the crystal thereby become obscured. One may improve speculation on the nature of these crystal-entrapped products by using more than one solvent, by thermal anneal techniques,[3,4] and by release of labeled entities by volatilization or thermal decomposition of the target.[5] The choice of potassium azide for this investigation was predicated upon the above considerations. First, a study of the radiation chemistry of KN_3 in thermal columns of nuclear reactors has been reported;[6] it therefore becomes possible to estimate the likelihood of radiation affecting the radiocarbon products in the target. Second, KN_3 has a relatively low decomposition temperature (355°) which permits the use of thermal decomposition as an alternative to solvent dissolution to release entrapped C^{14} products. Further, the complexity of the radiocarbon product distribution is limited by the presence of but two elements, nitrogen and potassium.[7,8] Recent investigations on metal nitrides relevant to the present study on KN_3 have been reported.[3,5,9,10]

Experimental Section

Sample Preparation and Irradiation. Potassium azide obtained from Eastman Organic Chemicals was recrystallized three times from water,[11] then oven dried at 110°. A 10-g sample of the purified KN_3 was placed within a necked quartz ampoule and heated under vacuum at 220° for 1 hr; then it was sealed off under helium at ambient pressure. The specimen was irradiated in the thermal column of the Los Alamos Omega West reactor for 113 hr in a neutron flux of $\sim 5 \times 10^{11}$ n cm^{-2} sec^{-1} (integrated flux of $\sim 1.5 \times 10^{17}$ n cm^{-2}); the ambient temperature in the thermal column was between 60 and 70°. The ampoule was opened in a drybox and stored in a desiccator under helium between experiments. Preliminary operations such as sample weighings were made in the drybox.

Aqueous Dissolution of Target Samples. All aqueous dissolutions were carried out in neutral or weakly alkaline media (*i.e.*, aqueous KN_3 is weakly alkaline). Carriers were added either in aqueous solution or as gases preparatory to their separation and radioanalysis. In general, no more than four carriers were added and separated in a given experiment (see ref 8).

Cyanide, Cyanamide, and Hydrolyzable Activities. A solution containing dissolved target, KCN, and cyan-

(1) Department of Chemistry Contribution No. 61-70.

(2) (a) F. Cacace and A. P. Wolf, *J. Amer. Chem. Soc.*, **84**, 3202 (1962); (b) R. D. Finn, H. J. Ache, and A. P. Wolf, *J. Phys. Chem.*, **74**, 3194 (1970).

(3) R. D. Finn, H. J. Ache, and A. P. Wolf, *ibid.*, **73**, 3928 (1969).

(4) G. Harbottle and N. Sutin, "Advances in Inorganic Chemistry and Radiochemistry," Vol. 1, Academic Press, New York, N. Y., 1959, pp 268-312.

(5) G. Stöcklin and K. Vogelbruch, *Radiochim. Acta*, 177 (1968).

(6) J. Cunningham, *Trans. Faraday Soc.*, **62**, 2423 (1966).

(7) Compare, for example, hydrazine sulfate,[8] which contains N, H, S, and O; 12 one-carbon products each with greater than 3% of the total radioactivity were found.

(8) J. D. Vaughan and V. T. Lieu, *J. Phys. Chem.*, **68**, 2497 (1964).

(9) J. G. Kuhry and J. P. Adloff, *Bull. Soc. Chim. Fr.*, 2402 (1967).

(10) J. G. Kuhry and J. P. Adloff, *ibid.*, 3414 (1967).

(11) E. A. Secco, *Can. J. Chem.*, **40**, 2191 (1962).

amide was divided into equal aliquots. Aliquot 1 was acidified with 1 *M* nitric acid; excess aqueous 1 *M* $AgNO_3$ was added to precipitate AgCN. The solution was filtered and the precipitate was discarded. The filtrate was made alkaline with 3 *M* NH_4OH, causing silver cyanamide (Ag_2CN_2) to precipitate. This precipitate was collected and dissolved in 6 *M* H_2SO_4, with the resulting solution being neutralized by 3 *M* NH_4OH to reprecipitate Ag_2CN_2. The cycling of the cyanamide ion precipitation was a purifying procedure. The dried Ag_2CN_2 was combusted over copper oxide at 800° to yield CO_2 which was trapped in aqueous NaOH, then precipitated as $BaCO_3$ preliminary to counting. A stream of air was swept through aliquot 2 into an acidified 1 *M* $AgNO_3$ solution and then on through a 1 *M* NaOH trap. The solution containing the dissolved target and carriers was acidified with dilute H_2SO_4 while being warmed, causing HCN to distil into the $AgNO_3$ solution precipitating AgCN. Carbonate activity resulting from dissolved CO_2 or from acid hydrolysis was caught in the NaOH trap. The AgCN was combusted over copper oxide and collected as $BaCO_3$. Gaseous CO_2 introduced into the air stream served as a carrier for the hydrolyzable fraction.

Formic Acid, Carbon Dioxide, Carbon Monoxide, Methane, and Guanidine. Procedures given elsewhere were used.[8,12]

Methylamine. An aqueous solution containing target, methylamine, and excess sodium hydroxide was distilled. The distillate was condensed into saturated aqueous picric acid. The methylamine picrate derivative was recrystallized from water, combusted over copper oxide, and collected as $BaCO_3$. A preliminary experiment indicated that guanidine does not distil over to form guanidine picrate.

Urea. The oxalate derivative of urea[3] was prepared, recrystallized from water, then converted into $BaCO_3$ after combustion over copper oxide.

Methylenimine. A solution containing target and formaldehyde carrier in a closed pressure compensated system was made 7 *N* in H_2SO_4[3] and refluxed for 1 hr. The methone derivative of formaldehyde[12] was then prepared, recrystallized in aqueous ethanol, and converted into $BaCO_3$ by combustion at 800° over copper oxide.

Thermal Anneal. Samples of KN_3 were heated under vacuum at 300° for periods ranging from 1 to 10 hr in a Lindberg Hevi-Duty furnace. Decomposition of KN_3 proceeds readily at 355° but occurs on the surface at a very slow rate at lower temperatures.[11] For that reason, anneal at temperatures higher than 300° and for longer periods than 10 hr was not investigated.

Thermal Decomposition. Samples of KN_3 were placed in a flat-bottom glass tube (1-cm cross section) which was fitted with a U-tube cold trap (−195°) connected to the vacuum line. The system was evacuated and then a Lindberg crucible furnace at 400° was elevated to cover the flat-bottom tube. Heating was continued for 3 hr. In a control experiment, it was found that decomposition of 0.07 g of irradiated KN_3 was essentially complete after 2 hr at 400°, but that longer periods were required to complete the decomposition of nonirradiated KN_3 at this temperature (see ref 5 for a similar observation on Cu_3N). After decomposition, the U-tube was removed and warmed, and the contents were swept into a copper oxide furnace at 800°. The residue in the flat-bottom tube was dissolved in water and analyzed for nonvolatile components.

Radioactivity Determination. All separated carriers were converted into $BaCO_3$ prior to counting. CO_2 evolutes from the various $BaCO_3$ specimens[12] were counted in a LND-2 proportional counter[13] with methane as the counter gas. Some specimens were counted in an ionization chamber using the Cary 31 vibrating reed electrometer. Radioactivity determinations for carriers were computed on the basis of total recovered $BaCO_3$ for each carrier, necessitating, therefore, no correction for carbonate blank.

Total Target Specific Activity. The total C^{14} activity per gram of irradiated KN_3 was determined by alkaline permanganate oxidation to carbonate. During reflux, a carbon dioxide-free air stream swept volatile or gaseous compounds through a furnace tube containing copper oxide at 800° into a 1 *M* NaOH trap. After refluxing 1 hr, the permanganate solution was acidified with excess H_2SO_4, and the carbon dioxide was trapped in 1 *M* aqueous NaOH. The total activity per gram of KN_3 determined in two runs was $3.087 \times 10^6 \pm 0.028 \times 10^6$ counts $min^{-1}\,g^{-1}$.

Results

The results of experiments on irradiated potassium azide can be divided into two classes according to the mode of target dissolution prior to product analysis. In the first class, target samples with or without thermal anneal were dissolved in water. In the second class, target samples were heated to and held at 400° for 3 hr, leading initially to melting and subsequently to decomposition of the KN_3 to $N_2(g)$ and K(s). The melt in the second class of experiments had the same role as the solvent in the first class, that is, the entrapped precursors were free to react (or not react) with the surrounding medium. After decomposition, the residues were dissolved in water before analyzing for labeled compounds.

Aqueous Dissolution. Table I gives the distribution of C^{14} among one-carbon postdissolution products for unannealed target samples. The products listed in Table I account for ~100% of the total C^{14} activity produced in the target; here the activity attributed to CO_2 is also part of that attributed to hydrolyzable.

(12) P. E. Yankwich and J. D. Vaughan, *J. Amer. Chem. Soc.*, **76**, 5851 (1954).

(13) LND, Inc., Oceanside, N. Y.

Of the seven labeled compounds with yields greater than 1%, only cyanide and cyanamide ions are free of hydrogen and/or oxygen from the solvent. However, these two products account for 63% of the activity. Table II gives the distribution of labeled compounds found when target samples were annealed for varying periods at 300° prior to aqueous dissolution. Although the data are erratic for the shorter time periods, several trends are evident. Cyanide gradually faded to less than a third of its original (unannealed) value (Table I) in 8 hr of anneal. Methylamine dropped from 25 to 0% within an hour. Cyanamide ion more than doubled in yield within an hour, then gradually climbed to nearly 80% after 8 hr. One would suspect that the loss in methylamine was gained by cyanamide ion. The hydrolyzable activity increased to about six or seven times its original value after 3 hr of anneal, but then dropped back to a low 2–3% after 5 hr.

Table I: Distribution of C^{14} among One-Carbon Compounds: Aqueous Dissolution of Unannealed KN_3

Compound	Number of separate determinations	Total activity, %
$C^{14}N^-$	3	45.7 ± 0.7
$C^{14}N_2^{2-}$	5	17.0 ± 0.6
$C^{14}H_3NH_2$	6	24.8 ± 1.0
$HC^{14}OOH$	1	~2.1
$C^{14}O(NH_2)_2$	3	4.4 ± 1.0
$C^{14}H_4 + C^{14}O$	3	3.8 ± 1.1
$C^{14}H_2NH$	1	<1
$C^{14}H_2O$	1	<1
$C^{14}NH(NH_2)_2$	1	0
$C^{14}O_2$	1	~1.5
Hydrolyzable	3	3.2 ± 1.4

Table II: Distribution of C^{14} among One-Carbon Compounds: Aqueous Dissolution of Annealed KN_3; 300°

Time, hr	Total activity, % CN^-	CN_2^{2-}	Hydrolyzable	Recovered
1[a]	43.4	44.4	1.1	88.9
2	50.8	39.7	4.7	95.2
3	39.5	31.9	22.3	93.7
3	17.6	60.4	16.9	94.9
4	24.8	50.0	14.2	89.0
5	18.5	73.0	2.6	94.1
6	15.6	72.5	2.2	90.3
8	13.9	78.4	2.2	94.5
10	5.2	76.9	4.2	86.3

[a] Methylamine activity was zero after 1-hr anneal.

The origin of the hydrolyzable activity found in the annealed and unannealed samples could be cyanate and/or carbonate ions. In acidic solution, cyanate undergoes hydrolysis to carbonate rapidly. None of the other one-carbon compounds appearing in Tables I and II undergoes transformation to CO_2 under the mild conditions that yielded the hydrolyzable activity. In control experiments, aqueous formic acid, formaldehyde, and urea each in the presence of potassium azide were refluxed for 1 hr in 6 *M* sulfuric acid; no hydrolysis occurred.

Thermal Decomposition. The results of the thermal decomposition experiments are given in Table III. It is interesting that in runs 2 and 3 the combined yields of cyanamide ion and cyanide ion total less than the total solution compounds (TS); in other runs, cyanamide ion yields rose above 80% of the total C^{14} production. In a ninth run, the decomposate was analyzed for methylamine and guanidine; no activity was recovered for either. In run 4, parallel analyses were made for cyanamide ion, with the indicated good agreement. Since melting occurs before decomposition, it was of interest to ascertain if the final distribution of labeled compounds was obtained at the instant of melting or required the decomposition process. In run 10, a sample of target was subjected to a temperature of 400°, then quenched after 5 min. The sample was observed to melt but did not have time to decompose. In run 10, the cyanide ion yield was 49.2% and that for cyanamide ion was 29.2%, the results of which were not markedly different from those in the aqueous dissolution of unannealed target. In run 11, a sample held at 400° for 1 hr gave 30.0% cyanide ion and 61.7% cyanamide ion.

Discussion

The recoiling C^{14} leaves the site of the nuclear event with a kinetic energy of *ca.* 40 keV, most of which it must lose through ionization, electronic excitation, and finally collision before it can enter stable (or metastable) chemical combination.[14] Recent experimental evidence[15] indicates that a recoil atom must stop in a very short time (picoseconds) and that the rate of dissipation of energy from the terminal hot zone[4] will depend on the insulating properties of the target. Recoil events in metal foils do not exhibit high hot zone temperatures because of rapid energy loss arising from very high thermal conductivity.[15] In ionic solids, such as potassium azide, the thermal conductivity is much smaller than in metals, so that hot zone temperatures would be higher. Finn, Ache, and Wolf[3] estimated that the hot zone temperature could be as high as 2500°K for about 10^{-11} sec for C^{14} recoil reactions. If such high temperatures obtain in terminal hot zones in irradiated potassium azide, local decomposition of the salt would begin, so that the stopped C^{14} atom could begin to react with highly excited azide ions,[16] nitrogen

(14) P. E. Yankwich, *Can. J. Chem.*, **34**, 301 (1956).
(15) C. H. W. Jones, *J. Phys. Chem.*, **74**, 3347 (1970).
(16) P. Gray, *Quart. Rev. Chem. Soc.*, **XVII**, 441 (1963).

Table III: Distribution of C^{14} among One-Carbon Compounds: Thermal Decomposition of KN_3 at 400°; 3 Hr

	Total activity, %								Average,
	1	2	3	4	5	6	7	8	%
CN_2^{2-}	75.4	66.5	68.8	87.2 86.0	93.0	88.0	84.0	89.0	88.0
CN^-	2.8	1.5	4.1						2.8
Hydrolyzable	3.0	1.1							1.6
Cold trap	0	0	0						
TS[a]		94.8	96.5						95.7

[a] TS refers to total solution components, obtained by permanganate combustion of an aliquot of the dissolved decomposition residue.

molecules, and perhaps potassium atoms. Quenching of the hot zone due to rapid cooling could stop some of the reactions short of completion,[4] leaving the hot atom in an activated metastable chemical combination. Dissolution of the target in water would then lead to vigorous reactions between the metastable precursors and the solvent to produce characteristic secondary labeled products.[12] If the target were thermally annealed prior to dissolution in water, permitting further reaction of the precursors in the crystal,[4] a different spectrum of labeled products would result.

The product distributions observed for unannealed and annealed target samples conform well to the above arguments. Methylamine (Table I) is clearly the product of a reactive precursor and water. The thermal anneal process should favor C^{14} entities most like lattice ions. Both the azide ion and cyanamide ion are linear, each with two equivalent bonds of 1.16 Å.[17] Thus, azide sites could be occupied by cyanamide ions without strain. The large yields of cyanamide attending long-term anneal supports this viewpoint. Since methylamine activity is reduced from 18 to 0% in 1 hr while cyanamide increased from 17 to 44% in the same interval, we can postulate that the methylamine precursor is transformed to cyanamide ion by the temperature increase. The precursor could be C^{14} linked to two nitrogen atoms, trapped during quench under strain. Attack by water could then release the highly activated entity with such impetus that one C^{14}–N link is severed (to form ammonia) and the other undergoes fivefold protonation to methylamine.

The gradual reduction of cyanide yield with annealing time suggests that this ion is itself slowly transformed into cyanamide ion in the crystal. The C–N bond in KCN is 1.13 Å;[17] in the unannealed target, the bond could be weaker and slightly longer than the fully bonded form,[3] yet strong enough to resist attack by water. Annealing of the crystals might cause displaced azide ions to react with the cyanide precursor to produce CN_2^{2-} with C–N bonds of 1.16 Å. We suggest that the increased yield of the hydrolyzable fraction after 3 or 4 hr of heating is a consequence of the formation of cyanic acid, HOCN, upon dissolution of the target. The precursor could be an intermediate in the transformation of cyanide ions to cyanamide ions, with C–N bond lengths appropriate to the particular path leading to HOCN. With anneal longer than 4 hr, the intermediate would presumably be converted into cyanamide.

In their study of magnesium nitride, Finn, Ache, and Wolf[3] found methyleneimine in large yield in annealed target and moderate yield in unannealed target. Methylenimine was found in insignificant yield in unannealed potassium azide. Further, the large recovery of identified products in annealed potassium azide indicates that methylenimine could have been only a minor product if present at all. The markedly different annealing characteristic of the two targets, despite their elemental similarity, is probably a consequence of the presence of compound ions in potassium azide and the different crystal structures of the targets.

In the decomposition experiments, the large yield of labeled cyanamide appears to be a consequence of the reaction of cyanide and azide ions in the hot melt. Thus

$$C^{14}N^- + N_3^- \longrightarrow C^{14}N_2^{2-} + N_2$$

A process similar to but slower than this could account for the proposed transformation of $C^{14}N^-$ to $C^{14}N_2^{2-}$ in the annealing process.

Of the minor products found in the aqueous dissolution of unannealed target, it is worth noting that urea is a hydrolysis product of cyanamide. In the dissolution process, cyanamide, activated by strain, could undergo hydrolysis to urea.

Cunningham[6] determined reactor radiation-induced decomposition of potassium azide in a reactor thermal column, under conditions similar to the target irradiation for this study.[18,19] After 110-hr exposure at 2.5×10^{12} n cm^{-2} sec^{-1} (10^{18} n cm^{-2} integrated flux), 5×10^{-4} mol of N_2 per mol of KN_3 and 0.9×10^{-6} mol of

(17) "Tables of Interatomic Distances and Configurations in Molecules and Ions," No. 11, L. E. Sutton, Ed., The Chemical Society, London, 1958, p M116.

(18) γ Radiation at the target location in the thermal column is attributable principally to neutron capture by carbon in the graphite moderator.[19] No measurement of this γ flux was made.

(19) H. T. Williams, Los Alamos Scientific Laboratory, Los Alamos, N. M., private communication.

C^{14} per mol of KN_3 were produced.[6] The probability of encounter of a C^{14} recoil atom with N_2 relative to its encounter with N_3^- is therefore estimated to be $5 \times 10^{-4} = (0.9 \times 10^{-6} \times 5 \times 10^{-4}/0.9 \times 10^{-6} \times 1)$.

The per cent decomposition of the target studied by Cunningham amounted to only $(2/3) \times 5 \times 10^{-2}\%$. Since the rates of reactions between recoil atom species and radiolytically produced species are diffusion controlled in crystalline targets,[2a] the contribution of radiation chemical effects to the recoil product distribution would be negligible in the potassium azide target. This conclusion is in agreement with the experimental observation of Finn, Ache, and Wolf on their magnesium nitride target.

Acknowledgment. This research was supported in part by U. S. Atomic Energy Commission Grant AT-(11-1)-1620. We wish to thank the Los Alamos Scientific Laboratory for irradiating the potassium azide specimen and Mr. W. A. Smith, Jr., for carrying out some of the preliminary experiments.

Hot-Atom Chemistry of Carbon-14 in Solid Benzene at Kinetic Energies between 5 and 100 Electron Volts[1]

by Helmut M. Pohlit, Wallace Erwin, Tz-Hong Lin, and Richard M. Lemmon*

Laboratory of Chemical Biodynamics, Lawrence Radiation Laboratory, University of California, Berkeley, California 94720 *(Received January 29, 1971)*

Publication costs assisted by the U. S. Atomic Energy Commission

The yields of seven major hydrocarbon products from the interaction of energetic carbon-14 ions with solid benzene (−196°) were determined for carbon ion energies between 5 and 100 eV. As one goes toward the lower kinetic energy, the yields of benzene, biphenyl, and diphenylmethane appear to remain essentially constant, that of phenylcycloheptatriene appears to increase, and those of toluene, cycloheptatriene, and phenylacetylene definitely decrease by a factor of 5 to 10. These results are additional support for previously postulated mechanisms and lead to the conclusions that (1) hydrogen and carbon pickup reactions proceed up to rather high kinetic energies (50–100 eV), and (2) insertion into carbon–hydrogen or carbon–carbon bonds with preservation of the adduct is limited to energies below 5 eV.

Introduction

In two previous papers we reported the identities, the yields between 100 eV and 15 keV, and the partial degradations of the eight major products of energetic ^{14}C ions and atoms (from an ion accelerator) in solid benzene: benzene (B), toluene (T), cycloheptatriene (CHT), phenylacetylene ($C_6H_5C{\equiv}CH$), "U-2" (subsequently identified as benzaldehyde),[2] biphenyl ($(C_6H_5)_2$), diphenylmethane ($(C_6H_5)_2CH_2$), and phenylcycloheptatriene (PCHT).[3,4] As a result of recent improvements in the ion accelerator used in this work,[5] we have extended our studies to the 100–5 eV kinetic energy range. This paper reports the yields of the hydrocarbon products at these lower energies.

Experimental Section

The procedures for irradiations and yield determinations were identical with those described previously.[3] "Yield" is defined as the per cent of the activity in an aliquot portion (of the target) that appears in the glpc peak of the product. The total activity in the target after an irradiation is roughly equal (80–100%) to the time integral of the $^{14}C^+$ beam intensity.

The toluene degradations were performed *via* oxidation to benzoic acid followed by the hydrazoic acid (Schmidt) reaction to aniline and CO_2; the latter two compounds were purified by gas–liquid partition chro-

(1) The work reported here was supported by the U. S. Atomic Energy Commission and by a grant to one of us (H. M. P.) from the Bundesministerium für Wissenschaftliche Forschung and the Deutscher Akademischer Austauschdienst of West Germany.

(2) The increasing yield with decreasing energy of this product indicates, as does the appearance of oxygen, an origin foreign to the expected hot-atom chemistry. Its appearance will be the subject of a forthcoming paper.

(3) H. M. Pohlit, T. H. Lin, W. R. Erwin, and R. M. Lemmon, *J. Amer. Chem. Soc.*, **91**, 5421 (1969).

(4) H. M. Pohlit, T. H. Lin, and R. M. Lemmon, *ibid.*, **91**, 5425 (1969).

(5) H. M. Pohlit, *et al.*, *Rev. Sci. Instrum.*, **41**, 1012 (1970).

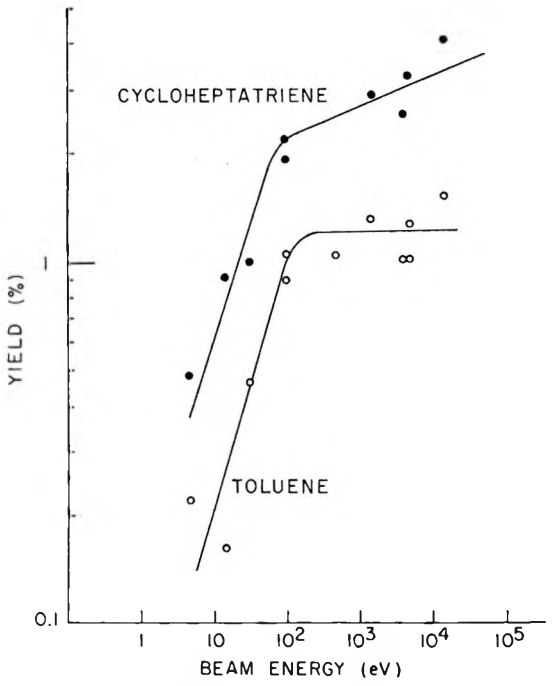

Figure 1. Yields of cycloheptatriene (●) and toluene (○) *vs.* $^{14}C^+$ ion energy.

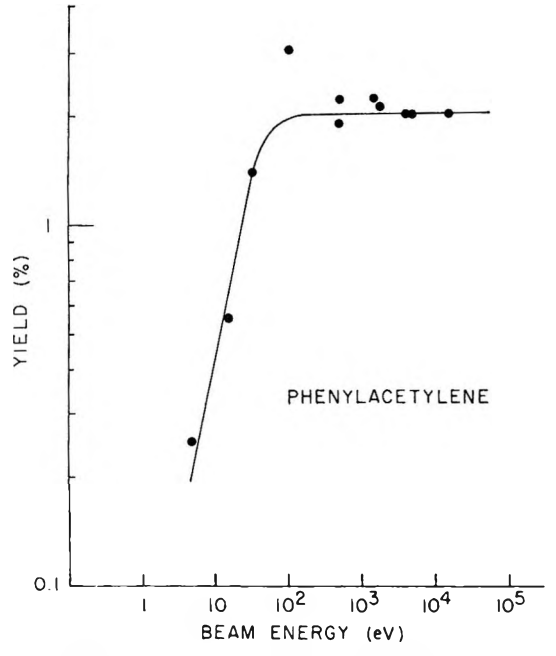

Figure 2. Yields of phenylacetylene *vs.* $^{14}C^+$ ion energy.

matography, and the activity was determined in a liquid scintillation counter. Details of these procedures are given in the Ph.D. thesis of Lin.[6]

A recent report describes the electronic and mechanical details of the ion accelerator and includes a discussion of the chemical identity (as well as the charge state) of the irradiating carbon species.[5]

Results

The yields of the products, as a function of the kinetic energy of the irradiating carbon, are shown in

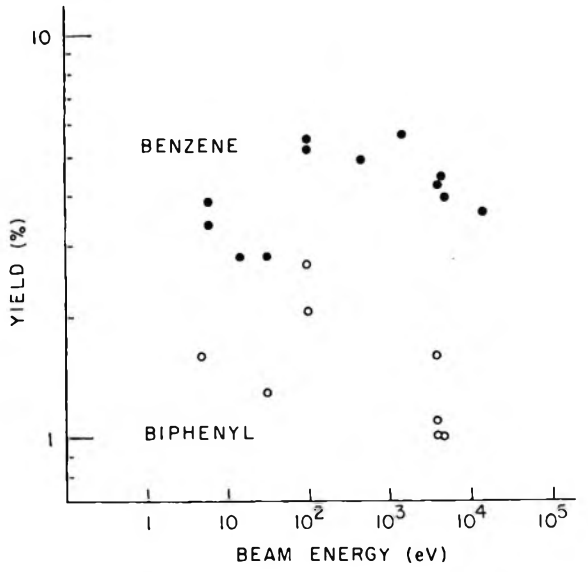

Figure 3. Yields of benzene (●) and biphenyl (○) *vs.* $^{14}C^+$ ion energy.

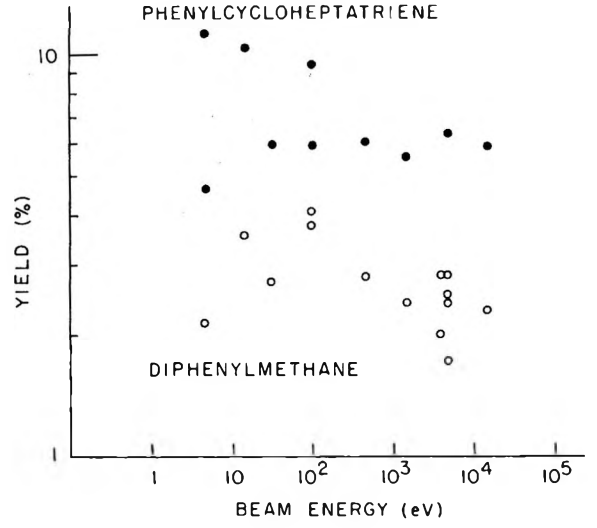

Figure 4. Yields of phenylcycloheptatriene (●) and diphenylmethane (○) *vs.* $^{14}C^+$ ion energy.

Figures 1–4. The energy measurements are accurate to within ±2 eV. Because of the possibility of imperfect charge neutralization at the target, the actual energies of our nominally 5-eV irradiations are more likely to be lower, rather than higher, than that figure. The yield data exhibit appreciable scattering; this is due to the trapping techniques for yield determinations[3] and apparently is also due to imperfectly controlled irradiation conditions, such as the beam's density. Each point represents the average of two to five yield determinations from one irradiation. It is extremely difficult to make estimates of the precisions of these yield determinations; however, we believe that almost all of them are valid to within ±25%.

(6) T. H. Lin, Ph.D. Thesis, UCRL-19335, University of California, Berkeley, 1969.

The activity distribution in the toluene product, as a function of the kinetic energy of the irradiating carbon, is shown in Table I. For comparison with our present results in the 5–100-eV range, we have included some earlier results obtained at higher energies.

Table I: Toluene-^{14}C Activity Distributions, %

Position	Kinetic energy of irradiation carbon, eV					
	5000[a]	4000	500[a]	100[a]	31	5
Me	85	84	82	80	83	29
Ring	13	14	16	15	12	66

[a] Previously reported in ref 4.

Discussion

We interpret the strong decrease in the yields of toluene and cycloheptatriene from 100 to 5 eV as being caused by a decreasing chance for the irradiating carbon atoms to pick up hydrogens, presumably in sequence, to form the assumed precursor CH_2. The same applies for the assumed precursor to phenylacetylene, C_2H_x. These precursors probably react with a ground-state benzene molecule, *via* insertion and/or substitution, without subsequent disintegration. Guideline classical-mechanical calculations (the subject of a forthcoming paper) suggest that the latter reactions (insertion and substitution) can occur only at kinetic energies below 5 eV; at higher energies the collision complex would have scant chance to survive. In contrast, hydrogen pickup reactions can proceed at rather high energies (possibly up to 50–100 eV); that is, the internal energy of the pickup product (CH, etc.) may be only a very small fraction of the product's kinetic energy. There is good support in the literature for a hydrogen-stripping mechanism in the formation of CH and CH_2 from C and CH, respectively.[7,8] The sharp decrease in our yields of phenylacetylene at carbon beam energies below 100 eV also indicates a C-stripping mechanism in the formation of C_2H_x.

Adduct formation is expected to require a substantial conversion of kinetic into internal energy, causing decomposition of the adduct unless its internal energy is only a little above bond energies ($\simeq$5 eV) so that subsequent collisions quickly stabilize the product. The apparently unchanged yield of $(C_6H_5)_2CH_2$ and increased yield of PCHT are, therefore, interpreted here as being due to this energy limitation for the formation of the assumed precursors, bencylidene (I) and cycloheptatrienylidene (II),[4] which subsequently react with another

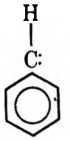

I

II

benzene molecule to form $(C_6H_5)_2CH_2$ and PCHT. The approximately constant yields of benzene and biphenyl point to intermediates in their formation of molecular weight similar to I or II. We are ignoring the "billiard-ball" hypothesis (which is, statistically, extremely unlikely) for the formation of our re-entry product, benzene. We believe that the intermediate to benzene-^{14}C is a short-lived C_7H_6 adduct, and, considering the small energy range (between activation energy and less than approximately 5 eV) within which the intermediate's formation occurs, it is not unreasonable to assume that the precursors to biphenyl and benzene, and to the above two carbenes I and II, are but different manifestations of the same short-lived intermediate. Examples of such possible intermediates have been proposed by Rose, *et al.*,[9] who studied the interactions of energetic ^{11}C with benzene and observed many of the products discussed here.

We do, however, have degradation data (Table I) from toluene formed in 5-eV experiments, and these data indicate a possible route, other than through a CH_2 intermediate, for toluene formation at or below that energy. (The degradation data for cycloheptatriene in this energy region, presented in the accompanying manuscript, are compatible with the CH_2 mechanism.) For the toluene, there is an essentially constant distribution of activity until the 5-eV region is reached; at this energy there is a great increase in ring activity (Table I). This is in contrast to toluene-^{14}C formed from photolytic $^{14}CH_2$ (with a maximum kinetic energy of 1.7 eV[4]); in this case the activity is entirely in the methyl group. One interpretation of these data is that a bare carbon atom, rather than CH_2, first interacts with benzene (in the below 5-eV region) in the mechanism leading to toluene. That such a process should suddenly appear only in the below 5-eV energy region is a matter for further investigation—it may be that a particular spin state of carbon is present only in the nominally 5-eV irradiations. A discussion of this possibility is given in the thesis of Lin.[6]

We have previously discussed the likelihood that the carbon ions of our beams are rapidly neutralized after the ions enter the target.[3] However, at lower energies, not only elastic collisions but possibly also reactive collisions may compete successfully with neutralization, and it might be argued that the decrease of yields of T, CHT, and $C_6H_5C{\equiv}CH$ is just a representation of this competition. Lack of space between the last decelerator lens and the target, coupled with the obvious difficulties in controlling the trajectories of a low kinetic energy ion beam, has so far hampered attempts to neutralize the low-energy beam and thereby ensure that only neutrals interact with the target.

(7) A. Henglein and G. A. Muccini, *Z. Naturforsch., B*, **18a**, 753 (1963).

(8) A. Henglein and G. A. Muccini, *ibid.*, **17a**, 452 (1962).

(9) T. Rose, C. MacKay, and R. Wolfgang, *J. Amer. Chem. Soc.*, **89**, 1529 (1967).

Partial Degradation of 1,3,5-Cycloheptatriene-^{14}C Obtained from Hot-Atom, Photolytic, and "Thermal" Reactions

by Helmut M. Pohlit and Richard M. Lemmon*

Chemical Biodynamics Laboratory, Lawrence Radiation Laboratory, University of California, Berkeley, California 94720 *(Received January 29, 1971)*

Publication costs assisted by the U. S. Atomic Energy Commission

1,3,5-Cycloheptatriene-^{14}C (CHT), one of the prominent products of fast ^{14}C atoms in benzene, was produced with $^{14}C^+$ ions (kinetic energies of 5, 31, and 100 eV) and was partially degraded. In the 5–100-eV energy range, over which the yield varies by a factor of about 6 to 8, the distribution of ^{14}C activity in the CHT product seems constant, *i.e.*, 31% in carbons 2–5. This value is compared with 45% obtained from 5000-eV $^{14}C^+$ ions, indicating secondary isomerization of CHT-^{14}C, at the higher energy, after its formation. In contrast, these same four carbons contain only 3.5% of the activity in CHT prepared by the photolysis of $^{14}CH_2N_2$ in benzene, and only 2.5% of the activity when the CHT is prepared by the catalytic decomposition of $^{14}CH_2N_2$ in benzene. It is concluded that (1) over the energy range from 5 to 100 eV only one mechanism is operative, (2) the last step, presumably the insertion reaction of CH_2 into benzene, does not proceed at energies above 5 eV, and (3) the effective energy available to the photolytically produced CH_2 must be well below 5 eV.

Introduction

A fast carbon ion entering a solid benzene target is neutralized and, when its energy is less than 100 eV, it begins to pick up hydrogen atoms from benzene molecules, forming CH_n radicals, of which CH_2 has been assumed to be the precursor to cycloheptatriene (CHT).[1,2] In the preceding paper we have indicated that hydrogen pickup may occur over a wide energy range, extending possibly up to 100 eV.[3] This was concluded from the rapid decrease of the yield of CHT when the irradiating $^{14}C^+$ ion's energy was decreased from 100 to 5 eV. However, our data are not extensive enough to rule out participation of other radicals, such as CH and CH_3.

CHT has been shown to be extensively isomerized if formed from $^{14}C^+$ ions of 5000 eV energy.[2] In the preceding paper,[3] it was also concluded that insertion reactions, such as that of CH_2 leading to CHT, have to occur below 5 eV. In other words, the range from 5 to 100 eV concerns only the formation of precursors. However, if there were more than one precursor involved (for example, a CH radical) in the formation of CHT, the relative abundances of these precursors would be expected to change and, very likely also, the degree of isomerization of CHT. We have, therefore, carried out the partial degradations of CHT obtained with $^{14}C^+$ ions between 5 and 100 eV. For comparison, CHT-^{14}C products from benzene and $^{14}CH_2$ *via* two different methods[4,5] ("thermal" and "photolytic") were also partially degraded.

Experimental Details and Results

The procedures for the irradiations and for the isolation of CHT-^{14}C have been described previously.[2] (For technical details concerning the ion accelerator see ref 6 and 7.)

The degradation procedure involves

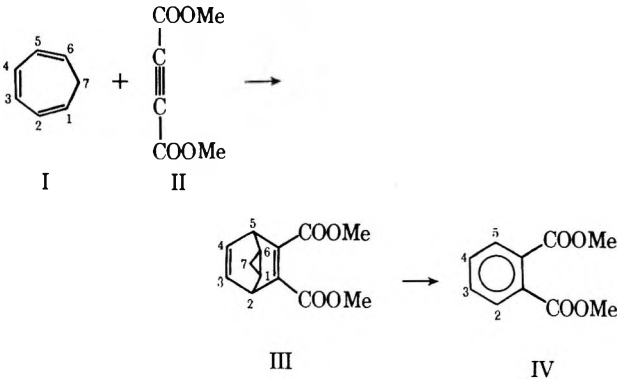

For experimental details, see ref 2 and 6. The ratio of specific activities of IV to III (or I) represents the relative abundance of labeling in positions 2, 3, 4, and 5 together. This ratio, in per cent, is denoted by α.

Catalytic Decomposition of $^{14}CH_2N_2$. For a detailed discussion of the catalytic decomposition of $^{14}CH_2N_2$, see ref 2.

Photolytic Preparation of CHT-^{14}C. Nitrosomethyl-^{14}C-urea (20 g, specific activity 10.8×10^5 dpm/mmol) was added slowly to 400 ml of benzene above a solution

(1) H. M. Pohlit, T. H. Lin, W. R. Erwin, and R. M. Lemmon, *J. Amer. Chem. Soc.*, 91, 5421 (1969).

(2) H. M. Pohlit, T. H. Lin, and R. M. Lemmon, *ibid.*, 91, 5425 (1969).

(3) H. M. Pohlit, W. R. Erwin, T. H. Lin, and R. M. Lemmon, *J. Phys. Chem.*, 75, 2555 (1971).

(4) E. Müller and G. Fricke, *Ann. Chem.*, 661, 38 (1963).

(5) R. Willstätter, *Ber.*, 31, 1544 (1898).

(6) H. M. Pohlit, Ph.D. Thesis, University of California, Berkeley, UCRL-18895, 1969.

(7) H. M. Pohlit, W. Erwin, F. R. Reynolds, R. M. Lemmon, and M. Calvin, *Rev. Sci. Instr.*, 41, 1012 (1970).

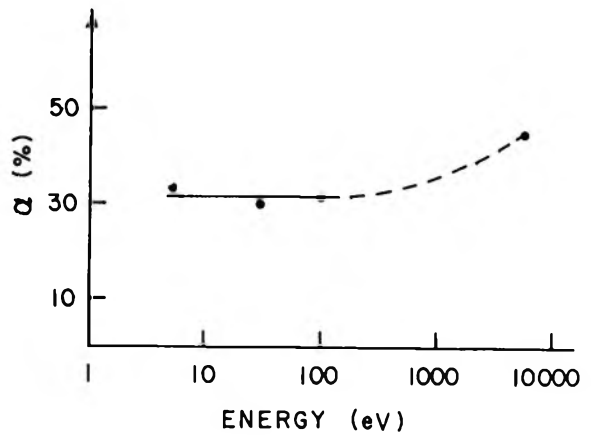

Figure 1. ^{14}C labeling in positions 2, 3, 4, and 5 of ^{14}C-cycloheptatriene *vs.* $^{14}C^+$ ion energy.

of 60 g KOH in 60 ml H_2O at *ca.* 6°. At the completion of the hydrolysis the yellow CH_2N_2 solution was decanted and irradiated at 6° for 4 hr with an unfiltered G.E. DXB "Photospot" lamp at about a 20-cm distance. The isolation of CHT-^{14}C was performed, as in ref 2, *via* preparative glpc; this is sample A.

Half of the above photolysis reaction mixture was irradiated under the same conditions for another 4 hr to check on possible isomerization of CHT-^{14}C after formation; this is sample B.

The values for α given in Table I, together with that reported earlier for a 5000-eV irradiation,[2] are plotted in Figure 1.

Discussion

If there is a real increase in α for energies higher than 100 eV (as is indicated by Figure 1), this increase may be due to increased "radiation damage" at the higher energies where the terminal "hot spot" will be larger. That is, there may be available, from diffusional processes at the end of the accelerated carbon's track, additional fragments, such as hydrogen atoms, whose availability may increase the yield of CHT.

Our interpretation of the yield drop from 2.5% at 100 eV to 0.3% at 5 eV (see Figure 1 of the ref 3) is that in this range precursors, presumably CH_2, are formed which produce CHT by insertion into the benzene ring.[3] Fewer of these precursors would be formed at the lower energies, where, for example, a bare carbon might interact with benzene before it could become CH_2. If this is correct and if α is a measure of the degree of isomerization (*via* hydrogen shifts) of CHT during or following the insertion reaction,[2] the constancy of α between 5 and 100 eV implies that the energy at which a CHT precursor (CH_2) reacts with benzene does not reflect the energy at which the precursor was formed. Therefore, the upper energy limit for insertion with appreciable success has to be below 5 eV. This constancy also implies that a possible "low energy mechanism" for CHT, such as insertion of C or CH into benzene—followed by hydrogen pickup,[2] cannot contribute appreciably to the formation of CHT in the 5–100-eV range because its relative contribution should have increased considerably at 5 eV. Since the CHT yield has decreased by a factor of 8 compared to what it is at 100 eV, the value of α should have changed unless both mechanisms produce separately exactly the same α. This is very unlikely.

The comparison of the "hot-atom" α with that of photolytically and catalytically produced CHT (3.5 and 2.5%, respectively)[2] suggests that either we are dealing with a different mechanism in the "hot-atom" case (which may be a difference in the electronic states of CH_2) or that the energy distribution of photolytically produced CH_2 is confined to a much lower energy range

Table I: Degradation of the Cycloheptatriene from Accelerated $^{14}C^+$ and Photolyzed $^{14}CH_2N_2$

Sample designation (and source)	Compound	Weight, mg	Specific activity, dpm/mol	Average α, %
A (photolytic prep.)	I	0.339	11.1×10^8	
	IIIa[a]	3.806	11.7×10^8	4.06[b]
		5.915	11.7×10^8	
	IV	3 787	4.92×10^7	
		2.497	4.59×10^7	
B (photolytic prep.)	IV	2.841	4.13×10^7	3.52
		0.547	4.15×10^7	
(100-eV $^{14}C^+$ ions)[a]	III	3.497	5.87×10^7	
	IIIa	3.686	5.94×10^7	
		3.244	5.97×10^7	31.3
		4.156	5.93×10^7	
	IV	1.821	1.87×10^7	
		3.450	1.86×10^7	
		2.94	1.88×10^7	
(31-eV $^{14}C^+$ ions)	IIIa[a]	4.161	9.15×10^7	
		4.090	9.00×10^7	
		4.428	9.23×10^7	30.0
	IV	3.676	2.73×10^7	
		3.443	2.70×10^7	
		4.188	2.79×10^7	
(5-eV $^{14}C^+$ ions)	IIIa[a]	5.196	4.8×10^7	
		1.161	5.22×10^7	
	IV	3.236	1.695×10^7	
		3.172	1.71×10^7	33.6
		2.860	1.68×10^7	

[a] IIIa is an isomer of III which does not decompose to IV (see ref 2 and 6). Its structure is most likely

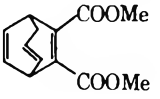

[b] The somewhat higher degree of isomerization in sample A is probably due to an accidental heating of the "buffer" of the Prepmaster, which was avoided in the isolation of sample B. Therefore, we have taken 3.5% as the upper limit for both A and B.

than that of hot-atom produced CH_2. There are estimates for photolytic CH_2 energies between 0.5 and 1.7 eV.[8] Since this energy does not seem sufficient to cause appreciable isomerization of CHT, nor of CHT to toluene,[9] the CHT obtained in the "hot-atom" chemical system must have been produced by CH_2 with energies well above 1.7 eV but below *ca.* 5 eV. Doering and Gaspar[10] found a certain amount of deuterium in carbons 1–6 of CHT prepared photolytically from CD_2N_2; however, they seem to attribute it mainly to photoisomerization of CHT after its formation.

The most reasonable interpretation of our results is that only one mechanism is operable for the CHT production and that CH_2 radicals with energies between about 0.5 and 5 eV are the precursors. Some of these precursors with energies >1.7 eV cause considerable isomerization in the CHT product.

Acknowledgements. This work was sponsored by the U. S. Atomic Energy Commission. One of us (H. M. P.) is also indebted for support from the Bundesministerium für Wissenschaftliche Forschung and the Deutscher Akademischer Austauschdienst of West Germany.

(8) H. M. Frey and G. B. Kistiakowsky, *J. Amer. Chem. Soc.*, **79**, 6373 (1957).

(9) R. M. Lemmon and W. Strohmeier, *ibid.*, **81**, 106 (1959).

(10) W. von E. Doering and P. P. Gaspar, *ibid.*, **85**, 3043 (1963).

The Effect of Olefins on the Reactions of Nitrous Oxide in γ-Irradiated Liquid Cyclopentane[1a]

by Fabio Busi*[1b] and Gordon R. Freeman

Chemistry Department, University of Alberta, Edmonton 7, Canada *(Received March 15, 1971)*

Publication costs borne completely by The Journal of Physical Chemistry

Addition of propylene or cyclopentene to solutions of nitrous oxide in cyclopentane has no effect on the nitrogen yields when the nitrous oxide concentration is <1 mol %, but it appears to increase the nitrogen yields slightly at nitrous oxide concentrations >1 mol %. The kinetics of the olefin effect cannot be explained by the association of an electron with an olefin molecule followed by transfer of the electron to nitrous oxide, as previously suggested. The effect is small, and if it is not an experimental artifact it must be due to unknown secondary reactions. Nitrous oxide does not react appreciably with hydrogen atoms, and monoolefins do not interact to a significant extent with electrons in the radiolysis of liquid saturated hydrocarbons at 25°. The initial yield of hydrogen from pure cyclopentane appears to be $G(H_2)_i = 5.7$. Essentially all ion–electron neutralizations in pure cyclopentane lead to hydrogen formation: G(H, olefin scavengable) ≈ 2.9; k(H + olefin)/k(H + c-C_5H_{10}) = 140 for both propylene and cyclopentene.

Introduction

It has been reported that addition of cyclohexene[2] or propylene[3] to a solution of nitrous oxide in liquid cyclohexane increased the γ-radiolysis yield of nitrogen. These results are surprising in view of the fact that the nitrogen yield was smaller from nitrous oxide solutions in pure cyclohexene than from solutions in cyclohexane at the same concentration.[2] It was suggested that olefins provide shallow traps for electrons in liquid alkanes and that such trapped electrons can be captured by nitrous oxide.[2,3]

$$e^-_{solv} + ol \longrightarrow (ol^-)_{solv} \quad (1)$$

$$(ol^-)_{solv} + N_2O \longrightarrow ol + N_2O^-_{solv} \quad (2)$$

$$N_2O^-_{solv} \longrightarrow N_2 + O^-_{solv} \quad (3)$$

(1) (a) This work received financial assistance from the National Research Council of Canada through Grant No. A1285. (b) To whom correspondence should be addressed at Consiglio Nazionale delle Ricerche, Laboratorio di Fotochimica e Radiazioni d'alta Energio, Bologna, Italy.

(2) S. Sato, R. Yugeta, K. Shinsaka, and T. Terao, *Bull. Chem. Soc. Jap.*, **39**, 156 (1966).

(3) M. G. Robinson and G. R. Freeman, *J. Chem. Phys.*, **48**, 983 (1968).

Here ol represents an olefin and $(ol^-)_{solv}$ may be a loosely bound olefin–electron complex rather than a stable negative ion.

Trapping of electrons by monoolefins is not a generally accepted concept, and neither of the previous reports[2,3] was unambiguous about the olefin result. An understanding of the olefin effect is an integral part of the elucidation of the mechanism of hydrocarbon radiolysis, so it is desirable to reinvestigate nitrous oxide–alkane–olefin systems. To this end we have studied the γ radiolysis of solutions of nitrous oxide in cyclopentane, cyclopentene, and various cyclopentane–olefin mixtures. The results are reported herein.

Experimental Section

Phillips Research Grade cyclopentane was purified by prolonged shaking with sulfuric acid, followed by washings with dilute potassium hydroxide and with water. The cyclopentane was dried over anhydrous magnesium sulfate, then distilled from lithium aluminum hydride in a nitrogen atmosphere.

Phillips Research Grade cyclopentene was distilled in a nitrogen atmosphere, then distilled and stored under vacuum.

Nitrous oxide (Matheson Co.) was purified by bubbling through a saturated solution of potassium hydroxide, then passed through a column of Drierite and one of potassium hydroxide pellets. It was finally distilled under vacuum and thoroughly degassed.

Propylene and ethylene (Phillips Research Grade) and hydrogen chloride (Matheson Co.) were degassed by distillation under vacuum, combined with freeze–pump–thaw cycles.

The Pyrex sample cells were filled by standard vacuum techniques. The 4-cm^3 cells each contained 2.0 cm^3 of solution.

The vacuum system contained metal needle valves with Teflon seats.

The Ostwald absorption coefficients of nitrous oxide in cyclopentane and cyclopentene were measured by the technique described by Hentz and Sherman;[4] the values obtained were 3.0 in cyclopentane and 3.7 in cyclopentene at ~25°.

For ethylene in cyclopentane an absorption coefficient of 3.9 at 25° was estimated by interpolation between the value 6.1 at 0° and 2.2 at 46°, calculated from data of Holroyd.[5]

It was assumed that all the propylene dissolved in the cyclopentane.

The samples were irradiated at 25° in a ^{60}Co Gammacell-220. The dose rate was 3.7×10^{17} eV/g min and the dose was 2.2×10^{18} eV/g.

Gaseous products that were volatile at −196° were separated by vacuum distillation, collected and measured in a McLeod–Toepler apparatus, and analyzed by gas chromatography. A 2.5-m Molecular Sieve 5A (Linde) column was used at 30° with helium carrier gas and a thermal conductivity detector.

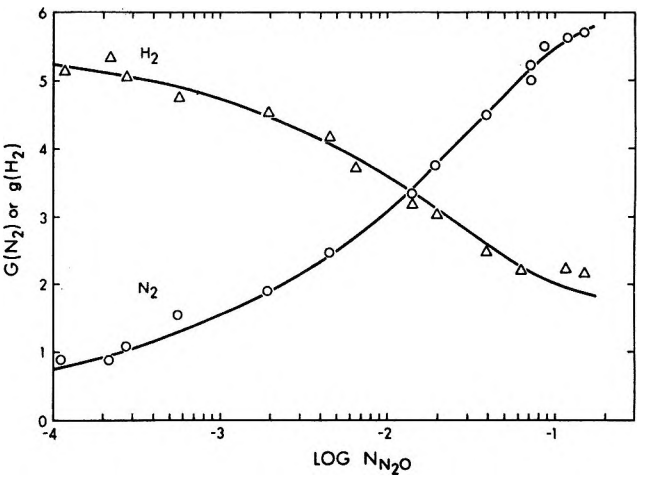

Figure 1. $G(N_2)$ and $g(H_2)$ from solutions of nitrous oxide in cyclopentane. N_{N_2O} is the mole fraction of nitrous oxide in the solution. $G(N_2)$ is based upon the total energy absorbed by the solution; $g(H_2)$ is based upon the energy initially absorbed by the solvent only. The curve drawn through the hydrogen yields has the equation $g(H_2) = 5.7 - 0.68G(N_2)$.

Results

The yields of nitrogen from the solutions are expressed as G values, based upon the total energy absorbed by the solution. The yields of hydrogen from the solutions are expressed as g values, based on the energy initially absorbed in the solvent only. When hydrogen was also a product of the solute radiolysis, $g(H_2)$ was corrected on the basis of the following yields for the pure liquid solutes: cyclopentene $g(H_2) = 1.2$;[6] propylene $g(H_2) = 0.8$;[7] ethylene $g(H_2) = 1.2$;[7] hydrogen chloride $g(H_2) = 6.5$.[8]

The nitrogen and hydrogen yields from the nitrous oxide–cyclopentane solutions are strongly dependent on the nitrous oxide concentration (Figure 1). The behavior of the nitrous oxide–cyclopentene solutions is similar, although the hydrogen yields are much lower and the nitrogen yields are slightly lower from the olefin solutions (Figure 2).

Cyclopentene was added to a number of cyclopentane–nitrous oxide solutions. Typical results are shown in Figure 3 (B–D). For example, when the mole fraction of nitrous oxide was 2.0×10^{-3}, addition of cyclopentene decreased the hydrogen yield by 40% but had no effect on the nitrogen yield. At a much higher nitrous oxide concentration, *e.g.*, $N_{N_2O} = 1.6 \times 10^{-1}$, addition of cyclopentene decreased $g(H_2)$ by about the

(4) R. R. Hentz and W. V. Sherman, *J. Phys. Chem.*, **72**, 2635 (1968).

(5) R. A. Holroyd, *ibid.*, **66**, 730 (1962).

(6) J. Y. Yang and I. Marcus, *J. Chem. Phys.*, **42**, 3315 (1965).

(7) M. G. Robinson, unpublished results.

(8) R. C. Rumfeldt and D. A. Armstrong, *J. Phys. Chem.*, **68**, 761 (1964).

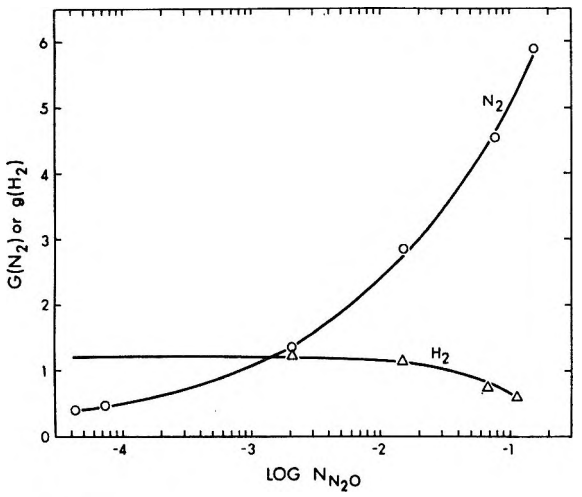

Figure 2. $G(N_2)$ and $g(H_2)$ from solutions of nitrous oxide in cyclopentene. N_{N_2O} is the mole fraction of nitrous oxide in the solution.

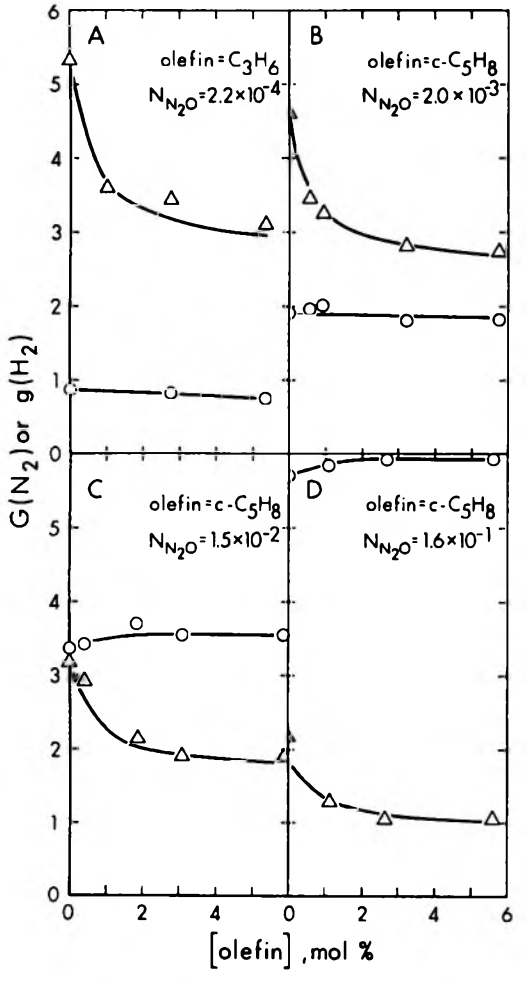

Figure 3. Nitrogen and hydrogen yields from nitrous oxidecyclopentane solutions, as functions of added olefin concentration: O, $G(N_2)$; △, $g(H_2)$. The curves through the hydrogen yields were calculated using $k(H + \text{olefin})/k(H + c\text{-}C_5H_{10}) = 140$.

same fractional amount; $G(N_2)$ appeared to increase slightly, but the effect was not much larger than the

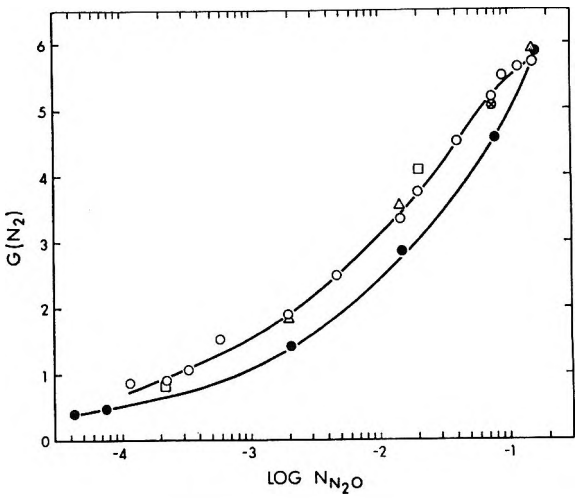

Figure 4. Nitrogen yields as functions of mole fraction nitrous oxide in cyclopentane (O), cyclopentene (●), and cyclopentane containing 3 mol % cyclopentene (△), 3 mol % propylene (□), or 3 mol % ethylene (×).

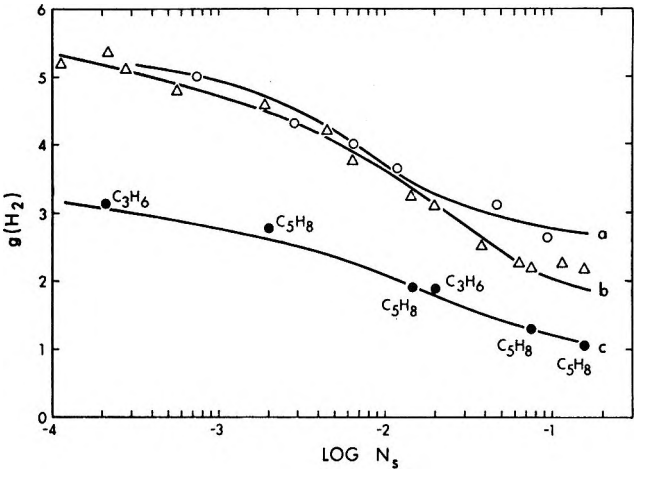

Figure 5. Hydrogen yields from cyclopentane containing various scavengers. The scavengers are: O, cyclopentene; △, nitrous oxide; ●, nitrous oxide plus a constant 5 mol % of cyclopentene or propylene. N_s is the mole fraction of solute, but in the ternary solutions ● refers to the nitrous oxide only. Curve a was calculated using $k(H + C_3H_6)/k(H + c\text{-}C_5H_{10}) = 140$ and $g(H) = 2.7$. Curve c corresponds to curve b lowered by a factor of 0.58.

average experimental scatter (Figure 3); addition of up to 30 mol % cyclopentene did not increase $G(N_2)$ further.

Addition of propylene to cyclopentane–nitrous oxide solutions had the same effect as had addition of cyclopentene; $g(H_2)$ was decreased at all nitrous oxide concentrations, and $G(N_2)$ was unaffected at low nitrous oxide concentrations but appeared to increase slightly when propylene was added at high nitrous oxide concentrations. A typical set of results is shown in Figure 3A.

The total Figure 3 displays the propylene and cyclopentene effects at values of N_{N_2O} from 2.2×10^{-4} to 1.6×10^{-1}.

The nitrogen yields from cyclopentane–nitrous oxide solutions containing 3 mol % of cyclopentene, propylene, or ethylene are compared with those from nitrous oxide in pure cyclopentane and pure cyclopentene solvents in Figure 4. Ethylene had no effect on the nitrogen yield even at high nitrous oxide concentration.

Different amounts of cyclopentene were added to cyclopentane and the hydrogen yields were measured. The results are shown in Figure 5. The hydrogen yields from cyclopentane–nitrous oxide solutions and from (cyclopentane + nitrous oxide + 5 mol % cyclopentene or propylene) solutions are also plotted for comparison. Cyclopentene depresses $g(H_2)$ by about the same amount as does nitrous oxide at low concentrations, but the former is less effective than the latter at high concentrations. Nitrous oxide and olefin together are much more effective than either additive alone.

The hydrogen yield from the purified cyclopentane was 5.3, independent of dose over the range 2×10^{18}–2×10^{19} eV/g. However, addition of hydrogen chloride increased $g(H_2)$ to 5.7, independent of hydrogen chloride concentration from 0.1 to 10 mol %. It appears that the initial yield of hydrogen from absolutely pure cyclopentane would be 5.7. Although most earlier workers reported yields in the vicinity of 5.3 for doses in the above region,[5,9-11] Hardwick[12] reported $g(H_2) = 5.78$ at 1×10^{18} eV/g.

Discussion

Cyclopentane–Nitrous Oxide Solutions. Taking $g(H_2)_0 = 5.7$ for pure cyclopentane, it appears that scavenging electrons by nitrous oxide can cause $g(H_2)$ to decrease by ≥ 3.6 (Figure 1). The total ionization yield in liquid hydrocarbons is about four ion pairs per 100 eV absorbed.[13-15] Thus nearly every ion–electron neutralization in the radiolysis of pure cyclopentane leads to hydrogen formation.

On the average $\Delta g(H_2) \approx 0.68\, G(N_2)$, as shown by the curves drawn in Figure 1.

Cyclopentane–Olefin–Nitrous Oxide Solutions. The data in Figures 3 and 4 demonstrate that the addition of cyclopentene or propylene has no effect on the nitrogen yields from solutions that have $N_{N_2O} < 10^{-2}$; there appears to be a small positive effect at higher nitrous oxide concentrations. There is the hint of a similar effect of ethylene on the yield of methyl radicals formed in methyl choride–cyclohexane solutions (Table I in ref 16). The methyl radicals were attributed exclusively to reaction 4. There was no effect of ethylene upon

$$e^- + CH_3Cl \longrightarrow CH_3 + Cl^- \qquad (4)$$

the methyl radical yields at the lower methyl chloride concentrations, but the addition of 1 mol % of ethylene to the 4 mol % methyl chloride solution increased $G(CH_3)$ by an amount (0.14 unit) several times greater than the experimental scatter (0.02 unit) shown by the other points.

The olefin effects are so small that one cannot be certain whether they are real or merely experimental artifacts. However, even if they are real the overall olefin effects cannot be explained by the occurrence of reaction 1 followed by 2 or 5.

$$(ol^-)_{solv} + CH_3Cl \longrightarrow ol + CH_3Cl^-{}_{solv} \qquad (5)$$

$$CH_3Cl^-{}_{solv} \longrightarrow CH_3 + Cl^-{}_{solv} \qquad (6)$$

These reactions would cause $G(N_2)$ and $G(CH_3)$ to increase by the same or greater amounts at low as at high nitrous oxide and methyl chloride concentrations, respectively. Furthermore, increasing olefin concentrations would be required to produce the effect as the electron scavenger concentration was increased. In fact the olefin effect had reached its maximum at 2 mol % of cyclopentene in both 1.5 and 16 mol % nitrous oxide solutions (Figure 3).

It is concluded that reactions 1, 2, and 5 do not occur to a significant extent with monoolefins.

Nitrous oxide has the same relative effect on the hydrogen yields from the cyclopentane–olefin solutions as on those from pure cyclopentane (Figure 5). It is clear that nitrous oxide and olefin do not react with the same intermediates.

It is well known that nitrous oxide reacts with electrons[17] and that olefins react with hydrogen atoms. The present work demonstrates that hydrogen atoms do not react with nitrous oxide and that electrons do not interact appreciably with monoolefins in liquid alkanes at room temperature.

Mechanism of Hydrogen Formation. The hydrogen formation mechanism may be presented in simplified form as follows.

	G	
$C_5H_{10} \xrightarrow{\sim\sim} C_5H_{10}^+ + e^-$	4	(7)
$\xrightarrow{\sim\sim} C_5H_{10}^*$	1.7	(8)
$C_5H_{10}^+ + e^- \longrightarrow C_5H_{10}^{\ddagger}$	4	(9)
$C_5H_{10}^* \longrightarrow H', H_2$, products	0.8	(10)
$\longrightarrow H + C_5H_9$	0.9	(11)

(9) S. Z. Toma and W. H. Hamill, *J. Amer. Chem. Soc.*, **86**, 1478 (1964).

(10) B. M. Hughes and R. G. Hanrahan, *J. Phys. Chem.*, **69**, 2707 (1965).

(11) L. G. Walker, Ph.D. Thesis, University of Alberta, 1967.

(12) T. J. Hardwick, *J. Phys. Chem.*, **66**, 1611 (1962).

(13) N. H. Sagert and A. S. Blair, *Can. J. Chem.*, **45**, 1351 (1967)

(14) G. R. Freeman and E. D. Stover, *ibid.*, **46**, 3235 (1968).

(15) J. M. Warman, K.-D. Asmus, and R. H. Schuler, *Advan. Chem. Ser.*, **No. 82**, 25 (1968).

(16) J. M. Warman, K.-D. Asmus, and R. H. Schuler, *J. Phys. Chem.*, **73**, 931 (1969).

(17) (a) F. S. Dainton and D. B. Peterson, *Proc. Roy. Soc., Ser. A*, **267**, 443 (1962); (b) G. Scholes and M. Simic, *Nature*, **202**, 895 (1964); (c) later work from many laboratories.

	G	
$C_5H_{10}^{\ddagger} \longrightarrow H', H_2$, products	2.0	(12)
$\longrightarrow H + C_5H_9$	2.0	(13)
$H' + C_5H_{10} \longrightarrow H_2 + C_5H_9$		(14)
$H + C_5H_{10} \longrightarrow H_2 + C_5H_9$	2.9	(15)

Here H′ is an atom that reacts while hot and is not scavengable by olefins; H possesses less energy than does H′ and is scavengable by olefins.

$$H + ol \longrightarrow Hol\cdot \quad (16)$$

The curves drawn through the hydrogen yields in Figure 3 and curve a in Figure 5 were drawn using the value $k_{16}/k_{15} = 140$ for both propylene and cyclopentene in reaction 16. The fraction of the residual hydrogen yield at a given nitrous oxide concentration that is scavengable by an olefin is about 50% at all nitrous oxide concentrations, the same as that in the absence of nitrous oxide.

Nitrous oxide inhibits hydrogen formation by intercepting reaction 9.

$$N_2O + e^- \longrightarrow N_2O^- \quad (17)$$

$$N_2O^- \longrightarrow N_2 + O^- \quad (3)$$

$$C_5H_{10}^+ + \text{negative ion} \longrightarrow \text{no H or } H_2 \quad (18)$$

The present results lead to the approximate G values listed after reactions 7–15 for pure cyclopentane. The value $G(H_2) = 5.3$ obtained from the purified cyclopentane in the present work, and the effect of added hydrogen chloride, indicate that a small amount of electron scavenger such as carbon dioxide remained in the cyclopentane.

Cyclopentene–Nitrous Oxide Solutions. The fact that the electron scavenging efficiency of nitrous oxide is lower in liquid olefins than in saturated hydrocarbons (Figure 4 and ref 2) is associated with the fact that the ion–electron separation distance in spurs is lower in the former than in the latter.[18] The smaller ion–electron separation distance results in a shorter geminate neutralization time and makes it more difficult for a solute molecule to intercept the electron before it reacts with its geminate ion.

(18) W. F. Schmidt and A. O. Allen, *J. Chem. Phys.*, **52**, 2345 (1970).

The Oxidation and Reduction of Organic Compounds by Ionizing Radiation: L-Penicillamine Hydrochloride

by Edwin E. Budzinski and Harold C. Box*

Biophysics Department, Roswell Park Memorial Institute, Buffalo, New York 14203 *(Received December 29, 1970)*

Publication costs assisted by the Public Health Service

Esr measurements on single crystals of L-penicillamine HCl X-irradiated and observed at 4.2°K reveal one reduced and two oxidized products. The oxidized products are "sulfur" radicals $SC(CH_3)_2CH(NH_3Cl)$-COOH and chlorine atoms. The reduced product is the anion $HSC(CH_3)_2CH(NH_3Cl)C(OH)O^-$. On warming, the yield of "sulfur" radicals is augmented by hole transfer from chlorine atoms to sulfur atoms. Dissociation of the anion also occurs on warming, producing the radical $HSC(CH_3)_2CHCOOH$. At room temperature the latter radical also disappears, and the final absorption is entirely due to "sulfur" radicals. It appears that processes initiated by both oxidation and reduction contribute to the formation of "sulfur" radicals. Altogether nine paramagnetic absorption spectra were observed in this study including several due to different conformations of the aforementioned radicals.

Introduction

In a previous paper[1] it was pointed out that it is often possible to stabilize the primary products of oxidation and reduction formed by ionizing radiation in organic compounds by maintaining the irradiated sample at the temperature of liquid helium (4.2°K). The damaged species can usually be identified using esr spectroscopy. In this investigation the technique was used to study radiation damage in single crystals of penicillamine HCl

$$HS\text{–}C(CH_3)_2\text{–}CH(NH_3^+Cl^-)\text{–}COOH$$

I

(1) H. C. Box, H. G. Freund, K. T. Lilga, and E. E. Budzinski, *J. Phys. Chem.*, **74**, 40 (1970).

The effect of ionizing radiation on sulfhydryls is of particular interest in radiation biology. Cysteine HCl,

$$HS\text{-}CH_2\text{-}CH(NH_3{}^+Cl^-)\text{-}COOH$$
II

which is a more biologically significant sulfhydryl compound, has been studied extensively. Wheaton and Ormerod[2] and Akasaka[3] have used esr spectroscopy to examine single crystals of cysteine HCl irradiated at liquid nitrogen temperature. However, this temperature is not low enough to stabilize the primary radiation damage products. We have irradiated and examined cysteine HCl at 4.2°K and found clear evidence that a more primitive stage of the radiation damage process can be observed at the lower temperature.[4] The esr absorption spectra are not as well defined, however, as those obtained from penicillamine. Consequently, we have concentrated our efforts on the latter compound. As an irradiated penicillamine HCl crystal is allowed to warm above 4.2°K various secondary reactions takes place. It is possible to follow the fate of both the oxidized and reduced species created by the ionization process. Ultimately the chain of chemical events initiated by oxidation *and* reduction leads to the formation of radicals of the type

$$S\text{-}C(CH_3)_2\text{-}CH(NH_3{}^+Cl^-)\text{-}COOH$$
IIIa

Altogether nine paramagnetic absorption spectra, including several associated with various conformations of the aforementioned radicals, were observed in this investigation.

Experimental Section

Single crystals of L-penicillamine HCl were obtained by slow cooling of supersaturated aqueous solutions. The crystals are monoclinic belonging to the space group $P2_1$ with two molecules per unit cell.[5] The asymmetric unit also contains a molecule of water.

A crystal, mounted on a Cu wire, was suspended along the axis of the cylindrical sample cavity of a K band esr spectrometer. The technique used to X-irradiate and measure the absorption in crystals at 4.2°K has been described previously.[1] A thermocouple embedded in the sample holder just above the crystal mount was used to record temperature during warming experiments. The temperature indicated by the thermocouple was probably somewhat above the actual crystal temperature.

Results

Five distinct stages in the radiation damage process could be observed in penicillamine HCl following irradiation at 4.2°K. The esr spectrum obtained at each stage for a particular crystal orientation is shown in Figure 1. The integrated absorption relative to the integrated absorption at the first stage is indicated. The sequence of events was as follows.

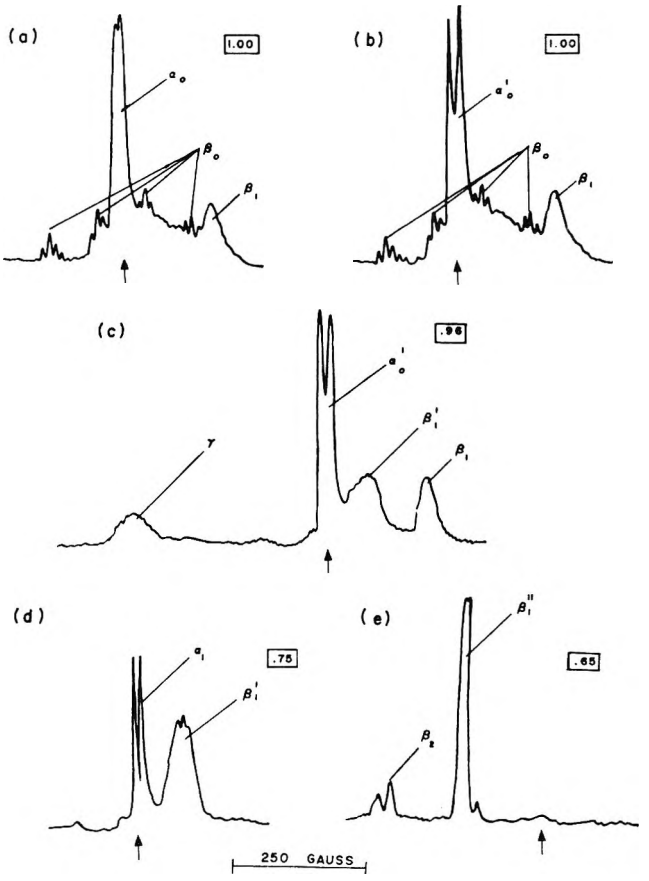

Figure 1. The sequence of esr spectra obtained from a single crystal of X-irradiated penicillamine HCl at 4.2°K. (a) Following irradiation at 4.2°K with no warming. (b) After warming to an indicated temperature of 65°K. (c) Warming to an indicated temperature of 200°K. (d) After warming to an indicated temperature of 235°K. (e) After warming to an indicated temperature of 275°K. These spectra were recorded with the magnetic field parallel to the (010) plane in a direction 31.4 and 135° away from the *a* and *c* axes, respectively. The numbers inclosed in boxes indicate the total integrated absorption relative to that meaured in (a). The arrows indicate the magnetic field correspding to free spin resonance.

First Stage. The esr absorption obtained at 4.2°K without warming is shown in Figure 1a. The absorption consists of three distinguishable components. The component labeled β_0 is due to chlorine atoms.[6] The

(2) R. F. Wheaton and M. G. Ormerod, *Trans. Faraday Soc.*, **65**, 1638 (1969).

(3) K. Akasaka, *J. Chem. Phys.*, **43**, 1182 (1965).

(4) Unpublished data.

(5) D. Crowfoot, C. W. Bunn, B. W. Rogers-Low, and A. Turner-Jones, "The Chemistry of Penicillin," Princeton University Press, Princeton, N. J., 1949, pp 310-367. More recently the crystal structure of L-penicillamine HCl has been investigated by R. Parthasarathy and F. Cole of the Center for Crystallographic Research, Roswell Park Memorial Institute.

(6) Esr spectra labeled with an α are associated with the reduction process; those labeled with a β are associated with the oxidation process. This notation is consistent with that used by K. Akasaka, *et al.*, *J. Chem. Phys.*, **40**, 3110 (1964), in their study of cystine HCl irradiated at 77°K. We have used primes, wherever necessary, to distinguish between spectra attributed to different conformations of the same paramagnetic species.

component labeled β_1 is attributed to the radical cation

$$HS^{+}\text{–}C(CH_3)_2\text{–}CH(NH_3{}^{+}Cl^{-})COOH$$

IIIb

or its neutralized form

$$S\text{–}C(CH_3)_2\text{–}CH(NH_3{}^{+}Cl^{-})\text{–}COOH$$

IIIa

The component labeled α_0 is attributed to the anion

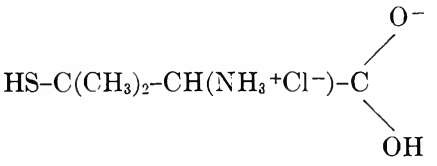

IV

The hyperfine structure associated with the β_0 absorption in Figure 1a clearly indicates that the absorption is due to atomic chlorine. There are four clusters of lines arising from the interaction of the unpaired electron with the chlorine nucleus. The two isotopes of chlorine, ^{35}Cl (75% abundant) and ^{37}Cl (25% abundant), have a spin of $^3/_2$ but slightly different magnetic moments. There is an additional interaction between the unpaired electron and two protons. Although the structure analysis[5] of penicillamine HCl has not determined the position of the hydrogen atoms, there is evidence of hydrogen bonding between the chlorine ion and oxygen atoms of a carboxyl group and two water molecules and between the chlorine ion and the nitrogen of an amino group. Two of these hydrogen bonds undoubtedly account for the proton hyperfine structure associated with the chlorine atom absorption. The protons are equivalently coupled for the crystal orientation used for Figure 1 and the interaction gives rise to a triplet hyperfine splitting in which the intensities of the lines are in the ratio of 1:2:1. Thus the hyperfine lines in the β_0 absorption in Figure 1a can be reconstructed by assigning two parameters: a hyperfine coupling of 87.0 G for the ^{35}Cl nucleus (and consequently 73.2 G for the ^{37}Cl nucleus) and a coupling of 12.1 G for the protons. A stick diagram of the computed hyperfine pattern is compared with the observed pattern in Figure 2. Since the hydrogen atoms involved in hydrogen bonding with the chlorine ion are easily exchangeable, the proton hyperfine pattern is absent in crystals grown from heavy water solution. The chlorine hyperfine pattern and the g value of the β_0 absorption are extremely anisotropic as would be expected for a Cl atom with the unpaired electron in a 3p state. For most crystal orientations the β_0 spectrum is much less well resolved than that shown in Figure 1a. Consequently, the tensors required to characterize this absorption fully were not determined.

The β_1 absorption has a large anisotropy associated with its g value. The principal values and direction

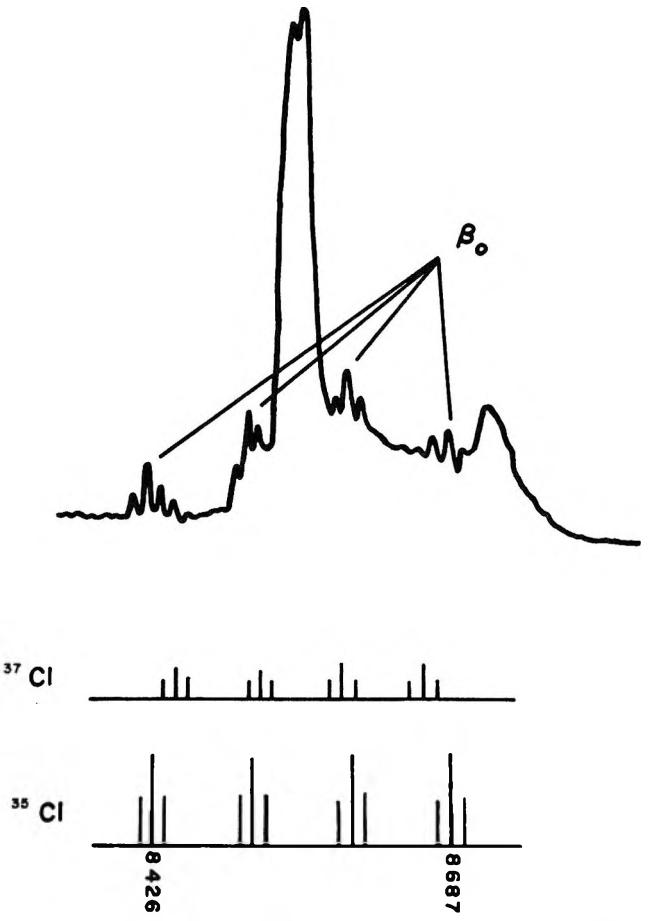

Figure 2. The spectra expected from chlorine atoms interacting with two protons indicated by stick diagrams for the two isotopes of chlorine. These two absorptions partially overlap to produce the hyperfine structure shown in the β_0 components of the esr absorption.

cosines for the principal axes of the g tensor are given in Table I. The g value characteristics suggest a radical in which the unpaired electron is localized on an atom of high atomic number (and consequently has a large spin-orbit coupling). Thus the β_1 absorption is attributed to the radical III in which the unpaired electron is localized mainly on the sulfur atom. Since there is no evidence of hyperfine coupling due to the sulfhydryl proton, it is more plausible to ascribe the absorption to the neutral form of the radical IIIa. The principal values of the g tensor for the β_1 absorption are very similar to the values (2.29, 1.99, 1.99) found by Akasaka[3] in cysteine HCl irradiated at 77°K for a radical attributed to the analog of IIIa.

As can be seen from Table I, the g value associated with the α_0 absorption is only slightly anisotropic. The hyperfine doublet is attributed to the exchangeable proton of the carboxyl group.[7] An experiment, which is described later, using a partially deuterated penicillamine HCl crystal confirms this interpretation. Anion

(7) J. W. Sinclair and M. W. Hanna, *J. Phys. Chem.*, **71**, 84 (1967); P. B. Ayscough and A. K. Roy, *Trans. Faraday Soc.*, **64**, 582 (1968).

Table I: Principal Values of g Tensors and Hyperfine Coupling Tensors (in Gauss) and Direction Cosines of Principal Axes Associated with Various Absorptions Shown in Figure 1[a]

		a'	b	c
α_0	2.0033	0.00	1.00	0.00
g value	2.0024	0.80	0.00	−0.60
	2.0016	0.60	0.00	0.80
α_0	10	0.0	1.0	0.0
hyperfine	10	−0.13	0.0	0.99
	6	0.99	0.0	0.13
α'_0	2.0031	0.00	1.00	0.00
g value	2.0023	0.13	0.00	−0.99
	2.0012	0.99	0.00	0.13
α'_0	20	0.85	0.00	−0.52
hyperfine	16	0.00	1.00	0.00
	13	0.52	0.00	0.85
β_1	2.297	0.25	0.95	0.20
g value	2.037	−0.74	0.05	0.67
	1.921	0.62	−0.32	0.72
β'_1	2.217	0.33	0.91	0.23
g value	2.000	0.72	−0.41	0.56
	1.983	−0.60	0.02	0.80
β''_1	2.058	0.96	0.12	0.25
g value	2.025	−0.19	−0.36	0.91
	2.002	−0.20	0.93	0.32
γ	2.248	0.07	0.44	0.89
g value	1.996	−0.70	0.66	−0.27
	1.978	0.71	0.61	−0.36
α_1	2.0037	0.49	0.84	0.23
g value	2.0022	0.86	−0.43	−0.28
	2.0008	0.14	−0.33	0.93
α_1	32	0.54	0.81	0.24
hyperfine	18	0.83	−0.46	−0.31
	7	0.14	−0.37	0.92
β_2	2.054	−0.44	0.35	0.83
g value	2.024	0.79	0.59	0.17
	2.000	−0.43	0.73	−0.54
C_3–S bond direction		0.228	0.937	0.258

[a] Direction cosines for the C_3–S bond direction are also given. The direction a' is orthogonal to b and c. There is another set of tensors related to this set by a twofold rotation about b.

IV is analogous to the anions observed in succinic acid[8] and amino acids[7,9] irradiated at low temperature.

Second Stage. By raising the crystal above the level of the liquid helium the crystal could be warmed to a temperature indicated approximately by a thermocouple embedded in the sample holder. Warming to 65°K and subsequent reimmersion in liquid helium produced the spectrum shown in Figure 1b. The only significant change is that the α_0 absorption has been replaced by another which is labeled α'_0. The g tensor and the hyperfine coupling tensor for the α'_0 absorption are given in Table I. The α'_0 absorption is attributed to a different conformation of the anion IV. Changes in the conformation of free radicals produced at low temperature are often observed as the temperature increases.[10] The hyperfine coupling is larger for the α'_0 absorption, indicating a reorientation of the anion such that the projection of O–H bond perpendicular to the carboxyl plane is larger.[7,11]

Third Stage. The β_0 absorption disappears when the crystal is warmed to 200°K and the absorption labeled β'_1 becomes apparent. The latter absorption is probably present even in the initial stage (Figure 1a) but is less intense and partially masked by the β_0 absorption. The principal values of the g tensors for the β_1 and β'_1 absorptions (Table I) are very similar. The β'_1 absorption is attributed to a different conformation of the radical IIIa. Experience teaches us to expect that free radicals produced by irradiation at low temperatures are likely to reorient or "relax" at higher temperatures.[2,7,10,12,13] For example, several conformations of the radical analogous to IIIa have been observed in cysteine HCl crystals irradiated with X-rays[2] or ultraviolet light[12] at low temperature and subsequently allowed to warm.

A new absorption labeled γ appears in Figure 1c. The large anisotropy associated with the g value for this absorption suggests a free radical with the unpaired electron localized on the sulfur atom. However, the principal axes of the g tensor for the γ absorption (Table I) are such that we are uncertain whether this absorption should be ascribed to an oxidation or a reduction product. This point is discussed more fully in the last section of this paper.

Fourth Stage. Warming to 235°K yields an absorption pattern, Figure 1d, consisting of two components. The γ and β_1 absorptions have disappeared and the β'_1 absorption is enhanced. The α'_0 absorption has also disappeared and a new absorption, labeled α_1 in Figure 1d, has appeared. The α_1 absorption has a well resolved and markedly anisotropic hyperfine doublet associated with it. Additional hyperfine lines appear at some crystal orientations which are due to forbidden transitions.[14] The anisotropic coupling and the existence of forbidden transitions (at K band) are characteristic of radicals in which the unpaired electron on a carbon atom interacts with the proton of a neighboring bonded hydrogen atom. The absorption is attributed

(8) H. C. Box, H. G. Freund, and K. T. Lilga, *J. Chem. Phys.*, **42**, 1471 (1965).

(9) H. C. Box, E. E. Budzinski, and H. G. Freund, *ibid.*, **50**, 2880 (1969).

(10) J. W. Wells and H. C. Box, *ibid.*, **46**, 2935 (1967).

(11) C. Heller and H. M. McConnell, *ibid.*, **32**, 1535 (1960).

(12) H. C. Box, H. G. Freund, and E. E. Budzinski, *ibid.*, **45**, 809 (1966).

(13) H. C. Box and H. G. Freund, *ibid.*, **44**, 2345 (1966).

(14) H. M. McConnell, C. Heller, T. Cole, and R. W. Fessenden, *J. Amer. Chem. Soc.*, **82**, 766 (1960).

to the radical

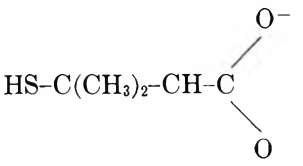

Va

or its neutralized form

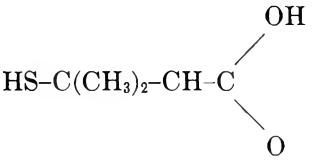

Vb

The characteristics of the g tensor and the hyperfine tensor for this absorption are given in Table I.

Fifth Stage. Finally after warming to 275°K an absorption is obtained which is relatively stable at room temperature. The major component of the absorption, β''_1 in Figure 1e, is attributed to the final "relaxed" conformation of the sulfur radical IIIa. The principal values of the g tensor for this absorption are nearly identical with the values (2.052, 2.025, 2.002) found by Akasaka[15] for the relaxed form of the radical analogous to IIIa produced in irradiated cystine HCl. For some crystal orientations a doublet hyperfine splitting is barely resolved which is probably due to a proton on a neighboring molecule.

A minor component of the final absorption, β_2 in Figure 1e, also shows considerable g value anisotropy and a doublet splitting for some crystal orientations.

The foregoing sequence of observations was repeated using a single crystal of penicillamine DCl grown from heavy water. The doublet splittings in the α_0 and α'_0 absorptions were not observed with the deuterated crystal showing that the doublet splitting originates with the proton of the exchangeable hydrogen atom in the carboxylic acid group of the anion IV. The doublet in the α_1 absorption remained, however, as would be expected for the radical V. Also the doublet associated with the β''_1 absorption was unaffected by deuteration.

Warming of the irradiated penicillamine crystals results in a gradual decrease in the integrated absorption as indicated in Figure 1. The decrease probably results from the recombining of electrons, released from traps, with oxidized species.

Structure Considerations

In this section spatial relationships between some of the tensors listed in Table I and the crystal structure of L-penicillamine HCl are discussed. According to an analysis by Kurita and Gordy[15] the direction of maximum g value for the sulfur radical IIIb should correspond to the direction of the C–S bond. Esr measurements of the absorption by the sulfur radical produced in cystine HCl by irradiation at low temperature showed that the direction of the C–S bond for the initial conformation of the radical is unchanged from the direction of the C–S bond in the undamaged molecule. Upon warming the C–S bond reorients drastically, however.[15] We find the same behavior manifested in penicillamine HCl. The direction of the C–S bond in the first two conformations of the penicillamine sulfur radical (corresponding to the β_1 and β'_1 absorptions) are close to the C–S bond direction in the undamaged molecule. The direction cosines of the C–S bond, and the direction cosines of the principal axes corresponding to maximum g value for the β_1 and β'_1 absorptions may be compared in Table I. The room temperature conformation of the sulfur radical (corresponding to the β''_1 absorption) is completely reoriented, however.

It is interesting to note that the α_0 and α'_0 absorptions attributed to the anion IV show no hyperfine structure due to the C_2–H proton. This result implies that the C_2–H bond lies approximately in the same plane as the carboxyl group of the anion. Examination of the structure of penicillamine HCl shows that some reorientation of molecule must occur upon addition of the electron in order to achieve coplanarity.

Discussion

We utilize the diagram in Figure 3 in an attempt to knit together the experimental results of the preceding sections into a coherent picture. The initial reduced species produced in irradiated penicillamine HCl and the products derived from the reduced species are listed on the right-hand side of the diagram. Products associated with the oxidation process are listed on the left-hand side of the diagram. Paramagnetic species, detectable by esr spectroscopy, are underlined and reference is made to the corresponding absorption pattern in Figure 1. The paramagnetic species are arranged vertically downward according to their order of appearance. Our main interest is to deduce the chemical or physical events which logically account for the appearance of each new paramagnetic species.

The initial reduced species observed in irradiated penicillamine HCl is the anion IV. There are two oxidation products: atomic chlorine derived from chlorine negative ions and the "sulfur" radical IIIa. We visualize that the sulfur radical derives from a cation but that a proton immediately dissociates leaving IIIa.

Consider first the oxidation side of Figure 3. The first definitive change is the disappearance of chlorine which occurs concurrently with an increase in the absorption attributed to sulfur radicals. A simple explanation of these two changes would be that holes migrate from chlorine to sulfur atoms. Verification of the hole migration process is difficult, however, because of other changes occurring simultaneously in the esr ab-

(15) Y. Kurita and W. Gordy, *J. Chem. Phys.*, **34**, 282 (1961); K. Akasaka, S. Ohnishi, T. Suita, and I. Nitta, *ibid.*, **40**, 3110 (1964).

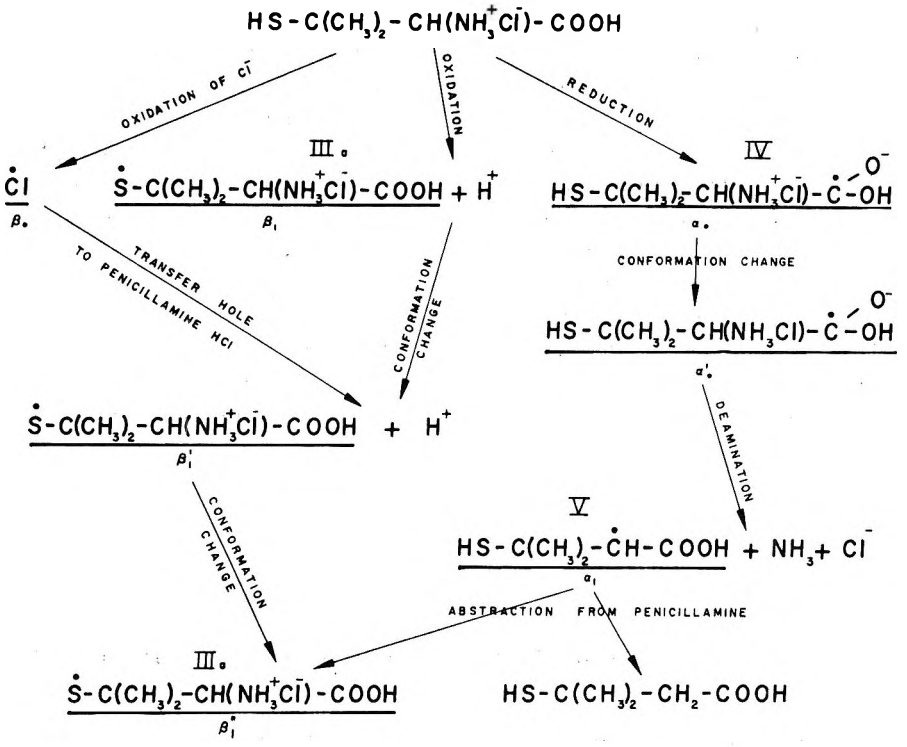

Figure 3. Diagram showing the sequence of processes which can account for the sequence of paramagnetic species observed in irradiated penicillamine HCl.

sorption, particularly a slight decrease in overall absorption and the appearance of the γ absorption (see Figure 1). Nevertheless, a causal relationship between the disappearance of the chlorine absorption and the enhancement of the sulfur radical absorption is strongly indicated. Subsequent changes in the oxidation products are rather trivial in that they can be attributed to changes in conformation of the sulfur radical. Such conformational changes are to be expected as the damaged molecule adjusts to its environment.[2,12]

We turn now to a consideration of the sequence of events initiated by the reduction process. After some reorientation the radical anion IV dissociates by deamination as shown in Figure 3. Because there are concurrent changes occurring in the oxidation chain a causal relationship between the disappearance of the anion absorption and appearance of the radical V was not rigorously demonstrable in this investigation. However, there is little doubt that the reduced amino acid dissociates by deamination.[9] In the last transformation on the reduction side of Figure 3 the radical V disappears. We cannot rule out the possibility that V disappears by some process involving the combination of unpaired electrons since there is an overall decrease in paramagnetic absorption as shown in Figure 1. It seems probable, however, that V is eliminated at least partially through an abstraction process which would contribute to the formation of IIIa. At room temperature one anticipates that the sulfur hydrogen from the sulfhydryl group of a penicillamine molecule migrates to the α-carbon atom of a neighboring radical (V).[16] Alternatively, hydrogen could be transferred from the sulfhydryl group to the α-carbon of V intramolecularly generating the radical

$$S\text{-}C(CH_3)_2\text{-}\dot{C}H_2\text{-}COOH$$
VI

An interesting speculation is that the minor absorption component, β_2, is due to radical VI.

Another remark needs to be made regarding the flow diagram in Figure 3. If ionization were the only effect of X-irradiation, we should expect to observe equal amounts of oxidized and reduced products at the initial stage of the radiation damage process. However, dissociation of the sulfhydryl bond in excited penicillamine molecules may occur. This process would also yield the radical III and atomic hydrogen. The atomic hydrogen would be expected to abstract another atom of hydrogen producing yet another sulfur radical. Thus, in Figure 1a, we can account for the fact that the integrated absorption of the oxidized products (β_0 and β_1 absorptions) exceeds that of the reduced product (α_0 absorption) at the first stage of the radiation damage process.

From a chemical analysis of cysteine irradiated in the solid state, Peterson, *et al.*,[17] drew several conclusions.

(16) H. C. Box, H. G. Freund, and E. E. Budzinski, *J. Chem Phys.*, **45**, 2324 (1966).

(17) D. B. Peterson, J. Holian, and W. M. Garrison, *J. Phys. Chem.*, **73**, 1569 (1969).

(1) Through oxidation and immediate loss of a proton sulfur radicals are generated directly. (2) Electron attachment to the carbonyl group of cysteine followed by dissociation of ammonia. (3) By intermolecular or intramolecular hydrogen transfer processes the radicals produced by deamination are destroyed and additional sulfur radicals are generated. All of these processes are verified in penicillamine HCl in the esr experiment reported here. These investigators also consider electron attachment to the sulfhydryl group as a competitive process to electron attachment at the carbonyl group. The possibility that the γ absorption, a relatively minor component of the total absorption in Figure 1c, is due to a sulfur cation was considered. However, the principal axes of the g tensor for the γ absorption show no obvious correlation with the structure of the penicillamine molecule, and no firm conclusion could be drawn concerning the nature of the γ absorption. Nevertheless, it is clear that overall our esr results are quite compatible with the processes postulated by Peterson, *et al.*,[17] from chemical analyses of irradiated cysteine.

Acknowledgments. This work was supported by Contract AT(30-1)3558 with the Atomic Energy Commission and Public Health Grant EC 00009.

Electron Spin Resonance Study of Irradiated Aqueous Solutions of Fumarate Ion. The Use of Fumarate for Radical Trapping[1]

by P. Neta

Radiation Research Laboratories, Mellon Institute of Science, Carnegie-Mellon University, Pittsburgh, Pennsylvania 15213 *(Received March 18, 1971)*

Publication costs assisted by Carnegie-Mellon University and the U. S. Atomic Energy Commission

Radicals produced by the reaction of fumarate ions with hydrated electrons, hydrogen atoms, hydroxyl radicals, carboxyl radicals, and a series of substituted alkyl radicals have been studied by electron spin resonance. The technique of *in situ* electron irradiation of aqueous solutions has been used for the formation of the radicals. Radicals produced from fumarate show a relatively slow second-order disappearance due to the double charge and were thus present at high steady-state concentrations. Spectra of three radicals were observed in irradiated dilute solutions of fumarate: $^{-}OOC\dot{C}HCH(OH)COO^{-}$ formed by addition of OH, $^{-}OOC\dot{C}HCH_2COO^{-}$ formed by addition of H, and

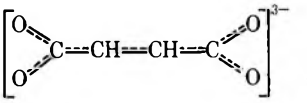

formed by reaction with e_{aq}^{-}. In concentrated solutions an additional spectrum was observed which was formed by addition of $^{-}OOC\dot{C}HCH_2COO^{-}$ and $^{-}OOC\dot{C}HCH(OH)COO^{-}$ to fumarate. The high radical concentrations found with fumarate suggest the use of this compound for radical trapping. The radicals $\dot{C}H_3$, $\dot{C}H_2Cl$, and $\dot{C}F_3$, which could not be observed in aqueous solutions directly, were successfully trapped by fumarate and the adduct positively identified through the hyperfine splittings of the hydrogen and halogen atoms. The rate constant for the addition of alcohol radicals to fumarate is estimated to be 10^7 M^{-1} sec^{-1}.

Introduction

The study of short-lived radicals by electron spin resonance spectroscopy is often limited by a low signal-to-noise ratio caused, for example, by low concentration of radicals or by line broadening. To overcome such limitations the method of spin trapping[2] has sometimes been used. In this method unstable radicals are added, for example, to a nitrone or a nitroso compound to form stable nitroxide radicals which are readily observed by esr. However, the spectra of these adduct radicals usually contain little information about the short-lived radical added and thus the positive identification of this latter radical is made difficult.

(1) Supported in part by the U. S. Atomic Energy Commission.

(2) See review by E. G. Janzen, *Accounts Chem. Res.*, 4, 31 (1971).

In a search for an alternative spin trap it was decided to study radical addition to fumarate ions. Although the adduct radical is not stable its second-order disappearance is about two orders of magnitude slower than that of an alkyl radical (probably because of the double charge).[3] This decrease in reactivity will increase the steady-state concentration considerably and make observation in the *in situ* radiolysis experiments relatively easy. Moreover, the unstable radical which adds to fumarate can often be identified through hyperfine splittings by its magnetic nuclei. It is also expected that the size of the radical being added will have an effect on the hyperfine splitting of the β hydrogen in the fumarate radical through changes in the average configuration with respect to internal rotation about the α-carbon–β-carbon bond.

In this work the formation of radicals and their addition to fumarate was studied by the *in situ* radiolysis of aqueous solutions developed in this laboratory.[4] As a preliminary step the radicals produced in irradiated solutions of fumarate have been studied in the absence of additives.

Experimental Section

The materials used were of the purest grade commercially available, usually from Baker; the gases were obtained from Matheson. Water was doubly distilled. Solutions were buffered with Baker Analyzed potassium hydroxide, sodium tetraborate, and sodium phosphates. Samples were deoxygenated by bubbling with nitrogen or were saturated with nitrous oxide. The latter is used to scavenge the hydrated electrons and to convert them into hydroxyl radicals. The irradiation with high-energy electrons was carried out directly in the esr cavity. The solution flowed through a flat silica cell. The irradiation arrangement and other details of the experiment were as previously described.[4]

Results and Discussion

The esr spectrum recorded with an irradiated aqueous solution of fumarate is shown in Figure 1. In this solution all the primary radicals of water radiolysis, OH, H, and e_{aq}^-, are expected to react with fumarate with rate constants $> 10^9\ M^{-1}\ sec^{-1}$,[5] and indeed three radicals can be identified from this spectrum. The 20.2 G doublet of 15.6 G doublets can be attributed to the OH adduct $^-OOC\dot{C}HCH(OH)COO^-$. Each line of this spectrum could be further resolved into a 0.2 G doublet due to the OH proton. The signal intensity of this spectrum was doubled by the addition of N_2O, which converts e_{aq}^- into OH radicals.

The second radical observed shows a 23.6 G triplet of 20.3 G doublets with no further splittings and its structure must be $^-OOC\dot{C}HCH_2COO^-$. The signal intensity of the spectrum of this radical was not affected by the addition of N_2O, an efficient electron scavenger. This finding rules out the possibility that this radical could be formed by the addition of e_{aq}^- to fumarate

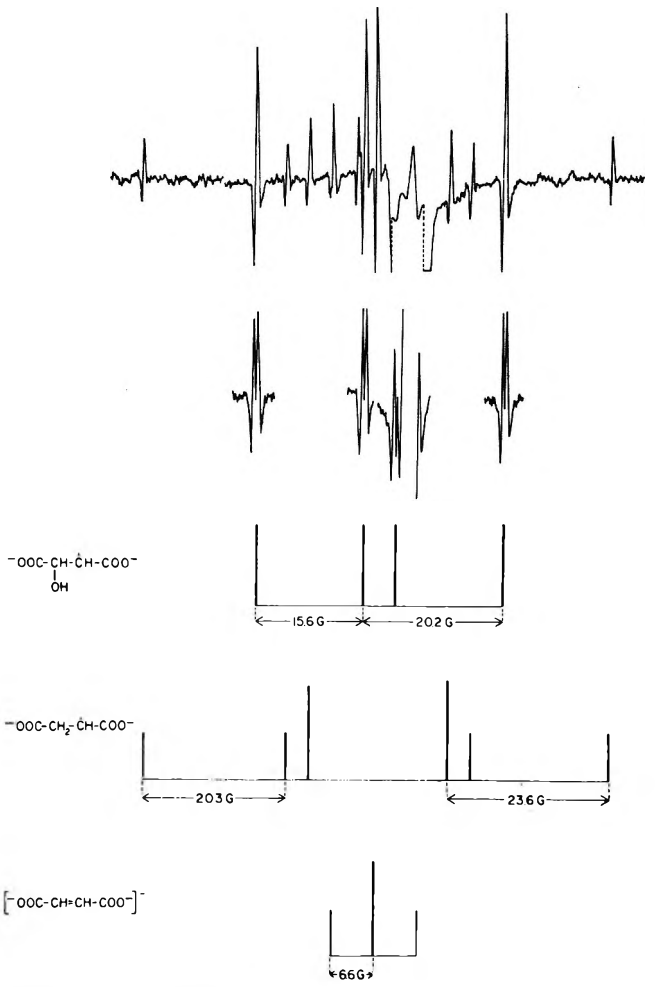

Figure 1. Second-derivative esr spectrum of an aqueous solution of fumarate (0.01 M) at pH 6.9 (phosphate buffer) during irradiation with 2.8-MeV electrons. Magnetic field increases to the right. The stick spectra show the relationship of the lines of the different radicals. The large signal from the silica cell is seen just above the center of the spectrum and is recorded at a gain 100 times less than the other portions. One line of the e_{aq}^- adduct spectrum and one doublet of the OH adduct spectrum are masked by the signal from the cell and cannot be seen in the continuous scan (top). These lines were resolved by use of lower modulation and slower scan and are shown below the main spectrum. Also shown below are the other doublets of the OH adduct, which appear as single lines in the main spectrum.

followed by rapid protonation. In line with this mechanism the signal intensity decreased upon increasing the pH because H atoms can be scavenged by OH^- and converted into e_{aq}^-. This decrease, however, was not very large because at all values of pH used H atoms react preferably with fumarate than with OH^- (rate constant ratio $\approx$ 1000).[5] No attempt was made to work at pH <6, where e_{aq}^- can be converted into H

(3) M. Simic, P. Neta, and E. Hayon, *J. Phys. Chem.*, **73**, 4214 (1969).

(4) K. Eiben and R. W. Fessenden, *ibid.*, **75**, 1186 (1971).

(5) M. Anbar and P. Neta, *Int. J. Appl. Radiat. Isotopes*, **18**, 493 (1967).

Table I: Hyperfine Constants of Radicals of the Type $^-OOC\dot{C}HCHRCOO^-$

R	g Factor[a]	Hyperfine constants[a] α H	β H	γ H	γ Halogen
e^- [b]	2.00357		6.61[b]		
H	2.00329	20.34	23.59		
OH	2.00321	20.21	15.56	0.20	
CO_2^-	2.00334	20.10	7.95		
CH_3	2.00324	20.15	10.21	0.73	
CH_2OH	2.00324	20.22	9.64	≤0.2	
$CH(OH)CH_3$	2.00331	20.06	7.30	0.31	
$C(OH)(CH_3)_2$	2.00325	20.00	5.45		
$CH(OH)CH_2OH$	2.00325	20.23	9.62	≤0.2	
CH_2NH_2	2.00324	20.15	9.00		
CF_3	2.00333	20.72	8.00		0.86
CH_2Cl	2.00334	20.34	8.83	0.41	0.41
$CHClCOO^-$	2.00324	20.12	10.26	0.49	
$CH(COO^-)CH_2COO^-$	2.00328	19.92	7.88	0.85	

[a] The g factors are measured relative to the peak from the silica cell and are accurate to ±0.00005. Hyperfine constants are given in gauss and are accurate to ±0.03 G. Second-order corrections have been made [R. W. Fessenden, *J. Chem. Phys.*, **37**, 747 (1962)]. [b] In this case e^- is not equal to R since it is not localized. The structure of the radical could probably be described by

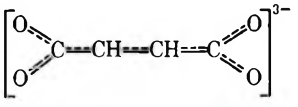

so that the two protons are equivalent and have a small splitting.

by reaction with H^+, because in acid solution the lifetime of the neutral radical $HOOC\dot{C}HCH_2COOH$ is short[3] and the steady-state concentration will be much smaller than that in basic solutions. The hyperfine constants of the $^-OOC\dot{C}HCH_2COO^-$ radical are in good agreement with those determined for the same radical obtained by hydrogen abstraction from succinate[6] or by e_{aq}^- reaction with $^-OOCCH(SH)CH_2COO^-$.[7] The steady-state concentration of the radical $^-OOC\dot{C}HCH_2COO^-$ under the present experimental conditions is considerably lower than that found[6] in irradiated solutions of succinate saturated with N_2O because in the latter case all the primary radicals of water radiolysis ($G \approx 6$) were directed into the formation of the $^-OOC\dot{C}HCH_2COO^-$ radical, while in the present study only the H atoms ($G = 0.6$) produce this radical.

The third radical identified in Figure 1 results from the reaction of fumarate with e_{aq}^-, because the signal intensity of its spectrum decreased with the addition of N_2O and other electron scavengers and slightly increased with increasing the pH (OH^- converts H into e_{aq}^-). This radical has a g factor slightly higher than those for the radicals discussed above, and the two protons are equivalent in this case, with a hyperfine constant of only 6.6 G. This spectrum suggests that the electron is not localized and the radical could be described by a resonance structure, probably

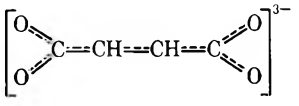

This resonance stabilization could probably account for the fact that the rate constant for reaction of e_{aq}^- with fumarate is over three orders of magnitude higher than that with ethylene.[5]

In concentrated solutions of fumarate (~1 M) an additional spectrum was observed, and the line intensities of the three primary spectra (shown in Figure 1) decreased. The spectrum of the new radical can be attributed to the dimer radical

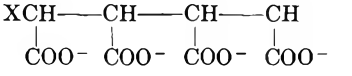

and the hyperfine constants are summarzed in Table I together with those of all the other radicals observed in this study. The fact that a concentration of fumarate of the order of 1 M was necessary for the formation of the dimer radical in competition with the radical–radical reaction ($2k \approx 10^7$ and 10^8 M^{-1} sec^{-1} for the OH adduct and H adduct, respectively)[8] suggests that this addition reaction has a rate constant of 10^3–10^4 M^{-1} sec^{-1}.

In order to investigate the addition of other radicals to fumarate, these radicals were produced in irradiated solutions by hydrogen abstraction (from formate, methylamine, and alcohols) by dehalogenation (of CH_3Cl, CF_3Cl, and CH_2Cl_2) or by electron addition (to acetone and acetaldehyde). The results are summarized in Table I.

(6) G. P. Laroff and R. W. Fessenden, *J. Chem. Phys.*, in press.
(7) P. Neta and R. W. Fessenden, *J. Phys. Chem.*, **75**, 2277 (1971).

Figure 2. Esr spectra of an aqueous solution of fumarate (0.01 *M*) and formate (0.1 *M*) saturated with N_2O at pH 10.1 during irradiation. The signal from the cell is recorded at a gain ten times less than the other portions.

Figure 2 shows the spectrum obtained in an irradiated aqueous solution containing fumarate and formate; the latter was present in excess to ensure scavenging of OH. The CO_2^- radicals formed from formate add to the double bond to form $^-OOC\dot{C}HCH(COO^-)_2$. This radical has a triple charge and was present in the solution at high steady-state concentration. The spectrum in Figure 2 was recorded at a gain ten times lower than most of the other spectra. The *g* factor and the hyperfine constant of the α proton determined for this radical are similar to those for the radicals obtained by H and OH addition, but the hyperfine constant of the β proton is greatly reduced. This reduction is most probably a result of both the size of the additional carboxyl group and its effect on the electron density distribution in the radical. However, the main effect seems to be that of the large size of the carboxyl group, which will change the average configuration of the hydrogen atom at the β position with respect to internal rotation about the α-carbon–β-carbon bond.

Another example is shown in Figure 3. In this case the spectrum was intentionally taken under conditions where most of the radicals formed in the system are present at about similar concentrations, so that their spectra are shown simultaneously. The concentrations were chosen such that the primary radicals react with both fumarate and chloroacetate. (Ratios of approximately 1:1.5 for e_{aq}^- and 3:1 for OH are estimated from the concentrations and rate constants of fumarate and chloroacetate, respectively).[6] The spectra of

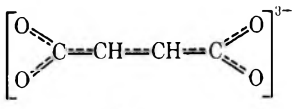

$^-OOC\dot{C}HCH_2COO^-$, $^-OOC\dot{C}H(OH)COO^-$, $\dot{C}H_2COO^-$, and $^-OOCCH\dot{C}HCOO^-$ (Cl on the CH) $ClCHCOO^-$

were all observed in the spectrum of Figure 3. The spectrum of $ClCHCOO^-$ was not observed under these conditions, probably because most of it added to fumarate. An increase in the concentration of chloroacetate caused the disappearance of the spectra of $^-OOC\dot{C}HCH_2COO^-$ and

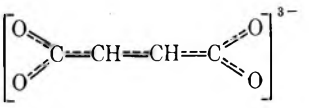

because of the increased competition for H and e_{aq}^- by chloroacetate. The addition reaction of $\dot{C}H_2COO^-$ to fumarate must be slower than that of $ClC\dot{H}COO^-$ because the adduct radical was not observed.

The radicals $\dot{C}H_3$, $\dot{C}F_3$, and $\dot{C}H_2Cl$ were produced by the reaction of CH_3Cl, CF_3Cl, and CH_2Cl_2 with hydrated electrons.[8] These radicals added to fumarate and all the spectra observed could be analyzed for the γ splittings of the hydrogen and halogen as summarized in Table I. The $\dot{C}H_2OH$, $\dot{C}H_2NH_2$, and $\dot{C}HOHCH_2OH$ radicals were produced by hydrogen abstraction from the parent compounds through reaction with OH. The radical $CH_3\dot{C}HOH$ was produced from a mixture of ethanol and acetaldehyde so that OH abstracted hydrogen from the alcohol and e_{aq}^- added to the carbonyl compound (which then protonated) and both form the same radical. Similarly, $(CH_3)_2\dot{C}OH$ was produced from a mixture of isopropyl alcohol and acetone. All these radicals were produced in the presence of a low concentration of fumarate where it did not interfere with their formation, and the adduct radicals could be observed.

The rate constant for the addition of an alcohol radical to fumarate was estimated from experiments with methanol. A solution was irradiated under such conditions that the spectra of both the $\dot{C}H_2OH$ and the adduct $^-OOC\dot{C}HCH(CH_2OH)COO^-$ were observed (1 *M* methanol and 0.01 *M* fumarate). The rate of production of $\dot{C}H_2OH$ was then changed by changing the irradiation dose rate (between 0.1 and 2.0 μA electron beam current). Assuming a competition between the radical–radical combination of $\dot{C}H_2OH$ with a rate constant of $2.4 \times 10^9\ M^{-1}\ sec^{-1}$ [9] and the addition of this radical to fumarate, it could be calculated that the rate constant for the addition is $\sim 10^7\ M^{-1}\ sec^{-1}$.

The hyperfine constants and *g* factors of all the adduct radicals observed are summarized in Table I. The slight variations in the *g* factors and the α H splittings do not seem to offer any indication on the nature of the radical added to fumarate. However, the β H splitting is considerably affected by the group R. In the series of the adducts of alcohol radicals the β H splitting decreases almost by a factor of two in going from R = $\dot{C}H_2OH$ to R = $\dot{C}(CH_3)_2OH$, and this decrease must be mainly the result of the decrease in the Ċ–C–H angle caused by the bulkier groups. Although the effect on the β H splitting is partly due to the change in the charge

(8) T. I. Balkas, J. H. Fendler, and R. H. Schuler, *J. Phys. Chem.*, 75, 455 (1971).

(9) M. Simic, P. Neta, and E. Hayon, *ibid.*, 73, 3794 (1969).

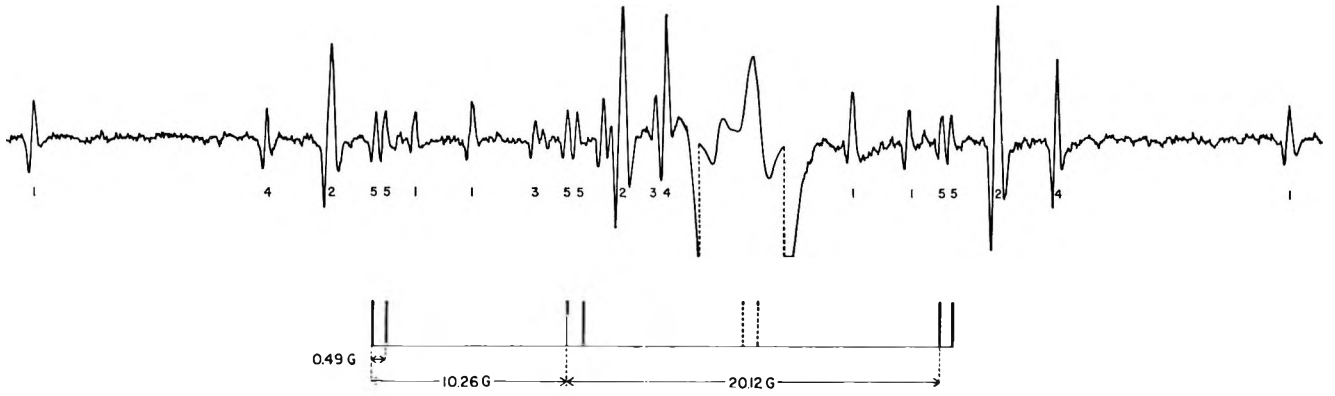

Figure 3. Esr spectrum of an aqueous solution of fumarate (0.01 M) and chloroacetate (0.1 M) at pH 9.8 during irradiation. The signal from the cell is recorded at a gain 100 times less than the other portions. The stick spectrum (5) shows the lines of the adduct of $ClĊHCOO^-$ to fumarate. The other lines in the spectrum are identified as: (1) $^-OOCĊHCH_2COO^-$; (2) $^-OOCĊHCHOHCOO^-$; (3) $[^-OOCCH{=}CHCOO^-]^-$; (4) $ĊH_2COO^-$.

distribution in the adduct radical caused by the particular R, it can be seen from the table that the geometric effects are also very pronounced.

The γ-hydrogen and γ-halogen splittings are also observed in most cases (Table I), and they are of great importance for the positive identification of R. The magnitude of these hyperfine constants varies between 0 and $\sim$1 G and thus could not be determined in some instances. The chlorine splitting with spin $^3/_2$ could be easily seen in the spectrum of the $ĊH_2Cl$ adduct but was not observed in the case of $ClĊHCOO^-$. The observation of the fluorine splittings in the spectrum of the $ĊF_3$ adduct $^-OOCĊHCH(CF_3)COO^-$ is important for the demonstration of the presence of $ĊF_3$ as intermediate in an irradiated aqueous solution of CF_3Cl. The immediate formation of $ĊF_3$ from the reaction of $CF_3Cl + e_{aq}^-$ and its hydrolysis into F^- on the 10-μsec time scale have been inferred from a recent pulse-conductivity study.[8] The fact that $ĊF_3$ radicals could be trapped by fumarate (0.001 M) despite their short lifetime[8] suggests that this trapping reaction is fast, probably close to $10^8\ M^{-1}\ sec^{-2}$.

In conclusion, it was found that many short-lived radicals add to fumarate to enable successful analyses of the adduct radicals Although these adduct radicals are not stable, they can be formed at relatively high steady-state concentration owing to the double charge of the fumarate. This latter compound can, therefore, be suggested as a possible radical trap. The rate constants for the addition of radicals to fumarate are of the order of $10^7\ M^{-1}\ sec^{-1}$ for the more reactive radicals. In order to observe the adduct radical the concentration of fumarate present should be high enough to compete with the radical–radical reactions, but, on the other hand, it should be low enough not to interfere with the formation of the radical to be added. The choice of concentrations is thus critical and in several cases studied no adduct radicals could be observed. For comparison, the possible use of dihydroxyfumarate and of acetylenedicarboxylate as radical traps was examined, but both of these compounds were found to be less adequate than fumarate because several spectra were found which could not be identified, and because of the lack of a β hydrogen (the hyperfine splitting of which is indicative of the size of the added radical). Maleate also seems to be slightly less successful because of a slower addition reaction. Despite its limitations as discussed above, the use of fumarate as a radical trap enabled the definite identification of $ĊH_3$, $ĊF_3$, $ĊH_2Cl$, and OH as intermediates in spite of the fact that the esr spectra of these radicals could not be observed in aqueous solutions. The advantage of fumarate over the nitrone as a radical trap lies in the fact that a more positive identification of the trapped short-lived radical is possible in many cases.

Acknowledgment. I wish to thank Professor R. W. Fessenden for many helpful discussions.

Radical Reactions in the Ligand Field of Metal Complexes. I. Electron Paramagnetic Resonance Spectra of Complex-Bonded Radicals Formed by Reaction of Cobalt(II) Acetylacetonate with *tert*-Butyl Hydroperoxide

by A. Tkáč,[1a] K. Veselý,[1b]* and L. Omelka[1a]

Institute of Chemical Physics, Slovak Technical University, Bratislava, Czechoslovakia, and Research Institute of Macromolecular Chemistry, Brno, Czechoslovakia *(Received May 22, 1970)*

Publication costs borne completely by The Journal of Physical Chemistry

The conditions of formation of long-lived complex-bonded radicals are described. The radicals are formed by the reaction of cobalt acetylacetonate with *tert*-butyl hydroperoxide in toluene. A maximum concentration of radicals was achieved at 25° (*ca.* 5×10^{15} spins/0.1 ml, *i.e.*, 1×10^{-4} mol/l.). Diamagnetic adducts are formed at low temperatures. They decompose when warmed up to room temperature, yielding the epr signal of the original intensity. The radical complex decomposes at elevated temperatures and the activation energy of this process is 28 ± 2 kcal/mol. The circumstances of the signal formation suggest that the observed radicals are the *tert*-$BuO_2\cdot$ radicals forming a complex with the cobalt central atom. Complex-bonded *tert*-BuO· radicals were prepared *via* reaction of cobalt acetylacetonate with di-*tert*-butyl peroxalate.

Introduction

Until recently it was assumed that the reaction

$$ROOH + M^{n+} \longrightarrow RO\cdot + M^{n+1} + OH^-$$

produces very short-lived radicals in the same way as the photolysis of diperoxide.

Chiang, *et al.*,[2] showed, however, that radicals formed *via* an analogous reaction of $H_2O_2 + M^{n+}$ have a lifetime of several seconds, whereas the lifetime of HO· radicals generated radiochemically is in the microsecond range. Later on Czapski, *et al.*,[3] proved that the $HO_2\cdot$ radicals formed by the fast consecutive reaction $HO\cdot + H_2O_2 \rightarrow H_2O + HO_2\cdot$ are complex-bonded. Brandon and Elliot[4] reported the formation of long-lived radicals produced by reaction of *tert*-butyl hydroperoxide or cumene hydroperoxide with naphthenates and acetylacetonates of manganese, cobalt, and vanadium in benzene. The radicals, when observed by epr, showed a singlet, $g = 2.0154 \pm 0.0004$, which the authors attributed to the *tert*-$BuO_2\cdot$ radical stabilized on the transition metal.

The purpose of our work was to study the reactions of radicals attached to metals. For this reason we first studied in some detail conditions for the formation and disappearance of the radical complexes produced by the reaction of cobalt acetylacetonate [$Co(acac)_2$] with *tert*-BuOOH.

Experimental Section

Chemicals. *tert*-BuOOH (Fluka, Switzerland) was dried over P_2O_5. Cobalt(II) acetylacetonate was prepared by the procedure described by Charles and Pawlikowski.[5] To remove water, the sample was heated at 100° under a pressure of 10^{-3} Torr. Toluene and benzene were washed with H_2SO_4, NaOH, and water and then dried over the molecular sieve A4.

Mixing of Components. The components were mixed under an atmosphere of argon or pure nitrogen to exclude moisture, or in the presence of oxygen. During these operations contact of solution with the metal was avoided. Two procedures were employed: (I) mixing in the epr cell (o.d. 4 mm) equipped with a three-way tap. Concentrated *tert*-BuOOH was added quickly to 0.2 ml of a 2% solution of Co $(acac)_2$. The mixing of samples was effected by an ultrasonic generator at the ambient temperature for 10 sec. Immediately after mixing, the cell was inserted into a Dewar vessel placed in the resonance cavity through which a stream of constant-temperature nitrogen was passing. (II) The sample of 0.4–2% solution of Co $(acac)_2$ was placed into a closed thermostated vessel equipped with magnetic stirring. A diluted solution of *tert*-BuOOH was then added stepwise, in small amounts.

Epr Spectra. A commercial X-band spectrometer Varian E3 equipped with 100-kHz field modulation was used. Samples were thermostated with a precision of ±1° from −100 to 150° using a Varian variable temperature accessory. The *g* values were calculated using

(1) (a) Slovak Technical University; (b) Research Institute of Macromolecular Chemistry.

(2) Y. S. Chiang, I. Craddock, D. Mickewich and I. Turkewich, *J. Phys. Chem.*, **70**, 3509 (1966).

(3) (a) G. Czapski and A. Samuni, *Israel J. Chem.*, **7**, 361 (1969); (b) G. Czapski, H. Levanon, and A. Samuni, *ibid.*, **7**, 375 (1969).

(4) R. W. Brandon and C. S. Elliot, *Tetrahedron Lett.*, 4375 (1967).

(5) R. G. Charles and M. A. Pawlikowski, *J. Phys. Chem.*, **62**, 440 (1958).

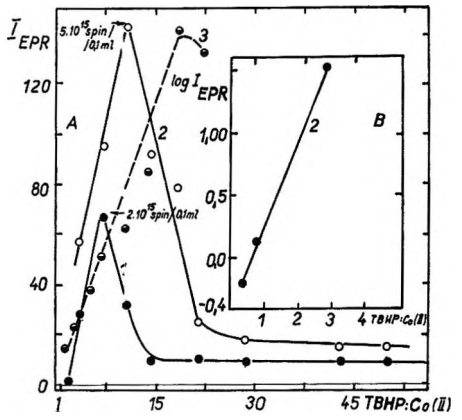

Figure 1. Dependence of the epr signal intensity upon the molar ratio *tert*-BuOOH/Co(acac)$_2$ in toluene at 23°: A, overall dependence; B, section of the curve 2 in logarithmic coordinates for low ratio *tert*-BuOOH/Co(acac)$_2$; 1, procedure I, Co(acac)$_2$ = 2%; 2, procedure II, Co(acac)$_2$ = 2%; 3, procedure II, Co(acac)$_2$ = 0.3%.

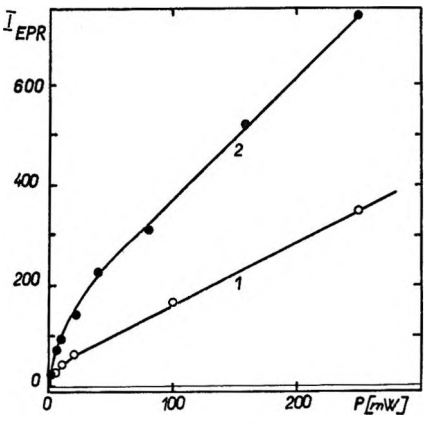

Figure 2. Dependence of the epr signal intensity upon the power of high-frequency radiation P (mW): 1, in Ar; 2, in dry air.

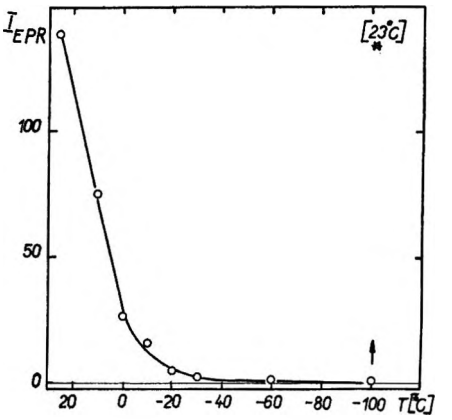

Figure 3. Change of the epr signal intensity with decreasing temperature of the sample. The sample was prepared by procedure I at 23°: *, the intensity of the signal after warming up the sample to 23°.

the standard Varian "pitch" as a calibration (g = 2.0028). The number of spins was determined by double integration of the signal area and by comparison of the result with a standard.

Results

A symmetrical singlet, bandwidth H = 20 Oe, g = 2.0147 ± 0.0005, can be seen immediately after mixing of the two components. The violet color of Co(acac)$_2$ solution becomes green within 2 sec. This signifies the presence of Co(III) in the mixture.

Influence of Molar Ratio. The intensity of the signal changes upon changing both the molar ratio of components *tert*-BuOOH–Co(II) and their absolute concentration. The curves are shown in Figure 1. Their maxima show that where procedure II was employed, *i.e.*, when there was no local excess of hydroperoxide after mixing, roughly twice the concentration of complex-bonded radicals was produced than when procedure I was used. The area of the signal represents 5 × 10^{15} spins/0.1 ml, *i.e.*, 1.2 × 10^{-4} mole-radicals/l. (±25%). The maximum appears at the molar ratio *ca.* 10:1 when procedure I is used but its position is shifted to the ratio 15:1 when procedure II is applied. The same signal intensity was obtained even when the overall concentration of both components was six times lower. The molar ratio *tert*-BuOOH:Co(II) at the maximum is, in this case, even higher and the maximum is spread. The section of Figure 1 shows that the epr signal was observed even when the molar ratio was smaller than 1:1.

Microwave Power. The dependence of signal intensity on the output of high-frequency radiation is shown in Figure 2. Continuous increase of the microwave power does not cause the saturation of the signal even with the maximum power from a 250-mW klystron. After a slight initial curvature the dependence is linear. This indicates a short relaxation time of the observed paramagnetic species, contrary to that measured for classical free radicals generated photo- or radiochemically. The dependence shown in Figure 2 is different from that observed for paramagnetic ions of transition metals, where the intensity of signal increases linearly with the power of the klystron without partial saturation of the signal. When the system had been saturated with atmospheric oxygen prior to measurement, the relaxation times were shortened and the slope of the curve was steeper.

Influence of Low Temperature. As shown in Figure 3, the intensity of the signal decreases as the temperature is lowered and at −100° the signal to noise ratio is already very low. When the sample is warmed up to room temperature again, the intensity of the signal is recovered. This change from paramagnetic to diamagnetic state and vice versa can be repeated many times.

Time Dependence of Signal Intensity at Various Temperatures. Under the given experimental condi-

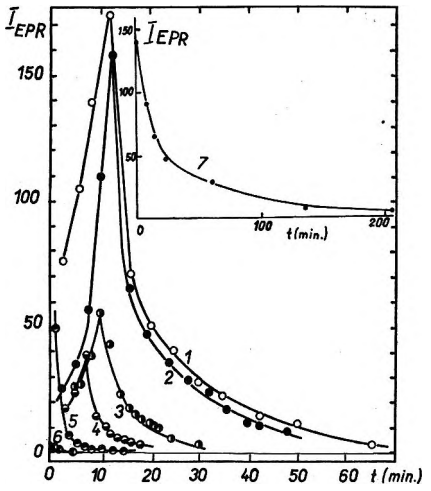

Figure 4. The plot of the epr signal intensity *vs.* time for different temperatures. Samples 1–6 were prepared using procedure I at 23°: 1, 27°; 2, 30°; 3, 35°; 4, 40°; 5, 45°; 6, 50°; 7, 24°, procedure II.

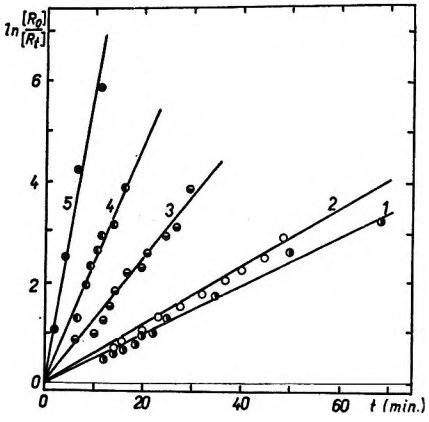

Figure 5. Decrease in the epr signal intensity expressed as the time dependence of ln (R_0/R_t) where R_0 is the original intensity of the epr signal proportional to the number of spins immediately after sample preparation at 23°; R_t is the signal intensity at time t. The notation of the curves is the same as in Figure 4.

tions, the time necessary for the sample to reach the equilibrium temperature is several minutes.

The changes in the epr signal intensity of the complex radicals as a function of time at temperatures from 27 to 50° are shown in Figure 4. During the first few minutes the singlet band narrows by 30–40%. At the same time the signal intensity increases. This effect may be connected either with the disappearance of dipolar interactions at elevated temperatures or with the primary processes that take place during the nonstationary conditions in the preparation of the sample. The decomposition of the radical complex is already so fast at 40° that no maximum can be observed. When the sample is prepared by procedure II, the intensity time curve at 24° does not show any maximum.

The decomposition of the radical complex between 24 and 50° is a first-order reaction (Figure 5) with the activation energy $E_a = 28 \pm 2$ kcal/mol.

Discussion

The results confirm the existence of long-lived radicals fixed to the cobalt atom in hydrocarbon solvents. This is supported by observing the dependence of the signal intensity upon the microwave power. This phenomenon has already been described by Chiang, *et al.*,[2] for the case of HO· and HO_2· radicals fixed to the Ti^{4+} atom. Further confirmation of the presence of complex-bonded radicals in our system follows from the dependence of epr signal intensity upon time at various temperatures. A new, so far undescribed phenomenon takes place when the temperature is lowered. Paramagnetism practically disappears within a relatively narrow temperature interval (10–0°). This completely reversible process can be explained in the same way as the antiferromagnetic effect, being due to the compensation of antiparallel spins during association. In this process no recombination of the complex-bonded radicals occurs.

The observed activation energy of complex decomposition shows that the radical–metal bond is relatively strong. Complexes of stable free radicals with metals have been described by Eaton[6] for semiquinones, and by Hoffman and Eames[7] for nitroxide radicals. Since, in our case, it was impossible to see any interaction of radicals with the cobalt central atom,[8] we suppose that the oxygen lone-pair electrons present in the radical form a coordination bond with the cobalt atom and that the unpaired electron is localized on the oxygen atom.

In the absence of peroxide in the toluene solution of $Co(acac)_2$, there is no signal due to a free $3d^7$ electron. This suggests that $Co(acac)_2$ is present in solution in the form of a dimer or multimer and that the equilibrium concentration of the monomer is below the sensitivity limit of our epr instrument. Thus the existence of a trimer, as predicted by Bullen, *et al.*,[9] as well as the value of its dissociation equilibrium constant determined cryoscopically by Bertrand, *et al.*,[10] should be viewed critically. The specific interaction of the acetylacetonate dimer, which forms a tetramer in the solid state with various solvents, indicates that cryoscopy is not a reliable method for these cases.

Brandon and Elliot[4] assume that the complex-bonded radical is the *tert*-BuO_2· radical. They came to this

(6) D. R. Eaton, *Inorg. Chem.*, **3**, 1268 (1964).

(7) B. H. Hoffman and T. B. Eames, *J. Amer. Chem. Soc.*, **91**, 5168 (1969).

(8) The magnetic moment of the ^{59}Co nucleus is $^7/_2$ and if a partial delocalization of the electron density of the free radical had occurred, a split leading to the formation of eight lines of equal intensity would have been observed.

(9) G. I. Bullen, R. Mason, and P. Pauling, *Inorg. Chem.*, **4**, 456 (1965).

(10) J. A. Bertrand, F. A. Cotton, and W. J. Hart, *ibid.*, **3**, 1007 (1964).

conclusion on the basis of measurement of the g value ($g = 2.015 \pm 0.004$); their result is practically identical with ours ($g = 2.0147 \pm 0.0004$).

The g values for oxygen-containing radicals have recently been determined by several authors.[11-15] The g values between 2.014 and 2.015 were attributed to the $RO_2\cdot$ radicals, whereas the radicals $RO\cdot$ are still a subject of controversy. Weiner and Hammond[14] observed radicals for which $g = 2.004$ when photolyzing *tert*-butyl peroxide. They assigned this value to the *tert*-BuO· radical. Takegami, *et al.*,[15] have photolyzed hydroperoxides and nitrites at very low temperatures. For the $RO_2\cdot$ radicals they found g values ranging from 2.010 to 2.017, whereas for the $RO\cdot$ radicals g values ranging from 2.005 to 2.009 were found. The radicals are observable up to −70°. Symons[16] tried to prove that the HO· and RO· radicals cannot be detected in the liquid phase by epr. The reason given was that these radicals have very short relaxation times and thus their epr signal appears in a form of a very broad band. Thus the author[16] attributed the observed signal to the ozonide radical *tert*-$BuO_3\cdot$.

Only a small difference between the g values of the free nitroxide radicals and their complexes with $AlCl_3$ was observed by Hoffman and Eames;[7] *e.g.*, *tert*-BuN–Ȯ free, $g = 2.0061$; complex with $AlCl_3$, $g = 2.0053$.

The assumption that the reaction *tert*-BuOOH + $Co(acac)_2$ gives bonded *tert*-$BuO_2\cdot$ radical and not *tert*-BuO· radicals has been confirmed by the study of di-*tert*-butyl peroxalate reaction with $Co(acac)_2$.

It is known[17] that di-*tert*-butyl peroxalate decomposes, producing *tert*-BuO· radicals and CO_2. The esr spectrum of the reaction mixture of di-*tert*-butyl peroxalate with Co $(acac)_2$, taken in inert medium, excluding moisture and reaction products, is seen as a singlet ($g = 2.0063 \pm 0.0004$) which is obviously due to the bonded *tert*-BuO· radicals. In the presence of traces of polar compound an octet appears in the spectrum. Although we intend to report on this particular reaction in some detail later on, this result is presented only to confirm that the radicals, formed through *tert*-BuOOH + $Co(acac)_2$ reaction, have a substantially different g factor and are obviously *tert*-$BuO_2\cdot$ fixed radicals.

The reaction of $Co^{III}(acac)_3$ and $Co^{III}(acac)_2OH$ with *tert*-BuOOH also yields radicals which can be seen in the epr spectrum as a singlet, $g = 2.0147$. In the former case the level of complex-bonded radicals is lower by an order of magnitude than in the case of $Co^{II}(acac)_2$.

Since the number of spins at the maximum in Figure 1 is 10^3–10^2 times lower than the concentration of $Co(acac)_2$, it may be assumed that either some parallel reaction (*e.g.*, oxidation without the formation of the radical complex) is operative or that the formation of diamagnetic associates occurs at room temperature (Figure 3). The existence of diamagnetic complexes of radicals with Ce^{3+} was also assumed by Czapski.[3]

The nmr analysis of the reaction mixture[18] revealed that even when *tert*-BuOOH was present in a considerable excess over $Co(acac)_2$, it completely decomposed, forming mainly *tert*-BuOH. The fact that the reaction is nonstoichiometric indicates the possible oxidation of cobalt, followed by its reduction to the original valency.

The reactions of *tert*-BuOOH with Co^{II}-2-ethylhexanoate[19] or with Co^{II}-acetylacetonate[20] are much faster in chlorobenzene and benzene than in acetic acid. Whereas the ratio $Co^{II}/(Co^{II} + Co^{III})$ is equal to 0.45–0.48 in nonpolar solvents,[19] the Co^{II} predominates in acetic acid. Co^{II}-acetylacetonate forms a very stable dimer, but in the solid state a tetramer structure was described by Cotton and Elder.[21] This tetramer can also exist in nonpolar solvents. Upon addition of a donor ligand (D), the following products are formed: $[Co(acac)_2]_2D$; $[Co(acac)_2D]_2$; $[Co(acac)_2]D_2$. Such a series of primary products is probably formed during the reaction of $Co(acac)_2$ with *tert*-BuOOH, and perhaps only some of them (1st or 2nd) will be reactive. This could account for the observed differences between procedures I and II. In our reaction scheme we denote the reactive components by simple formulas only which in fact denote dimers and higher diamagnetic associates, *e.g.* $(Co^{II})_2$, $(Co^{II}Co^{III})_2$, $(Co^{III})_2$, etc. The symbol Co^{III} means $Co^{III}(acac)_2OH$; $Co(acac)_2OH$ is a more powerful oxidizing agent than $Co^{III}(acac)_3$.[22]

The suggested reaction mechanism is based on that assumed by Richardson.[19]

Solvation of Complexes by Hydroperoxide

$$(Co^{II})_2 + 2ROOH \rightleftharpoons (Co^{II})_2(ROOH)_2 \quad (1)$$

$$Co^{II}Co^{III} + 2ROOH \rightleftharpoons Co^{II}Co^{III}(ROOH)_2 \quad (2)$$

$$(Co^{III})_2 + 2ROOH \rightleftharpoons (Co^{III})_2(ROOH)_2 \quad (3)$$

Formation of Free and Fixed Radicals

(11) F. A. Cotton and R. C. Elder, *Inorg. Chem.*, **4**, 1145 (1965); **5**, 423 (1966).

(12) K. U. Ingold and J. R. Morton, *J. Amer. Chem. Soc.*, **86**, 3400 (1964).

(13) P. D. Bartlett and G. Guaraldi, *ibid.*, **89**, 4799 (1967).

(14) S. Weiner and G. S. Hammond, *ibid.*, **91**, 2182 (1969).

(15) Y. Takegami, S. Insmura, F. Masuda, and Y. Watanabe, *Kogyo Kagaku Zasshi*, **72**, 1876 (1969); *Chem. Abstr.*, **72**, 21137 (1970).

(16) M. C. R. Symons, *J. Amer. Chem. Soc.*, **91**, 5924 (1969).

(17) P. D. Bartlett, E. P. Benzing, and R. E. Pincock, *ibid.*, **82**, 1762 (1960).

(18) L. Malik, private communication.

(19) W. H. Richardson, *J. Amer. Chem. Soc.*, **87**, 1096 (1965).

(20) Z. Osawa and T. Shibamiya, *Kogyo Kagaku Zasshi*, **73**, 115 (1970).

(21) F. A. Cotton and R. C. Elder, *Inorg. Chem.*, **5**, 423 (1966).

(22) J. Kotas, Thesis, Brno, 1971.

$$(Co^{II})_2(ROOH)_2 \longrightarrow R\dot{O}{\rightarrow}Co^{III}Co^{II}(ROOH) \begin{cases} \rightarrow R\dot{O}_2{\rightarrow}Co^{III}Co^{II} + ROH & (4) \\ \rightarrow R\dot{O}_2 + Co^{III}Co^{II}(ROH) & (5) \end{cases}$$

$$Co^{II}Co^{III}(ROOH)_2 \longrightarrow R\dot{O}_2{\rightarrow}(Co^{II})_2(ROOH) + H^+ \longrightarrow 2ROH + O_2 + Co^{II}Co^{III} \quad (6)$$

$$R\dot{O}{\rightarrow}(Co^{III})_2(ROOH) \begin{cases} \rightarrow R\dot{O}_2{\rightarrow}(Co^{III})_2 + ROH & (7) \\ \rightarrow R\dot{O}_2 + (Co^{III})_2ROH & (8) \end{cases}$$

$$(Co^{III})_2(ROOH)_2 \longrightarrow R\dot{O}_2{\rightarrow}Co^{II}Co^{III}(ROOH) \longrightarrow ROOR + O_2 + H^+ + (Co^{II})_2 \quad (9)$$

Monomolecular Decomposition of Fixed Radicals

$$R\dot{O}_2{\rightarrow}Co^{III}Co^{II} \longrightarrow R\dot{O}_2 + Co^{III}Co^{II} \quad (10)$$

$$R\dot{O}_2{\rightarrow}(Co^{III})_2 \longrightarrow R\dot{O}_2 + (Co^{III})_2 \quad (11)$$

Formation of Diamagnetic Dimer

$$2R\dot{O}_2{\rightarrow}Co^{III}Co^{II} \rightleftharpoons Co^{II}Co^{III}{\leftarrow}\underset{\displaystyle R}{\underset{|}{O}}{-}O \rightleftharpoons O{-}\underset{\displaystyle R}{\underset{|}{O}}{\rightarrow}Co^{III}Co^{II} \quad (12)$$

The present results do not permit us to draw any conclusions as to the step in which the bonded radicals are formed; *i.e.*, whether they are generated predominantly by reaction 4, 7, or 9. It is also difficult to decide if the monomolecular decomposition of these radicals occurs through reaction 10 or 11. Reactions 4, 5, 7, and 8 are fast, this being the reason for not observing the epr signal due to RO· bonded radicals.

Bartlett and Gunther[23] while studying the reaction of lead(IV) acetate with di-*tert*-butyl hydroperoxide, have observed the formation of unstable di-*tert*-butyl tetroxide that decomposed at −30°. In our case we expect the product of reaction 12 to have a similar structure; it decomposes, however, at higher temperature (*ca.* 0°). It follows from our results (Figure 3) that the stability of complex formed in reaction 12 increases when this complex is placed into a ligand field.

The problem of why the complex-bonded *tert*-BuO_2· radicals are formed preferably in nonpolar media is connected with the radical–metal bond strength. The replacement reactions of complex-bonded radicals caused by the presence of polar compounds will be described in the following communication.

(23) P. D. Bartlett and P. Gunther, *J. Amer. Chem. Soc.*, **88**, 3288 (1966).

Radical Reactions in the Ligand Field of Metal Complexes. II. Reactions of the *tert*-Butylperoxy Radical Bound to Cobalt(III)

by A. Tkáč,[1a] K. Veselý[1b]* and L. Omelka[1a]

Institute of Chemical Physics, Slovak Technical University, Bratislava, Czechoslovakia, and Research Institute of Macromolecular Chemistry, Brno, Czechoslovakia *(Received June 12, 1970)*

Publication costs borne completely by The Journal of Physical Chemistry

Reactions of the *tert*-butylperoxy radical bound to cobalt(III) hydroxyacetylacetonate have been examined. Polar solvents displace the *tert*-$BuO_2\cdot$ radical from the complex. Phenols can react with the *tert*-$BuO_2\cdot$ complex, forming phenoxy radicals. These can either form a complex with cobalt or, as in the case of dimethylphenol, produce polyphenylene oxide radicals. The reaction of N-phenyl-2-naphthylamine leads to the formation of a radical on the nitrogen. 4-Nitrosodiethylaniline gives stable nitrosyl radicals. Stable radicals showing the interaction of an unpaired electron with the aluminum nucleus are formed by reaction with triisobutylaluminum and triethylaluminum, respectively. A stable tri-*tert*-butylphenoxy radical can be fixed to Co^{II} acetylacetonate. An interaction of the unpaired electron with the cobalt nucleus then takes place.

Introduction

According to Brandon and Elliot[2] the reaction of *tert*-BuOOH with naphthenates and acetylacetonates of manganese, cobalt, and vanadium in nonpolar solvents produces long-lived radicals.

In our previous paper[3] we described conditions necessary for the production of complex-bound radicals by the reaction of *tert*-BuOOH with Co $(acac)_2$. We presented several reasons for the epr signal being due to complex-bound *tert*-$BuO_2\cdot$ radicals.

To characterize these radicals we studied both the exchange reaction and electron transfer reactions.

Whereas there is no information about exchange reactions of complex-bound radicals available, there are numerous reports on reactions of radicals which, being regarded as free, were in fact frequently bound to metal ions or to complexes. We pointed out that the equilibrium constant of radical complex formation will be affected very strongly by the environment.

Experimental Section

Chemicals. For $Co(acac)_2$ and *tert*-BuOOH, see our previous paper.[3] The tri-*tert*-butylphenoxy radical was prepared according to Müller and Ley.[4] The other chemicals used were commercial reagents.

Technique. The experiments were done in argon according to procedure I, described in our previous paper.[3] The spectra were taken using a Varian E3 X-band spectrometer.

Results and Discussion

Exchange Reaction of the Radical Complex. The influence of polar compounds upon the epr signal intensity was ascertained by adding various polar compounds into toluene solutions of *tert*-$BuO_2\cdot$ radicals complex-bound to $Co^{III}(acac)_2OH$. The data obtained directly after the ultrasound mixing of components are presented in Table I. Figure 1 shows the influence of different amounts of *tert*-butyl alcohol.

Table I

Added compound	The decrease in the epr signal after addition of the compound to *tert*-BuOOH in the ratio 1:1, %
Water	25
tert-Butyl alcohol	40
Ethanol	80
Methanol	80
Acetone	80
Cyclohexylamine	90
Pyridine	90

The original number of free spins contained in the radical complex was 5×10^{15} per 0.1 ml of sample. When the polar compounds are added in sufficient quantity into the toluene solution of cobalt acetylacetone before its reaction with the *tert*-BuOOH, the radical complex is not produced at all.

As far as polar compounds are concerned, we can only say that their solvation energy is higher than 28 kcal/mol, *i.e.*, higher than the bond strength[3] of the *tert*-$BuO_2\cdot Co(acac)_2OH$ bond in toluene solutions.

Generation of Phenoxy Radicals. The toluene solution of radical complex *tert*-$BuO_2\cdot Co(acac)_2OH$ (5×10^{15}

(1) (a) Slovak Technical University; (b) Research Institute of Macromolecular Chemistry.

(2) R. W. Brandon and C. S. Elliot, *Tetrahedron Lett.*, 4375 (1967).

(3) A. Tkáč, K. Veselý, and L. Omelka, *J. Phys. Chem.*, 75, 2575 (1971).

(4) E. Müller and K. Ley, *Chem. Ber.*, 87, 922 (1954).

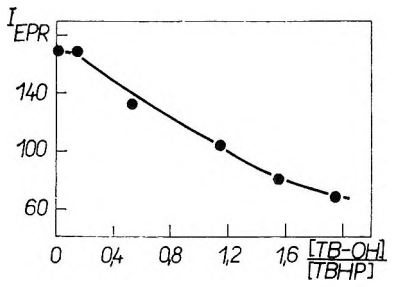

Figure 1. The epr signal intensity of the *tert*-BuO$_2$Co(acac)$_2$OH radical complex *vs.* the molar ratio *tert*-BuOH/*tert*-BuOOH; the amount of Co(acac)$_2$ is constant for all experiments. Measured at 24°, 1 min after ultrasound mixing.

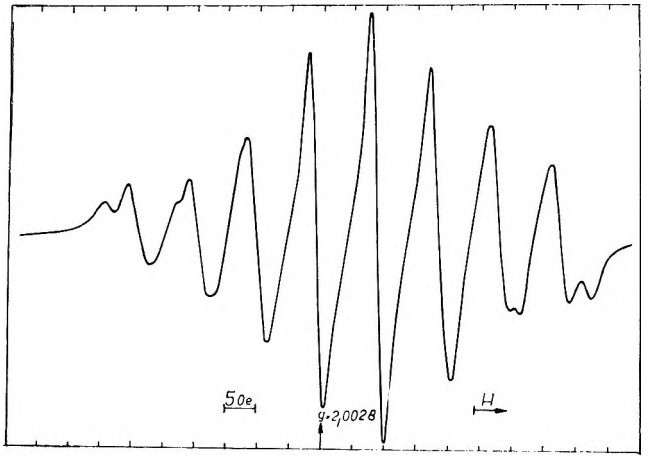

Figure 2. The epr signal generated by the interaction of *tert*-BuO$_2$Co(acac)$_2$OH with phenol (4% in toluene) at 23°. Modulation amplitude 1 Oe.

spin/0.1 ml) was used, 10 min after its preparation, to generate phenoxy radicals from phenol, 2,6-dimethylphenol, and tri-*tert*-butylphenol, respectively. After adding a phenolic compound, either in the form of toluene solution or directly as crystals, to the radical complex solution, a decrease in the intensity of the original signal (g = 2.0147) is seen immediately after mixing the components by ultrasound. New signals with lower g values are observed; their intensity corresponds to *ca.* ten times lower concentration of paramagnetic species (10^{14} spins/0.1 ml).

The phenoxy radical, formed by hydrogen abstraction from phenol, is stabilized on the cobalt atom (nuclear spin I = $^7/_2$) judging from hyperfine splitting (Figure 2). The shape of the spectrum, the number of lines, and their intensity distribution is different from that described by Butchatchenko[5] and Ayscough[6] for the case of free phenoxy radicals. A plausible interpretation of the observed spectrum is to visualize the signal as a superposition of two octets having the same g values but slightly differing coupling constants. A different line intensity will result as a consequence of this effect. It may be assumed that both resonance products are partially bonded to the cobalt nucleus with slightly different bond strengths.

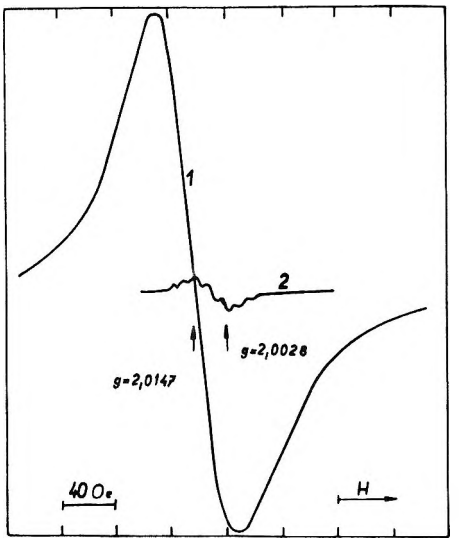

Figure 3. The epr signal due to a radical complex *tert*-BuO$_2$Co(acac)$_2$OH (1); the same signal after addition of 2,6-xylenol (2). Mixed by ultrasound for 30 sec at 24°.

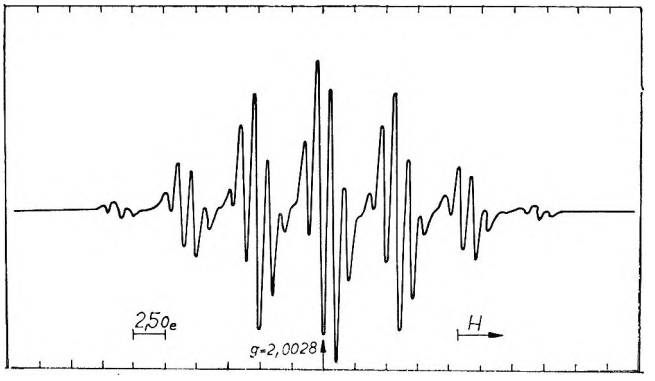

Figure 4. The epr signal of the polyphenyl ether radical prepared under the same conditions as in the previous case (see Figure 3).

When 2,6-dimethylphenol is added to the radical complex the intensity of the epr signal is reduced, as in the previous case (Figure 3). The radical formed here, however, is not stabilized by forming a bond with Co(III) but it forms a polyphenylene oxide radical whose epr signal appears as a characteristic septet (Figure 4). A septet induced by overlapping of two quartets is formed through the interaction of an unpaired electron on oxygen with the protons of two unequal methyl groups and two *meta* protons of the benzene ring with the coupling constants A(Me) = 5.77 Oe, A(Me′) = 4.77 Oe, and A(*meta* H) = 1.0 Oe. Such an interpretation has been given elsewhere.[7]

(5) A. L. Butchatchenko, "Stabilnyje radikaly," AN SSSR, Moscow, 1963, p 77.

(6) P. B. Ayscough, "Electron Spin Resonance in Chemistry," Methuen & Co. Ltd., London, 1967, p 298.

(7) A. Tkáč and J. Kresta, *Chem. Zvesti*, 24, 189 (1970).

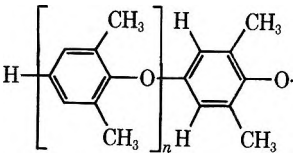

The oxidation reaction of tri-*tert*-butylphenol gives stable aryloxy radicals in good yield. These radicals can be characterized by a triplet whose line intensity ratio is 1:2:1, a consequence of the interaction of two protons in the *meta* position with the unpaired electron of oxygen. The epr signal due to the complex formed by reaction of tri-*tert*-butylphenol with *tert*-$BuO_2\cdot$ radicals fixed to cobalt is in fact a superposition of two spin systems: the aryloxy radical (g = 2.006) and the octet (g = 1.996) (see Figure 5). At sufficient dilution the central line shows a characteristic triplet with intensity ratio 1:2:1 (Figure 6). When suitably low modulation amplitude is employed each of the octet lines is further split to a doublet. Similar effects can be seen when a stable tri-*tert*-butylphenoxy radical is added to a toluene solution of $Co(acac)_2$ free from tri-*tert*-BuOOH.

Interaction of Stable Phenoxy Radicals with the Central Cobalt Atom in Acetylacetonate Cobalt(II) Complexes. Two overlapped epr signals can be seen when a spectrum of the mixture containing tri-*tert*-butylphenoxy radicals and $Co^{II}(acac)_2$ in inert medium is taken at room temperature (Figure 7). The signal, whose g = 2.006 and which is split into a triplet when suitable conditions are applied, can be ascribed to the tri-*tert*-butylphenoxy radical. The signal, consisting of eight lines of the same intensity (g = 1.996) and whose overall spectral width is 90 Oe, is due to the interaction of tri-*tert*-butylphenoxy radicals with the magnetic nucleus of cobalt (I = $^7/_2$). Increasing the temperature to 60° causes disappearance of the octet, whereas the triplet remains practically unchanged. The octet can be regenerated by cooling the sample down to the ambient temperature. As the original $Co(acac)_2$ is in the form of a dimer with compensated antiparallel spins and thus a diamagnetic compound, the observed paramagnetism in the presence of stable free radicals can be explained by assuming formation of a complex between free radicals and the cobalt dimer. At lower modulation amplitude each of the octet lines is split to a doublet of the same intensity. This split may be due to the proton of one acetylacetonate ligand. To prove the proposed interpretation it would have been necessary to determine the splitting constants as well as the g values in a microwave region different from that used for our experiments (3 cm).

Electron Transfer to Nitrogen. The cobalt radical complex can be used to generate stable free radicals from the commonly used antioxidant *N*-phenyl-2-naphthylamine. When 5% toluene solution of the antioxidant is added to the radical complex, immediately after a 10 sec mixing by ultrasound, then the

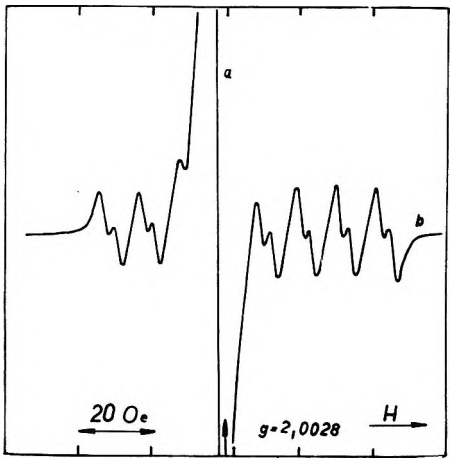

Figure 5. The epr spectrum consisting of two superimposed signals due to the stable tri-*tert*-butylphenoxy radicals (a) and the complex of the radical with dimer $[Co(acac)_2]_2$ (b). The radical was generated by reaction of *tert*-$BuO_2Co(acac)_2OH$ with 4% tri-*tert*-butylphenol in toluene solution at 24°.

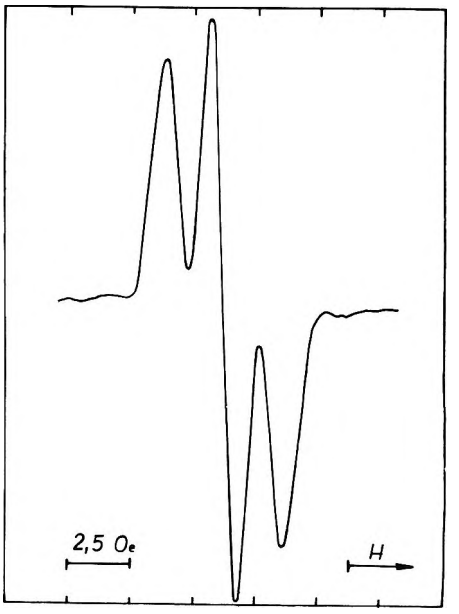

Figure 6. The epr spectrum of tri-*tert*-butylphenoxy radical generated as in Figure 5 (a), modulation amplitude 1 Oe, power 4 mW.

original signal (g = 2.0147) disappears and a new triplet of equal line intensity (g = 2.004) is seen (Figure 8). The homolytic fission of hydrogen from an amine group leads to the formation of an unpaired electron on nitrogen (nuclear spin I = 1). The radical complex enables us to compare relative stabilities of various types of free radicals in nonpolar media and to ascertain their inhibition effect by measuring their reactivity toward the $RO_2\cdot$ radicals which participate in all oxidative chain reactions.

By adding an excess of *p*-nitrosodiethylaniline to the toluene solution of *tert*-$BuO_2\cdot Co(acac)_2OH$, a 20% decrease in intensity of the original signal (g = 2.0147) is seen after a 4 min mixing by ultrasound at room

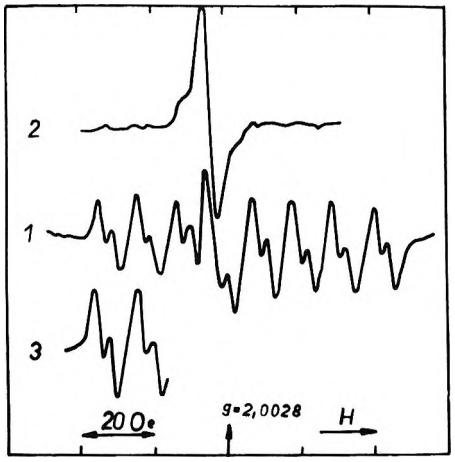

Figure 7. The epr signals due to the stable tri-*tert*-butylphenoxy radical forming a complex with $[Co(acac)_2]_2$ dimer. The stable radical was added into a toluene solution of $Co(acac)_2$ in the amount of 0.01% and mixed for 20 sec by ultrasound at 24° (1); the same signal observed at 50° (2); the same signal after cooling the sample down to room temperature (3). (Only the first two lines of the octet are shown.)

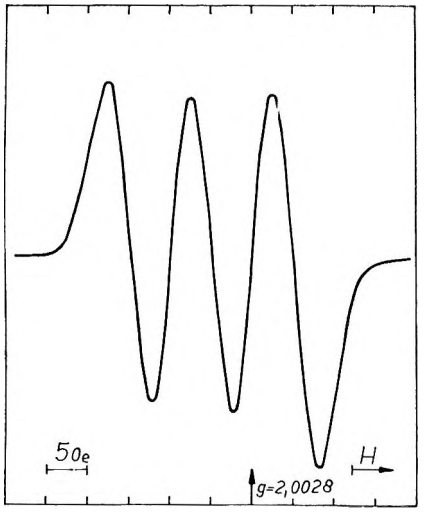

Figure 8. The epr spectrum of the stable radical generated by reaction of *tert*-$BuO_2Co(acac)_2OH$ with N-phenyl-2-naphthylamine in toluene solution at 24°; mixed by ultrasound for 30 sec.

temperature. A new, feeble signal due to another radical (g = 2.004) appears. After heating the mixture for 5 min at 50°, *i.e.*, at the temperature of decomposition of the radical complex,[3] the original signal disappears completely and a triplet of equal line intensity is observed. The triplet indicates the presence of the free electron interacting with a nitrogen nucleus (Figure 9).

Krajlič and Trumbore[8] have shown that *p*-nitrosodimethylaniline is a radical scavenger in radiochemistry. It is a selective scavenger of HO· radicals without reacting with HO_2· radicals.

Reaction with Alkylaluminum. After adding a ben-

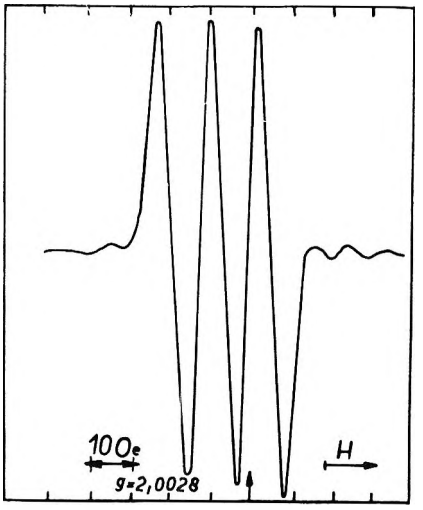

Figure 9. The epr spectrum due to nitrosyl radical generated by reaction of *tert*-$BuO_2Co(acac)_2OH$ with 2% *p*-nitrosodiethylaniline at 24°. Modulation amplitude 1 Oe.

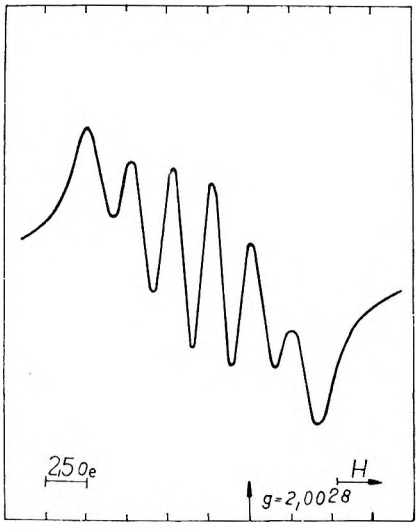

Figure 10. The epr spectrum generated by reaction of *tert*-$BuO_2Co(acac)_2OH$ with triethylaluminum in benzene solution at 24°. Modulation amplitude 1 Oe.

zene solution of triethylaluminum and triisobutylaluminum respectively under argon to a toluene solution of *tert*-BuO_2· cobalt-bonded radicals, the original signal (g = 2.0147) vanished and a new signal (g = 2.0041 ± 0.0005) appeared, the intensity of which was *ca.* 10% with regard to the original signal. The new signal is split into six lines of the same intensity, the coupling constant being 2.5 Oe (see Figure 10). This suggests the existence of the interaction of an unpaired electron with the aluminum nucleus (I = $^5/_2$).

Krusič and Kochi[9] have observed the formation of ethyl radicals during the photochemical generation

(8) I. Krajlič and C. N. Trumbore, *J. Amer. Chem. Soc.*, 87, 2547 (1965).

(9) P. J. Krusič and J. K. Kochi, *ibid.*, 91, 3942 (1969).

of *tert*-BuO· radicals in the presence of triethylaluminum at −100°. The ethyl radicals vanished immediately as soon as the irradiation was interrupted. The authors assume that the reaction proceeds *via* a four-coordinate intermediate R_3AlO-*tert*-Bu but they have not found any paramagnetic species showing hyperfine structure even at the lowest temperatures.

The fixed radicals observed by us are, at room temperature, even more stable than the original *tert*-BuO_2· radicals fixed to cobalt. It is likely that photochemically formed hot *tert*-BuO· radicals cannot be fixed to aluminum. It is possible, however, that in our case the *tert*-BuO_2· radicals are fixed to a bimetallic cobalt–aluminum complex.

Negative Ion Formation by Ethylene and 1,1-Difluoroethylene

by J. C. J. Thynne*[1] and K. A. G. MacNeil

Chemistry Department, Edinburgh University, Edinburgh, Scotland *(Received November 17, 1970)*

Publication costs borne completely by The Journal of Physical Chemistry

The formation of negative ions in ethylene and 1,1-difluoroethylene has been studied as a function of electron energy and various ionisation processes have been suggested to account for ion formation. The decomposition of a "compound-ion" state of $CH_2CF_2^{-*}$ is suggested to be responsible for the formation of several different ions at ~7 eV. The bond energy D(F–$CHCH_2$) has been calculated to be $\leq 5.0 \pm 0.3$ and electron affinities have been estimated for the species CH, C_2, C_2H, and C_2F.

Introduction

As part of a continuing program concerned with negative ion formation[2-4] as the result of low energy electron bombardment we have studied 1,1-difluoroethylene and ethylene. Tetrafluoroethylene has been studied previously in this laboratory;[5] consequently examination of these two molecules should be informative regarding the effect of fluorine atom substitution of an olefin upon the pattern of ion formation. Ethylene has been studied by other workers[6] but we are not aware of any investigation of 1,1-difluoroethylene.

In electron bombardment studies, when the electrons are produced from a heated filament, because of the energy spread of the electron beam uncertainties arise in the measurement of the appearance potentials of ions. This is partly due to the smearing-out effect of the high-energy tail of the electron energy distribution. We have developed an analytical technique to reduce this effect for negative ions[7] and have applied it to this investigation.

Experimental Section

The experiments were carried out using a Bendix time-of-flight mass spectrometer, Model 3015. The energy of the ionizing electrons was read on a digital voltmeter and the spectra were recorded on two 1-mV potentiometric recorders.

The electron current was maintained constant by automatic regulation over the whole energy range studied. Ionization curves were usually measured five times. The appearance potential at 4.2 eV of the O^- ion from SO_2 was used as the reference for energy scale calibration.[8,9]

The experimental data were treated by the deconvolution method described previously.[7] The electron energy distribution (which was needed to be known for this procedure) was measured using the SF_6^- ion formed by sulfur hexafluoride.[10,11] It was found that performing 15 smoothing and 20 unfolding iterations upon the basic data enabled satisfactory recovery of appearance potentials, resonance peak maxima, and peak widths (at half-height) to be made.

(1) Ministry of Technology, Abell House, John Islip Street, London, S.W.1, England.

(2) (a) J. C. J. Thynne, *J. Phys. Chem.*, **73**, 1586 (1969); (b) K. A. G. MacNeil and J. C. J. Thynne, *Int. J. Mass Spectrom. Ion Phys.*, **2**, 1 (1969).

(3) K. A. G. MacNeil and J. C. J. Thynne, *J. Phys. Chem.*, **74**, 2257 (1970).

(4) P. W. Harland and J. C. J. Thynne, *ibid.*, **73**, 4031 (1969).

(5) K. A. G. MacNeil and J. C. J. Thynne, *Int. J. Mass Spectrom. Ion Phys.*, **5**, 329 (1970).

(6) L. von Trepka and H. Neuert, *Z. Naturforsch. A*, **18**, 1295 (1963).

(7) K. A. G. MacNeil and J. C. J. Thynne, *Int. J. Mass Spectrom. Ion Phys.*, **3**, 35 (1969).

(8) K. Kraus, *Z. Naturforsch. A*, **16**, 1378 (1961).

(9) J. G. Dillard and J. L. Franklin, *J. Chem. Phys.*, **48**, 2349 (1968).

(10) W. M. Hickam and R. E. Fox, *ibid.*, **25**, 642 (1956).

(11) G. J. Schulz, *J. Appl. Phys.*, **31**, 1134 (1960).

Ethylene and 1,1-difluoroethylene were obtained from cylinders (Cambrian Chemicals Ltd. and the Pierce Chemical Co., respectively) and were used with no further purification.

Results and Discussion

Negative Ion Formation. (a) *Mass Spectra at 70 eV.* In Table I we show the negative ion mass spectra of ethylene, 1,1-difluoroethylene, and tetrafluoroethylene measured at 70 eV and 5×10^{-6} Torr. For comparison we have included the spectra of ethylene recorded by other workers.[6,12]

Table I: Mass Spectra of C_2H_4, $C_2H_2F_2$, and C_2F_4 Measured at 70 eV

			C_2H_4		
Ion	C_2F_4	CH_2CF_2	This work	Ref 6	Ref 12
H^-		25	80	600	
C^-	4.5		310	280	390
CH^-			240	156	260
CH_2^-			110	70	100
F^-	1000	1000			
C_2^-	1.4	340	1000	1000	1000
C_2H^-		108	740	725	770
CF^-	2.2				
F_2^-	<1				
C_2F^-		295			
CF_2^-	<1				
CF_3^-	<1				
$C_2F_3^-$	<1				

The three sets of ethylene data are in generally good accord when likely experimental differences such as source pressure, electron current, etc., are taken into account. The principal difference is in the H^- ion intensity; von Trepka and Neuert[6] found it to be the second most abundant ion. We recognize that, because of its low mass, H^- normally requires special focussing of the mass spectrometer; nevertheless, even under optimum conditions, the intensity quoted in Table I was never exceeded.

In the case of ethylene, anionic fragments containing two carbon atoms are more abundant than such species as C^- and CH^- and, for both C_2^-/C^- and C_2H^-/CH^-, the ratios are ~1.5.

Substitution of two of the hydrogen atoms in ethylene by fluorine atoms has a profound effect on the mass spectrum, and F^- becomes the principal ion rather than C_2^-. All hydrocarbon ions have fluorocarbon counterparts and the latter are the more abundant. This is partly due to the higher electron affinities of the halogenated ions although, since at 70 eV ion-pair processes are significant, it also reflects the fact that, since the ionization potential of hydrogen is less than that of fluorine, reactions such as *a* are more common than those of *b*.

$$RHF + e \xrightarrow{a} H^+ + RF^- + e$$
$$\xrightarrow{b} F^+ + RH^- + e$$

The low yields of CH_2^- and CF_2^- suggest that there is little symmetrical splitting which is somewhat unexpected since $D(CF_2{=}CH_2) < D(CH_2{=}CH_2)$.

F_2^- ion formation must occur *via* a rearrangement reaction; the very low intensity ion at $m/e = 33$ we attribute to CH_2F^- and must be formed as a result of fluorine migration. The absence of CF_2H^- indicates that the analogous migration involving hydrogen does not occur.

Tetrafluoroethylene forms a variety of ions although, with the exception of F^-, they are of very low intensity. Unlike C_2H_4 and $C_2H_2F_2$, in the case of C_2F_4 single carbon atom fragments are more abundant, C_2^-/C^- being ~0.3 and $C_2F^- \ll CF^-$. This suggests that the variation in the C=C bond strength is an important factor in determining the fragmentation patterns since the bond is weakest in the case of C_2F_4. F_2^- and CF_3^- must be rearrangement ions; this observation, in conjunction with our results for $C_2H_2F_2$ and the absence of ions such as H_2^- and CH_3^- in C_2H_4, suggests that while fluorine atom migration can occur fairly readily hydrogen atom migration is not a feature of negative ion mass spectra.

(*b*) *1,1-Difluoroethylene.* Ion formation by dissociative electron capture occurred over a broad range of electron energies; all of the observed ions exhibited two major maxima, the first close to 7 eV and the second in the 10–12-eV range. The ions observed and measured were H^-, F^-, C_2^-, C_2H^-, and C_2F^- and, at their respective resonance peak maxima in the 10–12-eV region, they were formed in the ratios 30:1000:49:65:830. Ionization efficiency curves for these species are illustrated in Figures 1 and 2. Because the data for the very low intensity H^- ions were found to be excessively noisy after only a few unfolding iterations the deconvoluted results for this ion have not been included in the Figures.

It can be seen that all of the negative ions exhibit a resonance peak at or close to 7 eV. This coincidence of peaks is attributed to the competitive dissociation of a single state of the unstable molecular negative ion $CF_2CH_2^-$. Such a "compound-ion" state can decompose by a variety of paths to form H^-, F^-, C_2^-, etc., but since each reaction path occurs with a different probability, although all the ions are observed at the same electron energy, they are formed with different intensities; some or all of these reactions probably occur with excess kinetic and/or excitation energy associated with the reaction products.

At higher electron energies the cluster of peaks between 10 and 12 eV is probably due to the formation of

(12) C. E. Melton and P. S. Rudolph, *J. Chem Phys.*, **31**, 1485 (1959).

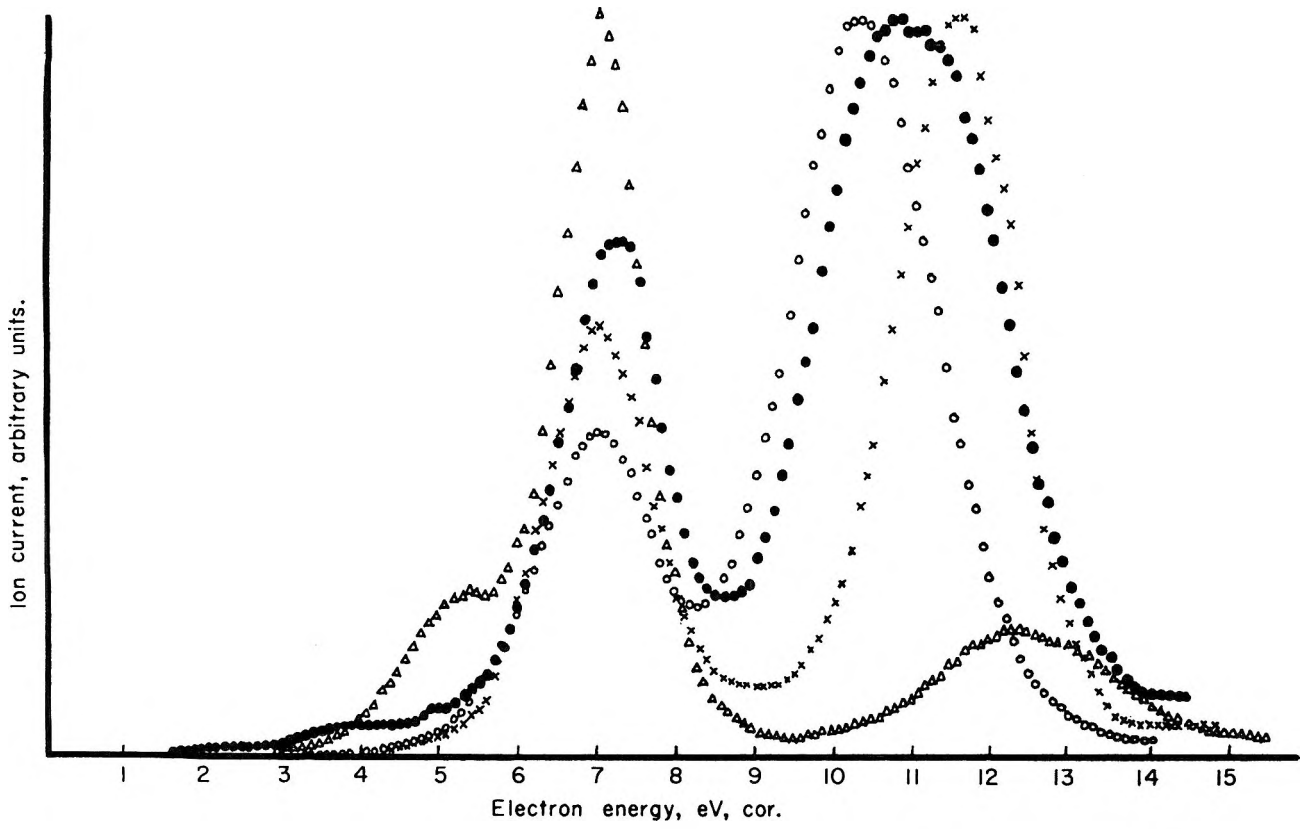

Figure 1. Ionization efficiency curves before deconvolution for the ions formed by CH_2CF_2: F^- (full circles); C_2F^- (open circles); C_2H^- (crosses), C_2^- (triangles).

one or two or even a band of closely spaced "compound-ion" states.

(*i*) F^-. Our deconvoluted data indicate that a low cross section process occurs at 1.6 ± 0.3 eV; between that energy and the onset of the major F^- resonance peak at 5.4 eV other low intensity dissociative attachment processes occur at 3.3 and 4.6 eV. The initial appearance of the ion is probably due to the reaction

$$CH_2CF_2 + e \longrightarrow F^- + CH_2CF \qquad (1)$$

and using a value of 3.4 eV for the electron affinity of fluorine,[13] we find that $D(F\text{–}CFCH_2) \leq 5.0 \pm 0.3$ eV. This result is in good accord with the general range of F–C bond strengths, *e.g.*, $F\text{–}C_2F_3 \leq 5.2 \pm 0.1$ [5] and 5.0 eV for $C_6H_5\text{–}F$.[14] At electron energies beyond the initial appearance of the ion the lack of thermochemical data for possible neutral fragments makes it difficult to identify the reactions responsible for ion production.

$$CH_2CF_2 + e \longrightarrow F^- + HF + C_2H \qquad (2)$$

$$\longrightarrow F^- + H + CHCF \qquad (3)$$

$$\longrightarrow F^- + F + CCH_2 \qquad (4)$$

The minimum enthalpy requirements for reactions 2 and 3 are 2.9 ± 0.3 and 3.2 ± 0.5 eV; one or both may be occurring in the low energy region and responsible for the onset noted at 3.3 eV. Because of the lack of data for $\Delta H_f(:CCH_2)$ we cannot estimate ΔH_4. A rough estimate [based upon $D(H\text{–}C{=}CH_2) \sim 4$ eV] suggests that $\Delta H_4 \geq \sim 5$ eV and we tentatively suggest that the onset of ionization noted at 5.4 eV is due to reaction 4.

Beyond 8.7 eV the ionization efficiency curve for F^- is very broad (~3 eV wide at half-height) and, on deconvolution, is resolved into two closely spaced peaks, having maxima at 10.6 ± 0.2 and 11.4 ± 0.2 eV. Since a precise onset cannot be deduced for the second resonance process, identification of the reaction responsible is made difficult but we may assume that the onset is greater than 8.7 eV, probably by ~1 eV.

For the first onset at 8.7 ± 0.3 eV possible reactions to be considered (together with their minimum enthalpy requirements) are

$$CH_2CF_2 + e \longrightarrow F^- + CF + CH_2$$

$$(7.8 \pm 0.3 \text{ eV}) \qquad (5)$$

$$\longrightarrow F^- + C + CH_2F$$

$$(7.9 \pm 0.3 \text{ eV}) \qquad (6)$$

$$\longrightarrow F^- + 2H + C_2F$$

$$(8.3 \pm 0.5 \text{ eV}) \qquad (7)$$

$$\longrightarrow F^- + H + F + C_2H$$

$$(8.8 \pm 0.5 \text{ eV}) \qquad (8)$$

(13) R. S. Berry and C. W. Riemann, *J. Chem. Phys.*, **38**, 1540 (1963).
(14) P. Smith, *ibid.*, **29**, 681 (1958).

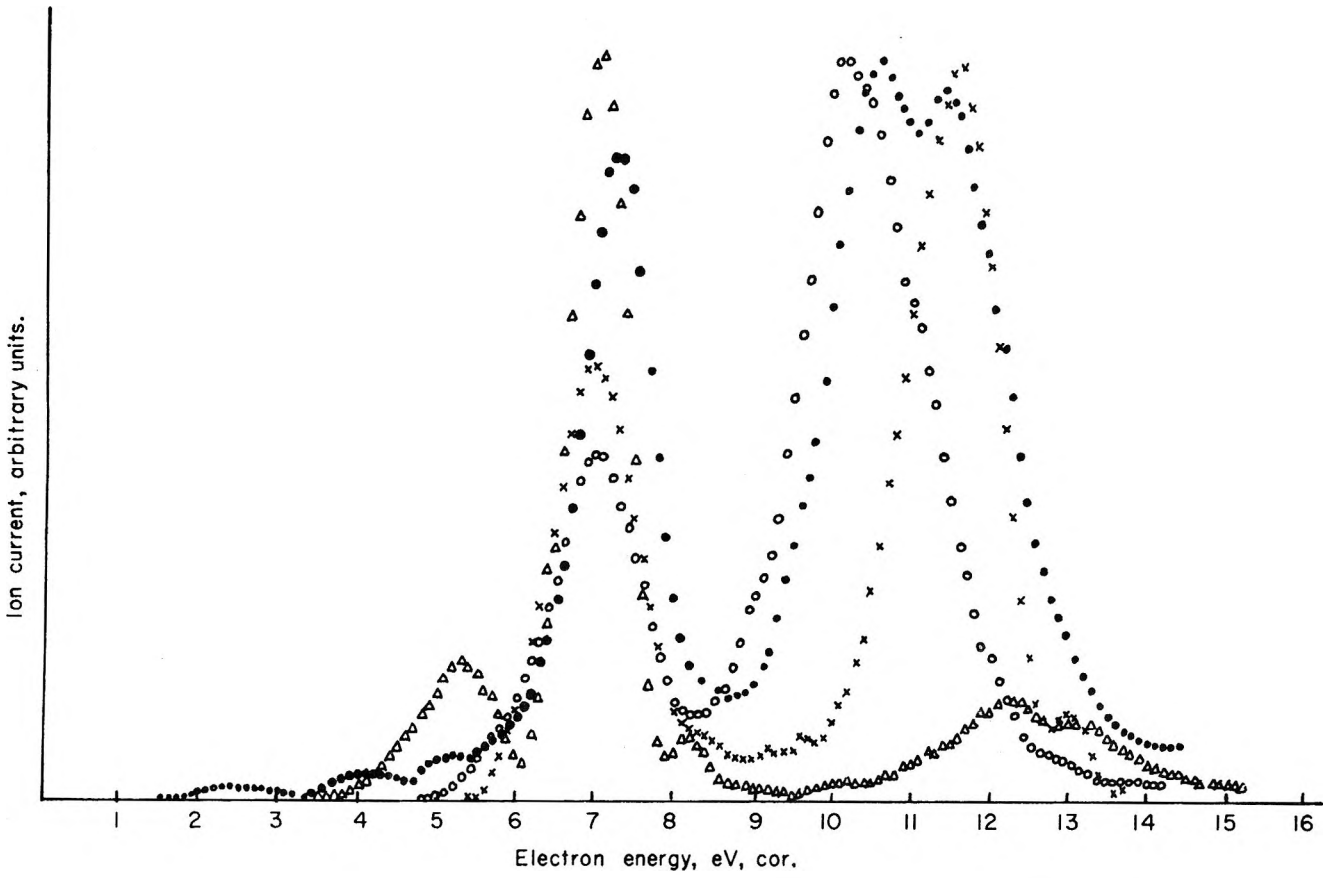

Figure 2. Ionization efficiency curves after deconvolution for the ions formed by CH_2CF_2: F^- (full circles), C_2F^- (open circles), C_2H^- (crosses), C_2^- (triangles).

At the second of the doublet of peaks possible reactions are

$$CH_2CF_2 + e \longrightarrow F^- + F + H_2 + C_2 \quad (10.3 \pm 0.3 \text{ eV}) \quad (9)$$

$$\longrightarrow F^- + C + H_2 + CF \quad (11.1 \pm 0.2 \text{ eV}) \quad (10)$$

$$\longrightarrow F^- + C + HF + CH \quad (11.6 \pm 0.1 \text{ eV}) \quad (11)$$

$$\longrightarrow F^- + C + H + CHF \quad (11.8 \pm 0.5 \text{ eV}) \quad (12)$$

It is unfortunate that for this ion, partly because of the complexity of the ionization curve and partly because of the paucity of thermochemical knowledge, none of the above processes can be positively identified although, for the second resonance peak, reactions 10–12 can probably be ruled out since $A(F^-) \sim 9$–10 eV.

(*ii*) C_2F^-. The interpretation of the formation of this ion should be considerably simpler than that of F^- since fewer reactions may be written to explain its formation. Our deconvoluted data for this ion are shown in Table II. Initially the ion appears at 4.9 ± 0.2 eV and may involve one of the reactions

$$CH_2CF_2 + e \longrightarrow C_2F^- + F + H_2 \quad (13)$$

$$\longrightarrow C_2F^- + H + HF \quad (14)$$

Reactions 13 and 14 require 7.1 ± 0.5 eV $- E(C_2F)$ and 5.8 ± 0.5 eV $- E(C_2F)$, respectively, which suggest that either $E(C_2F) \geq 2.2 \pm 0.7$ eV or $E(C_2F) \geq 0.9 \pm 0.7$ eV. Before deciding on which of these processes is the more likely, it is useful to examine the higher energy process at 8.3 ± 0.3 eV. Here only one reaction can be written

$$CH_2CF_2 + e \longrightarrow C_2F^- + F + 2H \quad (15)$$

requiring 11.7 ± 0.5 eV $- E(C_2F)$, indicating that $E(C_2F) \geq 3.4 \pm 0.8$ eV. Of reactions 13 and 14 the former is more consistent with this value for $E(C_2F)$ and probably also requires the simpler intramolecular rearrangement to form H_2. Reaction 14 cannot, however, be entirely discounted since it might occur with some 2 eV of excess energy.

(*iii*) C_2H^-. For formation of this species, reactions 16 and 17 may be written. These require 6.3 ± 0.5 eV $- E(C_2H)$ and 12.2 ± 0.5 eV $- E(C_2H)$, respectively.

$$CH_2CF_2 + e \longrightarrow C_2H^- + HF + F \quad (16)$$

$$\longrightarrow C_2H^- + 2F + H \quad (17)$$

Table II: Appearance Potentials (*A*), Resonance Peak Maxima (*PH*), and Peak Widths at Half-Height (*PW*) for Negative Ions Formed by 1,1-Difluoroethylene[a]

Ion	*A*	*PH*	*PW*
F^-	1.6 ± 0.3	~2.5	
	3.3 ± 0.3	~4.2	
	4.6 ± 0.3	~5.2	
	5.4 ± 0.3	7.3 ± 0.2	0.9 ± 0.1
	8.7 ± 0.3	10.6 ± 0.2	
	11.1 ± 0.3	11.4 ± 0.2	
C_2F^-	4.9 ± 0.2	7.0 ± 0.2	1.3 ± 0.1
	8.3 ± 0.3	10.2 ± 0.2	1.8 ± 0.2
C_2H^-	5.5 ± 0.2	7.0 ± 0.2	1.2 ± 0.1
	10.0 ± 0.2	11.6 ± 0.2	1.3 ± 0.1
C_2^-	3.5 ± 0.2	5.3 ± 0.2	1.2 ± 0.2
	6.1 ± 0.3	7.0 ± 0.2	1.0 ± 0.1
H^-	5.0 ± 0.3	7.2 ± 0.2	
	8.5 ± 0.3	10.7 ± 0.2	2.3 ± 0.3

[a] All values in electron volts.

Values of 2.7[5] and 2.8 eV[6] have been reported for the electron affinity of C_2H. This suggests that the onset of C_2H^- formation at 5.5 ± 0.2 eV is due to reaction 16, about 1.9 eV of excess energy being associated with the ion formation process. This supports our previous suggestion that many of the reactions leading to ion formation in the first "band" probably have excess energy distributed among the fragments.

If the large resonance peak at 10.0 ± 0.2 eV is due to reaction 17 then we may estimate that $E(C_2H) \geq 2.3 \pm 0.7$ eV, in reasonable accord with the values quoted above.

(*iv*) C_2^-. For this ion the first onset is at 3.5 ± 0.2 eV and must involve the reaction

$$CH_2CF_2 + e \longrightarrow C_2^- + 2HF \qquad (18)$$

which requires 6.4 ± 0.2 eV − $E(C_2)$. This process has a minimum energetic requirement which is about 6 eV lower than that of any other; even if the proposed rearrangement to give two molecules of hydrogen fluoride is unusual, it must be postulated in this case. On the basis of this reaction and the observed appearance potential, we may estimate the electron affinity of the C_2 species, $E(C_2) \geq 2.9 \pm 0.5$ eV.[15] Compared with monatomic carbon[16] [$E(C) = 1.1$ eV] this value seems high; however, Honig[17] has calculated that $E(C_2) = 3.1$ eV and, from an electron impact study of a number of hydrocarbons, von Trepka and Neuert[6] have also found that $E(C_2) \geq 2.9$ eV. The reasonable value of $E(C_2)$ obtained confirms that reaction 18, although unusual, is the reaction responsible for C_2^- ion formation.

At higher electron energies other possible reactions, together with their calculated minimum appearance potentials [assuming $E(C_2) = 2.9 \pm 0.5$ eV], are

$$CH_2CF_2 + e \longrightarrow C_2^- + H_2 + F_2 \quad (9.1 \pm 0.8 \text{ eV}) \qquad (19)$$

$$\longrightarrow C_2^- + HF + H + F \quad (9.4 \pm 0.8 \text{ eV}) \qquad (20)$$

$$\longrightarrow C_2^- + H_2 + 2F \quad (10.7 \pm 0.8 \text{ eV}) \qquad (21)$$

$$\longrightarrow C_2^- + F_2 + 2H \quad (13.7 \pm 0.8 \text{ eV}) \qquad (22)$$

$$\longrightarrow C_2^- + 2F + 2H \quad (15.3 \pm 0.8 \text{ eV}) \qquad (23)$$

Since the next possible process cannot occur below about 9 eV it is unlikely that the major C_2^- peak onsetting at 6.1 ± 0.3 eV can be due to any reaction other than (18) but with about 2.6 eV of excess energy.

Other low-intensity resonance processes leading to C_2^- formation occur at 9.5 and 10.6 eV and may be due to reactions 19, 20, and 21. Reaction 23 probably requires more energy than is available since our measurements did not go beyond 15 eV.

(*v*) H^-. This ion is formed at very low intensity over the energy range 5–14 eV. Because of its low abundance the H^- ion data were too noisy for the deconvolution procedure to be applied and the ionization curve shown in Figure 3 is that obtained after 20 smoothing iterations of the directly observed data. From the diagram certain gross features may be distinguished, namely a low-intensity resonance process with an appearance potential of about 5 eV reaching a maximum value at 7.2 ± 0.2 eV and a second process of much larger cross section at 8.5 eV reaching a peak value at 10.7 ± 0.2 eV. This second resonance peak is very broad (the width of the resonance curve at half-height being 2.3 eV) and deconvolution of the curve suggests, though in a rather inconsistent manner, that there are at least two dissociative attachment processes included within the broad peak.

For the lowest energy onset at about 5 eV several possible reactions can be written although the lack of thermochemical data makes definite identification impossible.

$$CH_2CF_2 + e \longrightarrow H^- + CHCF_2 \qquad (24)$$

$$\longrightarrow H^- + F + CHCF \qquad (25)$$

$$\longrightarrow H^- + CH + CF_2 \qquad (25a)$$

Assuming the electron affinity of hydrogen[18] $E(H)$ to be 0.75 eV then reaction 25 requires 5.8 ± 0.7 eV. If

(15) F. M. Page and G. C. Goode, "Negative Ions and the Magnetron," Wiley, New York, N. Y., 1969, p 138.

(16) S. Geltman, *Phys. Rev.*, **111**, 504 (1958).

(17) R. E. Honig, *J. Chem. Phys.*, **22**, 126 (1954).

(18) E. A. Hylleraas and J. Midtdal, *Phys. Rev.*, **103**, 829 (1956).

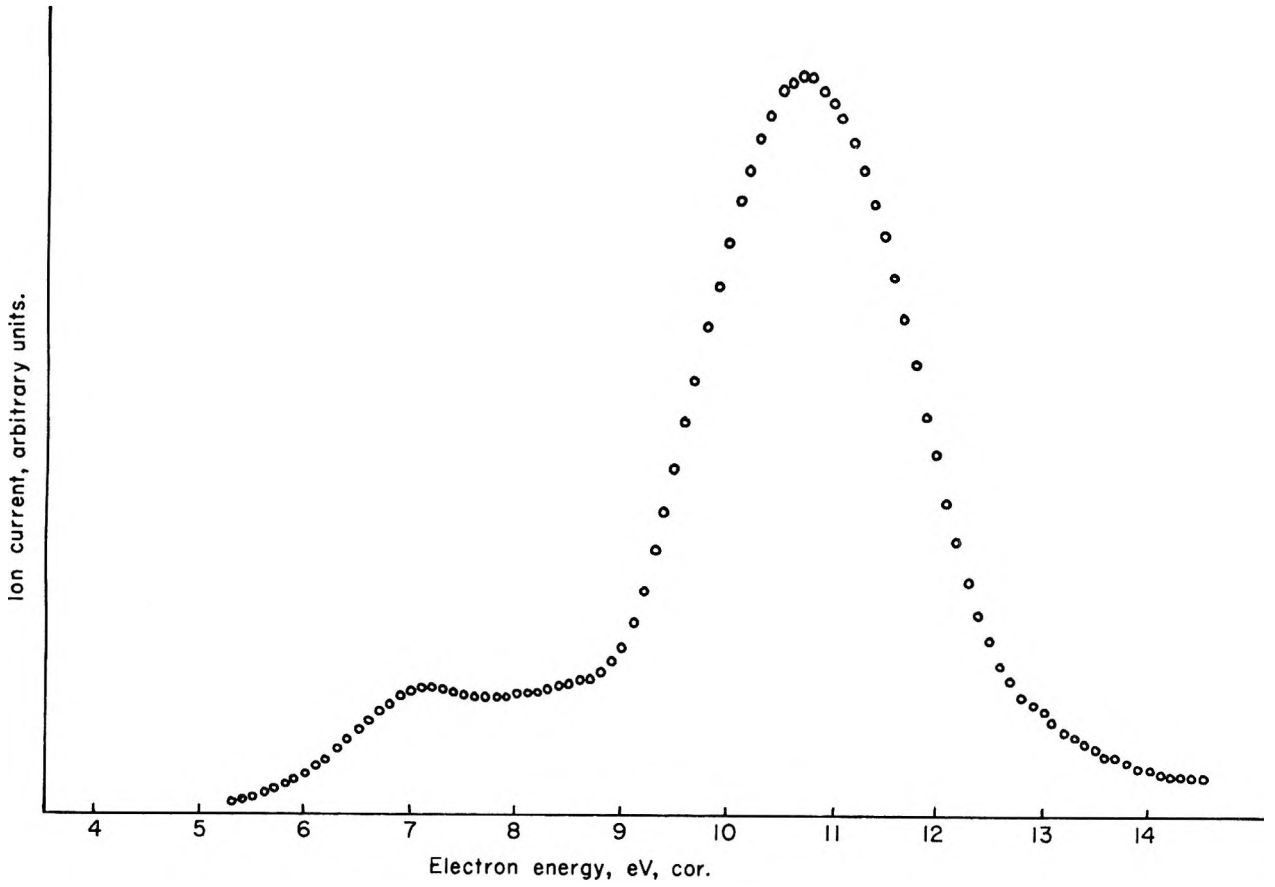

Figure 3. Ionization efficiency curve (after smoothing) for H^- ion formed by CH_2CF_2.

$D(H\text{–}CHCF_2) \sim 4.7$ eV (*i.e.*, similar to $H\text{–}C_2H_3$) then reaction 24 will have a minimum appearance potential of about 4 eV. It is therefore likely that the initial ionization process is due to reaction 24. For the second process at 8.5 ± 0.3 eV a variety of reactions can be written; probably the most likely reaction responsible is either (25) with about 2.7 eV of excess energy or reaction 25a which has a calculated appearance potential of 9.5 ± 0.5 eV. On balance we are inclined to favor reaction 25.

(*c*) *Ethylene.* In ethylene all of the negative ions detected as products of dissociative electron capture processes were formed in very low abundance. The mass spectrum measured at 70 eV is shown in Table I; at low electron energies the ions observed were H^-, CH^-, CH_2^-, and C_2H^- in the ratios 35:750:670:1000 but of these H^- was not sufficiently intense to be measured further. An interesting feature of ion formation is that C_2^- is only formed at high electron energies, presumably *via* an ion-pair process.

Ionization efficiency curves (before and after deconvolution) for CH^-, CH_2^-, and C_2H^- are shown in Figures 4 and 5 and the appearance potential data are summarized in Table III together with those of von Trepka and Neuert.[6]

(*i*) C_2H^-. At low electron energies C_2H^- is the most abundant ion and three dissociative attachment processes are noted at 6.9 ± 0.3, 8.8 ± 0.3, and 9.8 ± 0.3 eV. The second of these is not given explicitly by von Trepka and Neuert[6] although their ionization efficiency curve for C_2H^- suggests a small peak in this region.

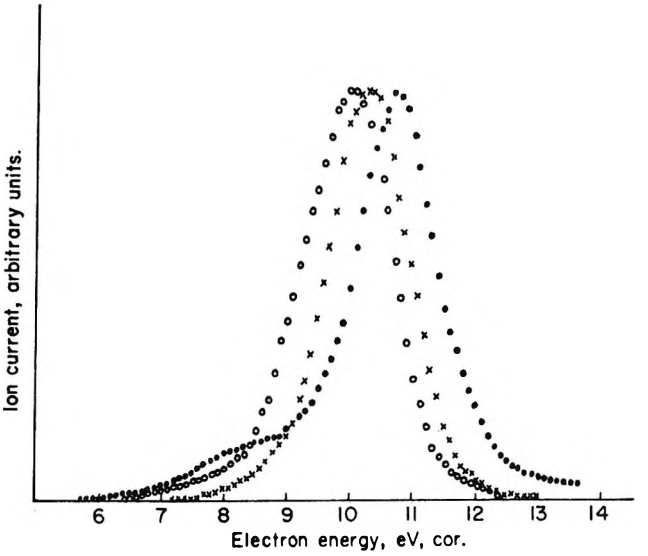

Figure 4. Ionization efficiency curves before deconvolution for ions formed by C_2H_4: C_2H^- (full circles), CH^- (open circles), CH_2^- (crosses).

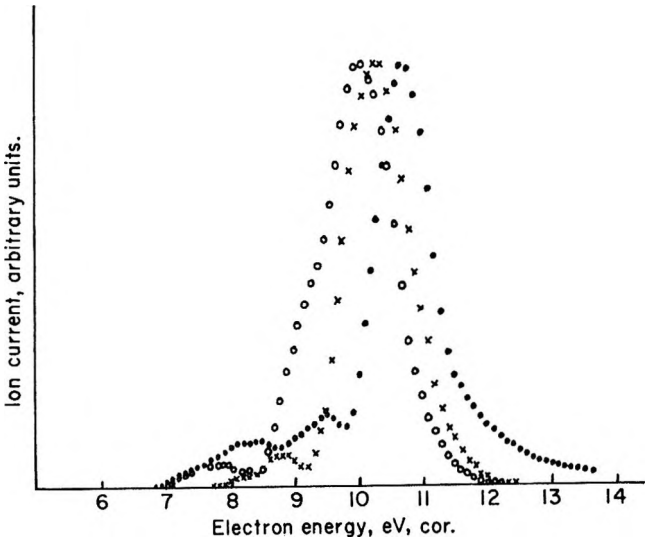

Figure 5. Ionization efficiency curves after deconvolution for ions formed by C_2H_4: C_2H^- (full circles), CH^- (open circles), CH_2^- (crosses).

Table III: Appearance Potentials (*A*), Resonance Peak Maxima (*PH*), and Resonance Peak Widths at Half-Height (*PW*) for Negative Ions Formed by Ethylene

Ion	*A*	*A* (ref 6)	*PH*	*PW*
CH^-	7.0 ± 0.3	7.3 ± 0.4	7.9 ± 0.3	
	8.4 ± 0.3	8.7 ± 0.3	10.1 ± 0.3	1.2 ± 0.2
CH_2^-	7.8 ± 0.3		8.8 ± 0.2	
	9.1 ± 0.3	8.8 ± 0.3	10.3 ± 0.3	1.2 ± 0.2
C_2H^-	6.9 ± 0.3	7.1 ± 0.4	8.5 ± 0.3	
	8.8 ± 0.3		9.5 ± 0.3	
	9.8 ± 0.3	10.0 ± 0.3	10.7 ± 0.3	1.0 ± 0.2

[a] All values in electron volts.

For formation of this ion the reactions can be written

$$C_2H_4 + e \longrightarrow C_2H^- + H_2 + H \quad (26)$$

$$\longrightarrow C_2H^- + 3H \quad (27)$$

which require 6.7 ± 0.4 eV − $E(C_2H)$ and 11.3 ± 0.4 eV − $E(C_2H)$, respectively. Using the value of $E(C_2H) \geq 2.3 \pm 0.7$ eV deduced above it is likely that the initial appearance of the ion is due to reaction 26 with about 2.5 eV of excess energy. The second appearance potential is compatible with reaction 27 occurring with zero excess energy and $E(C_2H) \geq 2.5 \pm 0.7$ eV; this electron affinity is in good accord with the value of ≥ 2.3 ± 0.7 eV deduced from the CH_2CF_2 study. The principal ionization process onsetting at 9.8 ± 0.3 eV could either be reaction 26 with 5.4 eV of excess energy or 27 with 0.8 eV excess energy. The latter reaction might appear to be favored since there would seem to be sufficient excess energy in reaction 26 to dissociate any molecular hydrogen formed. This, however, is an over-simplified view since all of the 5.4 eV of excess energy will not necessarily be deposited in the hydrogen molecule, unknown amounts being distributed between the fragmentary species as (where appropriate) translational, vibrational, and rotational energy. Since we are unable to evaluate the possible contributions due to such sources we cannot definitely attribute the second appearance potential to either reaction.

(*ii*) CH^-. Two appearance potentials at 7.0 ± 0.3 and 8.4 ± 0.3 eV are associated with formation of this ion together with an inflection in the ionization curve at about 9 eV. Possible reactions to be considered (together with their energy requirements) are

$$C_2H_4 + e \longrightarrow CH^- + CH_3$$
$$(7.1 \pm 0.1 \text{ eV} - E(CH)) \quad (28)$$

$$\longrightarrow CH^- + CH_2 + H$$
$$(12.0 \pm 0.3 \text{ eV} - E(CH)) \quad (29)$$

The value of 1.65 eV for $E(CH)$ obtained from an early study of methane[19] has been widely quoted;[20-22] however, it is informative to reexamine this value. An appearance potential of 10.2 ± 0.3 eV was obtained for CH^-/CH_4 by Smith,[19] who attributed ion formation to the reaction

$$CH_4 + e \longrightarrow CH^- + 3H \quad (30)$$

Recent thermochemical data show the calculated appearance potential of reaction 30 to be 13.7 ± 0.1 eV and this, together with a redetermination of 9.6 ± 0.3 eV for $A(CH^-)$ by von Trepka and Neuert,[6] suggests that $E(CH) \geq 4.1 \pm 0.4$ eV. This value seems excessively high and we prefer the value von Trepka and Neuert[6] obtained from a range of hydrocarbons, namely $E(CH) \geq 3.1$ eV.

Using this latter value we find that reactions 28 and 29 have minimum appearance potentials of 4.0 and 8.9 eV, respectively. This suggests that about 3 eV of excess energy are associated with the first ionization process which is due to reaction (28). If (29) is responsible for the major dissociative process at 8.4 eV then it implies that $E(CH) \geq 3.6 \pm 0.6$ eV, a value in reasonable accord with the results of von Trepka and Neuert.

(*iii*) CH_2^-. This ion, which must be formed by symmetrical splitting of ethylene, appeared at two energies 7.8 ± 0.3 and 9.1 ± 0.3 eV. The initial appearance was due to a reaction of very low cross section and has not been reported by other workers.

$$C_2H_4 + e \longrightarrow CH_2^- + CH_2$$
$$(7.7 \pm 0.4 \text{ eV} - E(CH_2)) \quad (31)$$

$$\longrightarrow CH_2^- + CH + H$$
$$(12.1 \pm 0.3 \text{ eV} - E(CH_2)) \quad (32)$$

(19) L. G. Smith, *Phys. Rev.*, 51, 263 (1937).
(20) H. O. Pritchard, *Chem. Rev.*, 52, 529 (1953).
(21) N. S. Buchel'nikova, *Usp. Fiz. Nauk.*, 65, 351 (1958).
(22) V. I. Vedeneyev, L. V. Gurvich, V. N. Kondrat'yev, V. A. Medvedev, and J. L. Frankevich in "Bond Energies, Ionisation Potentials and Electron Affinities," Edward Arnold, London, 1966.

To evaluate these reactions energetically we need to know $E(CH_2)$, and this value is uncertain. Early work on methane[19] has suggested that $E(CH_2) = -0.95$ eV but recent thermochemical data in conjunction with a redetermination of $A(CH_2^-)$ from CH_4[6] suggest $E(CH_2) \geq 0.9 \pm 0.4$ eV. Using this value then reactions 31 and 32 have minimum appearance potentials of 6.8 ± 0.8 and 11.2 ± 0.7 eV, respectively. Reaction 32 may therefore be discounted and both appearances are probably due to reaction 31, the first onset possibly occurring with a small amount of excess energy. Since the major onset occurs with about 2.3 eV of excess energy it is possible that the neutral CH_2 is formed in an excited state, possibly the triplet state.

(*d*) *Thermochemical Data.* The following heats of formation at 298°K have been used in calculations (all values in eV): F (0.8); C (7.4); H (2.3); CH (6.2); CH_2 (4.1); CH_3 (1.4); C_2H (4.9); C_2H_4 (0.5); HF (−2.8); CF (2.9); CF_2 (−1.6); CHF (1.3); CF_2H (−3.0); CH_2F (−0.3); C_2F (2.9); C_2F_2 (−3.2); C_2 (8.6); C_2HF (0.1); CH_2CF_2 (−4.3).

The heats of formation of CHF and C_2HF have been assumed to be the mean of CF_2 and CH_2 and of C_2F_2 and C_2H_2, respectively; all other values are taken from ref 23.

(23) J. L. Franklin, J. G. Dillard, H. M. Rosenstock, J. T. Herron, K. Draxl, and F. H. Field, NSRDS-NBS, 26 (1969).

Electronic Spectra of Ion-Radicals and Their Molecular Orbital Interpretation.

I. Aromatic Nitro-Substituted Anion-Radicals

by Tadamasa Shida* and Suehiro Iwata

The Institute of Physical and Chemical Research, Wako-shi, Saitama, Japan *(Received December 31, 1970)*

Publication costs assisted by The Institute of Physical and Chemical Research

A number of hitherto unknown electronic spectra have been observed for aromatic nitro-substituted anion-radicals produced in γ-irradiated rigid solutions at 77°K and are compared with an SCF–MO calculation. It is found that the strong character of the nitro group has a decisive influence on the whole electronic states of the ions and that the transitions can often be characterized clearly with simple excitation modes such as charge resonance and charge transfer between nitro groups and between nitro and hydrocarbon constituents. Systematic effects of alkylation and of twisting the nitro group are found for many cases and are accounted for consistently by the theory.

Introduction

Although quantum-mechanical calculations have had remarkable success in explaining esr spectra of ion-radicals, the interplay between theory and experiment on the excited electronic states of the radicals is rather slim. This is partly because of insufficiency of the experimental data. The observation of the electronic spectra is not easy in general owing to the high reactivity of the radicals under the usual experimental conditions.

We have established a method to produce ion-radicals by γ-ray irradiation of glassy solutions frozen at 77°K. Unambiguous spectra of the elusive radicals can be measured reliably for a variety of substances.[1,2] Utilizing the technique, we have undertaken a systematic study on the electronic state of radicals. Recently Zahradnik and Carsky[3] have begun similar studies on odd-electron systems. In our work emphasis will be placed on the presentation of informative experimental data as well as on the exploration of molecular orbital theory for the open-shell molecule. In this paper we present the results of the study on aromatic nitro anions. The reasons for choosing the system are as follows. (1) Compared with the ions of aromatic hydrocarbons, the system containing heteroatoms has been less frequently studied. (2) The existence of a multitude of nitro compounds enables us to compare isomers and related derivatives. (3) There are plenty

(1) W. H. Hamill, "Radical Ions," E. T. Kaiser and L. Kevan, Ed., Interscience, New York, N. Y., 1968, p 321.

(2) T. Shida, *J. Phys. Chem.*, **73**, 4311 (1969).

(3) R. Zahradnik and P. Carsky, *ibid.*, **74**, 1235, 1240, 1249 (1970), and succeeding papers.

of esr data of the anions to be used for the test of validity of the theory employed.

It is found that the anions show very characteristic spectral features according to the number of nitro substituents, the position of substitution, and the additional substitution by alkyl groups. These results have been successfully explained by an SCF–MO calculation.

Theoretical Section

The standard restricted SCF–CI procedure[4] was programmed using FORTRAN IV. For each symmetry the total number of 40 configurations was chosen out of the first 100 low-energy configurations of one- and two-electron excitations.[5] Of necessity, the molecular configuration of the ions was constructed with the standard bond lengths and angles of the neutral molecules. Unless otherwise stated, all the π electron systems were taken as planar. For the ions having sterically hindered functional groups, *e.g.*, the anion of *o*-dinitrobenzene, the skew angle was chosen rather arbitrarily.

As a check of our computer program we carried out calculations for several aromatic hydrocarbon anions adopting the Pariser–Parr approximation and obtained very close agreement with the result of Carsky and Zahradnik.[3] Similar calculations for the nitro compounds, however, yielded a serious disagreement with experiment when we fixed the one-center integrals as in eq 1 and 2 and changed the resonance integrals β_{C-N} and β_{N-O} within a tolerable range

$$W_\pi = -I_\pi \quad (1)$$

$$\gamma_{\pi\pi} = I_\pi - A_\pi \quad (2)$$

where I_π and A_π are the valence state ionization potential and the electron affinity of the π electron. A possible effect of charge heterogeneity in anion radicals on the one-center integrals has been examined critically and an explicit dependence of the integrals upon the density of electrons on each atom has been derived. This is a variation of Brown and Heffernan's variable electronegativity method,[6] and the details will appear elsewhere.[7] In effect, however, the heterogeneity of charge distribution itself does not account a great deal for the discrepancy between the calculated and experimental results.

However, the agreement was achieved by subtracting 1.5 eV and 2.0 eV from the one-center core integrals of nitrogen and oxygen atoms, respectively. Although the origin of the necessitated adjustment of the core integrals is not known at present, the systematic agreement with the experiment for all the ions studied seems to indicate that the parametrization may be justified by reasons yet to be found.

The two-center Coulomb repulsion integral was estimated using the Nishimoto–Mataga approximation for planar molecules, the extrapolation being made to the one-center repulsion integral modified by our treatment. For nonplanar molecules we assumed declined pairs of spheres and applied the Nishimoto–Mataga formula to each combination of spheres.

Experimental Section

It is known that the pure glassy 2-methyltetrahydrofuran (MTHF) at 77°K shows on γ irradiation a strong absorption of $\gamma_{max} \cong 1.2\ \mu$. The absorption is ascribed to the electron metastably trapped in the amorphous matrix. When the ether glass has been doped with solutes prior to irradiation, the electron band is replaced by the absorption band of solute anions. At solute concentrations of 10–100 mM, practically all the electrons liberated by irradiation are scavenged by the solute to form the anion, and clean absorption spectra of the solute anion are observed for longer wavelengths, the visible–near-infrared regions. For the near-uv–uv regions the spectra are less clean-cut because the positive ion of the matrix molecule, the counterpart product of the electron, decomposes to radical fragments which absorb in this spectral region. Moreover, most solute molecules absorb in the uv regions, so that the initial absorption of sample is too high to observe the optical change caused by the irradiation. Despite this, we attempted to extend the measurement of the spectra of solute anions to shorter wavelengths by reducing the solute concentration and the cell thickness to 0.5 mm. As the initial concentration was reduced, electrons were not completely scavenged and a residual absorption of the trapped electron appeared along with the absorption of the solute anion. The electron band, however, was easily photobleached by the red light of a tungsten lamp ($\lambda > 700$ mμ); thereby the absorption of solute anion was enhanced by the electrons released from the trap.

Since the yield of the electron per unit energy absorbed is known to be $G = 2.55$ for MTHF,[2] the yield of the solute anion is also equated to $G = 2.55$ by the assumption that all the electrons are scavenged at sufficiently high solute concentrations (10–100 mM). Therefore, the measurement of the total energy absorbed and the optical density of the anion give the extinction coefficient (ϵ) of the ion. All the ϵ values in this work have been obtained on the basis of $G(e^-) = 2.55$ and the dosimetry using the Fricke solution. Other details of the optical measurement as well as the irradiation procedure have been described elsewhere.[2] A Cary spectrophotometer, Model 14 RI, was used which was particularly suitable for the measurement of absorptions at longer wavelengths.

(4) H. C. Longuet-Higgins and J. A. Pople, *Proc. Phys. Soc., London, Sect. A*, 68, 591 (1955).

(5) We wish to thank Mr. S. Katsumata for his thorough check of the matrix element involving the two-electron excitation and of our computer program.

(6) R. D. Brown and M. L. Heffernan, *Trans. Faraday Soc.*, 54, 757 (1958).

(7) S. Iwata and T. Shida, to be published.

Table I: Nitrobenzene

	Calcd				Obsd, kK
	kK	Polarization[a]	Oscillator strength	Character[b]	
a	17.1	y	0.003	0.93 (6 → 7) pure CT	17.0
b	20.6	x	0.076	0.83 (6 → 8) − 0.40 (5 → 6)	21.2
c	28.6	y	0.075	0.94 (3 → 6) pure back CT	27 sh
d	31.4	x	0.123	−0.38 (6 → 8) − 0.40 (5 → 6) + 0.66 (4 → 7)	30.6
e	36.5	x	0.195	−0.51 (5 → 6) + 0.63 (6 → 9)	

[a] x and y are the long and the short axes of nitrobenzene, respectively. [b] Only configurations whose coefficient in the total wave function exceed 0.3 are shown in the tables. The numbers in parentheses refer to the orbitals in Figure 2. The electronic configuration (4 → 7) has two doublet states. The unprimed refers to $(4 \rightarrow 7) = 1/\sqrt{2}[|4\bar{6}7| - |4\bar{6}\bar{7}|]$, while the primed refers to $(4 \rightarrow 7)' = 1/\sqrt{6}[-2|4\bar{6}7| + |4\bar{6}\bar{7}| + |46\bar{7}|]$. This rule applies to the other cases also. The notation CT stands for the charge transfer from the nitro group to the hydrocarbon constituent. The transfer of the reverse direction will be called back CT.

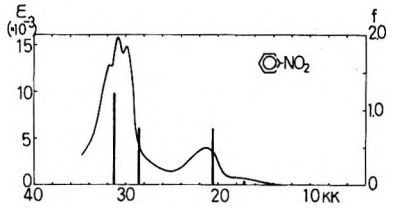

Figure 1. Absorption spectrum of nitrobenzene anion at 77°K. The sticks represent the calculated transitions shown in Table I.

Results and Discussion

(*1*) *Nitrobenzene.* Figure 1 shows the spectrum of nitrobenzene anion produced in the MTHF matrix at 77°K. The band at about 21 kK can be identified with the transition of λ_{max} 465–435 nm reported by Chambers and Adams,[8] and by Kemula and Sioda.[9] The other bands, not known previously, are also ascribed to the anion because of the general agreement with the calculated result shown in the figures and in the accompanying Table I. Although the ion produced in the presence of alkali metal cations is known to form the ion pair, Na^+, A^-, and show spectral shifts depending upon the cation,[8,10] the ions produced in the present work are free from such complication and the observed spectra can be compared with the theoretical calculation for the free ion.[11]

Figure 2 illustrates the character of the first several transitions listed in Table I. The molecular diagram and the horizontal line represent each SCF molecular orbital and its order of energy. Up to the broken line the orbitals are filled with two electrons and the orbital just above the line is half-filled in the ground state. The circles in the diagram show schematically the coefficient on each atom in each orbital. As is seen in Table I, the first few transitions can be characterized with a single or at most two or three dominant components. Thus, with these diagrams one can visualize the nature of transition. This clear-cut composition of the transition is a rather remarkable feature observed for all the ions studied in this work.

Comparison with the observed spectrum suggests that the predicted c band is overshadowed by the strong d band. This somewhat optimistic view is given credence by the result of alkylated nitrobenzenes which will be discussed in the following section. The band predicted at about 36 kK could not be detected because of the background absorption of the nitrobenzene molecule.

(*2*) *Alkylated Nitrobenzenes.* The family of spectra in Figure 3 shows the spectral shift as a function of alkylation. Since *o*-nitrotoluene is most plausibly nonplanar, the noticeable red shift of the visible band may be associated with the nonplanarity. The onset of the uv band at about 29 kK is relatively insensitive to the alkylation. If this band corresponds to the transition d of nitrobenzene anion, the insensitivity may be related to the fact that the transition consists chiefly of the local excitation of benzene anion.

The ions of 2,6-dimethylnitrobenzene and nitromesitylene are strikingly similar, both showing two bands in the near-uv region at about 29 and 31 kK and a visible band at about 18 kK. It seems that the visible bands correspond to the b bands of nitrobenzene anion and that they overshadow the longest wavelength absorption corresponding to the a band of nitrobenzene ion. The band at 18 kK of nitromesitylene is favorably compared with the absorption spectrum observed for the ion by Kemula and Sioda.[9] We presume that the bands at 28 and 31 kK correspond to the c and d bands of nitrobenzene. The manifestation of the c band may partly be due to the reduction of intensity of the d band. To support the presumption we carried out a calculation for the nitromesitylene anion. The calculation is essentially the same as that for nitrobenzene anion ex-

(8) J. Q. Chambers and R. N. Adams, *Mol. Phys.*, 9, 413 (1965).

(9) W. Kemula and R. Sioda, *Bull. Acad. Pol. Sci., Ser. Sci. Chim.*, 11, 395 (1963).

(10) E. J. Land, "Progress in Reaction Kinetics," Vol. 3, G. Porter, Ed., Pergamon Press, Elmsford, N. Y., and Oxford, 1965, p 378.

(11) T. Shida, "Proceedings of the Fourth International Congress of Radiation Research," J. F. Duplan and A. Chapiro, Ed., Gordon and Breach, New York, N. Y., 1971.

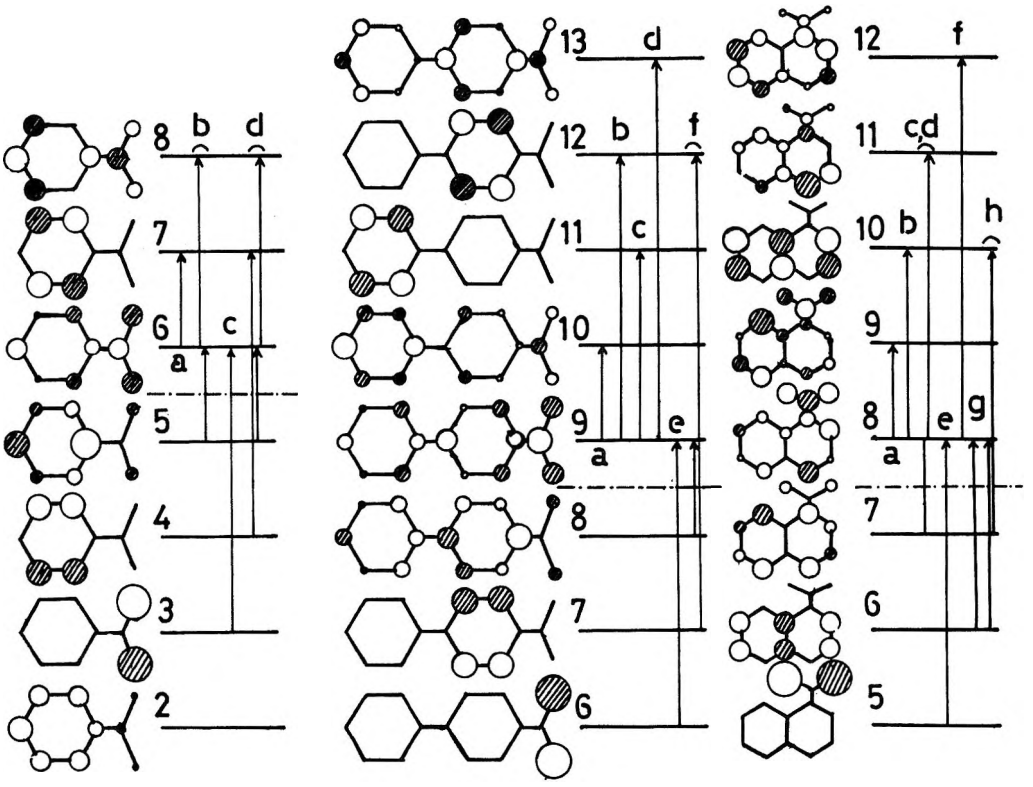

Figure 2. Molecular orbitals of nitrobenzene, *p*-nitrobiphenyl, and 1-nitronaphthalene anions and the modes of excitation. The broken line indicates that the orbitals below it are filled and the one just above it is half-filled in the ground electronic state of the ions. The vertical lines indicate the major configurations in which the molecular orbitals connected by the lines are involved in the π electron excitation. The letters correspond to the transitions in Table I.

Table II: Nitromesitylene[a]

	Calcd				Obsd, kK
	kK	Polarization	Oscillator strength	Character	
a	18.1	*y*	0.002	0.95 (6 → 7)	
b	19.0	*x*	0.076	0.89 (6 → 8)	18.0
c	29.2	*x*	0.036	0.59 (4 → 7) − 0.43 (5 → 6)	27.5
d	30.7	*y*	0.067	0.89 (3 → 6)	30.6

[a] The presence of methyl groups is ignored, and the plane of the nitro group is twisted by 60° from the plane of the benzene ring.

cept that the nitro group was assumed to be skewed by 60° out of the plane of benzene owing to the two ortho methyl groups. The calculated result shown in the stick spectrum and in Table II seems to account for the following features of the observed spectrum relative to that of nitrobenzene anion: (1) the longest wavelength absorption presumed to be overshadowed by the visible band does not shift appreciably to red; (2) the visible band shifts to the red; (3) the two near-uv bands do not shift significantly but the intensity of the absorption decreases considerably.

The result of Figure 3 indicates that the alkylation affects the spectra of anions much more profoundly than those of the corresponding neutral molecules. More examples of the effect of alkylation will be presented later.

(*3*) *Dinitrobenzenes.* The observed absorption spectra of *p*-dinitrobenzenes appear in Figure 4. The absorption at 20–32 kK of *p*-dinitrobenzene anion may be decomposed into three bands to get fair agreement with the calculation (Table III). The strong band at 10.8 kK is the prototype of the corresponding bands of the homologous *p,p'*-dinitrobiphenyl and *p,p'*-dinitrostilbene (see Figure 5 and Table IV). This is characterized as a transition between the states split from the degenerate states of AA^- and A^-A (A denoting the moiety of the three molecules mentioned above), and will be called the charge resonance (CR) band. The methylation of *p*-dinitrobenzene smears the marked vibrational structure and suppresses the intensity of absorption (Figure 4).

The calculation for *o*-dinitrobenzene was carried out

Table III: *p*-Dinitrobenzene

	Calcd				Obsd,
	kK	Polarization	Oscillator strength	Character[a]	kK
a	10.1	x	0.393	0.95 (8 → 9) CR	10.8
b	20.0	y	0.012	0.72 (4 → 8) − 0.41 (5 → 9)′ pure back CT	
c	26.0	x	0.351	0.84 (6 → 8)	23.8
d	27.3	y	0.013	0.88 (7 → 8) CT	29.0

[a] Refer to Figure 9 for the numbers in parentheses.

Table IV

	Calcd				Obsd
	kK	Polarization[a] deg	Oscillator strength	Character[b]	kK
			p,p′-Dinitrobiphenyl		
a	3.6	x	0.431	0.96 (11 → 12) CR	8.6
b	18.5	y	0.000	0.95 (11 → 15)	16.3
c	21.5	y	0.037	0.72 (5 → 11) − 0.35 (6 → 12)′	18.1
d	24.8	x	0.326	−0.33 (11 → 16) + 0.78 (10 → 11) CR	20.8
e	29.1	x	0.191	0.89 (11 → 16) + 0.33 (10 → 11) CR	
			p,p′-Dinitrostilbene (trans)		
a	3.0	5[c]	0.486	0.96 (12 → 13) CR	8.2
b	20.0	4[c]	0.002	0.97 (12 → 16)	14
c	21.8	6[c]	0.539	0.85 (11 → 12) CR	17
d	25.3	85[c]	0.031	0.93 (12 → 17)	

[a] See footnote *a*, Table I. [b] Refer to Figure 10 for the numbers in parentheses. [c] The angle measured counterclockwise from the C → N direction. The same rule applies to the other cases.

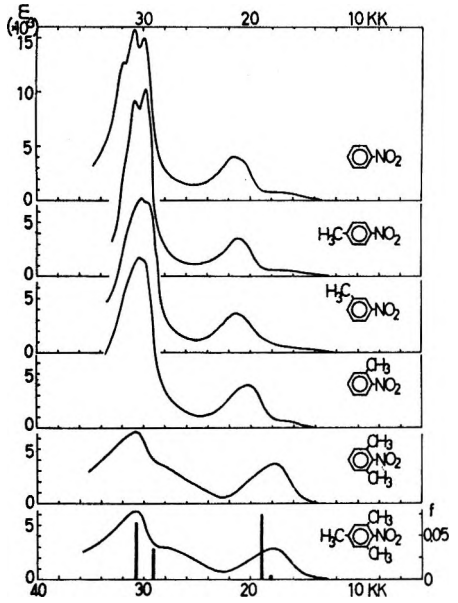

Figure 3. Absorption spectra of the anions of nitrobenzene and its alkylated derivatives.

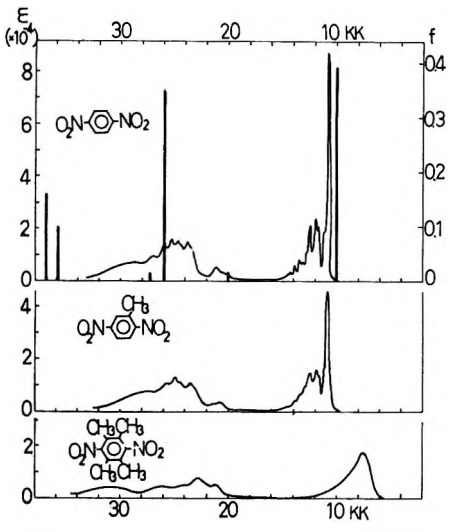

Figure 4. Absorption spectra of anions of *p*-dinitrobenzene and its alkylated derivatives.

assuming a nonplanar configuration (see footnote *a*, Table V). With this choice of configuration reasonable agreement between theory and experiment was obtained (Figure 6 and Table V). The set of spectra in Figure 7 shows the effect of alkylation on the *m*-dinitrobenzene anion. It is noted that the longest wavelength absorption ascribable to charge resonances (see Table VI) shifts to the blue with the increase of the number of

Table V: *o*-Dinitrobenzene[a]

	Calcd				Obsd, kK
	kK	Polarization[b]	Oscillator strength	Character[c]	
a	6.5	x	0.069	0.95 (8 → 9) CR	9.2
b	19.7	z, x	0.032	0.67 (8 → 10) + 0.51 (5 → 8)	~18 sh
c	20.0	y	0.010	0.78 (4 → 8)	
d	20.6	z, x	0.013	−0.59 (8 → 10) + 0.62 (5 → 8)	
e	22.9	y	0.100	0.92 (8 → 11)	22.8
f	29.8	x	0.073	0.84 (7 → 8)	28.4
g	32.3	y	0.027	0.74 (6 → 8) − 0.40 (7 → 9)′	
h	37.6	y	0.025	−0.43 (7 → 9)′ + 0.53 (8 → 12) + 0.46 (7 → 10)	37.8

[a] The plane of the two nitro groups is twisted by 30° in the same sense from the plane of the benzene ring. [b] The x is the symmetry axis; y is in the plane of benzene and perpendicular to x; z is perpendicular to the plane of benzene. [c] Refer to Figure 9 for the numbers in parentheses.

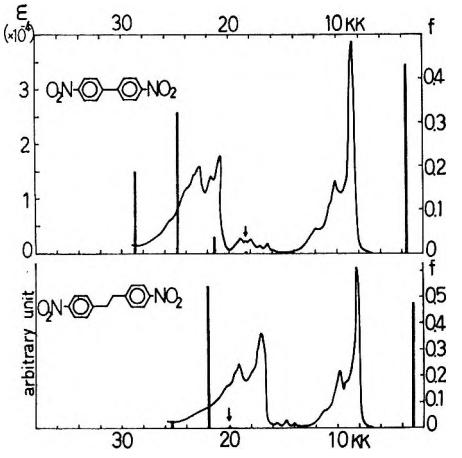

Figure 5. Absorption spectra of anions of p,p'-dinitrobiphenyl p,p'-dinitrostilbene. Owing to the poor solubility, dinitrostilbene did not scavenge electrons completely, which precluded the determination of ϵ (see Experimental Section).

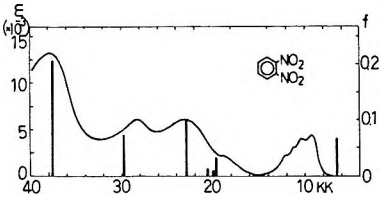

Figure 6. Absorption spectrum of *o*-dinitrobenzene anion.

methyl groups, contrary to the case of *p*-dinitrobenzene. The gradual decrease in the intensity of absorption is also noteworthy.

(4) *Mononitro- and Dinitrobiphenyls.* The survey of Figure 2 reveals that the a band of nitrobenzene anion splits to two in *p*-nitrobiphenyl (b and c bands of the latter). Similarly, the b, c, and d bands of nitrobenzene correspond to d, e, and f bands of nitrobiphenyl, respectively. The f band of nitrobiphenyl is characterized as a local excitation band of benzene anion, similar to the d band of nitrobenzene anion. If the observed band at about 25 kK (Figure 8) corresponds to

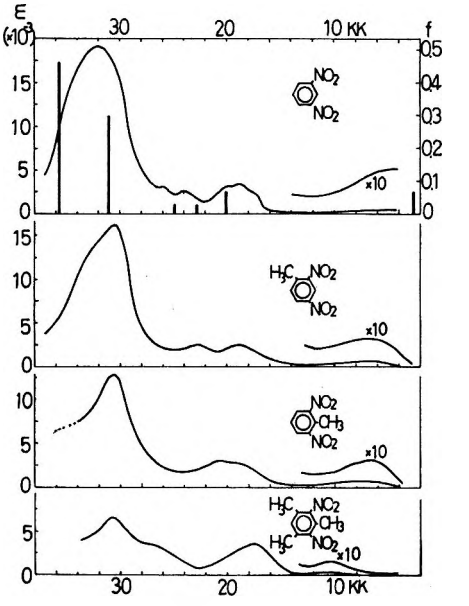

Figure 7. Absorption spectra of anions of *m*-dinitrobenzene and its alkylated derivatives.

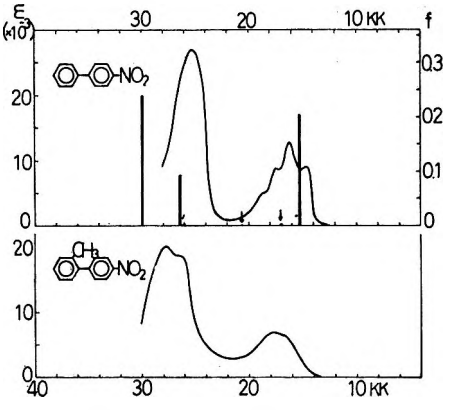

Figure 8. Absorption spectra of anions of *p*-nitrobiphenyl and its alkylated derivatives.

the f band, the discrepancy with the calculated value of 29.8 kK (Table VII) is significant. The introduction of the methyl group at the ortho′ position of *p*-nitrobi-

Table VI: *m*-Dinitrobenzene

	Calcd				Obsd, kK
	kK	Polarization[a]	Oscillator strength	Character[b]	
a	2.8	x	0.069	0.97 (8 → 9) CR	~5
b	20.0	x	0.072	0.92 (8 → 10)	18.8
c	22.8	y	0.026	0.83 (8 → 11)	24
	24.8	x	0.004	0.69 (4 → 8) + 0.41 (5 → 9)′	
d	25.0	y	0.023	0.70 (5 → 8) + 0.41 (4 → 9)′	26
e	31.1	x	0.298	0.83 (6 → 8)′ − 0.35 (7 → 8)	32
f	34.5	x	0.457	0.67 (7 → 8) − 0.34 (8 → 12)	32
g	34.8	y	0.094	−0.38 (8 → 11) + 0.56 (6 → 8) + 0.42 (7 → 9) − 0.35 (7 → 11)	32

[a] The x is the symmetry axis; y is in the plane of benzene and perpendicular to x. [b] Refer to Figure 9 for the numbers in parentheses.

Table VII: *p*-Nitrobiphenyl

	Calcd				Obsd, kK
	kK	Polarization[a]	Oscillator strength	Character[b]	
a	15.3	x	0.202	0.26G + 0.83 (9 → 10) + 0.35 (9 → 13)	15
b	17.0	y	0.003	0.96 (9 → 12)	
c	20.6	y	0.001	0.91 (9 → 11)	
d	26.0	x	0.002	0.75 (9 → 13)	
e	26.4	y	0.090	0.90 (6 → 9) back CT	~25
f	29.8	x	0.239	0.69 (8 → 9) + 0.36 (7 → 12) CT + LE (benzene)	~25

[a] See footnote *a*, Table I. [b] LE stands for local excitation.

phenyl, which will destroy the planar biphenyl skeleton, causes the blue shift of all the bands, making the spectrum somewhat similar to that of the nitrobenzene anion (lower spectrum of Figure 8). On this ground the discrepancy mentioned above seems to be associated with the biphenyl bond linking the two phenyl groups.

Comparison of the molecular diagram for *p*-dinitrobenzene (Figure 9) with that of *p,p′*-dinitrobiphenyl (Figure 10) shows that the a, b, and c bands of the form correspond to the a, c, and d bands of the latter. Similar correlation can be extended to *p,p′*-dinitrostilbene. However, the agreement of experiment with calculation becomes progressively poorer as the molecule becomes longer (Figure 5).

For *o*-nitro- and *o,o′*-dinitrobiphenyl the calculation was carried out assuming that the two phenyl groups were twisted by 60° around the biphenyl bonds. (Table VIII) The nonplanarity assumed as in footnote *c*, Table VIII gives fair agreement with the experimental result in Figure 11. It is noted that the intensity of absorption of *o*-nitro- and *o,o′*-dinitrobiphenyl is smaller than those of the meta and para isomers, similar to the case of the three dinitrobenzenes.

Both *o,o′*- and *p,p′*-dinitrobiphenyl anions have a charge resonance band at < 10 kK. Contrastingly, the *m,m′*-dinitrobiphenyl anion gives a spectrum similar to that of nitrobenzene anion (Figure 12). The calculation for the *m,m′*-dinitrobiphenyl ion gives a negative transition energy for the CR excitation (the energy becomes negative whether the anion is assumed to be trans or cis. The general comparison of the calculated result with experiment favors the trans form (Table IX). The unrealistic result suggests that the interaction between the two *m*-nitrophenyl groups is so weak as to give no appreciable level splitting for the CR band and that the negative value is a sheer calculational artifact. Therefore, we maintain that the CR band, if it occurs at all, appears in the inaccessible far-ir region. The first observable band next to the CR band is calculated to be at 11.2 kK. This band and the succeeding ones at 19.8, 25.1, and 30.5–34.4 kK have similar characters of the a, b, c, and d bands of nitrobenzene anion respectively (*cf.* Tables I and IX). The observed similarity of spectra is, thus, rationalized.

(*5*) *Mono- and Dinitronaphthalenes.* Figure 2 shows that the bands a, b, c + d, e, and h of 1-nitronaphthalene ion can be related with the bands a, b,+ c,

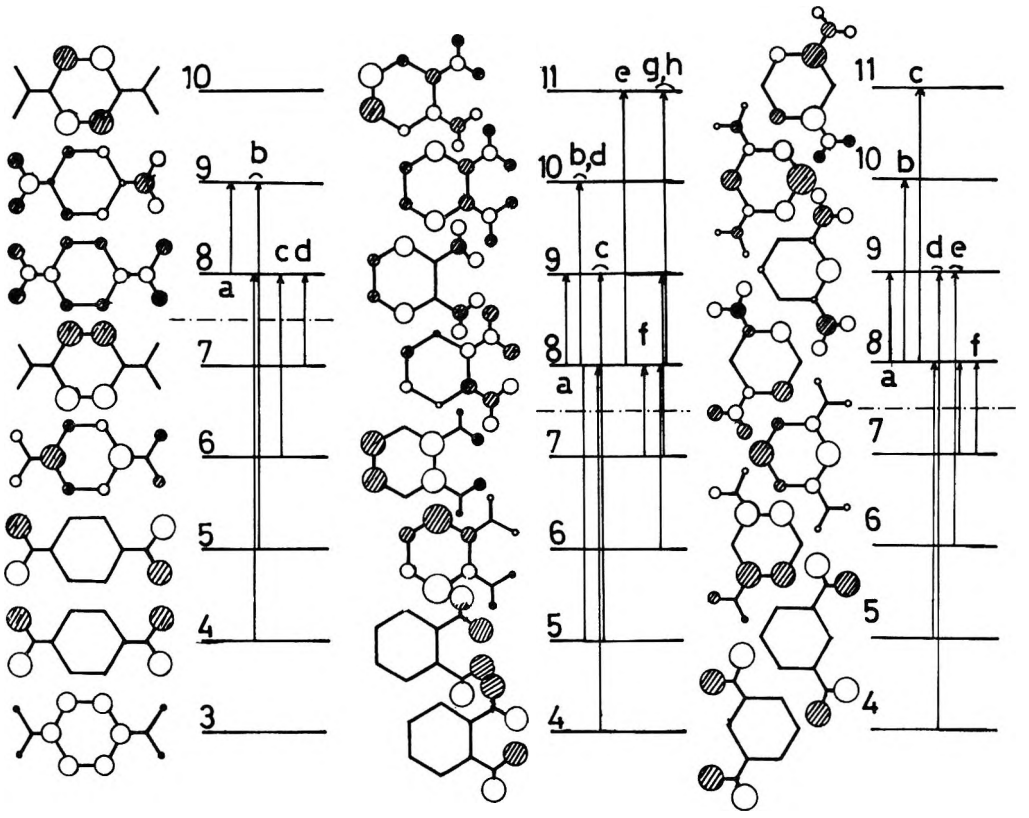

Figure 9. Molecular orbitals of dinitrobenzene anions and the modes of excitation (see the caption for Figure 2).

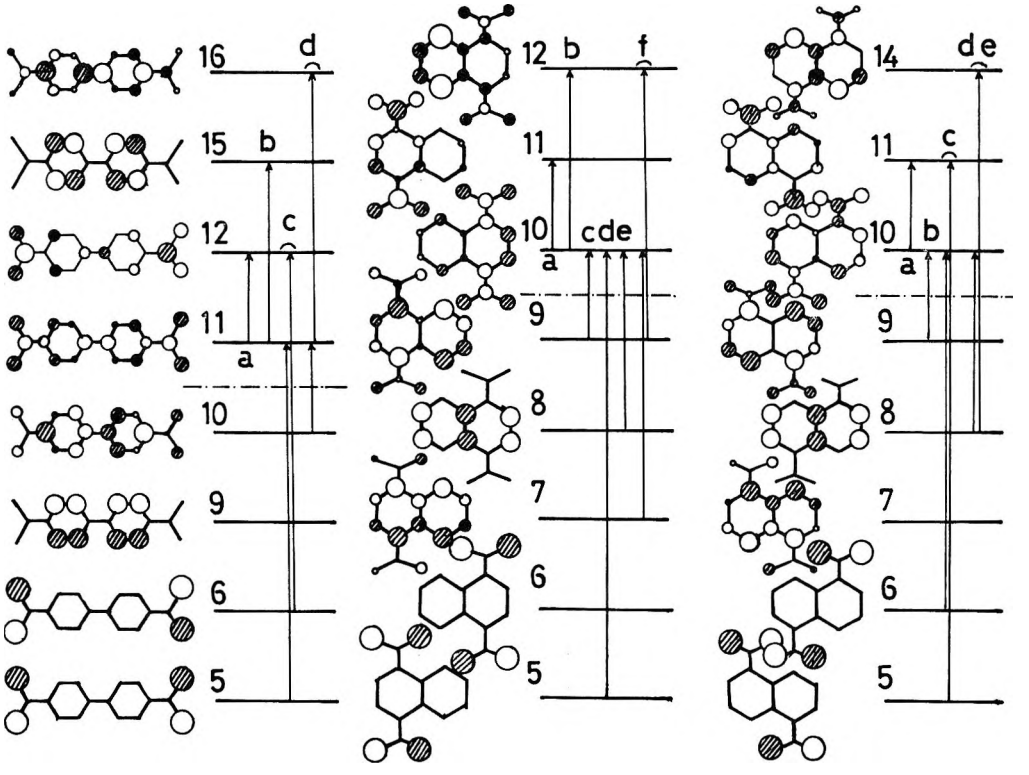

Figure 10. Molecular orbitals of anions of *p,p'*-dinitrobiphenyl and 1,4-and 1,5-dinitronaphthalene, and the modes of excitation.

d, e, and f of *p*-nitrobiphenyl ion, respectively. The latter, in turn, is closely related with the nitrobenzene anion. Thus the three ions in Figure 2 clearly demonstrate the dominant character of the nitro group. Several pieces of correspondence with the benzene and biphenyl derivatives are also seen in Figures 2 and 10.

Table VIII

Calcd				Obsd, kK
kK	Polarization, deg	Oscillator strength	Character	
			o-Nitrobiphenyl[b]	
17.0	37	0.012	0.63 (9 → 10) + 0.63 (9 → 12) − 0.38 (9 → 11)	14.0
20.4	0, Z	0.113	0.86 (9 → 13)	19.4
24.3	−46	0.001	0.50 (9 → 10) + 0.84 (9 → 11)	
25.7	36	0.013	−0.50 (9 → 10) + 0.67 (9 → 12)	27 sh
30.3	−83	0.002	0.62 (6 → 11) + 0.39 (6 → 10)	28.6
33.7	89	0.109	0.94 (5 → 9) back CT	31.2
34.5	−32	0.023	0.42 (9 → 15) + 0.45 (7 → 12) + 0.34 (7 → 10)	
38.9	1, Z	0.263	0.62 (8 → 9) + 0.50 (7 → 9) − 0.38 (9 → 15)	
			o,o'-Dinitrobiphenyl (cis)[c]	
1.6	*x*, *z*[a]	0.023	0.97 (11 → 12)	7.2
17.5	*y*[a]	0.009	0.96 (11 → 13)	15.0
20.9	*x*, *z*[a]	0.018	0.78 (11 → 14) − 0.44 (11 → 16)	20 sh
21.9	*y*[a]	0.033	0.84 (11 → 15)	22 sh
23.0	*x*[a]	0.046	−0.39 (11 → 16) + 0.65 (5 → 11) − 0.36 (6 → 12)'	
23.4	*y*[a]	0.026	0.73 (6 → 11) − 0.36 (5 → 12)' + 0.38 (6 → 12)	
23.9	*x*, *z*[a]	0.014	0.47 (11 → 14) + 0.58 (11 → 16) + 0.38 (5 → 11)	26 sh
30.6	*z*[a]	0.036	0.41 (11 → 16) + 0.62 (10 → 11) + 0.32 (10 → 13)	
32.7	*y*[a]	0.057	0.54 (10 → 12)' + 0.51 (9 → 12)' + 0.34 (8 → 11)	31.0
33.0	*x*[a]	0.015	0.44 (8 → 12)' + 0.47 (10 → 11) + 0.52 (9 → 11)	
35.2	*z*[a]	0.015	0.43 (10 → 13) + 0.35 (11 → 18)	
36.3	*y*[a]	0.123	0.54 (7 → 11) + 0.46 (10 → 12)	
36.8	*x*, *z*[a]	0.165	0.74 (8 → 12)'	

[a] The symmetry axis (C_2) is taken as x; y is the long axis of biphenyl; z is perpendicular to both x and y. [b] The plane of the phenyl group is twisted by 60° from the planar nitrophenyl group. [c] The two nitrophenyl groups are twisted by 60°.

Table IX

	Calcd				Obsd, kK
	kK	Polarization, deg	Oscillator strength	Character	
				m-Nitrobiphenyl	
a	13.6	−14	0.013	0.85 (9 → 10) + 0.41 (9 → 12) pure CT	14.5
b	20.1	12	0.109	0.61 (9 → 12) + 0.67 (9 → 13)	20.0
c	23.6	46	0.000	0.97 (9 → 11)	
d	27.0	−3	0.012	0.39 (9 → 10) + 0.58 (9 → 12) + 0.43 (9 → 13)	28 sh
e	30.9	6	0.018	0.64 (5 → 11) + 0.36 (8 → 10) + 0.36 (5 → 11)'	
f	31.8	89	0.089	0.97 (6 → 9) back CT	31.6
g	34.8	1	0.007	0.63 (8 → 11) + 0.38 (4 → 11)	
h	35.0	−1	0.035	−0.44 (5 → 11) + 0.39 (8 → 10) − 0.36 (8 → 11) − 0.32 (8 → 9)	
				m,m'-Dinitrobiphenyl (trans)	
	(−1.3)[a]	−30	0.149	0.97 (10 → 12) CR	
	11.2	12	0.025	0.98 (11 → 13)	~15
	19.8	−7	0.154	0.90 (11 → 15)	19.8
	22.7	57	0.050	0.97 (10 → 12)'	
	25.1	−7	0.034	0.40 (5 → 12)' + 0.75 (6 → 11)	~26
	28.0	60	0.002	−0.33 (11 → 15) + 0.51 (9 → 12)' + 0.49 (10 → 13)	
	30.5	6	0.117	0.74 (9 → 12)' − 0.46 (10 → 13)	30.6
	34.4	−17	0.489	0.53 (8 → 11) + 0.37 (9 → 12)	

[a] The ground state is assumed to have the *ungerade* symmetry. For the negative value of the first CR transition, see text.

Table X

	Calcd				Obsd, kK
	kK	Polarization, deg	Oscillator strength	Character[a]	
				1-Nitronaphthalene	
a	13.9	−29	0.091	0.87 (8 → 9) CT	13.4
b	18.1	90	0.006	0.94 (8 → 10) back CT	
c	25.5	−28	0.057	−0.34 (8 → 9) + 0.69 (7 → 8) + 0.53 (8 → 11)	22.2
d	27.1	6	0.093	−0.43 (7 → 8) + 0.56 (8 → 11)	27 sh
e	27.8	−70	0.075	0.87 (5 → 8) back CT	27 sh
f	31.6	26	0.010	0.71 (8 → 12)	30.5 sh
g	34.3	−33	0.052	0.75 (6 → 8)	32 sh
h	34.8	−8	0.134	0.32 (6 → 8) − 0.42 (7 → 10) + 0.40 (4 → 8)	34.2
i	39.0	49	0.075	0.84 (7 → 9)′	35.5
				2-Nitronaphthalene	
a	11.3	9	0.055	0.92 (8 → 9) CT	~12
b	20.2	31	0.091	0.90 (8 → 10) CT	18.4
c	24.8	−1	0.044	0.63 (7 → 8) − 0.53 (7 → 9) CT	24.0
d	25.9	74	0.014	0.83 (8 → 11) back CT	~25 sh
e	29.0	−58	0.103	0.91 (5 → 8) back CT	30.4
f	32.8	12	0.168	0.51 (7 → 8) + 0.55 (8 → 12) − 0.43 (7 → 10)	34.8

[a] Refer to Figure 10 for the numbers in parentheses.

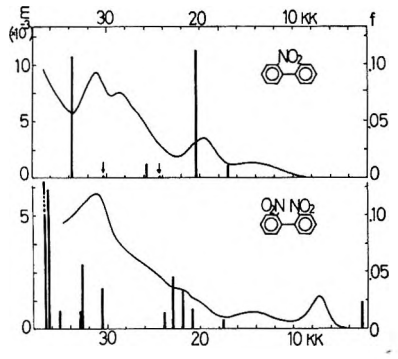

Figure 11. Absorption spectra of anions of *o*-nitro- and *o,o′*-dinitrobiphenyl.

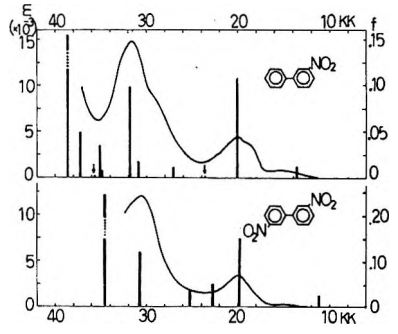

Figure 12. Absorption spectra of anions of *m*-nitro- and *m,m′*-dinitrobiphenyl.

The distinct difference between the observed spectra of 1- and 2-nitronaphthalene is well accounted for by the calculation (Figure 13 and Table X). The spectrum of 2-nitronaphthalene agrees roughly with the spectrum reported by Kemula and Sioda.[8]

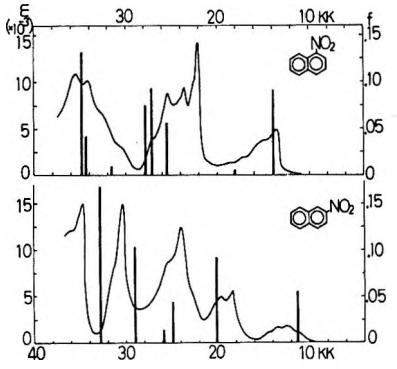

Figure 13. Absorption spectra of anions of nitronaphthalenes.

Discussion

Several features are prominent in the present work; the agreement between theory and experiment is, as a whole, satisfactory. The strong character of the nitro group has a decisive influence on the whole electronic state of the ion. Compared with neutral molecules, alkylation causes significant effects upon the electronic states of the unsubstituted ion. In most cases the first several transitions can be characterized clearly with a few excitation modes such as charge resonance, charge transfer, and local excitation. For the ions having the symmetry of D_{2h} (or near to it) a strong CR band appears as the longest wavelength abosrption, *e.g.*, *p*-dinitrobenzene, *p*-dinitrobiphenyl, and 1,4-dinitronaphthalene (Figure 14 and Table XI). When the forced

Table XI

	Calcd				Obsd, kK
	kK	Polarization[a]	Oscillator strength	Character	
				1,4-Dinitronaphthalene	
a	9.8	x	0.226	0.91 (10 → 11)	11.8
b	21.2	y	0.027	0.90 (10 → 12)	
c	21.4	x	0.276	0.83 (9 → 10)	18.0
	21.7	x	0.009	0.79 (10 → 13) + 0.39 (6 → 10)	
d	22.5	y	0.049	0.81 (5 → 10)	25
	22.8	x	0.006	0.71 (6 → 10) + 0.39 (5 → 11)	
e	28.4	y	0.043	0.86 (8 → 10)	
f	31.0	x	0.204	0.71 (7 → 10) − 0.40 (9 → 12)	30.4
				1,5-Dinitronaphthalene	
a	5.3	−30	0.163	0.95 (10 → 11)	6.7
b	20.9	−25	0.136	0.86 (9 → 10)	17.3
c	22.5	75	0.030	0.73 (6 → 10) + 0.33 (5 → 11)′ − 0.47 (5 → 11)	22
d	28.9	−28	0.125	0.75 (8 → 10) − 0.46 (10 → 14)	26.2
e	30.7	12	0.120	0.44 (8 → 10) + 0.75 (10 → 14)	
	32.7	16	0.008	0.72 (10 → 15) + 0.44 (8 → 12)	
	39.3	43	0.150	0.55 (7 → 11)′ + 0.68 (9 → 12)	
	40.8	33	0.280	0.53 (7 → 11)′ − 0.51 (9 → 12) − 0.40 (9 → 13)′	39
				1,8-Dinitronaphthalene[b]	
	4.9	x	0.032	0.96 (10 → 11)	6.8
	15.0	y	0.097	0.89 (10 → 13) − 0.39 (9 → 10)	~16
	15.2	x	0.007	0.95 (10 → 12)	17.2
	23.4	y	0.000	0.66 (5 → 10) − 0.40 (6 → 11)′	
	23.4	x	0.011	0.67 (6 → 10) − 0.39 (5 → 11)′ + 0.34 (6 → 13)	20.8
	24.5	x	0.004	0.83 (10 → 14)	
	24.6	y	0.258	0.34 (10 → 13) + 0.81 (9 → 10)	22.1
	29.5	y	0.022	0.79 (10 → 15) + 0.40 (8 → 12)	26.0
	31.8	x	0.003	0.60 (8 → 10) − 0.56 (9 → 11)′ − 0.35 (9 → 11)	
	32.2	x	0.041	0.62 (8 → 10) + 0.46 (9 → 11)′ + 0.37 (9 → 11)	29.7
	33.7	x	0.004	−0.41 (10 → 14) − 0.45 (9 → 11)′ + 0.58 (7 → 10)	
	40.0	y	0.003	0.92 (8 → 11)′	
	39.7	x	0.281	0.36 (7 → 10) + 0.82 (9 → 12)	~40

[a] The line connecting the two nitrogens is taken as the y axis, and the line perpendicular to it as the x axis. For 1,8-dinitronaphthalene, the short axis of naphthalene is taken as the y axis. [b] The two nitro groups are twisted by 30° in the same direction from the plane of naphthalene.

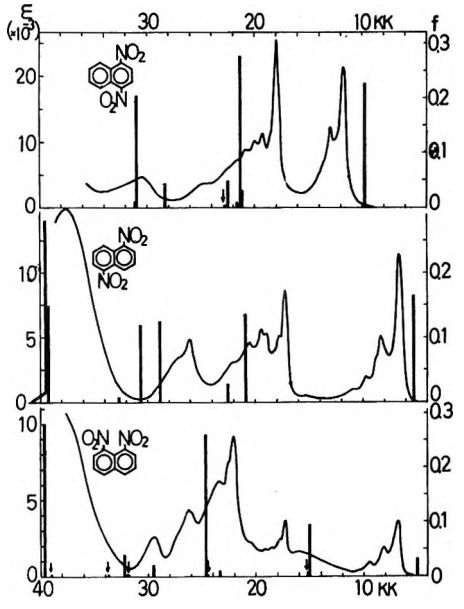

Figure 14. Absorption spectra of anions of dinitronaphthalenes.

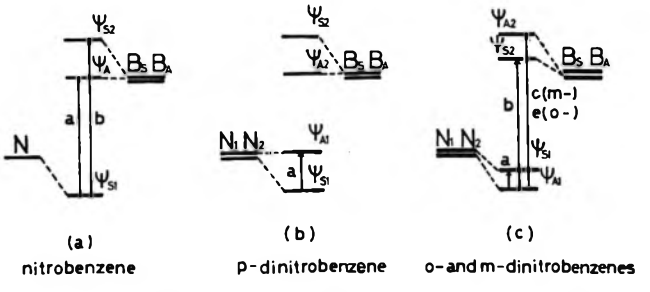

Figure 15. Schematic representation of the first few transitions of mono- and dinitrobenzene anions in terms of the one-electron model. The levels at the right and the left represent the lowest vacant orbitals of neutral benzene and nitro group, respectively. The levels at the middle represent the ground and the first few states of the aromatic nitro anions.

twisting of the molecule destroys the coplanarity of the nitrophenyl group with other parts of the molecule, the spectrum of the ion tends to be similar to that of nitrobenzene, *e.g.*, 2′-methyl-*p*-nitrobiphenyl and *o*-nitro-

biphenyl. Twisting of the nitro group out of the plane of the benzene ring tends to decrease the intensity of the LE band of benzene at about 30 kK, *e.g.*, nitromesitylene, dinitrodurene, and *o*-dinitrobenzene.

The overall survey of the results reveals that even a simple one-electron model suffices for the description of the first few transitions. For example, the first two transitions of nitobenzene anion are understandable by the simple diagram of Figure 15a. Consider the lowest vacant orbitals of neutral nitro group N and of benzene molecule, B_S(symmetrical e_{2u}) and B_A(asymmetrical e_{2u}). Then N and B_S of the same symmetry interact to yield the two levels, ψ_{S_1} and ψ_{S_2}. The two transitions indicated by the vertical lines accord well with the a and b transitions in Figure 2. Similarly, the characters of the three dinitrobenzene ions can be described roughly by the diagrams of Figures 15b and 15c. Let the orbital of two nitro groups be N_1 and N_2 and symmetrize them as N_S, $N_A = 1/\sqrt{2}(N_1 \pm N_2)$. Both N_S and N_A will be split by the respective interaction with B_S and B_A. The amount of split becomes greater as the coefficient (c) of the carbon atoms of B_S and B_A to which the nitro groups are attached becomes larger (in absolute magnitude). The coefficient for *p*-dinitrobenzene are $c_S^2 = 1/2$ and $c_A^2 = 0$, while for *o*- and *m*-dinitrobenzene, $c_S^2 = 1/12$ and $c_A^2 = 1/4$. Therefore, the interaction between N_S and B_S is larger than that between N_A and B_A for *p*-dinitrobenzene to make ψ_{S_1} the ground state as shown in Figure 15b. The reverse is true for ortho and meta isomers (Figure 15c). The transition between ψ_{S_1} and ψ_{A_1} is designated the charge resonance transition in the above discussion. Only the CR transition is allowed for *p*-dinitrobenzene, while three transitions are allowed for ortho and meta isomers, which accounts for the simpler spectrum of the former. (Note that the excitation character of the c band of *p*-dinitrobenzene is beyond the capacity of the simplified description in terms of the one-electron model.)

The spin density of the ground electronic state has been calculated for all the anions studied in this work except for the alkylated derivatives and compared with the experimental result of Rieger and Fraenkel.[12] The calculated spin density plotted against the experimental splitting constant yields a straight line similar to that in Figure 1 of the cited reference. However, the proportionality constant, $Q_{CH}{}^H$, connecting the experimental proton hyperfine splittings, a^H, and the calculated spin density, ρ^π, turned out to be 27.8 instead of 23.7 of ref 12 where the spin density was calculated by the McLachlan procedure.

Acknowledgment. The authors wish to acknowledge the comments of Dr. M. Imamura and Dr. M. B. Robin.

(12) P. H. Rieger and G. K. Fraenkel, *J. Chem. Phys.*, **39**, 609 1963).

Microwave Absorption and Potential Barrier for Orientation. Sulfur Dioxide Adsorbed on Sodium Chloride and Potassium Chloride

by Tsvia Ron and M. Folman*

Department of Chemistry, Technion-Israel Institute of Technology, Haifa, Israel *(Received January 11, 1971)*

Publication costs borne completely by The Journal of Physical Chemistry

Microwave absorption of SO_2 adsorbed on finely powdered NaCl and KCl has been investigated in the 3000-MHz region. From T tan δ *vs.* temperature dependence the relaxation time and free energy of activation for orientation were calculated. The energy of interaction of the molecule with the solid adsorbent was computed for different adsorption sites and orientations of the adsorbate and as a function of angle of rotation. The computed values of heat of adsorption and potential barrier for orientation were in good agreement with the experimental ones.

Previous work from this laboratory was concerned mainly with microwave absorption of molecules adsorbed on silica-type adsorbents.[1-3] This substrate is not suitable for quantitative treatment, due to its irregular structure. Recently, work concerned with COS adsorbed on NaCl crystals was reported,[4] in which calculations of adsorbent–adsorbate interactions and dielectric absorptions were described.

(1) U. Feldman, Ch. Schonfeld, and M. Folman, *Trans. Faraday Soc.*, **59**, 2394 (1963).
(2) U. Feldman and M. Folman, *ibid.*, **60**, 440 (1964).
(3) I. Lubezky, U. Feldman, and M. Folman, *ibid.*, **61**, 940 (1965).
(4) I. Lubezky and M. Folman, *ibid.*, **67**, 222 (1971).

In the present work microwave absorption measurements were carried out on SO_2 adsorbed on NaCl and KCl crystals. The extended Fröhlich model[5] was used to describe the absorption mechanism. The free energy of activation for reorientation of the adsorbate was derived by calculating the adsorption potentials as a function of the orientation and the distance of the adsorbed molecule from the surface.

For a complete rotation of the SO_2 molecule in the $x = 0$ or $y = 0$ plane around an axis parallel to the surface, two minima, one at 0° and the other at 180° separated by a maximum at 100°, were found. The angle of rotation α was that between the axis of the molecule and the normal to the surface. The free energy of activation for orientation was calculated from the difference between the values of adsorption potentials at 180 and 100°. The lower minimum at 0° which represents the equilibrium orientation agreed well with the experimental values of the heats of adsorption. Experimental values for $\Delta F^{\ddagger}$ calculated by means of the Debye expression for dilute solution, which is identical with the one obtained by means of the present model, were in good agreement with the theoretical ones.

Experimental Section

The dielectric absorption was measured by means of a microwave system operating at a frequency of 3000 MHz. The apparatus was based on a sensitive heterodyne beat method, in which the solid adsorbent is placed inside a resonance cavity.[1] The cavity, operating in the TH_{01} mode, was of transmission type made of brass and silver plated on the inside. The coupling of the cavity to the microwave system was through loops of silver wire passing in vacuum-tight Teflon leads. A more detailed description of the cavity and the method of measurements were given previously.[6]

The configuration of the electric field in the cavity requires a rod-shaped adsorbent. Accordingly, a sample of this shape was sited in a cylindrical Teflon basket with thin, perforated walls. This basket was connected to an iron holder to lift it into a vacuum-sealed quartz tube, when desorption was carried out. During desorption of the sample an electric furnace was placed around the tube and the sample was heated up to 475°K. Measurements were done in the temperature range 150 to 230°K. The temperature was controlled to within 0.5°K.

Theory of Measurement

To calculate the loss tangent, expressions derived by Jackson, *et al.*,[7] for a partially filled cavity were used. For such a case, the loss factor, tan δ, is given by

$$\tan \delta = K\left(\frac{1}{Q} - \frac{1}{Q_1}\right) \tag{1}$$

where Q and Q_1 are the quality factors of the cavity containing the sample at any surface converage and the bare adsorbent, respectively. Q_1 was evaluated from the resonance curve displayed on a double beam oscilloscope, its half-power width being measured with the help of frequency markers obtained by using a highly stabilized C.W. oscillator. Q can be expressed in terms of Q_1 and the power transmitted through the cavity. If the energy level on the scope is kept constant during adsorption by means of a calibrated precision attenuator connected in series with the cavity, eq 1 may be written as

$$\tan \delta = \frac{K}{Q_1}(10^{\Delta/20} - 1) \tag{2}$$

where Δ is the difference in readings of the attenuator. K is given by[7]

$$K = \frac{\left(\frac{a}{b}\right)^2 + F^2\left(\frac{\epsilon_1}{\epsilon_0} - 1\right)}{\frac{\epsilon_1}{\epsilon_0}F^2\left[1 + \frac{J_1^2(\beta_1 b)}{J_0^2(\beta_1 b)}\right]} \tag{3}$$

where a is the cavity radius, b the radius of the adsorbent sample, ϵ_1 and ϵ_0 are the dielectric constants of the sample and the free space, respectively. J_1 and J_0 are Bessel functions of the first order, $\beta_1 = \beta_0\sqrt{\epsilon_1/\epsilon_0} = 2\pi/\lambda_0\sqrt{\epsilon_1/\epsilon_0}$, λ_0 is the free space wavelength, and F is defined by

$$F \equiv [Y_0(\beta_0 a)J_0(\beta_0 b) - Y_0(\beta_0 b)J_0(\beta_0 a)]\frac{\beta_0 \pi a}{2} \tag{4}$$

where Y_0 is the second-order Bessel function. The ratio ϵ_1/ϵ_0 is a complicated function of a and b. Provided, however, that the sample radius and the ratio ϵ_1/ϵ_0 to be determined are not too large,[7] the explicit expression may be used

$$\frac{\epsilon_1}{\epsilon_0} = 1 + \frac{\left(\frac{a}{b}\right)\frac{J_0(\beta_0 a)}{J_1(\beta_0 b)}}{F\left[1 + \frac{(\beta_0 b)^2}{8}\right] + \frac{(\beta_0 b)^2}{8}\frac{a}{b}\frac{J_0(\beta_0 a)}{J_1(\beta_0 b)}} \tag{5}$$

To check the validity of the described procedure, the dielectric constant of NaCl and KCl was obtained by inserting a rod-shaped sample (made of pressed powder) of known dimensions into the center of the cavity and measuring the resonance frequency. Using eq 5, ϵ_1 was calculated for the powdered salt. By means of the Böttcher equation[8] for powders, the dielectric constant for the bulk phase was obtained. The so obtained ϵ

(5) J. D. Hoffman and H. G. Pfeiffer, *J. Chem. Phys.*, **22**, 132 (1954).

(6) T. Ron and M. Folman, *J. Phys. Chem.*, **75**, 532 (1971).

(7) F. Horner, T. A. Taylor, R. Dunsmuir, J. Lamb, and W. Jackson, *J. Inst. Elec. Eng.*, **93**, 53 (1946).

(8) C. J. F. Böttcher, "Theory of Electric Polarisation," Elsevier, Amsterdam, 1952.

values were $\epsilon_{NaCl} = 5.24$ and $\epsilon_{KCl} = 4.30$. The corresponding values taken from the literature[8] are 5.7 and 4.7, respectively. Taking into account the fact that the Böttcher equation gives approximate values only and that the values given in the literature are for much lower frequencies, the agreement may be considered good enough to justify the use of the procedure described.

Materials and Sample Preparation. The NaCl and KCl adsorbents were of analytical grade. The salts were heated to about 400°K to remove adsorbed water; then they were ground in a ball mill for 24 hr in a dry atmosphere. From the fine powder, tablets were obtained by means of a hydraulic press. The tablets were piled in a Teflon basket, thus forming a rod-shaped sample 20 mm in diameter and about 50 mm high. The sample was evacuated at 475°K for 8 hr prior to any measurement.

The specific surface areas obtained by the B.E.T. method, using argon as adsorbate were 1.7 and 0.50 m^2/g for the NaCl and KCl sample, respectively. The total weights were 23.9 g for NaCl and 27.0 g for KCl.

SO_2 of spectroscopic grade was supplied by J. N. Matheson and Co. It was further purified by bulb-to-bulb distillation and multiple freezing.

Results and Discussion

The adsorption isotherms of SO_2 on NaCl and KCl samples are shown in Figures 1 and 2. From these, isosteric heats of adsorption q^{st} were calculated. The q^{st} were practically constant for the range of surface coverages measured and equal to 8.85 kcal/mol for SO_2 adsorbed on pressed NaCl powder and 7.15 kcal/mol for the loose powder. The isosteric heat for adsorption on KCl loose powder was 6.9 kcal/mol. The tan δ values as a function of surface coverage at different temperatures are given in Figures 3 and 4.

Since the absorption of the solid adsorbents is very low, the Debye equation for dilute solutions of a polar solute in a lossless solvent was used. The expression for $T \tan \delta$ is

$$T \tan \delta = \frac{(\epsilon + 2)^2}{\epsilon} \frac{4\pi\mu^2 cN}{27k} \frac{\omega\tau}{1 + \omega^2\tau^2} \qquad (6)$$

where ϵ is the dielectric constant of the adsorbate–adsorbent system, k the Boltzmann constant, μ the

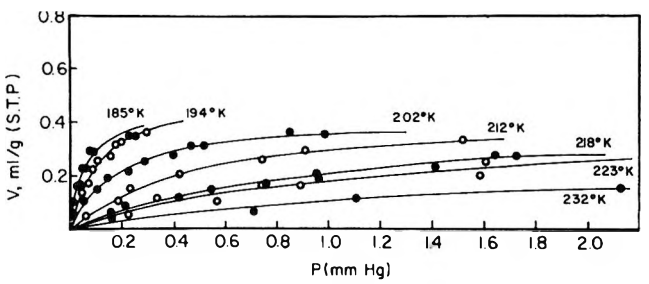

Figure 1. Adsorption isotherms of SO_2 on NaCl.

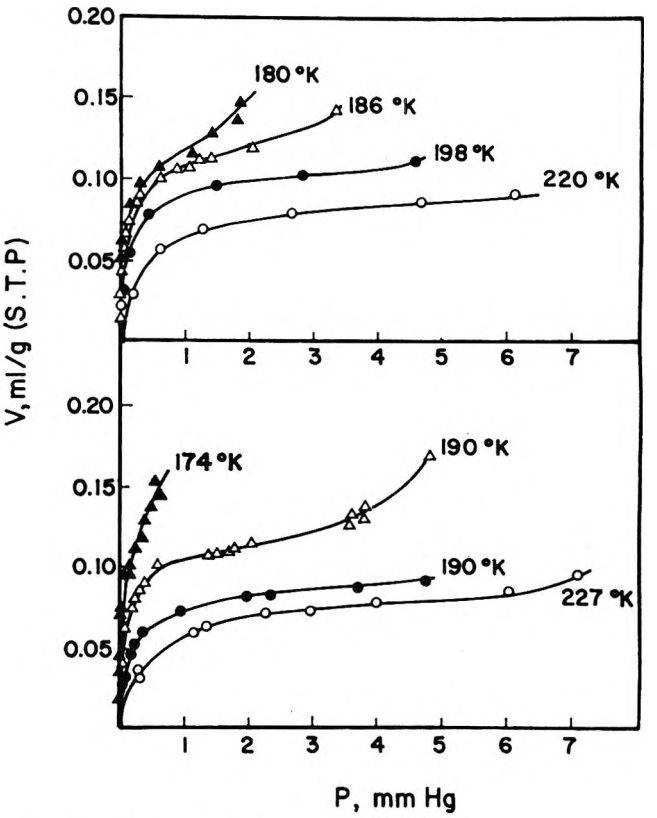

Figure 2. Adsorption isotherms of SO_2 on KCl.

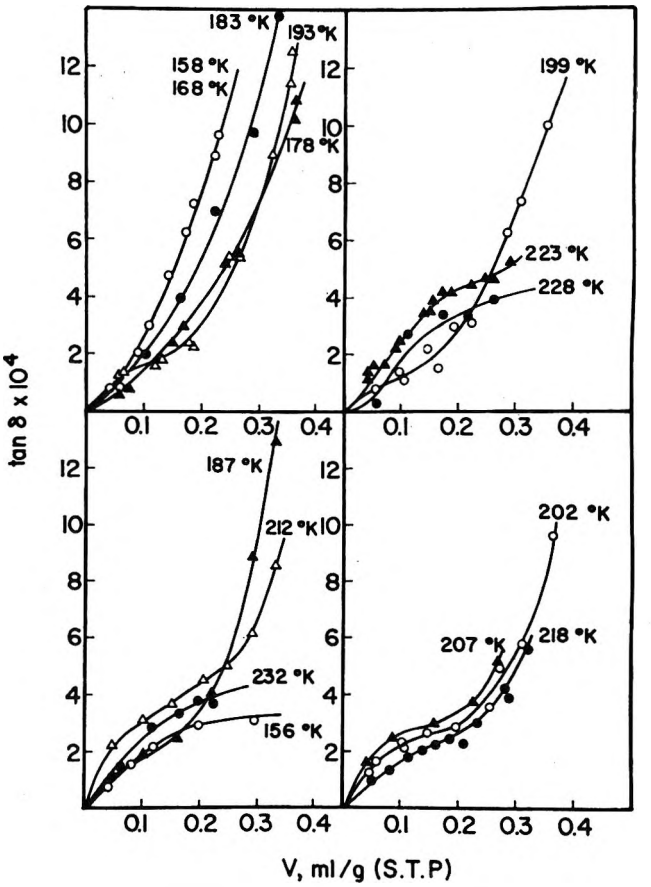

Figure 3. Plots of tan δ *vs.* volume of SO_2 adsorbed on NaCl at 3000 MHz.

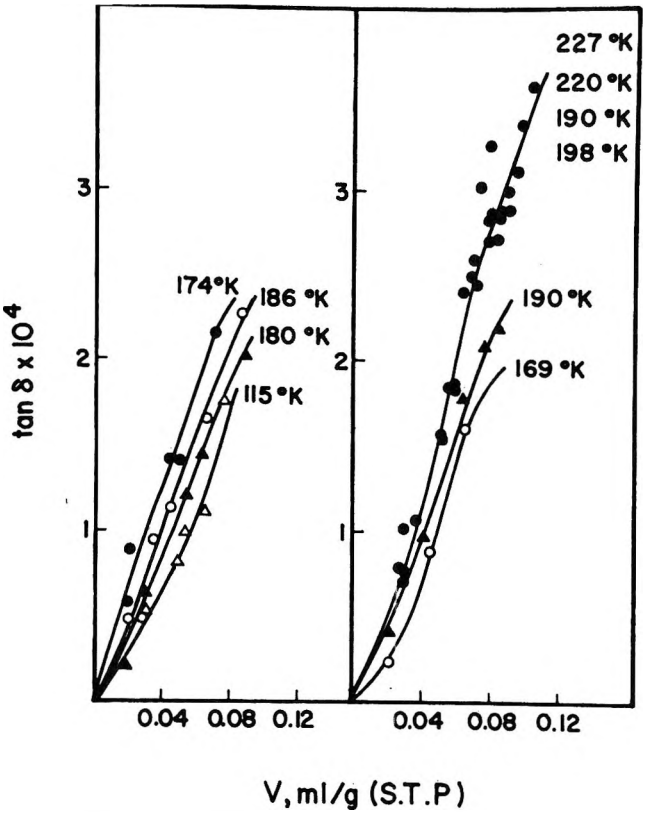

Figure 4. Plots of tan δ *vs.* volume of SO_2 adsorbed on KCl at 3000 MHz.

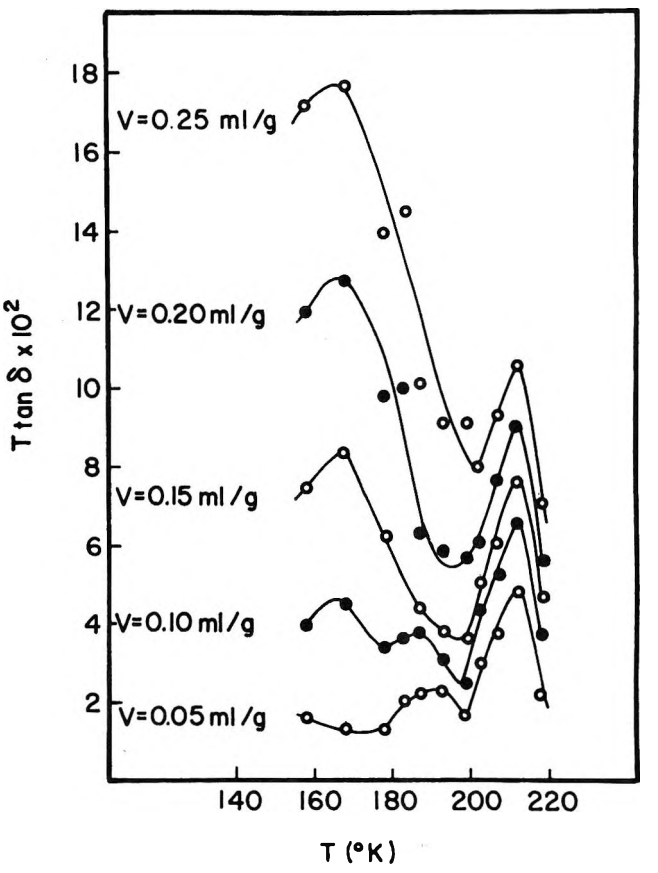

Figure 5. T tan δ *vs.* temperature plots at 3000 MHz for SO_2 adsorbed on NaCl, at constant coverages.

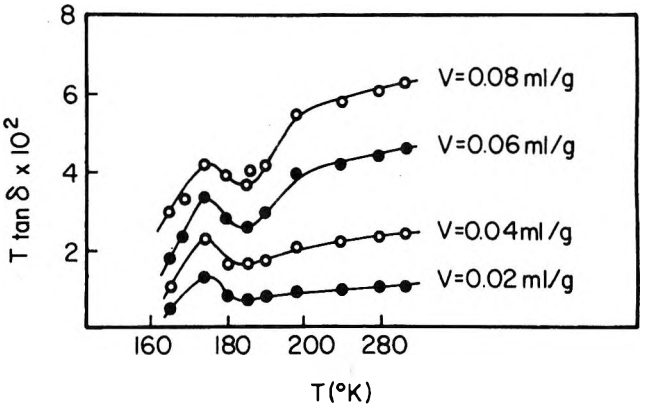

Figure 6. T tan δ *vs.* temperature plots at 3000 MHz for SO_2 adsorbed on KCl, at constant coverages.

dipole moment, c the concentration in moles per milliliter, ω the frequency of the system, and τ the relaxation time. As it was stressed already in the introduction, this equation may be derived from Fröhlich's model.

It may easily be shown that the curve of T tan δ as a function of T (or ω) will reach a maximum at the point where $\omega\tau = 1$. Since ω is known, the relaxation time, τ, can be obtained. From the expression of the reaction rate theory[5]

$$\tau = \frac{h}{kT} \exp \frac{\Delta F^{\ddagger}}{RT} \qquad (7)$$

$\Delta F^{\ddagger}$, the free energy of activation, may be calculated.

Plots of T tan δ against temperature at constant coverages are given in Figures 5 and 6. Figure 5 shows that SO_2 adsorbed on NaCl has two absorption regions, with maxima at 213 and 168°K. The $\Delta F^{\ddagger}$ values calculated by means of eq 7 are 2.30 and 1.75 kcal/mol, respectively.

Figure 6 (SO_2 on KCl) shows the existence of one maximum at 174°K followed by an increase in T tan δ at higher temperatures. In the region 198–227°K, T tan δ remains constant. $\Delta F^{\ddagger}$ calculated from the maximum at 174°K was 1.83 kcal/mol.

Adsorption Potentials and Activation Energies for Reorientation. Adsorption potentials for SO_2 adsorbed on the two adsorbents were calculated for several sites, of which Na^+ and K^+ cations were found to be the most energetic ones. The energies of adsorption on the Cl^- ion on KCl, in the center of the unit cell and the center of the cell edge, were found less than half the energy obtained for the cations.

The adsorption potential was taken as a sum of dispersion, induction, dipole, quadrupole, and repulsion potentials

$$\phi = \phi_D + \phi_E + \phi_I + \phi_Q + \phi_R \qquad (8)$$

The assumption of additivity of the different potentials was successfully used by other investigators.[9]

The dispersion potential, ϕ_D, has been calculated using the Kirkwood–Müller formula,[10] which for interactions between the adsorbate and the adsorbent is given as a sum of pair interactions with each lattice point of the adsorbent. When written in terms of the lattice parameter, a, and $\rho = r/a$ where $-r$ is the distance of the absorbent molecule from the surface, the equation becomes

$$\phi_D = \frac{6mc^2}{a^6}\left[\frac{\alpha_0\alpha_+}{\alpha_0/\chi_0 + \alpha_+/\chi_+} S_+(\rho) + \frac{\alpha_0\alpha_-}{\alpha_0/\chi_0 + \alpha_-/\chi_-} S_-(\rho)\right] \quad (9)$$

where m is the mass of the electron, c the velocity of light, α is polarizability of the interacting particles, and χ the magnetic susceptibility. The subscripts 0, +, and − refer to the adsorbate, the alkali ion, and the halogen ion, respectively. $S_+(\rho)$ and $S_-(\rho)$ are summations of the inverse sixth power of the distances of the adsorbate and the interacting ions. Summation was done over 550 ions using a computer.

An additional contribution to dispersion potential is given by the induced dipole–quadrupole interaction as[11]

$$\phi_D' = -\frac{1}{a^8}\frac{45h^2}{32\pi^2 m}\left\{\alpha_0\alpha_+\left[\frac{1}{2\left(\frac{\alpha_0}{\chi_0}\Big/\frac{\alpha_+}{\chi_+}\right)+1} + \frac{1}{2\left(\frac{\alpha_+}{\chi_+}\Big/\frac{\alpha_0}{\chi_0}\right)+1}\right] S_+'(\rho) + \alpha_0\alpha_-\left[\frac{1}{2\left(\frac{\alpha_0}{\chi_0}\Big/\frac{\alpha_-}{\chi_-}\right)+1} + \frac{1}{2\left(\frac{\alpha_-}{\chi_-}\Big/\frac{\alpha_0}{\chi_0}\right)+1}\right] S_-'(\rho)\right\} \quad (10)$$

where $S_+'(\rho)$ and $S_-'(\rho)$ are summations of the inverse eighth power of the distances.

The induction, dipole, and quadrupole potential depend on the electrostatic field above the crystal surface. The electrostatic potential for a (100) plane of an fcc lattice is given by Lennard-Jones and Dent[12] as

$$\phi = \frac{4\nu e}{2a}\left[\sum_{l,m}\frac{(-1)^{(l+m)/2}}{l^2+m^2}\cos\pi\times\left(\frac{lx}{a}+\frac{my}{a}+\frac{l+m}{2}\right)\frac{\exp(-\pi\rho\sqrt{l^2+m^2})}{1+\exp(-\pi\sqrt{l^2+m^2})}\right] \quad (11)$$

where l and m are integers, ν is the valence of the two ions, and e is the charge of the electron. Due to the rapid converge of this expression the summation may be performed only over l and m such at $l^2 + m^2 = 2$.

The induction potential is given by

$$\phi_I = -{}^1/_2\alpha_0 F^2 \quad (12)$$

where $F = -\text{grad}\ \phi$, α_0 is the mean polarizability of the adsorbate.

The dipole potential is given by

$$\phi_E = -\vec{\mu}\cdot\vec{F} \quad (13)$$

The quadrupole potential is

$$\phi_Q = {}^1/_2 Q\frac{\partial^2\phi}{\partial t^2} \quad (14)$$

where Q is the quadrupole moment of the adsorbate and t is taken along its axis of symmetry.

The repulsion potential was taken in the usual way as a geometrical mean of the repulsion functions of the adsorbent and the adsorbed molecule in the gas state. The usual expression of repulsion potentials, $B\exp(-cr)$, was used for the crystal ions, while the repulsion term in the Lennard-Jones potential, $4\epsilon(\sigma/r)$,[12] was taken to describe the adsorbate repulsion. The final expression for the repulsion potential was given by

$$\phi_R = (4\epsilon B)^{1/2}\left(\frac{\sigma}{\rho}\right)^6\frac{1}{a^6}\exp\left(-\frac{ca\rho}{2}\right) \quad (15)$$

where B, c, ϵ, and σ are characteristic constants. The values of ϕ_R decrease rapidly so that summation over 20 ions is practically sufficient. Nevertheless, as it was convenient to calculate it in conjunction with the dispersion terms, the summation was done over 550 ions as well.

The model used for the calculations was that of a rigid linear dipole with a single axis of rotation. Since the geometrical center of SO_2 overlaps with the center of mass, this was taken as the center of interaction for all the potentials given above.

The dipole was allowed to rotate around an axis parallel to the surface. It may be shown that for the described model, the potential function will not change with rotation around a perpendicular axis, if the molecule is situated on a lattice point.

The values of parameters used in the calculations are given in the Appendix.

The Q value used in the calculations was taken from the literature.[13] There it was obtained by assuming that a single scalar would describe the molecular quadrupole moment and must be regarded as an effective value. It is, however, believed that this approximation is quite acceptable in view of the used model.

(9) D. M. Young and A. D. Crowell, "Physical Adsorption of Gases," Butterworths, Washington, D. C., and London, 1962.

(10) A. Müller, *Proc. Roy. Soc., Ser. A*, **154**, 624 (1936).

(11) N. N. Avgul, A. A. Isirikyan, A. V. Kiselev, I. A. Lygina, and D. P. Poshkus, *Bull. Acad. Sci. USSR, Div. Chem. Sci.*, 1314 (1957).

(12) J. E. Lennard-Jones and B. M. Dent, *Trans. Faraday Soc.*, **24**, 92 (1928).

(13) D. E. Stogryn and A. P. Stogryn, *Mol. Phys.*, **11**, 371 (1966).

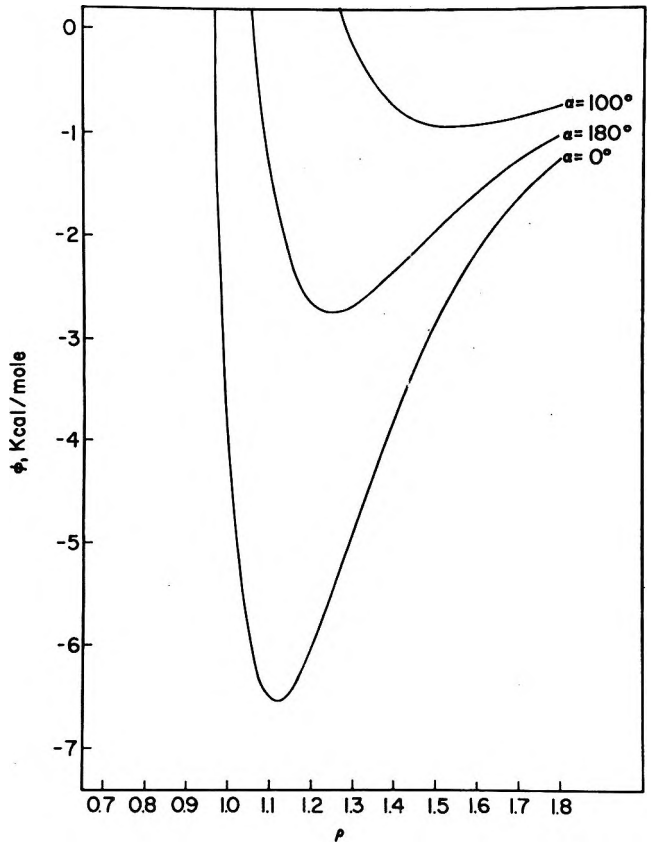

Figure 7. Adsorption potential curves of SO_2 on (100) plane of NaCl in different orientations.

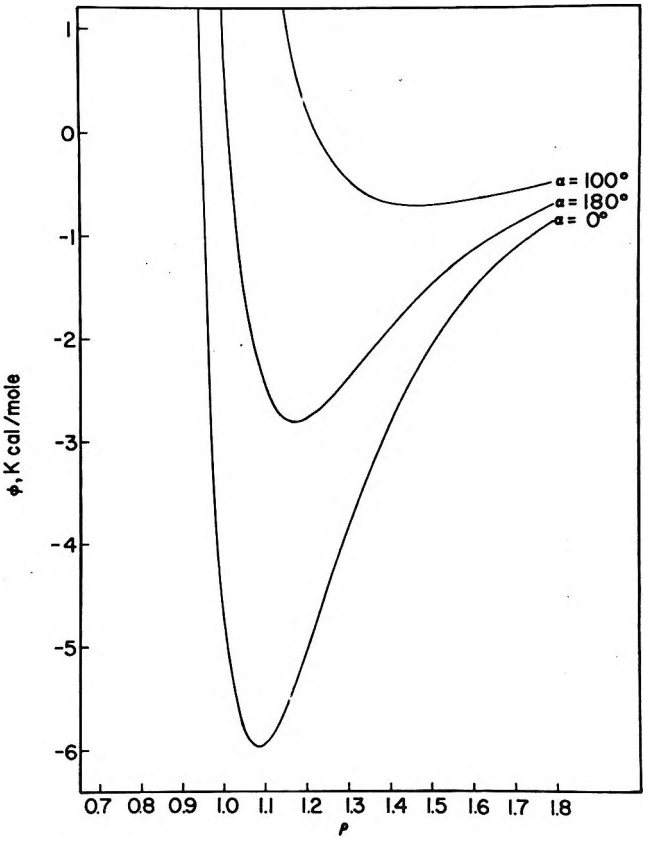

Figure 8. Adsorption potential curves of SO_2 on (100) plane of KCl in different orientations.

The total adsorption potential was plotted as a function of the distance from the surface, for different orientations of the adsorbate. These potentials are shown in Figures 7 and 8 for orientations of $\alpha = 0$, 100, and 180°. The potential at the minimum of the curve is related to the adsorption heat for a given orientation by

$$\Delta H = (\phi_{min} + \epsilon_0) - RT \qquad (16)$$

where ΔH is the enthalpy of adsorption, ϵ_0 is the zero-point energy (per mole) and is $^1/_2Nh\nu$. ν, the vibrational frequency normal to the surface, is given by $(^1/_{2\pi})\sqrt{f/m}$, where f is the force constant and m is the mass of the SO_2 molecule. The force constant was derived using the assumption of a parabolic shaped potential near the minimum.

ϕ_{min} as a function of the angle of rotation is given in Figures 9 and 10. It is clearly seen that the lowest energy is obtained for $\alpha = 0°$ (when the O atoms are pointing to the cation). It was also found that in connection with the rotation process, the equilibrium distance of the molecule from the surface oscillates between its values at the $\alpha = 0$ and 100° positions.

For SO_2 adsorbed on NaCl the following values were obtained at $\alpha = 0°$: $\rho^\circ_{min} = 1.15$ ($r = 3.24$ Å), $\phi^\circ_{min} = -6.55$ kcal/mol and $\nu^\circ = 2.8 \times 10^{12}$ sec^{-1}. ΔH obtained by means of eq 16 is -6.75 kcal/mol, which is in good agreement with the experimental isosteric heat of 7.15 kcal/mol obtained for loose powder, whereas strongly pressed tablets gave q^{st} of 8.85 kcal/mol. At $\alpha = 180°$ another minimum exists where $\rho_{min}^{180} = 1.26$ ($r = 3.53$ Å), $\phi_{min}^{180} = -2.76$ kcal/mol, and $\nu^{180} = 1.29 \times 10^{12}$ sec^{-1}. The adsorbed molecule has to overcome a potential barrier while rotating. This barrier is obtained at $\alpha = 100°$ with $\rho_{min}^{100} = 1.55$ ($r = 4.36$ Å), $\phi_{min}^{100} = -0.93$ kcal/mol, and $\nu^{100} = 0.46 \times 10^{12}$ sec^{-1}.

It seems that among the existing theories of dielectric absorption in solids, the theory of Fröhlich[14] is most adequate for the purpose of adaptation for the adsorbed state. According to this theory, there exist several equilibrium positions separated by potential barriers, for dipoles in a polar solid. In the absence of an external electric field all these orientations are energetically equivalent. When an external field is applied, the potential minima are changed slightly; this in turn affects the population of these states, and therefore the system becomes polarized. The rate of change of this polarization with time leads to a kinetic expression which defines the relaxation time of the process

$$\frac{1}{\tau} = K = A \exp\left(-\frac{\Delta E}{RT}\right) \qquad (17)$$

(14) H. Fröhlich, "Theory of Dielectrics," 2nd ed, Oxford Clarendon Press, London, 1958.

where ΔE is the height of the potential barrier separating two equilibrium positions, τ is the relaxation time, and K is the rate constant for the process. This equation is analogous to the well-known expression of the absolute rate theory (eq 7).

Fröhlich's model has been extended to the case where the orientational sites are not equivalent.[5] For the simple case of only two different orientational sites τ is given by

$$\tau = \frac{1}{(K + K')} \tag{18}$$

where K and K' are the rate constants for the orientation of the dipole from position (site) 1 to position (site) 2, and in the reverse direction, respectively. Since K depends exponentially on $\Delta F^{\pm}$, it is possible to neglect K' in eq 18 as compared to K if the difference between the two $\Delta F^{\pm}$ values is large as compared to RT. Then, the whole relaxation process is governed by the rate constant corresponding to the lower value of $\Delta F^{\pm}$. From Figure 9 it is seen that the rate-determining magnitude will be $\Delta F^{\pm}$ connected with the difference between $\phi_{min}{}^{100}$ and $\phi_{min}{}^{180}$. After correction for vibrational and $T\Delta S^{\pm}$ terms, $\Delta F^{\pm}$ is given by

$$\Delta F^{\pm} = \Delta H^{\pm} - T\Delta S^{\pm} =$$

$$\phi_{min}{}^{100} - \phi_{min}{}^{180} + \epsilon_0{}^{100^\circ} - \epsilon_0{}^{180^\circ} - T\Delta S^{\pm} \tag{19}$$

$\Delta S^{\pm}$ was calculated by assuming that only the vibrations normal to the surface contribute to the entropy term. In the case of SO_2 adsorbed on Na^+ ion on NaCl, $\Delta F^{\pm}$ equals 1.48 kcal/mol.

For SO_2 adsorbed on K^+ ion, the values obtained are summarized. At the lowest minimum: $\alpha = 0°$, $\rho^\circ{}_{min} = 1.08$ ($r = 3.39$ Å), $\phi^\circ{}_{min} = -5.98$ kcal/mol, $\nu^\circ = 2.04 \times 10^{12}$ sec^{-1}, $\Delta H = -6.24$ kcal/mol. At the second minimum: $\alpha = 180°$, $\rho_{min}{}^{180} = 1.17$ ($r = 3.67$ Å), $\phi_{min}{}^{180} = 2.81$ kcal/mol, $\nu^{180} = 1.25 \times 10^{12}$ sec^{-1}. At the maximum: $\alpha = 100°$, $\rho^{100} = 1.46$ ($r = 4.58$ Å), $\phi_{min}{}^{100} = -0.71$ kcal/mol, $\nu^{100} = 0.43 \times 10^{12}$ sec^{-1}. From Figure 10 it is evident that the rate-determining magnitude is $\Delta F^{\pm}$ connected with the difference $\phi_{min}{}^{100} - \phi_{min}{}^{180}$, and from eq 19 $\Delta F^{\pm}$ is obtained as 1.69 kcal/mol.

The good agreement between calculated and experimental results obtained for the adsorption of SO_2 on the two alkali halides seems to prove the validity of the model used. In the case of the NaCl adsorbent the experimental results showed two maxima. For the first, at 168°K, an experimental value of $\Delta F^{\pm}$ (obtained by means of eq 7) was 1.75 kcal/mol, which is in good agreement with the $\Delta F^{\pm}$ value calculated from the adsorption potentials (1.52 kcal/mol). The isosteric heat of adsorption for the NaCl powder (7.15 kcal/mol) fits the calculated value of ΔH well. The second maximum at 213°K may be connected with molecules adsorbed on some other sites. These are probably Na^+ ions located at different positions such as the edges of the crystals or Na^+ ions located on a different crystal plane. An analog to this minimum was not found with the KCl adsorbent. This may be explained by the fact that the crystallites were much larger than in the case of NaCl which decreased the proportion of the energetic sites.

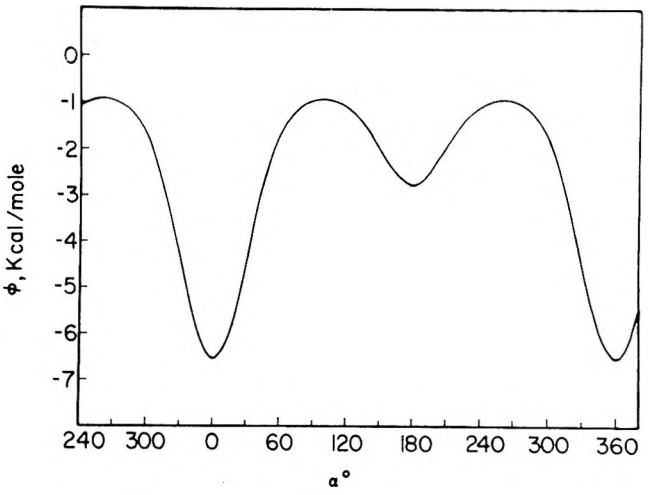

Figure 9. Adsorption potential of SO_2 adsorbed on Na^+ ion as a function of the angle of rotation.

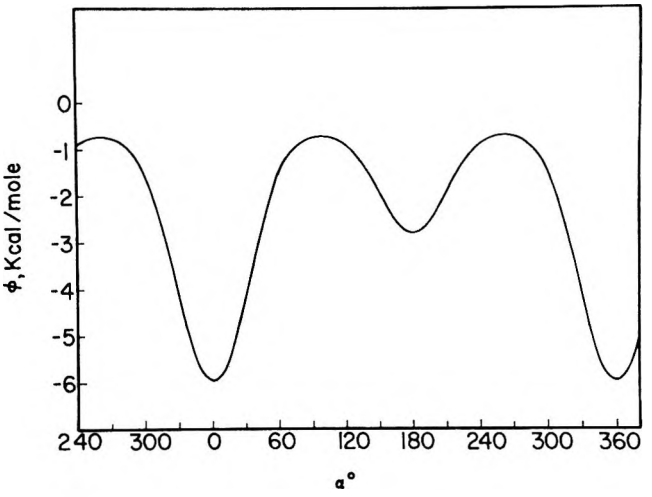

Figure 10. Adsorption potential of SO_2 adsorbed on K^+ ion as a function of the angle of rotation.

Summary

The dieletric absorption of SO_2 adsorbed on NaCl and KCl crystals was explained by assuming that the molecule is adsorbed in two rotational positions separated by a potential barrier.

Calculation of adsorption potential as a function of angle of rotation shows that the two positions are not equivalent.

The free energy of activation for orientation was calculated and found in good agreement with the experimental value obtained from measurements at microwave frequencies.

The existence of two absorption regions of unequal intensity in the case of NaCl adsorbent was explained as due to two different adsorption sites of unequal abundance.

Appendix

The parameters used in the calculations of adsorption potentials are listed.

$$\alpha_0(||) = 54.9 \times 10^{-25} \text{ cc/molecule}^{15}$$

$$\alpha_0(\text{av}) = 37.2 \times 10^{-25} \text{ cc/molecule}^{15}$$

$$\alpha_+(Na^+) = 2.2 \times 10^{-25} \text{ cc/molecule}^{16}$$

$$\alpha_+(K^+) = 9.7 \times 10^{-25}\ ^{16}$$

$$\alpha_-(Cl^-) = 30.0 \times 10^{-25}\ ^{16}$$

$$\chi_0 = -18.2 \times 10^{-6} \text{ cgs}^{17}$$

$$\chi_+(Na^+) = -6.1 \times 10^{-6} \text{ cgs}^{18}$$

$$\chi_+(K^+) = -14.6 \times 10^{-6} \text{ cgs}^{18}$$

$$\chi_-(Cl^-) = -24.2 \times 10^{-6} \text{ cgs}^{18}$$

$$\mu(SO_2) = 1.62 \text{ D}^{16}$$

$$Q = -4.42 \times 10^{-26} \text{ esu}^{13}$$

$$B_+^{1/2}(Na^+) = 12.63 \times 10^{-6} \text{ erg}^{18}$$

$$B_+^{1/2}(K^+) = 31.02 \times 10^{-6} \text{ erg}^{18}$$

$$B_-^{1/2}(Cl^-) = 71.9 \times 10^{-6} \text{ erg}^{18}$$

$$C = \frac{1}{0.345}^{18}$$

$$\epsilon/k = 347°\text{K}^{15}$$

$$\sigma = 4.04 \text{ Å}^{15}$$

$$a_{NaCl} = 2.815 \text{ Å}^{17}$$

$$a_{KCl} = 3.14 \text{ Å}^{17}$$

(15) J. O. Hirschfelder, C. F. Curtiss, and R. B. Bird, Wiley, New York, N. Y., 1965.

(16) A. J. Dekker, "Solid State Physics," Prentice-Hall, Englewood Cliffs, N. J., 1957.

(17) "Handbook of Chemistry and Physics," The Chemical Rubber Co., Cleveland, Ohio, 1965.

(18) M. L. Huggins and J. E. Mayer, *J. Chem. Phys.*, **1**, 643 (1933)

Infrared Spectra of $LiAlF_4$ and $NaAlF_4$

by S. J. Cyvin, B. N. Cyvin,

Technical University of Norway, Trondheim, Norway

and A. Snelson*

IIT Research Institute, Chicago, Illinois 60616 *(Received April 1, 1971)*

Publication costs assisted by the IIT Research Institute

The infrared spectra of the vapors over heated mixtures of $^7LiF + AlF_3$, $^6LiF + AlF_3$, and $NaF + AlF_3$ have been obtained using the matrix isolation technique. In the spectral region 4000–190 cm^{-1}, eight frequencies were assigned to $LiAlF_4$, and seven frequencies to $NaAlF_4$. A normal coordinate analysis, based on a molecular model with C_{2v} symmetry, was performed. Agreement between the observed and calculated frequencies though fairly good, was insufficient to prove the assumed molecular geometry. Mean amplitudes of vibration based on the assumed force fields are given for both compounds. A possible structure for the $(MAlF_4)_2$ dimer is suggested.

Introduction

Several mass spectroscopic studies have been made to determine the nature of the vapor species present over heated mixtures of $LiF + AlF_3$[1,2] and $NaF + AlF_3$.[2-5] At about 600° the major vapor species present in both systems are the mixed halides $LiAlF_4$ and $NaAlF_4$, with small though somewhat uncertain amounts of a dimer $(MAlF_4)_2$. The molecular symmetry of $NaAlF_4$ was determined as C_{2v} in a high-temperature electron diffraction study.[6] In this configuration the AlF_4 group

(1) R. F. Porter and E. E. Zeller, *J. Chem. Phys.*, **33**, 858 (1960).

(2) A. Buchler and J. B. Berkowitz-Mattuck," Advances in High Temperature Chemistry," Vol. 1, L. Eyring, Ed., Academic Press, New York, N. Y., 1967, p 133.

(3) L. N. Sidorov, E. V. Erokhin, P. A. Akishin, and E. N. Kolosov, *Dokl. Akad. Nauk SSSR*, 173, 370 (1967).

is essentially tetrahedral, being joined to the sodium atom *via* a planar ring containing the atoms NaF_2Al. In a high-temperature infrared gas-phase study[7] of the vapors over LiF + AlF_3 and NaF + AlF_3, two frequencies were assigned to each of the species $LiAlF_4$ and $NaAlF_4$. Both these molecules are expected to have more than two infrared active vibration frequencies and for this reason the spectra of these compounds have been reexamined using the matrix isolation technique.

Experimental Section

The matrix isolation cryostat and molecular beam furnace used in the investigation have been described elsewhere.[8] Research grade neon was used for the matrix gas and liquid helium for the refrigerant. Knudsen cells were made of graphite with effusion orifices 0.037 cm in diameter. In all experiments the ratio of effusate surface area in the Knudsen cell to effusion orifice area was at least 100:1. Reagent grade sodium fluoride and aluminum fluoride were obtained from Baker and Adamson. ^{6}LiF and ^{7}LiF were obtained from Oak Ridge National Laboratory with stated isotopic purities of 99.3% and 99.99%, respectively. Knudsen cell temperatures between 750 and 950° were used. Deposition times for the matrices varied from 1.5 to 5 hr. Matrix gas flow rates were usually about 5×10^{-2} mol/hr. Spectra were recorded on a Perkin–Elmer 621 spectrophotometer. Reported frequencies are believed accurate to ± 1 cm^{-1}.

Results

A. Lithium Fluoride and Aluminum Fluoride. A total of 14 experiments were made in which mixtures of ^{6}LiF + AlF_3 and ^{7}LiF + AlF_3 were vaporized in the 750–950° temperature range and the spectra recorded. In most experiments a 1:1 mole ratio of the lithium and aluminum fluorides was used. Matrix dilutions varied from about 1000:1 to 15,000:1 with deposition times from 2 to 5 hr. Typical spectra from equimolar mixtures of ^{6}LiF + AlF_3 and ^{7}LiF + AlF_3 mixtures are shown in Figures 1–3. In these figures, absorption bands of LiF[9] and AlF_3[10] have been omitted. When equimolar mixtures of the two halides were vaporized the LiF and AlF_3 absorption bands were very weak compared with other absorption bands appearing in the spectra. In a few experiments in which nonequimolar mixtures of the two halides were vaporized the only observable effect on the spectra was an enhancement in the absorption band intensities of the component in excess of the 1:1 ratio.

The spectrum shown in Figure 1 was obtained with the Knudsen cell maintained at 750°, under equilibrium conditions, whereas the spectra shown in Figures 2 and 3 were obtained with the vapor superheated under nonequilibrium conditions at 950°. It is evident from Figures 1 and 2 that superheating the vapor over

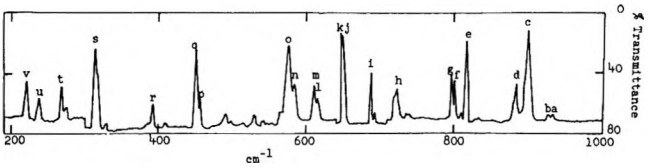

Figure 1. Infrared spectrum of the vapor species over an equimolar mixture of ^{6}LiF and AlF_3 in a neon matrix. Deposition time, 5 hr at 750°. Matrix dilution approximately 13,000:1.

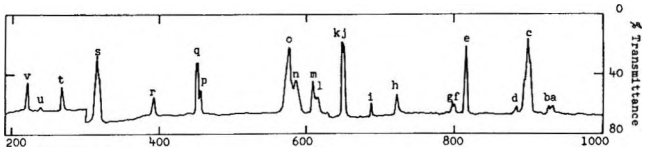

Figure 2. Infrared spectrum of the vapor species over an equimolar mixture of ^{6}LiF and AlF_3 in a neon matrix. Deposition time, 5 hr at 950°. Matrix dilution approximately 12,000:1.

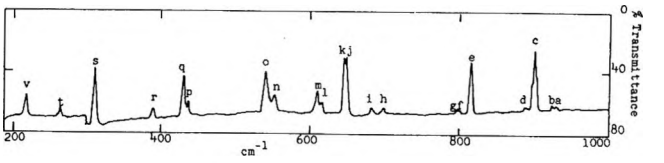

Figure 3. Infrared spectrum of the vapor species over an equimolar mixture of ^{7}LiF and AlF_3 in a neon matrix. Deposition time, 4 hr at 930°. Matrix dilution approximately 12,000:1.

^{6}LiF + AlF_3 markedly reduces the intensities of some absorption bands with respect to others. Since matrix dilutions were approximately the same in both experiments, the changes in relative intensities cannot be attributed to matrix effects. The reduction in absorption intensity of certain bands under superheat conditions suggests, therefore, the presence of two or possibly more species vaporizing from the ^{6}LiF + AlF_3 mixture. Enhancement of absorption band intensities which showed dimunition under superheating conditions could be achieved, though to a less marked degree, by performing experiments at low matrix dilutions in which the isolation efficiency was relatively poor. This behavior suggests that these absorption features may be attributed to polymeric species. From these observations, together with the known vapor phase composition

(4) L. N. Sidorov and E. N. Kolosov, *Zh. Fiz. Khim.*, **42**, 2622 (1968); *Russ. J. Phys. Chem.*, **42**, 1382 (1968).

(5) L. N. Sidorov, E. N. Kolosov, and V. B. Shol'ts, *Zh. Fiz. Khim.*, **42**, 2626 (1968); *Russ. J. Phys. Chem.*, **42**, 1386 (1968).

(6) V. P. Spiridonov and E. V. Erokhin, *Zh. Neorg. Khim.*, **14**, 636 (1969); *Russ. J. Inorg. Chem.*, **14**, 332 (1969).

(7) L. D. McCory, R. C. Paule, and J. L. Margrave, *J. Phys. Chem.*, **67**, 1086 (1963).

(8) A. Snelson, *J. Phys. Chem.*, **73**, 1919 (1969).

(9) A. Snelson, *J. Chem. Phys.*, **46**, 3652 (1967).

(10) A. Snelson, *J. Phys. Chem.*, **71**, 3202 (1967).

of this system from mass spectral data, it appears reasonable to conclude that the stronger absorption features in the LiF + AlF_3 spectra can be assigned to $LiAlF_4$, and the weaker to a dimer $(LiAlF_4)_2$. One experiment was performed in which an equimolar mixture of ^6LiF, ^7LiF, and AlF_3 was vaporized and the spectra of the superheated vapors were recorded. Only a few new weak absorption bands appeared which were not common to the ^6LiF + AlF_3 and ^7LiF + AlF_3 spectra separately, providing further evidence for assigning the stronger absorption features to a species containing only one lithium atom. The possibility that some of the weaker absorption features may arise from matrix agglomeration effects rather than a dimer species cannot be excluded.

In Table I the frequencies of all absorption bands appearing in the spectra of the superheated vapor species over mixtures of ^6LiF + AlF_3 and ^7LiF + AlF_3 are given. On the assumption that the more intense absorption bands in the mixed halide spectra are due to $LiAlF_4$, relative absorption band intensity ratios were used to identify all the bands that could be assigned to this species. To this end, relative absorption band intensity ratios, with respect to the 901-cm^{-1} band, were determined for most absorption features in the ^6LiF + AlF_3 spectra. The results obtained from five different spectra obtained under varying experimental conditions are presented in Table II. Previous experience with matrix spectra[11] has shown that if the deviation from the mean for a set of relative intensity ratios is $\leq \pm 7\%$, the two absorption bands may be assigned reasonably to the same species. Based on this criterion, eight of the absorption bands listed in Table II are assigned to the same species, presumably $^6LiAlF_4$. They are the bands with maxima at 901, 818, 651, 577, 453, 316, 269, and 222 cm^{-1}. Similar relative intensity measurements made on the ^7LiF + AlF_3 spectra resulted in eight bands at 900, 817, 649, 541, 433, 313, and 221 cm^{-1} being assigned to $^7LiAlF_4$.

In both the ^6LiF + AlF_3 and the ^7LiF + AlF_3 spectra some of the absorption bands assigned to the $LiAlF_4$ species appeared as doublets. Since measured relative intensity ratios for each of the doublets remained essentially constant in the different spectra, it might seem reasonable to assign each component of the doublets to a different vibrational mode of the $LiAlF_4$ molecule. These doublets were observed at 651–649, 588–577, and 458–453 cm^{-1} in the ^6Li spectra, with corresponding pairs at 649–647, 552–541, and 438–433 cm^{-1} in the ^7Li spectra. However, these doublets are believed to arise from matrix splitting of single frequencies for the following reasons. (a) The separation of the two maxima in corresponding sets of doublets in the ^6Li and ^7Li spectra are the same. A similar constant separation in matrix split isotopic frequencies has been observed in the ^6Li and ^7Li spectra of the dimers of Li_2F_2[9] and $NaLiF_2$.[11] (b) If each frequency in each pair of corresponding doublets represents a different vibrational mode of the molecule then essentially the same isotope shift is observed for each component of the doublets in

Table I: Frequencies of Absorption Bands in the Spectra of the Vapor Species Over Mixtures of ^6LiF + AlF_3, ^7LiF + AlF_3, and NaF + AlF_3

Absorption band designations in Figures 1, 2, and 3	Frequency, cm^{-1}		Absorption band designation in Figure 4	Frequency, cm^{-1}
	^6LiF + AlF_3	^7LiF + AlF_3		NaF + AlF_3
a	932	929	a	921
b	928	923	b	903
c	901	900	c	884
d	885	882	d	858
e	818	817	e	811
f	801	801	f	809
g	798	798	g	791
h	724	698	h	740
i	689	683	i	721
j	651	649	j	903
k	649	647	k	674
l	616	616	l	625
m	611	611	m	616
n	588	552	n	600
o	577	541	o	473
p	458	438	p	379
q	453	433	q	372
r	393	393	r	323
s	316	313	s	302
t	269	268		
u	239			
v	222	221		

Table II: Relative Intensity Measurement for Some of the Absorption Bands in the Spectrum of the Vapor Species over ^6LiF + AlF_3

	Frequencies of absorption bands used to derive intensity ratios	Equipment number					Std dev from the mean ± percentage
		9	10	11	12	16	
1	901/932		16.0	13.9	33.0		28.6
2	901/928		14.6	12.3	28.4		27.2
3	901/885	8.22	6.33	10.9	3.62	3.93	43.6
4	901/818	1.11	1.06	1.31	1.02	1.20	4.4
5	901/801		5.00	8.75	2.43	3.70	27.1
6	901/798		4.06	6.05	2.21	3.12	20.7
7	901/724	6.60	4.05	5.26	2.13	2.26	28.3
8	901/689	7.44	4.37	6.87	2.73	2.52	28.6
9	901/651	0.91	0.92	0.97	0.90	0.80	2.2
10	901/611		2.44	2.90	3.63	7.83	17.4
11	901/577	1.19	1.02	1.16	1.21	1.35	3.4
12	901/453	2.16	1.77	2.03	2.13	2.60	4.2
13	901/393	8.50	4.50	4.53	4.90	6.95	13.6
14	901/316	1.10	1.08	1.04	1.16	1.18	1.8
15	901/269	4.82	3.53	3.20	3.00	4.38	6.3
16	901/222	2.49	2.17	1.77	2.56	2.39	4.4

[a] It was not possible to obtain intensity ratios for all bands since some were too weak to allow meaningful measurements to be made.

(11) S. J. Cyvin, B. N. Cyvin, and A. Snelson, *J. Phys. Chem.*, **74**, 4338 (1970).

the ^{6}Li and ^{7}Li spectra. Although such behavior is not impossible, it may be considered unlikely for all three sets of frequencies. (c) If each frequency in each pair of corresponding doublets represents a different vibrational mode in the two isotopic molecules it is not possible to account for the observed isotope shifts in terms of any reasonable model for an $LiAlF_4$ molecule.

Although the above observations do not eliminate the possibility that two of the maxima in one of the three sets of doublets may indeed correspond to two different genuine vibrational modes of the $LiAlF_4$ molecule, the normal coordinate analysis presented later suggests this to be unlikely.

B. Sodium Fluoride and Aluminum Fluoride. Five experiments were made in which a mixture of NaF + AlF_3 was vaporized in the 800–870° temperature range and the spectra recorded. In all experiments equimolar mixtures of the two fluorides were used. Matrix dilutions varied from about 1000:1 to 15,000:1 with deposition times of from 2 to 5 hr. A typical spectrum is shown in Figure 4, in which absorption bands due to NaF and AlF_3 have been omitted. Absorption band frequencies are listed in Table I. Under varying experimental conditions the spectra showed the same type of behavior as was observed for the LiF + AlF_3 mixtures with regard to absorption band intensity changes. Mass spectrometric studies of the NaF + AlF_3 system indicate the most prevalent vapor phases species to be $NaAlF_4$, and it was assumed that the stronger absorption bands in the matrix spectrum could be assigned to this molecule. Relative absorption band intensity ratios with respect to the feature at 884 cm^{-1} were obtained to determine which absorptions were related to the same molecular species. From these measurements, seven frequencies occurring at 884, 811, 674, 379, 372, 323, and 302 cm^{-1} were assigned to the $NaAlF_4$ molecule.

Normal Coordinate Analysis. The normal coordinate analyses for $LiAlF_4$ and $NaAlF_4$ are based on a molecular model with C_{2v} symmetry as shown in Figure 5. For $NaAlF_4$ the C_{2v} symmetry has been confirmed in a high temperature, gas phase, electron diffraction study.[6] The resulting structural parameters were: $D(Al–F_{ext})$ = 1.69 Å, $R(Al–F_{br})$ = 1.69 Å, $S(Na–F)$ = 2.11 Å, and $\angle(F–Na–F)$ = 82°. These values require $\angle(F_{br}–Al–F_{br})$ = 110°, which is very near the tetrahedral angle. The $\angle(F_{ext}–Al–F_{ext})$ was assumed at the tetrahedral value of 109.47°. For $LiAlF_4$ no structural data are available. Evidence for C_{2v} rather than C_{3v} symmetry for this species has been presented elsewhere.[12] Structural parameters were estimated using data from related molecules.[13] $S(Li–F)$ = 1.68 Å and $\angle(F–Li–F)$ = 107° were assumed equal to the values in Li_2F_2 $D(Al–F_{ext})$ = 1.65 Å and $R(Al–F_{br})$ = 1.65 Å were taken as equal to the bond length in the Al–F monomer of 1.65437 Å.[13] This value is intermediate between the Al–F bond distances in AlF_3 (1.63 ± 0.02 Å) and in

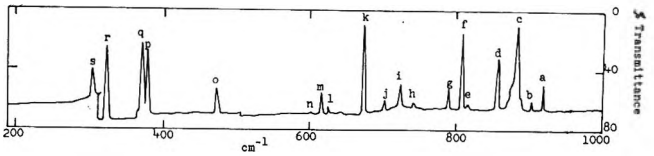

Figure 4. Infrared spectrum of the vapor species over an equimolar mixture of NaF and AlF_3 in a neon matrix. Deposition time, 5 hr at 870°. Matrix dilution approximately 14,000:1.

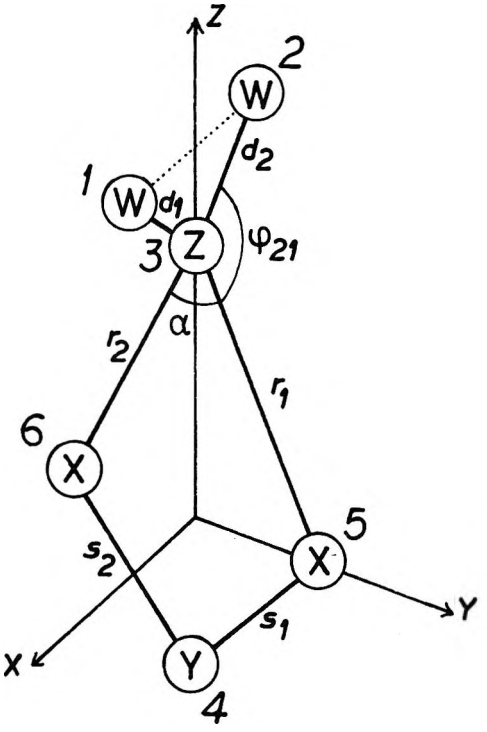

Figure 5. The $LiAlF_4$ and $NaAlF_4$ molecular model; symmetry C_{2v}. Equilibrium parameters: $R(X–Z)$, $S(X–Y)$, $D(W–Z)$, $2A(\angle XZX)$, and $2F(\angle WZW)$.

$NaAlF_4$ (1.69 ± 0.02 Å). From these assumed values the $\angle(F_{br}–Al–F_{br})$ = 109.88°, very close to the value in $NaAlF_4$. The $\angle(F_{ext}–Al–F_{ext})$ was set at 109.47°.

The equality of the $Al–F_{ext}$ and $Al–F_{br}$ distances may be questioned since in other known bridge structures (*e.g.*, Al_2Cl_6 and B_2H_6) the bridge bond distances are about 10% larger than the external bond distances. However, equal Al–F bond lengths in $NaAlF_4$ were reported as giving the best agreement between the theoretical and experimental intensities in the electron diffraction investigation.[6] In any event some possible inaccuracies in the selected structural parameters are believed to have a relatively minor influence on the normal coordinate analysis.

A complete set of symmetry coordinates was constructed using the following valence coordinates (*cf.*

(12) S. J. Cyvin, B. N. Cyvin, D. B. Rao, and A. Snelson, *Z. Anorg. Allg. Chem.*, 380, 212 (1971).

(13) K. S. Krasnov, V. S. Timoshinin, T. G. Danilova, and V. S. Khandozhko, "Molecular Constants of Inorganic Compounds," Izd. Khimiya, Lenignrad, 1968.

Figure 5). Stretching modes of the r, s, and d types, and the angle bending α, are indicated in Figure 5. The four φ type bendings are completely defined by their atom numbers as ϕ_{11} (1-3-5), ϕ_{12}(1-3-6), φ_{21}(2-3-5), and φ_{22}(2-3-6). The ring deformation coordinate, denoted by w, is given in terms of cartesian displacements as

$$w = x_3 + x_4 - x_5 - x_6$$

The symmetry coordinates are distributed according to the representation

$$\Gamma_{vib} = 5A_1 + A_2 + 3B_1 + 3B_2$$

Of the 12 fundamental vibrational frequencies, only the A_2 mode is infrared inactive. With the orientation of cartesian axes shown in Figure 1, the B_1 and B_2 species contain the out-of-plane and in-plane ring vibrations, respectively, as referred to the YZ plane.

The complete set of symmetry coordinates is specified as

$$S_1(A_1) = 2^{-1/2}(r_1 + r_2)$$
$$S_2(A_1) = 2^{-1/2}(s_1 + s_2)$$
$$S_3(A_1) = 2^{-1/2}(d_1 + d_2)$$
$$S_4(A_1) = R\alpha$$
$$S_5(A_1) = {}^1/_2(RD)^{1/2}(\varphi_{11} + \varphi_{12} + \varphi_{21} + \varphi_{22})$$
$$S(A_2) = {}^1/_2(RD)^{1/2}(\varphi_{11} - \varphi_{12} - \varphi_{21} + \varphi_{22})$$
$$S_1(B_1) = 2^{-1/2}(d_1 - d_2)$$
$$S_2(B_1) = {}^1/_2(RD)^{1/2}(\varphi_{11} + \varphi_{12} - \varphi_{21} - \varphi_{22})$$
$$S_3(B_1) = w$$
$$S_1(B_2) = 2^{-1/2}(r_1 - r_2)$$
$$S_2(B_2) = 2^{-1/2}(s_1 - s_2)$$
$$S_3(B_2) = {}^1/_2(RD)^{1/2}(\varphi_{11} - \varphi_{12} + \varphi_{21} - \varphi_{22})$$

In constructing symmetry coordinates two types of important ring bending coordinates have been omitted in order to avoid redundancies. Although the above set of symmetry coordinates is convenient as a basis for the specification of a final harmonic force field to be used in calculating molecular force constants, it is not too convenient as a basis for an initial force field calculation. This is particularly true since a diagonalized F matrix is probably a poor approximation because of the omitted ring bending coordinates. Therefore, a force constant matrix on the basis of a redundant set of valence coordinates was chosen for the initial approximation. In addition to the valence coordinates given above, the YXZ bendings (β) and the XYX bendings (δ) were included.

$LiAlF_4$. For the preliminary analysis of $LiAlF_4$, force constants were tried which were transferred directly from Li_2F_2[11] and AlF_3.[10] This approach was essentially unsuccessful, and for this reason the following proposed assignment must be considered as somewhat tentative. An analysis was therefore attempted using the following assumptions. (1) All the observed frequencies assigned to the two lithium aluminum fluoride species are indeed fundamentals. (2) The absorption bands occurring at the highest frequencies, 901 and 900 cm^{-1}, for the ^6Li and ^7Li compounds, respectively, may be composed of more than one fundamental each. (3) The bands at 541–577 cm^{-1}, and those at 433–453 cm^{-1} which display large isotope effects can be assigned to the symmetrical and asymmetrical Li–F stretching modes, respectively. (4) An unknown number of fundamentals frequencies may be present below 190 cm^{-1}.

After several approximations a force field with the following nine nonvanishing constants was found to give reasonable results: $f_d(Al–F_{ext}) = 4.5$, $f_r(Al–F_{br}) = 3.5$, $f_s(Li–F) = 0.6$, $f_\alpha = 0.5$, $f_\varphi(sym) = 0.5$, $f_\varphi(asym) = 0.2$, $f_\beta = 0.1$, $f_\delta = 0.3$ and $f_w = 0.1$; all in mdyn/Å. Comparison of these force constants with those occurring in other molecules containing bridge-type structures suggests the above values to be not unreasonable. This force field when converted into the symmetrized F matrix resulted in the appearance of a number of relatively large off-diagonal constants which would have been difficult to estimate in advance. The calculated frequencies from this initial approximate force field are shown in Table III along with a tentative assignment for the observed frequencies.

The frequency ratios from the Teller–Redlich product rule for $^7LiAlF_4$ and $^6LiAlF_4$ are given in Table IV. Unfortunately, the differences between the theoretical ratios for the various species are too small to be of any effective help in the assignment. An adjustment of the symmetry force constants to fit the observed frequencies exactly for $^7LiAlF_4$ did not change the main features of the F matrix. Table V gives the resulting symmetrized F matrix which is considered as the final force field. Complete sets of calculated frequencies for $^7LiAlF_4$ and $^6LiAlF_4$ from the final force field are included in Table III. For two of the frequencies in A_1 the differences between observed and calculated values for $^6LiAlF_4$ would in general be unacceptable. In view of the uncertainties in the experimental data on which the present normal coordinate analysis is based, the extent of the agreement between the observed and calculated frequencies is about as good as can be expected.

$NaAlF_4$. The normal coordinate analysis of this molecule was made largely on the basis of the force constants determined for the lithium species. Thus, in the initial approximate force field analysis, all the force constants obtained for $LiAlF_4$ were used, with the addition that $f_s(Na–F) = 0.48$ mdyn/Å. The results are shown in Table VI. Although no quantitative agreement between the observed and calculated frequencies can be expected in such an approximation, the data served as a guide in making the tentative fre-

Table III: Tentative Assignment for the Observed and Calculated Frequencies of $^7LiAlF_4$ and $^6LiAlF_4$ (cm^{-1})

	$^7LiAlF_4$			$^6LiAlF_4$		
	Calcd			Calcd		
Species	Approx	Final	Obsd	Approx	Final	Obsd
A_1	874	900	900	874	900	901
	661	649	649	685	671	651
	556	541	541	573	558	577
	424	313	313	427	315	316
	162	162	Unobsd (<190)	162	162	Unobsd (<190)
A_2	232	232	Inactive	232	232	Inactive
B_1	905	900	900	905	900	901
	297	266	266	300	268	269
	151	151	Unobsd (<190)	160	159	Unobsd (<190)
B_2	815	817	817	816	818	818
	505	433	433	537	460	453
	257	221	221	257	221	222

Table IV: Ratios from the Teller–Redlich Product Rule for $^7LiAlF_4$ and $^6LiAlF_4$

Species	Theoretical	Observed
A_1	0.9302	0.928[a]
A_2	1.0000	
B_1	0.9395	0.932[b]
B_2	0.9399	0.950

[a] Assuming the lowest frequency in both isotopic molecules to have the same value. [b] Using calculated values for lowest frequency.

Table V: Symmetry Force Constants (mdyn/Å) for Lithium Tetrafluoroaluminate

Species A_1					A_2
4.716					0.200
−1.228	1.752				
−0.100	−0.066	4.426			
0.574	−0.595	0.237	0.638		
0.040	−0.026	−0.059	0.082	0.482	

Species B_1			Species B_2		
4.407			3.490		
−0.031	0.175		0.105	0.485	
−0.016	−0.013	0.093	−0.053	−0.004	0.151

Table VI: Tentatively Assigned Observed Frequencies and Calculated Frequencies for $NaAlF_4$ (cm^{-1})

	Calcd		
Species	Approx	Final	Obsd
A_1	871	884	884
	608	674	674
	447	379	379
	280	302	302
	158	158	Unobsd (<190)
A_2	232	232	Inactive
B_1	905	884	884
	289	323	323
	104	104	Unobsd (<190)
B_2	812	811	811
	337	372	372
	244	244	Unobsd (?)

Table VII: Symmetry Force Constants (mdyn/Å) for Sodium Tetrafluoroaluminate

Species A_1					A_2
4.588					0.200
−0.495	0.871				
0.435	0.035	4.893			
0.297	−0.369	0.082	0.698		
0.027	0.014	−0.030	0.044	0.487	

Species B_1			Species B_2		
4.361			3.568		
0.055	0.235		0.038	0.841	
0.020	0.014	0.106	0.009	−0.025	0.205

quency assignments shown in Table VI. The force constants were further adjusted to fit the observed frequencies, and the final force field in terms of the symmetrized F matrix is given in Table VII. Finally, it should be recognized the normal coordinate analysis for $NaAlF_4$ is even more uncertain than that of the lithium compounds.

Comments on a Molecular Model for the Dimer. Based on the electron diffraction data for the $NaAlF_4$ monomer,[6] a structure for the dimer $Na_2Al_2F_8$ was proposed.[4] In this model, the F atoms that are "external" in the monomer structure form a total of four angular Al–F–Al bridges, with the Na atoms located at opposite ends of the dimer molecule. Presumably a similar structure might also be postulated for $Li_2Al_2F_8$. If these proposed structures for the dimers are correct, then the spectra of both species should not exhibit absorption bonds characteristic of the external Al–F bonds in the monomers. In the monomer, the stretching frequencies for such bonds lie at about 900 and 884 cm^{-1}, respectively, in the Li and Na compounds. In

the spectra obtained from mixtures of LiF + AlF_3 and NaF + AlF_3 absorption bands appeared at about 885 and 858 cm^{-1}, respectively, which from their behavior under differing experimental conditions, could clearly be assigned to species vaporizing from the Knudsen cell, presumably the dimers $Li_2Al_2F_8$ and $Na_2Al_2F_8$. If this latter conclusion is correct then it must be inferred that the absorptions bands at 885 and 858 cm^{-1}, which are characteristic of Al–F_{ext} type vibrations, are not consistent with previously proposed dimer model. If indeed the above interpretation of the matrix spectra is correct, a molecular model for the dimer must include external Al–F bonds. A possible structure which satisfies this latter condition would consist of two tetrahedal AlF_4 groups in which two of the F atoms in each AlF_4 unit are connected to each other *via* two Al–F–M–F–Al bridges. Such a structure differs from that of the monomer only in so much as the metal atom in the latter is joined to two fluorine atoms on the same AlF_4 tetrahedron, while in the dimer, the metal atoms are joined to two fluorine atoms on different AlF_4 tetrahdera.

Mean Amplitudes of Vibration. The cited electron diffraction work[6] on $NaAlF_4$ does not give any observed mean amplitudes of vibration. Such data would have been interesting for comparison with calculated mean amplitudes from a spectroscopic analysis. Calculated mean amplitudes would also be useful in further refinement of the electron diffraction data in a reinvestigation of the structure. Thus, in spite of the uncertainties in the normal coordinate analyses it is believed that the calculated mean amplitudes[14] from the final force fields of the present investigation may be useful in future studies. The mean amplitudes of vibration for lithium tetrafluoroaluminate are given in Table VIII and those for the sodium compound in Table IX.

Table VIII: Mean Amplitudes of Vibration (Å Units) for Lithium Tetrafluoroaluminate

	Temp, °K				
Distance	0	298.16	500	1000	1500
Al–F_{ext}	0.042	0.044	0.047	0.059	0.071
Al–F_{br}	0.045	0.046	0.051	0.065	0.077
^{7}Li–$F_{(br)}$	0.083	0.093	0.109	0.147	0.178
^{6}Li–$F_{(br)}$	0.085	0.094	0.110	0.147	0.178
Al···^{7}Li	0.077	0.087	0.102	0.136	0.165
Al···^{6}Li	0.079	0.088	0.102	0.137	0.165
F_{br}···F_{br}	0.063	0.074	0.089	0.121	0.147
F_{ext}···F_{ext}	0.082	0.126	0.159	0.223	0.272
F_{ext}···F_{br}	0.073	0.099	0.122	0.169	0.207
^{7}Li···$F_{(ext)}$	0.101	0.146	0.183	0.254	0.310
^{6}Li···$F_{(ext)}$	0.104	0.147	0.183	0.254	0.310

Table IX: Mean Amplitudes of Vibration (Å Units) for Sodium Tetrafluoroaluminate

	Temp, °K				
Distance	0	298.16	500	1000	1500
Al–F_{ext}	0.042	0.043	0.047	0.058	0.069
Al–F_{br}	0.044	0.045	0.049	0.063	0.075
Na–$F_{(br)}$	0.068	0.083	0.101	0.139	0.169
Al···Na	0.062	0.077	0.094	0.129	0.157
F_{br}···F_{br}	0.061	0.070	0.083	0.113	0.137
F_{ext}···F_{ext}	0.081	0.125	0.157	0.220	0.268
F_{ext}···F_{br}	0.069	0.090	0.110	0.152	0.185
Na···$F_{(ext)}$	0.084	0.138	0.176	0.246	0.301

Acknowledgment. One of the authors, A. Snelson, gratefully acknowledges the support of the Air Force Office of Scientific Research under Contract No. AF49(638)-1718 in funding this study.

(14) S. J. Cyvin, "Molecular Vibrations and Mean Square Amplitudes," American Elsevier, New York, N. Y., 1968.

Dielectric Relaxation in α,ω-Dibromoalkanes in Benzene Solution[1]

by Suresh Chandra* and Jai Prakash

Department of Physics, University of Gorakhpur, Gorakhpur, India *(Received February 1, 1971)*

Publication costs borne completely by The Journal of Physical Chemistry

The dielectric constant and loss of 1,3-, 1,4-, 1,5-, and 1,6-dibromoalkanes in dilute benzene solutions have been measured at 35° at the frequencies 450 kHz, 3.9 GHz, 24.7 GHz, and 36.8 GHz. It has been observed that the dielectric behavior of these α,ω-dibromoalkanes can be represented by a skewed arc plot which is interpreted as a result of intramolecular cooperative relaxation phenomena.

1. Introduction

Molecular behavior as derived through dielectric relaxation measurements in liquids has long been a subject of controversy because of the ambiguity concerning the form of internal field correction.[2] In pure polar liquids the internal field effects are quite pronounced due to a large dipolar field. The situtation is simplified if the dielectric behavior of a polar molecule is studied in a nonpolar solvent. This allows the solute molecules to be examined in a quasiisolated state. The value of the dipole moment in solution is close to the gaseous value and the relaxation time is microscopic. In general, it is less complicated to analyze the dilute solution dielectric data. In this paper the values of the dielectric constant and loss of four α,ω-dibromoalkanes (namely 1,3-dibromopropane, 1,4-dibromobutane, 1,5-dibromopentane, and 1,6-dibromohexane) in benzene solution at different frequencies and 35° are reported. An asymmetric distribution of relaxation time has been obtained in all these cases giving skewed arcs when dielectric loss is plotted against dielectric constant in a complex plane. The results are discussed in terms of characteristic relaxation time and asymmetric distribution parameter which may be either due to intramolecular cooperative relaxation phenomena or multiple relaxation times.

2. Experimental Section

The value of the dielectric constant and loss at 35° of these substances in benzene solution was determined at 450 kHz, 3.87 GHz, 24.65 GHz, and 36.81 GHz. The experimental arrangement was essentially the same as used by us[3,4] earlier. The standing wave method was used for evaluating the complex dielectric constant. The refractive index was measured at 35° using an Abbe refractometer.

Substances of the Purum grade were obtained from M/S Fluka AG (Switzerland) which were further purified by fractional distillation. Benzene supplied by M/S BDH (India) was fractionally distilled thrice before use.

3. Results and Discussion

The dielectric behavior is generally represented as a plot between ϵ'' and ϵ' in a complex plane. For dilute solutions, some authors[5,6] have preferred a plot between a'' and a', where a'' and a' are the dielectric loss and dielectric constant slopes, respectively. The values of a' and a'' can be evaluated from the experimental values of ϵ' and ϵ'' for dilute solutions of different concentrations. Five dilute solutions of varying concentrations in the mole fraction range (0–0.0510) have been used to obtain the values of a' and a''. These values are given in Table I. The accuracy of measurement of a' is $\pm 1\%$ and of a'' $\pm 5\%$. Plots of a'' *vs.* a' for the four α,ω-dibromoalkanes in benzene solution are given in Figure 1 which are obviously asymmetric (skewed arcs).

The skewed arcs can be analyzed in terms of either (i) Davidson–Cole representation which may result from inter- or intramolecular cooperative phenomena or (ii) superposition of two or more noninteracting Debye-type relaxations. For the present case two probable relaxations are due to end-over-end molecular rotation and end group–CH_2Br group rotation.

The Davidson–Cole[7] type formula is

$$\frac{a^* - a_\infty}{a_0 - a_\infty} = \frac{1}{(1 + i\omega\tau_{cs})^{\beta_{sol}}} \qquad (1)$$

where $a^* = a' - ia''$, β_{sol} is the asymmetric distribution parameter associated with the characteristic re-

(1) This paper forms a part of the Thesis submitted by Jai Prakash for the Ph.D. degree, Gorakhpur University, 1969.

(2) (a) C. P. Smyth, "Dielectric Behaviour and Structure," McGraw-Hill, New York, N. Y., 1955; (b) N. E. Hill, W. E. Vaughan, A. H. Price, and M. Davies, "Dielectric Properties and Molecular Behaviour," Van Nostrand-Reinhold, London, 1969.

(3) S. Chandra and D. Nath, *J. Chem. Phys.*, **51**, 5299 (1969).

(4) S. Chandra and J. Prakash, *ibid.*, **54**, 5366 (1971).

(5) W. M. Heston, Jr., A. D. Franklin, E. J. Hennelly, and C. P. Smyth, *J. Amer. Chem. Soc.*, **72**, 3443 (1950).

(6) W. F. Hassel, M. D. Magee, S. W. Tucker, and S. Walker, *Tetrahedron*, **20**, 2137 (1964).

(7) D. W. Davidson and R. H. Cole, *J. Chem. Phys.*, **19**, 1484 (1951).

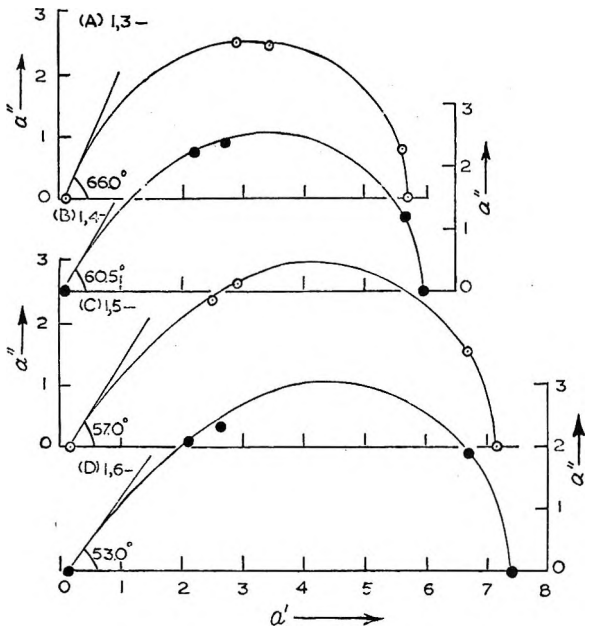

Figure 1. Complex plot of a'' *vs.* a' of some α,ω-dibromoalkanes in benzene solution at 35°.

Table I: Complex Slopes of Some α,ω-Dibromoalkanes in Benzene Solution at 35°

Substance	Frequency of measurement	a'	a''
1,3-Dibromopropane	450 kHz	5.71 (a_0)	
	3.87 GHz	5.60	0.77
	24.65 GHz	3.44	2.42
	36.81 GHz	2.89	2.48
	Optical	0.09 (a_∞)	
1,4-Dibromobutane	450 kHz	5.96 (a_0)	
	3.87 GHz	5.66	1.18
	24.65 GHz	2.71	2.39
	36.81 GHz	2.18	2.22
	Optical	0.07 (a_∞)	
1,5-Dibromopentane	450 kHz	7.14 (a_0)	
	3.87 GHz	6.70	1.50
	24.65 GHz	2.92	2.60
	36.81 GHz	2.50	2.35
	Optical	0.18 (a_∞)	
1,6-Dibromohexane	450 kHz	7.41 (a_0)	
	3.87 GHz	6.68	1.88
	24.65 GHz	2.64	2.30
	36.81 GHz	2.12	2.07
	Optical	0.13 (a_∞)	

laxation times (τ_{cs}) in solution, and a_0 and a_∞ are the static dielectric constant and optical dielectric constant slopes, respectively. a_∞ has been determined from a' *vs.* a''/ω plots and given in Table I. a_∞ can also be evaluated from a plot between concentration and square of the refractive index provided that $\epsilon_\infty = n^2_D$. The values of a_∞ calculated by both these methods agree, which suggests that for these cases $\epsilon_\infty = n^2_D$ is a valid approximation.

Separating real and imaginary parts of eq 1 and rearranging, we get

$$\omega\tau_{cs} = \tan\left[\frac{\tan^{-1}\dfrac{a''}{a' - a_\infty}}{\beta_{sol}}\right] \qquad (2)$$

Equations 1 and 2 can be used for finding the values of β_{sol} and τ_{cs}. The locus of eq 1 is a semicircle at the low-frequency end which asymptotically reduces to a straight line at the high-frequency end. This line makes an angle $\beta_{sol}\pi/2$ with the real axis, thus giving the value of β_{sol}. Then, τ_{cs} is evaluated using eq 2.

The calculated values of β_{sol} and τ_{cs} are given in Table II. The increasing value of β_{sol} with decreasing chain length means that the molecules tend to behave more and more as rigid spherical molecules with decreasing chain length. Similar behavior is also obtained by Vaughan, Lovell, and Smyth[8] for *n*-alkyl bromides. The decreasing value of β_{sol} with increasing chain length suggests that the segmental reorientations become increasingly possible as the number of C–C bonds increases. This is in conformity with the results obtained in the pure liquid state for these substances.[4] The value of τ_{cs} is found to increase with the increasing chain length, which is due to the increase in the molecular size. Similar behavior has also been observed for some α,ω-dichloroalkanes in pure liquid and benzene solution by us.[9] An idea about the effect of the dipolar field can be sought by comparing the dielectric relaxation parameters of a substance in pure liquid state and dilute solutions in nonpolar solvent. Table II also presents such a comparison. The values of β are higher for solution showing that the distribution of relaxation time decreases or becomes more symmetrical. The values of τ_{cs} are lower than the corresponding values in the pure liquid because of the presence of a relatively smaller dipolar field in solution. The smaller value of τ_{cs} in solution also suggests that there is little contribution from the rotation of the molecule as whole.[10]

A new distribution function for analyzing dielectric relaxation parameters in the systems exhibiting intramolecular rotating groups has been suggested by Higasi, *et al.*,[11] and Vaughan, *et al.*[8] They have been able with this distribution function to explain successfully the dielectric behavior of *n*-bromoalkanes. This distribution function, however, has been found to fail for α,ω-dibromoalkanes.[12]

The present dielectric behavior can also be analyzed in terms of superposition of two noninteracting Debye-type dispersions[13] which could not be done by us with

(8) W. E. Vaughan, W. S. Lovell, and C. P. Smyth, *J. Amer. Chem. Soc.*, 90, 6318 (1968).

(9) S. Chandra and R. A. Yadav, unpublished work.

(10) G. P. Johari, J. Crossley, and C. P. Smyth, *J. Amer. Chem. Soc.*, 91, 5197 (1969).

(11) K. Higasi, K. Bergmann, and C. P. Smyth, *J. Phys. Chem.*, 64, 880 (1960).

(12) S. K. Garg and C. P. Smyth, unpublished work.

(13) A. Budo, *Phys. Z.*, 39, 706 (1938).

Table II: Comparison of the Dielectric Relaxation Parameters in Pure Liquid and Benzene Solution of Some α,ω-Dibromoalkanes at 35°

Substance	State[a]	β	$\tau_0 \times 10^{12}$, sec	$\tau_1 \times 10^{12}$, sec	$\tau_2 \times 10^{12}$, sec
1,3-Dibromopropane	L[b]	0.57	20.7	12.9	2.5[c]
	B	0.73	7.3	6.4	2.8
1,4-Dibromobutane	L[b]	0.55	33.0	22.2	2.5[c]
	B	0.67	12.3	9.1	3.1
1,5-Dibromopentane	L[b]	0.54	37.5	23.0	2.5[c]
	B	0.63	15.0	11.2	2.8
1,6-Dibromohexane	L[b]	0.53	47.4	26.4	2.5[c]
	B	0.59	20.7	14.4	3.2

[a] L and B stand for "pure liquid" and "benzene solution," respectively. [b] S. Chandra and J. Prakash, *J. Chem. Phys.*, **54**, 5366 (1971). [c] Average value.

certainty due to lack of measurements at the higher frequency side. However, an approximate value of τ_1 (end-over-end relaxation time) and τ_2 ($-CH_2Br$ group rotation relaxation time) can be obtained from a plot between a' *vs.* $a''\omega$ as suggested by Cole.[14] The plot between a' *vs.* $a''\omega$ in the present case is found to consist of two slopes from which τ_1 and τ_2 have been calculated. These values are also given in Table II. Within the uncertainties[15] inherent in the experiment and method of analysis the value of τ_2 can be considered to be independent of chain length. The values of τ_2 in solution and pure liquid agree and hence it can be identified with $-CH_2Br$ group rotation relaxation which is expected to be independent of the surrounding. This value is also comparable to the $-CH_2Cl$ group rotation relaxation[16] value (3.0×10^{-12} sec and 3.6×10^{-12} sec) which is a similar group. The value of τ_1 is increasing with the chain length as τ_{cs} and hence can be identified with the end-over-end rotation relaxation time. The values of τ_1 in solution are lower than τ_1 in pure liquid as expected.[2a] However, it may be remarked that τ_1 and τ_2 obtained by such an analysis are only approximate and no knowledge about the relative weight factors of the two relaxation processes can be had.

Thus, it is seen that both the representations in terms of a Davidson–Cole plot or two relaxation mechanism explain the results equally satisfactorily. The accuracy of the measurement is such that it cannot establish the preference of one model over the other. However, the evidence that τ_2 in solution and pure liquid are approximately the same gives weight to the two relaxation model though intramolecular cooperative phenomena cannot be completely ruled out.

Acknowledgments. We thank Professor D. Sharma for his keen interest, Professor Krishnaji for helpful discussions, and Dr. S. C. Srivastava for his help in the measurements.

(14) R. H. Cole, *J. Chem. Phys.*, **23**, 493 (1955).

(15) M. D. Magee and S. Walker, *Trans. Faraday Soc.*, **62**, 3093 (1966).

(16) S. Dasgupta and C. P. Smyth, *J. Amer. Chem. Soc.*, **90**, 6318 (1968).

Viscosity of the Cyclohexane–Aniline Binary Liquid System near the Critical Temperature[1]

by Charles C. Yang and F. R. Meeks*

Department of Chemistry, University of Cincinnati, Cincinnati, Ohio 45221 *(Received May 26, 1970)*

Publication costs assisted by the Petroleum Research Fund

The viscosity of the binary liquid system cyclohexane–aniline has been measured in the region just above the coexistence curve for three compositions: 0.430, 0.445, and 0.460 mole fraction aniline. The temperature control was better than ±0.001°; the data produced a typical branch of a λ-shaped curve, and typically, the viscosity is anomalously high as the phase separation temperature is approached. Neither logarithmic nor exponential behavior of the viscosity is followed for the full range of temperatures investigated (0.001–0.3° above phase separations).

I. Introduction

Anomalous increase of the viscosity of binary liquid systems near the critical mixing point has long been a matter of record.[1,2] For binary liquid mixtures the anomalous increase of the viscosity is of the order of 15–20% at the critical mixing point.

In 1945 Mondain-Monval and Quiquerez[3a] investigated the viscosity and opalescence of binary and ternary systems in the critical region. Systems found to possess abnormally high viscosity while still in the "homogeneous" region but near the critical point included water–aniline–ethanol, water–benzene–ethanol, water–toluene–ethanol, aniline–cyclohexane, nitrobenzene–hexane, water–acetone–cyclohexane, and ether–acetone–petroleum ether. The first five systems showed marked opalescence correlated with the viscosity increase, but the last two showed no critical opalescence. The systems showing abnormal viscosity are believed to possess a colloidal structure in the critical region, which becomes visible as opalescence only when the refractive indices of the constituents differ by more than 0.04.[3b]

Reed and Taylor[4] have observed an anomalous increase in the viscosity of isooctane–perfluoroheptane mixtures. The viscosity exhibits an anomalous increase up to 25%. The anomalous behavior can be detected as far away as 10° from the critical temperature. However, other investigators found that for some systems the anomaly occurs only at temperatures much closer to the critical point.

Semenchenko and Zorina[5] investigated the viscosity of nitrobenzene–hexane mixtures. The results showed that the range of temperature and concentration in which the critical phenomena were observed was 1.0 to 1.5° and 10 mol %. The peak of viscosity in that critical region was at least 20% in excess of the value that would correspond to a linear increase (from much higher temperatures).

Campbell, *et al.*,[6] have studied the aniline–hexane system. They report that the phenomenon of anomalously high viscosity is observed over a temperature range of 2.4° above the critical solution temperature and over the concentration range of 37–58.5 mol % hexane.

The object of the present work is to establish a precise viscosity curve near the critical temperature. As the temperature approaches the critical point, viscosity readings were made at temperature intervals of the order of 0.001° as compared to 0.01° reported earlier for other systems.[5,7,8]

It is hoped that these more precise data may be helpful in testing theories of the critical state and, incidentally, in determining whether the viscosity is a useful criterion for establishing the correct phase separation temperature (and ultimately, the critical solution temperature) for binary mixtures.

II. Experimental Section

A. Reagents. Both the aniline and the cyclohexane

(1) Taken in part from the doctoral dissertation of C. Yang, University of Cincinnati, 1970.

(2) (a) M. S. Green and J. V. Sengers, *Nat. Bur. Stand. (U. S.) Misc. Pub.*, 273 (1966), see especially, in connection with the present work, pp 9, 21, and 165; (b) D. E. Tsalakatos, *Bull. Soc. Chim. Fr.*, 5, 397 (1909).

(3) (a) P. Mondain-Monval and J. Quiquerez, *Bull. Soc. Chim.*, 12, 380 (1945); (b) *ibid.*, 11, 26 (1944).

(4) T. M. Reed and T. E. Taylor, *J. Phys. Chem.*, 63, 58 (1959).

(5) V. K. Semenchenko and E. L. Zorina, *Dokl. Akad. Nauk SSSR*, 73, 331 (1950); 80, 903 (1951).

(6) A. N. Campbell, *et al.*, *Can. J. Chem.*, 46, 2399 (1968).

(7) J. Brunet and K. E. Gubbins, *Trans. Faraday Soc.*, 65, 1255 (1969).

(8) G. Arcovito, C. Faloci, M. Roberti, and L. Mistura, *Phys. Rev. Lett.*, 22, 1040 (1969).

were Chromato quality reagents with 99.9 and 99.8% purity, respectively. They were obtained from Matheson Coleman and Bell Co., Norwood, Ohio.

Calcium oxide powder was Baker Analyzed reagent obtained from J. T. Baker Chemical Co., Phillipsburg, N. J.

A single bottle of each of the above three reagents was used for the preparation of all the samples in this experimentation.

Extensive purification and drying of the cyclohexane–aniline mixtures were carried out in an elaborate vacuum system described elsewhere.[9] Although high purity is an extremely desirable attribute for reagents used in critical phenomena work, it is well known that reproducibility of the temperature of coalescence, as observed visually, is a *sufficient* guarantee for the cyclohexane–aniline system. (Variations in the absolute value of the temperature of phase separation from laboratory to laboratory are not unknown; indeed the response characteristics of the same apparatus can vary from year to year. It is felt that differences between physical properties of samples from the same bottles, further purified and dried in the same way and measured within a relatively short period of time in the same thermostat, give information relative to one another as valuable as would be that from mixtures of absolutely pure components.)

B. The Constant Temperature Bath. The constant temperature bath consisted of a large "fish tank" which contained approximately 90 l. of distilled water. It is described elsewhere.[9]

C. Temperature Measurements. The temperatures of the water bath were measured by two different, supplementary methods using (1) a Beckmann thermometer and (2) a Wheatstone bridge with a thermistor.

The Beckmann thermometer was standardized by using sodium sulfate ($Na_2SO_4 \cdot 10H_2O$) which has a decomposition temperature of 32.384°. The use of a Gaertner microscope equipped with a movable vernier permitted observation of temperature of the water bath to 0.001°, but the Beckmann thermometer responded to temperature change rather slowly. It was believed that the Beckmann thermometer gave only a "mean" temperature over a small time period, instead of an "instant" temperature at a specific moment. Besides, the readings of the Beckmann thermometer could vary from one observer to the other. Therefore, a thermistor was used to supplement the Beckmann.

The Wheatstone bridge consisted of one galvanometer, one thermistor, one carbon-film resistor, two resistance boxes, one switch and two 1.35-V mercury batteries in series. The highly sensitive galvanometer was obtained from the Rubicon Division of Minneapolis, Honeywell Co. Inc.

The thermistor was Type GA51P8 obtained from Fenwal Electronics Inc., Framingham, Mass. The resistance of the thermistor was approximately 76,000 ohms at 30°. As the temperature of the bath increased, the resistance of the thermistor decreased. The standardized Beckmann thermometer was used to establish the relationship between the temperature of the water bath and the resistance of the thermistor. The plot of temperature *vs.* resistances showed a straight line in the temperature range of our interest. This standard straight line was then used to convert the resistance readings of the thermistor back to the actual temperatures. Due to the extremely high sensitivity of the galvonometer and the high resistance of the thermistor, the precision of the temperature measurements was estimated to be approximately ±0.0003°.

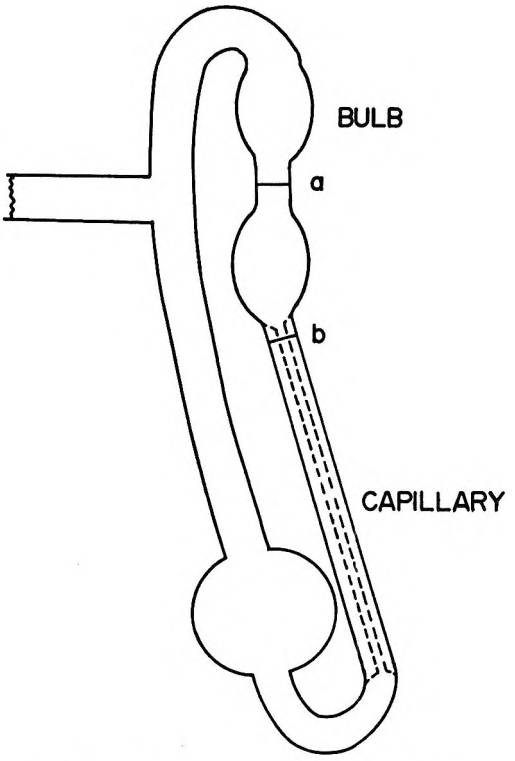

Figure 1. The modified Cannon-Fenske viscometer.

D. The Viscometer. A Cannon-Fenske viscometer, size 100, was obtained from the Cannon Instrument Co., State College, Pa. The viscometer was further modified for measurements of viscosity under vacuum (Figure 1). According to the manufacturer, the radius of the capillary of the viscometer is 0.0315 cm and the volume of the efflux bulb is 3.15 ± 0.15 cm^3.

The viscometer was attached to a submersible support with a chain which allowed it to rotate 360°. By rotating the viscometer into a downward position, the bulb above "a" in Figure 1 was filled with the sample. The viscometer was allowed to remain in the constant temperature bath for 1 hr. It was then returned to a vertical position by means of a chain control. The sample was allowed to flow freely down past etch mark

(9) D. N. Stoneback and F. R. Meeks, *J. Phys. Chem.*, in press.

"a" and a stopwatch was used to measure the time for the meniscus to pass from mark "a" to mark "b."

In the design of the viscometer, attention was paid to the capillary diameter in order to avoid shear affects and separation or beating of the sample during the flow time from mark to mark. Radii less than that chosen (0.0315 cm) would of course increase flow times and therefore minimize the percentage of error in them. However, uniformity of bore becomes a problem, as well as uncertainty about the presence of Newtonian flow. Larger capillaries, it was felt, would simply reduce flow time unnecessarily. Repetitive measurements on the three samples gave high reproducibility, so that the limiting factor in error seems to be thermostatic control of the bath.

A Swiss-made "Breno" stopwatch was used. It could be read to 0.1 sec and easily estimated to 0.05 sec. A stopwatch holder obtained from the Precision Scientific Co., Chicago, added convenience to the use of the stopwatch.

The viscometer was calibrated with deionized water under vacuum at a constant temperature of 30.0°; the viscometer constant was calculated to be 0.012052 cSt/sec.

A legitimate question can be raised as to whether the temperature of the thermostat and that within the sample were the same, to within less than 0.001°. In the heat capacity work reported in ref 9, the sample was considerably larger, and there was always at least one thermistor inside the sample itself at all times. No discrepancy between bath and sample temperature was observed in that research.

E. The Vacuum System. The vacuum system and purification procedure are described elsewhere.[9]

III. Results and Conclusions

The viscosities of three samples, A, B, and C, with aniline mole fractions of 0.430, 0.445, and 0.460, respectively, were measured. The results are given in Figures 2–4. A relative viscosity was defined as the ratio of the kinematic viscosity at a temperature T to the maximum kinematic viscosity which occurred at the phase separation temperature, T_c. Therefore, all three samples would have a relative viscosity of 1.000 at T_c. Thus T_c is to be distinguished in this work from the critical consolute temperature, presumed (as seen below) to occur at a mole fraction of aniline very nearly 0.445. The temperature difference between T and T_c is called ΔT. When T is higher than T_c, ΔT has a positive sign. When ΔT was 0.3°, all three samples were clear. As ΔT decreased, the samples became cloudier and the kinematic viscosity increased. At the phase separation temperature, where ΔT became zero, the samples were opaque and the kinematic viscosity was the highest. When ΔT became negative, the kinematic viscosity started to decrease. A visible meniscus did not always appear at the same temperature as the drop of the kinematic viscosity. Sometimes it appeared at a temperature one or two thousandths of a degree lower. This discrepancy is probably caused by the opalascence of the samples.

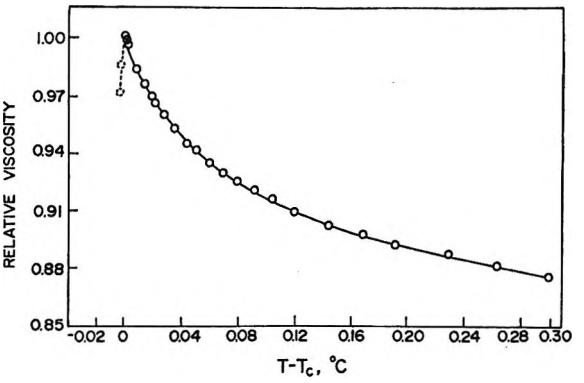

Figure 2. Relative viscosity of sample A.

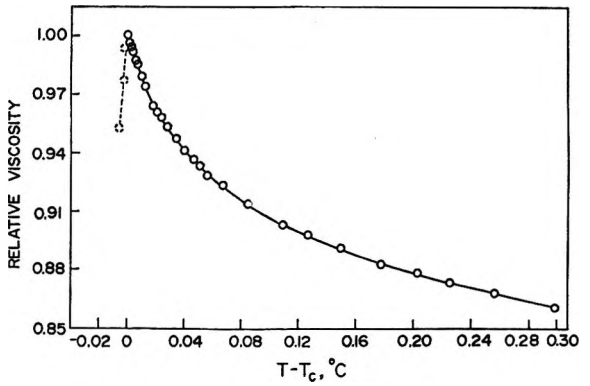

Figure 3. Relative viscosity of sample B.

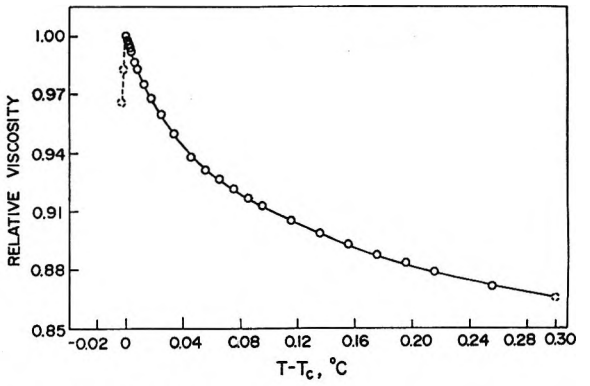

Figure 4. Relative viscosity of sample C.

Figures 2 to 4 show the relative viscosity *vs.* ΔT curves for the three samples. The slope becomes increasingly negative as the temperature decreases. A distinct discontinuity occurs at the critical solution temperature.

The viscosity data were curve-fitted for polynomial equations of degree six using an IBM 360 computer. The program used was R-02-2, University of Cincinnati, March 1969, which was revised form BMD05R, version of the Dec 1965 Health Science Computation Facility, UCLA.

Table I summarizes the experimental data in the form of a sixth-order computer-fitted polynomial in $T - T_c$. From the coefficients given in Table I, the original data can be regenerated to within an error of less than about 1% at the lower value of $T - T_c$ (~0.001°) and an error of considerably less than 1% for values of $T - T_c$ of the order of 0.3°.

Table I: Polynomial Coefficients for the Relative Viscosities

$$\chi_{rel} = \sum_{n=0}^{6} K_n(T - T_c)^n$$

	Sample A	Sample B	Sample C
k_0	0.99989	0.99941	0.99992
k_1	−2.05785	−2.31437	−2.18194
k_2	27.5215	29.1288	26.3122
k_3	−247.730	−241.313	−207.754
k_4	1251.52	1141.26	937.610
k_5	−3194.58	−02789.58	−2201.25
k_6	3197.93	2723.68	2078.23

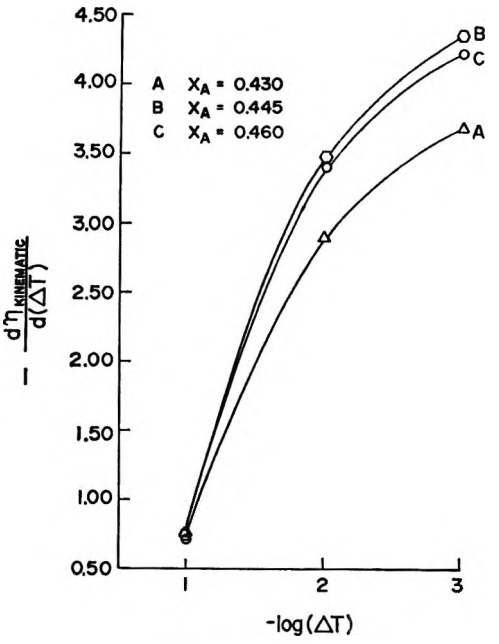

Figure 5. A comparison of the slopes.

The curve-fitted equations were used to calculate the slopes of the viscosity curves at any specific temperatures. At a temperature 0.1° above the critical temperature the slopes of all three curves are approximately equal. However, when ΔT is only 0.001°, sample B, which has 0.445 mole fraction of aniline, has the largest slope (Figure 5). The slope of sample C, which has 0.460 mole fraction of aniline, is the second largest and sample C with 0.430 mole fraction of aniline the smallest. It is interesting to see that the maximum slope change occurs at a concentration which is in the middle of a critical concentration range, 0.430–0.465 mole fraction of aniline, as reported by Atack and Rice.[10,11] It can be concluded that if there is only one critical concentration instead of a range of critical concentrations, then this critical concentration is very near, if not at, 0.445 mole fraction of aniline.

The results of this work have been compared with two recent publications in this field. Brunet and Gubbins,[7] in investigating the viscosity of four binary liquid systems near the critical mixing point, have measured the viscosity of a series of aniline–cyclohexane mixtures from 0.4 to 20° above the critical solution temperature. However, they emphasize the approximate location of the viscosity anomaly instead of the exact quantitative aspects of the anomaly. Arcovito, Faloci, Roberti, and Mistura[8] conclude that the viscosity above the critical solution temperature is quite well fitted over three decades by a logarithmic law

$$\Delta\eta = -A \ln [(T - T_c)/T_c] + B$$

where $\Delta\eta$ is the excess shear viscosity, $A = 0.16$, and $B = 0.30$ cSt. This equation was tested using present viscosity data; unfortunately, the results were unsatisfactory. A possible discrepancy may be in the fact that the temperature bath which they used was controlled only to ±0.01° while in the present work we measured the viscosity of the mixtures at a temperature as close as 0.001° above the critical solution temperature. This temperature range is probably beyond the "*three* decades of a logarithmic law" as claimed in ref 8.

The kinematic viscosity of an aniline–cyclohexane mixture with a composition of 0.440 mole fraction aniline was estimated to be 1.48 cSt near the critical solution temperature, if there were no viscosity anomaly.[7] In the present experimentation the kinematic viscosity of a similar mixture is 1.93 cSt at the critical solution temperature and 1.70 at $\Delta T = 0.2°$. These mean a viscosity anomaly of 30 and 15% at the respective temperatures.

Fixman[12] was the first to treat the viscosity of critical mixtures quantitatively on a theoretical basis. His method involves a calculation of the entropy production through diffusion which results when a mixture in a state of composition fluctuation is caused to have a velocity gradient. The long wavelength part of the spectrum of composition fluctuation is intense and very easily distorted by a velocity gradient in the critical region. The return to uniform composition through diffusion dissipates energy, and the loss is interpreted as an excess viscosity. Botch and Fixman[13] investigated the dependence of viscosity on the velocity gradient based on the Fixman's theory. They estimated that

(10) D. Atack and O. K. Rice, *Discuss. Faraday Soc.*, **15**, 210 (1953).
(11) D. Atack and O. K. Rice, *J. Chem. Phys.*, **22**, 382 (1954).
(12) M. Fixman, *ibid.*, **36**, 310 (1962).
(13) W. Botch and M. Fixman, *ibid.*, **36**, 3100 (1962).

$T - T_c$ must be 0.2° in order that a 15% decrement be found in the excess viscosity.

A calculation for the present system based on Fixman's theory is not yet feasible due to lack of sufficiently accurate data (partial molar volumes, etc.) for the aniline–cyclohexane system. These should be regarded as necessary parameters to be obtained in order to test the applicability of Fixman's calculation for viscosity in the critical region.

Efforts were made, using both the Wang electronic calculator and the IBM 360, to fit the data of the present work to an equation of the form

$$\eta = A\left(\frac{T - T_c}{Tc}\right)^{-\alpha} + B\left(\frac{T - T_c}{T_c}\right) + C$$

with unsatisfactory results. This equation is incapable of giving sufficiently acute variation in η in the lower ranges of $T - T_c$. However, a plot of ln η *vs.* ln $(T - T_c)$ gives a moderately good straight line such that

$$\lim_{T \to T_c}\left[\frac{\ln \eta}{\ln (T - T_c)}\right] = 0.033$$

Discussion of the physical significance of this result will have to be postponed until comparable data are obtained for other binary systems.

Anomalous Freezing Behavior of Polymer Gels and Solutions

by D. J. Solms

Department of Chemistry, University of Cape Town, Rondebosch C.P., South Africa

and A. M. Rijke*

Department of Materials Science, University of Virginia, Charlottesville, Virginia 22901 *(Received December 2, 1970)*

Publication costs assisted by the National Science Foundation

An experimental and theoretical study is reported of the anomalous freezing point depression of polymer solutions and gels crosslinked in the presence of large amounts of diluent. It is found that all solutions and gels freeze at temperatures lower than would be predicted on the basis of their known thermodynamic properties. The results for dilute solutions and highly swollen, dilute solution-crosslinked gels can be satisfactorily explained by assuming that rapid annealing accompanies the growth of solvent crystallites that are prevented from growing larger by the surrounding polymer filaments. These frozen systems are assumed to be crystals in which each individual polymer chain is embedded and immobilized. Annealing is supposed to be slower and less extensive in the more concentrated systems. The freezing-point depressions of swollen natural rubber vulcanizates are larger than predicted by the theory of Kuhn, probably due to extensive interpenetration of network chains, but the presence of diluent at the time of crosslinking reduces this depression well below the theoretical value. The effect of chain interpenetration can also be observed in solution-crosslinked gels if the amount of diluent is sufficiently reduced.

Introduction

Gels and solutions of polymers exhibit anomalous freezing behavior in that they freeze at temperatures lower than would be predicted from conventional thermodynamic considerations. In crosslinked networks swollen to equilibrium, the chemical potential of the solvent inside the gel must, by definition, be equal to that of the pure solvent and hence no freezing point depression would be expected. In polymer solutions the effect of the solute on the chemical potential of the solvent is accessible both by theoretical treatments and by direct experimental measurement. The observed freezing points of such solutions are, however, consistently lower than predicted.[1-4]

These observations have failed to attract much attention, mainly because, in most cases of dilute systems, the freezing point lowering is too small to be of use as a method for providing reliable thermodynamic information. The larger freezing point depressions measured for more concentrated systems are obscured by such uncertainties as the inhomogeneity and time-

(1) J. W. Breitenbach and A. J. Renner, *Monatsh. Chem.* **81**, 454 (1950).

(2) T. Kawai, *J. Polym. Sci.*, **32**, 425 (1958).

(3) H. Ozasa, Y. Yamamoto, and A. Yamaoka, *Himeji Kogyo Daigaku Kenkyu Hôkoku*, **10**, 33 (1958).

(4) D. Craig and N. M. Trivisonno, *J. Polym. Sci., Part B*, **1**, 253 (1963).

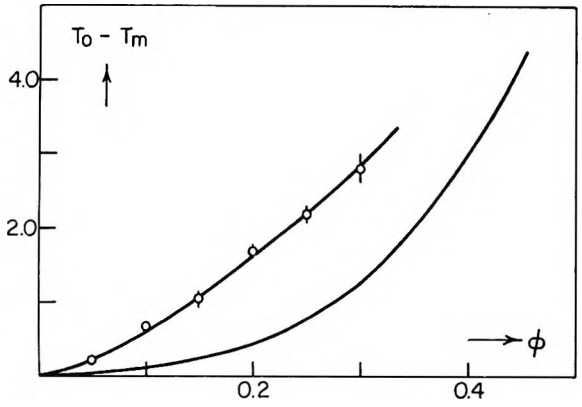

Figure 1. Freezing point depression of benzene solutions of natural rubber as a function of volume fraction polymer: upper line, experimental; lower line, according to eq 1 where $\chi = 0.41$.

dependent heat transfer in the viscous media. Nevertheless, the available data show clearly that most polymer–solvent systems freeze well below the temperatures predicted by thermodynamic requirements over a wide range of concentration. An example is provided by Figure 1 where the freezing point depression of benzene in acetone-extracted natural rubber solutions is plotted as a function of volume fraction polymer. All points fall well above the theoretical line as given by the equation

$$\frac{1}{T_m} - \frac{1}{T_0} = -(R/\Delta H_f)[\ln (1 - \phi) + \phi + \chi\phi^2] \quad (1)$$

where T_m is the freezing point of the solution, T_0 that of pure solvent, R the gas constant, ΔH_f the molar heat of fusion of the solvent, and ϕ the volume fraction polymer. The Huggins interaction parameter χ is known from vapor pressure measurements to be constant for this system over almost the entire range of concentration.[5] In order to make the experimental points fit the theoretical curve, values ranging from about -0.7 to 0.1 would have to be assigned to the interaction parameter. Such low values cannot be explained by the difference in operating temperature between the cryoscopic and vapor pressure measurements. Alternatively, a negative partial molar heat of dilution or a sharp decrease in the entropy contribution to χ with increasing concentration would accommodate these values. Whereas the former is known to be positive,[5] a pronounced concentration dependence of the entropy contribution must be rated most unlikely. Similar results have been found for solutions of other polymers.

Ozasa and coworkers[3] observed for polystyrene–benzene and poly(vinyl alcohol)–water solutions which they assumed to be ideal that the concentrations at which the incipient abnormal depression occurs are molecular-weight dependent. They postulated that these concentrations are probably equal to the so-called critical concentrations in the case of viscosity measurements of the dilute solutions.

Craig and Trivisonno[4] have attempted to explain their large freezing point depressions in terms of "segmental" weights, but such an approach neglects the very considerable amount of theory which has already been used successfully to explain the nonideality of polymer solutions.

Kawai[2] has collected cryoscopic data for a number of polymer–solvent systems to study the interaction parameter over a wide concentration range using eq 1. With the exception of the system poly(vinyl acetate)–benzene, his χ values are all considerably smaller than those inferred from vapor pressure measurements and osmometry.

Whereas the freezing point depressions for polymer solutions are almost invariably larger than can be accounted for on the basis of their accepted thermodynamic quantities, the observed depressions for gels crosslinked in the dry state are even larger. The freezing points of these gels, swollen to equilibrium in pure solvent, lie not only well below that of the solvent, but also at least an order of magnitude below that of a solution of the same polymer concentration. Kuhn[6,7] has reported that a gel consisting of 4% poly(vinyl alcohol) and polyacrylic acid in water shows a freezing point depression of 0.9°, whereas a solution of the same uncrosslinked polymers of the same concentration in water has a freezing point depression of only a few hundredths of a degree. At such concentrations the polymer chains in solutions are entirely interpenetrating, so that there is no difference in concentration distribution of polymer between gel and solution.

The abnormal freezing-point depression of gels has been at least semiquantitatively explained by Kuhn,[7] who postulated that solvent nuclei can grow undisturbed inside the meshes of a gel until the crystallite sizes become comparable to the mesh dimensions. Further growth is hampered by the chains between the crosslinks, unless the temperature is lowered enough to render subsequent growth around the chains thermodynamically feasible. In actual practice, however, such low temperatures would simultaneously induce rapid nucleation in all meshes and effective growth beyond the range of each mesh can therefore be ruled out. As a result of this, the crystallite dimensions are essentially determined by the chain lengths between crosslinks and efforts have been directed toward correlating the observed freezing point depression with the Young's modulus of elasticity. Kuhn has proposed the Gibbs–Thomson equation for the freezing

(5) G. Gee and L. R. G. Treloar, *Trans. Faraday Soc.*, **38**, 147 (1942).

(6) W. Kuhn and H. Majer, *Angew. Chem., Int. Ed. Engl.*, **64**, 345 (1956).

(7) W. Kuhn, *Helv. Chim. Acta*, **39**, 1071 (1956); *J. Polym. Sci.*, **16**, 539 (1955).

point depression of cubic microcrystals of edge length a, which reads

$$\Delta T = \frac{4 \times 10^3 E \sigma_{cl}}{\rho_c R T_0 a} \quad (2)$$

where ΔT is the freezing point depression, E the molar freezing point depression constant of the solvent, σ_{cl} the interfacial energy between the crystalline and liquid solvent, and ρ_c the density of the crystalline solvent. The edge length a can be estimated from modulus measurements on dry or swollen gels using the existing statistical mechanical theories of rubber elasticity and swelling or, inversely, the validity of controversial issues in these theories can, at least in principle, be further assessed by the determination of freezing-point depressions.

Kuhn's experimental results have indicated that there is a discrepancy of a factor 3.5 between observed and calculated values for the freezing-point depressions.[8] The uncertainty in the value to be assigned to σ_{cl} could very well account for this difference, but a more likely explanation could be offered by reconsidering the assumption that a equals the distance between two crosslinks. Because of the extensive interpenetration of the network chains many more crosslinks can be found within a sphere of radius $(\overline{r^2})^{1/2}$ around each crosslink. Here, $(\overline{r^2})^{1/2}$ represents the root-mean-square end-to-end distance of a chain between two crosslinks in a swollen gel. This would result in an increase in freezing point depression in agreement with the experimental observation.

Butenuth[9] and Westlinning tested Kuhn's theory using a suitable series of benzene-swollen rubber vulcanizates. The theory was successful in accounting for the result, but since the mesh size was accessible only indirectly, the agreement is less striking than it might have been if an independent physical measurement had been used to evaluate the mesh size.

The relation between crystallite size and mesh dimensions is complicated by the kinetic factors controlling the nucleation and growth mechanism. Kanig and Karge[10] have indicated that using slow cooling rates (1°/hr) results in large undercoolings. Initially, nucleation takes place mainly in the larger meshes. The growing crystallites will shove part of the network material together, forming thicker threads and bands, affecting the mesh dimensions in neighboring interstices, and ultimately cause stretching, disentangling, and possibly rupture of some of the linkages. Thus, the original mesh size distribution and in general the network topology will be affected by slow cooling rates. As a result, appreciable differences between melting and freezing behavior have been reported when following this procedure. In contrast, fast cooling rates will not allow larger crystallites time enough to grow at the expense of the adjacent regions—possibly due to difficulties in heat transfer—before the temperature corresponding to a nucleus size equal to or smaller than the average mesh size is reached. Therefore, upon fast cooling, nucleation and growth will occur in many meshes at about the same moment, the crystallite size distribution will more resemble the mesh size distribution, and the network will have suffered less deformation and damage. Very fast cooling rates, on the other hand, will tend to obscure the real freezing point because crystallization rates are not infinitely fast and large temperature gradients will cause distortion within the network.

Additional measurements have been made to arrive at an independent estimate of the crystallite size in frozen gels. Good agreement among the maxima in mesh size distribution curves for polystyrene gels in a number of solvents was found from electron microscopy and small angle X-ray diffraction, but no unique relationship with the freezing-point depression could be established owing to the uncertainty in the values of σ_{cl}.[10] Kuhn, *et al.*, have studied the broadening of the X-ray diffraction peaks in an effort to detect the presence of microcrystals in frozen gels.[11] Their results failed to indicate the existence of crystallites smaller than 800 Å in these systems, about an order of magnitude too large to account for the observed freezing-point depressions. Also, on subsequent heating, it was observed that the melting point depressions were considerably smaller than the freezing point depressions. This has been explained by assuming that the crystallites which are prevented from growing larger by the surrounding filaments of the gel are orientated parallel in a crystallographically exact manner toward their supporting crystal. Upon reaching the necessary size, they anneal into larger crystalline regions encasing the polymer filaments. This would explain the observed sharpness of the X-ray peaks as well as the smaller melting-point depressions. The occurrence of this type of annealing is further supported by the observation reported by Boonstra, *et al.*[12] These authors did not detect any annealing of benzene crystals in rubber vulcanizates over a period of 1 hr at a temperature of −30°, but on warming above −10°, annealing occurred quite rapidly as evidenced by the diminishing width of the 19.5° peak in the X-ray diffractograms. Even over long periods at −30° the character of the principle peak appeared to change.

The anomalous freezing point depression of polymer solutions, although less spectacular than that of gels, has frequently been attributed to the same cause, *i.e.*,

(8) W. Kuhn, E. Peterli, and H. Majer, *Z. Elektrochem.*, **62**, 296 (1958).

(9) G. Butenuth and H. Westlinning, *Rubber Chem. Technol.*, **37**, 311 (1964).

(10) G. Kanig and H. Karge, *J. Colloid Interface Sci.*, **21**, 649 (1966).

(11) W. Kuhn, R. Block, and P. Moser, *Experientia*, **18**, 197 (1962).

(12) B. B. Boonstra, F. A. Heckman, and G. L. Taylor, *J. Appl. Polym. Sci.*, **12**, 223 (1968).

Table I: Network Parameters of Poly(methyl methacrylate) Gels

Code	Volume fraction MMA	% DVB by vol of MMA	M_c	$\phi = q^{-1}$, equilib	q_0	ΔT, obsd	Cube size, $a = (\bar{r}^2)^{1/2}$, Å	Cube size, $a' = \left[\frac{2qM_c}{N_A\rho_p}\right]^{1/3}$, Å
W_1	0.125	3.3	11,700	0.0400	17.08	0.61	91.0	93.4
W_2	0.125	4.0	10,290	0.0459	14.57	0.71	85.4	85.5
W_3	0.125	4.7	9,450	0.0546	11.99	0.85	82.1	78.4
W_4	0.125	5.4	8,750	0.0550	11.52	0.86	79.6	76.2
X_1	0.150	1.3	19,300	0.0352	17.03	0.47	125.1	115.2
X_2	0.150	1.8	15,300	0.0401	15.65	0.56	108.3	102.1
X_3	0.150	2.2	13,470	0.0455	13.96	0.69	100.7	97.8
X_4	0.150	2.7	11,900	0.0515	11.64	0.83	96.2	86.3
Y_1	0.175	1.2	15,000	0.0410	14.88	0.53	108.2	100.6
Y_2	0.175	1.5	13,300	0.0464	13.12	0.74	101.5	92.8
Y_3	0.175	1.8	12,100	0.0515	11.52	0.86	97.2	86.8
Y_4	0.175	2.2	10,940	0.0578	9.84	0.99	93.3	80.8
Z_1	0.200	1.0	11,590	0.0431	15.94	0.53	90.3	90.8
Z_2	0.200	1.3	10,520	0.0518	12.54	0.83	87.4	82.7
Z_3	0.200	1.6	9,700	0.0603	9.86	1.11	86.0	76.5
Z_4	0.200	2.1	9,200	0.0695	8.29	1.46	84.6	71.5

that the growth of macrocrystals of freezing temperature T_0 is impeded by the presence of polymer chains. Although the growth of solvent nuclei is less restricted in solutions than in gels as a result of the greater mobility of uncrosslinked chains, it is reasonable to assume that the final crystallite dimensions will be affected by the conformation and concentration of the interpenetrating polymer solute.

We have studied the freezing and melting behavior of a number of polymer solutions as well as a series of swollen poly(methyl methacrylate) networks which were crosslinked in solution. This latter enabled us to vary the degree of crosslinking while maintaining a high degree of swelling. We have compared some of the specific topological features of these networks with those of gels crosslinked in the dry state.

Some theoretical considerations are presented which are capable of explaining our experimental observations.

Experimental Section

Preparation and Characterization of the Poly(methyl methacrylate) Networks. Methyl methacrylate and divinylbenzene were copolymerized in benzene solutions in various ratios (see Table I) following previously described techniques.[13] The equilibrium degrees of swelling of the resulting PMMA gels in pure benzene were determined by equilibrating cubic pieces of gel in benzene for 3–4 days at 25°. The gels were removed and weighed in closed bottles containing tissue paper to remove adherent solvent. They were then placed in an oven at 80° and dried until constant weight is attained. Assuming that the volume of the polymer and solvent are additive, the values for the degree of swelling, q, in pure benzene were then calculated from $q = V/V_0$, where V is the volume of the swollen gel and V_0 is that of the dry gel.

The properties of each of the 16 gels were characterized by measuring the extent of deswelling when the gels were equilibrated in dilute solutions of PMMA. The experimental procedure and the theoretical basis for this determination have been reported in detail in an earlier paper.[13] Values for M_c, the molecular weight between crosslinks, and q_0, the "relaxed" degree of swelling, are listed in Table I. The interaction parameter χ was determined separately from osmometric studies.

Determination of Freezing Point. A 0.5-ml sample of swollen gel or about 1 ml of polymer solution was placed in a small Pyrex vial and a thermocouple junction inserted *via* a rubber stopper. The assembly was placed inside a large empty boiling tube which was surrounded by a suitable Dry Ice bath. A reference thermocouple was immersed in a mixture of pure ice and degassed distilled water contained in a Dewar vessel. The output of the two thermocouples was connected to a Sargent X-T recorder using an amplification such that full scale deflection was obtained for a potential difference of 1.25 mV. The recorder was calibrated using the freezing points of pure water, pure benzene, and a series of standard naphthalene–benzene solutions. Sufficient time was allowed for the solutions to become homogeneous and their concentration was determined gravimetrically at the end of a run. Typical cooling curves, shown in Figure 2, exhibit slightly convex plateaus, signifying that there

(13) A. M. Rijke, *J. Polym. Sci., Part A*, 3, 2523 (1965).

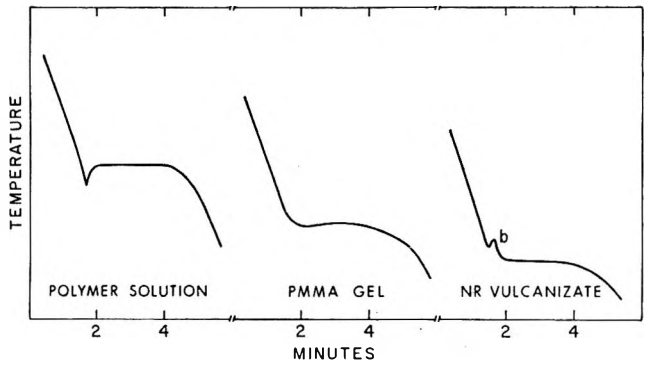

Figure 2. Typical freezing curves of polymer solutions, solution-crosslinked gels, and rubber vulcanizates.

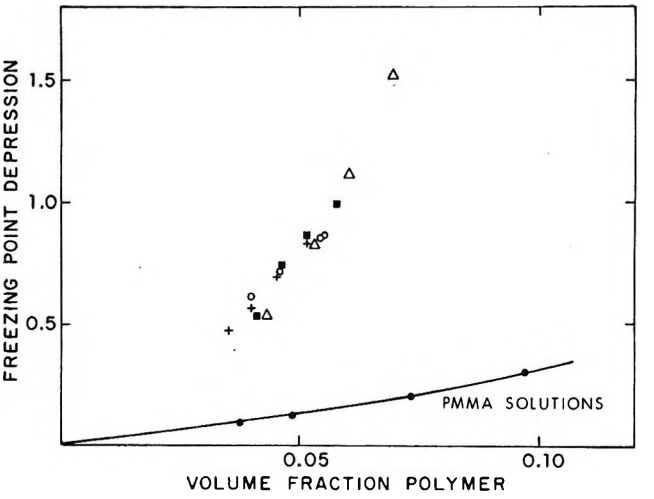

Figure 3. Plot of freezing point depression of benzene solutions *vs.* volume fraction polymer for PMMA solutions and gels: O, W series; +, X series; ■, Y series; Δ, Z series.

was a time during which the temperature remained steady. The small blip (b) is thought to represent the freezing of a small sheath of benzene surrounding the thermocouple wires in the gel.

Results and Discussion

The effect of the cooling rate on the observed values for ΔT and their reproducibility has been investigated in order to determine the freezing mechanism of our procedure and possible network damage. It was found that the results were markedly dependent on cooling rate if the samples were large, but no dependence was observed within a range of 0.2–16°/min for samples of 1 ml or less. For the gels, the reproducibility of the measurement, as determined by repeated freezing and melting of the same sample specimen and subsequent reswelling, was found to be independent of cooling rate, indicating that no appreciable extent of network damage occurred on freezing. No effect of cooling rate was noted for the solutions at concentrations below about 10% but there is a tendency for the freezing point depression to increase at the faster cooling rates near a concentration of 20%. For very viscous solutions ΔT becomes unusually large and the reproducibility of the measurement becomes very poor at cooling rates which gave perfectly satisfactory results for the less viscous solutions.

The freezing point depressions of the solutions and the four series of gels are graphically shown in Figure 3 as a function of volume fraction polymer. It is seen, even at high degrees of swelling (low crosslink density), that the freezing-point depressions of our solution-crosslinked gels are many times larger than those of the corresponding solutions, but significantly smaller than the ΔT values found for dry-crosslinked gels.[8] The former is in agreement with Kuhn's findings on polyacrylic acid–poly(vinyl alcohol) gels and solutions in water.[6]

In an attempt to elucidate the anomalous freezing-point depression of polymer gels and solutions we consider that there can be no doubt that eq 1 gives correctly the temperature T_m at which *large* crystals of pure solvent are in equilibrium with solution. As experimentally a lower equilibrium T_m* is found we can therefore conclude that the solid phase is not present in the form of continuous large crystals. The obvious explanation is that, owing to the presence of polymer chains, the solvent crystals are sufficiently small to reduce the equilibrium temperature as a result of interfacial effects. Although these considerations apply to a first approximation to gels and can be described quantitatively (eq 2), in no way do they accommodate the experimental anomalous freezing point depression of solutions other than by stating that the solute somehow impedes the growth of large solvent crystals. In view of this we propose to consider the thermodynamics of the phase transition from the point of equilibrium between a liquid solution on the one hand and a frozen, solid solution on the other in which the individual polymer chains are embedded and immobilized in the annealed, crystalline matrix of the solvent. Our proposition is based on the evidence that: (1) the experimentally observed freezing and melting point depressions are the same within experimental error and reproducible for moderately concentrated solutions and all solution-crosslinked gels and therefore represent a true equilibrium; (2) the crystallite dimensions from X-ray diffraction patterns,[11,12] even at −30°, are many times larger than inferred from the freezing point depression as given by eq 2; and (3) the annealing of small solvent crystallites can be observed directly at different temperatures by studying the diminishing width of the 19.5° peak in the X-ray diffractograms.[12]

The assumption that the polymer is not part of the solvent crystal lattice implies that, as a consequence, a large interface between amorphous polymer and crystalline solvent is developed upon freezing. Following a reasoning analogous to the derivation of the Gibbs–

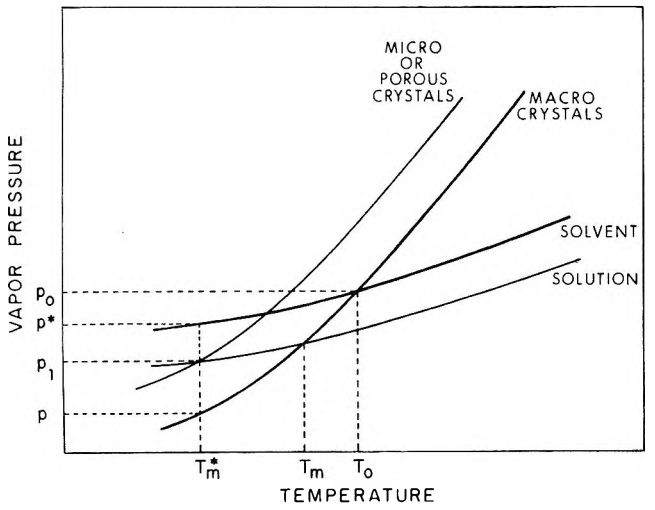

Figure 4. Vapor pressure curves for pure solvent, polymer solution, large solvent crystals, and very small or porous solvent crystals.

Thomson equation we can state that if a finite interfacial energy is involved in this interface a large vapor pressure and therewith a lower freezing point will ensue as a result of a greatly increased surface-to-volume ratio of the crystalline solvent phase. A frozen polymer solution of (macroscopic) unit volume may conveniently be conceived to form by sublimation of a solvent crystal of volume $(1 - \phi)$ at T_m^* where its vapor pressure is p, isothermal compression of the vapor from p to p_1, and subsequent condensation on the lattice sites in the solution crystal (see Figure 4). The amount of work involved in this isothermal distillation can be expressed as

$$\Delta W = [(1 - \phi)\rho_c/M]RT_m^* \ln p_1/p \quad (3)$$

and equals the energy involved in the newly created interface

$$\Delta W = \sigma S \quad (4)$$

where ρ_c is the density of the solvent crystal, M the molecular weight of the solvent, σ the interfacial energy, and S the new interfacial area. An accurate evaluation of S in terms of volume fraction of polymer appears to be impossible, but a rough estimate, with at best approximate value only, can, however, be made from the polymer dimensions, if some oversimplifications are made. We will assume that no polymer segments other than the immediately adjoining ones of the same chain occur as first neighbor pairs. This may be expected to hold to some extent for dilute solutions in good solvents. Further, we will neglect solvation of the chain by solvent molecules as there appears to be no way of assessing solvation without making certain rather arbitrary assumptions.[14] Both simplications, however, affect σ and S and, according to eq 4, an error in the one will be numerically compensated in the other. This also applies to our final result (eq 12) provided that S increases linearly with volume fraction of polymer. Writing then $S = 2\pi r_0 L$ and inserting in eq 4 yields, after equating eq 3 and 4

$$\ln p_1/p = KM\sigma[\phi/(1 - \phi)] \quad (5)$$

where

$$K = 2(\pi\rho_p N_A l_0/M_0)^{1/2}/RT_m^*\rho_c$$

where ρ_p is the density of the polymer, N_A Avogadro's number, l_0 the length and M_0 the molecular weight of a polymer unit, r_0 the "average" radius of the circular cross section of the polymer chain, and L the sum of the lengths of all chains.

For small values of $(p_1 - p)/p$ eq 5 may be rewritten

$$p_1 = p[1 + KM\sigma\phi/(1 - \phi)] \quad (6)$$

The vapor pressure p at temperature T_m^* is given by the Clausius–Clapeyron equation

$$p = p_0(1 - \Omega\Delta T/RT_0^2) \quad (7)$$

where $T_0 = T_m^* + \Delta T$ is the freezing temperature of pure solvent at pressure p_0 and Ω is the molar heat of sublimation. Inserting eq 7 in eq 6 then gives

$$p_1 = p_0[1 - \Omega\Delta T/RT_0^2 + KM\sigma\phi/(1 - \phi)] \quad (8)$$

as both $\Omega\Delta T/RT_0^2$ and K are very much smaller than unity. By considering that the melting temperature of the crystalline solvent in the frozen solution is the temperature at which the crystalline and liquid phase have the same vapor pressure p_1, we may write for the composition of the melt

$$\ln p_1/p^* = \ln (1 - \phi) + \phi + \chi\phi^2 \quad (9)$$

Here p^* represents the vapor pressure of the pure liquid solvent at T_m^* and is given by

$$p^* = p_0(1 - \Lambda\Delta T/RT_0^2) \quad (10)$$

Λ being the molar heat of evaporation of the solvent. Inserting eq 10 in eq 9 and expanding ln $(1 - \phi)$ with omission of powers of ϕ higher than the second, yields for small values of $(p_1 - p^*)/p^*$

$$p_1 = p_0[1 - \Lambda\Delta T/RT_0^2][1 - (1/2 - \chi)\phi^2] \quad (11)$$

Combining eq 11 and 8 and solving for ΔT gives finally, upon rearrangement

$$\Delta T(1 - \phi)/\phi = 10^3 KE\sigma + 10^3(E/M)(1/2 - \chi)\phi(1 - \phi) \quad (12)$$

where $E = 10^{-3}MRT_0^2/(\Omega - \Lambda)$ is the molar freezing point depression constant of the solvent. This result indicates that the freezing point depression is proportional to the interfacial energy between polymer and crystalline solvent and some properties of the polymer and solvent as reflected in K, χ, and E. Equations

(14) W. R. Moore and B. M. Tidswell, *J. Polym. Sci.*, **27**, 459 (1958).

Table II: Parameters for the Freezing Point Depression and Interfacial Energies of Some Polymer–Solvent Systems

System	$E_{solvent}$, deg/mol	$K \times 10^3$, cm² mol/erg	$\sigma_{interface}$, erg/cm²	$\sigma_{polymer}$ from parachor, ergs/cm²	$\sigma_{crystalline\ solvent}$, ergs/cm²	χ from slope	χ osmo. or vapor press.
Natural rubber–benzene	5.12	2.90	0.38	~36	~35	0.43	0.41[a]
cis-1,4-Polybutadiene–benzene		3.20	0.21	~35		0.43	0.34
PMMA–benzene		2.02	0.20	~44		0.38	0.44[b]
PVA–water	1.86	3.66	0.32	~94	~103	0.39	0.49[c]

[a] See ref 5. [b] See ref 13. [c] I. Sakurada, A. Nakajima, and H. Fujiwara, *J. Polym. Sci.*, **35**, 497 (1959).

9 to 12 can be generalized to include the effects of the presence of crosslinks. Prior to the gel point all of the polymer is soluble, the concentration will be determined by the available liquid volume, and the above equations will retain their validity. Beyond the gel point the system will exhibit limited swelling and a modification of the chemical potential of the solvent due to the elastic reaction of the network structure[15] should then be introduced in eq 9. Thus

$$\ln p_1/p^* = \ln (1 - \phi) + \phi + \chi\phi^2 + k(\phi^{1/3}/q_0^{2/3} - \phi) \quad (9a)$$

where k stands for the ratio between the molar volume of the solvent and that of the chains between crosslinks. If the gel is swollen to equilibrium the elastic term will balance the first three terms occurring in the right-hand member of eq 9a so that $p_1 = p^*$. This leads to

$$\Delta T(1 - \phi)/\phi = 10^3 KE\sigma \quad (12a)$$

The freezing point depressions of benzene in solutions of three different polymers have been determined over as wide a range of concentration as was experimentally accessible. The results are shown graphically in Figure 5 where $\Delta T(1 - \phi)/\phi$ is plotted against $\phi(1 - \phi)$ for benzene solutions of acetone-extracted natural rubber, *cis*-1,4-polybutadiene, and poly(methyl methacrylate). Also included in Figure 5 are some results from measurements on solutions of polyvinyl alcohol in water as reported by Ozasa and coworkers.[3] According to eq 12 these plots should be linear, which is borne out by experiment up to concentrations as high as 20%. Although the data beyond this concentration become increasingly inaccurate, there is a tendency to larger freezing points. In the light of the approximative nature of the assumptions underlying eq 12, deviations from the linearity are not surprising. The freezing point depressions are somewhat larger than those measured by Kawai[2] on similar systems for a corresponding concentration range. The difference is about 0.2–0.4° and can probably be attributed to the difference in sample size and measuring technique. From the slopes of the lines in Figure 5 values for χ can be calculated and are listed in Table I. They are

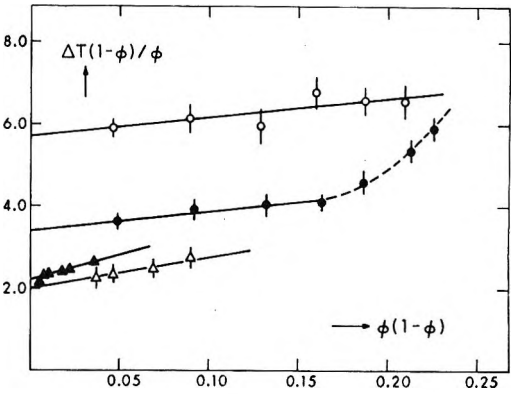

Figure 5. Plots of $\Delta T(1 - \phi)/\phi$ against $\phi(1 - \phi)$ according to eq 12 for polymer solutions: ○, natural rubber in benzene ($\bar{M}_n > 10^6$); ●, *cis*-1,4-polybutadiene in benzene ($\bar{M}_n = \bar{M}_w = 190{,}000$); △, poly(methyl methacrylate) in benzene ($\bar{M}_n = 152{,}000$); and ▲, polyvinyl alcohol in water ($\bar{M}_n = 68{,}000$) from the data of Ozasa, *et al.*[3]

all significantly larger than those calculated[2] using eq 1 and compare favorably with χ values derived from osmometric and vapor pressure measurements. The effect of difference in measuring temperature is considered to be negligible within the limits of error. Values for the interfacial energy σ can be obtained from the intercepts and are listed in Table II. Unfortunately, there are no data for σ from other experimental sources available in the literature to serve as an independent check on our results. However, it is possible to calculate approximate values for σ from the difference in surface free energy between crystalline solvent and amorphous polymer, provided that the chains are not solvated. The surface free energy of ice and benzene can be obtained from the theoretical considerations suggested by de Reuck.[16] They are listed in Table II. The surface free energies of amorphous polymers have been determined only for a small number of polymer liquids at temperatures well above their melting points.[17] However, when extrapolated

(15) J. J. Hermans, *J. Polym. Sci.*, **59**, 191 (1962).

(16) A. V. S. de Reuck, *Nature*, **179**, 1119 (1957).

(17) R. H. Dettre and R. E. Johnsen, *J. Colloid Interface Sci.*, **21**, 367 (1966).

to room temperature, these values are in satisfactory agreement with surface free energies calculated from the parachor and the liquid density extrapolated from above the melting point.[18] The surface energy of our polymer samples thus calculated are all close to the estimated surface energy of the crystalline solvents, *viz.*, about 35 ergs/cm² for benzene[8] and about 103 ergs/cm² for ice.[16] These and the values for the polymer surface energies are approximations only, owing to the assumptions made in the theoretical derivation and the sensitivity to the choice of group increments contributing to the parachor values.[19] The data show that our experimental values are about an order of magnitude smaller than those calculated, but the large uncertainty in the differences between the calculated surface energies does not warrant any further interpretation.

The freezing point depressions of gels, as described by eq 12a, indicate that the term $\Delta T(1 - \phi)/\phi$ should be constant for each polymer–solvent system swollen to equilibrium and independent of the number of crosslinks. This is borne out by our experimental data for the W series, which show a straight line passing through the origin if ΔT is plotted against $\phi/(1 - \phi)$. From the slope a value for σ of 1.42 ergs/cm² can be calculated, indicating that the interfacial energy (or interfacial area) may well be dependent on chain conformation. Similar plots for the X, Y, and Z series also exhibit straight lines, but with progressively larger slopes and intercepts on the abscissa indicating that the simplifying assumptions underlying eq 12a become less justified when the amount of diluent during crosslinking is reduced (see Figure 6). A probable explanation may be provided by the effect of the increasing number of polymer–polymer segment contacts in these systems, which will affect the value of σ and introduce an additional term on the right-hand side of eq 12a.

The freezing point depressions of the gels according to eq 2 is shown in Figure 7 where ΔT is plotted against $1/a$. Here a is assumed to be equal to $(\bar{r}^2)^{1/2}$ and calculated from M_c using

$$(\bar{r}^2)^{1/2} = \alpha(q/q_0)^{1/3}(\bar{r_0}^2)^{1/2} \qquad (13)$$

α is the molecular expansion factor, which, according to Stockmayer and Fixman,[20] equals

$$\alpha^3 - 1 = 2z \qquad (14)$$

where the perturbation parameter z, to a first approximation, is given by

$$z = 2(^3/_{2\pi})^{3/2}N_A^{-1}(\bar{r_0}^2/M_c)^{-3/2}A_2M_c^{1/2} \qquad (15)$$

where $(\bar{r_0}^2)^{1/2}$ is the root mean square end-to-end distance of the unperturbed chain of length M_c. A_2 is the second virial coefficient derived from osmometric measurements. For sufficiently large values of M_c, $(\bar{r_0}^2/M_c)^{1/2}$ can be considered to be constant at constant temperature. A value[13] of $(\bar{r_0}^2/M_c)^{1/2} = 665 \times 10^{-11}$ was used to calculate $(\bar{r_0}^2)^{1/2}$.

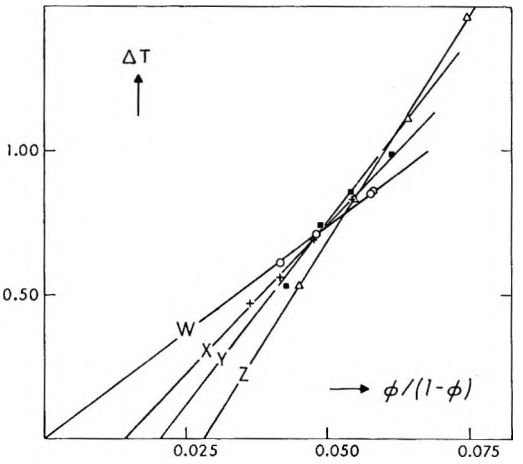

Figure 6. Freezing point depressions of solution-crosslinked PMMA gels in benzene, plotted according to eq 12a.

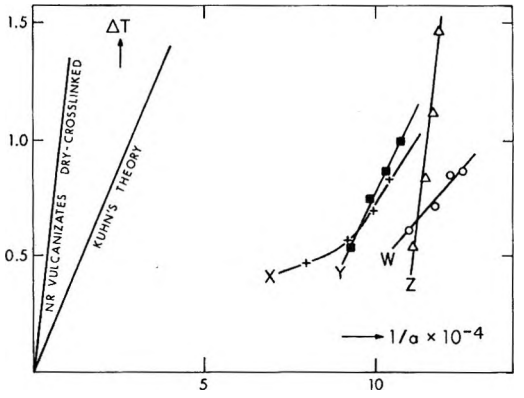

Figure 7. Freezing point depressions of solution-crosslinked PMMA gels in benzene, plotted according to eq 2, compared with natural rubber vulcanizates and theory.

The plots of ΔT against $1/a$ are linear over the freezing temperature range investigated in agreement with eq 2. According to this equation the freezing point depression is related to the network topology only in that ΔT is inversely proportional to a. The experimental results on natural rubber vulcanizates crosslinked in the dry state confirm this prediction, but our ΔT values for solution-crosslinked gels do not. For larger values of a a relation other than the one represented graphically seems to hold for these gels. Some indication of this is perhaps provided by the gel X_4. Unfortunately, further experimental investigation into the range of even more loosely crosslinked gels becomes increasingly prohibitive owing to difficulties in handling the samples.

The presence of diluent at the time of crosslinking not only lowers the freezing point depression but also affects the slopes of the lines in Figure 7. Smaller

(18) R. J. Roe, *J. Phys. Chem.*, 69, 2809 (1965).

(19) O. R. Quayle, *Chem. Rev.*, 53, 439 (1953).

(20) W. H. Stockmayer and M. Fixman, *J. Polymer Sci., Part C-1*, 137 (1963).

amounts of diluent cause the slopes to increase. One would expect the lines to move to the left when the amount of diluent is reduced and ultimately to coincide with the line found for the vulcanizates. This tendency is borne out by the set W, X, and Y, but the line representing the Z series is displaced to the right. This may well be explained by considering that the chains become increasingly intertwined when the amount of diluent during crosslinking is reduced, which will decrease the experimental values of M_c. An assessment of the interpenetration of chains can be made by comparison with a rock salt lattice-like manner of distributing the crosslinks in the gel.[8] The distance between two crosslinks calculated in this manner equals $a' = [2q(M_c/N_A\rho_p)]^{1/3}$. The data listed in Table I show that a and a' differ by less than 3% for series W but by about 7, 9, and 11% for the other series. This indicates that the statistical coils formed in the presence of decreasing amounts of diluent become increasingly interpenetrating. Apparently, in this dilution range, the interpenetration is more effective in reducing elastically active chain lengths than in inhibiting the growth of micro crystals. The latter probably becomes more pronounced when the percentage diluent during crosslinking is still further reduced.

On the basis of the experimental results reported here the anomalous freezing point depression of polymer solutions and gels can be interpreted by assuming that the freezing of the solvent is affected by the presence of the polymer chains in the following manner. For not too concentrated solutions nucleation of the solvent crystals takes place in the interstices between the chains. On subsequent growth the relatively mobile chains are pushed aside to some extent, but the actual crystallite sizes are severely limited by the presence of the chains. Rapid annealing of the crystallites takes place. The recorded freezing temperature (which equals the melting temperature) is the temperature at which the crystallites grow to their mature size and anneal into a macroscopic crystal with a very large internal surface area. Annealing may be limited by the chains in very concentrated solutions. A similar process takes place in gels crosslinked in the presence of very large amounts of diluent (more than about 85% for our gels) and probably also for other gels at very high degrees of swelling. When the amount of diluent during crosslinking is systematically reduced, the annealing of the crystallites takes place slower and to a lesser extent due to the restrictions imposed by the increasingly interpenetrating chains. Ultimately, annealing will be so slow that the freezing point depression will essentially follow eq 2, and a discrepancy between freezing point and melting point will be observed. Annealing will take place only to sizes less than about ten times the original crystallite size. For gels crosslinked in the absence of diluent, extensive interpenetration of chains will cause a to be much smaller than $(\bar{r^2})^{1/2}$.

The above conclusions are based on admittedly scarce experimental data. It should be borne in mind, however, that several areas, such as that of very highly swollen, loosely crosslinked gels are not experimentally accessible and that the correct evaluation of M_c and a becomes increasingly uncertain in the presence of smaller amounts of diluent.

A Thermodynamic Study of the Formation of Electron Donor–Acceptor Complexes by Gas–Liquid Chromatography[1]

by Claude Eon, Claude Pommier, and Georges Guiochon*

Ecole Polytechnique, Department of Chemistry, Paris, France *(Received January 18, 1971)*

Publication costs borne completely by The Journal of Physical Chemistry

A new more accurate theoretical treatment has been derived to study the equilibria of complex formation in solutions by gas chromatography. To check the validity of the equations derived, an experimental study of the electron donor–acceptor interactions between dibutyl tetrachlorophthalate and volatile derivatives of furan, thiophene, and pyrrole has been made. Experimental results are in very good agreement with those predicted by the theoretical equations. The results are discussed as a function of the structure of the compounds studied. An excellent correlation has been obtained between the equilibrium constants derived from gas chromatographic measurements and the aromaticity of these compounds evaluated from nmr data.

Introduction

Homogeneous equilibria in liquid phase can be studied by gas chromatography: if a volatile solute, B, is eluted through a column containing a nonvolatile complexing agent, A, mixed with an inert solvent, S, the retention time of B depends on the concentration of A in the stationary phase. In the simplest case of a 1:1 association

$$A + B \rightleftarrows AB \qquad (1)$$

Equation 2, relating the equilibrium constant K of this reaction, the chromatographic partition coefficient K_R on the mixture of A and S used as stationary phase, and the molar concentration (A) of this mixture, is usually accepted

$$K_R = K_R^\circ[1 + K(A)] \qquad (2)$$

where K_R° is the partition coefficient of B on the pure inert solvent, S.

This method of determination of equilibrium constants was first described by Chalkley, *et al.*[2a] It has been generalized by Purnell[2b] and used in studies on olefin–Ag^+ complexes,[3-7] on charge-transfer complexes[8,9] in organic solvents as well as on metallic chloro complexes in fused salts.[10,11]

However, eq 2 does not take into account either the activity coefficients of the various species in solution (the nonvolatile complexing agent A, the solute B, and the complex AB) or the entropic effects resulting from the differences in the molecular sizes of the two stationary phase components A and S. So, important errors can be made when equilibrium constants are calculated by this way. Eventually, this method may even lead to calculate values of equilibrium constants which are significantly different from zero in cases where no complex may occur, from gas chromatographic retention data obtained on mixtures of two liquid phases of various concentrations.

In this work, a new theoretical treatment is developed to account for these effects; the more general equations obtained are then illustrated by the study of the interactions between dibutyl tetrachlorophthalate and various derivatives of thiophene, furan, and pyrrole. The experimental results are compared with those derived from the theoretical relationships and discussed in term of the aromaticity of the solutes determined from nmr measurements.

Theoretical

We shall derive the general equations in the simplest case of a single 1:1 association between the volatile solute B and the additive A as written in eq 1. Similar derivation for successive complexes can easily be made and for them only the results will be given.

1. Equilibrium Constant and Partition Coefficient. The thermodynamic equilibrium constant K of complexing reaction 1 is related to the molar fractions X_i

(1) Presented at the 161st National Meeting of the American Chemical Society, Los Angeles, Calif., Mar 1971.

(2) (a) B. W. Bradford, D. Harvey, and D. E. Chalkley, *J. Inst. Petrol., London*, **41**, 80 (1955); (b) J. H. Purnell, "Gas Chromatography 1966," A. B. Littlewood, Ed., The Institute of Petroleum, London, 1967, p. 3.

(3) M. A. Muhs and T. F. Weiss, *J. Amer. Chem. Soc.*, **84**, 4697 (1962).

(4) E. Gil-Av and J. Herling, *J. Phys. Chem.*, **66**, 1208 (1962).

(5) A. N. Genkin and B. I. Buguslavskaya, *Neftkimiya*, **5**, 897 (1965).

(6) R. J. Cvetanovic, J. F. Duncan, W. E. Falconer, and R. S. Irwin, *J. Amer. Chem. Soc.*, **87**, 1827 (1965).

(7) H. Schnecko, *Anal. Chem.*, **40**, 1391 (1968).

(8) F. W. Willmott and A. B. Littlewood, *Anal. Chem.*, **38**, 1031 (1966).

(9) D. F. Cadogan and J. H. Purnell, *J. Chem. Soc. A*, 2133 (1968).

(10) R. S. Juvet, V. R. Shaw, and M. A. Khan, *J. Amer. Chem. Soc.*, **91**, 3788 (1969).

(11) C. Pommier, C. Eon, H. Fould, and G. Guiochon, *Bull. Soc. Chim. Fr.*, 1401 (1969); *C. R. Acad. Sci., Ser. C*, **268**, 1553 (1969).

and the activity coefficients γ_i of the various species by[12]

$$K = \frac{X_{AB}}{X_A X_B} \frac{\gamma_{AE}}{\gamma_A \gamma_B} \quad (3)$$

The partition coefficient K_R is defined in gas chromatography as the ratio of the total concentration of B (under either uncomplexed or complexed forms) in the liquid phase to the concentration of B in the gas phase.[13] From these definitions, the following relationship between K, K_R, and X_A can easily be derived

$$K_R = \frac{RT}{f_B^\circ v_{A,S}^\circ \gamma_B}\left[1 + KX_A\frac{\gamma_A\gamma_B}{\gamma_{AB}}\right] \quad (4)$$

In this equation f_B° is the fugacity of the pure B vapor in equilibrium with pure B liquid at the column temperature T and $v_{A,S}^\circ$ is the molar volume of the mixture A,S of molar fraction X_A.

It is most often possible to choose the inert solvent S so that the solution A,S has a quasiideal behavior and a molar volume varying linearly with the molar fraction

$$v_{A,S}^\circ = v_S^\circ + (v_A^\circ - v_S^\circ)X_A \quad (5)$$

where v_S° and v_A° are molar volumes of pure S and A, respectively.

The measurements were carried out by analytical gas chromatography; the solute B is infinitely diluted in the solution so that in eq 4 γ_B and γ_{AB} are activity coefficients at infinite dilution and will thus be denoted hereafter by γ_B^∞ and γ_{AB}^∞, respectively. The activity coefficient of B in the mixture A,S is classically expressed as the product of a thermal term ${}^t\gamma_{B(A,S)}^\infty$ and an athermal term ${}^a\gamma_{B(A,S)}^\infty$.[14] The athermal part of the activity coefficient at infinite dilution is given by the simplified Flory and Huggins equation[14]

$$\frac{1}{{}^a\gamma_{B(A,S)}^\infty} = \frac{v_{AS}^\circ}{v_B^\circ}\exp\left[\frac{v_B^\circ}{v_{AS}^\circ} - 1\right] \quad (6)$$

Practically, the molar volume of the solute is small compared with the molar volumes v_A° and v_S° of the heavy components A and S of the stationary phase which are not very different from each other. In these conditions it is easily shown, either by an expansion of the exponential function and neglecting the second-order terms or by numerical calculations, that the rather complicated expression obtained by combining eq 5 and 6 is practically equivalent to a linear variation of $1/{}^a\gamma_{B(A,S)}^\infty$ with X_A, so it can be written

$$\frac{1}{{}^a\gamma_{B(A,S)}^\infty} = \frac{1}{{}^a\gamma_{B(S)}^\infty} + \left[\frac{1}{{}^a\gamma_{B(A)}^\infty} - \frac{1}{{}^a\gamma_{B(S)}^\infty}\right]X_A \quad (7)$$

The logarithm of the thermal part of the activity coefficient ${}^t\gamma_{B(A,S)}$ is proportional to the enthalpy of mixing of the solute B in the stationary phase as an uncomplexed species. For solutes which do not give complex formation, we observed that this enthalpy does not vary significantly with the composition of the liquid phase if the solvent S is chosen so that eq 5 is valid. Then we can write

$${}^t\gamma_{B(A,S)}^\infty \simeq {}^t\gamma_{B(S)}^\infty \quad (8)$$

Combining eq 4, 7, and 8, we obtain the eq 9 which shows a linear variation of $K_R v_{A,S}^\circ$ *vs.* the mole fraction X_A

$$v_{A,S}^\circ K_R =$$

$$v_S^\circ K_R^\circ\left[1 + \left(\psi + K\frac{\gamma_{A(A,S)}\gamma_{B(S)}^\infty}{\gamma_{AB(A,S)}^\infty}\right)X_A\right] \quad (9a)$$

In this equation

$$K_R^\circ = \frac{RT}{f_B^\circ \gamma_{B(S)} v_S^{c\infty}} \quad (9b)$$

is the partition coefficient of B on the pure inert solvent and

$$\psi = \frac{\gamma_{B(S)}^\infty}{\gamma_{B(A)}^\infty} - 1 \quad (9c)$$

Contrary to what is often stated, especially when eq 2 is used, it is not possible to derive the equilibrium constant from measurements of gas chromatographic retention data, as can be seen from eq 9: the partition coefficient is a linear function of the mole fraction of the complexing additive but the slope of the linear plot of $v_{A,S}^\circ K_R$ *vs.* X_A does not give the equilibrium constant. It gives only

$$K\frac{\gamma_{A(A,S)}\gamma_{B(S)}^\infty}{\gamma_{AB(A,S)}^\infty} \quad (10)$$

We know however that we can define alternatively the activity coefficient γ_i^* of the species i in the pure solvent S using as reference state for the chemical potentials the infinitely diluted solution.[12] A thermodynamic constant K^* can then be defined as

$$K^* = \frac{X_{AB}}{X_A X_B}\frac{\gamma_{AB}^*}{\gamma_A^*\gamma_B^*} \quad (11)$$

It is easily shown that the activity coefficients γ_i^* and γ_i are proportional and that

$$\gamma_i^* = \frac{\gamma_i}{\gamma_i^\infty} \quad (12)$$

Combining eq 3, 11, and 12 gives

$$K^* = K\frac{\gamma_A^\infty\gamma_B^\infty}{\gamma_{AB}^\infty} \quad (13)$$

(12) J. E. Leffler and E. Grunwald, "Rates and Equilibria of Organic Reaction," Wiley, New York, N. Y., 1963, p 315.

(13) R. Juvet and S. Dal Nogare, "Gas Chromatography," Interscience, New York, N. Y., 1962.

(14) E. A. Guggenheim, "Mixtures," Oxford University Press, Oxford, 1954, Chapters X and XI.

Whenever the solution A,S is quasiideal so that $\gamma_{A(A,S)}$ is not appreciably different from γ_A^∞, eq 9a may be written

$$v_{A,S}^\circ K_R = v_S^\circ K_R^\circ [1 + (\psi + K^*)X_A] \quad (14)$$

and the constant K^* can be measured from gas chromatographic retention data. Although K^* is in one sense less general than K since it is defined by reference to the particular solvent S it is also a thermodynamical constant. It will be especially useful to consider these constants in practice for the comparative study of the behavior of derivatives of the same chemical family for example.

In the case of successive reactions of complex formations

$$\begin{aligned} A + B &\rightleftarrows AB \\ A + AB &\rightleftarrows A_2B \\ A + A_{n-1}B &\rightleftarrows A_nB \end{aligned} \quad (15)$$

with equilibrium constants $K_1, K_2, \ldots, K_n$, respectively, a similar treatment leads to the following relationship

$$v_{A,S}^\circ K_R = v_S^\circ K_R^\circ \left[1 + \left(\psi + K_1 \frac{\gamma_{A(A,S)}\gamma_{B(S)}^\infty}{\gamma_{AB(A,S)}^\infty}\right)X_A + K_1K_2 \frac{\gamma_{A(A,S)}^2\gamma_{B(S)}^\infty}{\gamma_{A_2B(A,S)}^\infty}X_A^2 + \ldots + K_1K_2\ldots K_n \frac{\gamma_{A(A,S)}^n\gamma_{B(S)}^\infty}{\gamma_{A_nB(A,S)}^\infty}X_A^n\right] \quad (16)$$

2. Influence of the Temperature. The specific retention volume V_g is related to the enthalpy of solution $\Delta H_{A,S}^d$ of the solute in the liquid stationary phase by the well known equation[13]

$$\frac{d}{d\frac{1}{T}} \ln V_g = \frac{-\Delta H_{A,S}^d}{R} \quad (17)$$

The specific retention volume is related to the partition coefficient K_R and the density of the liquid phase $d_{A,S}$ by the equation[12]

$$V_g = \frac{273K_R}{Td_{A,S}} \quad (18)$$

Finally the enthalpy ΔH^r of the reaction of complex formation is given by

$$\frac{d}{d\frac{1}{T}} \ln K = -\frac{\Delta H^r}{R} \quad (19)$$

whereas the excess enthalpy ΔH^E of this reaction[12] is given by

$$\frac{d}{d\frac{1}{T}} \ln \frac{\gamma_{A(A,S)}\gamma_{B(A,S)}}{\gamma_{AB(A,S)}} = -\frac{\Delta H^E}{R} \quad (20)$$

Differentiating eq 9 and 18 *vs.* $1/T$ and combining with eq 17, 19, and 20 gives

$$\Delta H_{A,S}^d = \Delta H_S^d + \frac{(\Delta H^r + \Delta H^E)K\frac{\gamma_{A(A,S)}\gamma_{B(S)}}{\gamma_{AB(A,S)}}X_A}{1 + \left(\psi + K\frac{\gamma_{A(A,S)}\gamma_{B(S)}}{\gamma_{AB(A,S)}}X_A\right)} \quad (21)$$

when ΔH_S^d is the enthalpy of solution of the solute in the pure inert solvent.

Using the equilibrium constant at infinite dilution in the pure inert solvent, K^* defined by eq 11, we obtain

$$\Delta H_{A,S}^d = \Delta H_S^d + \Delta H^{r*}\frac{K^*X_A}{1 + (\psi + K^*)X_A} \quad (22)$$

The enthalpy of dissolution $\Delta H_{A,S}^d$ of the solute B in the solvent A,S is a homographic function of the molar fraction of the stationary phase. This enthalpy accounts for both the chemical and the physical thermal effects occurring when the gaseous solute dissolves and is partially complexed in the liquid phase.

Experimental Section

A laboratory-made gas chromatograph has been used for the experimental measurements of partition coefficients; special care has been taken to control column temperature (±0.2° in 1 day, gradient less than 0.5° along the column), inlet and outlet pressures. The eluted vapors are detected by a flame ionization detector. Experiments have been carried out in the temperature range 60–100°.

The columns used are metal tubes (2 mm i.d., 0.5–2 m long), filled with Chromosorb P, 80–100 mesh, acid washed, treated with dimethyldichlorosilane, and coated in the ratio of 40 g of squalane–dibutyl tetrachlorophthalate (DBTC) mixture for 100 g of solid support; the following molar fractions of DBTC have been used: 0, 0.094, 0.168, 0.322, 0.447, 0.68, 0.90, and 1. The solid support was provided by Johns-Manville, New York, N. Y., the dibutyl tetrachlorophthalate by Varian Aerograph, Walnut Creek, Calif., and the squalane by Touzart et Matignon, Paris, France. The DBTC sample was pure as ascertained by its uv and ir spectra and by tlc; squalane samples were checked for squalene and rejected if traces were found.

The exact amount of liquid phase coated on the support is determined by Soxhlet extraction from a weighed fraction of the impregnated solid. After using a column several weeks a similar treatment is made on the stationary phase unpacked from the inlet of the column. We observed no significant change in the liquid to solid ratio nor in the squalane to DBTC ratio so that the liquid phase seems really to remain stationary in the conditions whose the measurements have been carried out.

Table I: Partition Coefficients K_R and Enthalpies of Solution ΔH^d (kcal/mol) at 80.3°

Solute	$X_{DBTC} = 0$		$X_{DBTC} = 0.094$		$X_{DBTC} = 0.168$		$X_{DBTC} = 0.322$		$X_{DBTC} = 0.447$		$X_{DBTC} = 0.680$		$X_{DBTC} = 0.90$		$X_{DBTC} = 1$	
	K_R	$-\Delta H^d$	K_R	$-\Delta H^d$	K_R	$-\Delta H^d$	K_R	$-\Delta H^d$	K_R	$-\Delta H^d$	K_R	$-\Delta H^d$	K_R	$-\Delta H^d$	K_R	$-\Delta H^d$
Cyclopentene	39.3	6.25	39.6	6.22	39.9	6.22	40.4	6.23	41.0	6.23	42.2	6.26	43.5	6.25	44.3	6.26
Cyclopentadiene	30.9	6.04	31.8	6.18	32.6	6.31	34.4	6.61	36.0	6.85	39.5	7.32	43.8	7.77	46.1	7.99
Diethyl ether	23.0	6.31	23.2	6.30	23.4	6.32	23.8	6.37	24.2	6.40	25.0	6.35	26.1	6.33	26.7	6.45
Divinyl ether	14.3	5.75	15.1	5.75	15.7	5.79	17.1	5.87	18.5	5.92	21.5	6.03	25.0	6.11	27.0	6.16
2,5-Dihydrofuran	56.5	7.24	59.7	7.26	62.4	7.30	68.6	7.38	74.3	7.44	87.0	7.56	102	7.64	110.6	7.68
Furan	17.2	5.56	18.5	5.62	19.6	5.69	22.0	5.83	24.3	5.92	29.3	6.09	35.3	6.22	38.7	6.28
2-Methylfuran	45.7	6.66	48.6	6.74	51.0	6.82	56.7	6.98	61.9	7.09	73.4	7.32	87.2	7.48	95	7.56
Tetrahydrothiophene	270	8.47	284	8.46	297	8.46	326	8.46	353	8.50	411	8.52	482	8.53	522	8.53
Thiophene	88	7.06	95.3	7.17	101	7.26	116	7.45	129	7.58	158	7.81	193	7.97	213	8.05
2-Methylthiophene	212	8.24	228	8.36	242	8.46	274	8.69	304	8.84	369	9.12	448	9.32	492	9.41
3-Methylthiophene	228	8.22	246	8.33	260	8.43	294	8.64	325	8.78	394	9.03	477	9.23	524	9.31
2,5-Dimethylthiophene	482	9.32	520	9.45	552	9.56	627	9.79	696	9.96	848	10.24	1030	10.45	1135	10.54
2-Ethylthiophene	446	9.31	477	9.36	502	9.43	561	9.56	616	9.65	736	9.83	880	9.95	963	10.02
2-Chlorothiophene	337	8.49	367	8.82	392	8.91	450	9.08	503	9.20	621	9.41	760	9.56	843	9.63
2,5-Dichlorothiophene	1080	10.0	1160	10.11	1220	10.20	1375	10.38	1510	10.51	1815	10.73	2180	10.90	2380	10.99
2-Bromothiophene	672	9.29	740	9.46	798	9.60	929	9.86	1050	10.04	1320	10.33	1640	10.53	1820	10.63
3-Bromothiophene	772	9.40	860	9.60	933	9.76	1105	10.05	1260	10.25	1610	10.56	2020	10.78	2260	10.87
3,4-Dibromothiophene	6190	10.95	7210	11.44	8080	11.78	10060	12.34	11870	12.68	15880	13.18	20700	13.51	23430	13.64
2-Iodothiophene	1610	9.83	1810	10.13	1980	10.36	2360	10.77	2720	11.04	3510	12.51	4450	11.74	4980	11.86
Pyrrole	103	8.30	129	8.39	152	8.52	210	8.83	270	9.09	426	9.64	650	10.15	795	10.39
1-Methylpyrrole	126		143		157		191		223		297		393		451	
Benzene	87.2	7.02	93.7	7.13	99.2	7.23	111	7.44	123	7.58	149	7.83	179	8.03	197	8.09

All experimental parameters, column temperature, column inlet and outlet pressures, gas flow rate, and mass of stationary phase, are controlled and/or measured carefully so that the specific retention volumes and the partition coefficients can be calculated with a relative error less than 0.5% at the 95% confidence level.[15] A Varian HA-100 nmr spectrometer has been used to record at 80° the spectra of the solutes dissolved in squalane. No significant changes have been observed in the spectra when the ponderal concentration of the solutes was increased from 2.5 to 10%.

Results

1. Gas Chromatographic Measurements. We have measured the partition coefficients of furan, thiophene, pyrrole, and substituted derivatives on dibutyl tetrachlorophthalate–squalane mixtures covering the full range of molar fraction.

Electron donor–acceptor complexes are known to form between benzene derivatives and DBTC[9] and it was expected that the aromatic heterocyclic compounds studied form similar complexes.

The values of K_R and $\Delta H_{A,S}{}^d$ were derived from the retention data by the usual equations.[13] Table I gives the values of K_R and $\Delta H_{A,S}{}^d$ at 80° on each of the eight stationary phases used. The measured densities of the liquid phases are given in Table II so that K_R can be calculated at each temperature. As expected from theoretical eq 9 and 14, a linear variation of $v_{A,S}{}^\circ K_R$ with the molar fraction X_A is observed when a single 1:1 complex is formed. This is the case of the furan and thiophene derivatives studied. A parabolic variation is found when two successive associations occur as happens with the pyrrole derivatives. These results are illustrated by Figures 1 and 2.

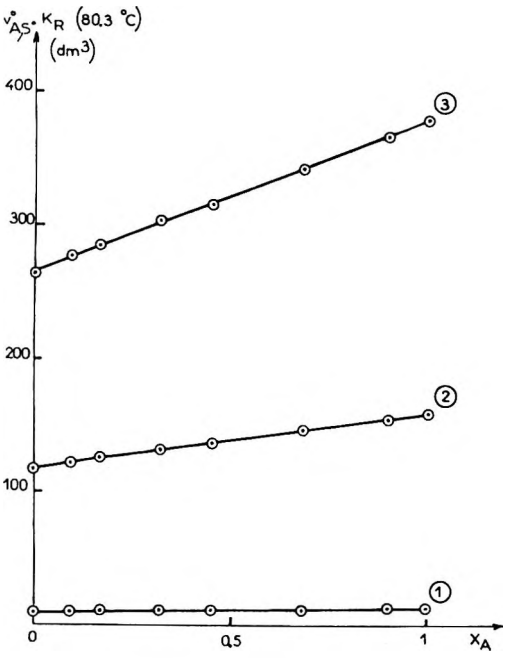

Figure 1. Variation of $v_{A,S}{}^\circ K_R$ with the composition of the liquid stationary phase: values at 80.3° for furan (1), 2-methylthiophene (2), and 2,5-dimethylthiophene (3).

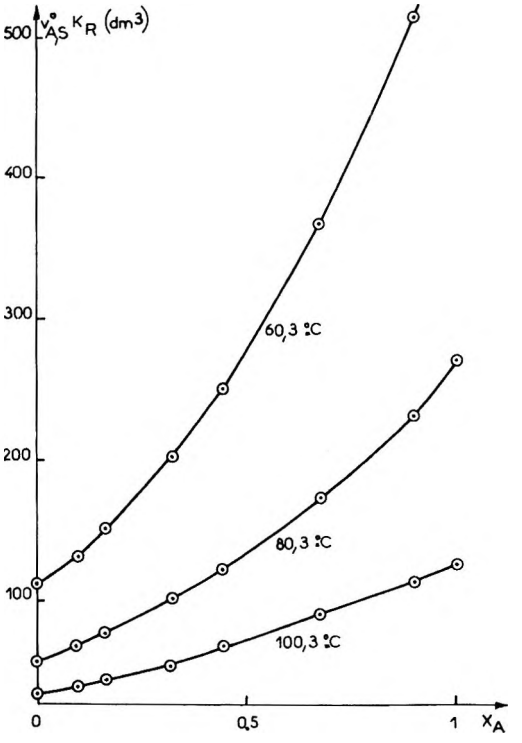

Figure 2. Variation of $v_{A,S}{}^\circ K_R$ with the composition of the liquid stationary phase for pyrrole at various temperatures.

Table II: Density of Mixtures of Squalane and Dibutyl Tetrachlorophthalate Used as Stationary Phases

	T, °C				
X_{DBTC}	60.3	70.3	80.3	90.3	100.3
0	0.784	0.777	0.770	0.763	0.757
0.094	0.814	0.806	0.798	0.790	0.782
0.168	0.839	0.831	0.823	0.815	0.807
0.322	0.896	0.888	0.880	0.871	0.863
0.447	0.949	0.940	0.931	0.923	0.914
0.68	1.061	1.052	1.044	1.035	1.025
0.90	1.200	1.189	1.179	1.168	1.158
1	1.281	1.270	1.260	1.249	1.238

To determine the equilibrium constants K^* using eq 11, the ψ values have been calculated from the measured molar volumes $v_A{}^\circ$, $v_B{}^\circ$, and $v_S{}^\circ$ by the equation

$$\psi = \frac{v_A{}^\circ}{v_S{}^\circ} \frac{\exp[v_B{}^\circ/v_A{}^\circ]}{\exp[v_B{}^\circ/v_S{}^\circ]} - 1 \qquad (23)$$

The values of the equilibrium constants and of the derived thermodynamic functions of the reaction at infinite dilution in squalane are reported in Table III for the 22 solutes studied. It should be pointed out that if this procedure is applied to the retention data of alkanes or cyclohexane, a null value is obtained for the

(15) M. Goedert and G. Guiochon, *Anal. Chem.*, 42, 962 (1970).

Table III: Equilibrium Constants K^* and Thermodynamic Functions of Complexation Reactions with DBTC

Solute	K^* 60.3°	70.3°	80.3°	90.3°	100.3°	$\Delta G^{*\,a}$ (80.3°)	$\Delta H^{*\,a}$	$\Delta S^{*\,b}$
Cyclopentene	7.10^{-3}	6.10^{-3}	$4.8.10^{-3}$	$4.2.10^{-3}$	$3.5.10^{-3}$			
Cyclopentadiene	0.42	0.29	0.21	0.15	0.11	0.11	−8.20	−26.3
Diethyl ether	6.10^{-2}	1.7×10^{-2}	5×10^{-3}	2×10^{-3}	6×10^{-4}	3.65	−28.4	−90.8
Divinyl ether	0.50	0.47	0.46	0.44	0.42	0.55	−1.00	−4.39
2,5-Dihydrofuran	0.545	0.521	0.499	0.479	0.461	0.49	−1.03	−4.30
Furan	0.776	0.730	0.690	0.653	0.620	0.26	−1.39	−4.65
2-Methylfuran	0.680	0.624	0.575	0.533	0.495	0.39	−1.95	−6.62
Tetrahydrothiophene	0.491	0.489	0.488	0.487	0.485	0.50	−0.069	−1.62
Thiophene	0.928	0.858	0.796	0.742	0.694	0.016	−1.79	−5.52
2-Methylthiophene	0.866	0.783	0.712	0.651	0.597	0.024	−2.29	−7.14
3-Methylthiophene	0.843	0.765	0.698	0.640	0.590	0.25	−2.20	−6.93
2,5-Dimethylthiophene	0.881	0.792	0.716	0.651	0.595	0.023	−2.42	−7.40
2-Ethylthiophene	0.662	0.618	0.580	0.545	0.515	0.38	−1.55	−5.47
2-Chlorothiophene	0.946	0.884	0.838	0.770	0.726	0.012	−1.63	−5.02
2,5-Dichlorothiophene	0.748	0.685	0.630	0.583	0.541	0.32	−2.00	−6.45
2-Bromothiophene	1.15	1.04	0.946	0.864	0.794	0.039	−2.29	−6.59
3-Bromothiophene	1.33	1.19	1.07	0.980	0.896	−0.052	−2.40	−6.66
3,4-Dibromothiophene	2.16	1.84	1.60	1.35	1.16	−0.33	−3.86	−10.0
2-Iodothiophene	1.51	1.33	1.18	1.02	0.90	−0.12	−3.24	−8.84
Pyrrole K_1	1.81	1.87	1.93	2.00	2.06	−0.46	+0.78	+3.52
Pyrrole K_2	1.57	1.20	0.94	0.74	0.59	0.045	−6.09	−17.4
1-Methylpyrrole K_1	1.04	1.11	1.19	1.26		−0.12	+1.56	+4.75
1-Methylpyrrole K_2	0.715	0.355	0.183	0.099		1.18	−15.87	−48.3
Benzene	0.822	0.747	0.683	0.627	0.580	0.27	−2.16	−6.88

[a] In kcal/mol. [b] In cal/mol.

constant K^* which does not occur when eq 2 is used, which proves that our theoretical treatment is sound and that the behavior of the DBTC–squalane solutions is quasiideal.

K^* is determined with a relative standard deviation which is less than 0.25% in most cases and about 0.5% for the most volatile solutes. A very good linear variation of ln K^* *vs.* $1/T$ is observed even when two successive complexes are formed as with pyrrole derivatives. ΔH^{r*} can be calculated with a good precision (relative standard deviation $\leq 1\%$) and reactions are exothermic except the first complexation reaction of pyrrole derivatives (Figure 3). The validity of eq 22 has been checked by calculating Φ from the expression

$$\Phi = \left[\frac{\Delta H^{r*}K^*}{\Delta H_{A,S}{}^{d} - \Delta H_S{}^{d}} - (\psi + K^*)\right]X_A = 1 \quad (24)$$

As shown in Table IV for some solutes taken as examples, a good agreement with the theoretical equation is obtained. The same agreement was observed with all compounds. The disagreement observed at low mole fraction of DBTC results from the low precision on the difference $\Delta H_{A,S}{}^{d} - \Delta H_S{}^{d}$.

2. Nuclear Magnetic Resonance Measurements. As in aromatic compounds, the internal chemical shift of ring protons measured in heterocyclic derivatives characterizes the ring current and its absolute value increases when aromaticity increases.[16,17] Nmr measurements have been made on proton 4 for 2-monosubstituted furans and thiophenes and some 2,5-disubstituted derivatives of thiophene. The anisotropic effect of methyl and chloro substituents is small and the additivity rules are verified in these last compounds. Results are given in Table V. Because of the small proton 4 unshielding in 2-methylfuran and of the large difference in the resonance energies of furan and thiophene it

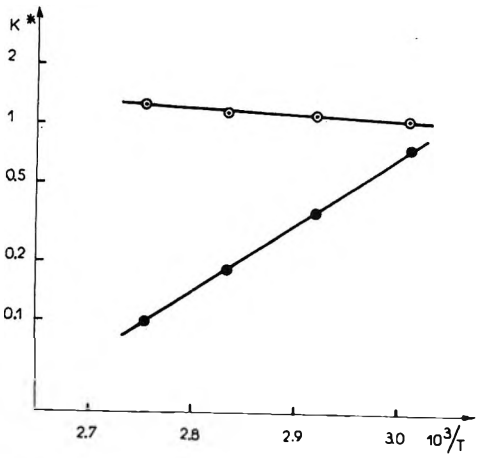

Figure 3. Influence of the temperature on the equilibrium constants of 1-methylpyrrole with DBTC: ○, first equilibrium; ●, second equilibrium.

(16) Y. Pascal, J. P. Morizur, and J. Wiemann, *Bull. Soc. Chim. Fr.*, 2211 (1965).

(17) J. P. Morizur and Y. Pascal, *ibid.*, 2296 (1966).

Table IV: Variation of the Function Φ (Eq 24 with the Mole Fraction of DBTC at 80.3°)

X_{DBTC}	Thiophene	3-Bromothiophene	2-Iodothiophene
0.094	1.26	1.12	1.10
0.168	1.13	1.07	1.05
0.322	1.03	1.01	1.02
0.447	1.02	1.00	1.01
0.68	0.99	0.99	1.01
0.90	1.00	0.99	1.02
1	0.99	0.99	1.02

seems reasonable to establish a single increasing aromaticity scale of the investigated compounds in the order they appear in Table V.

Table V: Nmr Measurements at 80° in Squalane of Proton 4 Chemical Shifts (in ppm)

Solute	δ	Δδ
Furan	6.32	0
2-Methylfuran	6.20	−0.12
Thiophene	6.92	0
2-Methylthiophene	6.68	−0.24
2-Ethylthiophene	6.70	−0.22
2-Chlorothiophene	6.66	−0.26
2-Bromothiophene	6.65	−0.27
2-Iodothiophene	6.58	−0.34
2,5-Dimethylthiophene	6.33	−0.59
2,5-Dichlorothiophene	6.52	−0.40

Discussion

As shown, the experimental results are in excellent agreement with the theoretical relationships derived, which confirm the validity of the theoretical treatment given above.

1. Furan and Thiophene Derivatives. Except for pyrrole derivatives, all aromatic compounds studied show a single, exothermic, 1:1 association with dibutyl tetrachlorophthalate. We can expect that such associations are of the same type as those previously described between trinitrobenzene and thiophene,[18] *i.e.*, a $\pi-\pi$ complex between the two parallel planar rings. If this is so, the stability of the complexes should increase with the aromaticity of the donor at least as long as no steric hindrance occurs. This is well verified for the fundamental five-membered rings giving 1:1 associations (Table VI). However, it is observed that the listing of the substituted derivatives by increasing order of K^* differs from the listing by increasing order of known electron donor ability of these compounds. For example, 2-ethylthiophene forms a less stable complex than furan does, although it is more aromatic. Such anomalies cannot be explained by a steric hindrance of the reaction. They can probably be accounted for by preferential orientations of the substituted heterocyclic rings above the DBTC plane, depending on dipole–dipole interaction. This assumption is supported by the following results. It is a well-known semiempirical fact in the thermodynamics of reactions that, for a given reaction, there is a linear relationship between the reaction enthalpies ΔH^r and entropies ΔS^r for substituted derivatives of the same family.[12]

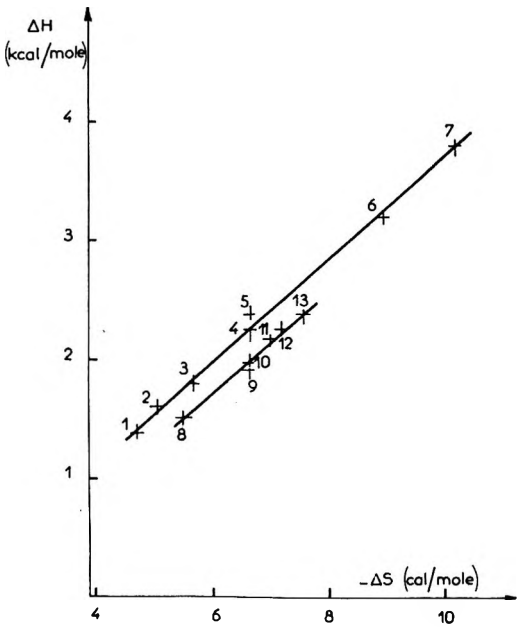

Figure 4. Relationship between enthalpy and entropy of complexing reactions: 1, furan; 2, 2-chlorothiophene; 3, thiophene; 4, 2-bromothiophene; 5, 3-bromothiophene; 6, 2-iodothiophene; 7, 3,4-dibromothiophene; 8, 2-ethylthiophene; 9, 2,5-dichlorothiophene; 10, 2-methylfuran; 11, 3-methylthiophene; 12, 2-methylthiophene; 13, 2,3-dimethylthiophene.

Table VI: Equilibrium Constants and Resonance Energies of Fundamental Five-Membered Rings

Compound	K^* (80°)	E_R, kcal/mol
Cyclopentadiene	0.21	3.5
Furan	0.69	23
Thiophene	0.80	29
Pyrrole	0.94[a]	24

[a] Second equilibrium constant.

As shown on Figure 4, when ΔH^r is plotted *vs.* ΔS^r for all the compounds studied here, it is observed that the points fall on two portions of straight lines, corresponding to two different reaction mechanisms. Each

(18) A. Kraak and H. Wynberg, *Tetrahedron*, **24**, 3881 (1968).

population of solutes can be classified in increasing order of K^*

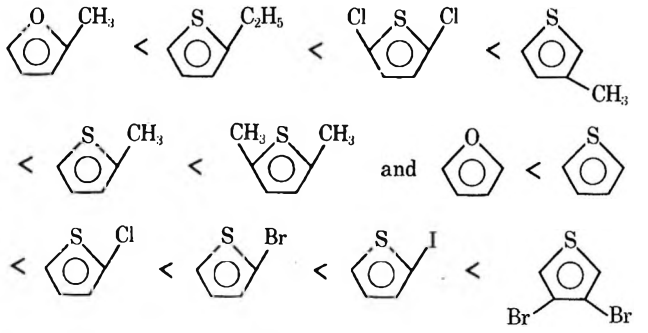

and there should be a correlation in each series with the order of increasing aromaticity. Indeed it is observed that in each of these two series, the aromaticity of the molecules increases in the same order as K^*, except for 2,5-dichlorothiophene which has an aromaticity lower than that predicted from K^* value.

In the first group are all compounds containing substituents with inductive effect; in the second group are fundamental rings and substituted derivatives containing substituents with mesomeric effect (except 2,5-dichlorothiophene). The slight difference in reaction mechanism can probably be ascribed to differences in electrostatic interaction between the substituents of the DBTC molecule and the substituents of the electron donor which are differently charged in the two series of molecules. The presence of 2,5-dichlorothiophene in the first series can be explained by a resonance effect between the two chlorine atoms decreasing the charges appearing on these atoms

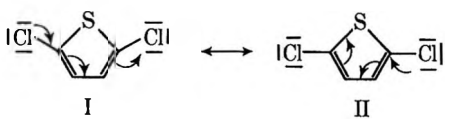

I II

A similar resonance in 3,4-dibromothiophene will require mesomeric forms

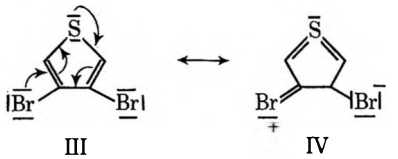

III IV

which are less stable than for forms I and II, which may explain why this compound is in the first series.

2. Pyrrole Derivatives. Pyrrole and methylpyrrole react with dibutyl tetrachlorophthalate to form two successive complexes: PyDBTC and $Py(DBTC)_2$. Pyrroles have been found to give a 1:1 complex with aromatic compounds such as thiophene; in this complex the two rings are orthogonal or at least nonplanar, thus different from a π–π charge-transfer association.[19] As remarked above, the first association of pyrrole with DBTC is endothermic, whereas all π–π complex formations observed with other heterocyclic aromatic compounds are exothermic. Thus, it is probable that the first equilibrium deals with a dipole–dipole interaction of the two molecules and that the second reaction is a π–π charge transfer, with a parallel approach of the two planar rings. If this is so, the aromaticity of the first molecule of pyrrole is increased because of the increased negative charge on the nitrogen atoms and the second equilibrium constant should be larger than expected from the resonance energy of the pyrrole ring. Values reported in Table VI show that this is in agreement with the experimental results. Otherwise, we can remark that the points relative to the second complexation of pyrrole derivatives in the $\Delta H/\Delta S$ plot do not fall on one or the other lines corresponding to furans and thiophenes.

3. Other Derivatives. A few nonaromatic compounds (ethers, hydrocarbons, hydrogenated furans, and thiophenes) have also been investigated. The experimental results are reported in Tables I and III. General laws cannot be drawn from the results obtained because of the diversity of the derivatives but it should be noted that rather stable associations are formed when the solute molecule has a heteroatom bearing an unshared pair of electrons, except if a steric hindrance occurs such as with diethyl ether. For example, an association is formed between tetrahydrothiophene and DBTC which is probably a π–n complex, involving the shared pair of electrons of the sulfur atom and the π electrons of the acceptor. When the molecule contains also one or two double bonds, it is not possible with the available information to predict how the association is formed nor even if there is a parallel or nonparallel approach of the two molecule planes.

Conclusion

The reaction of complex formation in the liquid phase can be studied and equilibrium constants can be measured with high precision by gas–liquid chromatography. As we have shown elsewhere[20] the values obtained by this method are in very good agreement with those derived by a conventional method from measurements made in ultraviolet spectroscopy, but gas–liquid chromatography results are easier and faster to obtain, and much more precise. Moreover, because the chromatographic process is a separation technique, rigorous purification of the solutes is not necessary as in the case of classical techniques. This not only saves time but also can enhance the accuracy of the method. This precision justifies a refined theoretical treatment and allows a more subtle analysis of the structure of the studied complexes than is possible with the conventional methods.

(19) R. B. Jones, *Advan. Heterocycl. Chem.*, in press.

(20) C. Eon, C. Pommier, and G. Guiochon, *C. R. Acad. Sci., Ser C*, 270, 1436 (1970).

Appendix

List of Symbols

f_i° fugacity of the constituent i
(i) molar concentration of the solute i
K equilibrium constant of the complexing reaction
K^* equilibrium constant defined with all species infinitely diluted in an inert solvent S
K_R gas chromatographic partition coefficient
K_R° partition coefficient on the pure solvent S
X_i mole fraction of the solute i
v_i° molar volume of i
$\gamma_{i(m)}$ activity coefficient of the solute i dissolved in m
${}^a\gamma_{i(m)}^\infty$, ${}^t\gamma_{i(m)}^\infty$ athermal and thermal terms of the activity coefficient of i infinitely diluted in m
$\Delta H_m{}^d$ enthalpy of dissolution in the liquid m
ΔH^E excess enthalpy of the complexing reaction
ΔH^r enthalpy of the complexing reaction
ΔH^{r*}, ΔG^{r*}, $\Delta S^{r\Delta*}$ thermodynamic functions, enthalpy, free enthalpy, and entropy, of the reaction in the solvent S, same reference state as for K^*

Correlation of Heterogeneous Charge-Transfer Rate Constants and Homogeneous Rate Constants for Removal of Coordinated Water in the Ac and Dc Polarographic Study of Some Irreversibly Reduced Complex Ions in Aqueous Solution

by A. M. Bond

Department of Inorganic Chemistry, University of Melbourne, Parkville, 3052, Victoria, Australia
(Received December 17, 1970)

Publication costs borne completely by The Journal of Physical Chemistry

To test the potential usefulness of a previously proposed simple polarographic method for determining the nature and stability of irreversibly reduced complex ions, which relies on heterogeneous charge-transfer rate constants being independent of ligand concentration, it was necessary to study the mechanism of reduction of the aquo and complexed metal ions. In this regard, the importance of the removal of coordinated water is shown by the extremely good correlation found between the homogeneous rate constant for this reaction and the heterogeneous charge-transfer rate constant. In general, when the rate constant for water removal in the aquo complex is greater than 10^8 sec^{-1}, a reversible electrode process is observed; for rate constants in the range 10^8 to 10^7 sec^{-1}, the electrode process is quasireversible; for rate constants less than 10^7 sec^{-1}, the electrode process is irreversible. Conclusions from this correlation are given. In the presence of nonadsorbable complex forming ligands, the heterogeneous charge-transfer rate constants do not appear to be altered greatly compared with those for the aquo complex and the simple calculation method can be used to qualitatively assess the strength of such systems, as is shown with Co(II), Mn(II), and Fe(II). For systems where no change in rate constants occurs on complex formation, and for which it is believed that the slow removal of water remains rate determining, the simple calculation method can be used to obtain stability constants. Such is the case for some complexes of Ni(II). The use of conventional and rapid ac and dc polarographic techniques in these studies is described.

Polarographic reduction of aquo and complexed metal ions has received considerable attention in the past.[1-3] The electrode processes for reduction of complexes may be classified in three general categories: (1) reversible; (2) quasireversible; and (3) irreversible.

Reversible and quasireversible electrode processes, being based in the main on parameters of thermodynamic significance, such as the reversible half-wave potential, $E_{1/2}{}^r$, which is closely related to the standard

(1) I. M. Kolthoff and J. J. Lingane, "Polarography," Vol. I and II, 2nd ed, Interscience, New York, N. Y., 1952.

(2) J. Heyrovsky and J. Kuta, "Principles of Polarography," Academic Press, New York, N. Y., 1966.

(3) A. A. Vlcek, *Progr. Inorg. Chem.*, **5**, 211 (1963).

reduction potential, E^0, can be treated adequately and simply for most systems.

In general, polarographic methods for the direct study of irreversibly reduced complexes to determine solution equilibria are rather complex because they have to introduce kinetic considerations as well as thermodynamic ones and although the theory has been worked out for many irreversible electrode processes, examples where applications have been made using the theories are extremely rare. Certainly applications are mainly confined to specialists in the field. Saraiya and Sundaram[4] have tabulated the complex ion systems studied polarographically and reviewed many of the available polarographic methods for study of complexes. Examination of this comprehensive review illustrates the limited nature of studies on irreversibly reduced complexes.

Recently, the author[5] has suggested an extremely simple calculation method for study of complex ions from irreversible electrode processes. The method, however, requires several conditions to hold before being applicable and the general usefulness has yet to be ascertained. One of the major conditions necessary is that the heterogeneous rate constant, k_e^0, should not change markedly with addition of ligand to the aquo complex. Obviously, a systematic study of the kinetics and/or mechanism of reduction of aquo complexes is necessary as a preliminary to making any predictions as to the potential usefulness of the method. Such a study was therefore undertaken and the results are reported in this paper along with a theoretical account of the use of ac polarography and controlled drop time techniques to assist in the study of irreversible electrode processes.

Experimental Section

All chemicals used were of reagent grade purity. Metal ions were added as the perchlorate salts where available, otherwise nitrate salts were used. Sodium perchlorate, 1 *M* (pH 5), was used to study the electrode processes of species known not to be susceptible to hydrolysis, otherwise, suitable mixtures of sodium perchlorate and perchloric acid were used. All ligands were added as the sodium salts.

All measurements on complex ion systems were made at an ionic strength of 1.0 maintained by sodium perchlorate and at (25.0 ± 0.1)°. Argon was used to deaerate the solutions.

Polarograms were obtained using Metrohm Polarecord E 261. Ac polarography was carried out using the Metrohm ac Modulator E393 and an ac voltage of 10 mV, root mean square, at 50 Hz. To minimize cell impedance, the modulating ac voltage was applied through an auxiliary tungsten electrode. Rapid polarographic techniques with controlled drop times of 0.16 sec were achieved with a Metrohm Polarographie-Stand E 354. Potentials in dc polarography were compensated for the ohmic *iR* drop with Metrohm IR Compensator E 446. Potentials in ac polarography are reported without *iR* compensation.

Theory

(*i*) *Dc Polarography.* The equation to an irreversible dc polarographic wave may be described by the expression

$$E_{dc} = E_{1/2} + 2.303\frac{RT}{\alpha nF}\log\left[\frac{(i_d - i)}{i}\right] \quad (1)$$

$E_{1/2}$ is related to $E_{1/2}^r$ as follows

$$E_{1/2} = E_{1/2}^r + 2.303\frac{RT}{\alpha nF}\log k_e^0\sqrt{\frac{t}{D}} \quad (2)$$

provided α is independent of potential. In the above equation: E_{dc} = dc potential; $E_{1/2}$ = half-wave potential; $E_{1/2}^r$ = reversible half-wave potential; α = transfer coefficient; t = drop time; D = diffusion coefficient; k_e^0 = heterogeneous rate constant. Other symbols are those used conventionally.

$E_{1/2}$ can be measured either as the potential of E_{dc} at $i = i_d/2$ or more rigorously from a graphical plot of E_{dc} *vs.* log $[(i_d - i)/i]$.

From eq 2 it can be seen that if for a series of measurements made at variable ligand concentration, k_e^0, α, t, and D remain constant, then the change in half-wave potential, $\Delta E_{1/2}$, is equal to $\Delta E_{1/2}^r$, and this provides the basis of the simple method proposed by the author.[5]

In the previous work it was shown that if $\Delta E_{1/2}^r$ could be calculated in the above manner, then the method of Lingane[6] for evaluation of complex ions, in which $\Delta E_{1/2} = \Delta E_{1/2}^r$ is plotted against the logarithm of the ligand concentration, could be used. However, a more exact treatment of De Ford and Hume[7] could also be used.

The equation of De Ford–Hume can be expressed in a simplified form as

$$F_0(X) = \sum_{j=0}^{j}\beta_j C_x^j = \text{antilog}\, 0.4343\frac{nF}{RT}[(E_{1/2}^r)_f - (E_{1/2}^r)_c] \quad (3)$$

where $F_0(X)$ is introduced for convenience to represent the experimentally measurable quantity on the right-hand side of the equation, β_j is the formation constant of the jth complex, C_x the concentration of complex forming ligand, and the subscripts f and c refer to the free ion and complexed ion, respectively. $(E_{1/2}^r)_f - (E_{1/2}^r)_c$ is the change in half-wave potential $\Delta E_{1/2}^r$ and provided $\Delta E_{1/2} = \Delta E_{1/2}^r$ for an irreversible electrode

(4) S. C. Saraiya and A. K. Sundaram, "A Review of the Study of Complexes by Polarography," Government of India Atomic Energy Commission Report, B.A.R.C.-410, Bombay, India, 1969.

(5) A. M. Bond, *J. Electroanal. Chem.*, **28**, 433 (1970).

(6) J. J. Lingane, *Chem. Rev.*, **29**, 1 (1941).

(7) D. D. De Ford and D. N. Hume, *J. Amer. Chem. Soc.*, **73**, 5321 (1951).

process, eq 3 should be solvable in the form

$$F_0(X) = \sum_{j=0}^{j} \beta_j C_x{}^j = \text{antilog } 0.4343\frac{nF}{RT}\Delta E_{1/2} \quad (4)$$

Equation 4 is applicable only when reduction of the metal complex proceeds directly to the metal, so that the overall electrode process for reduction of the aquo ion is

$$M(H_2O)_n{}^{z+} + xe \rightleftharpoons M(0) + nH_2O \quad (5)$$

from which $(E_{1/2})_f$ is measured.

In the presence of a complex-forming ligand, L^-, the overall electrode process can be represented as follows

$$[M(H_2O)_{n-y}L_y]^{(z-y)+} + xe \rightleftharpoons M(0) + (n - y)H_2O + yL^- \quad (6)$$

From this electrode process $(E_{1/2})_c$ is obtained, and $\Delta E_{1/2} = (E_{1/2})_f - (E_{1/2})_c = \Delta E_{1/2}{}^r$, if $k_e{}^0$, t, α, and D are approximately the same in the presence and absence of ligand.

The drop time, t, the transfer coefficient, α, and diffusion coefficient, D, are simply checked experimentally to see if they are constant. If t changes, then this can be overcome by using a controlled drop time method of measurement. D does not usually change markedly with inorganic complexes, but using a constant concentration of depolarizer and measuring i_d at the various concentrations of ligand will show any changes in this parameter. Application of eq 1 should reveal any changes in α or alternatively this can be checked even more simply by measurement of $(E_{1/4} - E_{3/4})$ on all solutions, as this difference in potential is equal to $(2.303RT/\alpha nF)$ log 9. $k_e{}^0$ is undoubtedly the parameter most likely to vary markedly on addition of ligands.

The electrode process of the type in eq 5, in which reduction of the aquo complex occurs, is normally measured in noncomplexing perchlorate or nitrate media. Perchlorate is not strongly adsorbed at mercury electrodes and in the absence of adsorption phenomena the rate-determining step has been attributed to the removal of coordinated water.[8,9]

In the presence of a ligand, as in eq 6, the rate of the electrode process could be expected to be similar to the electrode process in eq 5 if the rate-determining step remains the removal of coordinated water and ligand formation is not significantly involved in the overall electrode process.

If any adsorption occurs in the presence of a ligand, then the rate would almost certainly be altered,[9-16] so that the approximation $\Delta E_{1/2} = \Delta E_{1/2}{}^r$ would not be expected to apply. Thus nonadsorbable ligands such as nitrate, fluoride, sulfate, etc., would appear to be the most suitable for this study. Alternatively, negatively charged ligands such as chloride, bromide, and iodide, although strongly adsorbed at potentials positive to the electrocapillary maximum (ecm), are not adsorbed significantly if the reduction occurs at sufficiently negative potentials to the ecm, and if irreversible electrode processes are to be studied by the simple calculation method, then it is probably desirable that they have fairly negative $E_{1/2}$ values (*i.e.*, more negative than about 1.0 V *vs.* the saturated calomel reference electrode) and all systems studied comply with this.

(*ii*) *Ac Polarography.* Theoretical studies for irreversible ac electrode processes[17-19] have slight quantitative differences. However, they are in complete agreement regarding the important quantitative prediction that a measurable ac wave of $k_e{}^0$-independent magnitude and shape will be observed with irreversible systems. The sole influence of $k_e{}^0$ is to determine the position of the wave on the dc potential axis. The direct proportionality between the fundamental harmonic current magnitude and the charge-transfer coefficient is also a significant result of theoretical treatment.

The summit potential E_s of an irreversible ac wave is given by

$$E_s = E_{1/2}{}^r + \frac{RT}{\alpha nF}\ln\left(\frac{1.349k_e{}^0t^{1/2}}{D^{1/2}}\right) - \frac{RT}{2\alpha nF}\ln Q \quad (7)$$

where $Q = 1.907(\omega t)^{1/2}$ and ω = applied angular frequency. It thus follows from eq 2 that

$$E_s = E_{1/2} - \frac{RT}{2\alpha nF}\ln Q$$

Hence, it can be deduced that E_s is displaced cathodically by a substantial amount from the dc polarographic half-wave potential, but importantly, on addition of ligand, $\Delta E_s = \Delta E_{1/2}$ and this could also be equal to $\Delta E_{1/2}{}^r$. Thus if the simple calculation method is applicable, results from ac polarography should be identical with those from dc polarography when ΔE_s values are used.

(8) I. U. Nelson and R. T. Iwamoto, *J. Electroanal. Chem.*, **6**, 234 (1963).

(9) R. E. Connick and C. P. Coppel, *J. Amer. Chem. Soc.*, **81**, 6389 (1959).

(10) N. S. Hush and J. W. Scarrot, *J. Electroanal. Chem.*, **7**, 26 (1964).

(11) J. E. B. Randles and K. W. Somerton, *Trans. Faraday Soc.*, **48**, 951 (1952).

(12) B. Breyer, F. Gutman, and S. Hacobian, *Aust. J. Sci. Res., Ser. A*, **4**, 595 (1951).

(13) A. J. Engel, J. Lawson, and D. A. Aikens, *Anal. Chem.*, **34**, 269 (1965).

(14) J. J. Lingane, *J. Amer. Chem. Soc.*, **61**, 2099 (1939).

(15) E. D. Moorhead and W. M. MacNevin, *Anal. Chem.*, **34**, 269 (1962).

(16) B. Breyer and H. H. Bauer, "Alternating Current Polarography and Tensammetry," Interscience, New York, N. Y., London, 1963, pp 141-147, 153-155, 169-170, 185.

(17) B. Timmer, M. Sluyters-Rehbach, and J. H. Sluyters, *J. Electroanal. Chem.*, **14**, 169 (1967).

(18) B. Timmer, M. Sluyters-Rehbach, and J. H. Sluyters, *ibid.*, **14**, 181 (1969).

(19) D. E. Smith and T. G. McCord, *Anal. Chem.*, **40**, 474 (1968).

An expression for the ac peak magnitude, I_p, is[19]

$$I_p = \frac{1.644\alpha n^2F^2AC(\omega D)^{1/2}\Delta E}{RT(1 + Q^{1/2})^2} \quad (8)$$

where A = area of electrode, C = initial concentration of electroactive species, ΔE = amplitude of ac potential. For measurements made at constant C, I_p should change similarly to the dc value of i_d unless α is changing and this can be used to verify one of the approximations which must hold for application of the simple calculation method.

For the quasireversible ac electrode process, I_p is a function of k_e^0 [20] and measurement of I_p compared with i_d can provide information on the constancy or otherwise of k_e^0 with added ligand.

Results and Discussion

Reduction of Aquo Complexes at the Dropping Mercury Electrode. The aquo complex, when reduced to the metal, undergoes the overall electrode process

$$M(aq)^{z+} + xe \rightleftharpoons M(0) + aq$$

where aq = H_2O. During this electrode process the bonds between the metal and water must be broken, and the rate of the electrode process is likely to be governed by the equilibria of water exchange such as

$$M(H_2O)_n^{z+} + H_2O^* \rightleftharpoons [M(H_2O)_{n-1}H_2O^*] + H_2O \quad (9)$$

If the rate of exchange of water is extremely fast then a reversible electrode process will probably result, because the removal of water will not be involved in the rate of the electrode process and other steps will be rate determining. However, if removal of water is sufficiently slow this will most likely result in the observation of an irreversible electrode process. Lyons has studied in detail the electrodeposition from aqueous solutions,[21,22] and considered the role of coordinated water, as have several other workers in polarographic studies.[8-10,13,15,23-25]

The close similarity between eq 9 and the electrode process can be appreciated, and correlations between rates of electrode processes and equilibria in eq 9 could be anticipated. Figure 1 shows some characteristic rate constants (half-lives) for H_2O substitution in the inner coordination sphere of metal ions as measured by Eigen.[26] These half-lives or rate constants can be used as a measure of the rate of exchange of the first water of coordination.

The values are, however, obtained from homogeneous equilibria and are not strictly relatable to heterogeneous equilibria present with a dropping mercury electrode and its associated electric field. Despite this, however, some extremely interesting correlations are apparent.

Species in the extreme right-hand side of Figure 1 with rate constants of the order of 10^8 to 10^{10} sec^{-1} (half-life 10^{-8} to 10^{-10} sec) are in general reversibly reduced (or almost so) at the dropping mercury electrode. The polarographic reduction of $Cd(aq)^{2+}$ is classically regarded as a reversible one. $Cu(aq)^{2+}$ reduction is close to reversible in sodium perchlorate.[27] The reversibility of mercury is uncertain because measurements are made at a mercury electrode itself, but available evidence in perchloric acid is that the electrode process is fast.[28-30] Reduction of aquo alkali metal ions, $Li(aq)^+$, $Na(aq)^+$, $K(aq)^+$, $Rb(aq)^+$, and $Cs(aq)^+$ is also reversible as shown by the wave shapes and the observed agreement of half-wave potentials with the theoretical values computed from the standard potentials of the solid metals, their solubilities in mercury, and the free energies of the amalgams.[31] Rate measurements by Randles and Somerton[11] for reduction of $Na(aq)^+$, $K(aq)^+$, and $Cs(aq)^+$ give values of k_e^0 in the range 0.1 to 0.4 cm sec^{-1}, also indicating these electrode processes are reversible. Results obtained with the ac polarographic method by Schwabe and Jehring[32] also show that reduction of $K(aq)^+$ and $Na(aq)^+$ are fast electrode processes. Heyrovsky and Kuta[33] have concluded that reduction of $K(aq)^+$, $Na(aq)^+$, $Cs(aq)^+$, and $Rb(aq)^+$ is reversible. Reduction of the aquoalkaline earth metal ions has not been particularly well characterized, but certainly reduction of $Ca(aq)^{2+}$, $Sr(aq)^{2+}$, and $Ba(aq)^{2+}$ is fast[34] and at least for $Ca(aq)^{2+}$ and $Sr(aq)^{2+}$ is probably reversible.[34-37]

In moving left across Figure 1, to aquo complexes with rate constants for removal of coordinated water less than 10^8 sec^{-1}, it can be seen that the group zinc, manganese, and lanthanum have values in the range 10^7 to 10^8 sec^{-1} (half-lives between 10^{-7} and 10^{-8} sec). Polarographic reduction of $Zn(aq)^{2+}$ in perchlorate media has been shown to be quasireversible[5,38] as has

(20) D. E. Smith, *Electroanal. Chem.*, **1**, 1 (1966).
(21) E. H. Lyons, Jr., *J. Electrochem. Soc.*, **101**, 363 (1954).
(22) E. H. Lyons, Jr., *ibid.*, **101**, 376 (1954).
(23) A. A. Vlček, *Chem. Listy*, **50**, 828 (1956).
(24) J. Dandoy and L. Gierst, *J. Electroanal. Chem.*, **2**, 116 (1961).
(25) L. Gierst and H. Hurwitz, *Z. Elektrochem.*, **64**, 36 (1960).
(26) M. Eigen, *Pure Appl. Chem.*, **6**, 97 (1963).
(27) A. M. Bond, *J. Electroanal. Chem.*, **23**, 277 (1969).
(28) K. Rosenthal and V. Ershler, *Zh. Fiz. Khim.*, **22**, 1344 (1948).
(29) H. Gerischer and K. E. Staubach, *Z. Phys. Chem.*, **6**, 118 (1956).
(30) K. B. Oldham, *Trans. Faraday Soc.*, **53**, 80 (1957).
(31) See ref 1, Vol. II, p 425.
(32) K. Schwabe and H. Jehring, *Z. Anal. Chem.*, **173**, 36 (1960).
(33) See ref 2, pp 531–547.
(34) See ref 1, pp 431–434.
(35) G. Kumura, *Collect. Czech. Chem. Commun.*, **4**, 492 (1932).
(36) I. Zlotowski and I. M. Kolthoff, *J. Phys. Chem.*, **49**, 386 (1945); *J. Amer. Chem. Soc.*, **66**, 1431 (1944).
(37) J. Heyrovsky and S. Berezicky, *Collect. Czech. Chem. Commun.*, **1**, 19 (1920).
(38) A. M. Bond, *J. Electroanal. Chem.*, **20**, 109 (1969).

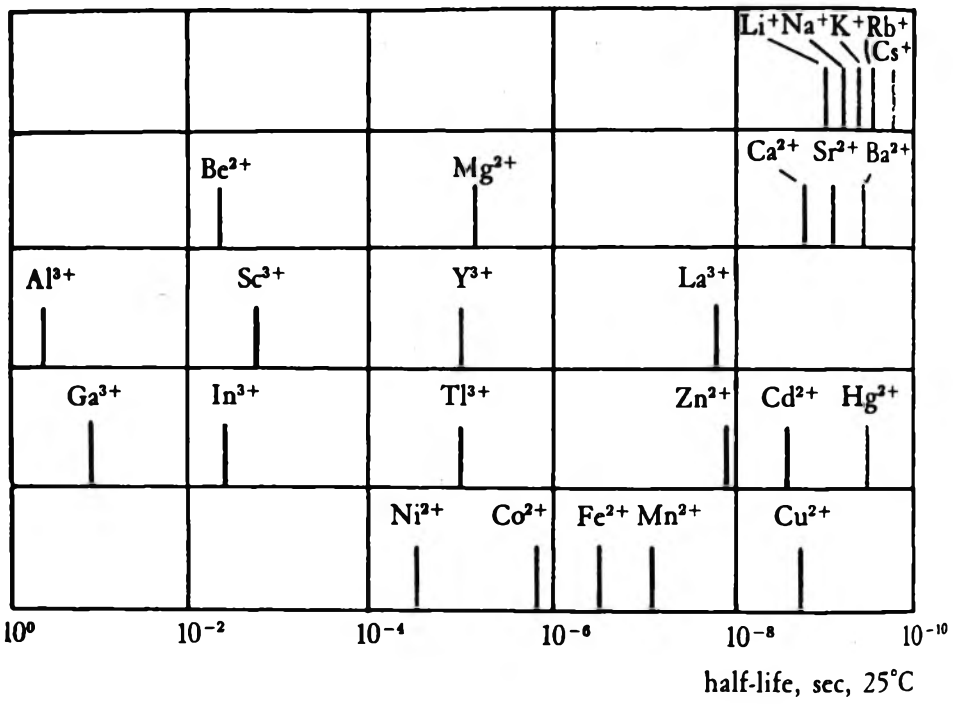

Figure 1. Characteristic half-lives for H_2O substitution in the inner coordination sphere of metal ions. Data taken from ref 26 and reproduced by permission of the copyright holder and author.

that for $Mn(aq)^{2+}$ (shown later in this paper). In "neutral" media Sancho and Almagro,[39] using ac polarography, concluded that the reduction process of La(III) was irreversible, but at the pH of their work it is not clear what species was actually being reduced so the reduction process for the aquated $La(aq)^{3+}$ ion is uncertain.

All other species in Figure 1 have rate constants for removal of water $<10^7$ sec^{-1} (half-lives $<10^{-7}$ sec), and reductions of $Co(aq)^{2+}$, $Ni(aq)^{2+}$, and $Fe(aq)^{2+}$ as well as all other species listed were confirmed to be irreversible in accordance with Heyrovsky and Kuta's data.[33]

Thus, an extraordinarily good correlation exists between homogeneous rate constants for loss of coordinated water and polarographic heterogeneous charge-transfer rate constants for all examples encountered in Figure 1. Reversible electrode processes with k_e^0 greater than 2×10^{-2} cm sec^{-1} [40] have rate constants for loss of coordinated water greater than 10^8 sec^{-1}. Quasireversible electrode processes with k_e^0 values in the range 2×10^{-2} to 5×10^{-5} cm sec^{-1} [40] have homogeneous rate constants for removal of water in the range of about 10^7 to 10^8 sec^{-1} and irreversible electrode processes with k_e^0 less than 5×10^{-5} cm sec^{-1} have homogeneous rate constants less than 10^7 sec^{-1}.

That such a correlation should exist between the two types of rate constant suggests strongly that the role of the mercury electrode is not particularly important for reduction of simple aquo cations in the absence of adsorption phenomena. Also it would appear from this correlation that it is the removal of the first coordinated water that is rate determining in polarographic reduction of aquo complexes.

Reduction of Metal–Ligand Complexes at the Dropping Mercury Electrode. A systematic survey of the reactions of solvated metal cations with various ligands has been carried out by Eigen and others,[26,41-48] and the rates of water removal in the presence and absence of ligand can be compared. The observed changes of k_e^0 in the presence of ligand could be expected to follow similar patterns to homogeneous rate measurements as has been found for reduction of aquo complexes, provided no complications are introduced because of adsorption phenomena.

It has been found that for reactions of alkali metals and most alkaline earths and other complex ions, for which the rate constants for removal of water are high ($>10^7$ sec^{-1}), small variations are observed in the presence of different ligands.

(39) J. Sancho and V. Almagro, *Ann. Real Soc. Espan. Fis. Quim.* **56B**, 115 (1960).

(40) P. Delahay, *J. Amer. Chem. Soc.*, **75**, 1430 (1953).

(41) M. Eigen, *Z. Elektrochem.*, **64**, 115 (1960).

(42) M. Eigen in "Advances in the Chemistry of Coordination Compounds," S. Kirschner, Ed., Macmillan, New York, N. Y., 1961, p 371.

(43) M. Eigen and K. Tamm, *Z. Elektrochem.*, **66**, 93 (1962).

(44) M. Eigen and K. Tamm, *ibid.*, **66**, 104 (1962).

(45) G. G. Hammes and J. I. Steinfeld, *J. Amer. Chem. Soc.*, **84**, 4639 (1962).

(46) G. G. Hammes and S. A. Levison, *Biochemistry*, **3**, 1504 (1964).

(47) B. Fleet and G. A. Rechnitz, *Anal. Chem.*, **42**, 690 (1970).

(48) R. E. Connick in "Advances in the Chemistry of the Coordination Compounds," S. Kirschner, Ed., Macmillan, New York, N. Y., 1961, p 15.

Table I: Polarographic Data for the Nickel(II)–Fluoride System (Ionic Strength = 1.0 Maintained by Sodium Perchlorate. All Potentials Reported *vs.* Ag|AgCl. Concentration of Nickel(II) = 8×10^{-4} *M*)

	Conventional dc			Rapid dc			Conventional ac			Rapid ac		
[NaF], *M*	$-E_{1/2}$, V	$F_0(X)$	$F_1(X)$	$-E_{1/2}$, V	$F_0(X)$	$F_1(X)$	$-E_s$, V	$F_0(X)$	$F_1(X)$	$-E_s$, V	$F_0(X)$	$F_1(X)$
0.00	1.0326	1.00		1.0405	1.00		1.0492	1.00		1.0424	1.00	
0.30	1.0405	1.85	2.83	1.0487	1.89	2.97	1.0575	1.91	3.03	1.0503	1.85	2.83
0.60	1.0466	2.98	3.30	1.0544	2.96	3.27	1.0617	2.65	2.75	1.0570	3.12	3.52
1.00	1.0506	4.06	3.06	1.0577	3.82	2.82	1.0658	3.64	2.64	1.0604	4.06	3.06

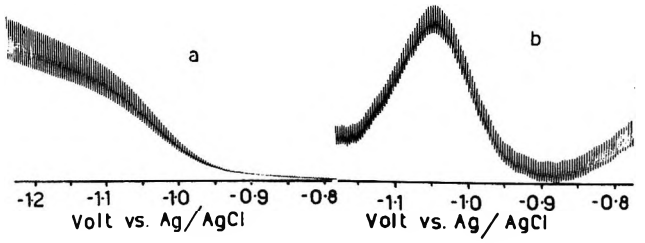

Figure 2. (a) Conventional dc polarogram of Ni(II) in 1 *M* $NaClO_4$. (b) Conventional ac polarogram of Ni(II) in 1 *M* $NaClO_4$.

Magnesium and several divalent transition metal complexes exhibit rate constants less than 10^7 sec^{-1}, but values are virtually independent of the nature of the ligand. Consequently k_e^0 values for some electrode processes $M(x) + xe \rightleftharpoons M(0)$ could be expected to be basically independent of ligand concentration in the absence of adsorption phenomena, and complexes of these metals, for example, could be studied by the simple calculation method.

With a third group of cations with rate constants of water removal that are extremely low (see species on left-hand side of Figure 1), it has been found that rate constants show a marked dependence on the nature of the ligand. It has been postulated that the hydrolysis of a water molecule in the coordination shell is the rate-determining step and that the rate constant is therefore dependent on the basicity of the anion. These systems presumably would not be suitable for study by the simple calculation method.

The Nickel(II) System. Figure 2 shows ac and dc polarograms of the reduction in 1 *M* $NaClO_4$. The wave is reasonably well defined in both the ac and dc cases, but is highly irreversible. With conventional polarographic techniques and with drop times varying between 1.3 and 10 sec, $(E_{1/4} - E_{3/4})$ was invariant at (66 ± 3) mV as was the shape of the dc wave. The shape of the ac wave was also drop-time independent, with a half-width of (120 ± 10) mV. Under the conditions of rapid polarography with controlled drop times of 0.16 to 0.32 sec, the shapes of dc and ac waves were also the same as with conventional polarography.

The loss of water from $Ni(H_2O)_n^{2+}$ is the slowest of the transition metal series considered in Figure 1, and because it is so slow, it is probably the most favorable case for water removal to remain the rate-determining step, even on addition of ligands.

Addition of fluoride, chloride, and nitrate was not observed to alter the polarographic characteristics in any way, and it would appear that the electrode process is entirely suited for the simple calculation method.

Table I shows the data for the nickel(II)–fluoride system. All results are in excellent agreement and one complex, $NiF(aq)^+$, is shown to exist with a stability constant, β_1, of 3.0 ± 0.3. This result is in excellent agreement with other data obtained under exactly the same conditions of ionic strength of 1.0 and temperature of 25°,[49] where, using the fluoride ion electrode potentiometric method,[50] a value $\beta_1 = 2.2 \pm 0.3$ was obtained. All data from Table I were obtained from an average of ten independently prepared solutions. E_s and $E_{1/2}$ values were usually observed to lie in a range of 3 to 4 mV for the ten readings, and average values had standard deviations of about 0.5 to 0.8 mV. The only other β values for the $NiF(aq)^+$ complex were obtained under slightly different conditions and values of $\beta_1 = 4.6$ ($I = 1.0$ ($NaClO_4$), $T = 20°$)[51] and 1.5 ($I = 0.5$ ($NaNO_3$), $T = 16°$)[50] were reported. The generally excellent agreement of polarographic values calculated by the simple method and other data can be seen.

For the nickel(II)–chloride system, extremely weak complex formation was observed as $E_{1/2}$ and E_s values in 1 *M* sodium perchlorate compared with 1 *M* NaCl differed by only 5 to 6 mV, the values in sodium chloride being the more negative. Analysis of the data gave a β_1 value for the complex $NiCl(aq)^+$ of 0.6 ± 0.1. Consideration of the method of measurement shows that this value can be considered only as an order of magnitude, and that nickel(II)–chloride complexes in water are extremely weak. Very little comparable data are available in the literature; however, an indirect polarographic[52] method gives $\beta_1 = 0.6$ ($I = 2.0$ ($NaClO_4$), $T = 25°$) as do potentiometric studies under identical conditions.[53] Other data[54] are

(49) A. M. Bond and G. Hefter, *J. Inorg. Nucl. Chem.*, in press.

(50) A. M. Bond and T. A. O'Donnell, *J. Electroanal. Chem.*, **26**, 137 (1970).

(51) S. Ahrland and K. Rosengren, *Acta Chem. Scand.*, **10**, 727 (1956).

(52) P. Kivalo and R. Luoto, *Suom. Kemistilehti B*, **30**, 163 (1957).

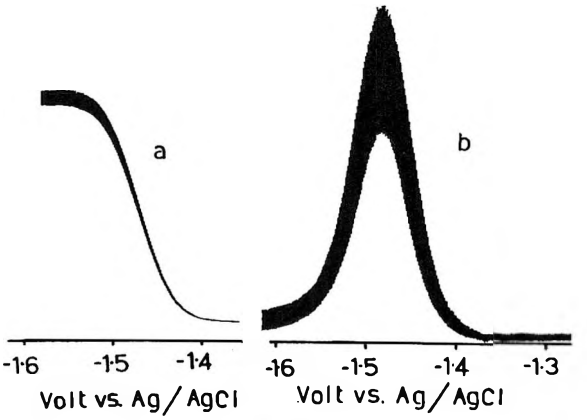

Figure 3. (a) Conventional dc polarogram of Mn(II) in 1 *M* $NaClO_4$. (b) Conventional ac polarogram of Mn(II) in 1 *M* $NaClO_4$.

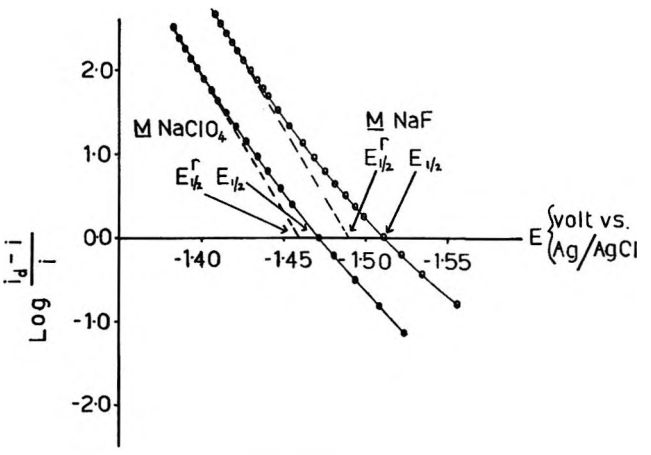

Figure 4. Analysis of conventional dc polarograms of Mn(II) in 1 *M* $NaClO_4$ and 1 *M* NaF.

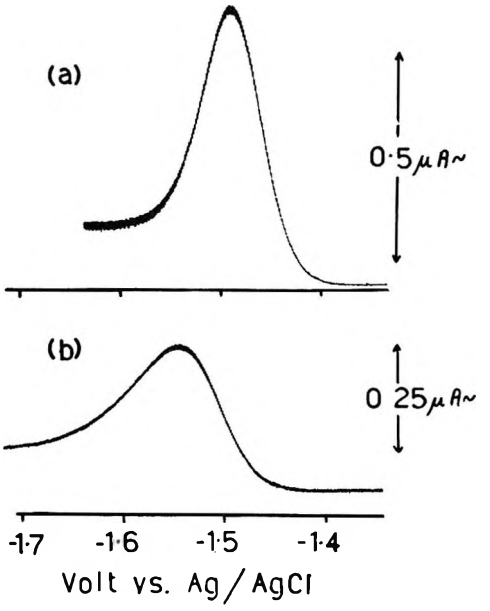

Figure 5. Comparison of rapid ac polarograms in (a) 1 *M* $NaClO_4$ and (b) 1 *M* NaF.

also consistent with weak complex formation and the polarographic result seems realistic.

Comparison of $E_{1/2}$ and E_s values in sodium nitrate–sodium perchlorate media at ionic strength of 1.0 indicates that the nitrate complex is even weaker than that of the chloride and a β_1 value of 0.4 ± 0.1 for the complex $NiNO_3(aq)^+$ was found. This value is again considered as only an order of magnitude. No comparable data are available[54] but the value seems chemically reasonable.

It is concluded therefore that the simple method of calculation is applicable to nickel(II) complexes with a high degree of precision, where adsorption phenomena are absent, and that the presence of ligands such as fluoride, chloride, and nitrate does not alter k_e^0 because removal of coordinated water remains the rate-determining step.

The Manganese(II) System. Figure 3 shows ac and dc polarograms of manganese(II) in 1 *M* sodium perchlorate. Table II shows some data in 1 *M* sodium perchlorate and 1 *M* sodium fluoride. Figure 4 shows a plot of $E_{d.e.}$ *vs.* log $(i_d - i)/i$ in both media, and the quasireversible electrode process is characterized by a curved plot with limiting slope at the more positive portion of the wave of (30.5 ± 2)mV which is the reversible or Nernstian slope for reduction. The theoretically calculated current–voltage curve became complex in the region where the maximum was encountered and this part was not included in Figure 4.

The reversible half-wave potential was calculated by extrapolation of the reversible slope to the potential axis. The ac wave is also quasireversible as shown by the half-width of 80 mV, this being made up of a contribution of 36 mV from the more positive half and 44 mV from the other side. As the electrode process is quasireversible, the peak height of the ac wave, I_p, provides a measure of k_e^0, and the large decrease in I_p on addition of fluoride suggests k_e^0 decreases significantly due to complex formation. The decrease in the dc i_d values is consistent with a change in the diffusion coefficient and so some decrease in the ac I_p value would be anticipated. However, the decrease is too great to be explained in terms of this parameter. The increases in dc $(E_{1/4} - E_{3/4})$ and ac half-width also verify the decrease in k_e^0. Figure 5 shows a comparison of rapid ac polarograms in 1 *M* $NaClO_4$ and 1 *M* NaF and the considerable change in rate can be appreciated. Considerable drop-time dependence of the wave which is another characteristic of quasireversible electrode processes can also be seen to occur by comparison of Figures 3 and 5.

The simple calculation method would not be completely valid for this system as k_e^0 is not independent

(53) M. W. Lister and P. Rosenblum, *Can. J. Chem.*, 38, 1827 (1960).

(54) "Stability Constants of Metal Ion Complexes," Special Publication No. 17, The Chemical Society, London, 1964

Table II: Polarographic Data for the Manganese(II)-Fluoride System (All Potentials Reported *vs.* AgA|gCl. Concentration of Manganese(II) = 4×10^{-4} *M*)

	Conventional dc				Rapid dc			Conventional ac			Rapid ac		
Medium	$-E_{1/2}$, V	$-E_{1/2}{}^{r}$, V	i_d, μA	$(E_{1/4} - E_{3/4})$, mV	$-E_{1/2}$, V	i_d, μA	$(E_{1/4} - E_{3/4})$, mV	$-E_s$, V	I_p, μA	Half-width, mV	$-E_s$, V	I_p, μA	Half-width, mV
1 *M* $NaClO_4$	1.472	1.461	5.75	35	1.486	3.16	39	1.481	1.63	80	1.489	0.635	80
1 *M* NaF	1.516	1.490	4.30	44	1.538	2.28	54	1.530	0.92	110	1.546	0.350	110

of fluoride concentration. Reversible $E_{1/2}$ values calculated from plots as in Figure 4 indicate one complex $MnF(aq)^+$ exists with β_1 equal to 10 ± 2. Assuming the simple method had been applicable, stability constants would have been calculated to be higher than this, but qualitatively the observation of a weak complex of manganese(II) would still have been correct.

The characteristics of the manganese(II) electrode process are very similar to that for zinc(II) considered previously.[5] Variations in k_e^0 for zinc(II) in different electrolytes are generally not particularly large,[55] but they could be significant in some cases if the proposed calculation method is to be used. With manganese(II) a similar situation probably applies and the simple method will be valid in some cases but not in others, although certainly in most cases at least a qualitative idea of the complex strength can be gained because changes in k_e^0 will not be particularly large.

The above suggestions that small changes in k_e^0 may occur in the presence of complexation for these two systems parallel changes in homogeneous rate constants for removal of water. The homogeneous rate constants are similar (see Figure 1) and for zinc(II),[26] at least, complexation is also known to cause slight variation in the values of the homogeneous rate constants. From this it seems likely that where rates of water exchange are rapid as for zinc and manganese and where k_e^0 values are correspondingly large, changes in k_e^0 are likely with complex formation and the simple calculation method will not be generally applicable, except in a qualitative fashion.

Cobalt(II) and Iron(II) Systems. In terms of homogeneous rate constants for removal of water, $Co(aq)^{2+}$ and $Fe(aq)^{2+}$ lie intermediate in behavior to the previously considered $Ni(aq)^{2+}$ and $Mn(aq)^{2+}$ systems as shown in Figure 1. Whether k_e^0 values are liable to change with complexation as for $Mn(aq)^{2+}$, or apparently remain constant as for $Ni(aq)^{2+}$, should provide an interesting result.

The ac and dc parameters for reduction of cobalt(II) in various media are summarized in Table III. Figure 6 shows typical polarograms. The electrode process in all media is shown to be irreversible by the considerable difference between $E_{1/2}$ and E_s values, the $(E_{1/4} - E_{3/4})$ values, and half-widths of ac polarograms. $E_{1/2}$ and E_s values were also markedly dependent on drop time as is expected for irreversible electrode processes, values

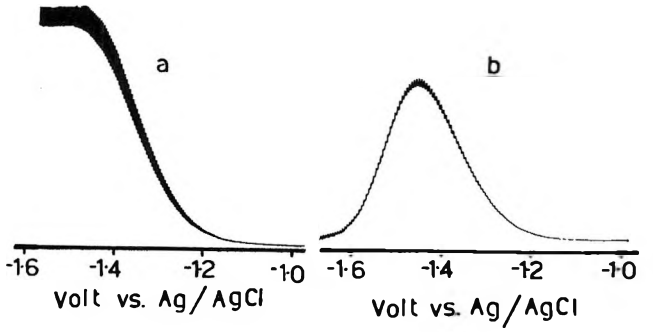

Figure 6. (a) Conventional dc polarogram of Co(II) in 1 *M* $NaClO_4$. (b) Conventional ac polarogram of Co(II) in 1 *M* $NaClO_4$.

becoming considerably more negative at the shorter drop times. Plots of i_d *vs.* square root of mercury column height were linear, indicating diffusion control.

Examination of changes in $E_{1/2}$ and E_s, and assuming them to be solely representative of complexation, qualitatively indicates that the strengths of the complexes are weak and in the order $ClO_4^- < NO_3^- < Cl^- < F^-$. This is in agreement with the limited amount of data available.[49,54] In nitrate media virtually no change in the parameters for polarographic reduction takes place compared with perchlorate media and any nitrate complexes must be extremely weak, and <0.5. On addition of chloride and fluoride to perchlorate solutions at constant ionic strength of 1.0, the ac polarographic waves were observed to become broader. Consequently, the simple calculation method is not applicable in the quantitative sense. Values of stability constants slightly larger than those obtained by other methods[49,54] would be obtained which, combined with polarographic data, indicates k_e^0 decreases with increasing chloride and fluoride in a similar fashion to the manganese(II)–fluoride system described previously.

Iron(II) also behaves similarly to cobalt(II) and manganese(II). Data for the iron(II)–fluoride system are given in Table IV. Figure 7 shows a dc polarogram in 1 *M* $NaClO_4$ and Figure 8 shows ac polarograms in 1 *M* $NaClO_4$ and 1 *M* NaF. Comparison of the two ac polarograms shows that the symmetrical ac wave in perchlorate becomes asymmetrical on addition of fluo-

(55) See ref 2, p 216.

Table III: Polarographic Data for Cobalt(II) in Various Media, Drop Time = 1.9 Sec, for Conventional Ac and Dc Polarography (All Potentials Reported *vs.* Ag|AgCl, Concentration of Cobalt(II) = 8×10^{-4} *M*)

	Conventional dc		Conventional ac		Rapid dc		Rapid ac	
Medium	$-E_{1/2}$, V	$(E_{1/4} - E_{3/4})$, mV	$-E_s$, V	Half-width, mV	$-E_{1/2}$, V	$(E_{1/4} - E_{3/4})$, mV	$-E_s$, V	Half-width, mV
1 *M* $NaClO_4$	1.352	94	1.435	206	1.400	100	1.453	200
0.7 *M* $NaClO_4$ + 0.3 *M* NaF	1.392	102	1.469	220	1.439	105	1.480	204
1 *M* NaF	1.408	102	1.508	220	1.463	110	1.517	220
1 *M* $NaNO_3$			1.438	208				
1 *M* NaCl			1.454	218				

Table IV: Polarographic Data for the Iron(II)–Fluoride System (All Potentials Reported *vs.* Ag|AgCl, Concentration of Iron(II) = 4×10^{-4} *M*)

	Conventional dc		Rapid dc		Conventional ac		Rapid ac	
Medium	$-E_{1/2}$, V	$(E_{1/4} - E_{3/4})$, mV	$-E_{1/2}$, V	$(E_{1/4} - E_{3/4})$, mV	$-E_s$, V	Half-width, mV	$-E_s$, V	Half-width, mV
1 *M* $NaClO_4$	1.396	70	1.465	82	1.469	200	1.487	196
1 *M* NaF	1.447	70	1.506	101	1.508	218	1.548	208

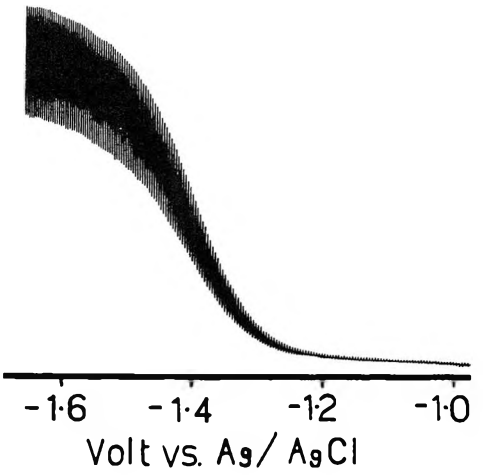

Figure 7. Conventional dc polarogram of Fe(II) in 1 *M* $NaClO_4$.

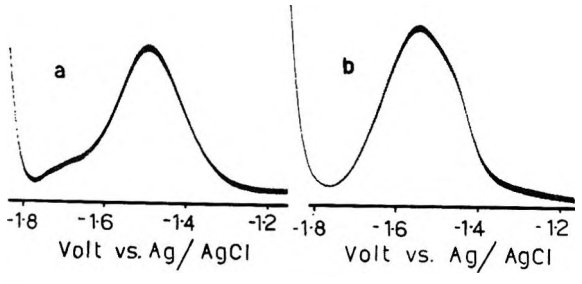

Figure 8. Comparison of rapid ac polarograms of Fe(II) in (a) 1 *M* $NaClO_4$ and (b) 1 *M* NaF.

ride, and that the parameters of the electrode process are altered by fluoride complexation. Qualitatively it can be concluded that weak fluoride complexation of iron(II) exists but the simple calculation method is not quantitatively valid. Dodgen and Rollefson[56] concluded from their measurements that β_1 for the complex $FeF(aq)^+$ was <30. Polarographic measurements made in this work are in agreement with this result. Shifts in $E_{1/2}$ and E_s are larger than that due solely to complexation. The observed shift therefore necessarily represents an upper limit of β_1 for the complex, and it is concluded that for the iron(II)–fluoride system β_1 is <30. Similarly for the cobalt(II)–fluoride system, β_1 for the complex $CoF(aq)^+$ must be <30.

Conclusions

For polarographic reduction of aquo complexes to the metal, the value of k_e^0 would appear to be closely related to the rate of removal of coordinated water, and the influence of the mercury electrode would not appear to be significant.

For reduction of complexes of the type $[M(H_2O)_n L_y]^{(z-y)+}$, in the absence of adsorption phenomena, the k_e^0 value may or may not be similar to the k_e^0 value for reduction of the simple aquo complex, $[M(H_2O)_n]^{z+}$, depending upon several variables. If removal of coordinated water is slow, such as with $Ni(aq)^{2+}$, then even after addition of ligand, removal of water rather than ligand will probably remain rate determining, and the k_e^0 value can remain essentially unaltered. However, in some cases removal of ligand, rather than water, could become rate determining, in which case k_e^0 will decrease as probably occurs with Co(II), Mn(II), and Fe(II). Alternatively, the presence of the ligand could catalyze the removal of coordinated water and lead to

(56) H. W. Dodgen and G. K. Rollefson, *J. Amer. Chem. Soc.*, **71**, 2600 (1949).

an increase in k_e^0, or else inhibit the rate of removal and decrease k_e^0.

The above considerations, of course, apply in the absence of adsorption phenomena and in the absence of any specific interaction of the complex or ligand with the mercury electrode. The changes in k_e^0, in the absence of the above phenomena, appear in general to be fairly small, so that changes in $E_{1/2}$ for irreversible electrode processes of this type can in most cases be used, at least in a qualitative sense, to determine whether complexes are "nonexistent," weak, or strong. Such was the case for some Co(II), Mn(II), and Fe(II) complexes considered in this work. In cases where k_e^0 does not alter significantly on addition of ligand, use of the simple method of calculation proposed previously by the author can be employed by the author to give data on the stability and nature of the complexes formed, such as for the fluoride, chloride, and nitrate complexes of nickel(II), and presumably for other species with slow removal of coordinated water.

Acknowledgment. The author wishes to acknowledge helpful discussions with Mr. K. A. Phillips during the course of this work.

Outer-Sphere Association Kinetics of Magnesium(II), Manganese(II), Cobalt(II), Nickel(II), Copper(II), and Zinc(II) *m*-Benzenedisulfonates in Methanol[1]

by Anthony Fanelli and Sergio Petrucci*

Polytechnic Institute of Brooklyn, Brooklyn, New York 11201 *(Received December 29, 1970)*

Publication costs borne completely by The Journal of Physical Chemistry

Measurements of the relaxation of ultrasonic absorption of Mg^{2+}, Mn^{2+}, Co^{2+}, Ni^{2+}, Cu^{2+}, and Zn^{2+} *m*-benzenedisulfonates in methanol at 25°, in the frequency range 15–185 MHz, have been interpreted as being due to the outer-sphere process of association between the solvated cations and BDS^{2-} anion. The forward and reverse rate constants are comparable with the calculated diffusion controlled rate constants according to the Smoluchowski–Debye–Eigen theories. The volume changes of reaction can be interpreted as being due to the elimination of one molecule of methanol from either the second coordination sphere of the cations or from the anion. The process has a barrier of energy equal to the one of viscous flow. This has been proven by measurements of the activation parameters, $\Delta H^{\pm}$ and $\Delta S^{\pm}$, by measuring the ultrasonic relaxation of MgBDS in methanol at −15 and −50°. Corresponding electrical conductance results in a comparable temperature range are reported for MgBDS in methanol in order to calculate the necessary association constants. The Fuoss–Kraus method has been employed for this purpose.

Introduction

The problem of the mechanism of ionic association and complexation in nonaqueous solvents is presently receiving much attention, after the corresponding study in aqueous media has provided a rather complete picture.[2]

One of the first queries to be answered is whether the complexation process involves ion pairs or outer-sphere intermediates as found for complexation involving divalent metal cations in water.[2] According to Eigen[2] the process starts with a diffusion-controlled approach of solvated ions. This is followed by stepwise elimination of molecules of solvent from between the ions.

The second question is whether the collapse of the outer-sphere complex with the penetration of the ligand into the first coordination sphere of the metal cation, in the case of octahedrally coordinated systems, occurs with a dissociative, D (SN1 lim), or with an interchange dissociative (Id) mechanism.[3] In the D mechanism an intermediate of reduced coordination is predicted in the transition state. The rate constant for solvent exchange, as determined by nmr, should correspond to the first-order rate constant of ligand penetration.[3] In the Id mechanism an interchange of ligands, solvent,

(1) This work is part of a thesis of A. Fanelli in partial fulfillment for the requirements of the degree of Doctor of Philosophy (Chemistry), Polytechnic Institute of Brooklyn, 1971.

(2) M. Eigen and L. DeMaeyer in "Investigation of Rates and Mechanism of Reactions," Vol. 8, A. Weissberger, Ed., Wiley, New York, N. Y., 1963, Part II.

(3) C. H. Langford and H. B. Gray, "Ligand Substitution Processes," W. A. Benjamin, New York, N. Y., 1965; T. R. Stengle and C. H. Langford, *Coord. Chem. Rev.*, **2**, 349 (1967).

and anion occurs in the transition state without formation of an intermediate of reduced coordination. The first-order constant of ligand penetration should differ by a statistical factor from the rate constant of solvent exchange. This factor should correspond to the solvation number of the cation in the second coordination sphere.[3,4]

Recent evidence[4,5] shows that some first-order rate constants of solvent substitution are $^1/_{20}$ times the rate of solvent exchange as determined by nmr. In other cases[6] an equality between the two rate constants has been reported for similar systems. While this problem is currently under experimental investigation in this laboratory the first equation, namely, the problem of the outer-sphere kinetics in nonaqueous solvents, has not been widely studied.

It is particularly important to perform such a study whenever possible to ascertain that the use of theoretically calculated outer-sphere association constants is justified. If one takes a two-step mechanism as the simplest scheme of a multistep reaction and assumes a preequilibration condition for the first step, the observed second-order rate constant, is related to the outer-sphere association constant K_{12}^{-1}, and to the first-order rate constant of ligand penetration, k_{23}, by the expression $k_f = K_{12}^{-1}k_{23}$. Much of the discrepancy between the substitution rate constants, k_{23}, and the rate constant of solvent exchange might arise from the use of incorrect outer-sphere association constants. This is an uncertainty to be clarified *before* speculating between the relative virtues of the D or Id mechanisms of solvent substitution in the first coordination sphere of metal cations.

Recently,[7] the electrical conductance of several M(II) *m*-benzenedisulfonates in methanol at 25° has been measured, providing useful parameters like association constants, collision diameters, and hydrodynamic radii. The pressure-jump relaxation kinetics of the same systems have been performed,[4] providing rate constants for inner-sphere complex formation. In order to extend this research, in the light of the above discussion, it was necessary to perform the study of the outer-sphere ion-pair formation. Ultrasonic relaxation has proved to be a suitable tool for such a study.

Experimental Part

The ultrasonic equipment and procedure for the work at 25° have been described elsewhere.[8-10] The conductance apparatus and technique have also been previously described.[7,11]

For the work at −15 and −45 or −50° special precautions and additional equipment have been used. A thermostat was built capable to perform within ±0.01° to −50°. This was built by surrounding a 2.5-gal. stainless steel beaker with 5-in. thick asbestos insulation. As the thermostat liquid stirred *n*-hexane was used. Cooling was done by a Cryo-cool C60 cryostat with a cold finger immersed in the liquid. A Bayley proportional thermoregulator was used to maintain the desired temperature. The temperature was measured within ±0.001° with a Pt thermometer (calibrated by the National Bureau of Standards) connected to a Leeds and Northrup Mueller bridge. Both the ultrasonic and the conductance cell were opened to be filled only when at room temperature in order to avoid moisture condensation.

The ultrasonic measurements were performed at low temperatures after the cell had remained immersed in the bath already at the desired temperature for at least 1 hr. Measurements were repeated at the same frequency with time to assure reproducibility. Eventually several solutions were reanalyzed[4] after the measurements in the ultrasonic cell to ensure that no significant condensation of water or change in composition occurred. Water content was checked by Karl Fischer reagent and was always found to be below 0.05%. The sound absorption of the solvent was measured to −78.5°. This last temperature was achieved by Dry Ice–acetone slush. A relaxation started to appear as shown below. Corrections of the concentrations for the density of the solvent at various temperatures were done in the calculations.

The conductance measurements were performed at low temperatures also in the constructed thermostat. *n*-Hexane proved to be a suitable bath fluid. No abnormal frequency dependence of the resistance was observed. On the contrary when acetone or methanol were first tried as bath liquids capacitance losses between the glass sealed-in leads of the conductance cell caused unreliable data even at the frequency of 1000 Hz, the frequency dependence becoming several per cent of the measured resistance at higher frequencies in the audio region. The liquid *n*-hexane was changed after each run to avoid capacitance leaks due to humidity condensation in the thermostat liquid. The temperature of the bath was held constant within ±0.01° at −15 and −45°, the lowest temperature obtainable with this precision. Therefore, conducatance data were performed at −15 and −45°, whereas the ultrasonic runs were preformed at −15 and −50°. At this last temperature a precision of ±0.05° was obtained. The association constant was extraplolated to −50° for the ultrasonic calculations.

(4) G. Macri and S. Petrucci, *Inorg. Chem.*, **9**, 1009 (1970).

(5) C. H. Langford and H. G. Tsiang, *ibid.*, **9**, 2346 (1970).

(6) R. G. Pearson and P. Ellgen, *ibid.*, **6**, 1379 (1967).

(7) R. Lovas, G. Macri, and S. Petrucci, *J. Amer. Chem. Soc.*, **92**, 6502 (1970).

(8) S. Petrucci, *J. Phys. Chem.*, **71**, 1174 (1967).

(9) S. Petrucci and M. Battistini, *ibid.*, **71**, 1181 (1967).

(10) G. S. Darbari, M. R. Richelson, and S. Petrucci, *J. Chem. Phys.*, **53**, 859 (1970); G. S. Darbari and S. Petrucci, *J. Phys. Chem.*, **73**, 921 (1969).

(11) S. Petrucci, P. Hemmes, and M. Battistini, *J. Amer. Chem. Soc.*, **89**, 5552 (1967).

Addition of further stock solution to the conductance cell was done in a drybox under a dry N_2 atmosphere *after* the cell had returned to room temperature. The cell constant was measured at 25°.[7] Corrections for the temperature change for the geometrical characteristic of the cell were done by calculation from the literature.[12] They were less than 0.05% of the cell constant value.

Results

The data for the sound absorption coefficient α (neper cm^{-1}) at the frequencies and temperatures investigated have been deposited in the microfilm edition of this journal.[13] The solvent properties pertinent to this work are density ρ (g/cc), dielectric constant ϵ, viscosity, η (P), longitudinal ultrasonic velocity V_0 (m/sec), and sound absorption coefficiency, $\alpha_0/$, expressed as α_0/f^2 (neper cm^{-1} sec^2). These constants are: at 25° $\rho = 0.7866$, $\epsilon = 32.66$, $\eta = 0.00547$, $V_0 = 1100$, $(\alpha_0/f^2) = 30 \times 10^{-17}$; at −15° $\rho = 0.8249$, $\epsilon = 39.1$, $\eta = 0.0105$, $V_0 = 1230$, $(\alpha_0/f^2) = 35 \times 10^{-17}$; at −50° $\rho = 0.8583$, $\epsilon = 46.3$, $\eta = 0.0237$, $V_0 = 1372$, $(\alpha_0/f^2) = 49 \times 10^{-17}$. In the above f is the frequency (Hz). The data of density, dielectric constant, and viscosity have been taken from the literature.[14] The sound velocities and attenuation, α_0, have been measured in this laboratory.

In Table I values of the equivalent electrical conductance Λ (mhos cm^2 $equiv^{-1}$) at the concentrations c (mol/l.) investigated for MgBDS at −15 and −45° are reported.

Table I: Equivalent Conductance Λ (mhos cm^2 $equiv^{-1}$) and Concentration c (mol/l.) for MgBDS in Methanol at −15 and −45°

MgBDS		
$c \times 10^4$, M	Λ	t, °C
2.211	32.092	−15°
3.798	27.618	
7.355	22.730	
10.844	20.217	
13.331	18.987	
16.693	17.844	
2.288	20.856	−45°
3.929	18.486	
7.609	15.707	
11.219	14.180	
13.791	13.424	
17.270	12.669	

Calculations and Discussion

I. Isothermal Study. The value of the solvent sound absorption has been measured as a function of the frequency at 25, −15, and −50°. In the range of frequency investigated (15–185 MHz) no relaxation of the solvent is present. At −50° however, an onset of a relaxation process at the highest frequency started to appear. In order to confirm this observation, the temperature of −78.5° was investigated. Here a relaxation was clearly visible starting at about 100 MHz. This relaxation is probably connected with a thermal and/or structural relaxation of the liquid. For the purpose of this work, however, namely in the temperature and frequency range where measurements were performed for the electrolyte solutions, the solvent absorption may be taken safely as constant.

In Figure 1 the ultrasonic results at 25° for the M^{II} BDS in methanol at 25° are reported in the form of $(\alpha_{exc}\lambda)$ *vs.* f, where $\alpha_{exc} = \alpha - \alpha_0$ is the excess sound absorption coefficient with respect to the solvent value, α_0, at each frequency f; λ is the sound wavelength, $\lambda = u/f$, and u is the sound velocity that has been approximated to the solvent sound velocity.

The solid lines in Figure 1 have been calculated for the theoretical function for a single relaxation

$$\alpha_{exc}\lambda = 2(\mu_{exc})_{max}\frac{\omega\tau}{1 + \omega^2\tau^2} \quad (1)$$

where τ is the relaxation time ($\tau^{-1} = 2\pi f_R$), f_R the relaxation frequency, and $(\mu_{exc})_{max}$ the maximum value of the excess sound absorption at $f = f_R$. Equation 1 has been fitted as a two-parameter equation to the data (Figure 1). The results of these calculations are reported in Table II. An error of ±5% may be associated with these results.

It may be noticed that the values of the relaxation frequency are concentration dependent, an indication that the process observed is not a first-order transformation but a bimolecular (or more complex) one. Ultrasonic data on $Ni(ClO_4)_2$, 0.09 M, in methanol at 25° show no relaxation and an insignificant excess sound absorption ($\Delta\alpha/f^2 \cong 1 \times 10^{-17}$) with respect to the solvent. Further, the relaxation frequency seems to be dependent on the charge of the cation. Indeed in Figure 2 data for K_2BDS and Cs_2BDS in the form of $(\alpha_{exc}\lambda)$ *vs.* f are reported. It may be seen that the relaxation frequencies are higher than the corresponding ones at the same concentration for the 2:2 salts.

The above proves the involvement of both M^{2+} and BDS^{2-} in the observed relaxation process. The hypothesis is advanced that the process is due to ionic association. On the other hand the elimination of methanol from the first coordination sphere of the

(12) R. A. Robinson and R. Stokes, "Electrolyte Solutions," Butterworths, Washington, D. C., 1965, p 97.

(13) Data for the sound absorption coefficient a (neper cm^{-1}) will appear following these pages in the microfilm edition of this volume of the journal. Single copies may be obtained from the Reprint Department, ACS Publications, 1155 Sixteenth St., N.W., Washington D. C. 20036, by referring to author, title of article, volume, and page number. Remit $4.00 for photocopy or $2.00 for microfiche.

(14) "International Critical Tables," and "Handbook of Chemistry and Physics," 48th ed, Weast, Ed., Chemical Rubber Publishing Co., Cleveland, Ohio, 1967.

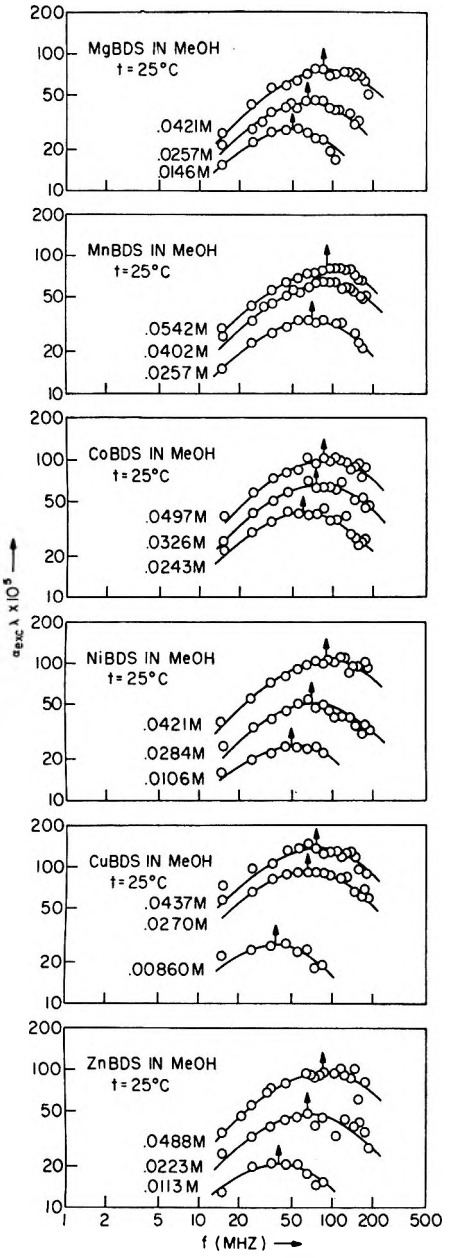

Figure 1. ($\alpha_{exc}\lambda$) *vs.* f (MHz) for $M^{II}BDS$ in methanol at 25°.

divalent metal cations studied in this work occurs in 10^{-3} to 10^{-4} sec,[15] therefore several orders of magnitude slower than the process observed here.

The hypothesis of ionic association must therefore correspond to outer-sphere complex formation, namely to the first step of the Eigen scheme[2]

$$M_s^{2+} + BDS_s^{2-} \underset{k_{21}}{\overset{k_{12}}{\rightleftharpoons}} M^{2+}S_6, BDS^{2-} \underset{k_{32}}{\overset{k_{23}}{\rightleftharpoons}} MS_5BDS \quad (2)$$

with S a solvent molecule.

The general solution of this mechanism in terms of the relaxation times is[2]

$$\tau_{I,II}^{-1} = {}^1/_2[S \pm \sqrt{S^2 - 4P}]$$

where

$$S = k_{12}\theta + k_{21} + k_{23} + k_{32}$$

$$P = k_{12}\theta(k_{23} + k_{32}) + k_{21}k_{32}$$

τ_I^{-1} corresponds to the fast relaxation time with the positive sign before the square-root term.

Table II: Maximum Excess Sound Absorption $(\mu_{exc})_{max}$, Relaxation Frequency f_R (MHz) and Isoentropic Volume Change ΔV_s for M^{II} BDS, K_2BDS, and Cs_2BDS in Methanol at 25°

Electrolyte	c, M	$(\mu_{exc})_{max}$ × 10^5	f_R, MHz	ΔV_s, cc/mol
MgBDS	0.0412	75	85	55.9
	0.0257	44	65	49.3
	0.0142	28	50	47.5
MnBDS	0.0542	83	90	54.2
	0.0402	65	80	52.5
	0.0257	34	70	46.0
CoBDS	0.0497	98	85	60.5
	0.0326	65	75	55.9
	0.0243	41	60	48.5
NiBDS	0.0421	108	90	66.8
	0.0284	52	70	52.0
	0.0106	25	50	49.2
CuBDS	0.0437	138	75	74.8
	0.0270	88	65	69.0
	0.0086	27	38	55.0
ZnBDS	0.0488	97	85	60.5
	0.0223	49	65	54.5
	0.0113	22	40	45.2
K_2BDS	0.0177	28	85	
Cs_2BDS	0.0182	34	100	

If k_{12}, $k_{21} \gg k_{23}$, k_{32} as it should be in our case then one has[2]

$$\tau_I^{-1} = k_{12}\theta + k_{21} \quad (3)$$

with

$$\theta = \sigma c f_\pm^2\left(2 + \frac{\partial \ln f_\pm^2}{\partial \ln \sigma}\right)$$

and

$$\tau_{II}^{-1} = k_{32} + k_{23}\frac{\theta}{\theta + K_{12}^{-1}}; \quad \left(K_{12}^{-1} = \frac{k_{12}}{k_{21}}\right) \quad (4)$$

In previous work[4] τ_{II} was measured for the same systems by pressure-jump relaxation kinetics. If the present hypothesis concerning the identification of the observed ultrasonic relaxation time with the first step of eq 2 is correct, then eq 3 should apply to the ultrasonic data. In the above σ is the overall degree of

(15) C. H. Langford and T. H. Stengle, *Annu. Rev. Phys. Chem.*, **19**, 193 (1968); R. G. Pearson, J. Palmer, M. M. Anderson, and A. L. Allred, *Z. Elektrochem.*, **68**, 110 (1960).

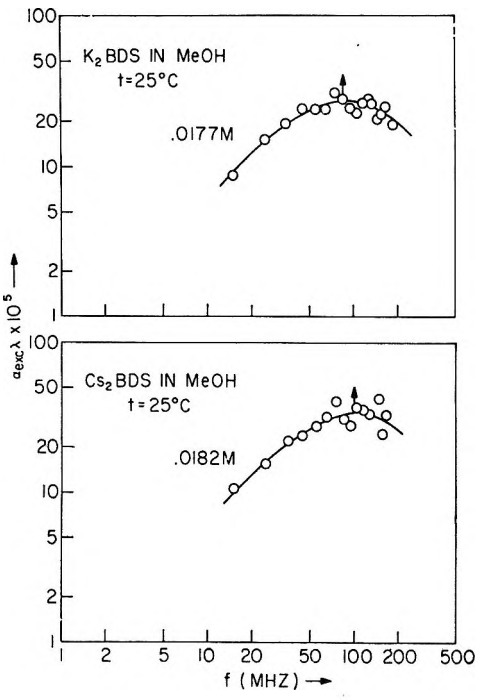

Figure 2. $(\alpha_{exc}\lambda)$ *vs.* f (MHz) for K_2BDS and Cs_2BDS in methanol at 25°.

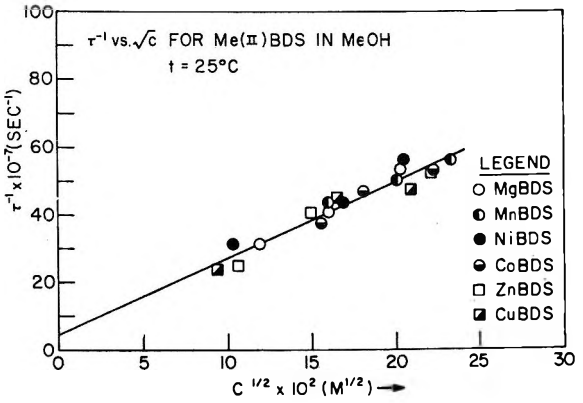

Figure 3. τ^{-1} (sec^{-1}) *vs.* $\sqrt{c}$ ($M^{1/2}$) for $M^{II}BDS$ in methanol at 25°.

dissociation of the electrolyte and $f_\pm$ the mean ionic activity coefficient.

The Debye–Hückel theory is the only available tool to calculate the unknown activity coefficient. Since this theory would give unreliable results in the concentration range studied in this work as pointed out elsewhere,[16] the following two types of calculations have been performed. As a first approximation it is assumed that $\theta \cong 2\sigma c$. Then, since $\sigma \cong 1/\sqrt{K}\sqrt{c}$, one may write $\theta \cong (2/\sqrt{K})\sqrt{c}$ with K the association constant of the electrolyte as determined by conductance.[7] Then

$$\tau^{-1} = \frac{2k_f}{\sqrt{K}}\sqrt{c} + k_R \tag{5}$$

where for simplicity k_{12} has been called k_f and k_{21}, k_R. Assumption of eq 5 is equivalent to taking $f_\pm^2 = 1$, $(\partial \ln f_\pm^2)/(\partial \ln \sigma) = 0$, and $\sigma \ll 1$. In Figure 3 the data for all the $M^{II}BDS$ in methanol at 25° are reported. They all appear to fall on a common line within experimental error. From the slope and the average[7] $K = (43{,}500 \pm 5000)\ M^{-1}$ one calculates $k_f = (2.37 \pm 0.16) \times 10^{11}\ M^{-1}\ sec^{-1}$ while the intercept gives $k_R = (4.5 \pm 2.7) \times 10^7\ sec^{-1}$. The solid straight line in Figure 3 has been calculated by least-square analysis.

If the process observed corresponds to a diffusion-controlled approach between ions then the Smoluchowski–Debye and Eigen equations should be applicable written in the form[8]

$$k_D = \frac{8NkT}{3000\eta}\left(\frac{-b}{e^{-b} - 1}\right) \tag{6}$$

$$k_{-D} = \frac{2kT}{\pi\eta a^3}\left(\frac{-b}{1 - e^{b}}\right) \tag{7}$$

with

$$b = \frac{|z_+z_-|e^2}{a\epsilon kT}$$

where N is the Avogadro number, k the Boltzmann constant, T the absolute temperature, η the solvent viscosity, ϵ the solvent dielectric constant, and a the minimum approach distance of free ions or the distance between the center of the ions in the ion pair due to the diffusion-controlled process; k_D and k_{-D} depend on the value of a chosen. Assuming $a = (R_+ + R_-) = 10$ Å, the sum of the hydrodynamic radii[7] or $a = a_J = 13$ Å, the collision parameter from the conductance coefficient, J,[7] the following results are obtained: $a = 10$ Å, $k_D = 8.2 \times 10^{10}\ M^{-1}\ sec^{-1}$, $k_{-D} = 3.6 \times 10^{-7}\ sec^{-1}$; $a = 13$ Å, $k_D = 6.3 \times 10^{10}\ M^{-1}\ sec^{-1}$, $k_{-D} = 6.1 \times 10^7\ sec^{-1}$. The corresponding Fuoss association constants[17] are $K_F = (k_D/k_{-D}) = 2280\ M^{-1}$ for $a = 10$ Å and $K_F = 1030\ M^{-1}$ for $a = 13$ Å, respectively.

It may be seen that within a factor of 3 to 4, k_f and k_D are comparable, a discrepancy not unreasonable as pointed out elsewhere for similar reactions.[16,18] k_{-D} and k_R are equal within experimental error.

The second calculation procedure adopted[16] is to retain the full expression for θ, calculating $f_\pm$ from the Debye–Hückel theory at the lowest concentration studied for $M^{II}BDS$. Some of these results are shown in Table III where k_f has been calculated from the eq 3 taking $k_R = k_f/K_{12}^{-1}$ and $K_{12}^{-1} = K_{Fuoss} = (4\pi Na^3/3000)e^b$. Then

$$k_f = \frac{\tau^{-1}}{(\theta + K_F^{-1})} \tag{8}$$

and K_{Fuoss} has been calculated for $a = 10$ Å and $a = 13$ Å. Again, the results for k_D and k_f are comparable

(16) G. S. Darbari and S. Petrucci, *J. Phys. Chem.*, **74**, 268 (1970).
(17) R. M. Fuoss, *J. Amer. Chem. Soc.*, **80**, 5058 (1958).
(18) A. Elder and S. Petrucci, *Inorg. Chem.*, **9**, 19 (1970).

Table III: Forward Rate Constant k_f (M^{-1} sec^{-1}) for Some $M^{II}BDS$ in Methanol at 25° Calculated from the Relation $k_f = [\tau^{-1}/(\theta + K_F^{-1})]$, at the Lower Concentration Studied and for $a = 10$ Å and $a = 13$ Å

	$a = 10$ Å, $K_F^{-1} = 4.39 \times 10^{-4}$				$a = 13$ Å, $K_F^{-1} = 9.71 \times 10^{-4}$		
Electrolyte	$\tau^{-1} \times 10^7$	$\theta \times 10^4$	$(\theta + K_F^{-1}) \times 10^4$	$k_f \times 10^{-11}$	$\theta \times 10^4$	$(\theta + K_F^{-1}) \times 10^4$	$k_f \times 10^{-11}$
NiBDS	31.4	2.56	6.95	4.51	3.19	12.90	2.43
ZnBDS	25.1	2.54	6.93	3.62	3.10	12.81	1.96
CuBDS	23.9	2.45	6.84	3.49	3.00	12.79	1.88
MgBDS	31.4	2.44	6.83	4.60	2.99	12.70	2.47

within a factor of 3 to 5. This also means that the previous approximation done in taking $\theta \cong (2/\sqrt{K})\sqrt{c}$ is not too unreasonable, much not having been gained by retention of the full expression for θ where applicable.

The conclusion might then be reached that a diffusion-controlled approach between the solvated ions to form an outer-sphere ion pair is the process whose relaxation has been observed.

A complication arises, however, in calculating the isoentropic volume change due to the reaction. The maximum excess sound absorption is bound to the concentration, degree of dissociation, and ΔV_s by the relation[2]

$$(\mu_{exc})_{max} = \frac{\pi}{2\beta_s} \frac{(\Delta V_s)^2}{RT} c\Gamma^* \qquad (9)$$

where

$$\Gamma^* = \frac{\sigma}{\sigma_{12}}[\Gamma/1 + \Gamma(\partial \ln f_\pm^2/\partial\sigma_{12})]; \quad \Gamma = \frac{\sigma_{12}(1 - \sigma_{12})}{2 - \sigma_{12}}$$

$$\Gamma^* \approx \frac{\sigma(1 - \sigma_{12})}{2 - \sigma_{12}} \cong \frac{1}{\sqrt{Kc}} \frac{1 - \sigma_{12}}{2 - \sigma_{12}}$$

σ_{12} is the degree of dissociation for the first step. Then

$$\Delta V_s = \left[\frac{2(\mu_{exc})_{max}\beta_s RT}{\pi\sqrt{c}} \sqrt{K}\right]^{1/2} \left(\frac{2 - \sigma_{12}}{1 - \sigma_{12}}\right)^{1/2} \qquad (10)$$

where $\beta_s = 1.065 \times 10^{-4}$ atm^{-1} for methanol at 25°. Values of ΔV_s were calculated by means of eq 10 using the data of Table II for $(\mu_{exc})_{max}$, $K_{Fuoss} = 2280\ M^{-1}$ for the estimation of σ_{12}, and the association constants determined by conductance.[7] Results are included in Table II. Also, ΔV_s and ΔV_T are related by[2]

$$\Delta V_s = \Delta V_T - \Delta H \frac{\alpha_p}{\rho c_p} \qquad (11)$$

with α_p the isobaric expansion coefficient, c_p the specific heat, and ρ the density of the solvent. ΔV_T and ΔH are the isothermal volume change and enthalpy of reaction, respectively. In water the enthalpic term is small with respect to ΔV_T.[2] In nonaqueous solvent this may not be the case due to the larger expansivity of the liquid.[2] In methanol $\alpha_p = 1.2 \times 10^{-3}$ deg^{-1}, $\rho = 0.7866$ g/cc, and $c_p = 0.60$ cal/deg g. This makes $(\alpha_p/\rho c_p) = 2.55 \times 10^{-3}$ cc/cal. Even allowing ΔH for the outer-sphere process to be the same as the ΔH for the overall process as determined by conductance (see below), *i.e.*, setting $\Delta H = 3800$ cal/mol, gives $\Delta H \cdot (\alpha_p/\rho c_p) = 9.7$ cc/mol. On the other hand if a molecule of methanol is eliminated during the observed process, then ΔV_T should roughly correspond to the molar volume of methanol, namely, 40.7 cc/mol. Examination of the data in Table II shows that this is the order of magnitude of the ΔV_s results. Because the enthalpic term must be smaller than the ΔV_T term, the rough numerical correspondence in order of magnitude between ΔV_s and ΔV_T supports the idea that one molecule of methanol is eliminated during the observed process.

The above discussion leads to the conclusion that the observed process corresponds to the diffusion controlled formation of an outer-sphere complex with simultaneous elimination of a molecule of methanol. This molecule could be loosely bound to the second coordination sphere of the cation or correspond to anion desolvation. While the present data do not allow distinction between these two possibilities, kinetically the problem arises as to whether one should write a single or double step for the observed process. A similar problem arises in water[19] in the interpretation of the sound absorption of the M(II) sulfates, *i.e.*, whether to take a two-step or a three-step overall mechanism.[19] The choice of three steps may be indicated if three distinct barriers of energy corresponding to diffusion, collapse of the outer sphere complex, and cation desolvation can be distinguished from the data or required to interpret the data. The determination of the activation parameters $\Delta H^\pm$ and $\Delta S^\pm$ should give an indication as to whether the barrier of energy for the observed process is larger or equal to the one of viscous flow, namely, to the minimal one for molecular encounter. To answer this question, such a study was performed for MgBDS in MeOH by a combination of ultrasonic relaxation and electrical conductance data.

II. Temperature Dependence. In Figure 4 the data of equivalent conductance Λ *vs.* $\sqrt{c}$ for MgBDS in methanol at 25–15° and −45° are shown. It may be

(19) L. G. Jackopin and E. Yeager, *J. Phys. Chem.*, **74**, 3766 (1970).

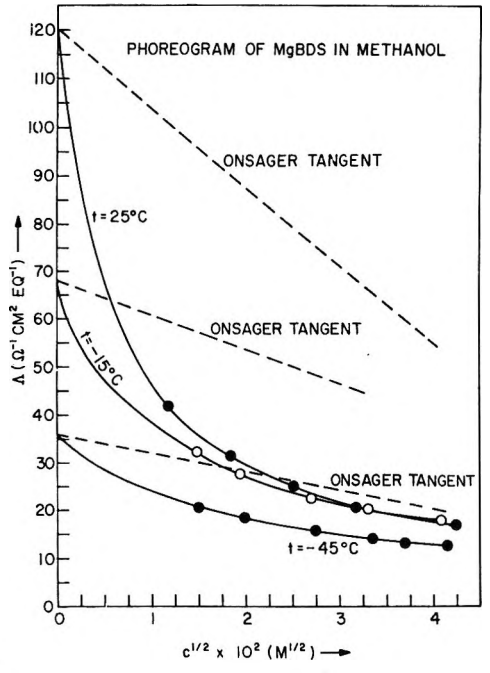

Figure 4. Λ (mhos cm^2 equiv^{-1}) *vs.* $\sqrt{c}$ ($M^{1/2}$) for MgBDS in methanol at 25, −15, and −45°.

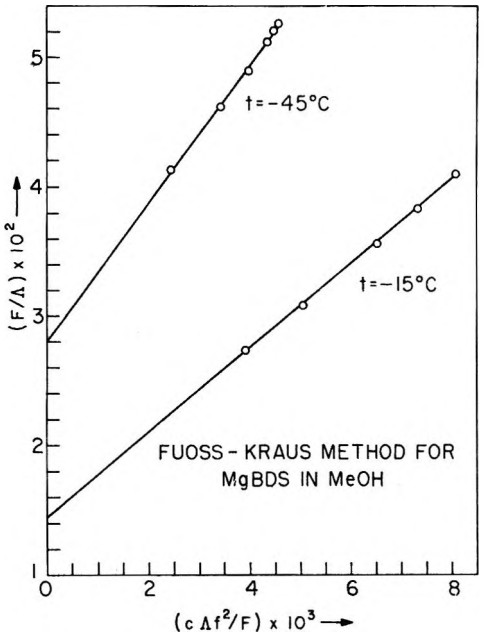

Figure 5. Fuoss–Kraus plot for MgBDS in methanol at −15 and −45°.

seen that by lowering the temperature the deviation from the Onsager tangent at the same concentration decreases. This in turn is a qualitative indication that the extent of ionic association must decrease by lowering the temperature. These data have been treated as before [7] at 25°, by the Fuoss–Kraus method. For values of the association constant K larger than a few thousand units the difference in K using the Fuoss–Kraus method or one of the more sophisticated forms of the conductance theory[20] becomes insignificant.[7]

In Figure 5 the $(F(z)/\Lambda)$ plot *vs.* $c\Lambda f_{\pm}^2/F(z)$ is shown for MgBDS at −15 and −45° where the symbols have their usual meaning. $f_{\pm}$ in this case is the limiting value of the Debye–Hückel activity coefficient, namely $\log f_{\pm} = -S_f\sqrt{c\alpha}$. The values of K and the limiting equivalent conductance, Λ_0, derived from the data are shown in Table IV. Notice that the Walden product, $\Lambda_0\eta$, is constant within 10%.

Table IV: Results at 25°, −15°, and −45° According to the Fuoss–Kraus Method of the Association Constant K (M^{-1}), of the Limiting Equivalent Conductance Λ_0 (mhos cm^2 equiv^{-1}). The Walden Product $\Lambda_0\eta$ at the Three Temperatures Is also Reported

t, °C	K, M^{-1}	Λ_0, mhos cm^2 equiv^{-1}	$\Lambda_0\eta$
25	48,500[7]	120.5[7]	0.667
−15	15,307 ± 44	68.7 ± 0.1	0.722
−45	6,771 ± 40	35.7 ± 0.1	0.725

A plot of log K *vs.* $(1/T)$ is linear within experimental error. The slope determined by least-squares analysis gives the enthalpy of the association process according to the relation

$$K = \exp\left(-\frac{\Delta H}{RT} + \frac{\Delta S}{R}\right) \qquad (12)$$

The result is $\Delta H = (3.8 \pm 0.5)$ kcal/mol. This may be used to calculate $\Delta S = (34 \pm 0.5)$ eu, which gives $\Delta G_{298} = -(6.4 \pm 0.5)$ kcal/mol.

With the value of the association constant so determined one may now proceed to the analysis of the ultrasonic data for MgBDS in methanol at various temperatures. Figure 6 reports the $(\alpha_{exc}\lambda)$ *vs.* f for this system at −15 and −50°. The results for the analysis by eq 1 are reported in Table V. Notice however that at −50° the background sound absorption from which the α_{exc} data have been computed is slightly different from the solvent value α_0. This nonrelaxing absorption α_{nr} has been computed by fitting the data first as a single relaxation curve by the relation[2]

$$\frac{\alpha}{f^2} = \frac{A}{1 + (f/f_R)^2} + B \qquad (13)$$

treated as a three-parameter equation in A, f_R, and B with $B = \alpha_{nr}/f^2$. These values are reported in Table V. We believe that this procedure, already done in other cases,[19,21] is the correct one to avoid distortions in the μ_{exc} function (1) that could simulate additional relaxation of a spurious nature. On the other hand if a

(20) R. M. Fuoss and F. Accascina, "Electrolyte Conductance," Interscience, New York, N. Y., 1959; R. F. Prini, *Trans. Faraday Soc.*, 65, 3311 (1969).

(21) P. Hemmes and S. Petrucci, *J. Phys. Chem.*, 74, 467 (1970); F. Fittipaldi, P. Hemmes, and S. Petrucci, *Acustica*, 23, 322 (1970).

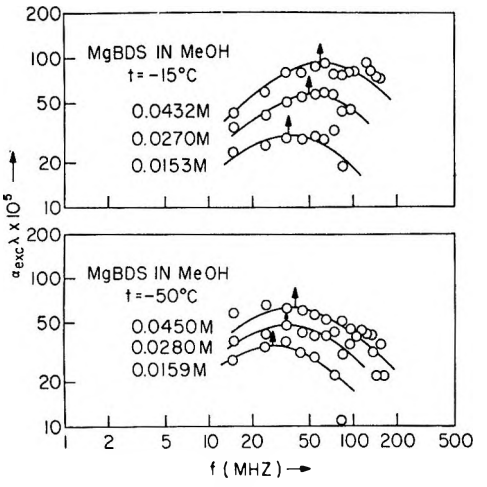

Figure 6. ($\alpha_{exc}\lambda$) *vs.* f (MHz) for MgBDS in MeOH at −15 and −45°.

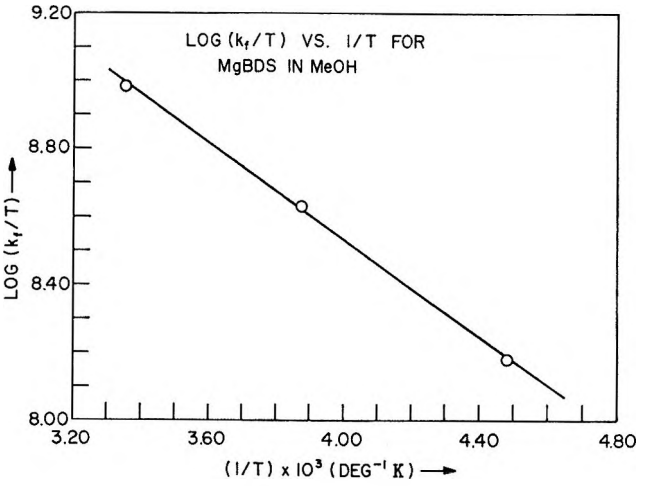

Figure 7. Log (k_f/T) (M^{-1} sec^{-1} °K^{-1}) *vs.* ($1/T$) (°K^{-1}) for MgBDS in methanol.

relaxation at high frequency has been masked by this procedure, the barrier of energy for the relaxation process should not correspond to the viscous flow as shown below but should be larger than it. This would result because the process corresponding to diffusion would have been cut off by the procedure of assuming B as the background absorption. As a general observation already clearly indicated by Eigen,[2] one should try to use the high-frequency absorption, not necessarily equal to the solvent absorption, as a background absorption. Indeed if one recalls the general relation valid for a Newtonian liquid[22]

$$\frac{\alpha}{f^2} = \frac{2\pi^2}{\rho V_0^3}(\eta_v + {}^4/_3\eta) \qquad (14)$$

where η_v is the compressional volume viscosity, it is enough to realize that ions may alter the structure of the solvent and therefore values of η_v and η to understand that $B = \alpha_0/f^2$ should not be taken as a rule.

Table V: $(\mu_{exc})_{max}$ and f_R at −15° and −50° for MgBDS in Methanol (the Nonrelaxing Portion of the Sound Absorption (α_{nr}/f^2) (cm^{-1} sec^2) Is also Reported Together with the Solvent Value (α_0/f^2) (cm^{-1} sec^2) for Comparison)

	MgBDS				
t, °C	c, M	$\mu_{exc\ max}$ × 10^5	f_R, MHz	α_{nr}/f^2 × 10^{17}, cm^{-1} sec^2	α_0/f^2 × 10^{17}, cm^{-1} sec^2
−15	0.0432	90	60	35	35
	0.0270	56	50	35	35
	0.0153	30	36	35	35
−50	0.0450	63	40	52	49
	0.0280	48	35	51	49
	0.0159	35	28	49	49

A plot of τ^{-1} *vs.* $\sqrt{c}$ for MgBDS in methanol at −15 and −50° gives for k_f and k_R: at −15°, $k_f = (1.1 \pm 0.2) \times 10^{11}$ M^{-1} sec^{-1} and $k_R = (1.0 \pm 5.5) \times 10^7$ sec^{-1}; at −50°, $k_f = (0.34 \pm 0.06) \times 10^{11}$ M^{-1} sec^{-1} and $k_R = (6.9 \pm 5.1) \times 10^7$ sec^{-1}. The scatter in k_R is characteristic of poor accuracy for the reverse rate constant when measured by relaxation tools. The above values have been obtained as slope and intercept by fitting the τ^{-1} *vs.* $\sqrt{c}$ plot by least-qsuares analysis.

With the determined values of k_f, Figure 7 shows a plot of log (k_f/T) *vs.* $1/T$. From the Eyring expression

$$k_f = \frac{kT}{h}\exp\left(-\frac{\Delta H^{\pm}}{RT}\right)\exp\left(\frac{\Delta S^{\pm}}{R}\right) \qquad (15)$$

and the determined slope from Figure 7, $\Delta H^{\pm} = (3.3 \pm 0.5)$ kcal/mol and $\Delta S^{\pm} = (5.3 \pm 1.0)$ eu. Similarly, from the viscosity data of methanol and the Eyring expression[22]

$$\eta = \frac{hN}{V}\exp\left(\frac{\Delta H_\eta{}^{\pm}}{RT}\right)\exp\left(-\frac{\Delta S_\eta{}^{\pm}}{R}\right) \qquad (16)$$

where V is the molar volume and h the Planck constant, one may calculate $\Delta H_\eta{}^{\pm} = 2.5$ kcal/mol and $\Delta S_\eta{}^{\pm} = 0.5$ eu. The accord between the two parameters, $\Delta H^{\pm}$ for the measured process and $\Delta H_\eta{}^{\pm}$, is good enough to suggest that the barrier of energy of viscous flow is the one to be attributed to the observed ultrasonic relaxation. The above calculation may be repeated in a different fashion through the Smoluchowski diffusion theory. Indeed from eq 6 neglecting e^{-b} with respect to 1, one may write

$$k_D \cong \frac{8NkT}{3000\eta}b = \frac{8N|z_1z_2|e^2}{a\epsilon 3000\eta}$$

and writing for η the Eyring expression (16) one has, taking the parameter a as independent of temperature

$$k_{D\epsilon} = \frac{8|z_1z_2|e^2}{3000a}\frac{V}{h}\exp\left(-\frac{\Delta H_\eta{}^{\pm}}{RT}\right)\exp\left(\frac{\Delta S_\eta{}^{\pm}}{R}\right) \qquad (17)$$

$$k_{D\epsilon} \cong \text{constant}\exp\left(-\frac{\Delta H_\eta{}^{\pm}}{RT}\right)$$

(22) T. A. Litovitz and C. M. Davis in "Physical Acoustics," Vol. 2, W. P. Mason, Ed., Academic Press, New York, N. Y., 1965, Part A.

A plot of log ($k_f\epsilon$) *vs.* $1/T$ gives as slope, $\Delta H^{\ddagger} = (2.8 \pm 0.5)$ kcal/mol, experimentally indistinguishable from the one calculated from viscosity data for the solvent. Taking into account change in V with temperature in eq 17 has a negligible effect on the determined value of $\Delta H^{\ddagger}$.

Conclusions

The observed relaxation for $M^{II}BDS$ in methanol is interpreted as a diffusion-controlled process of formation of an outer-sphere ion pair with the simultaneous elimination of a molecule of methanol. The same barrier of energy of viscous flow is observed. The agreement with theories based on a continuum for this step of the association is even more remarkable if one considers the numerical approximations introduced by our ignorance of the values of the ionic mean activity coefficients and their concentration dependence.

Zwitterion Formation upon Deprotonation in L-3,4-Dihydroxyphenylalanine and Other Phenolic Amines

by R. Bruce Martin

Chemistry Department, University of Virginia, Charlottesville, Virginia 22901 *(Received January 14, 1971)*

Publication costs borne completely by The Journal of Physical Chemistry

In weakly basic solutions L-3,4-dihydroxyphenylalanine (DOPA) exhibits two overlapping acidity constants of $pK_1 = 8.76$ and $pK_2 = 9.84$ as determined by potentiometric titration at 0.16 ionic strength and 25.0°. A new, simple method for evaluating acidity constants of overlapping deprotonations is described. By analyzing the increase in absorption near 295 nm due to the first phenolic ionization it is shown that the K_1 acidity constant is composed of 61% phenolic ionization and 39% ammonium deprotonation corresponding to a ratio of 1.6 zwitterionic to neutral forms of these two groups. From an analysis of both model compound and spectrophotometric results appearing in the literature it is concluded that the corresponding ratio for norepinephrine is about 3 and that for epinephrine about 4. Of the two bidentate metal ion binding loci in DOPA, Cu(II) appears to bind predominantly at the glycinate site in neutral solutions and in the catecholate mode in basic ones, while Mn(II) should chelate in the latter mode under both conditions.

Various compounds containing both amine and phenolic groups are found in biological systems. Examples are tyrosine, 3,4-dihydroxyphenylalanine (DOPA), epinephrine (adrenaline), and related compounds. The acidities of the phenolic and substituted ammonium groups are comparable so that their deprotonations often occur in the same pH region. As a result a special analysis is required to assess their relative contributions to the acidity (acid ionization) constants determined by titration. A complete resolution of the phenolic and ammonium deprotonations has been performed for tyrosine,[1] while no analysis appears to have been tried for DOPA, and most of the attempts on the catechol amines are incorrectly formulated. This paper describes a new method for evaluation of overlapping acidity constants, reports the first resolution of phenolic and ammonium deprotonations for DOPA, and presents a new analysis of data appearing in the literature for several phenolic amines. Preliminary studies of metal ion binding sites in DOPA are mentioned.

Results and Discussion

Evaluation of Macroconstants. Overlapping deprotonations require special methods for evaluation of acidity constants, several of which have been described.[2-4] A new method, especially suitable for cases to be discussed below, is here introduced for evaluation of macroconstants of two overlapping deprotonations. Concentrations of hydrogen and hydroxide ions are assumed negligible compared with the concentration of other acidic and basic species.

For two acidic groups let $\bar{h}$ be the mean number of protons removed per molecule. The relationship between $\bar{h}$ and the macroconstants is given by[2]

(1) R. B. Martin, J. T. Edsall, D. B. Wetlaufer, and B. R. Hollingworth, *J. Biol. Chem.*, **233**, 1429 (1958).

(2) J. T. Edsall, R. B. Martin, and B. R. Hollingworth, *Proc. Nat. Acad. Sci. U. S.*, **44**, 505 (1958).

(3) J. C. Speakman, *J. Chem. Soc.*, 855 (1940).

(4) F. J. C. Rossotti and H. S. Rossotti, "The Determination of Stability Constants," McGraw-Hill, New York, N. Y., 1961, pp 99–101 for projection strip method.

$$\bar{h} = \frac{(H^+)K_1 + 2K_1K_2}{(H^+)^2 + (H^+)K_1 + K_1K_2} \quad (1)$$

where $\bar{h}$ may take values from 0 to 2.

The titration curve for two acidic groups is symmetrical about the midpoint ($\bar{h} = 1.0$). We take two symmetrically related points on the titration curve, $\bar{h} = a$ and $\bar{h} = 2 - a$. Substitution into eq 1 and elimination of K_1 yields

$$(H^+)_a(H^+)_{2-a} = K_1K_2 \quad (2)$$

At the midpoint in the titration curve where $\bar{h} = 1.0$ eq 2 becomes

$$(H^+)_1^2 = K_1K_2 \quad (3)$$

On the other hand, if the product K_1K_2 is eliminated upon substitution into eq 1 we obtain

$$K_1 = \frac{a(H^+)_a - (2 - a)(H^+)_{2-a}}{1 - a} \quad (4)$$

Equation 4 permits a determination of K_1 without the necessity of approximating K_2. After determining K_1 from eq 4, K_2 may be found from eq 2 or 3. Equation 4 takes on the especially simple form when $a = {}^1/_2$

$$K_1 = (H^+)_{1/2} - 3(H^+)_{3/2} \quad (5)$$

Thus K_1 and K_2 may be evaluated from eq 3 and 5 by considering three well defined points on the titration curve at $\bar{h} = 0.5$, 1.0, and 1.5. Other points along the curve afford an opportunity for checks. Equation 4 is most useful when $\bar{h} < 1$. For $\bar{h} > 1$ it is more convenient to use the analogous equation for K_2 found by eliminating K_1 between eq 2 and 4.

Application of the above equations to the potentiometric titration curve obtained upon the addition of standard base to a solution containing DOPA yields $pK_1 = 8.76$ and $pK_2 = 9.84$ for a combination of the ammonium and first phenolic deprotonations at 25.0° and 0.16 ionic strength. These values agree closely with those of 8.71 and 9.74 obtained at the same temperature and 1.0 M ionic strength.[5] Under the latter conditions, the second phenolic ionization occurs with $pK_a = 13.4$ (due mainly to electrostatic effects) and the carboxylic acid ionization with $pK_a = 2.31$, so that they do not interfere with deprotonations occurring in the pH 6–11.5 region. Similar considerations apply to the other catecholamines discussed in this paper.

Resolution of Microconstants. Deprotonations from the phenolic and ammonium groups of phenolic amines may be described by equilibria shown in Chart I.

Chart I

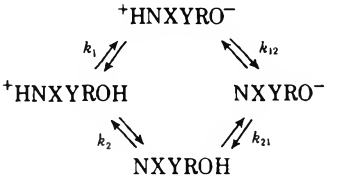

The letters X and Y designate hydrogen or other substituent on nitrogen. The acidity (acid ionization) constants defined by the scheme are termed microconstants. Their subscripts 1 and 2 refer to the phenolic and ammonium deprotonations, respectively. The four microconstants are related to the two acidity constants determined by titration, called macroconstants, by

$$\frac{(H^+)([{}^+HNXYRO^-] + [NXYROH])}{[{}^+HNXYROH]} = K_1 = k_1 + k_2 \quad (6)$$

$$\frac{[{}^+HNXYRO^-] + [NXYROH]}{(H^+)[NXYRO^-]} = K_2^{-1} = k_{12}^{-1} + k_{21}^{-1} \quad (7)$$

Due to the properties of a cyclic system, we also have

$$K_1K_2 = k_1k_{12} = k_2k_{21} \quad (8)$$

Only three equations relate the four microconstants and at least one item of additional information is required if the relative contributions of the phenolic and ammonium deprotonations are to be assessed.[2]

Two different approaches are possible for resolution of the microconstants shown in Chart I or similar systems. If the two acidic groups are associated with characteristic spectral properties, deprotonation of one group may be followed independently of the other as illustrated below for ultraviolet absorption. In the other method one of the two deprotonation modes in Chart I is blocked by substitution, often of a methyl group for hydrogen. The competing phenolic and ammonium deprotonations in tyrosine were resolved by a study of the ether *O*-methyltyrosine where only the ammonium or k_2 process in Chart I occurs with $pk_2 = 9.28$ as listed in Table I.[1,2] N methylation to yield the betaine *N*-methyltyrosine gave a pk_1 value that was about 0.15 log unit too high when compared with other, internally consistent results.[1] Thus model compound substitution studies must be employed with some caution.

Methyl blocked derivatives were employed by an Italian school to resolve a correctly formulated microconstant scheme similar to Chart I for norepinephrine and epinephrine (*N*-methylnorepinephrine).[6] The dimethyl ether was employed to estimate pk_2, and in conjunction with titration results for pK_1 and pK_2, pk_1 was calculated by use of eq 6–8. Their results are quoted in Table I. These same authors have also determined that for *N*,*N*-dimethylnorepinephrine $pk_1 = 8.88$ so that a comparison is possible with a betaine model. The results of our calculations for the betaine are shown in Table I, where the ether and betaine give

(5) J. E. Gorton and R. F. Jameson, *J. Chem. Soc. A*, 2615 (1968).

(6) C. Sinistri and L. Villa, *Farmaco, Ed. Sci.*, **17**, 949 (1962), quoted by P. Pratesi and E. Grana, *Advan. Drug Res.*, **2**, 127 (1965).

Table I: Acidity Constants for Phenolic Amines

	pK_1	pK_2	pk_1	pk_2	$R = k_1/k_2$	$pk_{21} - pk_1$	T, °C	μ	Method	Ref
p-Tyramine	9.61	10.65	9.70	10.32	4.2	0.24	25	0.10	Spectra	*a*
	9.53	10.78	9.66	10.11	2.8	0.54	20	0.10	Spectra	*b*
Tyrosine ethyl ester	7.33	9.80	9.42	7.33	0.008	0.38	25	0.16	Titration	*c*
Tyrosine	9.12	10.20	9.63	9.28	0.44	0.41	25	0.16	Spectra and ether	*c*
DOPA	8.76	9.84	8.97	9.17	1.6	0.46	25	0.16	Spectra	*d*
Dopamine	8.87	10.63	8.90	10.06	15	0.54	20	0.10	Spectra	*b*
Norepinephrine	8.73	9.84	8.92	9.18	1.8	0.47	25	~0	Ether	*e*
	8.73	9.84	8.88	9.27	2.5	0.43	25	~0	Betaine	*e*
	8.64	9.70	8.70	9.54	6.9	0.10	25	0.10	Spectra	*f*
	8.73	9.78	8.84	9.37	3.4	0.30	20	0.10	Spectra	*b*
Epinephrine	8.79	10.10	8.88	9.51	4.3	0.50	25	~0	Ether and betaine	*e*
	8.66	9.95	8.72	9.57	7.1	0.32	25	0.10	Spectra	*f*
	8.71	9.90	8.81	9.39	3.8	0.41	20	0.10	Spectra	*b*
Isopropylnorepinephrine	8.82	10.20	8.91	9.58	4.7	0.53	25	~0	Ether	*e*
	8.72	9.87	8.81	9.43	4.1	0.35	20	0.10	Spectra	*b*

[a] Calculated from ref 8 as described in text. [b] Calculated from ref 7 as described in text. [c] References 1 and 2. [d] This work. [e] Reference 6. [f] Calculated from ref 8 and 9 as described in text.

identical conclusions for epinephrine and somewhat different though similar answers for norepinephrine.

Phenolic group ionizations give rise to a marked increase in absorption at 295 nm. This absorption is perturbed little if at all by the ammonium group deprotonation in tyrosine,[1,2] and the same assumption is made for the molecules of this study. The phenolic ionization may be followed separately by ultraviolet absorption spectra and the results utilized to determine all micro- and macroconstants on the molecule of interest, independently of separate titration experiments, which may be employed as a check. The method, originally developed for application to tyrosine,[2] is described briefly for new results obtained with DOPA.

The fraction of all molecules with ionized phenolic groups is defined by

$$\alpha = \frac{[^+\text{HNXYRO}^-] + [\text{NXYRO}^-]}{[\text{all species in chart I}]}$$

We may also define a function M such that

$$M = \frac{(\text{H}^+)\alpha}{1 - \alpha} = \frac{k_1(\text{H}^+) + k_2k_{21}}{(\text{H}^+) + k_2} \qquad (9)$$

The last equality, following from the definitions of the microconstants, has been derived previously.[2] The function M would represent a simple acidity constant over a range of (H^+) if the phenolic ionization occurs separately either in solutions more acid (k_1) or more basic (k_{21}) than the ammonium deprotonation. In cases where the two ionizations are competitive M is not constant but varies with (H^+) according to eq 9.

Equation 9 may be written in logarithmic form to give

$$pM = \text{pH} - \log\frac{\alpha}{1 - \alpha} = -\log\frac{k_1(\text{H}^+) + k_2k_{21}}{(\text{H}^+) + k_2} \qquad (10)$$

A plot of pM *vs.* α would yield a horizonatal straight line if the phenolic ionization occurs without competition from any other. Figure 1 shows the results for DOPA; the curvature indicates that the phenolic and ammonium deprotonations occur in the same pH region. From eq 10 it is evident that the left-hand intercept of Figure 1 at high (H^+) yields pk_1 and the right-hand intercept at low (H^+) gives pk_{21}. From the intercepts of Figure 1 for DOPA, we obtain pk_1 = 8.97 and pk_{21} = 9.42. The shape of the curve in Figure 1 is determined by k_2 as indicated in eq 10 and several methods have been described for determining

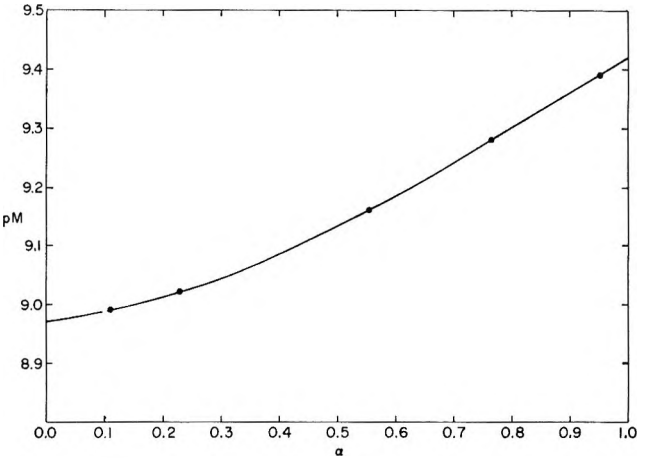

Figure 1. Plot of pM *vs.* fraction of molecules with ionized phenolic groups according to eq 5 for L-3,4-dihydroxyphenylalanine (DOPA). The data were obtained at 0.16 ionic strength and 25.0°.

the value of this constant.[1,2] For DOPA we obtain $pk_2 = 9.17$ and from eq 8, $pk_{12} = 9.62$. These four microconstant values determined by spectrophotometric titration may be combined according to eq 6 and 7 to yield $pK_1 = 8.76$ and $pK_2 = 9.83$. These calculated values for the macroconstants are in excellent agreement with the values determined directly by potentiometric titration at 0.16 ionic strength as described above in the section on macroconstants.

Table I includes results for the two macroconstants and two microconstants quoted as pk_1 and pk_2. The values of the two remaining microconstants, pk_{21} and pk_{12}, are easily calculated by eq 8 from the other values given and so are not listed in Table I. The ratio of molar concentration of zwitterionic to neutral forms, $[^+HNXYRO^-]/[NXYROH] = k_1/k_2 = R$, is tabulated in Table I for each method employed for every compound.

Two sets of workers measured the increase in absorption due to ionization of a phenolic hydrogen in a number of phenolic amines.[7,8] They did not formulate a microconstant scheme nor appreciate the variation in their calculated acidity constants with pH as a consequence of eq 10 as illustrated for DOPA in Figure 1. Both groups incorrectly assigned the acidity constant determined by standard methods for the phenolic absorption as K_1, but qualitatively consistent with the tendency of the phenolic group to ionize early in the titration curve of the two acidic groups for the compounds studied. Utilizing their data, we offer a reinterpretation of their results. We consider only those papers where two deprotonations are recognized in the pH 6–11 region of phenolic amines.

Let us assume that the spectrophotometrically determined acidity constants incorrectly assigned as K_1 represent an average of several determinations such that they correspond to a value of M in eq 9 where $\alpha = 0.5$, at the midpoint of phenolic ionization. We label as K_p this value of M at $\alpha = 0.5$ and note that K_p is some weighted average of k_1 and k_{21}. The acidity constant symmetrically related to K_p on the titration curve we label K_N. From eq 2 it is evident that $K_pK_N = K_1K_2$. By substitution of $M = K_p = (H^+)$ in eq 9 we obtain

$$K_p - K_N = k_1 - k_2 \qquad (11)$$

This equation when combined with eq 6 yields a solution to k_1 and k_2. Thus the results from the spectrophotometric studies can be reinterpreted to resolve the microconstant equilibria if we can assume that K_p corresponds to the point where $\alpha = 0.5$ in eq 9 and a value of K_1 is presented.

In his paper on ionization of sympathomimetic amines, Lewis remarks that pK_a values determined spectrophotometrically were higher than those determined by potentiometric titration.[7] This result is in accord with the equations presented in this paper which indicate that $K_1 > K_p$. Only for a phenolic ionization occurring unencumbered at more acid pH than ammonium deprotonation may K_p approach K_1. For five compounds for which Lewis gives pK_1 as well as pK_2 and pK_p values, the microconstants calculated with the aid of eq 6 and 11 are listed in Table I. Unfortunately in five monohydroxyphenylethanolamines, where the difference $pK_p - pK_1$ is of the order of 0.5, Lewis considered the equation he employed for overlapping macroconstants inapplicable and did not report pK_1 values. These five compounds, including synephrine (*p*-sympatol), are those in which the modes of deprotonation are most competitive. Since the five compounds exhibit similar values, we take averages of $pK_p = 9.57$ and $pK_N = 9.73$. Assuming $pK_1 = 9.07$ yields $pk_1 = 9.33$, $pk_2 = 9.42$, and $R = 1.2$. Though approximate, the value of R near unity provides a quantitative expression of the nearly equal proclivities of the phenolic and ammonium groups to deprotonate in these five monophenols.

In their paper on acidity of phenolic amines Kappe and Armstrong[8] do not consider the microconstant scheme and with one incidental exception report only pK_p and pK_N values (they incorrectly assign them as pK_1 and pK_2). In order to determine the microconstants from their paper, pK_1 values need be known and evidently are not generally available. Their description of experimental procedure mentions that $\bar{h} = 0.67$ at $pK_p = 9.74$ for *p*-tyramine. This information along with $pK_N = 10.52$ permits calculation of pK_1 by eq 4. This result and the microconstants evaluated are listed at the top of Table I. For norepinephrine and epinephrine the pK_p and pK_N values of these authors are combined with pK_1 and pK_2 values reported elsewhere in the literature[9] and obtained under identical conditions and with a similar sum to yield another set of values recorded in Table I for these compounds. The relatively high values of $R \sim 7$ probably indicate that the pK_p value is low.

The ratio R of zwitterionic to neutrally charged forms of the phenolic amines should be less dependent upon conditions than the microconstants from which the ratio is derived. Excluding the high values mentioned in the previous paragraph, there is excellent agreement among R values determined by totally different methods for the same compound. Even for *p*-tyramine (4-hydroxyphenylethylamine) the different values of 2.8 and 4.2 appear to exaggerate the difference between 74 and 81% zwitterionic form. Except for the two tyrosine compounds, the results of Table I indicate that the phenolic amines exist predominantly in the zwitterionic rather than the neutrally charged form of the two groups. In the pH 9–10 region these phenolic amines

(7) G. P. Lewis, *Brit. J. Pharmacol. Chemother.*, 9, 488 (1954).
(8) T. Kappe and M. D. Armstrong, *J. Med. Chem.*, 8, 368 (1965).
(9) R. F. Jameson and W. F. S. Nellie, *J. Chem. Soc.*, 2391 (1965).

are more aptly described as ammonium catecholates (or phenolates). Since both zwitterionic and neutral species bear identical net charges the R values are valid at all pH even when neither form predominates, as is the case at pH 7 for all compounds in Table I.

The reciprocal effects of a charged and uncharged ammonium group on the phenolic ionization and of an uncharged and charged phenolic group on the ammonium deprotonation are measured by the difference $pk_{21} - pk_1 = pk_{12} - pk_2$. Since the distance between these charge centers is nearly the same for all compounds listed in Table I, the pk differences should be similar and a further check is provided on the validity of the microconstant values.[1] As expected the pk differences tend to increase with decreasing ionic strength. Except for a low value in a result already mentioned as abnormal for norepinephrine, the close agreement among the pk differences indicates that the microconstant values listed present an accurate description of the equilibria involved.

Since the pk difference or the ratio $k_1/k_{21} = k_2/k_{12} \equiv S$ depends upon the structure of the compound, values may be estimated for a related series of compounds such as appear in Table I.[1,2] Unfortunately a knowledge of the ratio S does not provide the full fourth item of information to go with eq 6–8 required to resolve the four microconstant values. The relation among the two macroconstants and the ratios R and S is given by $(R + 1)^2/R = K_1/K_2S$. If the three values on the right-hand side are known, an ambiguity remains in a given case as to whether the solution of the equation yields R or $1/R$.

Experimental Section

L-3,4-Dihydroxyphenylalanine from Sigma Chemical Co. was 96% pure as determined by titration. Potentiometric titrations were performed at 5×10^{-3} M concentration with standard base at 25.0° in a thermostated reaction vessel under nitrogen passed through vanadous chloride scrubbers. Titration curves were recorded on a Radiometer TTT1a-SBR2b Titrator-Titrigraph combination. Spectrophotometric titrations were also performed under nitrogen. Absorbances were read on a Cary 11 spectrophotometer at 295 and 300 nm where, as illustrated for epinephrine,[7] the difference between ionized and un-ionized phenolic absorbances is nearly maximal and that of the acid form is off a steep slope. For the species of DOPA with one phenolic group completely ionized, an absorption maximum appears at 293 nm with ϵ 4400 near pH 11. The value of pk_1 obtained in Figure 1 was checked at each experimental point by the last equality of eq 8 in ref 2. Tris(hydroxymethyl)aminoethane and glycine buffers at about 0.01 M and DOPA at 1.6×10^{-4} M were employed to obtain the results plotted in Figure 1. In all experiments the ionic strength was controlled at 0.16 M with KCl, and the temperature was 25.0°.

In addition to the problem of proton binding sites in DOPA, there are two potentially chelating metal ion binding loci. On the basis of spectral comparisons with the alanine complex at pH 5 and the catechol complex at pH 9 it has been claimed that copper(II) chelates to DOPA in a glycinate mode at the lower pH and at the ortho phenolate groups at the higher pH.[5] The absorption scale in this reference is presented in arbitrary units so that a quantitative analysis is impossible. Nevertheless the absorption at 418 to 450 nm in the copper(II) complexes of catechol and DOPA at pH 9 seemed puzzling. The wavelength is much too short to be a ligand field band due to any oxygen donor atoms to copper(II). As a charge-transfer absorption band was a possibility, we undertook experiments to determine the molar absorptivities of the complexes. We find that solutions at pH >9 containing 2:1 molar ratios of either catechol or DOPA and Cu(II) exhibit absorption peaks at 400 and 418 nm, respectively, and that absorption in this region increases with time in the presence of air. Since intense absorption in the 400–450-nm region is typical of ortho-quinones in aqueous solutions and pyrocatechols are known to autoxidize easily to quinones and other products, the absorption may be accounted for. Some kind of Cu(II) complexes may also be involved, but we suggest that use of absorption spectra in the 400–450-nm region as a criterion for mode of metal ion binding in catechols be reinvestigated. An analysis of alternative bidentate binding modes based on estimated formation constants similar to that performed for histidine[10] suggests that for DOPA, Cu(II) binds predominantly at the substituted glycine locus in acid and neutral solutions with the catechol mode becoming dominant by pH 8 and increasingly so at higher pH. Though the overall binding is weaker, Mn(II) should bind predominantly in the catechol mode even in neutral solutions.

Acknowledgment. I thank Dr. Patsy Bostick Reed for performing the experimental measurements. This research was supported by a grant from the National Science Foundation awarded for other projects.

(10) E. W. Wilson, Jr., M. H. Kasperian, and R. B. Martin, *J. Amer. Chem. Soc.*, **92**, 5365 (1970).

Photometric and Mass Spectrometric Observations on the Reaction of Hydrogen Atoms with Cyanogen

by M. R. Dunn, C. G. Freeman, M. J. McEwan, and L. F. Phillips*

Chemistry Department, University of Canterbury, Christchurch, New Zealand *(Received March 8, 1971)*

Publication costs borne completely by The Journal of Physical Chemistry

The reaction is accompanied by a weak emission flame consisting of bands of the red and violet systems of CN. The intensity of CN emission at low cyanogen flows is proportional to $[H]^3/[H_2]$, as would be predicted by the proposed mechanism: $H + C_2N_2 \rightarrow HCN + CN$ (1); $CN + H_2 \rightarrow HCN + H$ (2); $H + H + CN \rightarrow H_2 + CN^*$ (3). The rate constant k_1 at room temperature is found to be $(8.6 \pm 3.0) \times 10^{-16}$ cm^3 molecule^{-1} sec^{-1}. This is consistent with a value of about 100 kcal for the heat of formation of the CN radical. With cyanogen in excess, reaction 2 competes with polymer formation, initiated by[1] $CN + C_2N_2 \rightarrow C_3N_3$ (4); the value of k_4, estimated from the point of onset of polymer formation, is about 1×10^{-14} cm^3 molecule^{-1} sec^{-1}.

Introduction

Haggart and Winkler[2] showed that the reaction of H atoms with cyanogen in the presence of excess H_2 involves the chain process

$$H + C_2N_2 \longrightarrow HCN + CN \qquad (1)$$

$$CN + H_2 \longrightarrow HCN + H \qquad (2)$$

Reaction 1 is stated to be fairly fast at room temperature.[3] For reaction 2 Hartel and Polanyi[4] estimated a value of about 7 kcal for the activation energy; this is reasonably consistent with Iwai, Pratt, and Broida's estimate[5] of 3×10^{-14} cm^3 molecule^{-1} sec^{-1} for the rate constant k_2 at room temperature. In a recent study of the H + ICN reaction in this laboratory[6] it was shown that the observed CN luminescence was excited by the termolecular process

$$H + H + CN \longrightarrow H_2 + CN^* \qquad (3)$$

The present photometric observations have shown that reaction 3 is also responsible for the blue-white luminescence that accompanies the $H + C_2N_2$ reaction, while both the photometric and the mass spectrometric observations are consistent with a mechanism of HCN production based on reactions 1 and 2, with the addition of polymer-forming reactions when C_2N_2 is in excess. Our mass spectrometric studies lead to a value of 8.6×10^{-16} cm^3 molecule^{-1} sec^{-1} for the rate constant k_1 at room temperature. On the assumption of a normal preexponential factor of about 10^{-10}, the rate constant found for reaction 1 is consistent with the "low" value of about 100 kcal given by a number of workers[7] for the heat of formation of the CN radical.

Experimental Section

The photometric[6] and mass spectrometric[8] apparatus and procedures were as previously described. Experiments were carried out at total pressures near 1 Torr. For the photometric studies H-atom concentrations were measured with an isothermal probe,[6] while in the mass spectrometric experiments the $H + NO_2$ titration[9] was used. Emission spectra were recorded with a McPherson Model 218 0.3-m monochromator, with an EMI 9558Q photomultiplier and a Keithley high-speed picoammeter. Low-resolution intensity measurements were made with a 1P21 photomultiplier plus a Corning 7-54 filter. Hydrogen was drawn from an Elhygen electrolytic generator (total impurities less than 10 ppm), or from a tank of commercial electrolytic hydrogen, *via* a tube of heated copper wool and a liquid air trap. The hydrogen was normally diluted, prior to the microwave discharge, with a large excess of either Matheson helium or welding-grade dry argon. The inert gases were purified by passage over heated BTS catalyst followed by successive towers containing sulfuric acid and P_2O_5. Matheson cyanogen (stated purity 99.1%, main impurities being HCN and CO_2, with 0.04% of CNCl and a trace of N_2) was used in the photometric experiments without further purification. For the mass spectrometric studies it was fractionated with a LeRoy still.

(1) D. E. Paul and F. W. Dalby, *J. Chem. Phys.*, **37**, 592 (1962).

(2) C. Haggart and C. A. Winkler, *Can. J. Chem.*, **37**, 1791 (1959).

(3) D. R. Safrany and W. Jaster, *J. Phys. Chem.*, **72**, 3305 (1968).

(4) P. Hartel and M. Polanyi, *Z. Phys. Chem., B*, **11**, 97 (1930).

(5) T. Iwai, D. W. Pratt, and H. P. Broida, *J. Chem. Phys.*, **49**, 919 (1968).

(6) R. F. C. Claridge, F. T. Greenaway, and M. J. McEwan, *J. Phys. Chem.*, **74**, 3293 (1970).

(7) V. H. Dibeler and S. K. Liston, *J. Chem. Phys.*, **47**, 4548 (1967); **48**, 4765 (1968); D. D. Davis and H. Okabe, *ibid.*, **49**, 5526 (1968); D. W. Setser and D. H. Stedman, *ibid.*, **49**, 467 (1968).

(8) C. G. Freeman and L. F. Phillips, *J. Phys. Chem.*, **72**, 3025 (1968).

(9) L. F. Phillips and H. I. Schiff, *J. Chem. Phys.*, **37**, 1233 (1962).

Results and Discussion

The blue-white reaction flame, consisting of bands of the red and violet systems of the CN radical, with no tail bands evident, typically extended along the full 50-cm length of the reaction tube (linear flow velocity about 8 m sec^{-1}) when H atoms were in excess. When the cyanogen flow was gradually increased the intensity increased quite rapidly until an optimum flow was reached. After about 30 sec of operation at the optimum flow rate the flame shortened, the CN intensity fell by about two orders of magnitude, and a weak greenish luminescence from a layer of polymer on the walls[6] became evident. The spectrum of the blue-white emission differed from the H + ICN flame, in that the ratio of violet to red intensities was greater with C_2N_2, and the intensity distribution among the bands showed marked differences in the population of vibrational levels of the upper state. This is illustrated in Figure 1 for the (v,v) sequence of the violet system. Since we are attributing the CN excitation to the same process in both cases, namely reaction 3, it is necessary to assume either that there is some specific process leading to rapid vibrational relaxation of excited CN in the H + ICN system, or that the ground-state CN radicals produced by reaction 1 differ from those produced in the H + ICN system in that they already possess some vibrational excitation.

The formation of CN polymer is believed to be initiated by the reaction[1]

$$CN + C_2N_2 \longrightarrow C_3N_3 \qquad (4)$$

Hence the steady-state concentration of CN radicals is given by

$$[CN] = k_1[H][C_2N_2]/(k_2[H_2] + k_4[C_2N_2]) \qquad (5)$$

The appropriate value of k_2 for insertion in this expression may be higher than the room temperature figure of 3×10^{-14} cm^3 $molecule^{-1}$ sec^{-1} because of the presence of vibrationally-excited H_2 from the discharge.[10] Under conditions where polymer formation can be neglected this expression reduces to $k_1[H][C_2N_2]/k_2[H_2]$, so that the intensity of CN emission due to reaction 3 becomes

$$I_{CN} = k_1k_3[H]^3[C_2N_2]/k_2[H_2] \qquad (6)$$

Hence, under conditions where sufficient time has elapsed for the steady state to be established with respect to [CN], but the actual consumption of C_2N_2 is small, the effect of varying [H] should be such that a graph of I_{CN} against $[H]^3/[H_2]$ is a straight line through the origin. An experimental test of this result is shown in Figure 2; a good linear dependence of I_{CN} on $[H]^3/[H_2]$ is found, except at high values of [H] where the consumption of C_2N_2 is likely to be important.

We have noted that as the flow of cyanogen was increased a point was reached at which the flame suddenly shortened and the buildup of a polymer deposit on the walls became noticeable. It may be assumed that at this point the rates of removal of CN by reactions 2

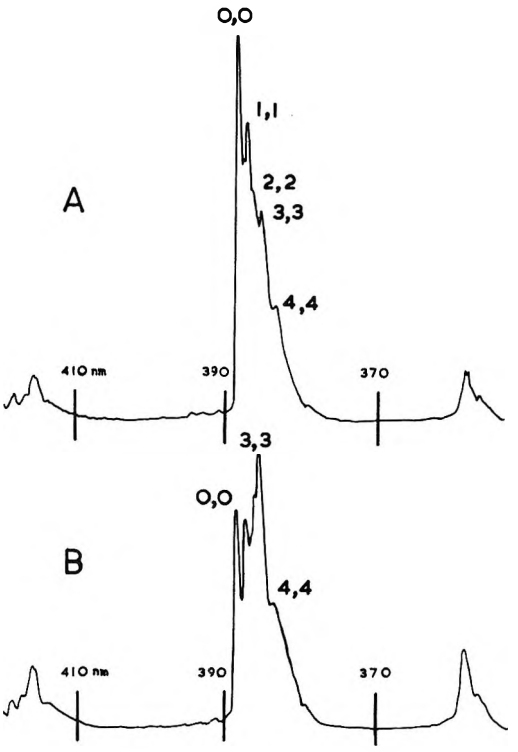

Figure 1. Low-resolution scan showing relative intensities of emission bands in the (v,v) sequence of the CN violet system: (A) H + ICN flame; (B) H + C_2N_2 flame.

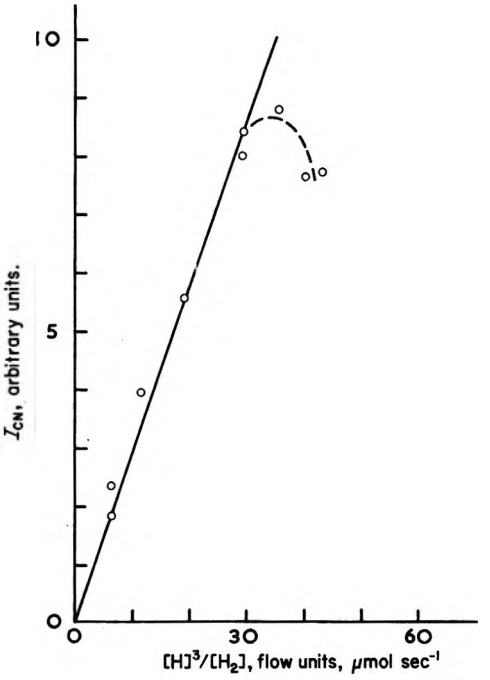

Figure 2. Graph of CN emission intensity *vs.* $[H]^3/[H_2]$ at t = 30 msec: $[C_2N_2] = 3.4 \times 10^{13}$, $[H_2] \sim 1.7 \times 10^{15}$, $[H] \sim 1 \times 10^{15}$. [H] was varied by varying the power supplied to the discharge.

(10) D. H. Stedman, D. Steffenson, and H. Niki, *Chem. Phys. Lett.*, 7, 173 (1970).

Table I: Evaluation of k_1;[a] Partial Pressures in Torr, Times, t, in Milliseconds

[Ar]	$[H_2]$	$10^3[C_2N_2]_0$	$10^3[C_2N_2]_t$	$10^3[H]_0$	t	$10^{16}k_1$
0.523	0.154	7.15	6.70	6.70	165	8.55
		12.51	11.7			8.7
		8.94	8.37			8.7
1.85	0.500	11.76	9.24	18.7	550	6.65
		6.30	4.70			8.1
		9.49	7.31			7.2
0.946	0.209	12.22	10.46	23.07	273	6.85
		23.66	20.66	24.27		5.8
		12.66	10.14	26.05		8.8
		12.98	10.51	22.21		9.9
		13.26	12.60	4.517		11.6
		3.645	2.804	25.68		10.6
		3.493	2.775	21.68		11.0
1.102	0.024	3.74	3.55	8.77	325	5.2
	0.076	13.44	10.62	20.57		6.3
1.152	0.076	5.02	4.155	22.13		7.45

[a] Mean $k_1 = 8.2 \times 10^{-16}$ cm^3 molecule^{-1} sec^{-1} (8.6×10^{-16} after correction for recombination of H, see text).

and 4 were comparable, so that if one of the two rate constants is known an estimate can be made of the other. In two typical determinations of the point at which the flame began to shorten the reactant concentrations (in particles cm^{-3}) were $[H_2] = 8.6 \times 10^{14}$, $[C_2N_2] = 3.4 \times 10^{14}$, $[H] = 1.7 \times 10^{15}$, and $[H_2] = 4.3 \times 10^{15}$, $[C_2N_2] = 8.6 \times 10^{14}$, $[H] = 3.8 \times 10^{15}$, respectively. Equating $k_2[H_2]$ with $k_4[C_2N_2]$, and taking $k_2 = 3 \times 10^{-14}$ cm^3 molecule^{-1} sec^{-1}, these determinations give k_4 values of 7.4×10^{-14} and 1.4×10^{-13}, respectively. Both values are considerably larger than the figure of 3.6×10^{-15} given by the Arrhenius expression of Paul and Dalby[1] at 300°K. The value of 3×10^{-12} estimated by Boden and Thrush[11] for k_4 at temperatures near 600°K is also greater, by a factor of about 150 in this case, than the corresponding value derived from Paul and Dalby's Arrhenius expression. Our estimates of k_4, and that of Boden and Thrush, should be reliable to within an order of magnitude; the observed discrepancies tend to confirm Boden and Thrush's suggestion that reaction 4 is partly heterogeneous.

The rate of reaction 1 at 300°K was determined mass spectrometrically in a flow system in which the walls were poisoned with phosphoric acid. The flow system was designed for the study of reactions with rate constants greater than about 10^{-14} cm^3 molecule^{-1} sec^{-1}, so that for the $H + C_2N_2$ reaction it was necessary to throttle down the flow speed (to about 100 cm sec^{-1}) by almost closing the lead to the pump. Preliminary measurements with no discharge showed that the reaction of C_2N_2 with H_2 could be neglected. From the data obtained using the microwave discharge, values of rate constants were calculated for reaction 1, on the assumption that the overall stoichiometry was

$$H_2 + C_2N_2 \longrightarrow 2HCN \qquad (7)$$

(*i.e.*, that H atoms were regenerated by reaction 2) and also for the termolecular reaction

$$H + H + C_2N_2 \longrightarrow 2HCN \qquad (8)$$

with no regeneration of H. The "rate constants" obtained for reaction 8 varied widely, and gave a mean value of 2×10^{-30} cm^6 molecule^{-2} sec^{-1} which is very large for such a reaction. On the other hand the values obtained for k_1 (see Table I) were reasonably consistent over a considerable range of initial [H] and $[C_2N_2]$ values. The mean value found for k_1 was 8.2×10^{-16} cm^3 molecule^{-1} sec^{-1}, with a standard deviation of 1.8×10^{-16}. The estimated error of the results is about 1.5 times the standard deviation. Systematic errors in the k_1 values would be introduced by the recombination of hydrogen atoms, which could have amounted to as much as 20% at $t = 500$ msec and not more than 10% elsewhere in Table I. This would cause the k_1 values to be too low by 5% at most. The H-atom concentrations might also have been overestimated by the NO_2 titration, which is subject to error in the presence of excess H_2.[12] A computer simulation of the titration reaction using the known rate constants[7,12,13] showed that under the typical conditions of our experiments ($[H] = 0.02$ Torr, $[H_2] = 0.15$ Torr) the concentration of [H] would have been overestimated by less than 5%. As a further check we measured the reduction in peak height at mass 2 when the discharge was activated, with and without NO_2 present, and found no significant variation except under the worst

(11) J. C. Boden and B. A. Thrush, *Proc. Roy. Soc., Ser. A*, **305**, 107 (1968).

(12) F. P. Del Greco and F. Kaufman, *Discuss. Faraday Soc.*, **33**, 128 (1962).

(13) M. A. A. Clyne and B. A. Thrush, *Proc. Roy. Soc., Ser. A*, **275**, 544, 559 (1963).

conditions of excess H_2, when an error amounting to a change of 5% in the value of k_1 may have been introduced. Making an allowance for these sources of error, we give our final k_1 value as $(8.6 \pm 3.0) \times 10^{-16}$ cm^3 molecule^{-1} sec^{-1}.

The activation energy of reaction 1 is an upper limit for the endothermicity of this reaction. If a preexponential factor of 10^{-10} is assumed the above value of k_1 is found to correspond to a value of not more than 99.6 kcal mol^{-1} for the heat of formation of the CN radical (for the other heats of formation we use the 0°K values listed in Davis and Okabe's Table IV;[7] the use of room temperature values would make a difference of at most 1 kcal in the calculated heat of formation of CN). A larger value of the heat of formation would appear to require an unreasonably large preexponential factor; for example, if the heat of formation is raised to 102 kcal the preexponential factor becomes 5×10^{-9}. Thus it is difficult to reconcile this k_1 value with the recent determination by Berkowitz, Chupka, and Walter[14] which gave a value of 105.5 kcal. The kinetic data of Boden and Thrush[11] also require a heat of formation near 100 kcal. On the other hand, our observation that reaction 1 is quite slow appears to dispose of the main argument given by Safrany and Jaster[3] in support of the "ultra-low" figure of 92.5 kcal for the heat of formation of CN.

Acknowledgments. This work was supported by the New Zealand Universities Research Committee and by Grant AF-AFOSR-1265-67 from the United States Air Force Office of Scientific Research.

(14) J. Berkowitz, W. A. Chupka, and T. A. Walter, *J. Chem. Phys.*, **50**, 1497 (1969).

Isomerization of Vibrationally Excited 3-Methyl-1-buten-1-yl Radicals *via* Hydrogen Atom Migration. Quantum Statistical Weight Effect[1]

by K. W. Watkins* and L. A. O'Deen

Department of Chemistry, Colorado State University, Fort Collins, Colorado 80521 *(Received March 15, 1971)*

Publication costs borne completely by The Journal of Physical Chemistry

The unimolecular rate constant for the isomerization by 1,4 hydrogen atom migration of the 3-methyl-1-buten-1-yl radical was measured. The radicals were generated with an average excess vibrational energy of ~34 kcal mol^{-1} by the addition of isopropyl radicals to acetylene at 53°. The average rate constant was 4.1×10^8 sec^{-1}. This rate constant, when compared with previous results for *n*-pentyl isomerization, provides a demonstration of the variation of elementary rate constants that occurs when the vibration–internal rotation frequency pattern is altered by substitution of a double bond for a single carbon–carbon bond. The best agreement between the rate constant as calculated by the RRKM theory and the experimental result was found when the threshold energy was chosen to be 17.1 kcal mol^{-1}. Other kinetic data reported are: the rate constant for addition of isopropyl to acetylene, $k_1 = 10^{11.30} \exp(-7600/RT)$ cm^3 mol^{-1} sec^{-1}; Δ(*i*-Pr, 1-penten-4-yl) = 0.4; Δ(1-penten-4-yl, *i*-Pr) = 0.3. The formation of benzene in this system is discussed.

Introduction

The isomerization of alkyl radicals *via* hydrogen atom migration has recently received much attention in both equilibrium[2] and nonequilibrium[3,4] reaction systems. Isomerization of alkenyl radicals offers a novel and important comparison to the study of alkyl radical isomerization. For the same or similar activated complexes the principal feature which determines the relative rates of two reactions in nonequilibrium systems, according to the RRKM formulation of unimolecular reactions, is the density of eigenstates, $N^*(E)$, of the molecule at the energy of interest.[5] Alterations in molecular structure which change the molecular vibration–internal rotation frequency pattern, but do not exert an appreciable mechanistic effect, are called quantum statistical weight effects. Pre-

(1) Abstracted from the M.S. Thesis of Louise A. O'Deen, Colorado State University, 1970.

(2) K. W. Watkins, *J. Amer. Chem. Soc.*, in press.

(3) K. W. Watkins and D. R. Lawson, *J. Phys. Chem.*, **75**, 1632 (1971).

(4) E. A. Hardwidge, C. A. Larson, and B. S. Rabinovitch, *J. Amer. Chem. Soc.*, **92**, 3278 (1970).

(5) B. S. Rabinovitch and D. W. Setser, *Advan. Photochem.*, **3**, 1 (1964).

vious investigations of quantum statistical weight effects in nonequilibrium unimolecular reactions have been on the replacement of D for H and F for H.[6] Specifically we will compare the rates of 1,4 hydrogen atom migration in the isomerization of pentyl-1 (P-1) and 3-methyl-1-buten-1-yl (3MB-1) radicals. Since 3MB-1 has three internal rotations and pentyl-1 has four, and because the energy levels for internal rotation are closely spaced ($\sim$200 cm^{-1}), then $N^*_{P\text{-}1}(E) > N^*_{3MB\text{-}1}(E)$ for similar energies. The fact that 3MB-1 has six degrees of freedom less than pentyl-1 also contributes to a lesser density of states than for pentyl-1. This is the first measurement of the effect of a double bond on the reaction of a chemically activated radical.

The activated complex (I) involved in the 1,4 hydrogen atom migration in 3MB-1 closely resembles that

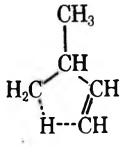

I

for the 1,4 hydrogen atom shift in pentyl-1. Isomerization of vibrationally excited pentyl-1 radicals has been studied previously.[5] Activation by the addition of alkyl radicals to ethylene and acetylene generates alkyl and alkenyl radicals with essentially equal energies. These conditions allow a study of the quantum statistical weight effect given by

$$\frac{k_E^{3MB\text{-}1}}{k_E^{P\text{-}1}} = \frac{\sigma_{3MB\text{-}1}}{\sigma_{P\text{-}1}} \times \frac{I_{3MB\text{-}1}}{I_{P\text{-}1}} \times \frac{\sum_0^{E\dagger} P(E_{vr}\dagger)_{3MB\text{-}1}}{\sum_0^{E\dagger} P(E_{vr}\dagger)_{P\text{-}1}} \times \frac{N^*(E)_{P\text{-}1}}{N^*(E)_{3MB\text{-}1}} \quad (I)$$

where $\sigma_{3MB\text{-}1}/\sigma_{P\text{-}1}$ is the ratio of reaction path degeneracies, $I_{3MB\text{-}1}/I_{P\text{-}1}$ is the ratio of the partition functions for the adiabatic degrees of freedom, $P(E_{vr}\dagger)$ is the sum of the vibration–rotation energy eigenstates at the energy $E_{vr}\dagger$ for the activated complexes, and the $N^*(E)$ are the densities of vibration–rotation energy eigenstates at the energy E for the activated molecules.

The addition of isopropyl radicals to acetylene was studied once previously by Dominguez and Trotman-Dickenson,[7] and the isomerization of the 3MB-1 radical was noted at that time. The reported average rate constant for isomerization of vibrationally excited 3MB-1 was $k_a = 2 \times 10^8$ sec^{-1} at 127°.[8] The results in the present work were obtained at 53° in order to minimize any thermal isomerization of stabilized 3MB-1. Also the use of a different precursor of isopropyl radicals from that used by Trotman-Dickenson allowed a more concerted effort to identify isomerization products.

Experimental Section

The experimental details were the same as described previously.[3,9] 3MB-1 radicals were generated by the vapor-phase photolysis of azoisopropane in the presence of acetylene over the temperature range 50–140°. Pyrex reactors of 2.01, 10.0, and 114 cm^3 were used. Runs were analyzed by gas chromatography using a 1.6-m alumina column. Conditioning of the column at 240° before each run was required to eliminate extraneous peaks. Authentic hydrocarbon samples were used for identification of the products. *trans*-2,5-Dimethyl-3-hexene, *cis*-2,5-dimethyl-3-hexene, 3,5-dimethyl-1-hexene, and 4,5-dimethyl-1-hexene were purchased from Chemical Samples Co. To ensure calibration of the detector a known amount of ethane was added to the product mixture before the analysis. The reaction conditions and rates of formation of products for the 53° runs are given in Table I.

Results

Reactions of Excited 3-Methyl-1-Butenyl Radicals. The addition of isopropyl to acetylene at 53° produces a 3MB-1 radical with an average energy of 33.8 kcal mol^{-1} (see Discussion). These radicals can either undergo unimolecular reaction, or be stabilized by collisional energy transfer. Because of a competition between isomerization and stabilization, stabilization products should predominate at high pressure, and isomerization products should "grow in" as the pressure is lowered.

At high pressure (200–500 Torr) the main products, besides those from C_3H_7 disproportionation and recombination, are 3-methyl-1-butene, *cis*-2,5-dimethyl-3-hexene, and benzene. The source of benzene will be discussed later. 3-Methyl-1-butene and *cis*-2,5-dimethyl-3-hexene are obvious products of 3MB-1. As the pressure was lowered (to 20–100 Torr) 1-pentene, 3,5-dimethyl-1-hexene, and 4,5-dimethyl-1-hexene appeared in increasingly greater yields. These must be the products of isomerization. 3,5-Dimethyl-1-hexene must result from the $\cdot CH_2CH(CH_3)CH{=}CH_2$ radical, which is formed from 3MB-1 after a 1,4 H atom migration. The products 1-pentene and 4,5-dimethyl-1-hexene must result from the $CH_3\dot{C}HCH_2CH{=}CH_2$ radical, which is formed from $\cdot CH_2CH(CH_3)CH{=}CH_2$ by a homoallylic rearrangement. Trotman-Dickenson observed 1-pentene, but the mechanism for its formation was explained later by Benson and DeMore.[10] Homoallylic

(6) F. H. Dorer and B. S. Rabinovitch, *J. Phys. Chem.*, 69, 1973 (1965), and references cited therein.

(7) J. A. G. Dominguez and A. F. Trotman-Dickenson, *J. Chem. Soc.*, 940 (1962).

(8) A. F. Trotman-Dickenson, R. R. Getty, and J. A. Kerr, *J. Chem. Soc. A*, 1360 (1967).

(9) K. W. Watkins and L. A. O'Deen, *J. Phys. Chem.*, 73, 4094 (1969).

(10) S. W. Benson and W. B. DeMore, *Annu. Rev. Phys. Chem.*, 19, 397 (1965).

Table I: Experimental Results, 53°

Run	Pressure[a] acetylene	Pressure azoisopropane	C_2H_6[b]	C_3H_8	3-M1B[c]	1-C_5H_{10}
30	17.1	4.1	15.1	18.4	0.32	0.066
31	20.1	4.2	29.6	33.7	0.608	0.098
32	25.8	5.2	...	36.2	1.46	0.295
33	36.1	9.2	15.5	20.0	1.12	0.10
34	42.0	8.3	11.0	11.0	1.18	0.084
35	44.8	9.9	12.6	14.3	1.59	0.190
36	80.2	16.4	19.0	24.5	4.43	0.183
37	86.9	19.2	31.0	26.3	5.27	0.298
38	121	25.2	25.3	...	7.10	0.226
39	130	25.9	21.3	23.6	5.76	0.16
40	132	28.4	18.3	21.0	6.63	0.076
41	197	37	33.9	42.3	13.1	0.79
42	424	87.1	36.3	46.6	23.3	0.36

	C_4H_6[d]	23DMB[e]	C_5H_8[f]	C_6H_6	*cis*-2,5-DM3H[g]	*trans*-2,5-DM3H	3,5-DM1H[h]	4,5-DM1H
30	Trace	26.3	0.083	0.058	0.012	0.012	0.025	0.308
31	0.000	50.8	0.104	0.079	0.025	0.012	0.050	0.508
32	0.013	54.4	0.363	0.086	0.131	0.035	0.018	0.643
33	0.004	28.5	0.135	0.15	0.171	0.052	0.039	0.471
34	...	19	0.122	0.090	0.046	0.013	Trace	0.487
35	...	21.0	0.185	0.105	0.021	0.01	0.038	0.570
36	0.000	32.6	0.280	0.293	0.243	0.083	0.061	0.817
37	0.000	45.3	0.305	0.246	0.296	0.028	0.030	0.883
38	0.000	40.8	0.440	0.481	0.868	0.070	0.003	0.976
39	...	34.8	0.386	0.346	0.683	0.021	0.010	0.658
40	0.000	32.6	0.377	0.398	0.470	0.063	0.06	0.725
41	0.000	60.2	0.53	0.987	0.970	0.041	0.07	1.00
42	0.000	53.2	1.05	1.76	1.43	Trace	0.33	0.71

[a] Reagent pressures, Torr. [b] Rates of formation of products, mol cm^{-3} sec^{-1} × 10^{12}. [c] 3-Methyl-1-butene. [d] 1,3-Butadiene. [e] 2,3-Dimethylbutane. [f] Pentadiene. [g] *cis*-2,5-Dimethyl-3-hexene. [h] *trans*-3,5-Dimethyl-1-hexene.

rearrangements have been extensively studied by Montgomery.[11] Cross-disproportionation and combination of $CH_3\dot{C}HCH_2CH{=}CH_2$ with i-C_3H_7 would explain the 1-pentene, pentadiene, and 4,5-dimethyl-1-hexene products. Trotman-Dicksnson did not find evidence for the $\cdot CH_2CH(CH_3)CH{=}CH_2$ radical. The 3,5-dimethyl-1-hexene reported here is the first evidence for its existence in this system.

Other minor products observed were isobutane, butadiene, and 3-methyl-1-butyne. A reaction scheme which can explain all of the products and their dependence upon pressure is given below. It incorporates the rearrangement mechanism of Benson and De-More.[10]

$$C_3H_7N_2C_3H_7\ (A) + h\nu \longrightarrow 2i\text{-}C_3H_7 + N_2$$

$$i\text{-}C_3H_7 + C_2H_2 \longrightarrow (CH_3)_2CHCH{=}\dot{C}H^*\ (3MB\text{-}1) \quad (1)$$

$$2i\text{-}C_3H_7 \longrightarrow C_6H_{14} \quad (2)$$

$$2i\text{-}C_3H_7 \longrightarrow C_3H_6 + C_3H_8 \quad (3)$$

$$(CH_3)_2CHCH{=}\dot{C}H^* + M \xrightarrow{\omega} (CH_3)_2CHCH{=}\dot{C}H + M\ (S) \quad (4)$$

$$(CH_3)_2CHCH{=}\dot{C}H + i\text{-}C_3H_7 \longrightarrow (CH_3)_2CHCH{=}CHCH(CH_3)_2 \quad (5)$$

$$(CH_3)_2CHCH{=}\dot{C}H + i\text{-}C_3H_7 \longrightarrow (CH_3)_2CHCH{=}CH_2 + C_3H_6 \quad (6)$$

$$(CH_3)_2CHCH{=}\dot{C}H + i\text{-}C_3H_7 \longrightarrow (CH_3)_2CHC{\equiv}CH + C_3H_8 \quad (7)$$

$$(CH_3)_2CHCH{=}\dot{C}H + A \longrightarrow (CH_3)_2CHCH{=}CH_2 + A\cdot \quad (8)$$

$$(CH_3)_2CHCH{=}\dot{C}H^* \xrightarrow{k_a} \cdot CH_2CH(CH_3)CH{=}CH_2^*\ (I) \quad (9)$$

$$\cdot CH_2CH(CH_3)CH{=}CH_2^* + M \longrightarrow \cdot CH_2CH(CH_3)CH{=}CH_2 + M \quad (10)$$

$$\cdot CH_2CH(CH_3)CH{=}CH_2 + i\text{-}C_3H_7 \longrightarrow (CH_3)_2CHCH_2CH(CH_3)CH{=}CH_2 \quad (11)$$

(11) L. K. Montgomery, J. W. Matt, and R. R. Webster, *J. Amer. Chem. Soc.*, **89**, 923 (1967).

$$\cdot CH_2CH(CH_3)CH{=}CH_2^* \longrightarrow CH_3\dot{C}HCH_2CH{=}CH_2^* \quad (12)$$

$$\cdot CH_2CH(CH_3)CH{=}CH_2^* \longrightarrow CH_2{=}CHCH{=}CH_2 + CH_3 \quad (13)$$

$$CH_3\dot{C}HCH_2CH{=}CH_2^* + M \longrightarrow CH_3\dot{C}HCH_2CH{=}CH_2 + M \quad (14)$$

$$CH_3\dot{C}HCH_2CH{=}CH_2 + i\text{-}C_3H_7 \longrightarrow (CH_3)_2CHCH(CH_3)CH_2CH{=}CH_2 \quad (15)$$

$$CH_3\dot{C}HCH_2CH{=}CH_2 + i\text{-}C_3H_7 \longrightarrow CH_3CH_2CH_2CH{=}CH_2 + C_3H_6 \quad (16)$$

$$CH_3\dot{C}HCH_2CH{=}CH_2 + i\text{-}C_3H_7 \longrightarrow CH_2{=}CHCH_2CH{=}CH_2 + C_3H_8 \quad (17)$$

Chemical Activation Rate Constant for Isomerization. In chemical activation systems the average rate constant k_a for a unimolecular reaction is given by $k_a = \omega_{eff}(I/S)$,[5,12] Where I is the rate of formation of the isomerization products, S is the rate of formation of the stabilization products, and ω_{eff} is the effective deactivation rate constant which is equal to the specific collision frequency of the excited radical with bath molecules times an efficiency factor β.[12] Acetylene may not be a strong collider ($\beta \sim 1.0$), but there are no data on its efficiency in chemical activation systems. Nitrogen, for example, was observed to have an efficiency of 0.53 in the deactivation of 2-methylbutyl-2 radicals.[13] Because of a lack of data we have assumed that $\beta = 1.0$. If β is actually closer to the value for N_2, then the true k_a would be about 0.5 of the k_a reported in this work.

In the case of isomerization reactions some back isomerization of the product must be considered. The reverse of reaction 9 is not likely to be significant compared with the forward reaction because of the unfavorable reaction path degeneracy ratio of 2/6, and the 8 kcal mol^{-1} higher threshold energy. Also we considered that only *cis*-3MB-1 could isomerize, because from a model it is evident that *trans*-3MB-1 cannot undergo 1,4 hydrogen atom migration.

The ratio I/S was calculated as follows. If the 3MB-1* radical is stabilized by collision the resulting products (S) follow from reactions 5–8. If 3MB-1* isomerizes before deactivation, then the resulting products (I) come from reactions 11, 13, and 15–17. Therefore, $S = R$(3-methyl-1-butene) + R(*cis*-2,5-dimethyl-3-hexene), and $I = R$(1-pentene) + R(pentadiene) + R(3,5-dimethyl-1-hexene) + R(4,5-dimethyl-1-hexene). Some error would be introduced if $CH_2CH(CH_3)CH{=}CH_2$, a precursor of I products, could abstract H atoms to give 3-methyl-1-butene, an S product. However, the combination product 3,5-dimethyl-1-hexene is always in minor amounts, which indicates that $CH_2CH(CH_3)CH{=}CH_2$ rapidly undergoes homoallylic rearrangement.

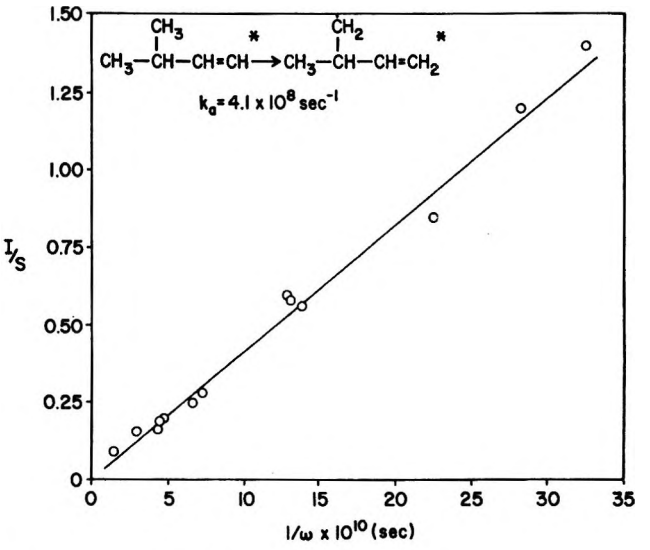

Figure 1. Plot of I/S *vs.* $1/\omega$ at 326°K.

A plot of I/S *vs.* $1/\omega$ from runs at 53° is shown in Figure 1. The collision diameters used to calculate the collision frequency of 3MB-1* were $\sigma(C_2H_2) = 4.22$ Å, σ(azo) = 7.50 Å, and σ(3MB-1) = 5.83 Å;[14] σ(azo) and σ(3MB-1) were chosen by analogy with σ values for *n*-octane and 3-methyl-1-butene, respectively.

A least squares treatment of the data gave an intercept of 0.014 and a 53° rate constant, $k_a = 4.1 \times 10^8$ sec^{-1}. We did not calculate a rate constant at 108° because of the strong possibility of thermal isomerization of previously stabilized radicals.

Rate Constant for Addition of Isopropyl to Acetylene. The rate constant for addition of isopropyl radicals to acetylene can be estimated from the expression

$$\frac{k_1}{k_2^{1/2}} = \frac{R(3MB\text{-}1)}{R(2,3\text{-}DMB)^{1/2}[C_2H_2]_0}$$

where R(3MB-1) is given by the sum of the rates of formation of all the products resulting from 3MB-1 radicals, and $[C_2H_2]_0$ is the initial concentration of acetylene. Less than 1% of the initial acetylene was consumed in a run. Values of $k_1/k_2^{1/2}$ *vs.* $1/T$ are tabulated in Table II, and Figure 2 is an Arrhenius plot of log $k_1/k_2^{1/2}$ *vs.* $1/T$. The activation energy difference $E_2 - {}^1/_2E$ was found from a least squares treatment to be 7.6 kcal mol^{-1}. Since E has been reported to be zero,[15] $E_2 = 7.6$ kcal mol^{-1}. The intercept gives log $A_1/A_2^{1/2} = 4.50$. Using log $A_2 = 13.8$[15] gives log $A_1 = 11.30$. The rate constant found was $k_1 = 10^{11.30} \exp(-7600/RT)$ mol^{-1} cm^3 sec^{-1}.

(12) C. W. Larson, D. C. Tardy, and B. S. Rabinovitch, *J. Chem. Phys.*, **49**, 299 (1968).

(13) D. C. Tardy and B. S. Rabinovitch, *ibid.*, **48**, 5194 (1968).

(14) J. O. Hirschfelder, C. F. Curtiss, and R. B. Bird, "Molecular Theory of Gases and Liquids," Wiley, New York, N. Y., 1964.

(15) E. L. Metcalfe and A. F. Trotman-Dickenson, *J. Chem. Soc.*, 4620 (1962).

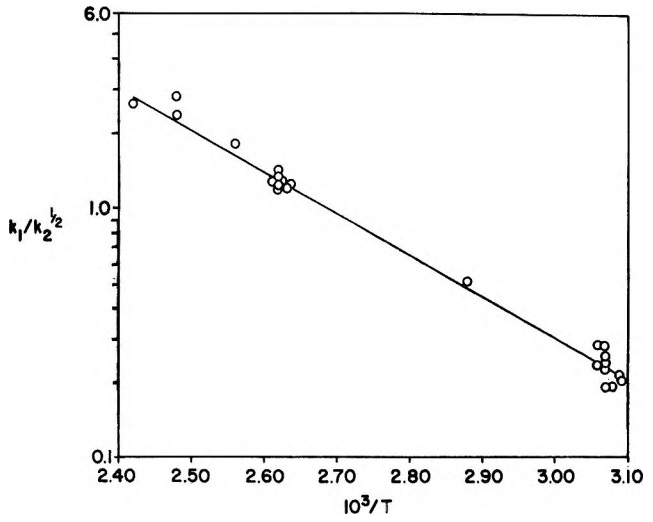

Figure 2. Addition of isopropyl radicals to acetylene; plot of log $k_1/k_2^{1/2}$ *vs.* $1/T$.

Table II: Relative Rate Constants

Run	$10^3/T$	R(3MB-1)[a]	$k_1/k_2^{1/2}$ [b]	I/S
10	2.42	16.5	2.61	...
11	2.48	35.4	2.80	...
12	2.48	180	2.37	...
13	2.56	26.1	1.84	...
14	2.62	9.95	1.27	...
15	2.62	12.4	1.44	...
16	2.62	25.7	1.22	...
17	2.62	25.1	1.26	...
18	2.62	26.7	1.13	...
19	2.62	32.2	1.17	...
20	2.62	3.16	1.28	...
21	2.62	4.40	1.25	...
25	2.62	8.40	1.23	...
26	2.62	9.03	1.33	...
27	2.64	9.74	1.34	...
28	2.88	5.02	0.512	...
30	3.10	0.89	0.202	1.4
31	3.12	1.48	0.207	1.20
32	3.06	3.05	0.287	0.85
33	3.08	2.25	0.192	0.576
34	3.07	2.02	0.225	0.569
35	3.06	2.81	0.279	0.608
36	3.07	6.40	0.282	0.286
37	3.07	7.35	0.256	0.272
38	3.07	10.2	0.268	0.206
39	3.09	8.04	0.210	0.190
40	3.07	8.74	0.235	0.166
41	3.06	17.5	0.232	0.170
42	3.07	29.1	0.189	0.100

[a] Rate of formation, mol cm^{-3} sec^{-1}. [b] Units: cm^3 mol^{-1} sec^{-1}.

This rate constant was determined only once previously. The value found was $k_1 = 10^{11.2} \exp(-6900/RT)$, from a study of the photolysis of isobutyraldehyde. In the isobutyraldehyde system the most important reaction of 3MB-1 besides isomerization is H atom abstraction from the aldehyde to give 3-methyl-1-butene. No products from 3MB-1 reactions with i-C_3H_7 were reported.

Cross Disproportionation and Combination of Isopropyl and 1-Penten-4-yl Radicals. Isopropyl radicals react with 1-penten-4-yl radicals by reactions 15–17. The rate constant ratios k_{16}/k_{15} and k_{17}/k_{15} were measured from the product ratios R(1-C_5H_{10})/R(4,5-DM1H) and $R(C_5H_8)/R$(4,5-DM1H), respectively. The averages from 31 runs are $k_{16}/k_{15} = 0.3 \pm 0.1$ and $k_{17}/k_{15} = 0.4 \pm 0.1$.

Benzene Formation. The product benzene makes up 3–6% of the yield of addition products at 53°, and 5–12% at 108°. Drew and Gordon[16] have studied the formation of benzene in mixtures of acetone and acetylene which were irradiated at temperatures between 200 and 500°. Benzene was the major product. From deuterium-labeling experiments, they suggested a mechanism in which a CH_3 radical added to acetylene, and the 3MB-1 radical added to acetylene in a typical free-radical polymerization reaction. Fessenden and Schuler[17] observed that vinyl radicals add much more readily to ethylene than alkyl radicals. When three acetylene molecules were added the radical would be large enough to undergo intramolecular reaction to yield benzene and a methyl radical. They noted that ethyl radicals also catalyzed the formation of benzene.

Our kinetic data are consistent with this mechanism in the following sense. If benzene is formed at the end of a chain sequence, and each step is in competition with combination reactions (such as reaction 5), then $R(C_6H_6)$ should be inversely proportional to the i-C_3H_7 concentration. At 53°, where addition does not compete significantly with combination, the rate of formation of benzene as given by the above mechanism reduces to $R(C_6H_6) \cong C'[C_2H_2]^3/[C_3H_7] \cong C[C_2H_2]^3/R$(2,3-DMB)$^{1/2}$ where C' is an algebraic collection of rate constants. A plot of the data at 53° gives a reasonable straight line of positive slope. At high acetylene pressures the relative amount of addition increases, and the slope decreases.

Discussion

Comparison of Theoretical Calculations with Experimental Results. Calculational procedures were described in detail previously when the data for n-pentyl were reported.[3] Figure 3 is a schematic potential energy diagram starting with $C_3H_7 + C_2H_2$ and leading to the observed products. This figure also serves to define the important quantities, E_{min}, E_{min}†, and E_0. The pertinent energy parameters for 3MB-1 isomerization are calculated in Appendix I. The details of the frequency assignments of the radical, association complex, and isomerization complex are given in Appendix II. All vibrational and internal rotational modes have

(16) C. M. Drew and A. S. Gordon, *J. Chem. Phys.*, **31**, 1417 (1959).
(17) R. W. Fessenden and R. H. Schuler, *ibid.*, **39**, 2147 (1963).

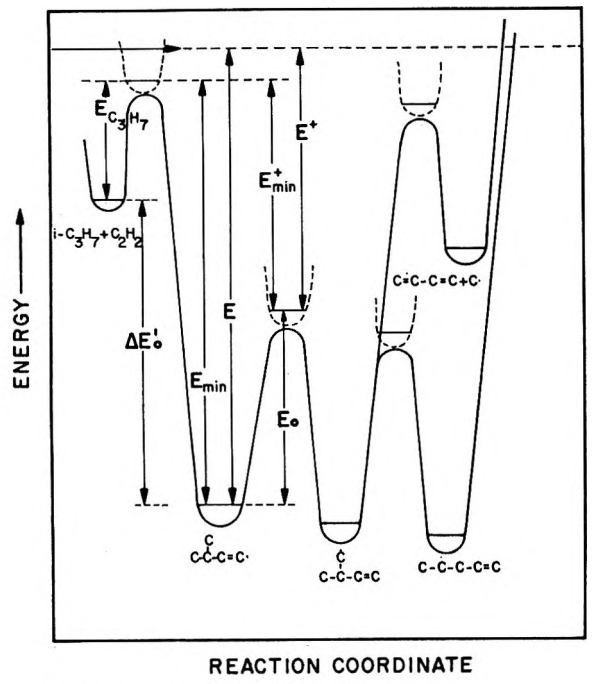

Figure 3. Schematic potential energy diagram.

been taken as active for both the energized radical and the activated complex. Table III (a) gives both the calculated and experimental rate constants. The agreement is not necessarily as good as it appears because the threshold energy is not known from other experiments, and so we have used the E_0 which gives the best agreement with experiment, using our model in Table IV. The best agreement is found for E_0(3MB-1) = 17.1 kcal mol^{-1}.

Table III

(a) Comparison of Calculated with Experimental Results

Reactant	$\langle E \rangle$[a]	E_0	k_a calcd	k_a exptl
P-1	34.1	19.0	2.8×10^6	3.3×10^6
P-1	34.1	18.8	3.2×10^6	3.3×10^6
3MB-1	33.8	17.1	4.2×10^8	4.1×10^8

(b) Ratios from Equation I

$$\frac{\sigma_{3MB-1}}{\sigma_{P-1}} = 3.0\frac{I_{3MB-1}}{I_{P-1}} = 1\frac{N^*(E)_{P-1}}{N^*(E)_{3MB-1}}^{b} = 50$$

$$\frac{\Sigma P(E_{vr}\dagger)_{3MB-1}}{\Sigma P(E_{vr}\dagger)_{P-1}}^{b} = 0.8\frac{k_E{}^{3MB-1}}{k_E{}^{P-1}} \text{ (calcd)} = 120$$

$$\frac{k_a{}^{3MB-1}}{k_a{}^{P-1}} \text{ (expt)} = 124$$

[a] In kcal mol^{-1}. [b] Evaluated at the average energy of the reacting molecules: 35.5 and 34.5 kcal mol^{-1} for P-1 and 3MB-1, respectively.

Quantum Statistical Weight Effect. The ratios of reaction path degeneracies, energy level densities, and activated complex sums as calculated at the average energy of the reacting radicals are given in Table III (b). The most important effect on the rate constant ratio is a result of the effect of the molecular vibration–internal rotation frequency pattern on the values of $N^*(E)$. For excited radicals at the same energy, for example E = 34.0 kcal mol^{-1}, the energy level density ratio is 33. The substitution of a stiff torsional mode for an essentially free rotation is the main contribution to the enhanced rate observed for 3MB-1. These experiments and calculations provide the first illustration of this type of quantum statistical weight effect.

The ratio of the sums of the energy eigenstates of the complexes is 1.3 at 34.0 kcal mol^{-1} for the case where the two threshold energies differ by 1.7 kcal mol^{-1}. For the threshold energy for 3MB-1 isomerization to be less than E_0 for the *n*-pentyl case is not unreasonable. The ring strain energy, which contributes to E_0 in both cases, is likely to be less for a ring containing a double bond. The strain energy in cyclopentene is 5.4 *vs.* 6.3 kcal mol^{-1} in cyclopentane.[18] Also a vinyl radical should have a lower activation energy for abstraction of a H atom than a primary radical, because of the stronger vinyl C–H bond energy. It is important to note that the difference in threshold energies of 1.7 kcal does not affect the dominant term which is the ratio of radical energy level densities. The difference only affects the ratio of the sums of energy eigenstates of the complexes.

Configuration of 3-Methyl-1-buten-1-yl. The configuration and configurational stability of alkenyl radicals is of general interest.[19] The vinyl radical has

Table IV: Frequency Assignments for the Isomerization Complex

Ring deformations (9)	CH stretch (8)	Ring CH_2 and CH motions (10)
Reaction coordinate	3060 (2)	CH_2 rock 1040
1623	2977 (2)	CH_2 wag 1300
1013 (2)	2950 (3)	CH_2 twist 1330
1100 (2)	2844	CH_2 bend 1450
870		CH bend (out of plane)
290		1330
		1020
		696
		CH bend (in plane)
		1319 (3)

Modes related to the methyl group (9)

CH_3 deformations	1477, 1455 (2)
CH_3 rock	1112 (3)
CC stretch	1000
CCH bend	1450
CCC bend	332
Torsion	198

(18) S. E. Benson, "Thermochemical Kinetics," Wiley, New York, N. Y., 1968.

(19) W. G. Bentrude, *Annu. Rev. Phys. Chem.*, 18, 283 (1967).

been studied in an argon matrix at 4°K, and shown to be sp^2 at the carbon bearing the odd electron.[20] When this fact is applied to 3MB-1, we can speak of a *cis*-3MB-1 and a *trans*-3MB-1, where the isopropyl group is cis or trans to the odd electron, and *cis*- and *trans*-2,5-dimethyl-3-hexene are produced by the combination of the respective radicals with isopropyl. In addition esr spectra indicate that vinyl radicals are interconverted by inversion of the radical.[17] In the case of 3MB-1

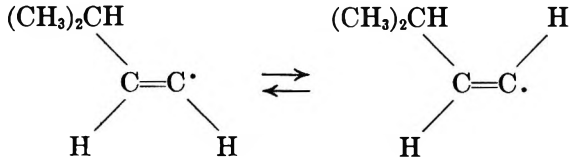

In the runs at 53° the ratio of *cis*- to *trans*-2,5-dimethyl-3-hexene decreases from about 20–30 at high pressure to 1.0 at the lowest pressure employed. An equilibrium ratio of *cis*- to *trans*-2,5-dimethyl-3-hexene would be about 0.35. However, the ratio of 20–30 could be the equilibrium ratio of *cis*- to *trans*-3MB-1. The free energies of formation of the radicals could differ more than those for cis and trans olefins. There are no experimental data on the free energies of formation of alkenyl radicals.

The stereoselectivity in favor of the cis product is quite common in some free radical additions to acetylene. In some cases the product is 100% cis.[19] The ratio of *cis*- to *trans*-2,5-dimethyl-3-hexene of 20–30 indicates that *cis*- and *trans*-3MB-1 are not interconverting faster than stabilization or combination (with isopropyl) at high pressure. As the pressure decreases the *cis*- to *trans*-2,5-dimethyl-3-hexene ratio decreases mainly because the precursor of *cis*-2,5-dimethyl-3-hexene is removed by isomerization.

Appendix I

Calculation of E_{min} and E_0. The quantity E_{min} can be seen from Figure 3 to be given by $E_{min} = \Delta E_0' + E_{C_3H_7}$, where $E_{C_3H_7}$ is the activation energy for addition of isopropyl radicals to acetylene. The value of $E_{C_3H_7}$ was determined in this work to be 7.6 kcal mol^{-1}.

The following heats of formation,[21] $\Delta H_f°$ (kcal mol^{-1}), at 0°K, were used to calculate $\Delta E_0'$: H, 51.62; 3-methyl-1-butene, −0.68; C_2H_2, 54.33; C_3H_8, −19.48.

The following bond dissociation energies were used: $D°_0$ (vinyl C–H) = 106.0[18] and $D°_0$ (i-C_3H_7 H) = 92.8[22] kcal mol^{-1}. Then $\Delta H_f°$ (3MB-1) = $\Delta H_f°$ (3-methyl-1-butene) − $\Delta H_f°$ (H) + $D°_0$ (vinyl C–H), $\Delta H_f°$ (3MB-1) = 53.7 kcal mol^{-1}, and $\Delta H_f°$ (i-C_3H_7) = $\Delta H_f°$ (C_3H_8) − $\Delta H_f°$ (H) + $D°_0$ (i-C_3H_7H), $\Delta H_f°$ (i-C_3H_7) = 21.7 kcal mol^{-1}. Therefore $\Delta E_0' = \Delta H_f°$ (i-C_3H_7) + $\Delta H_f°$ (C_2H_2) − $\Delta H_f°$ (3MB-1) and $\Delta E_0'$ = 22.3 kcal mol^{-1}. Thus, E_{min} = 22.3 + 7.6 = 29.9 kcal mol^{-1}. Note that E_{min} for *n*-pentyl* was 29.6 kcal mol^{-1}.

One can estimate the minimum E_0 as before.[3] Using the stain energy for cyclopentene given by Benson,[18] the minimum possible E_0 would be 14.4 kcal mol^{-1}.

Appendix II

Molecular Vibration Models. The vibration frequencies for a free radical are normally taken directly from the corresponding hydrocarbon by simply deleting three frequencies associated with the removal of a hydrogen atom. However, a complete vibration frequency assignment for 3-methyl-1-butene was not available. A procedure used by Rabinovitch[23] for assigning frequencies to the C–CH=CH_2 group was followed to establish the frequencies for the vinyl fragment. The remaining frequencies for the isopropyl group were taken directly from frequencies assigned to propane.[24] The frequencies (cm^{-1}) and their degeneracies assigned to 3MB-1 were: 3040 (2), 2963 (5), 2882 (2), 1642, 1465 (3), 1365 (3), 1295 (3), 1185, 1151, 1046, 995, 915 (2), 860 (2), 820, 747, 635, 435, 383 (2), 200 (2), 80. All three internal rotations were assigned as low vibrational frequencies, 200 cm^{-1} (2), 80 cm^{-1}.

The vibration frequencies for the dissociation complex (the reverse of reaction 1) were based on those for the radical. Eight modifications were made which were similar to those described previously.[3,23] The CCH bend of the isopropyl CH was lowered from 1300 to 650 cm^{-1}, and the CCH bend of the vinyl CH was lowered from 635 to 317 cm^{-1} in the complex. Two CCC skeletal bending frequencies at 435 and 383 cm^{-1} were lowered to 217 and 191 cm^{-1}. The torsional vibration frequency about the breaking C–C bond was reduced from 80 to 40 cm^{-1}, and the torsional frequency of the forming triple bond was raised from 995 to 1200 1200 cm^{-1}. The C–C stretch at 845 cm^{-1} associated with the reaction coordinate was set equal to zero. The C–C stretch associated with the forming triple bond was raised from 1642 to 1807 cm^{-1} in the complex.

This model gives a preexponential factor for the dissociation at 53° of $10^{14.32}$ sec^{-1}. Taking ΔS_0 to be −35.0 eu (standard state, 1 atm), which is −26.6 eu for a standard state of 1 mol l^{-1}, the preexponential factor for the bimolecular combination is $10^{11.5}$ mol^{-1} cm^3 sec^{-1}. This value is only 1.6 times greater than the experimental value reported here.

Vibration frequencies for the isomerization complex

(20) E. L. Cochran, F. J. Adrian, and V. A. Bowers, *J. Chem. Phys.*, **40**, 213 (1964).

(21) F. D. Rossini, "Selected Values of Physical and Thermodynamic Properties of Hydrocarbons," Carnegie Press, Pittsburgh, Pa., 1953.

(22) C. W. Larson and B. S. Rabinovitch, *J. Chem. Phys.*, **52**, 5181 (1970).

(23) M. J. Pearson and B. S. Rabinovitch, *ibid.*, **42**, 1624 (1965).

(24) J. H. Schnachtschneider and R. G. Synder, *Spectrochem. Acta*, **19**, 117 (1963).

were based on those of cyclopentene.[25] The nine ring deformation frequencies were assigned as in the pentyl-1 isomerization complex,[3] and the CH and CH_2 twists, wags, bends, and rocks were taken from cyclopentene. The frequency assignment for the isomerization complex is given in Table IV.

Acknowledgment. The authors are grateful to Mr. D. R. Lawson for his assistance with the computer calculations. We wish to thank Dr. C. W. Larson for his extremely helpful suggestions concerning the assignment of frequencies to the activated complex, and for pointing out errors in the original manuscript.

(25) C. W. Beckett, N. K. Freeman, and K. S. Pitzer, *J. Amer. Chem. Soc.*, **70**, 4227 (1948).

A Raman Spectral Study of Bisulfate–Sulfate Systems. II. Constitution, Equilibria, and Ultrafast Proton Transfer in Sulfuric Acid

by H. Chen and D. E. Irish*

Department of Chemistry, University of Waterloo, Waterloo, Ontario, Canada *(Received April 5, 1971)*

Publication costs borne completely by The Journal of Physical Chemistry

Species concentrations are reported for aqueous solutions of H_2SO_4 and H_2SO_4 + NaOH (or HCl) mixtures. These have been obtained from the relative integrated intensities of the 981-cm^{-1} Raman line of SO_4^{2-}. The apparent concentration quotients, Q_c, for the equilibrium have been computed and attempts to estimate K_2 from the data are discussed. Half-widths of the 981-cm^{-1} line and the 1050-cm^{-1} line of HSO_4^- have also been measured, and correlated with proton transfer processes occurring in the solutions. An apparent rate law

$$\text{rate}_R = k_R[H_3O^+](a_w)^z[SO_4^{2-}]$$

has been inferred, with $k_R^H = 6.4 \times 10^{11}\ M^{-1}\ \text{sec}^{-1}$. For $KDSO_4$–D_2O solutions $k_R^D = 10.4 \times 10^{11}\ M^{-1}\ \text{sec}^{-1}$. It is believed that for this system the Raman effect is providing uniquely detailed information about the mechanism of proton transfer along a chain of oriented water molecules.

Introduction

Concentrations of sulfate ion were previously determined from measurement of the relative integrated Raman intensity of the 981-cm^{-1} line [$\nu_1(A_1)$] of SO_4^{2-} for several bisulfate salts over a wide concentration range.[1] In addition to providing information about the apparent concentration quotient, Q_c, and the degree of formation[2] of sulfate ion ($\alpha = [SO_4^{2-}]/C$), the broadening of the 981-cm^{-1} Raman line was found to be directly proportional to the hydronium ion concentration in the solutions. This broadening was interpreted in terms of the ultrafast proton transfer between H_3O^+ and SO_4^{2-}, a phenomenon of considerable interest.[3-5] The work has now been extended by measurements on H_2SO_4 over the concentration range 0.261–14.20 M and for H_2SO_4–NaOH and H_2SO_4–HCl mixtures. Hydronium ion concentrations in some of these samples are considerably larger than in those previously studied and the data have provided a clearer picture of the mechanism of the proton transfer process.

The method of measurement of spectral parameters—frequency, half-width, and intensity—differs from that used in earlier studies[6] largely in the application of computer techniques for band contour analysis. The spectral region from 800 to 1300 cm^{-1} consists of a number of closely spaced and overlapping bands. (See Figures in ref 1.) The accuracy of species concentrations is dependent on the validity of the computer analysis of this region. Constancy or smooth monotonic changes of line parameters with changing composition give confidence in the analysis. Less intensity has been attributed to the sulfate ion in this work than in the earlier study[6] because weak lines at 948 and 1024 cm^{-1} are identified and recognized as arising from

(1) D. E. Irish and H. Chen, *J. Phys. Chem.*, **74**, 3796 (1970).

(2) The expression "degree of formation" prevalent in complex ion chemistry is used in preference to degree of ionization or degree of dissociation as the term relates expressly to the observed species, sulfate, whereas the latter terms are not well defined when other species such as ion pairs are formed on ionization.

(3) E. Grunwald, *Progr. Phys. Org. Chem.*, **3**, 317 (1965).

(4) W. J. Albery, *Progr. React. Kinet.*, **4**, 353 (1967).

(5) E. F. Caldin, *Chem. Rev.*, **69**, 135 (1969).

(6) T. F. Young, L. F. Maranville, and H. M. Smith in "The Structure of Electrolytic Solutions," W. J. Hamer, Ed., Wiley, New York, N. Y., 1959, p 35.

Table I: Data for H_2SO_4 Solutions

$[H_2SO_4]$	$[H_2O]$	$[SO_4^{2-}]^a$	$[SO_4^{2-}]^b$	$[H_3O^+]$	$[HSO_4^-]^c$	α^d	Q_c^e	I_c^f	$[w - w_0]_{981}^g$	w_{1050}^h
14.20	18.7	0.694	0.684	14.88	13.52	0.0482	0.753	15.6	26.6 ± 0.6	54.2 ± 0.2
13.07	22.1	0.980	1.04	14.11	12.03	0.0796	1.22	15.1	25.5 ± 1.1	51.3 ± 0.3
11.76	25.9	1.89	1.41	13.17	10.35	0.120	1.79	14.6	35.0 ± 1.5	50.7 ± 0.2
10.456	29.5	1.22	1.67	12.13	8.79	0.160	2.30	13.8	21.5 ± 0.5	51.0 ± 0.4
9.149	33.1	2.10	1.81	10.96	7.34	0.198	2.70	12.8	29.0 ± 1.0	45.8 ± 0.5
7.842	36.6	1.98	1.81	9.65	6.03	0.231	2.90	11.5	26.2 ± 1.0	44.1 ± 1.9
6.535	40.0	1.64	1.67	8.20	4.87	0.255	2.81	9.87	19.2 ± 0.5	42.0 ± 0.8
5.881	41.7	1.38	1.55	7.43	4.33	0.264	2.66	8.98	16.5 ± 2.3	40.7 ± 1.1
5.228	43.4	1.49	1.41	6.64	3.82	0.270	2.45	8.05	18.3 ± 0.2	40.0 ± 1.0
3.921	46.7	1.07	1.06	4.98	2.86	0.270	1.85	6.04	15.8 ± 0.5	32.5 ± 0.9
3.267	48.2	0.834	0.862	4.13	2.405	0.264	1.48	4.99	13.0 ± 0.4	31.9 ± 1.3
2.614	49.8	0.635	0.662	3.28	1.952	0.254	1.11	3.94	12.0 ± 0.4	30.7 ± 0.2
1.960	51.2	0.550	0.466	2.43	1.494	0.238	0.758	2.89	13.0 ± 0.2	31.0 ± 0.3
1.307	52.7	0.251	0.283	1.59	1.024	0.216	0.440	1.87	8.3 ± 0.7	26.7 ± 0.1
1.046	53.2	0.248	0.216	1.26	0.830	0.206	0.328	1.48	8.0 ± 0.9	28.9 ± 1.7
0.784	53.7	0.169	0.153	0.94	0.631	0.195	0.228	1.09	6.1 ± 0.6	27.9 ± 0.7
0.523	54.3	0.106	0.096	0.62	0.427	0.183	0.139	0.71	5.1 ± 1.3	28.6 ± 1.0
0.261	54.9	0.0438	0.045	0.31	0.216	0.172	0.065	0.35	2.5 ± 1.7	27.5 ± 0.5

[a] Mean values of $I_{981}/J_{981} = I_{981}/0.281$ in mol/l. [b] Least-squares fit based on 58 individual measurements. [c] $[H_2SO_4] - [SO_4^{2-}]^b$. [d] $[SO_4^{2-}]^b/[H_2SO_4]$. [e] $Q_c = (\alpha^2/1 - \alpha)[H_2SO_4]$. [f] I_c = ionic strength $= (1 + 2\alpha)[H_2SO_4]$. [g] Line width of the 981-cm^{-1} line (w) − line width in $(NH_4)_2SO_4$ solution (w_0). [h] Line width of the 1050-cm^{-1} line of HSO_4^-.

other species. One other Raman study of sulfuric acid has recently been reported but the interpretation is questionable.[7]

Experimental Section

Solutions were prepared from H_2SO_4 (C-I-L CP reagent), NaOH (Fisher Certified Reagent), and HCl (Baker and Adamson CP reagent) by standard quantitative techniques. Spectra and computer analyses were obtained as previously described.[1,8] Curve fitting was performed twice for a spectrum in which the 981-cm^{-1} line is intense and reasonably well separated from the 1050-cm^{-1} HSO_4^- line. More fittings were carried out when the 981-cm^{-1} line was weaker and broad, and the average and uncertainty were obtained.

Results and Discussion

Species Concentrations and Equilibria. Raman spectra of aqueous sulfuric acid solutions are qualitatively similar to those of $KHSO_4$, $NaHSO_4$, and NH_4HSO_4 illustrated previously.[1] No lines of H_2SO_4 molecules were detected in the concentration range studied. When hydronium concentrations exceed ~9.5 M the 1200-cm^{-1} line becomes noticeably broader and more intense. This observation is attributed to the vibration of H_3O^+ at ~1205 cm^{-1} [9] but has no effect on the intensity analysis.

The relative integrated intensities of the 981- and 1050-cm^{-1} lines of SO_4^{2-} and HSO_4^- were measured excluding contributions from the ~948- and ~1024-cm^{-1} lines to be discussed below. The 981-cm^{-1} intensity was converted into sulfate ion concentration by division by the molar intensity obtained from $(NH_4)_2SO_4$ solutions. The direct proportionality between relative integrated intensity and concentration of the latter salt has been illustrated elsewhere.[10] Species concentrations and derived quantities are presented in Table I. The concentration of H_2O has been obtained from the reported density.[11] A computer program was written to provide empirical equations for the sulfate ion concentration, of the form

$$M_{SO_4^{2-}} = A_1M_s + A_2M_s^2 + \ldots\ldots A_nM_s^n$$

where M_s stands for the stoichiometric concentration of the solutions, A_n are constants, and n is a positive integer. The Gauss criterion[12] was adopted to choose the best value of n. The equations for sulfuric acid and for the salts previously studied[1] follow.

$$M_{SO_4^{2-}} = 0.1575M_s + 0.05468M_s^2 - 0.007474M_s^3 + 0.0002170M_s^4 \quad (H_2SO_4\ 0\text{–}14.2\ M)$$

$$M_{SO_4^{2-}} = 0.3803M_s - 0.06904M_s^2 + 0.05253M_s^3 - 0.01654M_s^4 + 0.002068M_s^5 \quad (NH_4HSO_4\ 0\text{–}8\ M)$$

$$M_{SO_4^{2-}} = 0.3375M_s - 0.03936M_s^2 \quad (KHSO_4\ 0\text{–}3\ M)$$

$$M_{SO_4^{2-}} = 0.4904M_s - 0.6431M_s^2 + 0.3868M_s^3 - 0.07390M_s^4 \quad (KDSO_4\ 0\text{–}2.4\ M)$$

(7) N. G. Zarakhani and M. I. Vinnik, *Zh. Fiz. Khim.*, **37**, 503 (1963).

(8) More extensive details of the method and tables of primary data are contained in H. Chen, Ph.D. Thesis, University of Waterloo, Waterloo, Ontario, 1971.

(9) M. Falk and P. A. Giguère, *Can. J. Chem.*, **35**, 1195 (1957).

(10) D. E. Irish and H. Chen, *Appl. Spectrosc.*, **25**, 1 (1971).

(11) "Chemical Engineers Handbook," J. H. Perry, Ed., 4th ed, McGraw-Hill, New York, N. Y., 1963, pp 3–79.

(12) A. G. Worthing and J. Geffner, "Treatment of Experimental Data," Wiley, New York, N. Y., 1943, p 260.

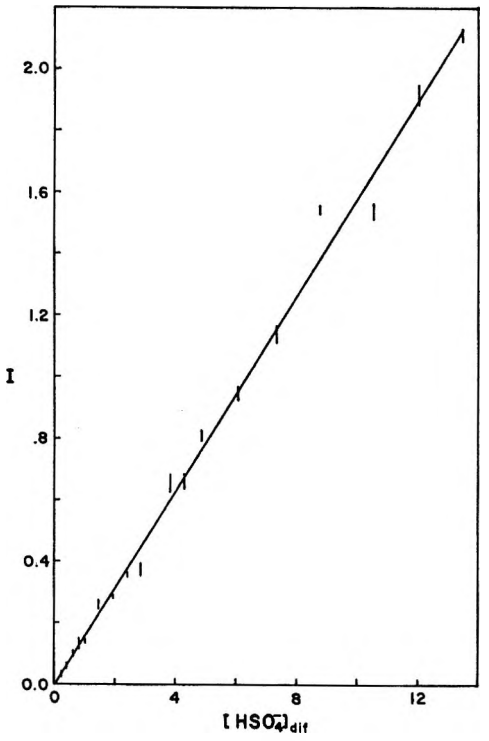

Figure 1. Intensity of the 1050-cm^{-1} Raman line of HSO_4^- *vs.* apparent concentration of the ion in H_2SO_4 solutions.

The difference between the stoichiometric concentration and the sulfate ion concentration provides the apparent concentration of the bisulfate ion, $[HSO_4^-]_{dif}$. This concentration is expected to be directly proportional to the intensity of the 1050-cm^{-1} line of HSO_4^- if the treatment of data is correct. The 1050-cm^{-1} intensity is more uncertain than the 981-cm^{-1} intensity because of greater overlap with other lines. However, direct proportionality was found (Figure 1). The molar intensity, J_{1050}, obtained from the slope, is 0.158. Values of 0.150 for NH_4HSO_4 and 0.144 for $KHSO_4$ and $KDSO_4$ were obtained. The average is 0.151 ± 0.007 with a deviation comparable to the experimental error. This value can be compared with 0.281 for the 981-cm^{-1} line of sulfate ion. Since the ion pair $H_3O^+ \cdot SO_4^{2-}$ has been postulated (see below), its concentration should be subtracted from $[HSO_4^-]_{dif}$ to obtain the "true" concentration of HSO_4^- for Figure 1. However, the 948-cm^{-1} line intensity is low and the concentration of the ion pair is probably no larger than the uncertainty in the measurements. Thus Figure 1 provides support for the general validity of the computer analysis of spectra and the applicability of the molar intensity value for sulfate obtained from $(NH_4)_2SO_4$ solutions.

Species concentrations are plotted in Figure 2. Comparison with other studies is provided. For comparison the similar plot for the bisulfate salts is given in Figure 3. The dependence of α on concentration is illustrated in Figure 4. For H_2SO_4 more concentrated than 8 *M*, the 981-cm^{-1} line appears only as a shoulder of the

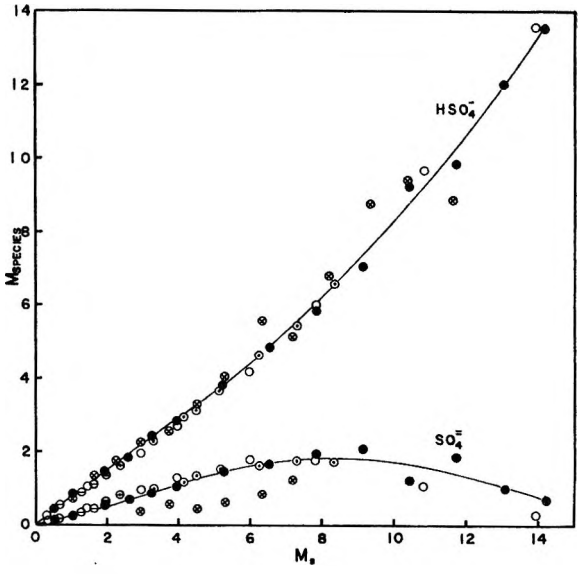

Figure 2. The ionic concentrations (*M* species) of SO_4^{2-} and HSO_4^- as functions of stoichiometric concentration of sulfuric acid: ●, this work; —, least-squares fit for the data of this work; ○, Raman data of Young, *et al.*;[6] ⊗, Raman data of Zarakhani and Vinnik;[7] ⊙, calculated from nmr data of Hood and Reilly;[13] ⊖, calculated from pmv data of Lindstrom and Wirth.[14]

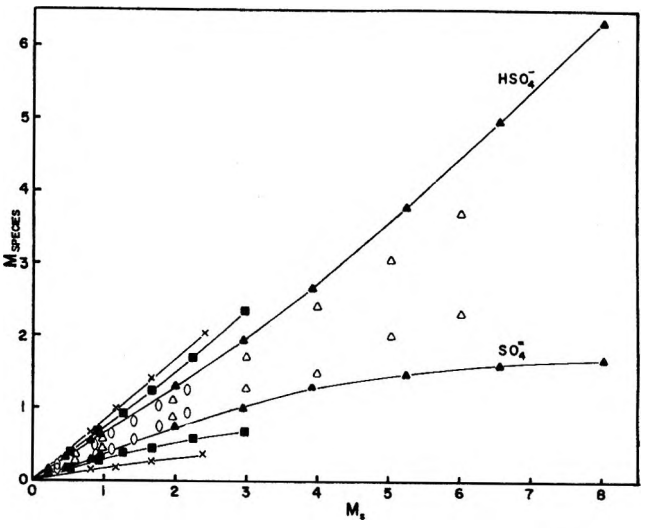

Figure 3. The ionic concentrations (*M* species) of SO_4^{2-} and HSO_4^- as functions of the stoichiometric concentration of NH_4HSO_4, $KHSO_4$, $KDSO_4$, and $NaHSO_4$ solutions: ▲, NH_4HSO_4, this work; △, NH_4HSO_4, Young, *et al.*,[6] ■, $KHSO_4$, this work; ×, $KDSO_4$, this work; 0, $NaHSO_4$, calculated from data of Lindstrom and Wirth.[14]

prominent 1050-cm^{-1} line and all lines are broadened. A greater uncertainty exists for the decomposition of these spectra and the points are more scattered. The maximum SO_4^{2-} concentration occurs at about 8.5 *M* rather than 7 *M* reported previously.[6] The α values calculated from nmr chemical shifts and mean partial molal volumes are dependent on the results of Young's Raman work. Hood and Reilly[13] have chosen their

(13) G. C. Hood and C. A. Reilly, *J. Chem. Phys.*, **27**, 1126 (1957).

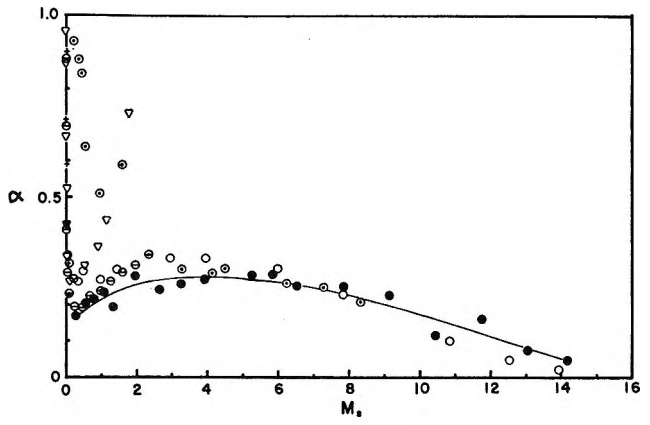

Figure 4. The degree of formation of sulfate, α, *vs.* stoichiometric concentration of H_2SO_4: ▽, M. Kerker, *J. Amer. Chem. Soc.*, **79**, 3664 (1957); +, R. M. Wallace, *J. Phys. Chem.*, **70**, 3922 (1966), other symbols as in Figure 2.

value of S_5 (a relation between the chemical shift of H_3O^+ and HSO_4^-) to provide the best agreement with the results of Young for $2 < C < 8$ *M*. However, below 3 *M* their relative values of α appear to be much too high. Lindstrom and Wirth[14] established their relation of ϕ_3 *vs.* $I^{1/2}$ guided by Young's Q_c data and obtained α for H_2SO_4 and $NaHSO_4$ solutions below 2.4 *M*. In Figure 4 it is interesting to note that α drops very rapidly, passes through a minimum, then rises slowly to a flat maximum at about 4 *M* and subsequently exhibits a smooth decrease. The reason for this shape is not clear. Possibly the explanation involves differences in proton hydration numbers in different concentration regions, as postulated by several workers.[15–18]

Present Raman techniques preclude doing any accurate intensity measurements on solutions sufficiently dilute to be treated with the Debye–Hückel theory. Thus accurate evaluation of K_2, the second acidity constant of sulfuric acid, from the present Q_c data is not possible. A plot of Q_c *vs.* molarity of the solutions indicates that the data for H_2SO_4, $KHSO_4$, and NH_4HSO_4 converge to a reasonable intercept at 0.010 (Figure 5). The plot of log Q_c *vs.* $\sqrt{I_c}$ is also presented for comparison (Figure 6). Attempts to estimate K_2 are discussed in the Appendix.

Raman Line Broadening and Ultrafast Proton Transfer. The half-width of the 981-cm^{-1} line of SO_4^{2-} is virtually independent of the concentration of $(NH_4)_2SO_4$ solutions. In a separate study[19] it has been shown that an increase of the viscosity by a factor of 500 does not broaden the line. Thus the value, w_0, for the salt solution can be adopted as the value of the half-width of the line, unbroadened by chemical processes. The same line broadens with increasing concentration of solutions of NH_4HSO_4, $KHSO_4$, $KDSO_4$, and H_2SO_4. The 1050-cm^{-1} line of HSO_4^- also increases in half-width, but to a smaller extent.

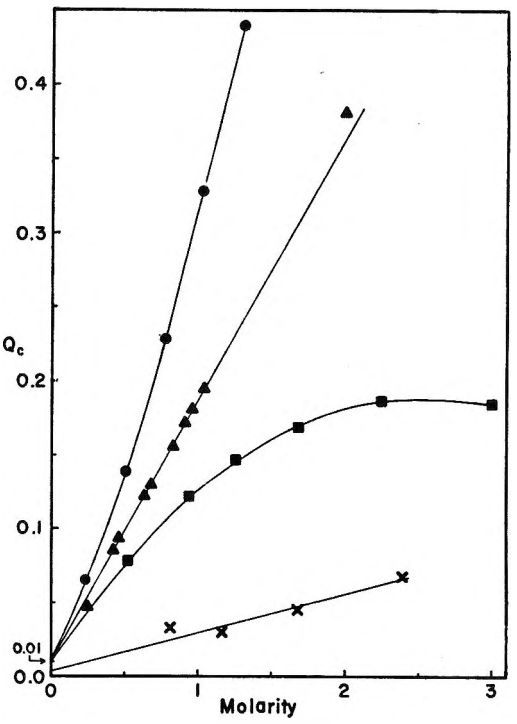

Figure 5. The dependence of the concentration quotient of HSO_4^-, Q_c, on the stoichiometric concentration of H_2SO_4, NH_4SO_4, $KHSO_4$, and $KDSO_4$ solutions; ●, H_2SO_4; ▲, NH_4HSO_4; ■, $KHSO_4$; ×, $KDSO_4$.

In the absence of rapid chemical reaction, collision broadening is the greatest contributor to the observed line width of a species in the liquid phase.[20] Collision broadening has been estimated to be of the order of 10 cm^{-1} [20,21] and generates a Lorentz line shape. Other factors, such as Doppler broadening due to thermal motions of the molecules, and natural line width as a consequence of the Heisenberg uncertainty principle, are negligible when compared with collision broadening. The Lorentz line shape can be modified and tends toward a Gaussian shape because of properties of a particular system or instrumental factors, such as finite slit widths.[20] Thus in practice, most of the vibrational line shapes are intermediate between Lorentzian and Gaussian, as found above. The Raman line broadening found in this study occurs under constant instrumental conditions and must be attributed to the systems. Collision broadening can account for the magnitude of

(14) R. E. Lindstrom and H. E. Wirth, *J. Phys. Chem.*, **73**, 218 (1969).

(15) E. Högfeldt, *Acta Cient. Venez.*, **17**, 13 (1966).

(16) E. Högfeldt, *Acta Chem. Scand.*, **14**, 1597 (1960).

(17) P. A. H. Wyatt, *Discuss. Faraday Soc.*, **24**, 162 (1957).

(18) E. B. Robertson and H. B. Dunford, *J. Amer. Chem. Soc.*, **86**, 5080 (1964).

(19) D. E. Irish and R. C. Meatherall, *J. Phys. Chem.*, **75**, 2684 (1971).

(20) K. S. Seshadri and R. N. Jones, *Spectrochim. Acta*, **19**, 1013 (1963).

(21) D. A. Ramsay, *J. Amer. Chem. Soc.*, **74**, 72 (1952).

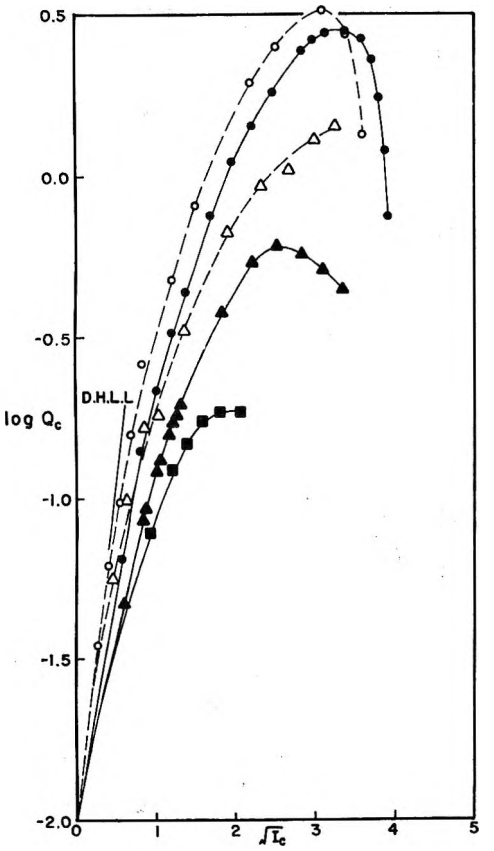

Figure 6. Log Q_c *vs.* $\sqrt{I_c}$ for H_2SO_4, NH_4HSO_4, and $KHSO_4$ solutions: ●, H_2SO_4, this work; ○, H_2SO_4, Raman data of Young, *et al.*,[6] ▲ NH_4HSO_4, this word; △, NH_4HSO_4, Raman data of Young, *et al.*;[6] ■, $KHSO_4$, this work.

w_0 but apparently is largely independent of concentration. Anions of other salts, nitrates and perchlorates, generate lines which broaden only by a few wave numbers when the concentration is increased from 0 to about 8 *M*. Thus collision broadening is not considered to be the cause of the appreciable increase observed in the acid systems. The proposal[22-24] that rapid proton transfer between acid molecule and conjugate base is responsible finds support from the data presented below.

If the mean lifetime of a vibrational state is short the uncertainty, Δt, is small and the uncertainty, ΔE, in the vibrational energy E of a given state will increase giving "breadth" to the energy state. This energy uncertainty exists both in the ground and the excited vibrational states, and thus the transition between two states does not produce a single vibrational frequency, but instead a range of continuous frequencies. Thus an increased half-width is observed for a vibrational line of a short-lived species. The broadening is given by

$$w - w_0 = \frac{1}{\pi c \tau} = 1.06 \times 10^{-11}(\tau)^{-1} \qquad (1)$$

where τ is the mean lifetime and c is the velocity of light. This equation is identical with that for slow exchange broadening of an nmr line,[25] and to that derived by Kreevoy and Meed[22,23] for Raman line broadening. The equation indicates that a τ of the order of 10^{-11} sec will cause a broadening of $\sim$1 cm^{-1}. Results of other studies have indicated that the rate of proton transfer along the hydrogen bond in water and ice is in the range 10^{11} to 10^{13} sec^{-1};[3,4,26-28] it is thus reasonable to assume that broadenings, ranging up to 30 cm^{-1} in acid systems, are caused by this phenomenon.

In addition to those stoichiometric solutions already mentioned, two more series of solutions were investigated to further unravel the nature of the proton transfer process. These solutions were designed with a variable ratio of the hydronium and sulfate ion concentrations. In the first series, various amounts of HCl were added to solutions of $(NH_4)_2SO_4$, maintained at 2.00 *M* $(NH_4)_2SO_4$. The results have been tabulated.[1] In the second series, solutions of 3.495 *M* H_2SO_4 were partially neutralized with NaOH or acidified with HCl. The data are presented in Table II. The data, from both this and the previous study,[1] clearly show that the broadening of the 981-cm^{-1} line of SO_4^{2-} is directly proportional to the hydronium concentration but not the SO_4^{2-} concentration. The comparison of the data for solutions of the same hydronium concentration, but differing amounts of sulfate ion, indicates that within experimental error the broadenings of the lines are the same. The broadening, $w - w_0$, is plotted against hydronium concentration in Figures 7 and 8. The possible reasons for the change of slope at about $[H_3O^+] = 2$ *M* and the higher value for the deuterated acid will be proposed in the discussion of the mechanism.

The apparent first-order rate law for proton transfer is

$$\text{rate}_R = (\tau_{SO_4^{2-}})^{-1}[SO_4^{2-}] \qquad (2)$$

where rate_R designates the overall rate of recombination of H_3O^+ and SO_4^{2-}. Introduction of the hydronium dependence of $(\tau_{SO_4^{2-}})^{-1}$ gives

$$\text{rate}_R = \pi c A [H_3O^+][SO_4^{2-}] \qquad (3)$$

A being the initial slope in Figures 7 and 8. We designate πcA as k_R, the overall rate constant for the

(22) M. M. Kreevoy and C. A. Mead, *J. Amer. Chem. Soc.*, **84**, 4596 (1962).

(23) M. M. Kreevoy and C. A. Mead, *Discuss. Faraday Soc.*, **39**, 166 (1965).

(24) A. K. Covington, M. J. Tait, and W. F. K. Wynne-Jones, *ibid.*, **39**, 172 (1965).

(25) J. A. Pople, W. G. Schneider, and H. J. Bernstein, "High Resolution Nuclear Magnetic Resonance," McGraw-Hill, New York, N. Y., 1959, p 221.

(26) M. Eigen and L. DeMaeyer in "The Structure of Electrolytic Solutions," W. J. Hamer, Ed., Wiley, New York, N. Y., 1959, Chapter 5.

(27) M. Eigen, W. Kruse, G. Maass, and L. DeMaeyer, *Progr. React. Kinet.*, **2**, 286 (1964).

(28) M. Eigen and L. DeMaeyer, *Proc. Roy. Soc., Ser. A*, **247**, 505 (1958).

Table II: Data for H_2SO_4–NaOH (or HCl)

$[H_2SO_4]$	[NaOH]	$[SO_4^{2-}]$	$[HSO_4^-]$	$[H_3O^+]$	Q_c	w_{1050}	w_{981}	$(w - w_0)_{981}$
3.495	5.988	2.63	0.87	0.13	0.393	28.7 ± 1.1	19.1 ± 0.5	1.1 ± 0.5
3.495	4.990	1.79	1.71	0.29	0.304	31.9 ± 2.5	20.1 ± 1.0	2.1 ± 0.1
3.495	3.992	1.22	2.28	0.72	0.385	32.5 ± 1.0	22.6 ± 0.6	4.6 ± 0.6
3.495	2.994	0.984	2.51	1.49	0.584	30.3 ± 0.0	26.9 ± 0.0	8.9 ± 0.0
3.495	1.996	0.799	2.70	2.29	0.677	30.5 ± 0.2	28.8 ± 0.3	10.8 ± 0.3
3.495	0.998	0.831	2.66	3.33	1.040	33.4 ± 0.2	32.2 ± 0.2	14.2 ± 0.2
	[HCl]							
3.495	5.490	0.767	2.73	9.75	2.74	38.6 ± 0.4	47.8 ± 0.2	29.8 ± 0.2
3.495	7.686	0.592	2.91	11.77	2.39	39.0	49.0 ± 0.8	31.0 ± 0.8

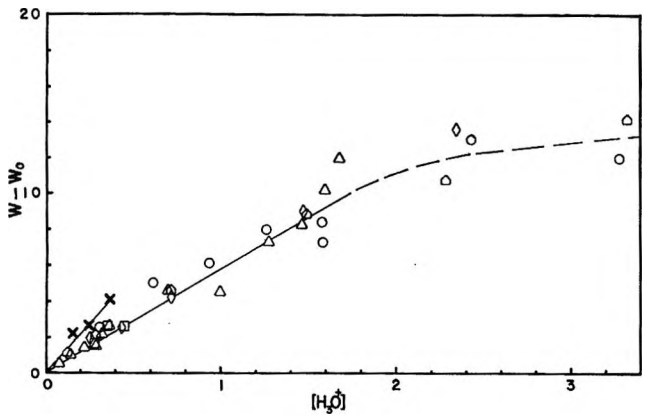

Figure 7. The dependence of the line broadening, $(w - w_0)$ cm^{-1}, of the 981-cm^{-1} line of SO_4^{2-} on hydronium concentration for $[H_3O^+] < 2\ M$. ○, H_2SO_4; ×, $KDSO_4$; ⌓, H_2SO_4 + NaOH; △, NH_4HSO_4; ◇, $(NH_4)_2SO_4$ + HCl; □, $KHSO_4$.

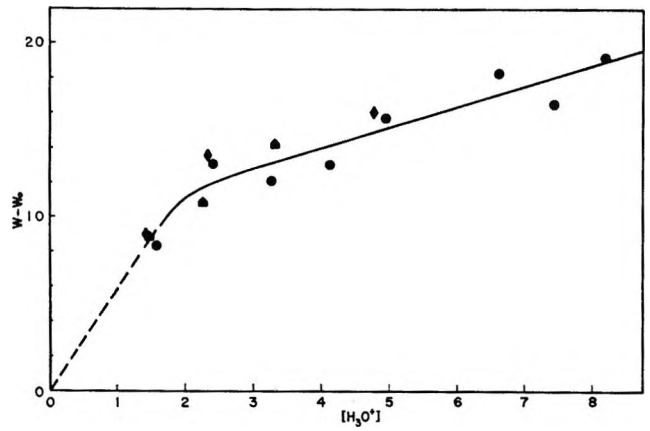

Figure 8. The dependence of the line broadening, $(w - w_0)$ cm^{-1}, of the 981-cm^{-1} line of SO_4^{2-} on hydronium concentration for $[H_3O^+] > 2\ M$: ●, H_2SO_4; ◆, $(NH_4)_2SO_4$ + HCl; ⬬, H_2SO_4 + NaOH.

recombination. For hydrogen acid systems, $A = 5.8$ $cm^{-1}\ M^{-1}$ when $[H_3O^+] < 2$, and ~ 11.3 $cm^{-1}\ M^{-1}$ for $KDSO_4$–D_2O. Thus $k_R^H = 5.5 \times 10^{11}\ M^{-1}\ sec^{-1}$ ($[H_3O^+] < 2$) and $k_R^D = 10.4 \times 10^{11}\ M^{-1} sec^{-1}$.

The broadening of the 1050-cm^{-1} line of HSO_4^- is not as great as that of the 981-cm^{-1} line, and there is more uncertainty in the measurements of the line width

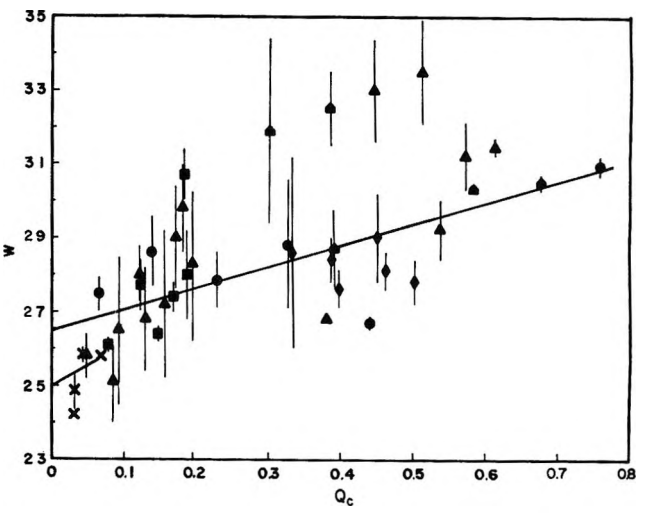

Figure 9. The dependence of the line width, w, cm^{-1}, of the 1050-cm^{-1} line of HSO_4^- on Q_c: ●, H_2SO_4; ×, $KDSO_4$; ⬬, H_2SO_4 + NaOH; ▲, NH_4HSO_4; ◆, $(NH_4)_2SO_4$ + HCl; ■, $KHSO_4$.

because of greater overlap. However, the consideration of the overall dissociation reaction by means of this broadening is still instructive. We designate the overall rate of dissociation as $rate_D$; then

$$rate_R = rate_D$$

$$(\tau_{SO_4^{2-}})^{-1}[SO_4^{2-}] = (\tau_{HSO_4^-})^{-1}[HSO_4^-]$$

$$\pi cA\,[H_3O^+][SO_4^{2-}] = \pi c(w - w_0)_{1050}[HSO_4^-]$$

$$(w - w_0)_{1050} = AQ_c \qquad (4)$$

$(w_0)_{1050}$ is not directly measurable because HSO_4^- always exists in the presence of SO_4^{2-} and H_3O^+. A plot of w_{1050} *vs.* Q_c is shown in Figure 9. It is evident that the uncertainty of the measurements (represented by the vertical lines) is great when compared with the magnitude of the broadening. Data of Figure 9 correspond to data of Figure 7 below 2 M H_3O^+. A straight line with the required slope ($A = 5.8$) can reasonably be drawn through the points. The internal consistency for the combined systems supports the interpretation. A value of $(w_0)_{1050}$ was estimated to be 26.5 ± 1 cm^{-1} by extrapolation. The linearity is

continued beyond that illustrated in Figure 9 up to $Q_c = 2.90$ ($C = 7.84$ M). Above this concentration Q_c falls with increasing concentration and the slope sharply becomes -5.8. The systems then contain, on the average, two or fewer water molecules per ion.

Conway[29] has reviewed the models which have been developed to describe the anomalous proton mobility observed in low-field conductance. He favors a mechanism involving field-assisted rotation of water molecules (the rate-determining step) followed by fast proton transfer, possibly by quantum mechanical tunneling. The process occurring in this study is similar but not identical with that for which the models were developed. The proton is being transferred over rather short distances, from water molecule to water molecule, in the *high* field of an ion with a double negative charge, SO_4^{2-}. We will assume a preliminary step involving partial rotation of water molecules followed by proton jumps along a chain of directed hydrogen bonds. The proportionalities between $(w - w_0)$ and $[H_3O^+]$ suggest that all hydronium and sulfate ions are always engaged in proton transfer to some extent and that the species do not need to diffuse together, prior to its onset. For concentrations above 2 M there are fewer than 11 water molecules per ion and ions must be separated by fewer than about four water molecules. The fields on the water molecules are large and alignments (step I) will be rapid. Steps II and III are written

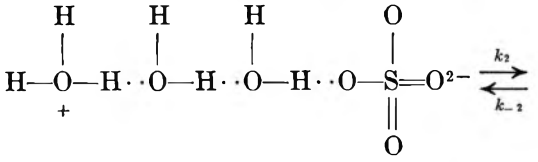

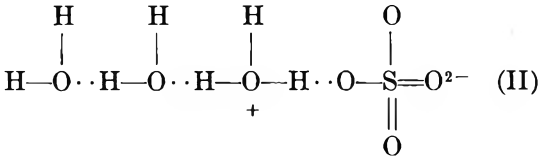

(II)

$$H_3O^+ \cdot SO_4^{2-} \underset{k_{-3}}{\overset{k_3}{\rightleftharpoons}} H_2O \cdot HSO_4^- \qquad \text{(III)}$$

In the present study the 948-cm^{-1} Raman line is attributed to the ion pair $H_3O^+SO_4^{2-}$. The lowering of the symmetric stretch of SO_4^{2-} by the force field from the adjacent hydronium ion is analogous to the lowering of the symmetric stretch of nitrate ion by ion pairing to cations.[30,31] The 948-cm^{-1} line is much greater in width than the 981-cm^{-1} line, suggestive of a shorter mean lifetime. The ion pair has also been postulated by Högfeldt[15] and is required in the stepwise mechanism —ionization of a weak acid followed by dissociation— advanced by Covington, *et al.*,[32] and Prue.[33] Because we have isolated the signal from the ion pair, the data for the 981-cm^{-1} line appear to be giving uniquely detailed information about steps I and II. (*i.e.*, k_3 has been excluded from the k_R observed, and the Raman effect measures all processes faster than 10^{11} sec^{-1}, possibly alignments and transfer.) The assignment[1] of the 1024-cm^{-1} Raman line to a fundamental of HSO_4 now appears most plausible.

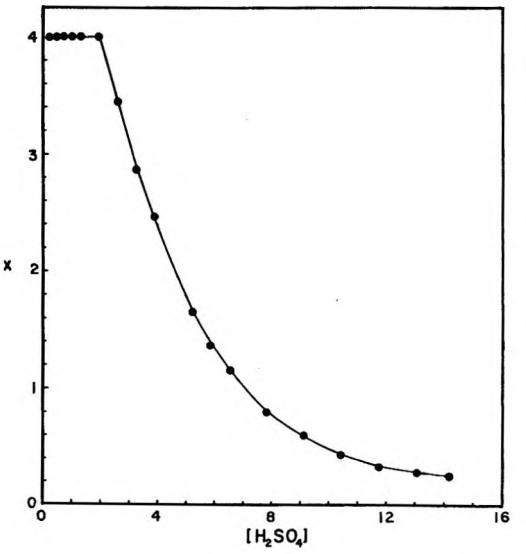

Figure 10. x *vs.* stoichiometric concentration of sulfuric acid.

Step II indicates that a water dependence should appear in the rate law. We will assume that the experimentally determined activity of water[34] gives a direct measure of the intervening water molecules in the system. The rate law is then written

$$\text{rate}_R = \pi cA\,[H_3O^+](a_w)^x[SO_4^{2-}] \qquad (5)$$

where x is a variable. For the concentration range $[H_3O^+] < 2$ M, a plot of $(w - w_0)_{981}$ *vs.* $[H_3O^+](a_w)^x$ is linear, and the slope is not sensitive to the value of x. Using smoothed data, the least-squares method based on a linear equation gave the best fit for $x = 4$ and yielded a slope of 6.75. The extension of this linear relationship to fit the data in the region $[H_3O^+] > 2$ M requires that x be less than 4, and decrease with increasing concentration. The variation of x with stoichiometric concentration of H_2SO_4, which gives the linearity, is illustrated in Figure 10. This variation suggests that in dilute solution the proton transfer may occur through four intervening water molecules but this number decreases as the concentration increases. It is consistent with the notion that the solvation number of H_3O^+ decreases with increasing concentra-

(29) B. E. Conway in "Modern Aspects of Electrochemistry," J. O'M. Bockris and B. E. Conway, Ed., Butterworths, London, 1964, No. 3, p 43.

(30) D. L. Nelson and D. E. Irish, *J. Chem. Phys.*, **54**, 4479 (1971).

(31) G. J. Janz, K. Balasubrahmanyam, and B. G. Oliver, *ibid.*, **51**, 5723 (1969).

(32) A. K. Covington, J. G. Freeman, and T. H. Lilley, *J. Phys. Chem.*, **74**, 3773 (1970).

(33) J. E. Prue, *Proc. Symp. Coord. Chem., 3rd, 1970*, **1**, 25 (1970).

(34) W. F. Giauque, E. W. Hornung, J. E. Kunzler, and T. R. Rubin, *J. Amer. Chem. Soc.*, **82**, 62 (1960).

tion.[15-18] It suggests that the change of slope in Figures 7 and 8 at ~2 M probably arises from the neglect of the role of the solvent in the reaction. It is interesting to note that Robertson and Dunford[18] postulate $H_{21}O_{10}^+$, the maximum average hydration number of the proton, at 2 ± 1 M and refer to drastic changes in the solution properties occurring in this region. The apparent rate constant for eq 5, which now fits the data from all systems over the entire range of compositions, is 6.4×10^{11} M^{-1} sec^{-1}. Eigen, *et al.*,[35] have reported on a proton transfer study of dilute H_2SO_4 solutions by means of the ultrasonic absorption relaxation technique. They give $k_R = 1.0 \times 10^{11}$ M^{-1} sec^{-1} in 0.1 M ionic strength. The present result is 6.4 times as large. Although one can argue that the agreement is good, the difference can possibly be accounted for by consideration of the concentration and the technique. At that low concentration structural diffusion would be a more important contributing step. The perturbation preceding the relaxation experiment could also disrupt the organization required for step II. Thus the experiment would "see" a greater contribution from the slower diffusion step.

Another interpretation bears consideration. A single 981-cm^{-1} line is generated by sulfate ion, whether existing as a solvent-separated ion pair as in step II or as "free" sulfate. Let us suppose that a preliminary diffusion step is required to bring SO_4^{2-} sufficiently close to H_3O^+ such that water molecule rotation can lead to step II. A preliminary equilibrium between the two types of sulfate must exist

$$H_3O^+ + H_2O + SO_4^{2-} \rightleftharpoons H_3O^+||SO_4^{2-}$$

The diffusion would be so slow ($<10^{11}$ M^{-1} sec^{-1}) that the 981-cm^{-1} line from "free" sulfate would be broadened to a negligible extent. Thus all of the observed broadening would arise from a *coincident*, broader line from the solvent-separated ion pair. If we adopt this two-line argument the observed 981-cm^{-1} half-widths are all too small because they would have been measured at a point farther up the band than the half-intensity point of that component arising from the solvent-separated ion pair. This criticism would be most valid for $C < 2$ M where the average ratio $[H_2O]:[\text{Ions}]_{\text{total}}$ is greater than 12:1. Line shape gave no indication of such a superposition of lines. The proportionality to total $[H_3O^+]$ and $[SO_4^{2-}]$ causes us to discount this possibility, and an interpretation based on it; the point of view that all sulfates are always experiencing step II to some degree is preferred.

The interpretation of sulfuric acid falls naturally into three concentration ranges. For $C < 2$ M, x in the term $(a_w)^x$ is four and water–ion ratios are high. For $2 < C < 7.84$, x falls from 4 to 0.8, and the rate expression of eq 5 fits the data. For $7.84 < C < 14.20$, eq 5 can again be made to fit the data. However there are, on the average, fewer than two water molecules per ion and the w_{1050} *vs.* Q_c plot is no longer given by eq 4. In this region it is probable that another proton transfer step becomes important.

$$SO_4^{2-} + H_3O^+\cdot HSO_4^- \rightleftharpoons HSO_4^- + H_3O^+\cdot SO_4^{2-} \quad \text{(IV)}$$

This step requires the existence of the ion pair $H_3O^+\cdot HSO_4^-$ which would generate intensity near the 1050-cm^{-1} envelope. Certainly, the latter band is very broad in this concentration range (44–54 cm^{-1}). The species would be a forerunner to molecular H_2SO_4 which exists when $C > 14$ M.[6] Generally, in solution chemistry, when one species concentration is diminishing with increasing stoichiometric concentration (in this case SO_4^{2-} when $8 < C < 14$ M; Figure 2) another is becoming significant. Thus, in the range 20–80 mol % of H_2SO_4, the existence of such a species is plausible and it, in turn, is being replaced by (H_3O^+)-(H_2SO_4).[36] Although the data may provide quantitative support for this type of extension of the mechanism, no thorough exploration of the consequences of this proposal has been attempted. It is noted, however, that for an approximately constant hydronium concentration, 1.5 M, and for different HSO_4^- concentrations, 1, 1.5, 2.5, and 3.8 M, the values of $(w - w_0)_{981}$ are 8.3, 9.0, 8.9, and 8.3 cm^{-1}, respectively, indicating independence of $[HSO_4^-]$ up to the change of slope in Figure 7. There are few data which permit such a comparison at higher concentrations but the independence of $[HSO_4^-]$ appears to also hold at 3.921 M and at 9.149 M H_2SO_4. The change of slope of the w_{1050} *vs.* Q_c plot is significant at concentrations above this where w_{981} is more difficult to measure and data for mixtures have not been obtained.

The observed D/H isotope effect has been used as a criterion for the correctness of models for proton transfer.[29] The isotope ratio of D/H mobilities is about 0.7. The ratio k_R^D/k_R^H is 0.6 for recombination rates in D_2O and H_2O, respectively,[27] and is similarly less than one for ice. For the processes in this work the D/H ratio is 1.9. Because these systems are acidic higher individual rates are expected. In their reviews, Bell[37] and Wiberg[38] cite many examples of acid- and base-catalyzed reactions which proceed faster in D_2O than in H_2O. In some cases the effect suggests a preequilibrium which favors higher concentrations of a conjugate acid in D_2O medium. Many of the accelerations are in the range 1.3 to 3.0.

(35) M. Eigen, G. Kurtze, and K. Tamm, *Z. Elektrochem.*, **57**, 103 (1953).

(36) T. F. Young and G. E. Walrafen, *Trans. Faraday Soc.*, **57**, 34 (1961).

(37) R. P. Bell, "Acid-Base Catalysis," Clarendon Press, Oxford, 1941, p 146.

(38) K. B. Wiberg, *Chem. Rev.*, **55**, 713 (1955).

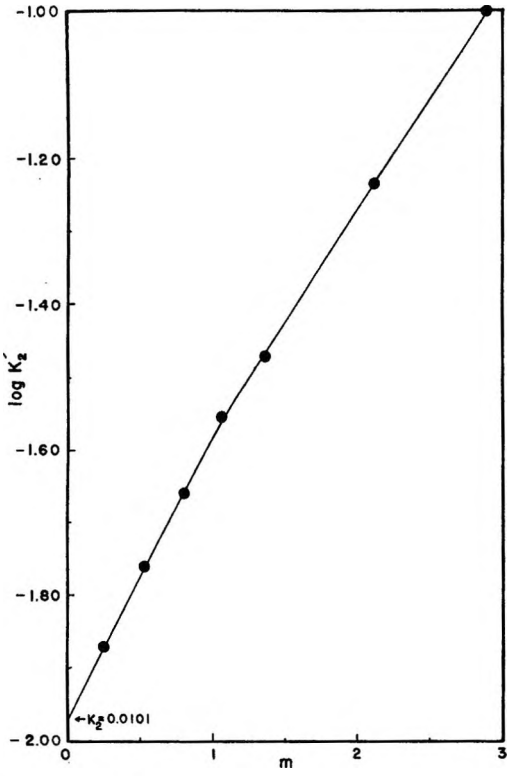

Figure 11. Log K_2' *vs.* m for sulfuric acid, based on method A.

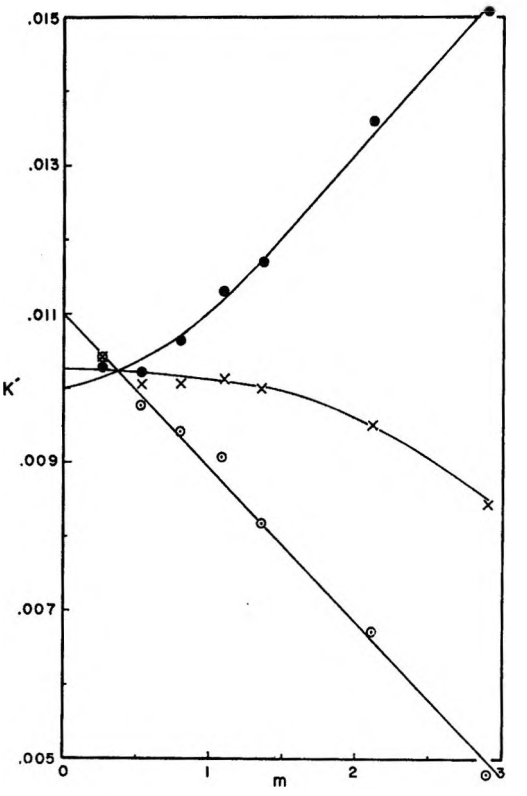

Figure 12. K' *vs.* m for sulfuric acid based on $(\gamma_\pm)_{HClO_4}$: K_{I_m}', O; $K_{m_{H^+}}'$, ×; $K_{m_\pm}'$, ●.

In the present case the system is such that there exists a secondary isotope effect and a medium effect, as well as the primary effect resulting from replacement of H^+ by D^+. Thus direct comparison of k_R^H and k_R^D is not expected to provide insight into any one of these factors.[39] The measured concentrations of SO_4^{2-} plus any $D_3O^+||SO_4^{2-}$ are less than those with hydrogen ion. Thus a preequilibrium does not appear to be the source of the effect.[40] The isotope effect would suggest that the proton transfer is *via* classical proton jumps with a required activation energy rather than by a nonclassical tunneling mechanism, if the transfer is rate determining. If the alignment is rate determining, which seems more probable,[41] the observed isotope effect is not unreasonable and tunneling could follow as a fast step. Albery[4] has suggested that the k^D/k^H ratio may be greater than one when the proton is close to the product. For $KDSO_4$–D_2O, directed hydrogen bonds may be stronger and shorter,[42] thus providing a more favorable path for the proton jump and the path may extend farther through the solution (a bigger cluster).[43]

Appendix

Attempts to Estimate K_2 for H_2SO_4 from Raman Data. In this Appendix we explore the possibility of estimating K_2 for H_2SO_4 from the Raman data obtained. Attention is paid to the use of the reported molal stoichiometric mean activity coefficients, $(\gamma_\pm)_{ST}$, as an aid in extrapolating the data obtained for moderately concentrated solutions. The equation for K_2 is[44]

$$K_2 = \frac{a_{H^+}a_{SO_4^{2-}}}{a_{H_2SO_4}} = \frac{4m}{(1-\alpha^2)}\frac{(\gamma_\pm)^3_{ST}}{\gamma_{H^+}\gamma_{HSO_4^-}} \qquad (6)$$

All of the quantities on the right are measurable except the single ion activity coefficients $\gamma_{H^+}\gamma_{HSO_4^-}$. Two different approximate approaches have been used to handle these quantities.

A. Elimination of γ_{H^+} and $\gamma_{HSO_4^-}$ Using the Debye–Hückel Expression (after Wallace[45]). At concentrations where the Debye–Hückel expression for log γ_i is valid rearrangement of eq 6 and introduction of log γ_i results in elimination of $\gamma_{H^+}\gamma_{HSO_4^-}$ and

$$K_2 = 4^{3/2}m(\gamma_\pm)_{ST}^2\left(\frac{\alpha}{1+\alpha}\right)^{1/2}\left(\frac{1}{1-\alpha}\right) \qquad (7)$$

Using values of α obtained in this study, and interpolated values of $(\gamma_\pm)_{ST}$ reported by Covington,

(39) E. L. Purlee, *J. Amer. Chem. Soc.*, 81, 263 (1959).

(40) A. J. Kresge and R. J. Preto, *ibid.*, 87, 4593 (1965).

(41) B. E. Conway, J. O'M. Bockris, and H. Linton, *J. Chem. Phys.*, 24, 834 (1956).

(42) E. Whalley, *Trans. Faraday Soc.*, 53, 1578 (1957).

(43) B. E. Conway and L. H. Laliberté, *J. Phys. Chem.*, 72, 4317 (1968).

(44) R. A. Robinson and R. H. Stokes, "Electrolyte Solutions," 2nd ed, Butterworths, London, 1968, pp 37–38.

(45) R. M. Wallace, *J. Phys. Chem.*, 70, 3922 (1966).

et al.[46] (Table II, third column, ref 46), approximate values, K_2', of K_2 were calculated from eq 7. A plot of log K_2' *vs.* m (Figure 11) is linear and extrapolates to $K_2 = 0.0101$ mol/kg of H_2O. The finite slope reveals the inadequacy of the assumption at the concentrations for which α has been measured, although eq 7 is expected to be valid for $I < 0.1$.

B. Use of Values of $\gamma_\pm$ for a Completely Ionized 1:1 Electrolyte. An approximate value for K_2 can also be obtained by using eq 6, if the value of $\gamma_{H^+}\gamma_{HSO_4^-}$ is assumed to be very close to $(\gamma_\pm)_{ST}^2$ of some completely ionized 1:1 electrolyte. We choose $HClO_4$, although the results would not be significantly different for HCl. The interpolated values of $(\gamma_\pm)_{ST}$ for $HClO_4$[47] have been chosen for three different conditions: for the same ionic strength as the H_2SO_4 solutions, for the same hydronium ion concentration, and for the same geometric mean ionic molality of 1:1 ions as that obtained using m_{H^+} and $m_{HSO_4^-}$ for a given H_2SO_4 solution.[8] Plots of K_2', designated K_{I_m}', $K_{m_{H^+}}'$ and $K_{m_\pm}'$, *vs.* m are given in Figure 12. Extrapolation suggests values for K_2 ranging from 0.010 to 0.011 mol/kg of H_2O. It is interesting to note that the hydronium ion concentration is apparently the best basis for choice of $\gamma_\pm$ at these concentrations. For salt solutions of moderate to high concentrations we have frequently observed that mass law concentration quotients are independent of concentration and ionic strength.[30] Such is not the case for acids, as illustrated here; the hydronium ion is responsible for the nonconstancy of the activity coefficient quotient in these systems.

Acknowledgments. This work was supported by the National Research Council of Canada. In the final stages of the work the authors had the benefit of stimulating conversations with a number of workers: A. K. Covington, E. Grunwald, J. E. Prue, D. H. Whiffen, and P. A. H. Wyatt. Their criticisms and suggestions are greatly appreciated. The cooperation and contribution of the Computer Science Division, University of Waterloo, and especially Mr. A. Weerheim to the curve resolving routine is gratefully acknowledged. The assistance given by W. L. Elsdon and D. J. Lockwood is also appreciated.

(46) A. K. Covington, J. V. Dobson, and W. F. K. Wynne-Jones, *Trans. Faraday Soc.*, 61, 2050 (1965).
(47) Reference 44, p 491.

A Raman Spectral Study of Bisulfate–Sulfate Systems. III. Salt Effects

by H. Chen and D. E. Irish*

Department of Chemistry, University of Waterloo, Waterloo, Ontario, Canada *(Received April 5, 1971)*

Publication costs borne completely by The Journal of Physical Chemistry

The degree of formation of sulfate in 1.357 *M* NH_4HSO_4 solutions containing various amounts of each of LiCl, NaCl, KCl, RbCl, CsCl, NH_4Cl, and NH_4Br has been measured by Raman spectrophotometry. The ionization is depressed by the salts in the order CsCl > RbCl ~ KCl > NaCl ~ NH_4Br > NH_4Cl ~ LiCl, if sufficient salt is added. For addition of small quantities of LiCl and NH_4Cl the ionization is enhanced.

Introduction

The equilibrium between an acid and its conjugate base is disturbed by addition of species foreign to the equilibrium. In most studies of the salt effect on acid–base equilibria, data have been obtained for dilute solutions and the ionization quotients have been obtained for the acid at infinite dilution.[1] Thus self-interactions of the acid and possible complex formation between ions of the acid and ions of the salt have been excluded. The addition of small amounts of a neutral salt then increases the extent of ionization in accord with the Debye–Hückel theory.[1,2]

Raman spectral data can only be obtained at concentrations well above those for which the extended Debye–Hückel theory is valid. Extrapolations to provide quantities which are directly comparable with those obtained from the dilute solution studies are not possible. The behavior at such concentrations is still of interest, however. In conjunction with Raman studies of the ionization of bisulfate[3,4]

(1) E. J. King, "Acid-Base Equilibria," Pergamon Press Ltd., Oxford, 1965, p 269.
(2) R. P. Bell, "Acid-Base Catalysis," Clarendon Press, Oxford, 1941, p 14.
(3) D. E. Irish and H. Chen, *J. Phys. Chem.*, 74, 3796 (1970).
(4) H. Chen and D. E. Irish, *ibid.*, 75, 2672 (1971).

we have measured the apparent concentration quotient, ${}_sQ_c$, for a fixed concentration of NH_4HSO_4 and various amounts of added salt. The alkali metal chlorides, ammonium chloride, and ammonium bromide were selected as these permit a comparison of univalent cations and no spectral manifestation of contact ion pairs was found.

Experimental Section

Solutions were prepared from NH_4HSO_4, NH_4Cl, LiCl, CsCl (Fisher Certified Reagent), NaCl (B & A ACS Reagent), KCl (B.D.H. Laboratory Reagent), RbCl (Fisher Purified Reagent), and NH_4Br (Matheson Coleman and Bell). Solutions of 1.357 *M* NH_4HSO_4 with inert electrolytes added were obtained by dissolution of a weighed amount of dried halide in 50.0 ml of 2.715 *M* NH_4HSO_4 followed by dilution to 100.0 ml; 1.357 *M* NH_4HSO_4 is an optimum low concentration for which intensities are still accurately measurable and spectral contours can be resolved. All solutions were treated with activated charcoal for at least 30 min and filtered through a 100-mμ Millipore filter before being transferred into the Raman cell. This eliminates any fluorescence and optical attenuation. On addition of the salts, some of the colorless, clear NH_4HSO_4 solutions became very pale yellow. The color is believed to result from a trace of $FeCl_4^-$, formed from impurity iron in the chlorides. The color causes absorption at 340.0 nm with a tail of the absorption band at the wavelength of the Raman exciting line and the Raman lines. The position of the absorption maximum agrees with that of dilute solutions of $FeCl_3$ in aqueous HCl.[5,6] The suppliers indicated iron impurity in the range 0.0001 to 0.002%. The faint color of some solutions had no effect on the data, as discussed below. Spectra of samples at 25° and computer analyses were obtained as previously described.[3]

Results

The degree of formation of SO_4^{2-}, α, can be related to the intensity ratio I_{981}/I_{1050} (the ratio of the intensities of the strong lines of SO_4^{2-} and HSO_4^-, respectively). For those solutions which were colored, this ratio is independent of color if the two lines are affected to the same extent by the low absorbance. Because of the closeness of the two lines, 455.3 and 456.7 nm, the difference in absorbance is not significant and no color correction has been applied. The expression for α is derived as follows

$$\frac{[SO_4^{2-}]}{[HSO_4^-]_{dif}} = \frac{I_{981}}{I_{1050}} \times \frac{J_{1050}}{J_{981}} = 0.534\frac{I_{981}}{I_{1050}}$$

$$[NH_4HSO_4] = [SO_4^{2-}] + [HSO_4^-]_{dif} =$$

$$[SO_4^{2-}]\left[1 + 1.87\frac{I_{1050}}{I_{981}}\right]$$

$$\alpha = \frac{[SO_4^{2-}]}{[NH_4HSO_4]} = \left[1 + 1.87\frac{I_{1050}}{I_{981}}\right]^{-1}$$

where J_i is the molar intensity of line $\bar{\nu}_i$ and these values have been measured.[3,4] The quantity I_{981}/I_{1050} is more sensitive to the uncertainty of curve resolving than measurement of I_{981} alone and thus α obtained from the above relation is less accurate than α measured directly.[3] More attempts were made to resolve a single spectrum and a mean value of the intensity ratio was taken. Data are presented in Table I. The sulfate ion concentration varies from 0.35 to 0.5 *M* in these solutions. Over this range the change of half-width resulting from proton transfer[4] is not significant. Thus the ratio of apparent peak heights serves as a check and confirmed the trends found from the ratio of integrated intensities. In the absence of salt, Q_c for 1.357 *M* NH_4HSO_4 is 0.252. The fractional change in Q_c is defined as $({}_sQ_c - Q_c)/Q_c = ({}_sQ_c - 0.252)/(0.252)$. A positive value indicates enhanced sulfate formation in the presence of the salt and *vice versa*. The plot of this function *vs.* salt concentration clearly shows how the different salts affect the degree of formation of sulfate (Figure 1). For the addition of sufficient salt, all salts depress the formation of sulfate in the order CsCl > RbCl ~ KCl > NaCl ~ NH_4Br > LiCl ~ NH_4Cl. In dilute salt solutions there is indication of enhancement of the concentration of sulfate.

Discussion

The equilibrium, in the presence of foreign salts, is described by the equation $K = {}_sQ_{cs}Q_y$ where K is the thermodynamic equilibrium constant and ${}_sQ_y$ is the activity coefficient quotient. Values of ${}_sQ_y$ are given in Table I; the value 0.010 is used for K at 25°. Log ${}_sQ_y$ is plotted against the square root of ionic strength in Figure 2. The broken curves represent approximately the trend of the salt effect for infinitely dilute weak acid solutions found in the literature.[1,7] The salt effect observed in this work is qualitatively in accord with those described in the literature. In the same figure, the data for the stoichiometric NH_4HSO_4 solutions are also shown for comparison (zero salt). For NH_4Cl and LiCl the first addition of salt increases the acid dissociation (decreases ${}_sQ_y$). On further addition the degree of formation of sulfate passes through a maximum and decreases; eventually dissociation is depressed from that observed for the acid in pure water. The initial increase was not observed for the other salts at the concentrations used, although a small enhancement may occur, judging from Figure 1. Both theory

(5) D. E. Metzler and R. J. Myers, *J. Amer. Chem. Soc.*, **72**, 3776 (1950).

(6) H. L. Friedman, *ibid.*, **74**, 5 (1952).

(7) H. S. Harned and B. B. Owen, "The Physical Chemistry of Electrolytic Solutions," 3rd ed, Reinhold, New York, N. Y., 1958, p 675.

Table I: Data for 1.357 *M* NH_4HSO_4 in Salt Solutions

Salt	M_{salt}	I_{981}/I_{1050}[a]	α	${}_sQ_c$	${}_sQ_y$[b]	log ${}_sQ_y$	$[SO_4^{2-}]$[d]	I_c	$\sqrt{I_c}$[c]
None	0.00	1.00	0.348	0.252	0.0397	−1.400	0.472	2.30	1.52
NH_4Cl	0.937	1.09	0.368	0.291	0.0344	−1.463	0.499	3.29	1.81
	2.000	1.03	0.355	0.265	0.0377	−1.423	0.482	4.32	2.08
	3.084	0.91	0.327	0.216	0.0463	−1.334	0.444	5.33	2.31
	4.107	0.82	0.304	0.180	0.0555	−1.255	0.412	6.29	2.51
NH_4Br	1.992	0.93	0.332	0.224	0.0444	−1.352	0.450	4.25	2.06
	3.007	0.82	0.304	0.180	0.0555	−1.255	0.412	5.19	2.28
	4.000	0.70	0.272	0.138	0.0725	−1.139	0.369	6.09	2.47
LiCl	1.191	1.14	0.379	0.314	0.0318	−1.498	0.514	3.58	1.89
	1.914	1.06	0.361	0.277	0.0361	−1.442	0.490	4.25	2.06
	2.750	0.96	0.339	0.236	0.0424	−1.372	0.460	5.03	2.24
	4.087	0.86	0.314	0.195	0.0513	−1.290	0.426	6.30	2.51
NaCl	1.988	0.91	0.327	0.216	0.0463	−1.334	0.444	4.23	2.06
	2.990	0.84	0.310	0.189	0.0529	−1.276	0.421	5.19	2.28
	4.044	0.72	0.278	0.145	0.0694	−1.158	0.376	6.15	2.48
KCl	1.411	0.91	0.327	0.216	0.0463	−1.334	0.444	3.66	1.91
	2.051	0.80	0.299	0.173	0.0568	−1.245	0.406	4.22	2.05
	2.426	0.76	0.289	0.159	0.0629	−1.201	0.392	4.57	2.14
	3.022	0.64	0.255	0.118	0.0847	−1.072	0.346	5.07	2.25
RbCl	1.651	0.86	0.314	0.195	0.0513	−1.290	0.426	3.86	1.96
CsCl	0.990	0.89	0.323	0.209	0.0478	−1.320	0.438	3.22	1.79
	1.862	0.79	0.297	0.170	0.0588	−1.230	0.403	4.02	2.00

[a] Average of four to eight curve resolvings with uncertainty of 0.02–0.04. [b] ${}_sQ_y = 0.010/{}_sQ_c$. [c] $I_c = {}^1/_2\Sigma M_i z_i^2 = M_{salt} + 1.357 + 2[SO_4^{2-}]$.

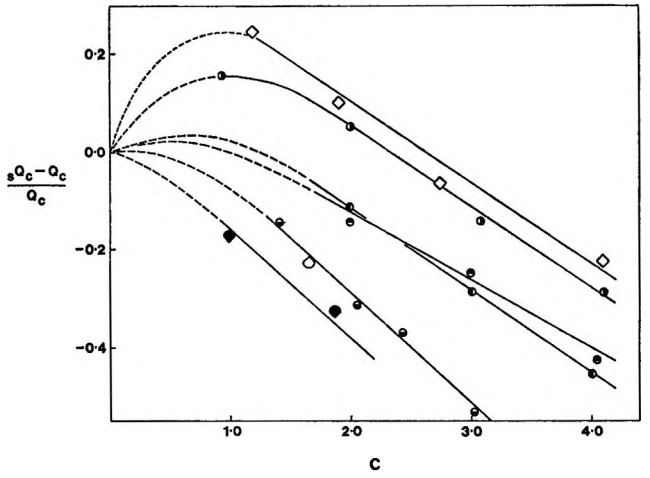

Figure 1. Effect of salt on the concentration quotient of the bisulfate–sulfate equilibrium, shown by: $({}_sQ_c - Q_c)/Q_c$ *vs.* the molarity of salt: ◑, NH_4Cl; ◇, LiCl; ◐, NH_4Br; ⊖, NaCl; ⊖, KCl; △, RbCl; ▼, CsCl.

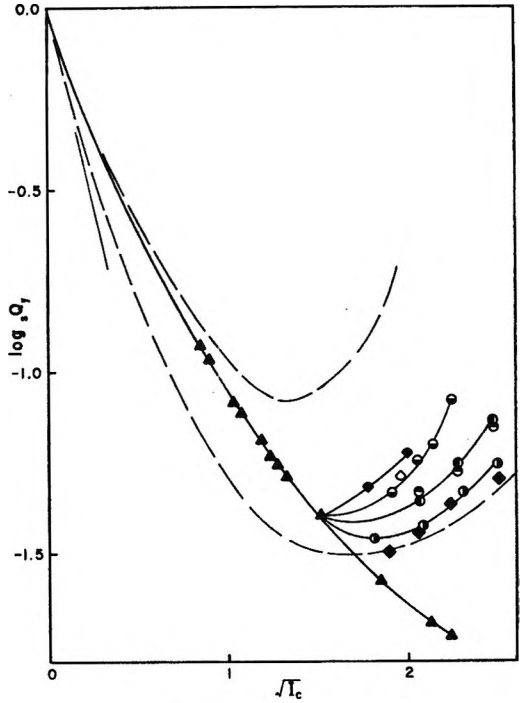

Figure 2. Log ${}_sQ_y$ *vs.* $\sqrt{I_c}$ for a 1.357 *M* NH_4HSO_4 solution with added foreign salts. Symbols defined in Figure 1: ▲, for stoichiometric solutions of NH_4HSO_4.

and experiment confirm an enhancement in dilute solutions in accord with the decrease of activity coefficients on increase of ionic strength.[1,2]

The same trend was reported by Harned and Robinson.[8] They reported that for NaCl–acetic acid solutions, the maximum in α was apparent for acid concentrations less than 5.4 *M* but not detected for 10.2 *M*. Working at much lower acid concentrations (0.2 *M*) than used in this study they found the increased dissociation to be in the order $BaCl_2$ > LiCl > NaCl > KCl. A rule,[8] valid for many studies, is that at a given ionic strength and acid concentration, ${}_sQ_y$ of a weak acid is greater in the solution of an alkali metal halide which in the pure solvent water possesses

(8) H. S. Harned and R. A. Robinson, *J. Amer. Chem. Soc.*, **50**, 3157 (1928).

the smaller mean activity coefficient. This rule cannot be extended to include ammonium salts, however. The mean activity coefficients of the salts in water decrease in the order LiCl > NaCl > NH_4Br > KCl > NH_4Cl > RbCl > CsCl. It is clear that NH_4Cl should be more comparable to KCl if the "rule" had wider significance.

Although the trends are consistent with the initial decrease and subsequent increase of activity coefficients as ionic strength increases the order and the magnitudes find no simple explanation. The order is not in keeping with a lowered dielectric constant of aqueous electrolyte solutions as proposed by Hasted, *et al.*;[9] the order for depressing the dissociation would have to be LiCl > NaCl > KCl ~ RbCl. Rationalization in terms of structure-making and structure-breaking ions is possible but this approach lacks in predictive capabilities.[10] One correlation which deserves further exploration concerns hydration of the ions. The less the "free" water (all water not bound to ions) the lower the degree of formation of sulfate. The free water concentration, ${}_FC_w$, is given by ${}_TC_w - hC_S - C_w'$. ${}_TC_w$ is the total water concentration, h is a total hydration number for salt of concentration C_S, and C_w' is the water bound by the proton, sulfate, bisulfate, and ammonium ions. For the ternary systems of this study ${}_TC_w$ is not known. The values for binary salt–water solutions, however, do permit estimation of ${}_FC_w$ values which lead to a correct sequence if spectroscopic estimates of h are used, *i.e.*, h of 4 for LiCl, 3 for NH_4Cl, and 5 or larger for the other halides of larger ionic radii.

Acknowledgments. This work was supported by the National Research Council of Canada.

(9) H. B. Hasted, D. M. Ritson, and C. H. Collie, *J. Chem. Phys.*, **16**, 1 (1948).

(10) H. Chen, Ph.D. Thesis, University of Waterloo, Waterloo Ontario, Canada, 1971, p 103.

NOTES

Viscosity Independence of the Half-Width of the $\nu_1(A_1)$ Raman Line of Sulfate Ion

by D. E. Irish* and R. C. Meatherall

Department of Chemistry, The University of Waterloo, Waterloo, Ontario, Canada *(Received April 5, 1971)*

Publication costs borne completely by The Journal of Physical Chemistry

The liquid state is characterized by random molecular motions. Transitions from one equilibrium position to another, hindered partial rotations, and collisions are occurring with a high frequency. The mean lifetime of a molecule between random reorientations has been linked to changes in the half-widths of Raman lines and infrared lines of liquids. Studies of pure organic liquids at different temperatures and of organic mixtures reveal a relationship between half-width and the reciprocal of viscosity.[1-3] Few width studies have been performed on aqueous electrolyte solutions. Concentration narrowing has been reported for alkali metal nitrite solutions and the inferred encounter rate constant increases with the solubility of these highly soluble salts.[4] Both specific and nonspecific dependences have been observed for the width of vibrational lines of alkali metal nitrates.[5]

The changes in width resulting from collisions and hindered motions generally do not exceed 10 cm^{-1}. These processes account for most of the width of vibrational lines of molecules in the liquid phase providing chemical processes are absent.[6] The latter include ultrafast proton transfer between hydronium ion and a base. Broadenings of more than 30 cm^{-1} result if the mean lifetime of the species is of the order of 10^{-12} sec.[7] In recent work on the bisulfate–sulfate equilibrium a proportionality has been found between the broadening of the 981-cm^{-1} symmetric stretching vibration of sulfate ion and the total hydronium ion concentration present.[8,9] The data have provided strong support for an interpretation in terms of ultrafast proton transfer and insight into the mechanism of the transfer process. It is important, in view of the literature cited above, to ensure that this interpretation is not in error

(1) A. V. Rakov, *Tr. Fiz. Inst. Akad. Nauk SSSR*, **27**, 111 (1964).

(2) I. I. Kondilenko, V. E. Pogorelov, and K. Khue, *Opt. Spectrosc.*, **28**, 367 (1970).

(3) S. Higuchi, S. Tanaka, and H. Kamada, *Nippon Kagaku Zasshi*, **89**, 849 (1968), *Chem. Abstr.*, **70**, 7706 (1969).

(4) D. E. Irish and M. H. Brooker, *Trans. Faraday Soc.*, **67**, 1916 (1971).

(5) D. E. Irish and A. R. Davis, *Can. J. Chem.*, **46**, 943 (1968).

(6) K. S. Seshadri and R. N. Jones, *Spectrochim. Acta*, **19**, 1013 (1963).

(7) E. Grunwald, *Progr. Phys. Org. Chem.*, **3**, 317 (1965).

(8) D. E. Irish and H. Chen, *J. Phys. Chem.*, **74**, 3796 (1970).

(9) H. Chen and D. E. Irish, *ibid.*, **75**, 2672, 2681 (1971).

because of a contribution to the broadening from viscosity.

The half-width of the 981-cm^{-1} line of sulfate ion (the same line studied in the proton transfer experiments) has been investigated for 1.2 *M* ammonium sulfate solutions containing different amounts of glucose, used to vary the viscosity. Ideally a colorless substance was desired which, when added in trace amounts, would increase the viscosity substantially. Neither glycerol nor Kelzan, a water soluble polymer supplied by the Kelco Chemical Co., were satisfactory. Aqueous glucose solutions have two broad bands located at 1070 and 900 cm^{-1}. It was possible to obtain a good 981-cm^{-1} line profile between these two. Five solutions were prepared. Each was 1.2 *M* in ammonium sulfate and contained sufficient glucose to provide viscosities of 2.0, 11.5, 85.0, 274.0, and 500.0 cP, respectively. The viscosity was measured in a Brookfield small sample chamber viscometer, jacketed for temperature control to 25 ± 0.1°. Solutions were contained in a Raman cell fitted with a water jacket and were maintained at 25 ± 1°. Spectra were excited by the 435.8-nm mercury line and obtained on the Cary 81 spectrophotometer. A slit width of 10 cm^{-1} was used.

The half-widths were measured, both manually and with the aid of a computer routine for the study of line shape.[8] For each solution a width of 14.5 ± 0.5 cm^{-1} was found. Within a wave number the half-width of the symmetric stretch of sulfate does not change when the viscosity of the medium changes from 2 to 500 cP. This independence is expected. The depolarization ratio of the symmetric stretch of a tetrahedral molecule is zero and the polarizability tensor is isotropic; in this case rotatory motions have no effect on the width of lines.[1] Any anisotropy, induced by the environment in the liquid phase, will be small.[10] In light of these results it is believed that the Raman line broadening data for sulfuric acid[9] and bisulfates[8] require no correction for viscosity.

(10) W. F. Murphy, M. V. Evans, and P. Bender, *J. Chem. Phys.*, **47**, 1836 (1967).

Replacement Reactions of Hot Chlorine Atoms in Chlorofluoromethanes

by S. C. Lee and C. O. Hower*

Department of Chemistry, University of Idaho, Moscow, Idaho 83843
(Received October 14, 1970)

Publication costs borne completely by The Journal of Physical Chemistry

In the last decade, the reactions of translationally hot tritium atoms, produced by nuclear recoil, have been used with great success to study the inertial and steric factors that affect hydrogen-atom reactions.[1] There is now considerable interest in extending these studies to hot halogen reactions in order to build a general model of the factors controlling the reactivity of monovalent chemical species. Recoil studies of chlorine atoms were initiated by Wai and Rowland[2-7] and by Spicer and Wolfgang.[8] Recoil fluorine has received relatively more attention.[9] Spicer, Todd, and Wolfgang have measured yields of hot fluorine replacement products in fluoromethanes[10] and hot chlorine replacement products in chloromethanes,[11] and discuss the trends observed in terms of steric factors and a "translational inertial" effect.

We report here the results of measurements made on the absolute yields of hot replacement products in chlorine-atom reactions with chlorofluoromethanes. These results represent the first systematic study of Cl for F replacement reactions and the first comparison of Cl for F with Cl for Cl replacements in the same molecule. Yield patterns are similar to those reported by Spicer, *et al.*, but some significant differences are also observed.

Experimental Section

Hot ^{38}Cl was produced by means of the $^{37}Cl(n,\gamma)^{38}Cl$ reaction using the 1-Mw reactor of Washington State University. Samples of the desired reactant were sealed in Vycor ampules along with small amounts of Ar, O_2, and dichloroethylene. All liquids were degassed in the vacuum system prior to use. Gases were obtained from Matheson Co. and used without purification. Dichloroethylene, used as a scavenger, was obtained from Eastman Co. Reagent grade CCl_4 was used directly.

Product analysis was by conventional radiogas chromatography using columns of either silicon GE SF-96 or silicon DC 550 on firebrick. Adsorption of halocarbons by stopcock grease is a frequent problem in this work, particularly if the compound being determined is present only at tracer levels. To eliminate this difficulty, the inlet system of the gas chromatograph was constructed using Teflon stopcocks.

(1) R. Wolfgang, *Progr. React. Kinet.*, **3**, 97 (1965).
(2) C. M. Wai, C. T. Ting, and F. S. Rowland, *J. Amer. Chem. Soc.*, **86**, 2525 (1964).
(3) C. M. Wai and F. S. Rowland, *J. Phys. Chem.*, **71**, 2752 (1967).
(4) C. M. Wai and F. S. Rowland, *ibid.*, **72**, 3049 (1968).
(5) C. M. Wai and F. S. Rowland, *J. Amer. Chem. Soc.*, **90**, 3638 (1968).
(6) C. M. Wai and F. S. Rowland, *ibid.*, **91**, 1053 (1969).
(7) C. M. Wai and F. S. Rowland, *J. Phys. Chem.*, **74**, 434 (1970).
(8) L. Spicer and R. Wolfgang, *J. Chem. Phys.*, **50**, 3466 (1969).
(9) See for example (a) C. F. McKnight, N. J. Parks, and J. W. Root, *J. Phys. Chem.*, **74**, 217 (1970); (b) T. Smail and F. S. Rowland, *ibid.*, **74**, 1859 (1970).
(10) L. Spicer, J. F. J. Todd, and R. Wolfgang, *J. Amer. Chem. Soc.*, **90**, 2425 (1968).
(11) L. Spicer and R. Wolfgang, *ibid.*, **90**, 2426 (1968).

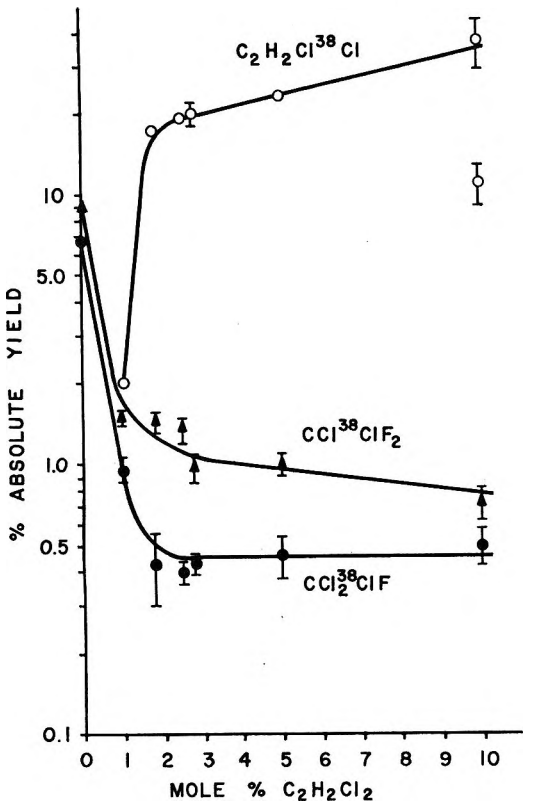

Figure 1. Dependence of product yields on dichloroethylene concentration for chlorine atom reactions with CF_2Cl_2. O_2 (1%) and Ar (1%) are also present.

Labeled compounds were detected with an external proportional counter. Absolute yields were determined by using the $^{40}Ar(n,\gamma)^{41}Ar$ reaction as an internal monitor. Both ^{41}Ar and ^{38}Cl were counted with the same detector and no correction was made for a difference in detection efficiency. These nuclides decay by high energy β transitions, and since the counter window was thin (5 mg/cm^2), error due to this assumption is small. We estimate a possible 5% error in the reported absolute yields from this source. An additional systematic error of 10% is estimated for the measurement of the ratio of argon to freon in the samples. Only errors due to counting statistics and data analysis are reported with the results.

Results and Discussion

The goal of this work was to measure the absolute yields of the hot Cl for Cl and Cl for F replacement reactions in the compounds studied. The assumption that these reactions proceed primarily by means of hot atoms was first tested by making scavenger and moderator studies. Dichloroethylene and oxygen were used as a scavenger combination following the experience of Wai and Rowland[3] in scavenging thermal Cl atoms from the CH_3Cl system. Figure 1 shows the dependence of product yields on $C_2H_2Cl_2$ concentration for a mixture of CF_2Cl_2, O_2 (1%), and Ar (1%). The results indicate that 3% $C_2H_2Cl_2$ and 1% O_2 is an efficient scavenger combination in CF_2Cl_2. This same combination was used with all of the reactant gases, the assumption being made that the scavenging efficiency would be about the same in the other reaction systems.

Table I: Replacement Product Yields for CF_3Cl as a Function of Neon Concentration

Neon, %	CF_3Cl yield, %	CF_2Cl_2 yield, %
0	0.74 ± 0.09	0.65 ± 0.06
65	0.44 ± 0.05	0.32 ± 0.03
88	0.03 ± 0.01	0.05 ± 0.01

Table I shows the effect on yields of adding neon to scavenged CF_3Cl. The yields of labeled CF_3Cl and CF_2Cl_2 decrease as neon concentration increases, and approach zero at high neon concentration. We are confident, therefore, that the replacement reactions measured in well-scavenged freons are due only to hot atoms.

Hot replacement reactions may frequently deposit sufficient excitation energy in the primary product to cause its subsequent decomposition. It has been demonstrated[9a,12,13] that F for F replacement reactions are followed by extensive decomposition, amounting in some cases to 80% of the total replacement yield. The extent of decomposition following hot chlorine replacement reactions is not known, but at least some decomposition may be assumed to occur. Decomposition will compete with stabilization by collision, and product yields may consequently be sensitive to pressure. It was therefore of interest to study product yields as a function of pressure. The yields of labeled CF_2Cl_2 and $CFCl_3$ from chlorine atom reactions with CF_2Cl_2 were measured at six different pressures in the range 3 to 46 cm. Yields were found to be independent of pressure within this range. This result cannot be interpreted to mean that decomposition is not occurring. It may be that these pressures were not high enough to bring about stabilization of a significant fraction of excited primary products. However, this does demonstrate that small variations in pressure from sample to sample will not perturb the yield patterns which we observe.

The absolute per cent yields of products resulting from Cl for Cl and Cl for F replacement reactions in CF_4, CF_3Cl, CF_2Cl_2, $CFCl_3$, and CCl_4 are given in Table II. Pertinent measurements by Spicer and Wolfgang on replacement reactions in chloromethanes are included in the table to facilitate comparisons. In all cases the reaction mixture consisted of the reactant molecule, 3% $C_2H_2Cl_2$, 1% O_2, and 1% Ar. Total pressures were about 60 cm. Reactions with CF_4 were studied in approximately equal molar mixtures of CCl_4

(12) C. F. McKnight and J. W. Root, *J. Phys. Chem.*, **73**, 4430 (1969).

(13) Y. N. Tang, T. Smail, and F. S. Rowland, *J. Amer. Chem. Soc.*, **91**, 2130 (1969).

Table II: Yields of Hot Chlorine Replacement Reactions

Reactant molecule (from ref 11)	Yield, %	Reactant molecule (this work)	Yield, %
	Cl for Cl Replacement		
CH_3Cl	2.4[a]	CF_3Cl	0.73 ± 0.05
CH_2Cl_2	1.7[a]	CF_2Cl_2	1.0 ± 0.15
$CHCl_3$	0.6[a]	$CFCl_3$	1.47 ± 0.15
CCl_4	0.6[a]	CCl_4	0.28 ± 0.10
	Cl for F Replacement		
		CF_4	0.92 ± 0.10
		CF_3Cl	0.64 ± 0.05
		CF_2Cl_2	0.43 ± 0.03
CH_3F	3.5	$CFCl_3$	0.20 ± 0.05

[a] Performed at 60% moderation with argon.

and CF_4; reported yields have been corrected for the mole fraction of reactant present. The yields reported in Table II are averages of two or more runs. In all cases duplicate runs gave results within the reported error limits. Error limits were obtained from counting statistics and uncertainties in base-line subtraction.

We assume as a framework for discussion that hot chlorine replacement reactions proceed as a fast one-step process. This assumption seems to be amply justified in the case of hot tritium reactions.[1] Several factors will then control the yield pattern in a series of compounds such as the freons. These are steric effects, inertial effects, and differences in the exent of decomposition of the primary products. The various factors have been discussed in detail in ref 1 and 11. These factors define the ability of a struck molecule to adjust to the intruding atom so that capture may be effected. The more rapid the molecular vibrational and rotational motions are, then the greater should be the efficiency for a one-step replacement reaction. It follows that as the number of heavy ligands in a molecule increases, the replacement yield should decrease. This is also, of course, the trend expected for steric effects.

In this work no attempt was made to identify secondary products resulting from decomposition, and hence the total replacement reaction yields are not known. It is therefore not appropriate to make quantitative interpretations of steric and inertial factors on the basis of the data at hand. The trends in the yields, however, are interesting. It is seen from the results of Spicer and Wolfgang that Cl for Cl replacement decreases in the chloromethanes as the number of Cl atoms increases, as expected from the previous discussion. These authors point out that this decrease is probably due primarily to the steric hindrance offered by the bulky chlorine atoms. In the freon series this trend should be much less evident because differences in mass and size between fluorine and chlorine ligands are much less than between hydrogen and chlorine. In fact, the trend is reversed; Cl for Cl replacement increases as the number of Cl atoms increases until there is an abrupt decrease with CCl_4. A possible explanation for this is that there is greater energy deposition, and consequently greater decomposition, in the fluorine-rich freons. This is reasonable because the more rapid vibrational motions of the fluorine atoms should permit more efficient energy transfer from the incoming hot atom to the struck molecule. It is also consistent with the observation of McKnight, *et al.*,[14] that the high deposition energies they observe in F for F replacement reactions indicate that energy transfer must involve the concerted motion of several atoms. We suggest, therefore, that the decomposition of primary products completely masks the observations of steric and inertial effects in Cl for Cl replacement in the freons. The sudden decrease in yield for CCl_4 is probably due to the steric effect reasserting its dominance.

The yields of Cl for F replacement products follow the trend expected from steric and inertial considerations. A striking feature of this series is that the yield per fluorine atom is a constant 0.2% within experimental error. This is not observed in the replacement reactions of the chloromethanes,[10] and may only be a coincidental result. It is also interesting to note the decrease in yields for the series CH_3F, CF_4, and $CFCl_3$. This trend is undoubtedly due to the dominance of steric factors. The observation of Spicer, *et al.*,[10] that replacement of the heavier atom is favored is supported by our results; product yields of Cl for Cl replacement are uniformly higher than for Cl for F replacement.

Further work should be undertaken to measure the extent of decomposition of primary products so that the study of steric and inertial factors can be put on a quantitative basis.

Acknowledgments. We wish to thank the Nuclear Radiation Center of Washington State University for the neutron irradiations used in this investigation. We also wish to thank Dr. C. M. Wai for many helpful suggestions and discussions throughout the course of our work.

(14) C. F. McKnight, N. J. Parks, and J. W. Root, *J. Phys. Chem.*, **74**, 217 (1970).

Equivalent Conductivity of Potassium Halides in Molten Acetamide

by Richard A. Wallace

Department of Materials Science and Engineering, Stanford University, Stanford, California 94305
(Received October 7, 1970)

Publication costs borne completely by The Journal of Physical Chemistry

The equivalent conductances of potassium halides in molten acetamide have been measured over concentra-

tion ranges between 0.001 and 0.23 N at 94°. Kohlrausch plots show complete dissociation for each halide salt and give substantial agreement with the Onsager limiting equation up to about 0.02 N. The series of decreasing relative equivalent conductances in molten acetamide, KI > KBr > KCl, has the same order as that found for these halides in N-methylacetamide,[1] but differs for the bromide and iodide ions in N,N-dimethylacetamide,[2] and dimethylformamide.[3]

Experimental Section

Apparatus. Conductances were measured at 1000 cycles with a shielded Jones bridge. A standard dipping cell, with lightly platinized electrodes, which had a cell constant of 0.1055 cm^{-1} as determined by the method of Jones and Bradshaw[4] was used. All measurements were made with the cell held in a silicone oil bath which was maintained at a constant temperature within ±0.1°. The conductance cell was sealed on the side of a 500-ml conical flask closed by a ground-glass cap fitted with a side arm through which prepurified dry nitrogen was passed to prevent the admission of air into the cell when the molten acetamide solutions were added to the cell. The solutions were kept below 110° to minimize any pyrolytic decomposition in molten acetamide over prolonged periods of time.

Acetamide Solutions. 1. Solvent. Analytical grade acetamide crystals (Mallinckrodt Chemical) were further purified by recrystallization in pure benzene. The resulting solvent (mp 80.0–80.5°) had a mean specific conductance of 8.5×10^{-6} ohm^{-1} cm^{-1} at 94°.

2. Halides. Analytical grade KI, KBr, and KCl (Mallinckrodt Chemical) were recrystallized from distilled water and fused.

Results and Discussion

Corresponding values of the equivalent conductance, ohm^{-1} cm^2 $equiv^{-1}$, and concentration, equiv/l., are presented in Table I. All conductances were corrected by subtracting the conductance of pure acetamide from that of the solutions. Λ_0 values were obtained by extrapolating Kohlrausch plots, Λ *vs.* $\sqrt{c}$, to infinite dilution for each halide. Figure 1 shows that each plot was linear within the experimental concentration range up to about 0.2 N.

The Onsager equation[5] for a uniunivalent electrolyte is

$$\Lambda = \Lambda_0 - \left[\frac{82.42}{(DT)^{1/2}\eta} + \Lambda_0\frac{8.204 \times 10^5}{(DT)^{3/2}}\right]\sqrt{c} \quad (1)$$

Substitution of the proper numerical values listed in Table II for the dielectric constant, the viscosity, and the absolute temperature into eq 1 yields the following equation for dilute solutions of electrolytes in molten acetamide at 94°

$$\Lambda = \Lambda_0 - [33.93 + 0.247\Lambda_0]\sqrt{c} \quad (2)$$

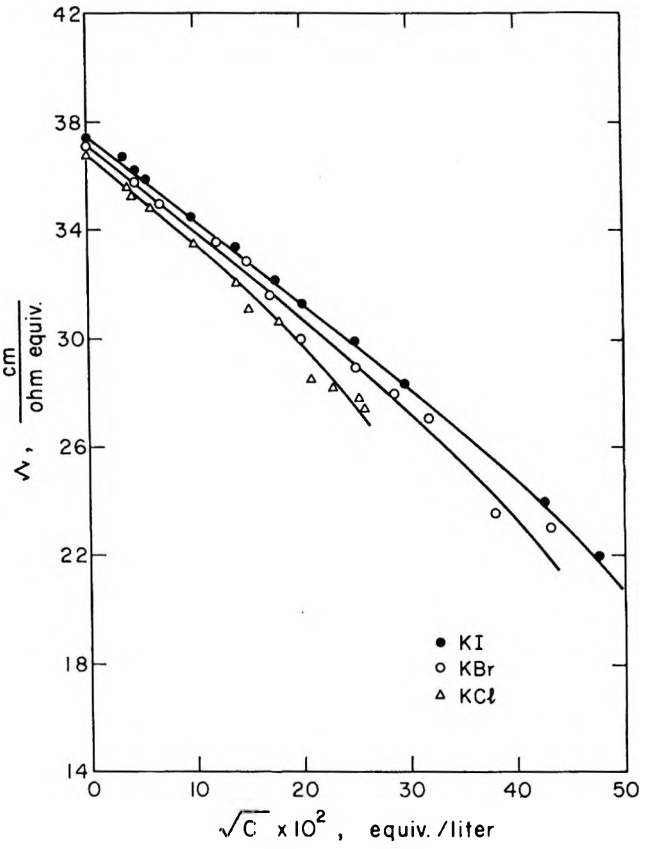

Figure 1. Equivalent conductance curves for potassium halides in molten acetamide at 94°. Experimental data fitted by least squares.

Table I: Equivalent Conductance of Potassium Halide Salts in Molten Acetamide at 94°

KI		KBr		KCl	
$C \times 10^4$, equiv $l.^{-1}$	Λ, ohm^{-1} cm^2 $equiv^{-1}$	$C \times 10^4$, equiv $l.^{-1}$	Λ, ohm^{-1} cm^2 $equiv^{-1}$	$C \times 10^4$, equiv $l.^{-1}$	Λ, ohm^{-1} cm^2 $equiv^{-1}$
2250	22.0	1890	23.0	655	27.4
1825	24.0	1450	23.5	635	27.7
870	28.3	1020	26.9	552	28.1
625	29.5	822	27.9	441	28.5
400	31.4	576	28.8	324	30.7
302	32.1	400	30.0	225	31.1
196	33.4	292	31.6	190	32.2
92.3	34.5	225	32.8	101	33.5
29.2	35.8	144	33.5	36.0	34.8
19.5	36.3	49.0	35.0	21.5	35.2
11.0	36.7	22.5	35.9	19.6	35.5
0.0	(37.4)	0.0	(37.1)	0.0	(36.8)

(1) L. R. Dawson, P. B. Sears, and R. H. Graves, *J. Amer. Chem. Soc.*, **77**, 1986 (1955).

(2) G. R. Lester, T. A. Glover, and P. G. Sears, *J. Phys. Chem.*, **60**, 1076 (1956).

(3) J. E. Prue and P. J. Sherrington, *Trans. Faraday Soc.*, **57**, 1795 (1961).

(4) G. Jones and B. C. Bradshaw, *J. Amer. Chem. Soc.*, **55**, 1780 (1933).

(5) L. Onsager, *Phys. Z.*, **28**, 277 (1927).

Table II: Physical Properties of Molten Acetamide

Temp, °C	Density, g/ml	Viscosity, P	Dielectric constant
86	0.990	0.0194	62.5
94	0.986	0.0163	60.6
105	0.980	0.0132	56.3

Compared with the theoretical slope of eq 2, $-[33.93 + 0.247\Lambda_0]$, less negative slopes (positive deviations) were observed indicating virtually complete absence of ion association. The large positive deviations from the Onsager limiting law may be accounted for by considering the extended conductance equation of Fuoss and Onsager.[6,7] This conductance equation predicts a positive deviation in our dilute concentration range caused by $c \ln c$ and c terms in their conductance function for 1:1 electrolytes in solvents of high dielectric constant above 30. Use of this extended conductance equation gives slopes for dilute potassium halide salts in acetamide which are in much closer agreement (within 10%) with the experimental slopes as shown in Figure 1.

Our viscosity measurements of KCl–acetamide and KBr–acetamide solutions at 94° showed that the bulk viscosity increased linearly with added KCl and KBr concentrations up to 0.3 *N*. No reduced viscosity or an acetamide depolymerization effect was detected. These experimental results indicate that the observed Onsager deviations cannot be explained using the assumptions of a locally reduced viscosity or any depolymerization action caused by potassium halide salts in molten acetamide.

At high potassium halide concentrations, the conductance against $\sqrt{c}$ curves in Figure 1 are all found to be slightly concave to the concentration axis. Ion-pair formation has probably occurred at these higher concentrations. It is well to point out that French and Glover[8] also reported a similar concavity to the concentration axis for *N*-methylacetamide at concentrations higher than 0.05 *N*. French and Glover[8] attributed this phenomenon to ion-pair formation. This ion-association effect illustrates again the similarity between molten acetamide and *N*-methylacetamide.

No reliable conductance data for dilute KBr and KCl acetamide solutions have been found in the literature. The equivalent conductance values for all KI–acetamide solutions are slightly higher than the corresponding values of Jander and Winkler,[9] who determined $\Lambda_0 = 36.5$ ohm^{-1} cm^2 equiv^{-1} for KI in molten acetamide at 94°. One source of error in conductance measurements is the presence of small amounts of water in acetamide solvent and solutions. Contamination of water in molten acetamide increases its residual conductance partly because of an increase in acetamide self-dissociation, given by eq 3, and partly because of a small decrease in viscosity.

$$2CH_3CONH_2 \rightleftharpoons [CH_3CONH_3]^+ + [CH_3CONH]^- \quad (3)$$

The series of decreasing relative equivalent conductances in molten acetamide KI > KBr > KCl has the same relationship as that found for these halides in *N*-methylacetamide.[1] However, published data[2,3] indicate that the iodide ion is less mobile than the bromide ion in dimethylformamide and *N*,*N*-dimethylacetamide. For example, Λ_0 KBr is 84.1 and Λ_0 KI is 82.6 in dimethylformamide at 25°. Similarly, Λ_0 KBr is 68.4 and Λ_0 KI is 67.0 in *N*,*N*-dimethylacetamide at 25°. It is suggested that each of these two solvents acts as a Lewis base in donating a pair of electrons to the iodide ion which behaves as a Lewis acid. It is possible that this acid–base interaction accounts for the decreased mobility of the iodide ion. A similar explanation was reported by Dawson[10] to account for the lower limiting equivalent conductance of potassium iodide relative to potassium bromide in dimethylformamide.

To what degree both potassium and halide ions in molten acetamide become solvated is uncertain; however, the fact that the halides are readily soluble[11] and the high[12] dipole moment (3.7 D) of the organic solvent may be considered as evidence of considerable solute–solvent interaction. Owing to solvation effects, the relative effective sizes of the solute ions in molten acetamide apparently are reversed with respect to the naked ions.

Table III presents the computed Walden products for potassium halides in molten acetamide at 94°. For comparison, the Walden product of KBr in *N*-methylacetamide is 0.613 at 35° and 0.608 at 45°.[8] Both of these organic solvents have high dipole moments which tend to promote solvation of salts.

From these results and others,[8,11] it is concluded that molten acetamide is a good electrolytic solvent,

Table III: Walden Products ($\Lambda_0\eta$) in Molten Acetamide at 94°

P-cm²/ohm-equiv		
KCl	KBr	KI
0.609	0.604	0.599

(6) R. M. Fuoss and F. Accascina, "Electrolytic Conductance," Interscience, New York, N. Y., 1959, Chapter XV, p 198.

(7) R. M. Fuoss, L. Onsager, and J. F. Skinner, *J. Phys. Chem.*, **69**, 2581 (1965).

(8) C. M. French and K. H. Glover, *Trans. Faraday Soc.*, **51**, 1427 (1955).

(9) G. Jander and G. Winkler, *J. Inorg. Nucl. Chem.*, **9**, 24 (1959).

(10) L. R. Dawson, in "Chemistry in Nonaqueous Ionizing Solvents," Vol. IV, G. Jander, H. Spandow, and C. C. Addison, Eds., Friedr. Vieweg und Sohn, Braunschweig, Germany, 1963, Part 3, p 281.

(11) R. A. Wallace and P. F. Bruins, *J. Electrochem. Soc.*, **114** (3), 209 (1967).

(12) J. W. Stout and L. H. Fischer, *J. Chem. Phys.*, **9**, 163 (1941).

strikingly similar to *N*-methylacetamide in its dissociating powers on electrolytes. Potassium halides are fully dissociated in dilute acetamide solutions. The series of increasing relative equivalent conductances KCl < KBr < KI indicates that KCl is the least mobile and hence the most highly solvated of the three halides.

Acknowledgments. This work was supported in part by the U. S. Air Force Office of Scientific Research, Grant AF-AFOSR 68-1360, by the Stanford University Center for Materials Research, and by the Office of Naval Research.

Effect of Propanol Upon the Absorption and Emission of Benzquinolines[1] in 3-Methylpentane

by John L. Kropp* and Jeffrey J. Lou

Systems Group of TRW Inc., Redondo Beach, California 90278
(Received February 1, 1971)

Publication costs assisted by the Systems Group of TRW

Recently we have reported the effect of added propanol upon the (π,π^*) fluorescence, phosphorescence, and T–T absorption of 1,2:5,6-dibenzacridine and 1,2:7,8-dibenzacridine in 3-methylpentane solution at 77°K and at room temperature.[2] The latter compound showed shifts in fluorescence spectra and large changes in the intensity of fluorescence, phosphorescence, and T–T absorption with the addition of propanol while the former showed little change in these properties even at propanol volumes up to 20% v/v. We attributed the difference in behavior to H bonding with a shift in ($n-\pi^*$) levels in the case of 1,2:7,8-dibenzacridine but not in the case of 1,2:5,6-dibenzacridine. However, no measurements of the strength of H bonding nor determinations of the energy of the lowest $^1(n,\pi^*)$ or $^3(n,\pi^*)$ levels are known to us for these two compounds.

The benzquinolines are a similar series of heterocyclics for which H-bond energies have been measured[3] and the energy of the lowest $^1(n,\pi^*)$ has been determined experimentally and calculated theoretically.[4]

There are three benzquinoline isomers, 3,4-benzquinoline (I), 5,6-benzquinoline (II), and 7,8-benzquinoline (III), that are derived from a common hydrocarbon, phenanthrene (IV).

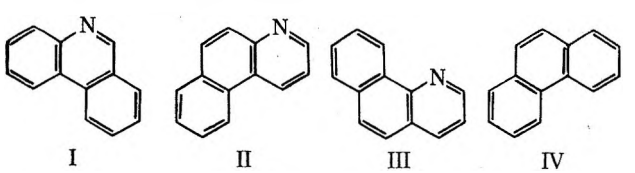

I II III IV

In this note we report the variation of fluorescence, phosphorescence, and T–T absorption intensities as propanol is added to 3-methylpentane (MP) solutions of these compounds.

The benzquinolines were obtained from Aldrich Chemical and were recrystallized before use. The absorption spectra of these purified compounds in ethanol or in hexane agreed with the published values[5] in the band position and extinction coefficient. Such agreement was used as a measure of spectroscopic purity. Solutions were prepared and measurements made in the same way as previously described.[2]

Results

We measured the absorption fluorescence and phosphorescence spectra of I, II, and III in pure MP and in various propanol–MP mixtures both at room temperature (23°) and at −196°. The values at −196° are given in Table I. The absorption spectra for II and III have been reported by Kanda and Shimada (KS)[6] in hexane and in ethanol at 20° and by Perkampus and Kortüm[7] (PK) in heptane. Our spectra in MP are in close agreement to the hexane spectra reported by KS and in heptane by PK. For all three benzoquinolines studied, the absorption at −196° shows a shift as propanol is added to the MP glass. Addition of propanol always shifts the spectrum to the red and the observed shift for 20% propanol solution relative to MP is about 300 cm^{-1} for I, II, or III. In contrast, at 23° the shift for I is about 200 cm^{-1} for propanol solutions of I, but only about 100 cm^{-1} for II and no shift for solutions of III.

Fluorescence spectra were measured at 23° and −196°. The wavelength structures of fluorescence spectra in MP are in agreement with those in heptane solution reported by PK. The fluorescence spectra in MP recorded at −196° are similar in wavelength distribution as those observed at 23°. However, all spectra shift uniformly to the red by about 300 cm^{-1} as propanol is added. This shift in energy is the same as observed in absorption spectra. Both shifts are attributable to H bonding of the particular benzquinoline with propanol.

The fluorescence yields (Φ_F) were determined for the benzquinolines at 23°. The values of Φ_F increase sharply as propanol is added at room temperature. A typical plot of fluorescence yield as a function of pro-

(1) Work supported under Contract AF 33615-69-C-1052 and ONR Contract N00014-67-C-0327.

(2) J. L. Kropp and J. J. Lou, *J. Phys. Chem.*, **74**, 3953 (1970).

(3) N. G. Coppens, J. Nasielski, and N. Sprecher, *Bull. Soc. Chim. Belg.*, **72**, 626 (1963).

(4) N. G. Coppens, C. Gillet, J. Nasielski, and E. Vanderdonct, *Spectrochim. Acta*, **18**, 1441 (1962).

(5) "U. V. Atlas of Organic Compounds," Plenum Press, New York, N. Y., 1966.

(6) Y. Kanda and R. Shimada, *Spectrochim. Acta*, **15**, 211 (1959).

(7) H. H. Perkampus and K. Kortüm, *Z. Phys. Chem. (Frankfurt am Main)*, **56**, 73 (1967).

Table I: Absorption, Fluorescence, and Phosphorescence Spectra of Benzquinolines at −196°

Compd	Absorption, cm⁻¹		Fluorescence, cm⁻¹		Phosphorescence, cm⁻¹	
3,4-Benzquinoline	29,160[a] (7.2)[c]	28,820[b]	29,160[a]	28,820[b]	21,740[a]	21,790[b]
	29,675 (2.6)	29,370	28,660		21,320	21,370
	29,805 (2.6)		28,410	28,170	20,940	21,505
	30,480 (6.7)	30,210	27,700	27,400	20,325	
	31,010 (3.4)	30,770	27,180	26,810	20,120	20,200
	31,150 (3.4)		26,660	26,040	19,760	19,800
	31,840 (5.0)	31,550		24,360	19,340	
					18,800	18,870
					18,550	
5,6-Benzquinoline	29,030 (13.5)	28,740	29,070	28,650	21,930	21,830
	29,410 (3.9)		28,650		21,530	21,410
	29,670 (5.4)	29,460	28,330	28,010	21,120	20,010
	30,000 (4.2)		27,970		20,580	20,490
	30,400 (11.0)	30,210	27,660	27,170	20,370	20,280
	30,820 (5.0)		26,950		19,980	19,860
	31,100 (6.0)	30,960	26,670		19,610	19,490
	31,800 (7.5)	31,540	26,320	25,970	19,230	
			24,940	24,690	19,010	18,900
			23,360		18,760	
7,8-Benzquinoline	28,940 (16.0)	28,650	29,800	28,570	21,740	21,830
	29,325 (4.9)		28,490		21,320	21,390
	29,680 (5.9)	29,325	28,250	27,930	20,940	21,050
	29,985 (4.6)		27,540	27,250	20,325	20,200
	30,350 (13.0)	30,000	26,840	26,660	20,120	
	30,760 (5.5)		26,100	25,830	19,760	19,800
	31,060 (5.9)		25,640		19,340	19,420
	31,350 (5.2)		24,750	24,510	18,800	18,870
					18,550	

[a] In pure 3-methylpentane. [b] In 3-methylpentane + 20% propanol. [c] Extinction coefficient; 3-methylpentane; the extinction coefficients in the mixed solvent are approximately the same.

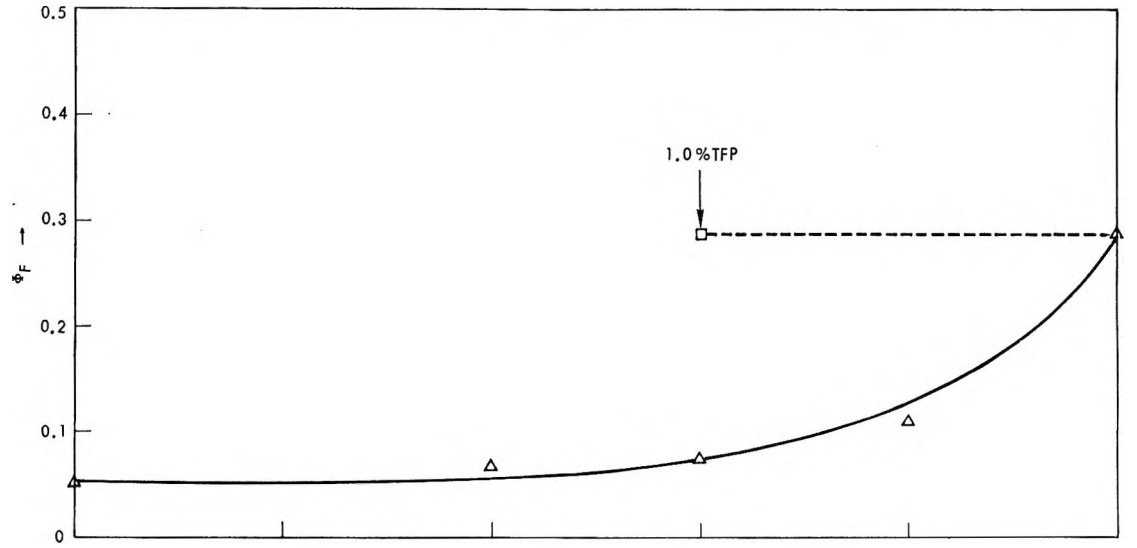

Figure 1. The fluorescence yield of 5,6-benzquinoline in 3-methylpentane solution at 23° as a function of added propanol.

panol concentration at 23° is given for II in Figure 1. The general features shown in Figure 1 are the same for all three isomers. For I the yield varies from 0.005 in MP to 0.175 in propanol, for II (Figure 1) from 0.05 to 0.30, and for III from 0.09 to 0.36. Figure 1 also shows the yield of 0.30 observed for II when 1% TFP (tetrafluoropropanol) is added to a pure MP solution. Corresponding yields of 1% TFP for I and III are 0.26 and 0.32. TFP is a very strong H-bonding substance and the high yield at 1% TFP indicates that at room

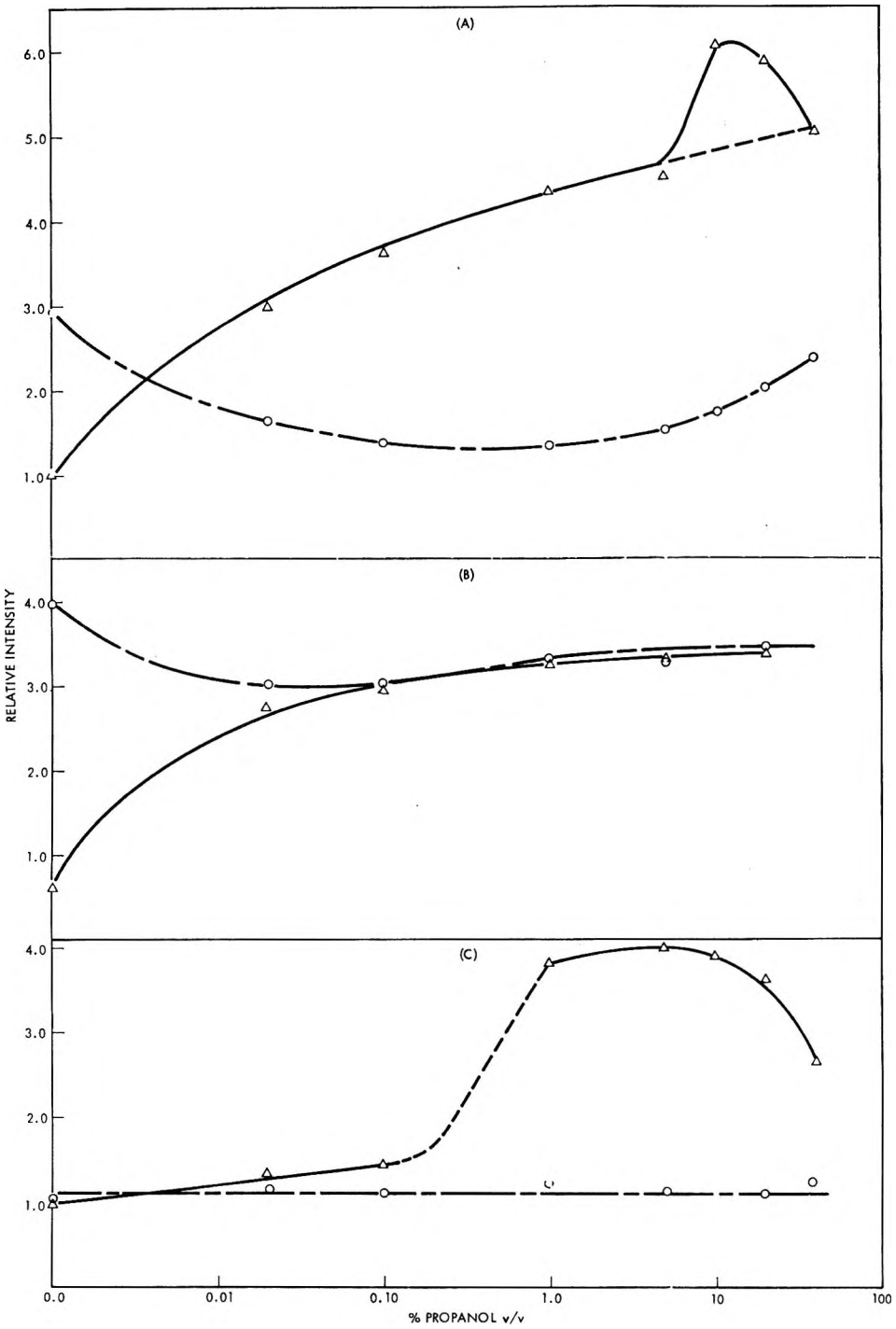

Figure 2. Fluorescence (——) and phosphorescence (— - —) intensities of 3,4-benzquinoline (A), 5,6-benzquinoline (B), and 7,8-benzquinoline (C) in 3-methylpentane at −196° as a function of added propanol.

temperature H-bonding is largely responsible for the increase in yield observed in propanol solutions.

Values of Φ_F were not measured at −196°. The fluorescence (F) an dphosphorescence (P) intensities at −196° for the three compounds studied are given in Figure 2. The relative intensities are corrected for phototube response. These curves show that for I and II the initial value of P is greater than F but that small quantities of propanol (0.1% v/v) decrease P while increasing F. However, for III the values of P and F are similar in pure MP. With increasing propanol concentrations P remains constant while F increases slowly up to 0.1% propanol.

The phosphorescence lifetimes (τ_p) in MP are 0.8, 2.4, and 1.75 sec for I, II, and III, respectively; in solutions containing any propanol (from 0.01 to 20%) these values increase to 1.1, 2.8, and 1.9 sec, respectively. Lim and Yu[8] have measured τ_p for II and III and our values are in fair agreement with theirs.

(8) E. C. Lim and J. M. H. Yu, *J. Chem. Phys.*, **47**, 3270 (1967).

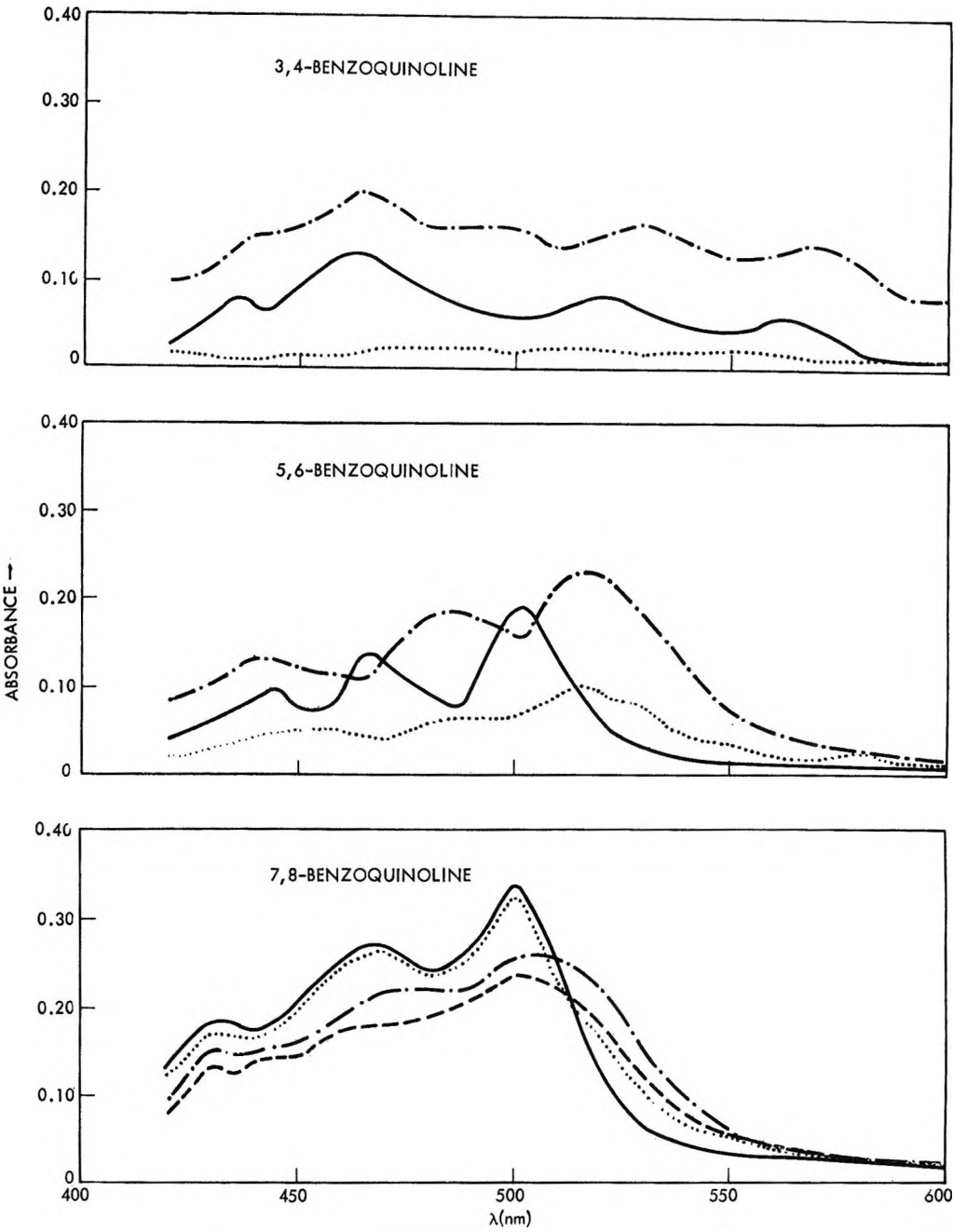

Figure 3. T-T absorption spectra of 3,4-benzquinoline, 5,6-benzquinoline, and 7,8-benzquinoline in MP glass at −196° as a function of propanol concentration: ——, 0% propanol; ····, 0.1% propanol; - - - - -, 1% propanol; — — — —, 20% propanol.

The T–T absorption of the three benzquinolines shows a dependence upon glass composition at −196°. For compounds I and II the T–T absorption decreases at low propanol concentrations just as is observed for P at low propanol concentrations; above 1% it increases again in intensity. However, for III there is little change in the total amount of T–T absorption. Figure 3 shows the results for typical propanol concentrations. Craig and Ross[9] have measured the T–T absorption for II and III. They reported that the absorption in a mixture of isopentane–methylcyclohexane was much weaker than in EPA. We observe that the intensity in MP is about as high (or higher) as that in 20% propanol solution. In fact, for II the intensity in pure MP is much higher than in MP solutions with up to 0.1% propanol. We have reproduced this measurement several times and are certain that the MP glass is not "wet." We also find no evidence of decomposition following a measurement of the T–T absorption as indicated by the absence of changes in absorption spectrum and the reproducibility of T–T absorption.

Discussion

The H-bond energies at room temperature for the benzquinoline–propanol complex in hexane have been

(9) D. P. Craig and I. G. Ross, *J. Chem. Soc.* (*London*), 1589 (1961).

determined as 4.7, 4.7, and 1.6 kcal/mol for I, II, and III, respectively.[3] The measured increases in Φ_F by factors of 35 for I and 6 and 4 for II and III show that while the efficiencies of H bonding are similar for I and II the enhancement of fluorescence yield by H bonding is far greater for I than either II or III. At −196° both I and II show a sharp increase in fluorescence and decrease in P and T–T absorption intensities at low propanol concentrations, but the magnitude of this effect is much greater for I than II. Thus an additional factor besides H bonding must contribute to give the effects we observe.

Lim and Yu[8] have shown that upper (n,π^*) states either triplet or singlet perturb the phosphorescence emission. Since H bonding raises the (n,π^*) levels much more than singlets, the relative interactions should be changed. Thus the H-bond strength and the strength of the (n,π^*) interaction should couple to perturb singlet and triplet state properties in hydroxylic solvents. Lim and Yu showed that either of two mechanisms could be operative. (1) The emitting $^1(\pi,\pi^*)$ state is coupled with the $^1(n,\pi^*)$ by vibrational coupling. In turn, the $^1(n,\pi^*)$ state is spin–orbit coupled to the lowest $^3(\pi,\pi^*)$ state. (2) The $^1(\pi,\pi^*)$ level is spin–orbit coupled to a $^3(n,\pi^*)$ level which is coupled to the $^3(\pi,\pi^*)$ emitting level. The positions of $^3(n,\pi^*)$ states intermediate in energy between the fluorescent $^1(\pi,\pi^*)$ level and the phosphorescent $^3(\pi,\pi^*)$ level are not known. The energy of the lowest $^1(n,\pi^*)$ level has been determined indirectly by Coppens, *et al.*[4] The lowest $^1(n,\pi^*)$ band in these compounds has been estimated to be 327 nm for I and II and 314 nm for III. Theoretically these authors calculate the energies to be 327 nm for I; 319 nm for II; and 314 nm for III.

Mechanism (1) of Lim and Yu seems to best fit our results. This follows from the fact that P and T–T absorption intensities decrease at very small propanol concentrations. If the $^1(n,\pi^*)$ state is responsible for the main interaction, then H bonding decreases the interaction energy decreasing the amount of triplet formation. However, if the main transfer process occurs *via* the $^3(n,\pi^*)$ we expect the intensity of P and T–T absorption to be increased at low propanol concentrations. (This is observed in our previous work for 1,2:7,8-dibenzacridine[2].) Thus, unless the $^3(n,\pi^*)$ level is fortuitously just lower in energy than the emitting $^1(\pi,\pi^*)$ level our data favor an interaction involving the $^1(n,\pi^*)$ level.

The interactions we observe can be understood in terms of both H bonding and the position of the $^1(n,\pi^*)$ level. For III there is a low H-bonding probability and the energy gap between the fluorescent level at 350 nm and the $^1(n,\pi^*)$ level at 314 nm is 3200 cm^{-1} while for I and II it is 2000 cm^{-1} and either 2000 or 2600 cm^{-1}. All of our data point to the fact that interaction is greater for I than for II.

Lim and Yu[8] also found that the degree of polarization of phosphorescence of I changed to a much larger degree than did that of II, indicating a much larger degree of vibronic spin–orbit interaction in I. These data all tend to show better agreement with the theoretical value of $^1(n,\pi^*)$ for II found by Coppens, *et al.*,[3] rather than the experimental value.

Significant changes occur in F and in T–T absorption at propanol concentrations above 1% at −196°. These seem to be due to a change in the structure of the glassy matrix. We have suggested this elsewhere[2] and it seems to be a general occurrence in most heterocyclics we have studied. The shifts in the T–T absorption spectrum of III can be attributed to the same effect. The shift in the T–T absorption of II occurs at too low a propanol concentration to be attributable to a change in glass composition. Also, the shift in phosphorescence is 100 cm^{-1} to lower energies compared with a 400-cm^{-1} shift in T–T absorption. The conclusion seems to be that the upper absorbing triplet level is itself shifted by the H bonding and it may be influenced by an $(n-\pi^*)$ level.

The Equilibrium Rate of Exchange of Water Molecules at the Air–Water Interface Using Nuclear Magnetic Resonance Spectroscopy

by Dinesh O. Shah

Departments of Chemical Engineering and Anesthesiology, University of Florida, Gainesville, Florida 32601
(Received February 12, 1971)

Publication costs borne completely by The Journal of Physical Chemistry

When water and its vapor are in equilibrium, the number of molecules leaving the water surface is the same as the number entering the water surface from the vapor. As a result, there is no net change in the number of molecules either in the vapor or in the liquid phase. In this study the equilibrium rate of exchange of water molecules at the air–water interface has been determined using nuclear magnetic resonance (nmr) spectroscopy. In nmr spectra, H_2O shows a resonance signal at τ 4.8 (ppm) with respect to external TMS, whereas D_2O does not.[1] Moreover, the area under a resonance peak is proportional to the number of protons present in the sample. Therefore, one can determine quantitatively the amount of H_2O present in D_2O.

Figure 1 schematically shows the experimental arrangement used to measure the rate of exchange of water molecules at the interface. A large glass tank (12-in. diameter; 12-in. height), containing water and an

(1) H. Inoue and T. Nakagawa, *J. Phys. Chem.*, **70**, 1108 (1966).

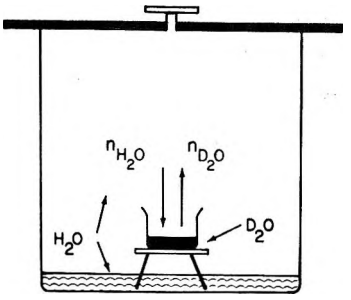

EQUILIBRIUM RATE of EXCHANGE of WATER MOLECULES AT THE AIR-WATER INTERFACE

Figure 1. A schematic diagram showing the experimental arrangement to measure the equilibrium rate of exchange of water molecules at the interface.

empty 50-ml capacity beaker placed on a stand, was kept covered for a period of 2–3 days to achieve equilibrium conditions between the water and its vapor at 25 ± 0.5°. D_2O (2 ml) (purity ≈ 99.8%) was delivered by a pipet through a hole in the cover to the beaker. In the actual experiment seven empty beakers were placed in the glass tank. The content of each beaker was taken out after a specific time interval (0, 5, 10, 15, 20, 40, or 60 min) and transferred to an nmr sample tube. The area under the water resonance peak in the nmr spectra increased with time, indicating the increase in water content of D_2O (Figure 2). The results were reproducible within ±5%, which essentially depended upon the reproducibility of the integrator of the nmr spectrometer. The inset in Figure 2 is a calibration plot of the area under the water peak and the volume per cent of H_2O in D_2O. The slope of the calibration plot indicates an increase of 11 units of area for each volume per cent of H_2O added in D_2O. The slope of the area under water peak *vs.* time plot gives an increase of 19.2 units of area per hour, which corresponds to 1.745 vol % H_2O in D_2O. Since the original amount of D_2O was 2 ml, its 1.745 vol % corresponds to 34.9 mg of H_2O. Hence, this suggests that the net amount of H_2O that entered the D_2O from vapor phase in 1 hr was 34.9 mg. Since the cross-sectional area of the beaker was 11.339 cm^2, *the net amount of H_2O exchanged per cm^2 per hour at equilibrium was 3.07 mg.*

The only assumption involved here is that, at equilibrium, the rate of exchange of molecules at the water vapor–water interface is the same as that at the water vapor–D_2O interface. This seems valid in view of the fact that both H_2O and D_2O have approximately the same surface tension, *i.e.*, 72.75 dyn/cm for H_2O and 72.80 dyn/cm for D_2O.[2] This suggests that molecules at the surface experience the same cohesive force in both liquids. It should be pointed out that the present experiment measures only the net number of H_2O molecules that enter and remain into D_2O liquid from the vapor phase as a result of exchange of molecules at the air–water interface when water vapor is at its equilibrium concentration, and does not measure the total number of molecules striking the interface from vapor phase or the number of molecules leaving the liquid phase. The rate of exchange of water molecules at the air–water interface at equilibrium (3.07 mg/cm^2 hr) determined in this work is much smaller than the rate of evaporation of water (30–72 mg/cm^2 hr depending upon the distance between the desiccant and the interface) observed in our own laboratory as well as by other investigators.[3] In the evaporation measurements a desiccant is suspended close to the water surface, which causes a gradient of partial pressures, and hence a faster rate of transport occurs. In equilibrium conditions, there is no such gradient involved. It is evident that the diffusion resistance of the boundary layer will decrease in the presence of a desiccant near the interface as compared with that in the equilibrium conditions. Therefore, the conditions at the interface would be strikingly different during evaporation as compared with those at equilibrium.

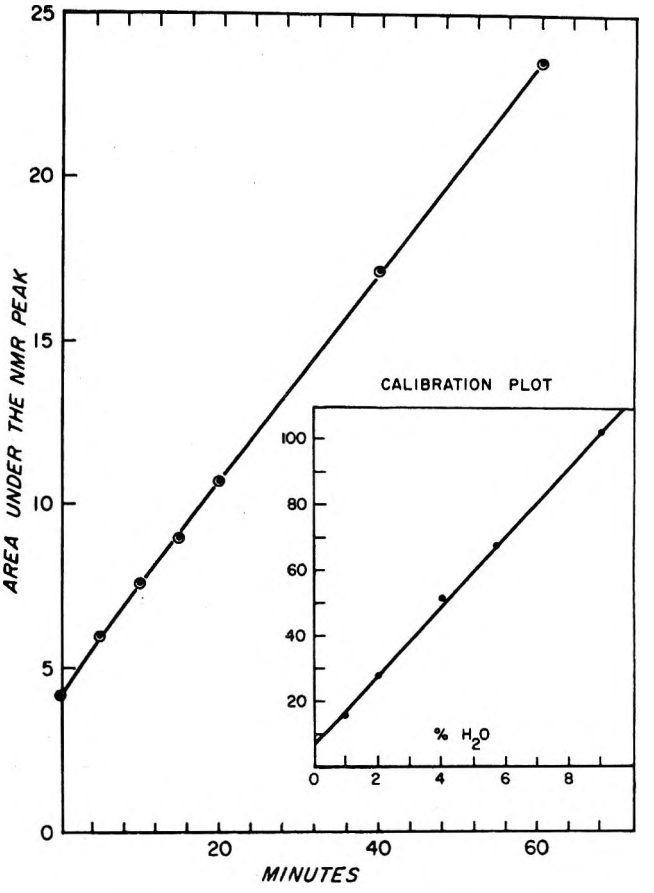

Figure 2. The plot of area under the water peak in the nmr spectra of D_2O from the beaker *vs.* time: *inset*, a calibration plot for the area under the water peak *vs.* volume per cent of H_2O added to D_2O.

(2) W. J. Moore, "Physical Chemistry," 3rd ed, Prentice-Hall, Englewood Cliffs, N. J., 1962, pp 453 and 229.

(3) R. J. Archer and V. K. La Mer, *Ann. N. Y. Acad. Sci.*, 58, 807 (1954).

For the exchange of molecules across the interface, one could conceptually consider that in half of the surface area the molecules go from the vapor to the liquid and in the other half from the liquid to the vapor phase. Therefore, it can be considered that in a 1-cm² area at the interface, 3.07 mg of H_2O molecules go into D_2O through a 0.5-cm² area, and from the other 0.5 cm² the same number of D_2O molecules goes to the vapor phase. In order to calculate the number of water molecules coming out of the interface from an area equal to that of a water molecule, we have to first determine the number of water molecules that can be accommodated in 0.5 cm² of area at the interface. Dividing the number of molecules that comes out of 0.5 cm² of the interface per second by the number that can be accommodated in 0.5 cm² gives the number of molecules that will come out of the area equal to that of a water molecule per second. Let us consider the number of H_2O molecules that can be accommodated in a 1-cm² area of the interface. Using the density of water at 25° (0.997 g/ml) and the Avogadro number, the number of H_2O molecules in 1 ml is found to be 0.337×10^{23}. The average thickness of the first layer of water molecules at the interface can be assumed to be 2.88 Å calculated[2] from van der Waals constant b or from measuring dimensions of scaled space-filling Fisher–Taylor–Hirschfelder molecular models in various orientations. The number of H_2O molecules present in a layer of 1 cm² area and 2.88 Å thickness was found to be 0.96×10^{15}. Therefore, the number of molecules in 0.5 cm² of the interface is 0.48×10^{15}. The average number of molecules that will come out of an area equal to that of a water molecule per second will be 2.8544×10^{16} (*i.e.*, the number of molecules leaving 0.5 cm² of area at the interface per second) divided by 0.48×10^{15}. This number is found to be 59.46. *This suggests that about 60 molecules per second escape from the interface from an area equal to that of a water molecule and hence the average residence time of a water molecule at the interface will be $^1/_{60}$th of a second.* Thus, the escape of water molecules from the liquid to the vapor phase seems to be a slow process as compared with other molecular processes. This may be related to the high surface tension of water (≈72 dyn/cm). In organic liquids having low surface tension, this process may be considerably more rapid. Theoretical calculations on the number of H_2O molecules striking the interface from the vapor phase and those entering into the liquid have been reported elsewhere.[4]

In summary, the present paper reports, using nmr spectroscopy, that the molecular exchange at equilibrium is a relatively slow process and that 3.07 mg of water is exchanged at the interface in equilibrium per cm² per hr at 25°, which corresponds to 60 water molecules leaving (or entering) the interface per second from an area equal to that of a water molecule.

Acknowledgment. I thank Professors R. D. Walker, J. P. O'Connell, J. H. Modell, and Dr. G. M. Sharma for their stimulating discussions and suggestions on this note. This work was supported in part by grant WP-15080 from the Federal Water Quality Administration and in part by funds from the Departments of Anesthesiology and Chemical Engineering of the University of Florida.

(4) D. O. Shah, Proceedings of 70th AIChE National Meeting, 1971, p 24.

Formation of Diamond. V. The Substitution of Nitrogen-15 for Nitrogen-14 in Diamond

by P. Cannon[1]

General Electric Research and Development Center, Schenectady, New York *(Received June 29, 1970)*

Publication costs assisted by the General Electric Co.

Comparison of defects and impurities in natural and synthetic diamond has attracted attention,[2] not only for the insights such study might afford on the origin of natural material but also for its value in understanding the mechanical properties of the crystals.

The theoretical work and studies of the peculiarities of spectra of particular natural crystals have proceeded further than the search for experimental generality. A difficulty occurs in the search for charged centers other than nitrogen, because the nitrogen display in spin resonance spectra includes a central line at $g = 2.002$ which would obscure the spectrum of trapped electrons if they were present. Experiments which might avoid this difficulty include: (1) compensation of the spin-active nitrogen with for example boron or aluminum; (2) study of the synthetic diamond formed in the absence of a catalyst in the hope that the concentration of nitrogen would be different; and (3) supposing the nitrogen to be chemically necessary to the nucleation of the diamond, study of diamonds synthesized in the presence of ^{15}N, which has a different nuclear spin and hence a different spin resonance spectrum (two esr lines symmetrically about $g = 2$).

Experiments of the first type have been done but have given no useful information, perhaps because the conditions needed for boron and aluminum diffusion also permit the out-diffusion of trapped electrons. The experimental challenge remaining is twofold: first,

(1) General Electric Co., West Lynn, Mass. 01905.

(2) See for example (a) W. V. Smith, P. P. Sorokin, P. L. Gelles, and G. T. Lasher, *Phys. Rev.*, **115**, 1546 (1959); (b) R. M. Deming, *Amer. Mineral.*, **46**, 740 (1961); (c) C. M. Huggins and P. Cannon, *Nature*, **194**, 829 (1962); (d) R. J. Cook and D. H. Whiffen, *Proc. Roy. Soc., Ser. A*, **295**, 99 (1966); (e) R. P. Messmer and G. D. Watkins, *Phys. Rev. Lett.*, **25**, 656 (1970).

can we demonstrate qualitative changes in the spin resonance spectrum by synthesizing diamond in the presence of ^{15}N, and, secondly, can we thus show the presence of defects other than nitrogen and open a way for further research?

Experimental Section

"Direct transition" diamond was prepared[3] by Bundy for the esr experiments. The conditions of preparation were 3300°, 130 kbars for a few milliseconds. Starting materials were spectroscopic graphite and a sample of the same material containing 0.1% of 99.8% pure boron. Samples of the diamond dust recovered from these experiments released iodine from iodoform during density measurements. Esr spectra were measured on milligram-sized samples of the dust.

Spectra obtained showed a broad absorption, 200 G wide, centered near $g = 2$ for the undoped specimen, and a single narrower line (~100 G wide or less) for the B-doped specimen. No resonance display characteristic of nitrogen was seen, though it must be remembered that the 200-G-wide absorption was broad enough to contain the entire ^{14}N triplet. The difficulties of working with the small quantities of this material led us back to the catalyzed synthesis method.

The bulk of the nitrogen in synthetic catalyzed diamonds derives from air gases adsorbed on the starting graphite. Starting mixes containing approximately 10^{19} N atoms/cc gave good yields of diamond containing 10^{20} N atoms/cc (analyses by vacuum fusion). Conversely, carefully degassed graphite (2700°, 1 hr, 10^{-7} Torr, cooled in argon) gave poor yields, as also did very high surface area graphitic carbons with starting nitrogen concentrations well over 10^{20} atoms/cc.

Control of the starting nitrogen concentration was finally achieved using nitrided catalyst powder and evacuated graphite. The conventional technique of nitriding metals by decomposing ammonia thereon was employed. Nickel was nitrided in the presence of 5 mm of ammonia for 24 hr at 600°. Poor but reproducible yields were obtained using Ni, Co, 1Ni–2Mn, and 1Co–2Mn catalyst compositions, all mixes having approximate nitrogen concentrations of 5×10^{20} atoms/cc. Similar experiments were done using isotopically tagged $^{15}NH_3$ (96+%). The metal catalyst and graphite assemblies were transformed into diamond in indirectly heated cells[4] at 1500°, 60 kbars.

The small yields of monocrystalline diamond were cleaned and examined qualitatively by esr spectroscopy. Slowly grown monocrystals prepared using an iron catalyst were kindly loaned by H. M. Strong for comparative purposes.

Regular commercial, quickly grown material[5] and the slowly grown monocrystals from iron-catalyzed systems are compared in dispersion mode esr spectra in Figure 1, while V-mode spectra for regular material and ^{15}N-nitride catalyzed material are shown in Figure 2. Obvious qualitative differences exist in these spectra. These include the single line X superposed on the central ^{14}N resonance in the slowly grown Fe-catalyzed specimen (Figure 1), and the narrower display, and the change in relative intensity of the inner and outer bands, in the ^{15}N case, compared with the ^{14}N case.

Figure 1. (a) Dispersion mode electron spin resonance spectra of man-made diamond "RVG". (b) Diamond prepared under controlled nucleation conditions.

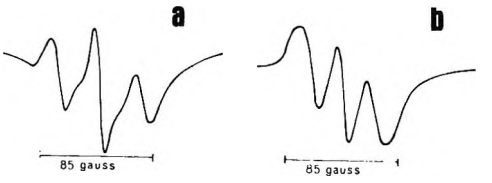

Figure 2. Electron spin resonance spectra in the vicinity of $g = 2$ for diamond prepared in the presence of nickel–manganese–graphite: (a) regular catalyst; (b) catalyst nitrided with $^{15}NH_3$.

Attempts to further induce charged defects by electron irradiation (10^{19} electrons cm^{-2}, 1.5 MeV, 50 min) resulted in no similarly visible changes in the esr spectra of these and boron-doped crystal specimens.

Implications

The spectra of those specimens prepared in the presence of ^{15}N show a change in the width of the hyperfine splitting which is consistent with the difference in the nuclear magnetic moments of ^{15}N and ^{14}N. Coupled with the chemical analytical evidence for the presence of nitrogen in these crystals, it appears certain that ^{15}N is appearing in the synthesized diamond in large quantity (the starting material is 96+% $^{15}NH_3$). The ^{15}N doped diamond still shows a threefold esr signal, but should show only two lines if no defects other than ^{15}N centers were present. The relative intensity of the inner and outer lines is different than in the ^{14}N case, but there is no simple interpretation of the central line which would involve atomic nitrogen or nitrogen–carbon interactions. The satellite absorptions which are visible in the regularly grown material (Figure 2a) are not visible in the spectrum of the ^{15}N-doped material. The central line in Figure 2b is thus to be ascribed to charged defects other than N, and single crystal experiments should permit its further resolution.

(3) F. P. Bundy, *J. Chem. Phys.*, **38**, 631 (1963).

(4) F. P. Bundy, *et al.*, *ibid.* **35**, 383 (1961).

(5) General Electric Co., Specialty Materials Department, Detroit, Mich.

The narrowness of the line X and its position in Figure 1b make it likely that there are ordered defects in these crystals (in addition to nitrogen) and that they are probably holes rather than electrons. Rather large concentrations may be involved (10^{20} defects/cc) and if spectral interpretation remains difficult some knowledge might still be gained by very accurate density measurements on catalyst-free specimens.

The use of ^{15}N in diamond synthesis has thus given results which will allow the further study of charged defects in synthetic diamond.

The curious role of nitrogen in the nucleation and growth processes of catalyzed diamond may be to allow spin reversal of other, disallowed transitions in carbon *via* CN formation; a lot of nitrogen would certainly block carbon transport paths by the formation of stable nitrides with catalysts, and thus reduce yields.

Acknowledgments. Thanks are extended to F. P. Bundy, H. M. Strong, and R. H. Wentorf for material assistance and critical discussion. E. T. Conlin supplied extensive skilled experimental help in the high pressure work.

Recoil Bromine Reaction. The Isomerization of Excited Cyclopropyl Bromide

by C. M. Wai* and R. L. Jennings

Department of Chemistry, University of Idaho, Moscow, Idaho 83843
(Received August 31, 1970)

Publication costs borne completely by The Journal of Physical Chemistry

Recoil bromine species activated by thermal neutron capture processes are able to undergo bimolecular substitution reactions in the gas phase for an atom or a group in hydrocarbon or alkyl halide molecules.[1-3] Very little information has been available regarding the internal excitation energies imparted to the product molecules during such hot bromine substitution processes. However, studies on recoil tritium and recoil fluorine substitution reactions with organic molecules have indicated that many hot products are indeed unstable and undergo secondary isomerization or decomposition by means of the high excitation energies left on the product molecules.[4-6] In this paper, we wish to report the isomerization of excited cyclopropyl bromide to allyl bromide induced by recoil Br^{80m} substitution reactions. The excited cyclopropyl bromide molecules were formed either by recoil Br^{80m} substitution for H in cyclopropane as in eq 1 or by recoil Br^{80m} substitution for Br in cyclopropyl bromide as in eq 2

$$Br^{80m} + \begin{matrix} CH_2 \\ / \quad \backslash \\ CH_2 - CH_2 \end{matrix} \longrightarrow \begin{matrix} CHBr^{80m} \\ / \quad \backslash \\ CH_2 - CH_2 \end{matrix} + H \qquad (1)$$

$$Br^{80m} + \begin{matrix} CHBr \\ / \quad \backslash \\ CH_2 - CH_2 \end{matrix} \longrightarrow \begin{matrix} CHBr^{80m} \\ / \quad \backslash \\ CH_2 - CH_2 \end{matrix} + Br \qquad (2)$$

Experimental Section

Neutron irradiations for this experiment were carried out in the thermal neutron flux of a TRIGA reactor for a period of 2–3 min at a flux of approximately 1×10^{12} n/cm² sec. Both Br^{80m} (half-life 4.5 hr) and Br^{82} (half-life 36 hr) activities were measured. Recoil Br^{80m} is produced by the $Br^{79}(n,\gamma)Br^{80m}$ process, whereas Br^{82} is produced mostly through isomeric transition from Br^{82m} (half-life 6.2 min).[7,8]

The preparation of samples and the radio gas chromatographic analysis of products followed the routine procedures for hot atom chemistry experiments.[9,10] A 16-ft silicon oil column operating at 40° was used for the separation of labeled products. The radioactivity was assayed by an internal gas-flow proportional counter. The retention times for allyl bromide and for cyclopropyl bromide in the column were 104 and 116 min, respectively. The long retention times for the major products were purposely arranged in order to minimize the counting of Br^{80} activity (half-life, 18 min) in the detector. When the separated products emerged from the column with such long retention times, initial Br^{80} activities in these products would decrease to a negligible small amount compared with Br^{80m} activities.

Two measurements were made for each sample; the first aliquot (for B^{80m}) was usually analyzed 4 hr after irradiation and the second aliquot (for Br^{82}) was analyzed after at least 40 hr, allowing most of the Br^{80m} to decay away. From the two measurements, correction for the Br^{82} activity in the first aliquot was made. To check our results, we also trapped the products (allyl bromide and cyclopropyl bromide) separated from the gas chromatograph in small loops and counted by a scintillation detector. This technique of counting Br^{80m} activity has been described by other investigators.[11] Our experimental result showed no difference

(1) A. A. Gordus and J. E. Willard, *J. Amer. Chem. Soc.*, **79**, 4609 (1957).

(2) J. E. Willard, "Chemical Effects of Nuclear Transformations," Vol. 2, International Atomic Energy Agency, Vienna, 1965, p 221.

(3) E. P. Rack and A. A. Gordus, *J. Phys. Chem.*, **65**, 944 (1961).

(4) E. K. C. Lee and F. S. Rowland, *J. Amer. Chem. Soc.*, **85**, 897 (1963).

(5) T. C. Ting and F. S. Rowland, *J. Phys. Chem.*, **72**, 763 (1968).

(6) C. F. McKnight and J. W. Root, *ibid.*, **73**, 4430 (1969).

(7) J. F. Emery, *J. Inorg. Nucl. Chem.*, **27**, 903 (1965).

(8) O. U. Anders, *Phys. Rev.*, **138**, B1 (1965).

(9) R. Wolfgang and F. S. Rowland, *Anal. Chem.*, **30**, 903 (1958).

(10) C. M. Wai and F. S. Rowland, *J. Amer. Chem. Soc.*, **90**, 3638 (1968).

(11) For example, see J. A. Merrigan and E. P. Rack, *J. Phys. Chem.*, **69**, 2795 (1965); T. E. Gilroy, G. Miller, and P. F. D. Shaw, *J. Amer. Chem. Soc.*, **86**, 5033 (1964).

Table I: Absolute Per Cent Yields of Radioactive Products from Recoil Br^{80m} Reactions with Cyclopropyl Bromide and with Cyclopropane

Sample descriptions[a]	Products			
	CH_3Br	$CH_2=CHBr$	$CH_2=CHCH_2Br$	$c\text{-}C_3H_5Br$
8 cm of $c\text{-}C_3H_6Br$ + 0.2 cm of Br_2	0.4	0.2	15.0	<0.1
8 cm of $c\text{-}C_3H_5Br$ + I_2 (sat. vapor)	0.2	0.1	13.2	<0.1
9 cm of $c\text{-}C_3H_6Br$ + 60 cm of Ne + I_2 (sat. vapor)	<0.1	<0.1	3.4	<0.1
65 cm of $c\text{-}C_3H_6$ + 5 cm of Br_2	0.25	0.10	1.42	<0.05
Liquid $c\text{-}C_3H_5Br$ + I_2	1.0	0.6	12.0	2.3

[a] Each gas sample contained 1 cm of Ar as a neutron monitor, utilizing the reaction $Ar^{40}(n,\gamma)Ar^{41}$.

in activity ratio of cyclopropyl bromide/allyl bromide between the two counting techniques.

Absolute yield measurements for Br^{80m} in the gas phase were obtained using the $Ar^{40}(n,\gamma)Ar^{41}$ nuclear reaction as an internal neutron monitor in the system. This technique of determining the hot yield has been applied previously to (n,γ) recoil Cl^{38} reactions in the gas phase.[10] Liquid phase yields were evaluated by comparison of the specific activity of allyl bromide (radioactivity of allyl bromide/unit mass of cylopropyl bromide) in the liquid phase with that in the gas phase under similar irradiation conditions.

Results and Discussion

Results of recoil Br^{80m} reactions with cyclopropyl bromide and with cyclopropane under different experimental conditions are given in Table I. The important observation in Table I is that no detectable amount (<0.1%) of labeled cyclopropyl bromide ($c\text{-}C_3H_5Br^{80m}$) has been found in any of the gas phase experiments. Instead, the isomerization product, allyl bromide ($CH_2=CHCH_2Br^{80m}$), is present as the major product in each experiment. None of the labeled 1-bromopropene-1 isomers (trans and cis forms of $CHBr=CHCH_3$) has been found in detectable amount in these experiments either. The gas phase results suggest that nearly every excited $c\text{-}C_3H_5Br^{80m}$ molecule formed by recoil Br^{80m} substitution for H or for Br in the cyclopropyl ring undergoes secondary isomerization to allyl bromide as in eq 3. The substitution of Br^{80m} for H

$$\begin{array}{c} CHBr^{80m} \\ \diagup \quad \diagdown \\ CH_2—CH_2 \end{array} \longrightarrow CH_2=CHCH_2Br^{80m} \qquad (3)$$

is less probable than the substitution of Br^{80m} for Br in cyclopropyl ring as shown in Table I. However, the internal excitation energy left on the product molecules in both processes is sufficient to cause secondary isomerization of the primary product. The activation energy for the isomerization of cyclopropyl bromide obtained from pyrolysis studies is about 47 kcal/mol.[12] Recoil Br^{80m} substitution reactions 1 and 2 must therefore leave at least 2 eV of excitation energy in the $c\text{-}C_3H_5Br^{80m}$ product. The essentially total loss of hot product by secondary isomerization has been observed in recoil tritium reaction with methyl isocyanide. The CH_2TNC molecules formed by the substitution of T-for-H in methyl isocyanide (CH_3NC) are not found under gas phase condition because of the easy isomerization (activation energy 38 kcal/mol) to methyl cyanide (CH_2TCN).[5] The high excitation energy in product following recoil Br^{80m} substitutions 1 and 2 is very similar to that of the recoil tritium substitution reaction.

An appreciable amount of $c\text{-}C_3H_5Br^{80m}$ is present only in the liquid phase experiments. The ratio of Br^{80m} labeled allyl bromide *vs.* cyclopropyl bromide in the liquid is about 85:15. If we assume that the mechanism of the recoil Br substitution reactions is the same in both the gas and liquid phases, then a fraction of the excited $c\text{-}C_3H_5Br^{80m}$ molecules (15%) formed by the primary substitution process might be stablized in the liquid phase because of the high collision frequencies in the liquid. The observation that the sum of the labeled $CH_2=CHCH_2Br^{80m}$ + $c\text{-}C_3H_5Br^{80m}$ yields is about constant between the gas phase and the liquid phases appears to support this mechanism. However, the "cage effect" and the slowness of diffusion in the liquid phase make it necessary to consider the possibility that the radioactive Br atom might combine with a cyclopropyl radical produced by its own energy transfer processes. The "cage effect" has been shown to play an important role in liquid phase recoil Cl reactions with alkyl halides.[13] The mechanisms for the reentry of recoil Br species in organic combinations in the liquid phase are not well understood yet. At present, no definite conclusion can be drawn regarding the forma-

(12) R. C. S. Grant and E. S. Swinbourne, *Chem. Commun.*, **17**, 620 (1966).

(13) C. M. Wai and F. S. Rowland, *J. Phys. Chem.*, **74**, 434 (1970).

tion of cyclopropyl bromide without extensive studies of recoil Br reactions in the liquid phase.

Rack and Gordus[3] have reported that the reaction of (n,γ) recoil Br^{80} with methane in the gas phase requires only kinetic energy and is not dependent on excited states or charge. Nicholas and Rack[14] have further indicated the absence of any isotopic effect between (n,γ) induced Br^{80m} and Br^{80} reaction in methane. These reports suggest that recoil Br^{80m} species can enter chemical combinations in the gas phase as neutralized atoms with excess kinetic energy. The decrease in Br^{80m} yield with the addition of inert gas Ne in cyclopropyl bromide vapor (Table I) is consistent with the moderation of kinetic energy of hot Br^{80m} atoms.

Acknowledgment. This research was partially supported by a grant from the Idaho State Office of Higher Education. We wish to thank the Washington State University Nuclear Reactor staff for their cooperation.

(14) J. B. Nicholas and E. P. Rack, *J. Chem. Phys.*, **48**, 4085 (1968).

Effects of Laminar and Turbulent Boundary Layer Buildup in Shock Tubes upon Chemical Rate Measurements

by Marvin Warshay

Lewis Research Center, National Aeronautics and Space Administration, Cleveland, Ohio 44135 *(Received March 19, 1971)*

Publication costs assisted by the National Aeronautics and Space Administration

The shock tube has been employed as a useful research tool for many years. In this period, shock tube research has attained a high level of sophistication. Nevertheless, the period of development is not yet over. For instance, in recent years, investigators of shock tubes have become increasingly aware of the departure of this device from ideal behavior.

In a recent paper, Mirels[1] applied a procedure previously developed by him[2,3] to calculate the variations of shock tube flow properties between the shock front and contact surface. In an ideal shock tube, the distance between the shock and contact surface increases linearly with distance from the diaphragm. However, in an actual shock tube, mass loss to the boundary layer causes the shock and contact surface to approach a limiting distance. The growing boundary layer creates, in effect, a diverging duct inside the shock tube through which the shocked gas flows subsonically. This tends to produce increases in pressure, temperature, and density, and a decrease in fluid particle velocity. The decreasing velocity affects the particle time-of-flight, or reaction time; this time is longer than is predicted by ideal shock tube theory (reaction time/laboratory time = ρ_{12} in ideal case).

These boundary layer effects on gas properties and time are particularly important for chemical rate studies where a knowledge of the true reaction time and the local state of the gas is essential. A changing fluid environment affects chemical rates whether brought about by the chemistry itself or by fluid dynamic influences resulting from boundary layer buildup. On the other hand, the boundary layer effect on reaction time is minor as long as rate studies are confined to the

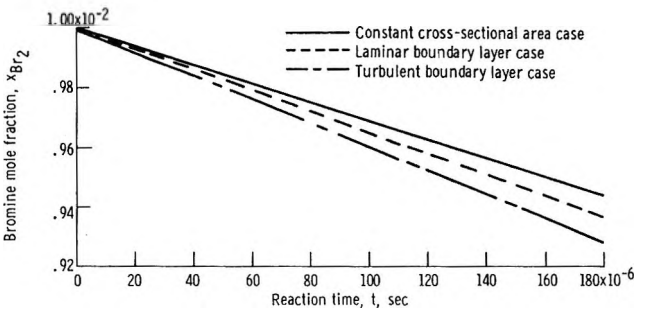

Figure 1. Comparison of mole fraction–time profiles for boundary layer and constant area cases. Initial temperature = 1264°K. Computed fluid property profiles for each case were used with Beer's law to convert the original measured intensity profile to the three mole fraction profiles shown. The effect of boundary layer is to cause more Br_2 to be consumed. However, quantitative conclusions regarding the effect upon k_D cannot be made on the basis of the relative positions of the curves because the fluid property histories of the three cases are different. For example, the temperature–time profiles of the three cases are different.

initial reaction periods corresponding to the zone close to the shock wave.

The present investigation examines the consequences of applying Mirels' theory in the translation of kinetic data into rate constants. The effects of the predicted flow nonuniformities due to boundary layer upon the rates of dissociation of bromine in a 1% bromine–99% argon mixture were studied. In this experiment,[4] the rates were obtained from initial slopes of light intensity against time curves (absorption measurements) which were corrected for the influence of endothermicity of the reaction, but not for any boundary layer effects. The enthalpy correction factor method of Palmer and Hornig[5] was employed to make the endothermicity corrections. As dissociation proceeds, the gas cools and all gas properties change. The initial slopes are affected by these changes. They are not the slopes at constant temperature and pressure. The enthalpy correction factor for each run establishes the rate constant at the initial shocked gas conditions (assuming no boundary layer effects). At 1% Br_2 concentrations

(1) H. Mirels, *Phys. Fluids*, **9**, 1907 (1966).
(2) H. Mirels, *ibid.*, **6**, 1201 (1963).
(3) H. Mirels, *AIAA J.*, **2**, 84 (1964).
(4) M. Warshay, NASA TN D-3502 (1966).
(5) H. B. Palmer and D. F. Hornig, *J. Chem. Phys.*, **26**, 98 (1957).

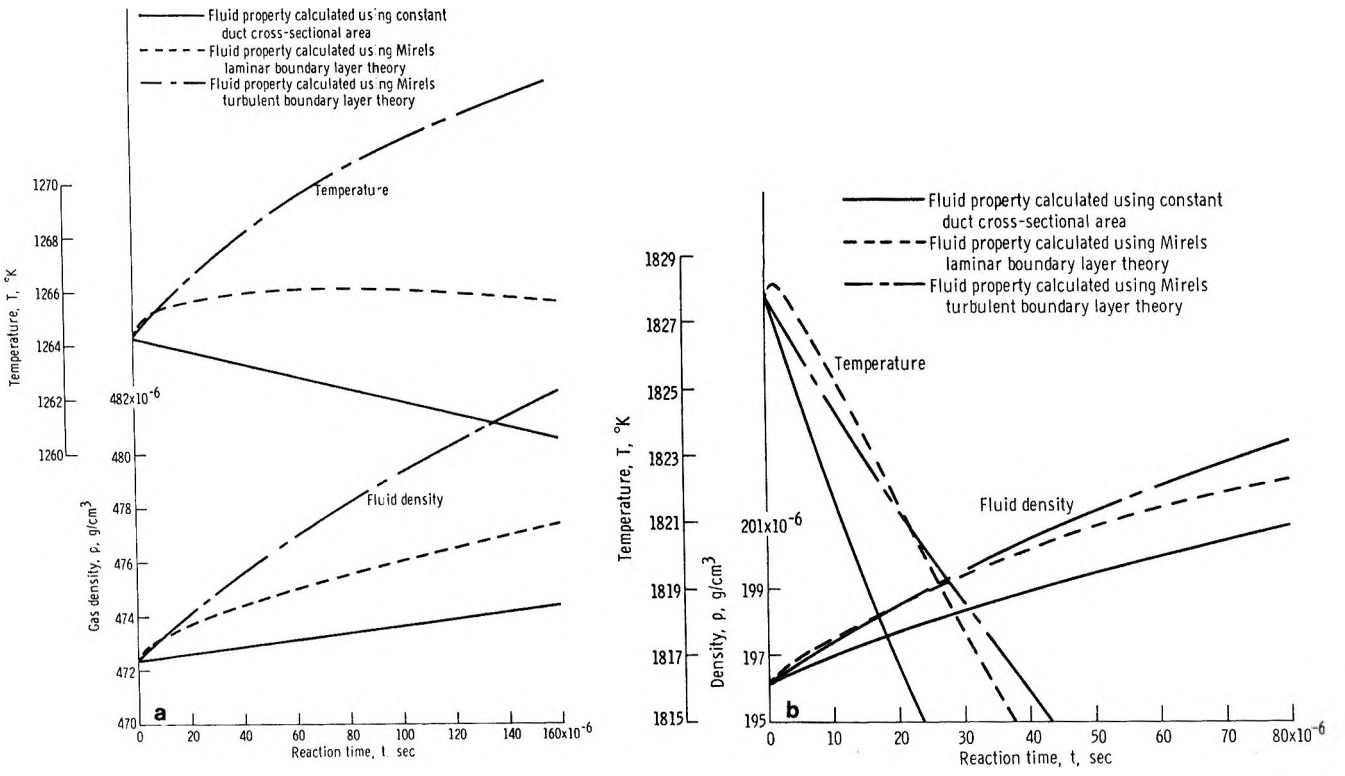

Figure 2. Effects of laminar and turbulent boundary layer buildup upon temperature and density. These data were calculated using the original k_D in the computer program. However, because of the large dilution of bromine by argon in this experiment, the fluid properties such as temperature, pressure, and density are insensitive to the degree of dissociation of bromine. The fluid dynamics due to boundary layer buildup governs fluid property variation; relatively large k_D variation does not change the profiles: (a) low temperature case; (b) high temperature case.

the corrections were small and varied very little with temperature ($1.07 < F < 1.13$). The chemical kinetic initial profiles have now been corrected for the particular boundary layer effects predicted by Mirels thereby establishing the magnitude of the effects of boundary layer buildup in the shock tube upon the measured dissociation rate constants.

Mirels developed the following relation to predict the effective area changes for a moving coordinate system.

$$A_{2s}/A_2 = 1 - (\ell/\ell_m)^n \quad (1)$$

$n = {}^1/_2$, laminar boundary layer

$n = {}^4/_5$, turbulent boundary layer

The equation gives the variations of equivalent free stream cross-sectional area, A_2, with distance behind the shock, ℓ, which constitutes the critical relationship required in the calculation of boundary layer effects. The maximum separation distance, ℓ_m, is achieved when the shock wave and contact surface velocities are equal. A_{2s} is the free stream cross-sectional area at the shock front. Based on experimental measurements on shocked gas flow accompanied by laminar boundary layer buildup, Fox, McLaren, and Hobson[6] concluded the Mirels' theory gives an adequate description of flow duration and attenuation. In addition, they concluded that Mirels' equation (eq 1) appears to be adequate in instances when the maximum separation distance is not attained.

Relationships proposed by Mirels in earlier papers[2,3] were used to calculate the laminar and turbulent ℓ_m values for the various shock conditions. The Mirels theory assumes that either a wholly laminar or a wholly turbulent boundary layer is created behind the incident shock wave. For the conditions of the bromine experiment, Mirels' simple criteria (based on tube diameter, initial gas pressure, and Mach number) indicated that the turbulent theory applied. However, the effects of both laminar and turbulent boundary layers were investigated. Calculation of the transition from laminar to turbulent boundary layer using published experimental data[7] indicated that in all probability the bromine measurements, which had been made close to the shock front, were made while a laminar boundary layer existed in the tube.

Computer calculations of fluid property *vs.* time profiles were made for the two boundary layer cases and for the original constant area treatment. These data were used with Beer's law to convert the measured intensity *vs.* time data of ref 4 into Br_2 mole frac-

(6) J. N. Fox, T. I. McLaren, and R. M. Hobson, *Phys. Fluids*, 9, 2345 (1966).

(7) R. A. Hartunian, A. L. Russo, and P. V. Marrone, *J. Aerosp. Sci.*, 587 (1960).

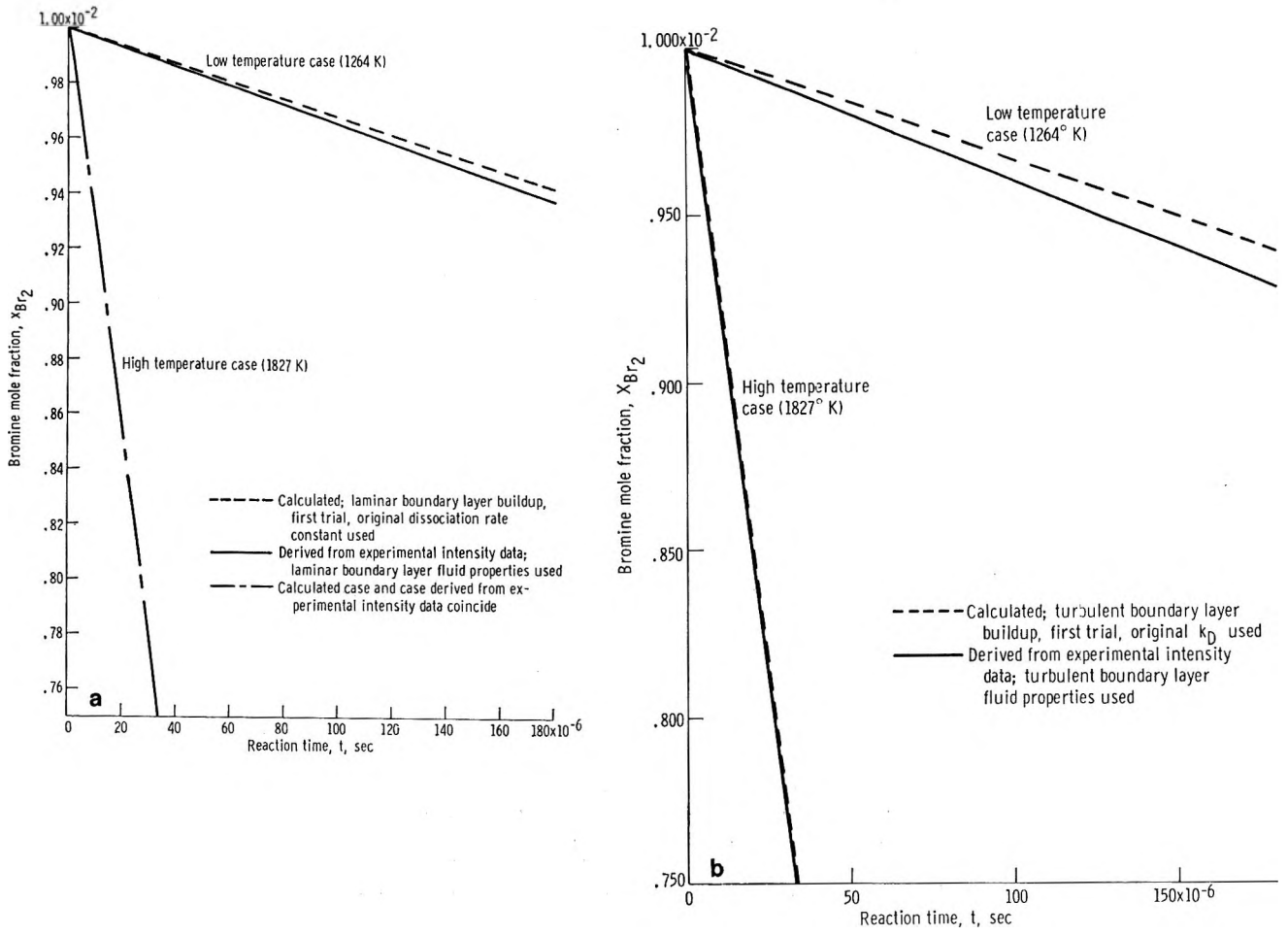

Figure 3. Initial slopes of bromine mole fraction–reaction time profiles. Laminar ℓ_m = 14,050 cm at 1264°K; ℓ_m = 3463 cm at 1827°K. Turbulent ℓ_m = 210 cm at 1264°K; ℓ_m = 146 cm at 1827°K. The ratio of the experimentally derived slope to the calculated first trial slope is a good measure of the boundary layer effect upon k_D; both the experimentally derived and the calculated profiles had identical fluid property histories. The Mirels correction upon the time coordinate had negligible effect upon these initial slopes. These runs represent the extremes of the temperature range investigated. Similar treatment of runs at intermediate temperatures produced the expected intermediate effect. The smaller effects of the laminar case compared with the turbulent case are attributable to the very much larger ℓ_m values for the former: (a) laminar; (b) turbulent.

tion (x_{Br_2}) *vs.* time profiles. More Br_2 is consumed when the presence of a boundary layer is assumed (Figure 1). This result stems from the higher density gradients produced by the boundary layer (Figure 2).

Ultimately, it developed that the steeper x_{Br_2}–time profiles of the boundary layer cases were associated with larger k_D values than was the original constant area profile. The degree of increase in k_D was temperature dependent; for each case it was established by feeding guesses of k_D to the computer program until the x_{Br_2} *vs.* time profile thereby generated matched the appropriate experimentally derived profile (Figure 3).

Figure 4 illustrated an alternate method which was also used to determine the boundary layer effects upon k_D. The results of this method, which involved computer-generated ln (I/I_0) *vs.* time profiles, and the mole fraction approach were in close agreement. (For more details about both methods see ref 8.)

The influence of Mirels' interpretation of boundary layer buildup upon the measured rate constant was as follows: at low temperatures (1264°K), where reaction rate slopes are shallow, the effect was significant for a turbulent boundary layer and small for the laminar boundary layer case; while at high temperatures (1827°K), where reaction rate slopes are steep, the effect was negligible in both cases (see Table I). A small displacement of a steep reaction rate curve hardly affects the slope, while a similar displacement of a curve which has a shallow slope may change the slope significantly. Over the temperature range covered (1264–1827°K) the following rate constant expressions were obtained for the three cases: (a) no boundary layer considered[4]

(8) M. Warshay, NASA TN D-4795 (1968).

$$k_D = 2.18 \times 10^{11} T^{1/2} \times \exp(-31.5 \text{ kcal/mol})/RT \quad \text{cm}^3/(\text{mol})(\text{sec}) \quad (2)$$

(b) laminar boundary layer case

$$k_D = 1.94 \times 10^{11} T^{1/2} \times \exp(-31.1 \text{ kcal/mol})/RT \quad \text{cm}^3/(\text{mol})(\text{sec}) \quad (3)$$

(c) turbulent boundary layer case

$$k_D = 1.45 \times 10^{11} T^{1/2} \times \exp(-30.0 \text{ kcal/mol})/RT \quad \text{cm}^3/(\text{mol})(\text{sec}) \quad (4)$$

The overall effects of boundary layer buildup upon k_D were evidently to decrease both the preexponential constant and E_a, the effects being much smaller for the laminar case.

Table I: Comparison of Laminar with Turbulent Boundary Layer Corrections of the Rate Constant k_D

	Initial gas temperature, °K	
	1264	1827
$\frac{k_D \text{ (laminar case)}}{k_D \text{ (no boundary layer)}}$	1.05	1.00
$\frac{k_D \text{ (turbulent case)}}{k_D \text{ (no boundary layer)}}$	1.20	-1.00

One is struck by the fact that the laminar case produced a smaller correction than the turbulent case. Belford and Strehlew[9] predicted the opposite. Certainly if the laminar and turbulent ℓ_m value were equal, eq 1 would indicate that the laminar effect would indeed be the more pronounced. However, for the conditions of this investigation the much larger laminar ℓ_m values (almost 70 times as large as the turbulent ℓ_m at 1264°K) overcame the effect of the exponent in eq 1. For other conditions, the turbulent correction could be the smaller one.

The bromine–argon mixture was used to illustrate the effects of boundary layer buildup upon k_D. Other 1% bromine–99% noble gas mixtures follow the same pattern. For each case the magnitude of the correction is governed by its ℓ_m (see eq 1). For higher Br_2 concentrations, where reaction rates are higher, the influence of boundary layer upon k_D diminishes. For example, for 100% Br_2 at 1264°K the boundary layer correction was calculated to be under 1%.

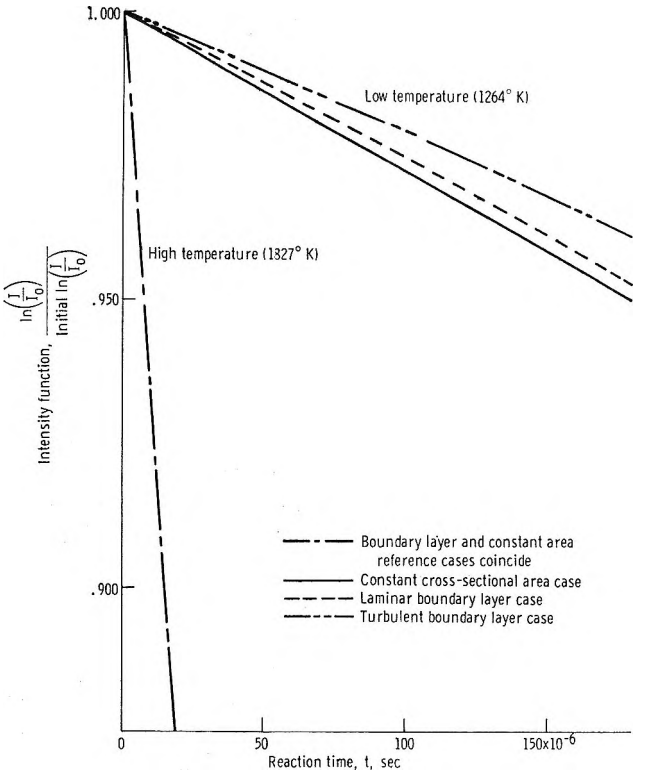

Figure 4. Calculated intensity function–time profiles. Original k_D used. These intensity profiles were derived from computed concentration–time and extinction coefficient–time profiles. The extinction coefficient (ϵ) profiles were derived from computed temperature variation and the known influence of temperature upon ϵ (ref 4). For any initial conditions, when the guessed k_D causes the boundary layer curve to match the constant area reference curve the effect upon k_D has been established. The relative positions of the curves prior to curve matching are not quantitatively related to the boundary layer effect upon k_D; unlike the constant area reference case, the boundary layer intensity profile is affected by fluid dynamic effects unrelated to Br_2 consumption but due solely to boundary layer buildup.

The initial slope technique of rate constant measurement apparently benefits from being in a region where the smaller influence of a laminar boundary layer prevails. In addition, time corrections due to boundary layer are minor there. In other experiments, *e.g.*, one which follows the reaction further toward equilibrium, the boundary layer effect could have greater influence.

(9) R. L. Belford and R. A. Strehlow, *Annu. Rev. Phys. Chem.*, **20**, 247 (1969).

COMMUNICATIONS TO THE EDITOR

Nitrosamine Anion Radicals

Publication costs assisted by the University of Puerto Rico

Sir: Recently several aliphatic nitro compounds have been reduced to their respective anion radicals.[1,2] To date no anion radicals of nitrosamines have been reported. Aliphatic nitrosamines are isoelectronic with amides, thionitrosamines, and *N*-cyanoamines, for all of which no anion radicals have been reported. We wish to report here the formation of the previously unknown nitrosamine anion radical.

When a 10^{-2} to 10^{-3} *M* solution of *N*-nitrosodiethylamine (**1**)[3] in dimethoxyethane (DME), distilled directly into the reaction vessel from the solvated electron, is shaken under high vacuum with a potassium mirror a light yellow solution results. This solution gives an 11-line esr spectrum[4] (Figure 1). The expected spectrum would be a nine-line triplet of triplets resulting from two nonequivalent nitrogens. The experimental spectrum is not consistent with this in that the line widths and intensities are not equal. Further the end lines are split.

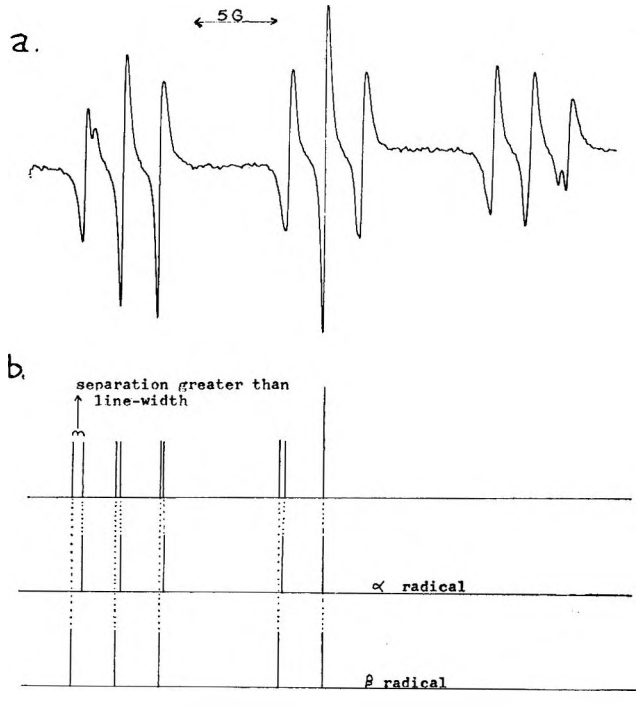

Figure 1. (a) Esr spectrum of **1** reduced by potassium in DME and recorded at room temperature. The line width of the center line is 0.28 G. The high-field lines are broader than the low-field lines due to *g*-tensor anisotropy. (b) Stick diagram for the low-field half of radicals α and β.

These results can be nicely interpreted in terms of two different radical anions in solution (α) and (β), both having identical *g* values, but (β) having slightly larger coupling constants for both nitrogens (Figure 1). This results in the $m = 0,0$ lines superimposing, thus, yielding a sharp center line. However, due to the small differences in the coupling constants, the $m = 0 \pm 1$ lines do not exactly overlap. The result is that these lines become broadened and less intense. The coupling constants differ by less than the line width. The large nitrogen coupling constants also differ by less than the line width, which results in slightly broader $m = \pm 1,0$ lines. Since the (β) anion radical has the larger coupling constants for both nitrogens, the differences are additive in the end lines, and the resulting difference in line positions becomes slightly larger than the line width. The coupling constants for the (β) radical are 12.60 and 2.40 G. Those for the (α) radical are 12.45 and 2.23 G. The two radicals can result from two different geometrical isomers or from two different ion pairs. If the two radicals were due to a hindered internal rotation as observed by McKinney and Geske[5] or some other intramolecular process, an increase in the temperature should time-average the two spectra. Experimentally this is not the case, for at +50° no coalescing of the lines is observed. In fact the lines narrow as the temperature increases and better separation of the end lines is observed (at +50° $\Delta W = 0.21$ G, and at +25° $\Delta W = 0.28$ G). This leads us to conclude that the two anion radicals are a tight ion pair (α) and a loose ion pair (β) as shown below.

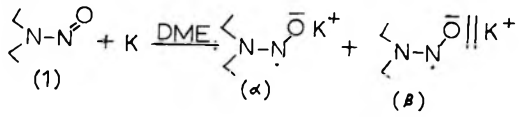

The esr spectrum of the loose and tight ion pairs of naphthalene anion radical have been observed simul-

(1) H. Zeldes and R. Livingston, *J. Amer. Chem. Soc.*, 90, 4540 (1968).

(2) L. H. Piette, P. Ludwig, and R. N. Adams, *ibid.*, 83, 3909 (1961).

(3) A. I. Vogel in "Practical Organic Chemistry," 3rd ed, Wiley, New York, N. Y., pp 426.

(4) The esr spectra were recorded on the x-band of a Varian E-3 spectrometer.

(5) T. M. McKinney and D. H. Geske, *J. Chem. Phys.*, 44, 2277 (1966).

taneously in solution by Chang and Johnson.[6] Both were in fast exchange conditions with the neutral molecule. Also two different ion pairs of the cyclooctatetraene anion radical in slow exchange have been observed in DME[7] and liquid NH_3.[8] Further support for the ion pair interpretation is obtained from the reduction of **1** in DME with Na. The esr spectrum of this solution shows a Na splitting of 0.88 G.

Reduction of **1** with K in tetrahydrofuran (THF) results in a nine-line spectrum, but with some line width and intensity distortions. This is due to the two radicals, but no splitting of the end lines is observed. Similar results were obtained from the reduction of *N*-nitrosodiisopropylamine (**2**) (see Table I). The reduction of *N*-methyl-*N*-nitrosoaniline (**3**) leads to nine lines all of equal intensity. However, the lines are broadened (line width = 2 G) due to the unresolved phenyl proton splittings. The coupling constants A_N and A_{M^+} for the various systems are shown in Table I.

Table I: Coupling Constants for Nitrosamine Anion Radicals

Metal–solvent	Compd	A_N (nitroso), G	A_N (alkylated), G	A_{M^+}, G
K-DME	1	12.60 ± 0.05	2.40 ± 0.02	
		12.45 ± 0.05	2.23 ± 0.02	
K-THF	1	12.57 ± 0.05	2.39 ± 0.02	
Na-DME	1	13.20 ± 0.05	2.43 ± 0.02	0.88
K-DME	2	12.50 ± 0.05	2.35 ± 0.05	
K-DME	3	11.4 ± 0.1	3.7 ± 0.1	

The s orbital spin densities were calculated from spectral data using the standard equation $\rho = A_N/510$, where A_N = 12.6 and 2.4 G (see Table II). s orbital spin densities obtained using an INDO treatment show good agreement with the experimental values.[9] Experimental π-electron spin densities are also shown in Table II. The results show that the odd electron resides predominantly on the nitroso nitrogen.

Table II: Calculated and Experimental Spin Densities

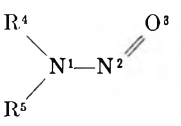

Position	Calculated s orbital spin density	Experimental s orbital spin density	Experimental π-electron spin density
1	+0.0002	0.0047	0.16
2	+0.0210	0.0247	0.84
3	+0.0067	0.0000	0.00
4	−0.0051		
5	−0.0030		

Acknowledgments. The authors are indebted to Dr. Alec Grimison for the molecular orbital calculations and to the University of Puerto Rico Research Fund for the support of this work.

(6) R. Chang and C. S. Johnson, Jr., *J. Amer. Chem. Soc.*, **88**, 2338 (1966).

(7) H. L. Strauss, T. J. Katz, and G. K. Frankel, *ibid.*, **85**, 2360 (1963).

(8) F. J. Smentowski and G. R. Stevenson, *J. Phys. Chem.*, **73**, 340 (1969).

(9) INDO calculations were carried out using the standard parameters.

UNIVERSITY OF PUERTO RICO
RÍO PIEDRAS CAMPUS
RÍO PIEDRAS, PUERTO RICO 00931

GERALD R. STEVENSON*
CARLOS J. COLÓN

RECEIVED FEBRUARY 19, 1971

Electron Spin Resonance of Atomic Silver on Porous Glass and Silica Gel Surfaces

Publication costs assisted by Leicester University

Sir: In their early esr studies of silver atoms formed by exposing silica gel treated with alcoholic silver nitrate to ^{60}Co γ-rays, Zhitnikov and Paugurt[1] suggested that two types of silver atom were trapped. However, Gardner, *et al.*,[2] have considerably extended these studies and have come to the conclusion that only one silver species is trapped, the extra features being shoulders characteristic of an axially symmetric unit with considerable g and A anisotropy. Their data are included in Table I. This result, as was stressed by Gardner, *et al.*, is of considerable significance with respect to the difficult problem of measuring the magnitude of the large electrostatic fields known to exist at the surface of catalyst materials.

We therefore felt that we should make known our reasons for considering that, after all, two distinct species are involved. First, the form of the spectra (Figure 1 of ref 2, and our Figure 1) is unusual for an asymmetric species of the type postulated since $|A_{\parallel}| < |A_{\perp}|$, which means that either A_{iso} or $2B$ must be negative. (For convenience, we are neglecting the fact that the nuclear moments for ^{107}Ag and ^{109}Ag are negative.) A_{iso} must surely be positive, and the interesting theory developed to explain the results[2] requires that $2B$ be positive also. This difficulty could be overcome by invoking equal participation from, say, p_x and p_y, but our results convince us that, in fact, the problem is an artefact. The coupling referred to as "perpendicular"[2] is very close to the isotropic coupling for free Ag^0, and the "parallel"[2] values lie between the

(1) R. A. Zhitnikov and A. P. Paugurt, *Sov. Phys. Solid State*, **8**, 1429 (1966).

(2) C. L. Gardner, E. J. Casey and C. W. M. Grant, *J. Phys. Chem.*, **74**, 3273 (1970).

Table I: Esr Parameters for Silver Atoms on a Silica Surface

Species	A value,[a] G	g value[a]	Comment
^{109}Ag	716 ± 5	2.002 ± 0.002	Can be seen on silica gel at any alcohol concentration
^{107}Ag	615.5 ± 5		
In environment 1 (or ⊥ features)[2]			
^{109}Ag	667 ± 10	2.001 ± 0.002	Only detected at fairly high alcohol concentrations
^{107}Ag	574 ± 5		
In environment 2 (or ∥ features)[2]			
Ag^{2+}	25 ± 3 = $A_{\|\|}$[3]	2.233 ± 0.002 = $g_{\|\|}$	Only detected after prolonged drying in a vacuum oven
^{109}Ag	619 ± 5	2.002 ± 0.002	Species obtained in ethanol at 77°K
^{107}Ag	534 ± 5		
In ethanol			

[a] Corrected using the Breit–Rabi equation.

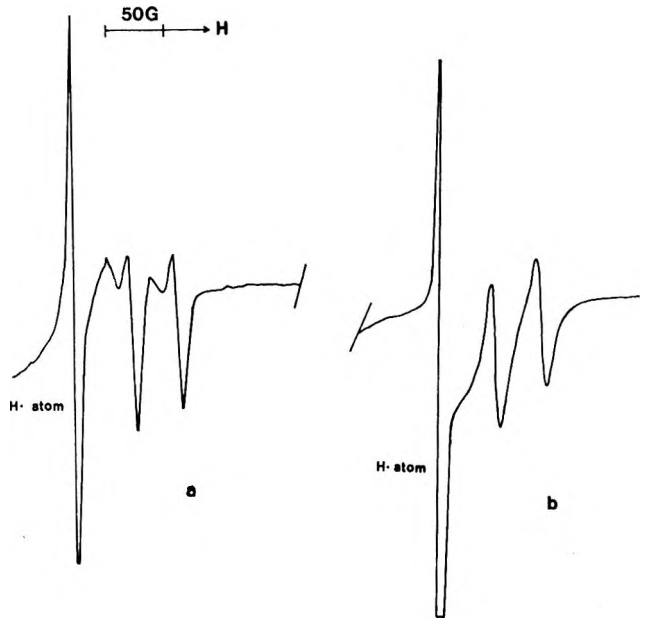

Figure 1. High-field part of the esr spectrum of γ-irradiated silica gel integrated with an alcoholic solution of silver nitrate: (a) after air drying at room temperature; (b) after prolonged drying in a vacuum oven prior to irradiation.

isotropic coupling for the free atoms and the value for the atoms in ethanol. Thus it seems likely that when Ag^+ is on a normal silica surface, uptake of an electron gives some atoms which are *remarkably* free of any environmental interaction. This is, surely, both surprising and informative. The other form, present in lower concentration, is formed from Ag^+ still partly solvated by ethanol. One of us has previously indicated how a ligand environment can cause a reduction in A_{iso},[3] and a similar mechanism no doubt applies in this case.[4]

We find that the relative yield of the two species is dependent upon the extent to which the silica gel is dried *in vacuo* (see Figure 1). This confirms the theory that two species are involved. Another interesting result is that after prolonged drying in the vacuum oven, followed by γ-irradiation, features characteristic of Ag^{2+} were obtained in addition to Ag^0. The $g_{||}$ and $A_{||}$ values are given in Table I. The perpendicular features were unfortunately completely hidden under other intense central lines. The magnitude of $g_{||}$ for Ag^{2+} is surely a function of the magnitude and symmetry of the local crystal field and might well prove to be a better indicator of the surface fields than, unfortunately, can be obtained from the Ag^0 spectra.

(3) M. C. R. Symons, *J. Chem. Soc.*, 1482 (1964).
(4) R. S. Eachus and M. C. R. Symons, *ibid.*, *A*, 1329, 1336 (1970).

DEPARTMENT OF CHEMISTRY H. C. STARKIE
THE UNIVERSITY M. C. R. SYMONS*
LEICESTER, LE1 7RH, ENGLAND

RECEIVED MARCH 17, 1971

Reply to "Electron Spin Resonance of Atomic Silver on Porous Glass and Silica Gel Surfaces" by H. C. Starkie and M. C. R. Symons

Publication costs assisted by the Defense Research Establishment, Ottawa

Sir: In the preceding communication Starkie and Symons[1a] have questioned our interpretation[1b] of the esr spectrum of atomic silver on porous glass and silica gel surfaces. Several of the points raised by these authors appear to have resulted from a misinterpretation of our paper and we wish to take this opportunity to make further clarification.

(1) (a) H. C. Starkie and M. C. R. Symons, *J. Phys. Chem.*, **75**, 2705 (1971); (b) C. L. Gardner, E. J. Casey, and C. W. M. Grant, *ibid.*, **74**, 3273 (1970).

1. It was not our intention to question in any way Zhitnikov and Paugurt's[2] observation that two silver species were trapped in their experiments. These they described as species A, due to Ag^0 on silica gel, and species B, due to Ag^0 in solution. Our experiments were carried out, using the method that Zhitnikov and Paugurt[2] describe, so that only species A was produced. All our results refer only to their species A.

2. While our calculation did yield positive values for B, the anisotropic hyperfine term, our main conclusion was that the method we used was not adequate. The method did show that cross terms can contribute negative terms to B and thus the calculation does not necessarily require B to be positive. Field gradient terms could also yield negative terms to B and may be important as well.

3. The major point raised by Starkie and Symons is, however, whether the unusual line shapes observed are due to an overlap of two (isotropic) lines as they suggest or due to g and hyperfine anisotropy as we have suggested.

In our opinion, the experimental results agree best with the latter suggestion for the following reasons. (a) In our experience the intensity ratio of the shoulder to the main peak does not change from sample to sample as might be expected from a mixture of two species. (b) In a "wet" sample, one observed the two species, A and B, as described by Zhitnikov and Paugurt.[2] Here again one does not see any noticeable change in intensities of the features in species A as might be expected from the model proposed by Starkie and Symons. Further, one might also expect that the field position of the features they ascribe to a partially solvated species would shift as the degree of solvation is increased if their suggestion is correct. We found no such shift.

4. It seems very possible that the vacuum drying technique used by Starkie and Symons to prepare "free" atomic silver could cause major changes in the surface distribution of the silver salts. Comparison of such results with those of undried samples may be misleading. Zhitnikov and Paugurt[2] have expressed the opinion that heat treatment and drying results in the formation of salt crystallites on the surface. Atomic silver formed in the symmetrical environment of a crystal might be expected to show less perturbation than that on a surface. Atomic silver in a metaphosphate host[3] has Hamiltonian parameters very close to those of the free atom for example.

In conclusion, it remains our opinion that the experimental results are best explained in terms of the model we proposed.

(2) R. A. Zhitnikov and A. P. Paugurt, *Sov. Phys. Solid State*, **8**, 1429 (1966).

(3) T. Feldmann and A. Treinin, *J. Chem. Phys.*, **47**, 2754 (1967).

DEFENSE RESEARCH BOARD
DREO, OTTAWA 4, CANADA

C. L. GARDNER*
E. J. CASEY
C. W. M. GRANT

RECEIVED MAY 4, 1971

Enhancement of Micellar Catalysis by Added Electrolytes

Publication costs assisted by the National Science Foundation

Sir: To date all experimental evidence has shown that electrolyte inhibition of micellar catalysis is a general phenomenon with no apparent exceptions (for general reviews of micellar catalysis see ref 1). This inhibition was rationalized by assuming that a counterion competes with an ionic reactant (*e.g.*, OH^-, H_3O^+, X^-) for a site on the ionic micelle, and in favorable cases electrolyte inhibition could be treated quantitatively in these terms.[2] Electrolytes increase the aggregation numbers of micelles, and therefore for a given detergent concentration reduce the number of micelles, but under the kinetic conditions micelles were in considerable excess over substrate, and it appeared that effects on micellar structure were much less important kinetically than exclusion of the reagent from the micellar pseudophase.[1,2]

We now report a significant exception to this behavior. The decarboxylation of the 6-nitrobenzisoxazole-3-carboxylate anion (I)[3] is markedly catalyzed by cationic micelles of 2×10^{-2} M cetyltrimethylammonium bromide (CTABr) at pH 9 (0.002 M NH_3 buffer, 25.0°), and this catalysis is unexpectedly enhanced by some salts. Not only do many salts actually increase micellar catalysis but others show rate maxima. Some examples are given in Figure 1 and Table I. These rate enhancements suggest that the traditional treatments of electrolytic inhibition are incomplete and that effects on micellar structure must be kinetically significant.

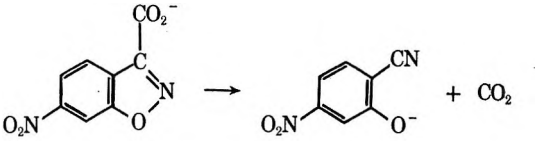

I

The salt effects depend upon the anion. Small hydrophilic anions enhance micellar catalysis at concentrations of 0–0.8 M, and their effectiveness increases in the order: no salt < $CH_3CO_2^-$ ≈ F^- < Cl^- < Br^- <

(1) H. Morawetz, *Advan. Catal.*, **20**, 341 (1969); E. M. Cordes and R. B. Dunlap, *Accounts Chem. Res.*, **2**, 329 (1969); E. J. Fendler and J. H. Fendler, *Advan. Phys. Org. Chem.*, **8**, 271 (1970).

(2) C. A. Bunton, E. J. Fendler, L. Sepulveda, and K-U. Yang, *J. Amer. Chem. Soc.*, **90**, 5512 (1968).

(3) C. A. Bunton and M. Minch, *Tetrahedron Lett.*, 3881 (1970).

Table I: Effects of Hydrophobic Anions and Organic Solutes[a]

Sodium Salt	10^3C_S, M	10^4k_ψ	Solute	10^2C_S, M	10^4k_ψ
		2.90	Testosterone	1.28[b]	2.50
β-Napthalenesulfonate	1.66	2.96	Testosterone	2.57[b]	2.20
β-Napthalenesulfonate	3.40	3.22	Estrone	4.45	3.43[c]
β-Napthalenesulfonate	5.50	3.50	Estrone	6.80	3.15[c]
β-Napthalenesulfonate	11.1	4.65	Urea	161	2.84
β-Napthalenesulfonate	15.2	3.72	Urea	321	2.71
β-Napthalenesulfonate	16.6	2.50	Urea	535	2.24
Cholate	1.19	2.73	Dioxane	133	3.07
Cholate	3.17	2.45	Dioxane	1785	2.65
Cholate	6.33	1.80	Dioxane	2300	2.20

[a] At 25.0° in aqueous 2×10^{-2} M CTABr, pH 9.0 except where specified; in the absence of detergent $10^6k_\psi = 3.0$ sec^{-1}. [b] With 10 M equivalents of dioxane. [c] At pH 12.5.

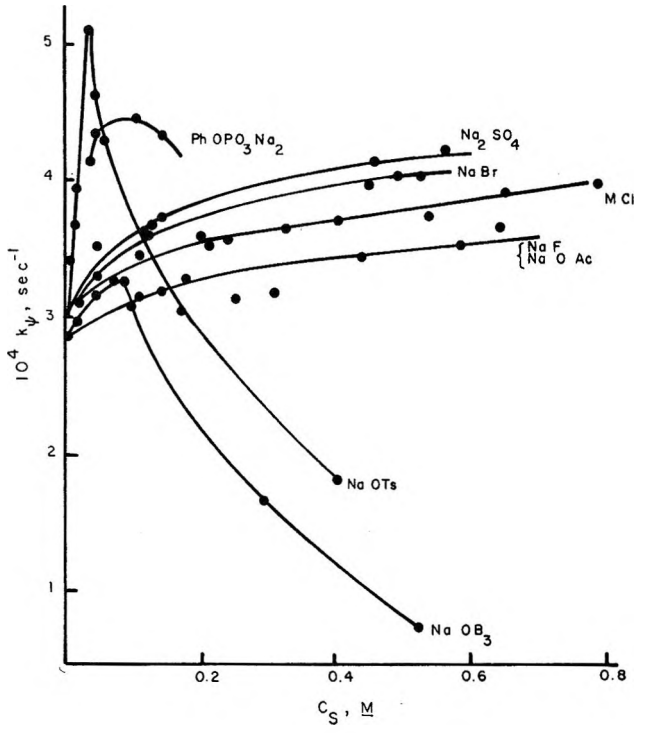

Figure 1. Effects of salts upon k_ψ, the first-order rate constant of decarboxylation (M = Li, Na, Me_4N).

SO_4^{2-}. The structure of the cation is relatively unimportant: Me_4NCl, NaCl, and LiCl all have the same effect on k_ψ. Less hydrophilic anions such as aryl sulfonates, phosphates, and carboxylates increase the catalysis up to a rate maximum characteristic of each anion (Figure 1 and Table I). The maximum catalysis increases in the order: benzoate < phenylphosphate dianion ≈ β-napthalenesulfonate < tosylate. Similar behavior was found at several CTABr concentrations and the salt concentration for maximum catalysis depended upon the concentration of CTABr. However, the strongly hydrophobic salt sodium cholate was an inhibitor at all concentrations (Table I). These salt effects are characteristic of the micellar-catalyzed decarboxylation; the rate constant in the absence of detergent is unaffected by added salt.[4]

These results show that at least for this reaction competition between the salt and the ionic substrate for the micelle is not all important, and it seems that the enhancement of micellar catalysis by added salts is caused by their changing the shape or reducing the charge density of the micelle. Salts decrease the cmc (critical micelle concentration) and increase the aggregation number of ionic micelles,[5,6] probably because increased screening by the counterions decreases the effective charge density of the micelle. Mixed micelles of CTABr and the uncharged detergent Igepal are better catalysts than either alone,[3] suggesting that there is a relation between the salt effects upon the charge density of the micelle and reaction rate.

Effects upon micellar structure are suggested by changes in viscosity, for example, the addition of NaOTS to 0.015 M CTABr markedly increases the viscosity to a maximum of *ca.* 120-fold at 0.03 M NaOTs; the viscosity then decreases. Similar relations between viscosity and tosylate concentration were observed over a wide range of CTABr concentrations. We suggest that incorporation of tosylate into the spherical CTABr micelles decreases charge repulsions and allows the ammonium head groups to come together so that the micelle becomes rodlike, with more effective bonding of the long alkyl chains, but at higher tosylate concentrations, the micelles become anionic and then again become more spherical. As confirmation of a strong micelle–anion interaction we find that CTABr (above the cmc) increases the uv absorbance of NaOTs in the region 2400–2800 Å.

The correlation of these viscosity, spectral, and kinetic changes suggests that they are all related to changes in micellar structure, showing that medium effects on micellar structure cannot be ignored in kinetic studies and that the overall electrolyte effect depends upon the ability of the counterion (i) to exclude ionic reagents from the micellar pseudophase and (ii) to

(4) D. S. Kemp and K. Paul, *J. Amer. Chem. Soc.*, 92, 2553 (1970).
(5) K. J. Mysels and L. H. Princen, *J. Colloid Sci.*, 12, 594 (1957).
(6) K. Shinoda, *J. Phys. Chem.*, 59, 432 (1955).

modify the micelle. The effects may combine or oppose each other.

The adducts need not be ionic, for example testosterone, although uncharged, is as effective an inhibitor as sodium cholate (Table I), but estrone, as its anion at pH 12, has little effect. Moreover, urea and dioxane have to be in appreciable concentration (>0.5 *M*) before they have significant kinetic effects (Table I), even though urea strongly affects the water structure and therefore the properties of micelles and macromolecules.[7]

It is not clear why salt inhibition of micellar catalysis has appeared to be so universal a phenomenon for ion–molecule as well as spontaneous reactions, or why the present spontaneous reaction appears to be so different from others. For example, the spontaneous hydrolysis of 2,4- and 2,6-dinitrophenylphosphate dianions was inhibited by all the salts examined,[2] and changes in micellar shape and size did not appear to be kinetically significant.[8] The decarboxylation of I is subject to very large solvent effects,[4] and therefore could be unusually sensitive to the nature of the micellar pseudophase. Our results show that added electrolytes and organic solutes have complex effects upon micellar catalysis which depend markedly upon the nature of the reaction; they also show how a reaction at a micellar surface can be controlled by chemically inert adducts, and provide a crude model for control of reactions at biological surfaces.

Acknowledgments. Support of this work by the National Science Foundation, the Arthritis and Metabolic Diseases Institute of the U. S. Public Health Service, The Fund for Overseas Research Grant Education, and the University of Chile–University of California Cooperative Program supported by the Ford Foundation is gratefully acknowledged.

(7) T. E. Wagner, C. Hsu, and C. S. Pratt, *J. Amer. Chem. Soc.*, **89**, 6366 (1967); F. M. Menger and C. E. Portnoy, *ibid.*, **90**, 1875 (1968).

(8) G. J. Buist, C. A. Bunton, L. Robinson, L. Sepulveda, and M. Stam, *ibid.*, **92**, 4072 (1970).

(9) National Institutes of Health Postdoctoral Fellow.

DEPARTMENT OF CHEMISTRY — C. A. BUNTON*
UNIVERSITY OF CALIFORNIA, SANTA BARBARA — M. MINCH[9]
SANTA BARBARA, CALIFORNIA 93106
FACULTY OF CHEMISTRY AND PHARMACY — L. SEPULVEDA
UNIVERSITY OF CHILE
SANTIAGO, CHILE

RECEIVED FEBRUARY 24, 1971

Relative Rates of Hydrogen Atom Abstraction by Near-Thermal Fluorine-18 Atoms

Publication costs assisted by the Division of Research, U. S. Atomic Energy Commission

Sir: Several recent investigations have been concerned with various theoretical and experimental aspects of the abstraction reactions of atomic fluorine with molecular hydrogen, hydrocarbons, and halocarbons, as in reaction 1.[1-6] However, despite the

$$^{18}F + RH \longrightarrow H^{18}F + R \qquad (1)$$

general interest in fluorine chemistry, relatively few studies of the abstraction reactions of thermal atomic fluorine have been completed, largely because of special experimental difficulties—the reactivity of HF, F_2, and other fluorinated species; the great exothermicity of most HF-forming reactions, with consequent temperature increases and difficulties in kinetic control; etc.[7-9] We have now carried out a series of measurements of the relative rates of the hydrogen abstraction reaction by near-thermal ^{18}F atoms with H_2, D_2, CH_4, CD_4, C_2H_6, and CH_3CF_3 by a method which appears capable of extension to most volatile molecules with little change in procedure.

The ^{18}F atoms have been formed as high kinetic energy atoms by the nuclear reaction $^{19}F(n,2n)^{18}F$, and 98% of them have been moderated to near-thermal energies through multiple collisions with SF_6,[10] the major component of all of the irradiation systems.[11-14]

$$^{18}F + CH{\equiv}CH \longrightarrow CH^{18}F{=}\dot{C}H \qquad (2)$$

$$CH^{18}F{=}\dot{C}H + HI \longrightarrow CH_2{=}CH^{18}F + I \qquad (3)$$

In the presence of 2:1 C_2H_2–HI as minor components, these moderated ^{18}F atoms add to C_2H_2 to form $CH^{18}F{=}\dot{C}H$, are stabilized by collisions at these pressures (>3000 Torr of SF_6), and are assayed by radio gas chromatography as $CH_2{=}CH^{18}F$.[11] The inclusion of an additional RH molecule in concentrations 2–10 times that of C_2H_2 diminishes the yield of $CH_2{=}CH^{18}F$ by the competition of (1) and (2). The tracer level of the experiments avoids most of the difficulties involved with corrosive materials and with the exothermicity of HF-forming reactions.[6,11-14] The temperature of the samples remained at 10° throughout the experiments.

(1) J. T. Muckerman, *J. Chem. Phys.*, **54**, 1155 (1971).

(2) R. L. Jaffe and J. B. Anderson, *ibid.*, **54**, 2224 (1971).

(3) T. P. Schafer, P. E. Siska, J. M. Parson, F. P. Tully, Y. C. Wong, and Y. T. Lee, *ibid.*, **53**, 3385 (1970).

(4) J. H. Parker and G. C. Pimentel, *ibid.*, **51**, 91 (1969).

(5) J. C. Polanyi and D. C. Tardy, *ibid.*, **51**, 5717 (1969).

(6) N. J. Parks, K. A. Krohn, and J. W. Root, *ibid.*, in press.

(7) G. C. Fettis and J. H. Knox, *Progr. React. Kinet.*, **2**, 1 (1964).

(8) P. D. Mercer and H. O. Pritchard, *J. Phys. Chem.*, **63**, 1468 (1959).

(9) G. C. Fettis, J. H. Knox, and A. F. Trotman-Dickenson, *J. Chem. Soc.*, 1064 (1960).

(10) The products known to be of "hot" origin—$SF_5{}^{18}F$ (~1%), $CH{\equiv}C^{18}F$ (<0.1%), $CH_3{}^{18}F$ from CH_4, etc.—are not included in the estimate of total well-moderated ^{18}F atoms.

(11) R. L. Williams and F. S. Rowland, *J. Amer. Chem. Soc.*, submitted for publication.

(12) T. Smail and F. S. Rowland, *J. Phys. Chem.*, **74**, 1866 (1970).

(13) T. Smail, G. E. Miller, and F. S. Rowland, *ibid.*, **74**, 3464 (1970).

(14) T. Smail, R. S. Iyer, and F. S. Rowland, *ibid.*, **75**, 1324 (1971).

All of the measurements were made in systems with about a 20-fold ratio of SF_6 to the other components. The interference with the acetylene addition reaction by HI alone was measured over the HI–C_2H_2 range from 0.1 to 5, and showed reasonably linear competition between reaction 1 with HI and 2. The slope of this line determined the relative rate for abstraction from HI *vs.* addition to acetylene, while the extrapolated intercept at zero HI was a measure of the rate of the abstraction from C_2H_2 itself. All of the other rates were determined in mixtures of SF_6, C_2H_2, HI, and RH, and corrections were made for the abstraction yields from C_2H_2 and HI. After such corrections—usually small—had been applied, reasonably linear behavior was again found for diminutions up to a factor of 3 in the $CH_2{=}CH^{18}F$ yields from the competition of RH with the acetylene-addition reaction. A 10-fold excess of Xe did not interfere in the scavenging of the ^{18}F atoms by acetylene, indicating negligible collisional stabilization under these conditions of a possible $Xe^{18}F$ intermediate. The relative rates of the abstraction reaction, per molecule and per hydrogen atom, are summarized in Table I. The error limits include an estimate of possible systematic variations.

Table I: Relative Rates of Hydrogen Atom Abstraction by Near-Thermal ^{18}F Atoms

	Relative rate[a]	
Substrate	Per molecule	Per hydrogen atom
HI	0.40 ± 0.05	0.40 ± 0.05
C_2H_2	0.12 ± 0.02	0.06 ± 0.01
C_2H_6	1.2 ± 0.2	0.20 ± 0.03
CH_4	0.43 ± 0.04	0.11 ± 0.01
CD_4	0.27 ± 0.04	0.07 ± 0.01
H_2	0.14 ± 0.02	0.07 ± 0.01
D_2	0.08 ± 0.01	0.04 ± 0.005
CH_3CF_3	0.05 ± 0.01	0.017 ± 0.003
Xe	0.00 ± 0.01	...

[a] Addition of ^{18}F to CH≡CH is the standard = 1.0.

Earlier measurements of the relative rates of hydrogen abstraction by fluorine atoms showed only small variations for different RH molecules—about a factor of 2 per H atom from the most easily abstracted (tertiary H in isobutane) to the least easily abstracted (H_2).[7-9] Our relative rates for the sequence C_2H_6–CH_4–H_2 show a somewhat wider variation than that found earlier, and the total range of about a factor of 25 per bond between HI and CH_3CF_3 is much larger than any previously published relative rate difference for such abstraction reactions by fluorine atoms. If the A factors are approximately equal, this factor of 25 at 10° represents an activation energy difference of 1.8 kcal/mol. The relatively low reactivity of CH_3CF_3 toward abstraction of H by thermal fluorine atoms has been previously described by Root, *et al.*, on the basis of scavenging curves for the reactions of hot ^{18}F atoms with CH_3CF_3, using $CF_3CF{=}CF_2$ as the scavenger.[6,15] The C–H bond in CH_3CF_3 has previously been shown to be relatively resistant to attack by thermal Br atoms, with an estimated bond dissociation energy about 5 kcal/mol higher than for CH_4.[16]

Our calculated k_H/k_D isotope effects for the relative rates of abstraction are 1.6 ± 0.2 for methane and 1.8 ± 0.2 for molecular hydrogen. The latter value is in reasonable agreement with the ratio calculated by classical trajectories on an LEPS surface of 1.59 ± 0.24,[1,17] but it is probably in small disagreement with the values of 1.41 and 1.34 calculated on the same surface using activated complex theory (classical and quantum reactant molecule partition functions, respectively).[1] No such isotope effect calculations have been performed as yet for the methane system.

The ^{18}F atoms in the 20:1 SF_6–RH systems are nearly thermalized, but measurements at ratios as high as 200:1 indicate some deviation from the relative rates given in Table I. This variation in relative rates indicates that our experiments effectively average over a distribution of ^{18}F atoms which includes a significant component not quite in thermal equilibrium with the environment. The trends in relative rates measured at 80% SF_6 and 95% SF_6 suggest that addition to acetylene has a lower activation energy than does abstraction from either HI or the hydrocarbons.

(15) N. J. Parks and J. W. Root, presented at the 161st National Meeting of the American Chemical Society, Los Angeles, Calif., Mar 1971.

(16) J. C. Amphlett and E. Whittle, *Trans. Faraday Soc.*, **64**, 2130 (1968).

(17) The apparent k_H/k_D factor for H_2 *vs.* D_2 of 25 at 300°K in the classical trajectory calculation of ref 2 is in error; the correct value is about 1.6 for that calculation (J. B. Anderson, private communication).

(18) This research was supported by A.E.C. Contract No. AT-(04-3)-34, Agreement No. 126.

DEPARTMENT OF CHEMISTRY[18]
UNIVERSITY OF CALIFORNIA
IRVINE, CALIFORNIA 92664

RONALD L. WILLIAMS
F. S. ROWLAND*

RECEIVED JUNE 18, 1971

FUEL CELL SYSTEMS—II

ADVANCES IN CHEMISTRY SERIES NO. 90

Thirty-one papers from the fifth of the biennial Fuel Cell Symposia sponsored by the Division of Fuel Chemistry, chaired by Bernard S. Baker. Topics include:

- **fuel cell power systems**
- **electrode structure**
- **use of hydrocarbons**
- **electrode catalysis and mechanisms**
- **high temperature fuel cells**
- **fuel cell systems**

Fuel cells are still doing their job well in the space program. Total energy, stationary fuel cell power plants seem worth a commercial push, and some hybrid devices look promising.

456 pages with index Cloth bound (1969) $17.50

Free set of L. C. cards with library orders upon request

Other books in the ADVANCES IN CHEMISTRY SERIES in fuel chemistry include:

No. 80 Chemical Reactions in Electrical Discharges. A wide range of topics is covered in 37 papers by chemists, physicists, and engineers—treatments of decomposition and dissociation reactions, ion-molecule reactions, chemical syntheses, and chemical engineering aspects and physics of reactions in electrical discharges. 514 pages
Cloth (1969) $15.00

No. 78 Literature of Chemical Technology. Forty articles discuss the literature of many aspects of chemical technology; seven of these are related to fuel cells, including electrochemistry of non-metals, noble metals, ceramics, enamels and glass, refractories, resources for petroleum chemicals, rocket propulsion, and rocket construction materials. 732 pages
Cloth (1968) $17.50

No. 69 Fuel Gasification. Waning natural gas supplies and the threat of nuclear fuels are renewing interest in converting solid fuels to high B.t.u. gas. Sixteen studies survey current research in the U.S. and elsewhere from which commercial processes seem imminent. 276 pages
Cloth (1967) $10.50

No. 64 Regenerative EMF Cells. Seventeen papers survey current progress and research on regenerative systems for converting and storing electrical energy. Principal emphasis is on thermally regenerative systems, but chemical and photochemical systems are considered. 309 pages
Cloth (1967) $11.00

No. 55 Coal Science. Forty-seven papers include coal origins, coal metamorphosis, coal as an organic rock, physical and chemical structure of coals, reactivity and reactions of coal in relation to structure and rank. 743 pages
Cloth (1966) $17.50

No. 54 Advanced Propellant Chemistry. Primarily directed toward the search for new oxidizers. Topics include theoretical approaches to advanced oxidizers, surveys of oxygen- and fluorine-containing oxidizers, fuels and binders, liquid systems. 290 pages
Cloth (1966) $10.50

No. 47 Fuel Cell Systems. New systems for the energy converter proving itself in military and space uses. Topics include fuel cells for submarines and satellites, hydrogen-bromine fuel cells, molten carbonate fuel cells, and a coal burning fuel-cell power plant. 360 pages
Cloth (1965) $10.50

No. 20 Literature of the Combustion of Petroleum. Twenty-one papers about the chemistry and kinetics of combustion, petroleum products as the fuel for engines, and combustion studies in engines. 295 pages
Paper (1958) $8.00

No. 5 Progress in Petroleum Technology. Survey of 25 years of progress at the ACS Diamond Jubilee. Thirty-two papers on all aspects of petroleum processing and products. 392 pages
Paper (1951) $8.00

Postpaid in U.S. and Canada; plus 30 cents elsewhere.

Order from:

SPECIAL ISSUES SALES
AMERICAN CHEMICAL SOCIETY
1155 SIXTEENTH ST., N.W.
WASHINGTON, D.C. 20036

Keep pace with the new...

through these basic research journals of the American Chemical Society

The Journal of the American Chemical Society

The premier American chemistry journal publishing original research papers in every field. Biweekly.

*ACS members:	U.S. $22.00	Canada, PUAS $26.50	Other nations $27.50
Nonmembers:	U.S. $44.00	Canada, PUAS $48.50	Other nations $49.50

The Journal of Organic Chemistry

Embraces the field, from synthesis to structure to behavior. Biweekly publication.

*ACS members:	U.S. $20.00	Canada, PUAS $24.50	Other nations $25.50
Nonmembers:	U.S. $40.00	Canada, PUAS $44.50	Other nations $45.50

The Journal of Physical Chemistry

Maintains a balance between classical areas of chemistry and modern structural quantum oriented areas. Biweekly.

*ACS members:	U.S. $20.00	Canada, PUAS $24.00	Other nations $25.00
Nonmembers:	U.S. $40.00	Canada, PUAS $44.00	Other nations $45.00

Biochemistry

Covers enzymes, proteins, carbohydrates, lipids, nucleic acids and their metabolism, genetics, biosynthesis. Biweekly.

*ACS members:	U.S. $20.00	Canada, PUAS $23.00	Other nations $23.50
Nonmembers:	U.S. $40.00	Canada, PUAS $43.00	Other nations $43.50

The Journal of Agricultural and Food Chemistry

Places special emphasis on the chemical aspects of agricultural and food chemistry. Bimonthly.

*ACS members:	U.S. $10.00	Canada, PUAS $13.00	Other nations $13.50
Nonmembers:	U.S. $20.00	Canada, PUAS $23.00	Other nations $23.50

The Journal of Medicinal Chemistry

Emphasis is on synthesis, mode of action and pharmacology of medicinal agents. Monthly.

*ACS members:	U.S. $15.00	Canada, PUAS $18.00	Other nations $18.50
Nonmembers:	U.S. $30.00	Canada, PUAS $33.00	Other nations $33.50

The Journal of Chemical and Engineering Data

Quarterly journal presenting data on properties and behavior of both new and known chemical systems.

*ACS members:	U.S. $15.00	Canada, PUAS $18.00	Other nations $18.50
Nonmembers:	U.S. $30.00	Canada, PUAS $33.00	Other nations $33.50

Inorganic Chemistry

Publishes original research, both experimental and theoretical, in all phases of inorganic chemistry.

*ACS members:	U.S. $18.00	Canada, PUAS $21.00	Other nations $21.50
Nonmembers:	U.S. $36.00	Canada, PUAS $39.00	Other nations $39.50

Macromolecules

Presents original research on all fundamental aspects of polymer chemistry. Bimonthly publication.

*ACS members:	U.S. $12.00	Canada, PUAS $15.00	Other nations $15.50
Nonmembers:	U.S. $24.00	Canada, PUAS $27.00	Other nations $27.50

American Chemical Society / 1155 Sixteenth Street, N.W., Washington, D.C. 20036

Please enter a one year subscription for the following journals:

1 _____ 2 _____ 3 _____

4 _____ 5 _____ 6 _____

7 _____ 8 _____ 9 _____

name _____ position _____

address _____

city _____ state/country _____ zip _____

your company _____ nature of company's business _____

☐ I am an ACS member ☐ I am not an ACS member ☐ Bill me for $ _____

☐ Payment enclosed (*payable to American Chemical Society*) in the amount of $_____. Payment must be made in U.S. currency, by international money order, UNESCO coupons, or U.S. bank draft; or order through your book dealer.

* NOTE: Subscriptions at ACS member rates are for personal use only.

72A